# Application of Niobium Compounds Towards the One-Step Synthesis of Methyl Isobutyl Ketone (MIBK) via Catalytic Distillation

by

William Kevin O'Keefe

A thesis
presented to the University of Waterloo
in fulfillment of the
thesis requirement for the degree of
Doctor of Philosophy
in
Chemical Engineering

Waterloo, Ontario, Canada, 2008

I hereby declare that I am the sole author of this thesis.

This is a true copy of the thesis, including any required final revisions, as accepted by my examiners.

I understand my thesis may be made electronically available to the public.

## ABSTRACT

Dispersed niobia catalysts were prepared via a non-aqueous synthesis route. The effects of the type of oxide support, the support thermal pre-treatment, the calcination temperature and the niobia loading on the activity and selectivity for mesityl oxide (MO) synthesis at 160°C were investigated in an autoclave reactor. The morphological and chemical properties of the catalysts were characterized via EDXRF, XRD, BET and Raman spectroscopy. The strength and nature of the acid sites were elucidated via *in situ* DRIFT spectra of the adsorption of pyridine as well as the temperature programmed desorption of $NH_3$ interacting with the surface oxide phase. All four catalyst parameters had significant effects on the catalytic properties. Significantly, the nature of the acidity was clearly linked to the catalyst activity and particularly the catalyst stability. Catalysts exhibiting predominantly Lewis acidity invariably deactivated despite good initial activity, with the final acetone conversion dependent on the catalyst formulation. In contrast, catalysts exhibiting Bronsted acidity showed no evidence of catalyst deactivation after 8 hours of reaction. A plausible mechanism which explains these observations is proposed.

Catalysts exhibiting Lewis acidity were more active when the supports were first activated at elevated temperature, likely due to a stronger support-surface oxide interaction as a consequence of increased surface coordinative unsaturation of the support. $SiO_2$ supported catalysts exhibiting Bronsted acidity were more active if the supports were initially activated at 100°C. Evidently, the hydroxyl groups on the oxide support contribute to the generation of Bronsted acidity. Different oxide supports gave rise to distinct acidic and catalytic properties in the niobia overlayer. The most striking example of this was the direct comparison of niobia dispersed onto two kinds of silica supports following the same preparative method. Unique and very strong acid sites were observed in niobia dispersed onto a commercial $SiO_2$ catalyst carrier that were not observed in niobia dispersed onto fumed $SiO_2$. For $SiO_2$ catalysts, the activity increased linearly with niobia loading regardless of calcination

temperature. In contrast, $Al_2O_3$ catalysts exhibited an initial increase in activity for MO synthesis with niobia loading followed by a decrease in activity after reaching a maximum activity below 1/3 monolayer coverage. The effect was more pronounced for catalysts exhibiting Bronsted acidity. It is proposed that adlineation sites are primarily responsible for catalytic activity in $Nb_2O_5/\gamma$-$Al_2O_3$ catalysts exhibiting Bronsted acidity.

Niobia catalysts were developed using commercially available catalyst carriers as supports. The macrokinetics of MO and MIBK syntheses were investigated in a benchtop fixed bed flow reactor. The catalysts showed excellent activity for MO and MIBK syntheses at 160°C, typically 0.9 to 1.3 [$g/hr*g_{cat}$]. However, the MIBK selectivity was constrained from 82 to 85% due to the coproduction of 2-propanol and diisobutyl ketone. The productivity for MO synthesis was found to be strongly dependent on the space velocity suggesting product inhibition. The intrinsic kinetics of the one-step synthesis of MIBK over a 15.2 wt% $Pd/Nb_2O_5/SiO_2$ catalyst was investigated in an autoclave reactor. A kinetic model was developed and is reported.

The one step synthesis of MIBK was investigated at the pilot plant scale via catalytic distillation (CD). An important finding was that while operating at 100% reflux, the accumulation of water in the reactive section resulted in the suppression of the DAA dehydration reaction. The *in situ* removal of water from the reactive section via an overhead distillate stream operating at 83 to 97% reflux directly resulted in an increase in MIBK productivity and hydrogen uptake efficiency by factors of about 20 yielding a moisture free reboiler product stream with as high as 53 wt% MIBK. The process was found to be controlled by the external mass transfer of hydrogen. Interestingly, the results suggest that the catalyst wetting efficiency affects the transport of hydrogen to the active sites as evidenced by the dependence of MO conversion on the reflux flow rate. The condition of minimum reflux flow rate and maximum hydrogen flow rate resulted in 97% MO conversion and 90 wt% MIBK selectivity.

## ACKNOWLEDGEMENTS

The author would like to express his sincerest appreciation to Professors Flora T.T. Ng and Garry L. Rempel for their steadfast support, patience and guidance throughout the course of this arduous research project. In particular, the author is grateful to his supervisors for extending a hand up, raising the author's research skills to higher levels and for providing the opportunity to join the catalysis community as a contributing member.

The author would like to thank the members of Professor Ng's research group, past and present, for sharing their knowledge and experience. Special thanks to Dr. Ming Jiang, an excellent researcher and the ultimate team player, for sharing his knowledge of physical chemistry, for teaching IR techniques, for his collaboration on some spectroscopic investigations and for always being willing to help out the students regardless of his own workload. Thanks to Dr. Donghua Zuo for sharing his knowledge of applied catalysis and FTIR and to Dr. Zhiwen Qi for helping out with gProms and CD experiments. Thanks to Dr. Prem Pal for helping with the TPD instrument and Dr. Kamalakar Gundar for sharing his knowledge of synthetic preparative chemistry and UV-Vis spectroscopy. Thanks to the other post docs who came and went through the years for their friendship as well as their advice and assistance: Dr. Yuxiang Zheng, Dr. Atuar Rhaman, Dr. Jin Nam Park and Dr. Manzoor Sultan. A special thanks to the other students, my friends, who shared the ride with me through the ups and downs; Dr. Amitava Sarkar, Dr. Deepyaman Seth, Dr. Taylor Xu, Dr. Roy Li, Greg Dechaine, Jen Moll, Tina Liu, Annie Zhang, Keir Thomas, Amir Arivani, Aijaz Baig and Chris Choi. The author would especially like to thank those who put their own research on hold to help out with the CD experiments, working long hard hours including night shifts in the pilot plant: Taylor, Amit, Deep, Greg, Donghua, Zhiwen, Ming, Peter, Kamalakar, Aijaz, Chris and Yuxiang!

Thanks to Professor I.E. Wachs, for his advice regarding the Raman spectroscopic analysis of niobia compounds. Thanks to Randy Fagan for his training and assistance with Raman Spectroscopy. Thanks to Brian Ellis for XRD training and assistance with the interpretation of the results. Thanks to Professor Legge for the use of his Karl Fischer Titrator and to Joe Clifford and Amanda Warboys for helping analyze the samples. Thanks to Jennifer Moll for EDXRF training and our undergraduate co-op students, Peter Rhebein and Amanda Warboys, who helped with the daily tasks and some BET and GC analysis. Thanks to Professors Eric Croiset and Bill Epling for the use of their GC/MS.

The author would like to thank the UW department of chemical engineering technicians and administrative staff for their assistance: Bert Habicher, Rick Hectus, Ralph Dickhout, Ravindra Singh, Ron Neil, Liz Bevan, Wendy Irving, Pat Anderson and Ingrid Sherrer.

The author would like to thank the members of his thesis advisory committee for their time and effort in reading this thesis as well as the PhD proposal and for providing constructive feedback to improve the quality of this work: Professors R.R. Hudgins, E. Croiset, T. Leung, J. J. Spivey, F.T.T. Ng and G.L. Rempel.

A special thanks to Rhonda and her family for being so supportive of the difficult decision to leave Husky Injection Molding Systems Ltd. in order to pursue higher education.

Financial support for this research provided to W. O'Keefe from the Government of Ontario, Ministry of Training Colleges and Students in the form of Ontario Graduate Scholarships is gratefully acknowledged. Financial support from the University of Waterloo in the form of University of Waterloo President's Graduate Scholarships and Faculty of Engineering Scholarships were very much appreciated. This research project was funded by the Natural Science and Engineering Research Council (NSERC) of Canada, Strategic Grants Program. Alumina and silica catalyst carriers were provided courtesy of Saint-Gobain Norpro.

## USE OF COPYRIGHTED MATERIAL

Some figures in this thesis have been reprinted from other sources with permission from the publishers. The permissions in writing are provided in Appendix G.

The DRIFT spectra in Figures 7-10 and 7-11, were obtained by Dr. Ming Jiang and used by permission from M. Jiang and F. T. T. Ng, "Adsorption properties of a $Pd/Al_2O_3$ catalyst", (2002) unpublished internal communication.

The schematic of the CD liquid sampling apparatus (Figure 8-5) was prepared by Suzanne K. Fines. The drawing was submitted in an unpublished internal communication (engineering report) to Prof. F.T.T. Ng as the principal deliverable of their design project intended for use by the UW catalytic distillation group. Used by permission.

## DEDICATION

This work is dedicated to my family; past, present and future…

For my mother, Eileen Margaret O'Keefe (1930-1997) for the countless sacrifices she made in order to provide a better life for my brother and I and for demonstrating the true meaning of strength. For my Aunts Judith Landers and Gwen Johnston, who were my greatest supporters in my pursuit of higher education. For my Aunt Betty and Uncle Ernie, who drove me to the hockey rinks before dawn and never missed a game. For my cousins Gail and Anne who sparked my interest in science at a very early age. For my many other uncles, aunts and cousins too numerous to name here, who have all helped me along the way. For Glenn and for Erin. For Rhonda and family.

*"…Come, my friends,*
*'Tis not too late to seek a newer world.*
*Push off, and sitting well in order smite*
*The sounding furrows; for my purpose holds*
*To sail beyond the sunset, and the baths*
*Of all the western stars until I die.*
*It may be that the gulfs will wash us down:*
*It may be we shall touch the Happy Isles,*
*And see the great Achilles, whom we knew.*
*Tho' much is taken, much abides; and tho'*
*We are not now that strength which in old days*
*Moved earth and heaven; that which we are, we are;*
*One equal temper of heroic hearts,*
*Made weak by time and fate, but strong in will*
*To strive, to seek, to find, and not to yield."*

- Excerpt from "Ulysses" by Alfred Lord Tennyson

# Table of Contents

Chapter Four: Study on the Effects of Niobia Catalyst Properties on the Activity, Selectivity and Stability for MO Synthesis

# List of Figures

## *Chapter One*



## *Chapter Two*



## *Chapter Three*

*Chapter Four*

*Chapter Five*

*Chapter Six*

*Chapter Seven*

*Chapter Eight*

*Appendix A*



*Appendix B*



*Appendix C*



*Appendix D*

*Appendix E*



*Appendix F*

# List of Tables

*Chapter One*



*Chapter Three*



*Chapter Four*

*Chapter Five*



*Chapter Six*



*Chapter Seven*

*Chapter Eight*

*Appendix A*



*Appendix B*

*Appendix C*



*Appendix D*



*Appendix E*

## NOMENCLATURE

***Acronyms***

cps = counts per second (dimensions of intensity of radiation)
CCD = central composite design (of experiment)
CD = catalytic distillation
$C_4$ = isobutylene
DAA = Diacetone Alcohol
DIBK = Di-isobutyl Ketone
DIPE = Di-isopropyl ether
DL = Detection Limit
DoE = Design of Experiment (implies statistical experimental design)
DRIFT = Diffuse Reflectance Infrared Fourier Transform (Spectroscopy)
EDXRF = Energy Dispersive X-Ray Fluorescence (Spectroscopy)
FBR = fixed bed reactor
FID = Flame Ionization Detector
FTIR= Fourier transform infrared (spectroscopy)
GC = Gas chromatography
HAc = acetic acid
HEX = denotes heat exchanger
HG = hexelene glycol
HHI = half hydrogenated intermediate
ICP = inductively coupled plasma (spectroscopy)
IMO= isomesityl oxide
IPA = isopropyl alcohol (IPA)
IPO = Isophorone
IR= infrared (spectroscopy)
KFT = Karl Fischer Titration
LEL = Lower Explosive Limit of a combustible gas
MIBC = Methyl Isobutyl Carbinol
MIBK=Methyl Isobutyl Ketone
MO = mesityl oxide
MS = Mass Spectroscopy
ODE = ordinary differential equation
PHO = phorone
QL = Quantitation Limit
RDS = rate determining step
RSD = Relative Standard Deviation; the standard deviation of a set of data or standard error of a regression model normalized by the mean value

$$RSD = 100\% * \frac{\sigma}{\overline{X}}$$

RSEE = relative standard error of estimate (of a predictive model)
sccm = standard cubic centimetres per minute
SMSI = strong metal support interaction
SOSI = surface oxide support interaction
STP = standard temperature and pressure

TBR = trickle bed reactor
TCD = thermal conductivity detector
TMB = Trimethyl Benzene (mesitylene)
TMP = 2,2,6,6-tetramethyl-r-pyrone
TOS = time on stream (hr)
TPD = Temperature Programmed Desorption

***Variables and Parameters***

a(t) = hydrogenation catalyst activity (dimensionless); defined in equation 8-13
a = activity (equations 2-10, 2-11); empirical model parameter in equation 5-1
A = Arrhenius pre-exponential factor
b=empirical model parameter in equation 5-1
$C_i$ = concentration (mol/L) of species "i" (eg. $C_W$ denotes water concentration)
$\overline{C}_p$ = mean heat capacity
$C_V$ = valve flow coefficient
$C_6^+$ = denotes the collective sum of the concentrations of higher molecular weight species from MO synthesis (phorones, mesitylene etc.) including unidentified species. "Other or Unknown $C_6^+$" refers to the collective sum of the concentrations (wt%) of all unidentified organic species excluding the known species
$d_p$ = particle diameter

$-\frac{dC_A}{dt}$ = rate of acetone consumption (eqn. 2-12)

$\frac{d\hat{C}_i}{dt}$ = specific rate of reaction to produce species "i" (i.e. productivity) [g/(hr*mL$_{cat}$)]

$\frac{dC_I}{dt}$ = rate of MIBK production (Eqn. 2-13)

$\frac{d_{DAA}}{dt}$ = rate of DAA production (Eqn. 2-10)

$D_{AB}$ = molecular diffusivity of solute A in solvent B (liquid phase)
$D_a$ = impeller diameter (m)
$D_{A,K}$ = Knudsen diffusivity of solute A
$D_e$ = effective diffusivity
$E_A$ = activation energy
$F_{A0}$ = acetone molar flow rate at reactor inlet
$F_A$ = acetone molar flow rate exiting the reactor
g = acceleration due to gravity (9.81 m/s$^2$)
$Ga_L$ = liquid phase Galileo number, defined in equation (8-6)
Ha = Hatta number defined in Equation (6-21)

$k_i$ = rate constant
$k'_s$ = pseudo first order rate constant for spent hydrogenation catalyst Eqn (8-13)
$k'_0$ = pseudo first order rate constant for fresh hydrogenation catalyst Eqn (8-13)
$k'_L$ or $K_L$ = liquid mass transfer coefficient (m/s)
$k_c$ = mass transfer coefficient
$K_c$ = equilibrium constant
L = reflux flow rate [g/min]
$M_i$ = molecular mass of species "i"
$\dot{m}_i$ = molar flow rate of species "i"
n = order of reaction
$n_i$ = number of moles of species "i"
N = agitation rate (revolutions/second)
$N_i$ = number of moles of species "i" (equations 6-9, 6-10 and 6-11)
$N_P$ = Power number (for agitated vessels, defined in Equation 6-20)
P = system pressure (absolute) [psia], used in equation (8-7)
P = power (watts)
Q = external heater duty [W], used in equation (8-7)
$\dot{Q}$ = condenser duty [W]
$Q_R$= reboiler duty [W]; equation (8-7)
r = reaction rate ($kmol/m^3*s$)
$r_{MO}$ = rate of mesityl oxide production (eqn 2-11)
r = pore diameter
r'= specific reaction rate (kmol/s*gcat) or
R= catalyst pellet radius
Re = modified Reynolds number equation (8-6); impeller Reynolds number equation (6-19)
S=standard deviation of analytical background response (Eqn. 3-1)
S = selectivity (eg. Eqn 6-2)
$S_H$ = hydrogenation selectivity (mol%) defined in Eqn. 6-1
Sc = Schmidt number (defined in Eqn. 6-17)
T = absolute temperature
$T_c$ = critical temperature
$T_m$ = temperature associated with the peak maximum of the TPD peak associated with the strongest acid sites (maximum mean desorption temperature)
U = superficial velocity
V = reactant volume
$V_A$ = molar volume of solute "A" at its normal boiling point
W = catalyst mass
WHSV = weight hourly space velocity =(mass flow rate / catalyst mass)
$X_{Ac}$ = acetone conversion
$X_i$ = mass fraction (wt%) of organic species "i" in the sample mixture
Z = total height of bed of distillation packing

***Greek Symbols***

$\beta_i$ = parameter in a regression model
$\Delta G$ = Gibbs free energy change
$\Delta H$= enthalpy change (Eqn 2-3)or latent heat of vaporization (Eqn. 6-18)
$\Delta P$ = pressure drop across bed
$\Delta S$ = entropy change
$\varepsilon$ = bed porosity (void fraction)
$\eta_{CE}$ = external catalyst wetting efficiency, defined in equation (8-6)
$\mu$ = dynamic viscosity [in cP or kg/ms]
$\nu_i$ =stoichiometric coefficient
$\xi_B$ = association factor for solute "B" in Wilke-Chang equation (6-22)
$\Phi$ = objective function in equation (6-12)
$\varphi$ = fractional monolayer coverage
$\rho$ = density
$\rho_b$ = catalyst bed density
$\rho_c$ = density of continuous (liquid) phase
$\sigma$ = standard deviation or constriction factor
$\sigma^2$ = variance
$\tau$= tortuosity

***Subscripts and other symbols***

A = acetone
ads = denotes adsorbed species (Scheme 1-1)
dads = denotes diadsorbed species (Scheme 1-1)
MO = MO
I = inhibitor (eg. $K_I$); (eg. MIBK in Eqn. 2-13)
pho = phorone
W = water
* = denotes an available active site (Scheme 1-1)

# Chapter One

## Introduction

### 1.1 MIBK, its Uses and Economic Outlook

4-methyl-2-pentanone, also known as methyl isobutyl ketone (MIBK), is a valuable derivative of acetone; third in consumption behind bisphenol and methyl methacrylate.[1] It is primarily used as a solvent in paints, inks, adhesives and other surface coatings as a consequence of its outstanding solvating properties for organic compounds and is also used as a precursor in the syntheses of pesticides, surfactants and other specialty chemicals such as methyl isobutyl carbinol (MIBC).[1] Recently, there has been an increasing demand for MIBK for use as a precursor in the syntheses of anti-ozonants for rubber products.[1,2] MIBK has particular utility in metallurgical and solvent extraction processes as is also used in the manufacture of antibiotics, pharmaceuticals and as a denaturant for rubbing alcohol.[1]

The commercial production of MIBK has been ongoing for over sixty years.[1] MIBK is a relatively inexpensive commodity (eg. $0.77 USD/lb in March 2004) that is produced on a large scale.[2] Currently, the global demand for MIBK is estimated to be greater than 350 000 t/a and is increasing due to demand from emerging economies in developing nations such as China and India.[3] In China, MIBK production units are small scale operations that are relatively inefficient.[4,5] Consequently, China continues to import most of its MIBK and its demand has more than doubled recently, from 17 000 tons in 2001 to 36 900 tons in 2004.[4] In 2005 the Jilin Chemical Group Fine Chemicals Co. Ltd. commissioned a 15 000 t/a MIBK plant in Jilin, which is now China's largest MIBK production facility.[4] Prior to this facility coming online in 2005, China's MIBK capacity was only 2 500 t/a.[4] In response to the increasing global demand for MIBK, Sasol Limited announced in December 2005 that it will be doubling its capacity for MIBK production to 60 000 t/a by

constructing a new MIBK plant in Sasolburg, South Africa, which is expected to come online in 2009.[3] Shell Oil, the world's largest producer of MIBK, has recently invested $50 M (US) to increase capacity in its oxygenated solvents plants by 55 million pounds per year, including its Deer Park Texas facility where MIBK is produced.[2,6]

Although global demand for MIBK is increasing, in developed countries the demand for MIBK remains unchanged as an increasing demand for MIBK for use in rubber applications is offset by a reduced demand for MIBK for use in solvent applications.[1,2] MIBK is non-toxic, however, it is known to contribute to the formation of ground level ozone and smog. Consequently, MIBK was designated a hazardous air pollutant in the US Clean Air Act Amendment (1990). As a result of this legislation, there has been a concerted effort by industry to reduce the amount of volatile organic compounds (VOC) including MIBK, in their products and processes. Regardless, US demand for MIBK increased steadily over the 1990's as chlorinated solvents were phased out in favour of oxygenated solvents and as industry best practices switched to an increased usage of "high solids coatings" where solvents with superior solvating properties, such as MIBK, are used but in lesser amounts.[2,7] The economic outlook for MIBK has recently been described as being flat with 0% market growth in developed countries over the short term, however its long term demand in developed nations will likely decline due to increasingly stringent environmental regulation and the drive to reduce the usage of VOCs.[2] In short, MIBK is a mature product and will remain in strong demand for the foreseeable future.

### 1.2 MIBK Synthesis

The synthesis of MIBK involves three major reaction steps. In the first step, acetone is dimerized to produce diacetone alcohol (DAA) via an aldol condensation reaction. This step is known to be extremely equilibrium limited with an equilibrium conversion of only 4.3 wt% at the normal boiling point of

acetone.[8,9] In the second step, which is also equilibrium limited,[10,11] DAA undergoes a dehydration reaction to produce mesityl oxide (MO) (an α,β-unsaturated ketone) and water. MO is accompanied by its isomer isomesityl oxide (IMO) with the material equilibrium strongly favouring the formation of MO. Lastly, the olefin bond of MO is selectively hydrogenated to produce MIBK. The acetone dimerization is slightly exothermic (-23 kJ/mol) , the DAA dehydration step is endothermic (+21 kJ/mol) and the hydrogenation step is strongly exothermic (-126 kJ/mol).[1] The heat effects from the first two reaction steps essentially negate each other; however, the overall MIBK synthesis is exothermic, primarily due to the strongly exothermic hydrogenation step.

MIBK production involves a relatively complex organic synthesis with numerous potential undesirable reactions as illustrated in Figure 1-1. MO, the immediate precursor to MIBK, may react with acetone to produce phorone and water via an aldol condensation reaction. The reaction of MO with acetone may also yield other isomers of phorone including 4,4-dimethyl-hepta-2,6-dione and 2,4-dimethyl-2,4-hetpadiene-6-one.[12] Phorone and its isomers may in turn react to form the cyclic isomers α-isophorone and β-isophorone and the cyclic compound mesitylene, also known as trimethyl benzene (TMB), via aldol condensation and Michael Addition reactions.[12-14] These cyclic compounds along with phorone and its isomers, may continue to react further to form numerous higher molecular weight species as well as thermal decomposition products including acetic acid and unsaturated hydrocarbons such as isobutylene.[14] Since phorone is an unsaturated molecule with two olefin groups and a ketone group, additional products may be obtained from its hydrogenation. The hydrogenation of one olefin group produces 2,6-dimethyl-2-heptene-4-one and the hydrogenation of both olefin groups produces diisobutyl ketone (DIBK), i.e. 2,6-dimethylheptan-4-one.[12] Isophorone may be hydrogenated to give 3,3,5-trimethyl-cyclohexanone. Similarly, the hydrogenation of mesitylene would yield 1,3,5-trimethyl cyclohexane.

The reaction of MO with acetone without the loss of water will produce "semi-phorone" (6-hydroxy-2,6-dimethyl-2-heptene-4-one) and its isomers (4,4-dimethyl-2,6-heptadione) and 2,2,6,6-tetramethyl-r-pyrone (TMP).[1] The dehydration of semi-phorone leads to the creation of pyran compounds.[1] DAA may also combine with acetone to form triacetone alcohol (TAA) or its isomer (4,6-dihydroxy-4,6-dimethyl,hept-2-one). The dehydration of TAA via the loss of one molecule of water leads to the production of semi-phorone and the loss of two water molecules results in phorone.[1] DAA may undergo a thermal decomposition reaction to produce acetic acid (HAc) and isobutylene ($C_4$) or may be hydrogenated to produce ethylene glycol (2-methyl-2,4-pentanediol).

Once the desired product has been obtained, MIBK may combine with acetone to form diisobutyl ketone (DIBK) or 2,6-dimethly-4-hydroxy-2-heptene (DMHA). These compounds may continue to react to form other oligomers. The direct hydrogenation of acetone producing 2-propanol, also known as isopropanol (IPA), is a significant undesirable parallel reaction commonly observed in processes for MIBK production. The secondary hydrogenation product, IPA, may dehydrate to form propene and water. Propene can be hydrogenated to produce propane. Alternatively, IPA molecules may react together to produce diisopropyl ether (DIPE) and water.

The ketone group of the desired product MIBK may be hydrogenated to form the saturated alcohol MIBC. Although it is possible that the ketone group of MO may be selectively hydrogenated without the hydrogenation of the olefin group to give the unsaturated alcohol 2-methyl-2-pentene-4-ol, this reaction pathway is very unlikely in the absence of promoters since the reactivity for hydrogenation of the olefin bond is known to be far greater than the reactivity of the ketone group in conjugated systems as a consequence of their relative adsorption strengths.[15] Thermodynamic considerations demonstrate that the C=C group in isolation is most easily hydrogenated followed by the C=C in a conjugated system, followed by the C=O group, which is most difficult to

hydrogenate.[16] Consequently, the unsaturated alcohol is rarely obtained using state-of-the-art hydrogenation catalysts designed to give high selectivity to the olefin hydrogenation.

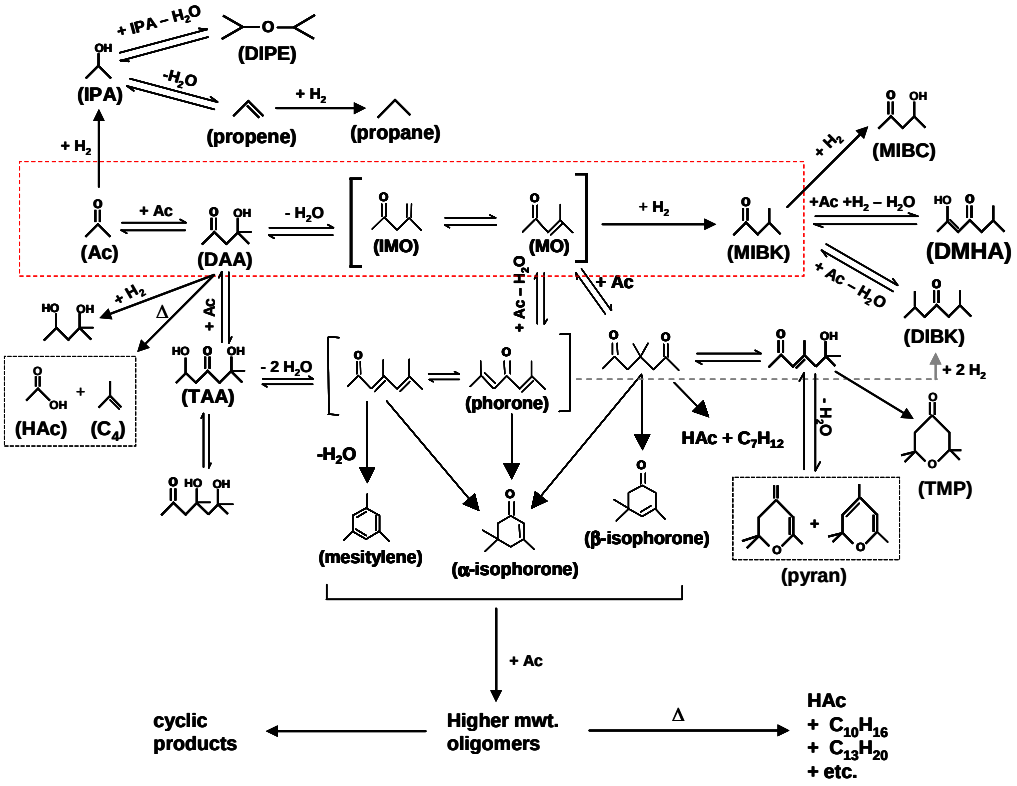


**Figure 1-1** Major Reaction Pathways for MIBK Synthesis[1,14]

The most successful hydrogenation catalysts for the selective hydrogenation of MO to MIBK are the group VIII B transition metals Pd, Pt and Ni. Pd is most commonly used since it typically gives the highest selectivity to MIBK. Other transition metals investigated for use in MIBK synthesis include the group VIII B elements Ru, Co and Rh. The group IIB metal Cu has also proven to be successful for MIBK synthesis. The observed trend of catalytic behaviour of these transition metals for MIBK synthesis can be explained by extension of the theory put forward by Delbecq and Sautet[15] for the selective hydrogenation of the olefin group of α,β-unsaturated aldehydes.

Upon adsorption, the conjugated C=C and C=O groups of α,β-unsaturated aldehydes and ketones compete for active sites. The prevalent adsorption mode will govern the activation of the substrate and hence its reactivity. In addition, the prevalent adsorption mode will constrain the possible reaction pathways and hence govern the reaction selectivity as well. Several adsorption modes are possible, as illustrated in Figure 1-2, as a consequence of the multiplicity of functional groups of the organic substrate.[15] Each of these adsorbed species exhibit unique adsorption strengths, which are also affected by the catalyst surface concentration of the substrates due to the effect of crowding. The prevalent adsorption mode is strongly dependent on the nature of the metal and the type of exposed crystal facet.[15] Moreover, the preferred adsorption mode may also be affected by the geometrical nature of the catalyst (i.e. structure sensitivity). It is generally believed that the most weakly bound species contribute to the hydrogenation reaction.[16]

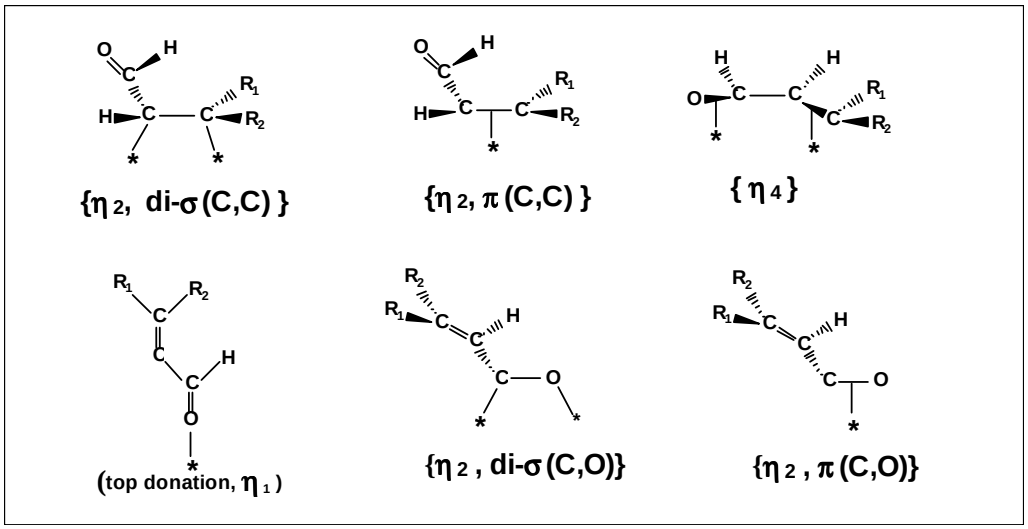


**Figure 1-2** Common adsorption modes of α,β-unsaturated aldehydes[15]
** denotes adsorption site*

Delbecq and Sautet[15] have postulated that the most thermodynamically favourable adsorption mode is governed by a competition between two-electron interactions which stabilize the adsorbed substrate and 4-electron interactions

which destabilize the adsorbed substrate. The two-electron interactions involve σ-donation and π-backbonding (Figure 1-3) resulting in a reduction in the total system energy as electrons from the d orbitals of the metal overlap with un-occupied π* anti-bonding orbitals of the substrate resulting in a decrease in electron density on the metal. The sigma donation results in the overlap of occupied s orbitals in the organic substrate with vacant d orbitals from the metal also reducing the total system energy while increasing the electron density on the metal. The four-electron interactions are repulsive interactions between occupied d orbitals on the transition metal and the occupied molecular orbitals of the organic substrate that have the correct energy and symmetry to overlap with the orbitals of the transition metal.

According to Delbecq and Sautet[15], a large d-band width implies a larger radial expansion of the filled d-orbitals of the metal resulting in greater spatial overlap with the orbitals of the organic substrate. Since the magnitude of the repulsive interaction between two filled orbitals is given by the square of their orbital overlap, a larger d-band width would result in greater 4-electron interaction and the suppression of the C=C hydrogenation by inhibiting its co-ordination while simultaneously promoting the co-ordination of the ketone group and its hydrogenation.[15] Thus, this theory allows the *apriori* prediction of catalytic behaviour for the selective hydrogenation of α,β-unsaturated aldehydes and ketones based on the d character of the transition metal. In the periodic table of the elements, the d-band width increases moving from right to left and moving from top to bottom. As predicted by this theory, the Group VIII elements Ni, Pd and Rh have been shown to give the highest initial selectivity for C=C bond hydrogenation, whereas Os has been shown to give the highest selectivity towards C=O hydrogenation.[16] Not surprisingly, Ni {[Ar]$3d^8 4s^2$} and Pd {[Kr]$4d^{10}$}, which are located in the periodic table of the elements at the top right corner of the group VIII metals, are commonly employed for the hydrogenation of MO. The IIB metal Cu {[Ar]$3d^{10} 4s^1$},

which is located immediately to the right of Ni on the periodic table, may also used for MIBK synthesis.

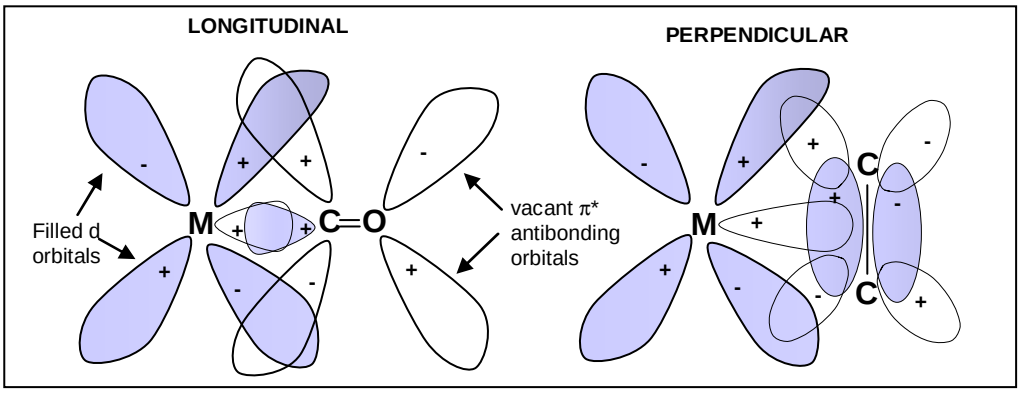


**Figure 1-3** Sigma donation and pi backbonding (based on drawing in Hegedus[17]) (left) longitudinal orientation involving carbon monoxide substrate; (right) perpendicular orientation involving an olefin substrate

MIBK is produced from the selective hydrogenation of the olefin group of MO. The author and co-workers[18] have recently proposed a novel reaction mechanism (Scheme 1-1) and mechanistic kinetic model (Eqn 1-1) for the liquid phase selective hydrogenation of MO over a $Pd/Al_2O_3$ catalyst. Since MO is an α,β-unsaturated ketone with conjugated C=C and C=O groups, the molecule may take several possible adsorption modes when coordinating with a heterogeneous catalyst. Quantum chemical calculations suggest that the most favourable adsorption mode of α,β-unsaturated aldehydes on a Pd (111) surface would be an $\eta_4$ diadsorbed species.[15]

Our proposed mechanism stipulates that a diadsorbed species arises due to the strong affinity of the ketone group for coordination with acidic sites and the necessary chemisorption of the olefin group to enable its hydrogenation.[18] If only a single site is available for adsorption, it is proposed that MO will coordinate preferentially via the ketone group and consequently, will act as an adsorbed inert. It is postulated that when adjacent sites are available, an $\eta_4$ diadsorbed species will result, with the olefin group forming an $\eta_2$(C,C) pi-complex at one site and the ketone group coordinating to the catalyst at an

adjacent active site forming an $\eta_2$(C,O) pi-complex. Alternatively, a similar diadsorbed species may be obtained by coordination of the carbonyl group to the catalyst via top donation $\eta_1$(C,O). MIBK is formed by the stepwise addition of dissociatively adsorbed atomic hydrogen to the diadsorbed organic substrate, first forming a half-hydrogenated intermediate (HHI), then the addition of atomic hydrogen to the HHI produces MIBK coordinated to the catalyst via the ketone group. The desorption of MIBK from the catalyst completes the reaction mechanism.

$$H_2 + 2^* \rightleftharpoons 2\,H_{ads}$$
$$MO + 2^* \rightleftharpoons MO_{dads}$$
$$MO_{ads} + H_{ads} \rightleftharpoons HHI_{dads} + *$$
$$HHI_{ads} + H_{ads} \rightleftharpoons MIBK_{ads} + 2^* \quad \text{(RDS)}$$
$$MIBK_{ads} \rightleftharpoons MIBK + *$$

**Scheme 1-1** Proposed mechanism for the selective hydrogenation of MO over a $Pd/Al_2O_3$ catalyst[18]

The mechanistic kinetic model of equation 1-1 was derived from the proposed mechanism in Scheme 1-1 via the Langmuir-Hinshelwood approach, assuming the second addition of hydrogen is the rate determining step. Incidentally, our proposed theory on the catalytic hydrogenation of MO, specifically the notion of the diadsorption of the organic substrate and the general form of the kinetic model (Eqn. 1-1) whereby the term expressing the fraction of available catalyst sites is raised to the fourth power, has been accepted as correct and has been subsequently used in the kinetic analysis of other researchers investigating MIBK synthesis. (eg. Talwalkar and Mahajani[19]). The requirement of the diadsorption of the substrate for hydrogenation implies that the reaction may be structure sensitive.

$$-r_A = \frac{kK_{AA}K_H C_A P_H}{\left[1 + K_A C_A + K_I C_I + \sqrt{K_H P_H}\right]^4} \qquad (1\text{-}1)$$

MO exists with its isomer, isomesityl (IMO). The author and coworkers[18] have shown that IMO is equally valuable as a precursor to MIBK exhibiting the same kinetics as MO. It is likely that IMO rearranges upon adsorption to the catalyst to form the same diadsorbed species that is created upon the adsorption of MO. As a consequence, IMO exhibits identical kinetic behaviour as MO.[18] Alternatively, it is possible that IMO is rapidly converted to MO in accordance with Le Chatelier's Principle as MO is hydrogenated to MIBK.

### 1.3 Conventional Processes for MIBK Production

Historically, MIBK has been produced in the multi-stage Hibernia-Schloven Process in which each of the three major reaction steps are carried out in separate reactors.[1] Since the first two reaction steps are equilibrium limited, a significant amount of unreacted material is present in the product streams. Consequently, distillation units are present downstream from the reactors in order to purify the product streams and to recover and recycle unreacted material. For example, the aldol condensation of acetone to produce DAA is typically carried out at as low a temperature as economically feasible (10 to 20°C) in order to maximize the chemical conversion.[1] However, only 8 to 15% acetone conversion is typically achieved at this temperature range with 20 to 60 minute residence times in a semi-batch reactor using a basic homogeneous catalyst such as sodium hydroxide.[1] The DAA dehydration step is carried out in a reactive distillation (RD) column at atmospheric pressure at 100 to 140°C using phosphoric acid as a homogenous catalyst.[1] In the third reaction stage, a solid catalyst is immobilized in the reactive section of a catalytic distillation (CD) reactor to facilitate the hydrogenation of MO at atmospheric pressure and 110°C.[1,20] Phase separators are required to remove water from the MO product stream prior to hydrogenation as well as to recover unreacted hydrogen from the MIBK product stream.

An advantage of the Hibernia-Schloven Process is that it offers the flexibility to allow the intermediate species DAA and MO to be extracted from

the process and sold as separate products if desired. DAA has a relatively high boiling point compared to MIBK, which may make it more desirable as a solvent from an environmental standpoint. In fact, DAA is currently used as an industrial solvent for resins and coating applications. Specifically, it is used for dissolving hot lacquers which have high molecular weight constituents, as a solvent for cellulose acetate, nitrocellulose and epoxy resins and is used as a precursor in the synthesis of hexelene glycol, which is a component in hydraulic brake fluid.[21] Since DAA is completely miscible with water, it is particularly useful for solvent applications requiring moisture tolerance.[1,21] MO is known to be relatively toxic. Consequently, its sale as a product for end use was terminated in the US in 1986.[21] However, MO is still valuable as a precursor for other value-added industrial chemicals such as isophorone and its derivatives and is used "captively", that is, being synthesized and chemically converted to another desired product or products at the same facility.[1,21]

The Hibernia-Schloven Process has clear disadvantages. In particular, the process is inherently inefficient and extremely energy intensive. The process requires significant capital investment and incurs substantial operating expenditures. The products from the first two reaction steps are produced in relatively low yield due to equilibrium limitations thus necessitating the further purification of the product streams by distillation and leads to a significant amount of material recycle. Since distillation is an extremely energy intensive process having a thermodynamic efficiency of less than 10%, additional distillation steps significantly add to the operating costs. The use of homogeneous catalysts is undesirable since these catalysts must be recovered from the product streams and recycled. Moreover, the DAA product stream from the first reaction step must be neutralized prior to the dehydration stage. In addition, these homogeneous catalysts create corrosion problems and inevitably lead to the generation of acidic and caustic waste streams.

Rising energy costs, increasingly strict environmental regulation as well as the continuous drive to reduce costs and improve the profitably of chemical processes has stimulated a gradual shift within the chemical industries towards sustainable development.[22] This trend is evident in the emergence of more efficient chemical processes with reduced emissions and reduced waste streams enabled by the development of novel catalyst and reactor technologies.[22] *Process Intensification*, is a principle of green engineering whereby two or more unit operations are combined into a single unit operation with the beneficial result of increased efficiency, reduced operating and capital costs and a reduction of waste and recycle streams. It is evident that the Hibernia-Schloven process for MIBK manufacture would benefit significantly from process intensification. Indeed, the Hibernia-Schloven process was the conventional technology for MIBK synthesis until the early 1970's at which point, "one-step" processes for MIBK synthesis emerged, for which the three major reaction steps producing MIBK from acetone are carried out simultaneously in a single reactor.[1] In this work, "one-step" synthesis is defined as a process where the production of MIBK from acetone and hydrogen is carried out in a single unit operation.

A one-step process for MIBK synthesis is made possible by a multifunctional catalyst that simultaneously facilitates the three major chemical transformations in a single reactor. The irreversible hydrogenation of MO breaks the equilibrium limitations of the previous reaction steps, thus shifting the reaction in favour of MIBK formation allowing acetone conversions much higher than the theoretical equilibrium conversion associated with the aldol condensation of acetone. The multifunctional catalyst typically consists of a transition metal such as Pd, Ni, Cu or Pt, which is responsible for the selective hydrogenation of MO, dispersed onto a support that contains acidic and or basic active sites that facilitates both the aldol condensation of acetone and the dehydration of DAA. Numerous catalysts have been investigated for this purpose including MgO and Mg-Al mixed oxides,[23-30] $CsOH/SiO_2$,[12,13] cation

exchange resins,[19,31-33] hydrotalcites and layered double hydroxides,[34-41] niobic acid ($Nb_2O_5 \cdot nH_2O$) and niobia ($Nb_2O_5$),[42-44] alumina and titania,[45,46] zirconium phosphate[47] and various zeolites.[48-54]

Due to its industrial importance, MIBK synthesis has been studied at length in both the liquid phase and the gas phase. The gas phase process is conducted in a fixed bed flow reactor at atmospheric pressure and temperatures typically less than 200°C but possibly as high as 290°C.[48] The low pressure operation is attractive from an economical perspective. However, gas phase processes give very low selectivity to MIBK, typically 60 to 80% and more importantly, gas phase processes for MIBK synthesis are severely limited by catalyst stability issues despite being investigated extensively.[43,49] State-of-the-art one-step processes for MIBK manufacture involve the liquid phase synthesis of MIBK in trickle bed reactors or multitubular fixed bed reactors at temperatures ranging from 100 to 160°C and pressures ranging from 1 to 10 MPa.[23-25] The liquid phase processes are robust with selectivities typically in excess of 90%.[23,24,42,48] However, the high pressure operation is economically detrimental.[23-25] In addition, the mass fraction of MIBK in the reactor product stream is typically less than 30 wt%, which necessitates further refining of the product stream and the recycle of unreacted material.[23,24] Consequently, there remains great incentive for the further development of novel catalysts and catalytic reactor technologies for the one-step synthesis of MIBK.

### 1.4 MIBK Synthesis via Catalytic Distillation

The goal of a highly efficient one-step process for MIBK synthesis remains an elusive but industrially important objective. This need is of heightened importance today in the current era of rising energy costs and increasingly stringent environmental regulation, presenting an excellent opportunity for the application of catalytic distillation (CD) technology. CD is a hybrid reactor technology which combines chemical reaction and product refinement in a single unit operation. The CD reactor consists of a distillation column, typically a packed column although tray column is also possible, within which

solid catalyst is immobilized inside one or more reaction zones (also known as *reactive sections*) within the column. It should be noted that the term "catalytic distillation" is reserved for those processes involving a heterogeneous catalyst while "reactive distillation" (RD) is usually reserved for those processes involving a homogeneous catalyst. However, some use the term "reactive distillation" as a general term encompassing both processes. Additionally, a third type of CD reactor has been disclosed whereby a solid powder catalyst is slurried in the feed stream and allowed to pass through the distillation column by convection within in the liquid phase.[55]

In the CD process, a continuous gas phase flows in a counter current mode with a discontinuous liquid phase. Rivulets and droplets of boiling liquid move down the column under the influence of gravity in the low interaction regime of trickle flow while wetting and spreading into thin films over the distillation packing and catalyst. Low interaction regime implies a weak interaction between gas and liquid phases. Consequently, the contribution of the gas-liquid interfacial drag forces and shear stresses to the wetting and spreading of liquid over the solid substrate are considered negligible. At the bottom of the column, a reboiler imparts energy to the system causing a reservoir of liquid to boil and a vapour stream to rise upwards through the packing contacting the liquid phase in a counter current fashion. The vapours are condensed in a condenser at the top of the column and some or all of the condensed liquid is refluxed to the column. Since a heterogeneous catalyst is used to facilitate the desired chemical transformations, the chemical reactions occur at or near liquid-solid, gas-solid and gas-liquid-solid interfaces within the mesoporous structure of the solid catalyst contained in the reactive sections. Chemical reaction does not occur in the non-reactive sections, which hold only inert distillation packing.

Since counter current flow is required, the heterogeneous catalyst must be supported on or contained within engineered structures in order to prevent an

excessive pressure drop and the subsequent flooding of the column. A minimum void fraction of 0.5 is required in order to ensure the feasibility of counter current operation in a fixed bed.[56] Random and structured distillation packing typically yield void fractions from about 0.7 to as high as 0.97.[56] Since catalyst particles larger than about 3 mm generally lead to intraparticle mass transfer limitations, smaller catalyst particles ranging between 1 to 3 mm are typically used in catalytic reactors.[57] Unfortunately, the direct loading of these small catalyst particles into a distillation column would result in an insufficient void volume (ca. 0.3 to 0.4) to prevent flooding. However, a plethora of design concepts have been applied for immobilizing heterogeneous catalyst within engineered structures in the reaction zones of CD columns in a manner which enhances the void fraction.

The catalysts may be supported within "envelopes" including porous cylinders or spheres containing catalyst, wire mesh bundles of various shapes including tubes and gutters, fibreglass bales (Chemical Research and Licensing Ltd.) or within monolithic structured packing such as KATAPAK® (Sulzer Chemtech Ltd.).[57] Alternatively, catalytically active distillation packing either monolithic or in the shapes of typical random packing media such as Raschig Rings or Berl Saddles can be produced either by coating the distillation packing with a thin film of catalytically active material, or by impregnation or even by the fabrication of the distillation packing directly from the catalyst material itself.[57]

Distillation is inherently a non-equilibrium process whereby the chemical potential of any given compound in the liquid phase is generally unequal to its chemical potential in the vapour phase. As a result, mass transfer occurs between the phases resulting in the less volatile species becoming increasingly concentrated towards the bottom of the column and the more volatile species becoming increasingly concentrated towards the top of the column. Therefore, if the desired products have much higher boiling points than the reactants, a

product stream can be withdrawn from the reboiler. Similarly, if the desired products are more volatile than the reactants, they will become highly concentrated in the overhead distillate. As in any distillation process, it is also possible to extract a product of intermediate composition as a side stream at some location on the column. However, a product side stream would likely require further refinement. The reactants are fed at one or more locations on the column. Since the locations of the feed streams affect the axial concentration and temperature gradients, they are specified in a manner to optimize the process performance. However, non-condensable gaseous reactants must be fed below the reactive section. Similarly, the size and location of reactive sections are selected to optimize reactor performance.

The distinguishing feature of CD is its ability to simultaneously conduct chemical reaction and product purification in a single unit operation. The process intensification provided by CD is a clear advantage compared to conventional reactor technology. In addition, the continuous removal of product from the reactive section due to the distillation action shifts the equilibrium in favour of product formation in accordance with Le Chatêlier's Principle, thus breaking any equilibrium limitations resulting in chemical conversions much higher than the theoretical equilibrium conversion and less catalyst being required to achieve a similar conversion in a conventional chemical reactor.[57,58] Conversions as high as 100% may be achieved for what would be otherwise equilibrium limited reactions.[57]

Higher selectivity may be achieved when undesirable consecutive reactions are possible as a consequence of the rapid removal of species from the reaction zone. The distillation action may possibly lead to significantly improved catalyst lifecycle if poisons are present in the feed stream. For example, if a liquid feed stream contains a known poison with a relatively high boiling point, the reactant mixture may be purified *in situ* by distillation and the

poison may be averted if the feed stream is located well below the reactive section.

Multicomponent mixtures exhibiting azeotropes may benefit from the *in situ* reaction facilitated by CD since the chemical reaction may shift the process away from the azeotropic condition.[57,58] This feature may lead to further process intensification since multicomponent mixtures whose purification by distillation is limited by an azeotrope would typically require an additional stage of purification by an alternative technology such as extractive distillation whereby an additional solvent is added to break the azeotrope or by some other technology such as membrane separation or adsorption.

Since the reaction occurs in a boiling medium, excellent temperature control may be achieved, which is often critical in organic synthesis. Conducting an exothermic chemical reaction in a boiling medium provides *inherent safe design* since the boiling solvent acts as a moderator which mitigates potential runaway reactions. Moreover, all of the energy liberated by the chemical reaction is efficiently converted *in situ* to drive the distillation process and may also prevent the formation of "hot spots" on the catalyst, which could possibly have an adverse affect on catalyst performance and lifecycle. Significant energy savings may be realized as a consequence of this enhanced energy integration as well as the inherent process efficiency. In addition, the reduced energy consumption indirectly may result in a reduction of greenhouse gas emissions due to reduced power requirements. Indeed CD is a salient example of *green engineering.*[58]

CD offers many potential advantages over conventional reactor technology in some instances. However, there are constraints and possible disadvantages associated with CD that limit its applicability. First, the reactants and products must have significantly different boiling points in order for distillation to be a practical separation method. Moreover, the relative

volatilities between reactants and products should be sufficient to ensure a high concentration of reactants and low concentration of products in the reaction zone. Second, there are an insufficient number of degrees of freedom to independently specify the reaction temperature and pressure. Consequently, CD processes will be constrained to those processes which can be carried out at the bubble point of the reactant mixture at relatively low to moderate pressures resulting in operating conditions that may not be optimal. Third, it must be practical and desirable to carry out the reaction in the low interaction regime of trickle flow. Finally, since distillation is energy intensive and expensive, CD is not suitable for reactions with long residence time requirements, in which case a reactor-separator arrangement would be more economical.[57] Possible applications of CD include alkylation, amination, carbonylation, chlorination dehydration and hydration, dimerization, esterification and transesterification, etherification, hydrogenation and dehydrogenation, hydrolysis, metathesis and disproportionation, polymerization and the synthesis of carbonates. Specific examples are outlined in recent reviews by Ng and Rempel[58] and by Hiwale et al.[59]

Recently, it has been suggested that CD is a promising reactor technology for the commercial production of MIBK.[32,60,61] The synthesis of MIBK meets many of the design criteria for CD. First, the overall reaction is strongly exothermic. Although this is not a requirement for CD, it is advantageous since it may lead to enhanced energy integration. It is of interest to ascertain whether the control of the reaction temperature due to the presence of the boiling medium and its moderating effect will enhance the reaction selectivity and catalyst performance for this complex organic synthesis. Second, MIBK has a much higher boiling point ($T_{nb}$=116°C) than the reactant acetone ($T_{nb}$=56°C) making distillation an appropriate technology for product purification. The large relative volatility ($\alpha_{AB}$=12) also ensures that it is possible to achieve a very high concentration of acetone in the reaction zone relative to the product MIBK. Third, MIBK synthesis in the liquid phase is typically carried out from

120 to 160°C.[23-25] Neglecting hydrogen, this would imply partial pressures of acetone ranging from about 0.59 to 1.34 MPa assuming the reaction temperature is at or near the boiling point of acetone and the reactant mixture is essentially pure acetone (a conservative first approximation). This suggests the operating pressure for a CD process will be relatively low compared to conventional processes for MIBK synthesis, which typically operate from 1 to 10 MPa.[23,33] However, these estimates suggest a reasonable range of operating pressure for a CD process within which the synthesis of MIBK is technically feasible. Lastly, MIBK is known to form azeotropes with water and other species, which may be present in the MIBK product.[62] Therefore, MIBK synthesis may benefit significantly from the application of CD technology.

It is known that the first two reaction steps are strongly equilibrium limited. Conventional reactors require the use of a multifunctional catalyst to effectively break these equilibrium limitations through the irreversible hydrogenation of MO, which shifts the equilibria in favour of product formation. The author and coworkers[63-65] have demonstrated that CD provides the flexibility to either produce MIBK in a single stage (Figure 1-4) by using a multifunctional catalyst in a single reaction zone or to produce MIBK using two distinct catalysts located in two discrete reaction zones; one for the production of MO from acetone and the other for the selective hydrogenation of MO.

There are potential advantages and disadvantages to both approaches. A possible advantage of using a multifunctional catalyst is that the rapid hydrogenation of MO upon its creation to MIBK may minimize the formation of undesirable by-products from which MO is a precursor including phorone and its isomers, mesitylene and other higher molecular weight species. Additionally, since the dehydration of DAA to produce MO is a relatively slow reaction for which the reverse reaction may be significant, the rapid hydrogenation of MO may possibly provide a synergistic effect leading to an enhanced catalyst activity. However for this reactor configuration to be

successful, the rate of hydrogen transport to the active sites must not be the limiting step. Otherwise, undesirable side reactions will become significant.

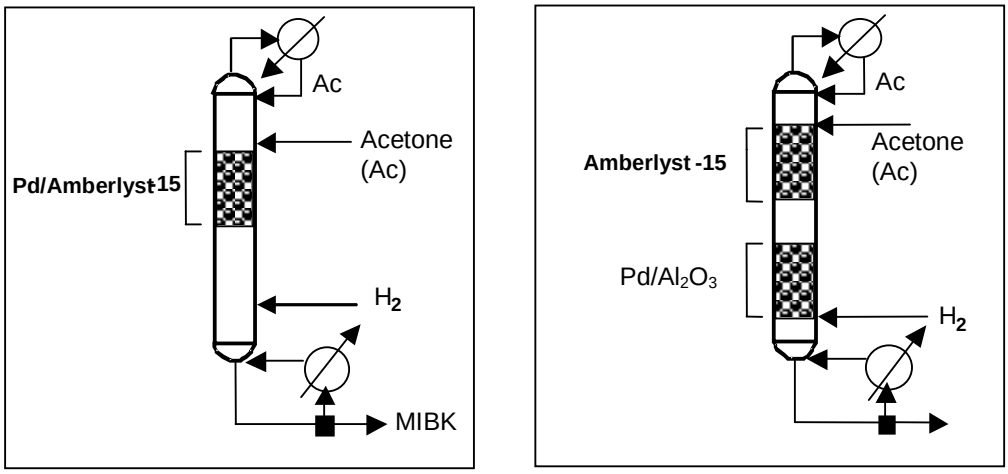


**Figure 1-4** Possible CD reactor configurations for MIBK synthesis, reprinted from O'Keefe et al.[65]♣ (left) single reaction zone utilizing a multifunctional catalyst (right) Two optimized zones using two distinct catalysts

For example, Lawson and Nkosi[32] reported selectivities to MIBK ranging from 15 to 67 (wt%) for various conditions of a batch CD process for the one-step production of MIBK. The highest selectivity was achieved only after 48 hours of batch distillation with the hydrogen volumetric flow rate maximized. Additionally, the high concentration of acetone in the reaction zone may lead to a greater rate of IPA production from the hydrogenation of acetone. The author and co-workers[18,63-65] have demonstrated previously that the direct hydrogenation of acetone is a significant competing reaction and that the relative rates of MO and acetone hydrogenation and hence the selectivity of the hydrogenation, is strongly dependent on the MO concentration (Figure 1-5).

The data in Figure 1-5 suggests that IPA and MO compete for the same active sites and that MO is hydrogenated preferentially. This implies that IPA production may be suppressed by first concentrating MO prior to its

hydrogenation or by increasing the competition for active sites by minimizing the palladium loading. Therefore, the two zone approach may be desirable since the hydrogenation zone may be located in the stripping section where MO would be more concentrated. However, the temperature at which the hydrogenation reaction will be carried out will also be higher. In contrast, the one zone approach requires all reaction steps to be carried out at essentially the same reaction temperature.

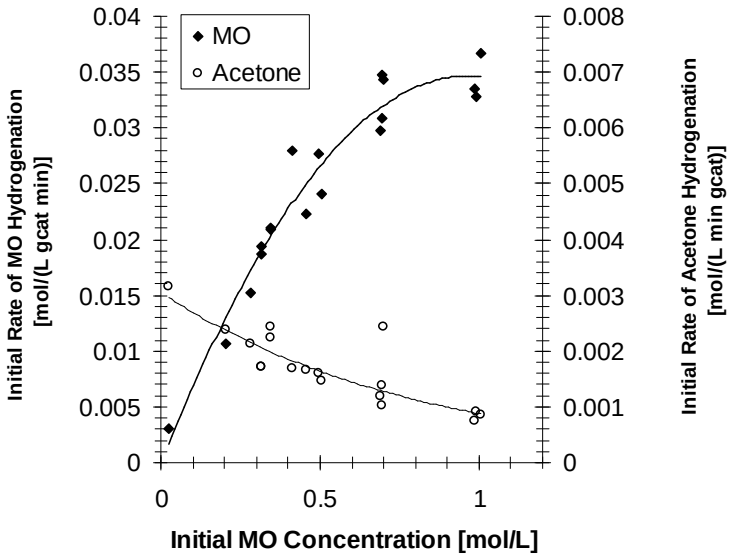


**Figure 1-5** Effect of the initial MO concentration on the initial specific rates of MO and acetone hydrogenation [T=100°C, $P_T$=4.23 MPa, ω=700 RPM, W=1 g 0.52 wt% $Pd/Al_2O_3$] Reprinted with permission from O'Keefe et al.[18]♣

Another advantage of the two zone approach is that it offers the simplicity and flexibility to independently optimize the catalysts for each reaction step, which may lead to a more efficient and robust process. Moreover, the hydrogenation catalyst may be designed in such a manner as to protect the active sites from known or potential poisons created in the previous reaction

♣ Figure 1-5 reprinted from W.K. O'Keefe, M. Jiang, F.T.T. Ng and G.L. Rempel, "Liquid Phase Kinetics of the Selective Hydrogenation of MO to Methyl Isobutyl Ketone in Acetone over a $Pd/Al_2O_3$ catalyst", *Chemical Engineering Science*, **60**, (2005), pp. 4131-4140. Used by permission of Elsevier Science. ©2005 Elsevier Science.

steps. In contrast, the use of a multifunctional catalyst introduces complexity. It has been frequently reported and is generally accepted that a careful balance of the strengths and densities between condensation and hydrogenation sites is needed to ensure an active, stable and selective catalyst for MIBK synthesis.[23,26,48,50]

Yang and Wu[49] have further suggested that not only is a careful balance between condensation and hydrogenation sites important but also that a close spatial proximity between the multi-functional sites is also needed. This implies that the condensation and hydrogenation sites act collectively as an ensemble to facilitate the desired chemical transformation. The fouling of a catalyst site within an ensemble may cause a desired reaction pathway to close while opening an undesirable pathway or may render the entire ensemble inactive. In the case of MIBK synthesis, the fouling of hydrogenation sites or large distances between an acid site and the nearest hydrogenation sites increases the probability that MO will combine with acetone at an acid site to produce phorone rather than react with hydrogen to produce the desired product. Yang and Wu[49] have asserted that increased distances between condensation and hydrogenation sites will lead to an increase in the production of IPA from the hydrogenation of acetone and lower catalyst selectivity.

## 1.5 Problem Definition

### *1.5.1 The CD Process and Catalyst Limitations for MIBK Synthesis*

The data disclosed by Lawson and Nkosi[32] has demonstrated that the one-step synthesis of MIBK via CD is technically feasible in a semi-batch mode of operation at 0.5 MPa and a reaction zone temperature of 127°C with hydrogen fed to the CD column at flow rates ranging from 7 to 55 L/hr (STP) using a catalyst consisting of 0.05 wt% Pd dispersed onto Amberlyst-15, a strongly acidic macroreticular cation exchange resin. However, the MIBK productivity and the selectivity to MIBK were poor as illustrated in Table 1-1. The average

MIBK productivity ranged from 0.09 to 0.12 (g/hr*$mL_{cat}$). The selectivity to MIBK (wt%) ranged from 33 to 68 (wt%) for acetone conversions ranging from 78 to 92 (wt%).

**Table 1-1** MIBK Productivity and Product Distribution for Batch CD Processes for MIBK Synthesis reported by Lawson and Nkosi[32]

| $H_2$ Flow (L/hr) @ STP | Batch Time [hr] | Acetone Conversion [wt%] | MO & IMO Selectivity [wt%] | MIBK Selectivity [wt%] | Others Selectivity [wt%] | MIBK Productivity♣ [g/hr*$mL_{cat}$] |
|---|---|---|---|---|---|---|
| 7 | 24 | 78.22 | 47.69 | 33.02 | 16.83 | 0.0850 |
| 12 | 24 | 62.80 | 31.60 | 45.00 | 22.20 | 0.0930 |
| 12 | 28 | 96.01 | 30.77 | 45.50 | 22.20 | 0.1233 |
| 55 | 24 | 48.69 | 29.2 | 64.9 | 5.6 | 0.1040 |
| 55 | 48 | 92.82 | 26.7 | 67.6 | 5.4 | 0.1033 |

The author and co-workers[63,64] conducted a preliminary pilot scale investigation into the synthesis of MO and MIBK in a single CD column operating in continuous flow mode utilizing two distinct catalysts in two separate reactive sections. These CD experiments are described and discussed in detail in Chapter Seven. Commercially available catalysts were used to obtain process benchmarks and to gain a cursory assessment of the effects of the main process variables on the productivity and product distribution. Amberlyst 15 was used to produce MO from acetone and a 0.5 wt% $Pd/Al_2O_3$ catalyst was used to facilitate the selective hydrogenation of MO. MIBK was produced in relatively low yield with a productivity ranging from 0.02 to 0.10 [g/hr*$g_{cat}$], which is comparable to the results reported by Lawson and Nkosi[32]. The low MIBK yield was attributed to the relatively low system pressures which ranged from 0.42 to 0.60 MPa. Since the reaction must occur at the bubble point of the mixture, the operating pressure was constrained by the thermal stability of the

♣ Productivity calculated from published data [32] by normalizing the amount of product obtained by the amount of catalyst used and the batch residence time

Amberlyst 15 cation exchange resin, which has a maximum recommended operating temperature of 120°C. The hydrogenation step was found to be limiting the overall CD process as evidenced by a relatively low conversion of MO, which ranged from 4.0 to 15.1 mol % and a very low hydrogen uptake efficiency less than 2 mol%.[63] The hydrogenation selectivity ranged from 84.4% (mol%) to 94.9%. Additionally, there was evidence of significant hydrogenation catalyst deactivation. DRIFT spectroscopic data indicates that MIBK interacts strongly with the Lewis acid sites of the $\gamma$-$Al_2O_3$ support.[64] The catalyst deactivation observed in the CD experiment may have occurred as a result of product inhibition and possibly coke formation due to the strong interaction of MIBK with the catalyst.

Cation exchange resins such as Amberlyst CH28, represent the state-of-the-art for catalysts for MIBK synthesis. However, there are several significant drawbacks of ion exchange resins for this application that justify further catalyst development. First, cation exchange resins exhibit poor lifecycle characteristics for MIBK synthesis requiring regeneration every 3 months and replacement every six months.[60] Second, since at least one mole of water is produced per mole of MIBK, the acid catalyst must exhibit excellent moisture tolerance. Unfortunately, acidic cationic exchange resins are known to deactivate in the presence of water.[19,33,66] Third, cation exchange resins have a very small characteristic particle size and must either be loaded within fibreglass or wire-mesh bags, or must be sandwiched between the corrugated metal sheets of a KATAPAK type packing, which significantly limits the amount of catalyst that can be charged to the reactor. Fibreglass and wire mesh bags lead to poor wetting characteristics and mass transfer limitations. Fourth, MIBK synthesis is a complex reaction involving many possible undesirable competing reactions. Therefore, the key to a successful one-step CD process is high selectivity to the desired product in order to avoid costly downstream refining. Preliminary CD experiments have shown that cationic exchange resins are not highly selective for the precursor MO. The selectivity was found to be constrained to a narrow

range of 83 to 90 wt%.[63] Consequently an acidic catalyst with improved selectivity to the precursor MO is needed. Lastly, and most importantly, an acidic catalyst with improved thermal stability compared to that of cation exchange resins is needed to allow higher operating pressures for the hydrogenation of MO, which currently limits the CD process. Clearly, a more robust hydrogenation catalyst is also needed.

### *1.5.2 Application of Niobia Compounds Towards MIBK Synthesis*

Niobic acid ($Nb_2O_5 \cdot nH_2O$) has gained much attention in recent years due to its striking and curious properties as a solid acid catalyst as well as consequence of unmistakable effects as a catalyst promoter for various reactions.[67] Niobic acid is a strongly acidic material with a Hammet index of $H_0$ = -5.6 which corresponds to approximately 70% of the strength of sulphuric acid.[67] However, unlike most solid acid catalysts that exhibit a diminution of acid strength in the presence of water, niobic acid maintains excellent activity for various reactions for which water is either liberated or consumed.[67] Consequently, niobic acid and supported niobia compounds are highly suited as catalysts for dehydration reactions, such as the case for MO synthesis. Moreover, since niobia is a metal oxide, this compound will provide the thermal stability needed for an improved CD process for MIBK synthesis.

Indeed, $Pd/Nb_2O_5$ and $Pd/Nb_2O_5/SiO_2$ have been identified as a promising catalysts for MIBK synthesis.[42-44] However, the fundamental relationships between the catalyst properties and the catalytic performance are not well understood. The effects of the most important catalyst parameters including the type of oxide support, the calcination temperature and the niobia loading on the catalyst performance remain largely unexplored for this reaction despite intriguing preliminary results reported in the literature. In fact, to the best of this author's knowledge, scientific investigation of supported niobia compounds for MIBK synthesis is constrained to a single study by Chen et al.[42] Paulis et al.[14] have studied niobic acid for the acid catalyzed aldol condensation of

acetone while Higashio and Nakayama[43] have studied the use of niobic acid for MIBK synthesis.

The interaction of the surface-phase niobium oxide with the metal oxide support may yield numerous niobium oxide species each with distinct geometrical structures and electronic properties. Fortunately, these niobia structures may be readily identified by spectroscopic methods and a well established science exists enabling the molecular control of their structure through the careful control of the synthesis method and catalyst parameters.[68-70] However, the active form or forms of niobia for MO synthesis is currently not known and more generally, the importance of the nature of the acidity ( i.e. Bronsted or Lewis) is not well understood for this reaction. Although numerous kinetic studies have been reported for the one step synthesis of MIBK, no kinetic models have been reported for this reaction when catalyzed by a niobium based catalyst.

### 1.6 Objectives and Scope of Study

It is evident from the results of the preliminary experiments as well as the data reported by Lawson and Nkosi[32] that a catalyst with improved thermal stability, moisture tolerance and improved selectivity is needed to improve the process. To this end, the objective of this research was the development and characterization of a superior catalyst for application towards the one step synthesis of MIBK via CD as well as the process analysis and reaction engineering that enabled the successful integration of this catalyst into a practical CD reactor. More generally, an objective of this research was to gain insight into the advantages and limitations of CD technology through its application towards a complex organic synthesis. An improved understanding of MIBK synthesis was ascertained through an integrated approach to catalyst design and reaction engineering realized the three project phases outlined below. An integrated approach implies that the three phases of study proceeded concurrently rather than in a sequential manner.[71] Thus, the

resultant catalyst design gave consideration to its performance at the reactor scale as well as the molecular scale.

***Phase I - Elucidation of structure activity relationships***

The first phase of research, a comprehensive investigation of the effects of the main catalyst parameters on the resultant catalyst performance for MO synthesis was conducted with a concerted effort directed towards the elucidation of the fundamental structure-activity relationships through a combination of catalyst activity/selectivity testing on the liquid phase synthesis of MO from acetone over powdered niobia catalysts in an autoclave reactor and detailed catalyst characterization. Specifically, the objectives of the first phase of research were to identify the active form or forms of niobia for MO synthesis and to determine the influences of the nature and strength of the acidity and other physicochemical properties on the resultant activity and product distribution. The first phase of research included catalyst screening on potential catalyst supports followed by more detailed investigation of catalyst formulation and synthesis on the most promising supports.

***Phase II – Reaction Kinetics and Catalyst scale-up***

In the second phase of research, promising catalytic materials and formulations identified in the first phase of research were further developed into multifunctional catalysts for MIBK synthesis by integration of Pd to their architecture in order to enable the hydrogenation function. The liquid phase kinetics of the overall MIBK synthesis was investigated in an autoclave reactor and predictive kinetic models were developed for future process analysis. Promising multifunctional catalysts were scaled up to the pellet scale using commercially available catalyst carriers and studied in continuous flow reactors in order to assess their long term stability, the effect of space velocity on the catalyst utilization and product distribution and to further improve the catalyst performance prior to pilot scale experimentation.

***Phase III - Pilot Scale Catalytic Distillation Experiments***

In the third phase of research, the catalyst performance was assessed at the pilot scale in a CD reactor under conditions of realistic space time and for substantial time on stream (TOS). Since MIBK production is a relatively complex organic synthesis, these experiments provided an excellent opportunity to test the potential advantages and limitations of CD technology. The secondary objectives of the pilot plant experiments were to assess the potential advantages and disadvantages of the possible reactor configurations (i.e. the two zone approach versus the single zone approach utilizing a multifunctional catalyst) and to assess the effects of process parameters on the catalyst utilization and product distribution.

# Chapter Two

## Literature Review

### 2.0 Synopsis

The principal focus of this research is the development and characterization of a $Pd/Nb_2O_5/X$ catalyst, where X denotes a metal oxide, to be applied towards the one-step synthesis of MIBK via catalytic distillation and in particular to elucidate the fundamental relationships between the nature of the niobia surface oxide phase and its resultant catalytic properties and kinetic behaviour. A comprehensive review of the scientific literature is presented in this chapter regarding the catalytic application of niobia compounds with particular emphasis on its use for MIBK synthesis. Relevant kinetic studies and the state-of-the-art of reactor technologies applied to MIBK synthesis are reviewed.

### 2.1 Niobium Compounds as Catalysts

#### *2.1.1 Thermodynamic Stability of Niobia*

The one-step synthesis of MIBK involves the selective hydrogenation of MO and is carried out industrially at hydrogenation pressures ranging from 1 to 10 MPa.[23,24] Since the niobia catalyst will be utilized in a reducing environment, and since it may also be subjected to a reduction process as a preparative step, its thermodynamic stability under these conditions is an important catalyst design criterion. Generally, metal oxides may decompose to produce a new metal oxide species for which the oxidation state of the metal is reduced. In the presence of hydrogen, niobium (V) oxide may be reduced following the reactions outlined in equation (2-1 and 2-2). The reduction of the metal will proceed spontaneously for conditions for which the Gibbs free energy change ($\Delta G$) is negative for the reduction reaction. $\Delta G$ is defined by equation (2-3).

$$Nb_2O_5 + H_2 \rightarrow 2NbO_2 + H_2O \quad (2\text{-}1)$$

$$NbO_2 + H_2 \rightarrow NbO + H_2O \quad (2\text{-}2)$$

$$\Delta G \equiv \Delta H - T\Delta S = \sum_i \nu_i \Delta G_f \quad (2\text{-}3)$$

Figure 2-1 from T.B. Reed[72] is a plot of the Gibbs free energy of formation ($\Delta G_f$) of various binary oxides including various niobium oxides, as a function of temperature. The relative stabilities of the compounds may be inferred from the figure. The most stable compounds correspond to those plotted lowest in the figure having the most negative Gibbs free energy of formation whereas the least stable compounds correspond to those plotted towards the top of the figure.

From this data in Figure 2-1, Ichikuni et al.[69] argued that niobium (V) oxide can not be reduced by hydrogen at any temperature. Indeed, $Nb_2O_5$ is very stable and is known to be much more difficult to reduce than Vanadium (V) oxide for example.[73] However, niobium (V) oxide may in fact be reduced, albeit at very high temperatures. Note that the Gibbs free energy of formations of NbO and $NbO_2$ indicated in Figure 2-1 are more negative than for $Nb_2O_5$. The reduction of $Nb_2O_5$ to produced $NbO_2$ (Eqn 2-1) can be carried out at 1073 to 1573 K while the further reduction of $NbO_2$ to produce NbO (Eqn 2-2) can occur at temperatures ranging from 1573 to 1973 K.[73] However, the reduction of $Nb_2O_5$ to $NbO_2$ is reversible.[73] It is evident that the reduction of niobium (V) oxide at low to moderate temperatures is not favourable and is therefore not likely to occur for the experimental conditions within a chemical reactor or during a reduction process in a calcinator at the mild temperatures used in this study.

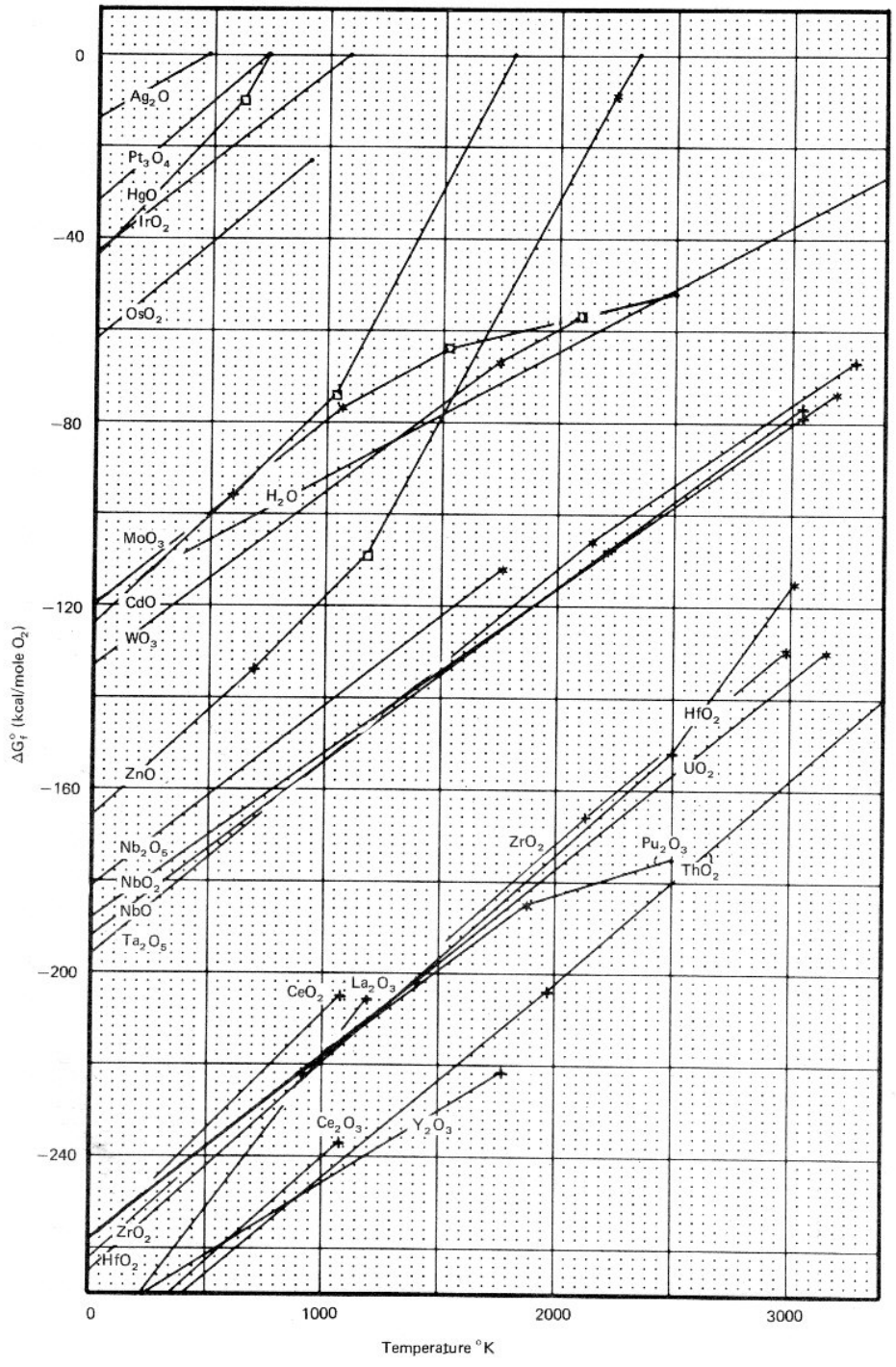


**Figure 2-1** The Gibbs Free Energy of Formation of Various Binary Oxides Reproduced from Reed[72]♠

♠ Reprinted from Thomas B. Reed, "Free Energy of Formation of Binary Compounds: An Atlas of Charts for High-Temperature Chemical Calculations", with permission from the MIT Press, © The MIT Press, Cambridge (1971).

*2.1.2 Polymorphism*

Niobia may adopt various, distinct geometrical crystalline structures, i.e. polymorphs, depending on the thermodynamic state of the system as well as the starting materials. The polymorphs of niobia are described in detail by Nowak and Ziolek[73] and are summarized here. At low temperature, Nb (V) oxide is amorphous. When heated to temperatures above around 500°C, niobia will crystallize and likely assume one of three principal crystal forms: the low temperature form T (or γ phase), the moderate temperature M form (or β phase) or the high temperature H form (α phase).[73,74] Tanabe[75] found via combined differential thermal analysis (DTA) and thermogravimetric (TG) analysis of niobic acid that the crystallization from the amorphous phase to the T form occurred around 550 to 570°C. The "M" form appears around 800°C and the high temperature "H" form appears around 1000°C.[74] These transitions between phases upon heating are irreversible and do not occur at well defined transition temperatures. The crystallization behaviour of niobia is dependent on the starting materials, impurities and the interaction of niobia with other materials, such as another oxide support.[74]

Within the low temperature γ phase, there is a further distinction between two low temperature forms; the "TT" and "T" forms. The TT form may appear around 500°C, while the T form appears near 600°C.[74] The T and TT forms are quite similar and have been considered by some to be the same form.[73] The TT form is a "less crystalline" form that is stabilized by impurities and does not always appear depending on the starting materials.[73] Aside from the three major crystal forms (T, M and H), other polymorphs may be synthesized and have been classified according to their distinct crystal habits. The B form (ζ phase) is assigned to those exhibiting a leaflet like habit, the N form is assigned to those exhibiting acicular habit (needles) and the P form (η phase) exhibit a prismatic habit.[73]

The amorphous form of hydrated niobium (V) oxide (i.e. niobic acid $Nb_2O_5 \cdot nH_2O$) is of particular interest in heterogeneous catalysis since this material exhibits very strong surface acidity ($H_0 \leq -5.6$; 70% the strength of sulphuric acid when calcined at moderate temperatures from 100 to 300°C) and significant catalytic activity for many reactions.[67,75-80] Crystallization of the amorphous structure upon heating at temperatures above 500°C is known to be accompanied by a significant loss of acidity and catalytic performance.[73,75,78]

*2.1.3 Catalytic Applications of Niobium Compounds*

Niobic acid and niobium compounds have gained much attention in recent years due to their unusual and striking properties as both catalysts and supports.[67,75-77] In fact, several entire volumes of the journal *Catalysis Today* ♠ as well as several international conferences have been dedicated solely to research into niobium chemistry and catalysis.[67,73] According to Tanabe and Okazaki[76], niobium compounds can be classified into one of five categories based on their catalytic properties: 1) promoter effect, 2) support effect, 3) acidity, 4) Redox and photocatalytic properties and 5) layered structure.

The addition of small amounts of niobium oxides to existing catalysts is known to increase the activity and selectivity of certain catalysts, significantly extend the lifecycle of some catalysts and in some cases improve their mechanical strength.[77] Most notable are the promoter and support effects of niobia for certain oxidation reactions, which has been described by Tanabe[76] as "remarkable". Examples of other reactions which may benefit or are known to benefit from the promoter effect of niobium oxide compounds include the oxidative dehydrogenation of alkanes and in particular the oxidative dehydration of ethane, which is of considerable industrial importance, as well as the oxidative coupling of methane, selective catalytic reduction (SCR) for $NO_x$ removal and ammoxidation.[67,73,77]

♠ The reader is referred to *Catalysis Today* volumes 8(1) , 16(3-4), 28(1-2), 57(3-4)

The dispersion of a metal or metal oxide catalyst onto a niobium oxide support often gives rise to a strong metal support interaction (SMSI) resulting in an enhancement of catalytic activity or selectivity. For example, a strong SMSI is known to affect the selectivity of $Co/Nb_2O_5$ catalysts for the Fischer-Tropsch synthesis giving high selectivity in the diesel range.[81] Other reactions which are known to benefit from the support effect of niobium compounds are described in recent reviews[67,73,76,77] and include hydrogenation, metathesis, hydrotreating including hydrocracking, hydrodesulphurisation (HDS) and hydrodenitrogenation (HDN), hydrogenolysis and the production of hydrocarbons and olefins from carbon monoxide and hydrogen.

Hydrated niobium pentoxide (niobic acid) is known to have a very strong surface acidity and consequently, can be utilized as a solid acid catalyst. Tanabe[75] has described niobic acid as an "unusual" solid acid catalyst noting that unlike most solid acid catalysts, which lose their acidity when exposed to water, niobic acid exhibits excellent moisture tolerance, not only retaining its acidity but often increasing in its acidity when exposed to moisture. Its strong acidity and synergistic affinity for water makes niobic acid and niobium oxide compounds ideal catalysts for reactions for which water molecules are either liberated or consumed including dehydration, hydration, hydrolysis, esterification and the Prins reaction.[67,73-79] From an industrial perspective, niobium compounds are promising as solid acid catalysts since they represent cost effective and environmentally sensitive alternatives to traditional homogeneous mineral catalysts used in petrochemical processes for the synthesis of fine chemicals.[67] Quite recently, Carniti et al.[82] demonstrated that niobic acid and niobium phosphate should be considered viable alternatives to homogenous acid catalysts for reactions in aqueous medium and in particular, fructose dehydration. Other reactions for which niobia compounds may serve as a solid acid catalyst include condensation, alkylation, isomerisation, ring-opening reactions and hydrogenolysis reactions.[67,73-77, 83]

If a very strong acidity is the principal catalyst design criterion, the reader is advised that niobium phosphate ($NbOPO_4$) calcined at moderate temperatures exhibits a much stronger surface acidity ($H_0$=-8.2; 90% the strength of $H_2SO_4$) than niobic acid.[84] In addition, niobium phosphate exhibits a similar water tolerance as niobic acid but has the advantage that it retains its acidic properties to higher catalyst pre-treatment temperatures.[84,85] $NbOPO_4$ is known to be active for several reactions including MTBE synthesis, esterification, alkylation and the isomerisation of 3,3-dimethly-1-butene.[84,85] Alternatively, Okazaki et al.[86] have demonstrated that the acidic properties of niobic acid could be enhanced and retained even upon exposure to temperatures as high as 600°C by pre-treatment with phosphoric acid, which delays the onset of crystallization to higher temperatures.

When niobia is present as a 2-dimensional surface oxide phase ( i.e. an "overlayer") dispersed onto another metal oxide, depending on the nature of the oxide support, certain niobia species might be present which exhibit sites that may facilitate oxidation and reduction reactions.[87] Oxidation reactions in particular may benefit from the redox properties of niobium compounds including the partial oxidation of methane and methanol oxidation.[67,68,73] The redox properties of niobia arise by virtue of an Nb atom's capacity to become reduced to a lower oxidation state and for the ability of niobium oxide species to lose and regain an oxygen atom throughout the course of a catalytic cycle. The +5 state is the most stable oxidation state for niobium however it may also take formal oxidation states from +5 to -1.[73]

According to Jehng and Wachs[68,87] the redox properties of the niobia are determined by the unique molecular structure of the niobium oxide species, which is in turn governed predominantly by the physicochemical interaction between the surface-phase niobium oxide and the metal oxide support. Therefore, the redox properties if any, of niobia dispersed onto a metal oxide are

governed by the nature of the metal oxide support. At low temperatures, only silica supported niobia exhibit redox sites whereas other metal oxide supports yield acid sites.[73] It is also known that the redox potential of a niobium oxide support may affect the redox properties of certain metals and metal oxides dispersed onto it.[73] In addition, some mixed metal oxides containing niobia are also known to exhibit redox properties.[76]

Certain niobium compounds such as potassium niobate ($K_4Nb_6O_{17}$), rubidium niobate ($Rb_4Nb_6O_{17}$) and others (eg. $HCa_2Nb_3O_{10}$, $K_{0.5}La_{0.5}Ca_{1.5}Nb_3O_{10}$) exhibit a layered structure, which gives rise to photocatalytic properties when doped with metals such as Ni, Pt, Ru and Cs that occupy the interlayer spaces.[67,76] Applications of niobium photocatalysts include hydrogen production via photocatalytic water splitting and the decomposition of organic waste compounds.[67]

### *2.1.4 Niobium Oxide Catalysts for MIBK Synthesis*

The fact the niobic acid and niobium compounds retain their strong acidity in the presence of water is an unexpected property for a solid acid catalyst, which makes niobium compounds excellent candidates as catalysts for reactions in which water is either liberated or consumed. It is not surprising therefore that niobia catalysts have been successfully utilized for MIBK synthesis.[43,44] In the case of MIBK synthesis, the most important catalytic properties of the niobia catalysts are their strong surface acidity as well as the support effect, which is purported to result in an enhanced hydrogenation activity and selectivity due to a strong metal support interaction.[67]

Higashio and Nakayama[43] conducted a series of experiments in a batch autoclave where the starting reactant was either acetone, DAA or MO and the experiment was carried out either with or without hydrogen. A multifunctional $Pd/Nb_2O_5 \bullet nH_2O$ catalyst for MIBK synthesis was created by calcining niobic

acid at 300°C and impregnating the niobic acid with palladium chloride to give 0.1 wt% Pd. The Pd was subsequently reduced with hydrazine.[43] The performance of this catalyst was compared to other catalysts consisting of Pd dispersed onto HY zeolite, $\gamma$-$Al_20_3$ and $SiO_2$-$Al_2O_3$. They found that niobic acid calcined at 300°C had the highest activity for DAA dehydration and of the catalysts investigated. They also found that a significant reverse aldol condensation reaction occurred resulting in the production of acetone from DAA. The reverse aldol condensation reaction was more pronounced on the alumina and zirconium catalysts and was attributed to the presence of basic sites on these supports.[43]

When a batch reactor was charged with 2 g of $Pd/Nb_2O5 \bullet nH_2O$ catalyst and 50 mL of acetone, pressurized with hydrogen to 20 kg/cm$^2$ and heated to 160°C for 2 hours, MIBK was produced in very high yield with 0.1 wt% MO and no DAA detected in the product.[43,44] This observation lead Higashio and Nakayama to the dubious conclusion that MIBK was synthesized directly from acetone without the formation of DAA as an intermediate.[43] This is not consistent with the reaction mechanisms proposed in the literature for MIBK synthesis over various catalysts.[19,23,50,53] However, DAA may be viewed as short lived intermediate under these reaction conditions. Their observation that DAA was not detected in the reaction mixture at 160°C and 20 kg/cm$^2$ pressure is not unusual nor is it a result unique to niobium oxide catalysts. Higashio and Nakayama[43] tested the long term stability of 100 mL of this catalyst for MIBK synthesis at 160°C and 20 kg/cm$^2$ in a fixed bed flow reactor with a 28 mL diameter with an acetone feed rate of 158 g/hr (i.e. LHSV=2 hr$^{-1}$) and hydrogen feed rate of 265 mL/min (STP). MIBK was produced with over 90% selectivity at an acetone conversion of about 33% for over 1500 hours time on stream without any apparent catalyst deactivation.[43]

Higashio and Nakayama[43] found that the $Pd/Al_2O_3$ catalyst with 0.1 wt% Pd resulted in a significant amount of 2-propanol (IPA) produced from the

direct hydrogenation of acetone whereas IPA was rarely detected in the case of the niobic acid catalyst with the same Pd loading. They concluded that a significant support effect between the niobic acid and the Pd crystallites resulted in an inhibition of the hydrogenation of the carbonyl group and a higher selectivity to the desired product. They surmised that the high selectivity of the bifunctional catalyst may have been influenced by the metal dispersion as well as the strong surface acidity of the support. Although Tanabe[67] has advised that a strong metal support interaction (SMSI) plays an important role in the synthesis of MIBK using a $Pd/Nb_2O_5 \bullet nH_2O$ catalyst, Higashio and Nakayama[43,44] apparently did not provide any direct evidence of such a SMSI nor did they characterize the Pd dispersion and morphological properties of the catalysts.

Paulis et al.[14] conducted a thorough investigation of the effects of the preparative variables in the synthesis of niobic acid via the hydrolysis of niobium ethoxide on the structural properties of niobic acid and its catalytic activity for the aldol condensation of acetone. They synthesized niobic acid from $PdCl_5$ and ethanol precursors with the hydrolysis pH and molar ratio of water to niobium as experimental variables. The catalysts were subsequently calcined at 400, 500, 700 and 900°C. The catalysts were characterized by BET, DRIFTS, XRD and ammonia TPD and then their activities tested for the gas phase aldol condensation of acetone in a fixed bed flow reactor at 250°C and 0.6 MPa pressure.

It is curious that they chose to explore such high calcination temperatures since it was well known at that time that the acidic and catalytic properties of niobia diminish significantly upon crystallization above 500°C. Indeed, their results confirmed this. Their XRD results revealed that the catalyst calcined at 400°C was amorphous whereas the catalysts calcined at 500°C had crystallized adopting a hexagonal structure.[14] The catalysts calcined at 700°C adopted an orthorhombic structure and the catalysts calcined at 900°C had a monoclinic

structure.[14] BET measurements showed that the surface area diminished significantly upon crystallization and continued to decrease with increasing calcination temperature. The surface area of the catalysts calcined at 400, 500, 700 and 900°C were 144, 79, 16 and 4 $m^2/g$ respectively.[14] The ammonia TPD data presented by Paulis et al.[14] shows very clearly that the catalyst calcined at 400°C exhibited a significant acidity, which diminished markedly upon crystallization of the niobic acid at 500°C and continued to diminish with increasing calcination temperature.

Not surprisingly, the amorphous catalyst calcined at 400°C had the highest activity for the aldol condensation of acetone being roughly 2.5 times more active than the catalyst calcined at 500°C and 14.6 times more active than the catalyst calcined at 900°C on a per gram of catalyst basis.[14] Paulis et al.[14] argued that if the reaction rates were normalized by the catalyst surface area rather than the catalyst mass, the results would suggest, with the exception of the catalyst calcined at 900°C, that the specific reaction rate increases slightly with increasing calcination temperature. However it seems the low nominal activities of the crystallized niobic acid would preclude them as potential commercial catalysts. It is interesting to note that the catalysts calcined at different temperatures each had distinct crystal structures which resulted in distinct product distributions in the reactor effluent.[14] The notion that the morphological properties of the niobia markedly affect the product distribution for this complex organic synthesis is intriguing.

Paulis et al.[14] studied the FTIR spectra of ammonia (rather than pyridine) adsorption on the niobic acid catalysts. The catalysts were activated by helium purge through the IR cell at room temperature. The catalysts were then saturated with ammonia also at room temperature. DRIFT spectra were obtained at temperatures from room temperature to 350°C. They assigned the band at 1663 $cm^{-1}$ to the N-H stretching vibration of $NH_4^+$, which are associated with Bronsted acid sites and the vibration at 1608 $cm^{-1}$ to the N-H stretching

vibration of $NH_3$, which are associated with Lewis acidity. Remarkably, Paulis et al.[14] reported the presence of some Bronsted acidity in all catalysts with the Bronsted acidity decreasing with increasing calcination temperature. Although the general trend of Bronsted acidity decreasing with increasing temperature is consistent with the findings of others, the presence of Bronsted acidity in a niobium oxide catalyst at such high calcination temperatures (400 to 900°C) is quite unexpected and perhaps questionable. It is generally accepted that for niobic acid, Bronsted acidity is maximized at low calcination temperature (ca. 100°C) and is essentially non-existent for calcination temperatures above around 400°C.[73,88] Niobic acid generally loses its strong acidic properties after crystallization from heating above 800 K (527 °C) and is essentially neutral in terms of total acidity when calcined above 500°C.[67,73,75,76,88]

Perhaps the most important finding of their investigation was their observation that the molar ratio of water to niobium in the hydrolysis of niobium ethoxide had a significant effect on the resultant surface area of the niobic acid. They found that the optimal molar ratio of water to niobium was around 80 and that relatively high surface area niobic acid could be synthesized without the need for a more complicated supercritical $CO_2$ extraction technique.[14] They also found that the pH of the hydrolysis solution did not affect the structural properties of the niobic acid.[14]

Although Pd supported on niobic acid has been demonstrated to be a good bifunctional catalyst for MIBK synthesis, it is of interest to explore niobia dispersed onto other supports in order to investigate the unique catalytic properties of highly dispersed nanostructured niobia towards MO and MIBK syntheses. To the best of this author's knowledge, scientific investigation of supported niobia compounds for application towards either MO synthesis or the one step synthesis of MIBK is limited to a single scientific study by Chen et al.[42]

Chen et al.[42] synthesized and characterized $Pd/Nb_2O_5/SiO_2$ catalysts whereby niobia was dispersed as a surface-phase oxide onto a high surface area silica support, based on non-aqueous synthesis techniques involving niobium (V) ethoxide precursor, disclosed previously by Ko et al.[89,90] After impregnation, the catalysts were dried in vacuum for 24 hours to remove the residual solvent. The organometallic precursor was decomposed in nitrogen at 400°C for 2 hours then the catalyst was calcined in air at 500°C for 2 hours. Catalysts were prepared with the surface-phase niobium oxide concentrations of 0.5, 1, 2 and 3 monolayer coverage. The effect of Pd loading was also investigated and varied from 0.03 to 0.3 wt%. $PdCl_2$ was used as a precursor and was deposited via aqueous impregnation for which the water was acidified. The catalyst was subsequently dried at 100°C for 24 hours then calcined in air at 400°C for 4 hours. The catalysts were characterized by BET, XRD and TPD using n-butylamine as a basic probe molecule. The catalysts were tested for activity for the one step synthesis of MIBK in the liquid phase at 160°C and 2.0 MPa in a batch autoclave. The long term stabilities of the catalysts were assessed in a fixed bed flow reactor (FBR) at 160°C and 2.0 MPa.

The results of the BET analysis showed that the specific surface area ($m^2/g_{cat}$) decreased with increasing niobia loading. However, when expressed on a per gram of silica basis, the results revealed that the surface area ($m^2/g_{SiO2}$) in fact increased with increasing loading up to a niobia loading equivalent to 2 monolayers coverage. From this observation it was concluded that the pores of the silica were not significantly blocked from the deposition of the surface niobium oxide phase.[42] The BET results revealed a relatively consistent mean pore size up to 2 monolayers coverage, which ranged between 16.8 and 17.5 nm, decreasing slightly with increasing loading.[42] XRD analysis of the catalysts showed that the onset of crystallinity did not occur until the catalysts were exposed to calcination temperatures in excess of 600°C. Moreover, crystallinity was only observed for the catalysts with niobia loading in excess of monolayer coverage.[42]

Crystallinity was observed at 700°C for a catalyst with a niobia loading equivalent to 3 monolayers coverage of niobia and was observed at 800°C for catalysts with 2 and 3 monolayers niobia coverage.[42] The catalyst with a single monolayer coverage exhibited the best thermal stability and did not show significant XRD peaks even after calcination at 800°C.[42] Their experimental observation that the onset of crystallinity was delayed to higher temperatures compared phase transitions observed for bulk niobic acid is consistent with the findings of Ko and Weissman[74] who found that Nb-O-Si linkages significantly stabilized the surface-phase niobium oxide of a $Nb_2O_5/SiO_2$ catalyst.

Ko and Weissman[74] observed that a catalyst consisting of a monolayer of niobia dispersed onto $SiO_2$ remained amorphous when calcined at 500°C and showed only very weak XRD peaks corresponding to the TT phase after calcination for 48 hours at 1000°C. They concluded that a strong interaction between the surface-phase niobia and the oxide support stabilized the amorphous niobia preventing crystallization and advised that in general, the strength of the interaction between the surface oxide phase and the oxide support governs the mobility of the niobia and hence its resultant structure and stability.[74] It is therefore perhaps expected that the degree of stabilization of the niobia afforded by the $SiO_2$ support for Chen et al.'s catalysts was less pronounced due to the higher niobia loading of 2 and 3 monolayers with the thermal stability of the amorphous niobia diminishing with higher niobia loading. Chen et al.'s[42] catalyst with a single monolayer coverage of niobia showed negligible crystallinity, which is consistent with the findings of Ko and Weissman.[74]

The TPD results indicated that the total acidity, both in terms of $\mu mol/g_{cat}$ and particularly in terms of $\mu mol/m^2_{cat}$, increased with increasing niobia loading beyond monolayer coverage with the catalyst having 3 monolayers of niobia coverage exhibiting the greatest total acidity.[42] Datka et al.[91] found that since silica does not exhibit acidic properties, the Lewis acidity of a $Nb_2O_5/SiO_2$

catalyst increased linearly with niobia loading for low niobia loading. However in contrast, they found that beyond monolayer coverage, the acidic properties diminished as the surface-phase niobia structure was replaced by $Nb_2O_5$ crystallites with inferior acidic properties causing the niobia structure to approach that of bulk niobium (V) oxide. In addition, they found that Bronsted acidity did not appear until a critical niobia coverage of around one half monolayer.[91] Although Bronsted acidity was detected by Datka et al.[91], only 5.5% of the acid sites were Bronsted sites for the catalyst with maximum Bronsted acidity. Asakura and Iwasawa[70] also carried out a thorough investigation of the acidic and catalytic properties of one monolayer niobia on silica and found no evidence of Bronsted acidity when the catalyst was calcined at 500°C. They concluded that the Bronsted acid sites were either unstable and or negligible at 500°C.[70] Other researchers have questioned whether Datka et al's spectroscopic data actually provides clear evidence of Bronsted acidity.[92]

Datka et al.[91] reported that both Bronsted and Lewis acidity were maximized at niobia concentration of 8 wt% for $Nb_2O_5/SiO_2$ catalysts, which was below monolayer coverage. Although both Datka et al.[91] and Chen et al.[42] calcined their $Nb_2O_5/SiO_2$ catalysts at 500°C, there is a significant distinction in their preparative method. Chen et al.[42] followed a non-aqueous synthesis technique disclosed by Ko et al.[89,90] using niobium ethoxide as a precursor whereas Datka et al.[91] used an aqueous incipient wetness impregnation technique using niobium oxalate as a precursor.

Although Chen et al.[42] reported the total acidity of their catalysts, they did not explain the nature of the acidity, whether Bronsted or Lewis, nor did they disclose any IR spectra. However, they assumed that their $Pd/Nb_2O_5/SiO_2$ catalysts exhibited both Bronsted and Lewis acidity, arguing that Shirai et al.[93] had demonstrated that niobia deposited on silica exhibited both Bronsted and Lewis acid sites, depending on the niobia loading. In doing so, they neglected the effect of calcination temperature on the nature of the catalyst acidity. Had

they scrutinized Shirai et al.'s work more carefully, they would have noted that their catalyst denoted "H", which exhibited both Bronsted and Lewis acid sites, was prepared by carrying out both the decomposition and attaching reactions at 200°C.[93] Moreover, Shirai et al.[93] presented a diagram outlining the effect of calcination temperature on the IR peak intensities assigned to Lewis and Bronsted acidity, which clearly demonstrated that the Bronsted acidity diminished linearly with pre-treatment temperature and was essentially non existent after treatment at 400°C. It is doubtful that the niobia catalysts prepared by Chen et al.[42] exhibited significant Bronsted acidity due to the high calcination temperature of 500°C. As mentioned previously, it is well known that Bronsted acidity is maximized at low calcination temperatures (ca. 100°C) and is essentially non existent after calcination above 400°C since protonic sites are lost as Lewis acid sites are created during dehydroxylation.

Chen et al.[42] compared the performances of their $Pd/Nb_2O_5/SiO_2$ catalysts to other catalysts consisting of Pd dispersed onto various supports with distinct acidic or basic character for both MIBK synthesis at 160°C and 2.0 MPa. The supports for these catalysts were tested for their activity for acetone condensation and separately for the dehydration of DAA at 160°C. Although they did not quantify or characterize the acidity/basicity of these catalysts, Chen et al.[42] argued that a $Pd/SiO_2$-$Al_2O_3$ catalyst exhibited Bronsted acidity, a Pd/CHT (calcined Mg/Al hydrotalcite) exhibited basicity, $Pd/Al_2O_3$ exhibited Lewis acidity and basic sites, a $Pd/CaO$-$Al_2O_3$ catalyst exhibited basic sites and the $Pd/Nb_2O_5/SiO_2$ catalysts exhibited both Bronsted and Lewis acid sites. They noted that a $Pd/Nb_2O_5/SiO_2$ catalyst with a niobia loading corresponding to a single monolayer showed the greatest activity and selectivity for MIBK synthesis. Also, they observed that the $Pd/Al_2O_3$-$SiO_2$ catalyst which apparently only exhibited Bronsted acidity had the lowest activity for MIBK synthesis while those catalysts with basic sites showed good activity for MIBK synthesis.

From these qualitative observations, Chen et al.[42] concluded that Bronsted acid sites alone are insufficient for MIBK synthesis and that Lewis acid sites were needed for formation of the enol form of acetone in the aldol condensation, which they assert is the controlling step in the one step synthesis of MIBK. Since the niobia catalyst exhibited the best result, they suggested that a catalyst with a combination of Lewis and Bronsted acid sites might be advantageous for MIBK synthesis since the Lewis acid sites catalyze the aldol condensation while the Bronsted acid sites catalyze the DAA dehydration.[42] Chen et al.[42] also found that the niobia catalysts showed the greatest activity for acetone condensation and DAA dehydration. All catalysts showed significant reverse reaction when DAA was the starting material with the basic catalysts producing the most acetone. However, the niobia catalysts were able to convert DAA to MO achieving mass fractions around 20 wt% MO after 2 hours. The $SiO_2$-$Al_2O_3$ support achieved around 10 wt% MO. The alumina support achieved a slight DAA conversion to MO while the CHT support achieved negligible DAA dehydration.

Aside from demonstrating that the niobia catalysts were more active and selective for MIBK synthesis as well as acetone condensation and DAA dehydration than the other catalysts prepared for this particular study, in this author's opinion, any inference on the role of the nature of the acidity or basicity from these experiments are inconclusive due to the qualitative nature of the study and particularly due to the dubious underlying assumption that the niobia catalyst investigated exhibited both Bronsted and Lewis acidity. In fact, from what is known about the effects of calcination temperature on the acidity of niobia compounds, their catalyst likely exhibited Lewis acidity only. Moreover, their conclusion that Bronsted acid sites alone are insufficient for MIBK synthesis is incongruous with other empirical evidence in the literature. For example, strongly acidic cation exchange resins, which exhibit only Bronsted acidity, currently represent the state-of-the-art of catalyst technology for MIBK synthesis. However, their assertion that a combination of both Lewis

and Bronsted acid sites might be advantageous for MIBK synthesis is both plausible and intriguing and warrants further investigation.

Chen et al.[42] studied the effect of Pd loading and reduction temperature on the performance of $Pd/Nb_2O_5/SiO_2$ catalysts for MIBK synthesis and found that the optimal loading was between 0.05 and 0.1 wt%. Below 0.05 wt% Pd, a significant amount of unreacted MO and other undesirable by-products were observed and at Pd loadings in excess of 0.1 wt%, a significant amount of IPA was observed.[42] The latter finding is consistent with that of O'Keefe et al.[18] who found that acetone and MO compete for Pd active sites with MO being hydrogenated preferentially. As the Pd loading increases, the competition for active sites decreases thus resulting in a greater IPA production rate. An increase in IPA production with increased Pd loading was also observed by Yang and Wu.[49] The effect of varying the reduction temperature (300, 400 and 500°C) for the $Pd/Nb_2O_5/SiO_2$ catalysts was investigated for the MIBK synthesis at 160°C and 2.0 MPa and was found to have a negligible effect on the acetone conversion, which ranged from 16.9 to 17.0%, and had a marginal effect on the MIBK selectivity, which ranged from 90.3 to 91.8% and was a maximum for the reduction temperature of 400°C.[42]

Chen et al.[42] carried out experiments whereby water was deliberately added to the reaction mixture and found that the acetone conversion achieved after an unspecified duration decreased linearly with the water concentration. In contrast, when the reaction was carried out in a fixed bed reactor, the conversion declined only slightly from 28 to 25 % after 177 hours time on stream. Thus, they concluded that the accumulation of water in the batch system resulted in the deactivation of the catalyst. They also found that the catalyst could be reactivated by flushing a stream of hydrogen at the reaction temperature of 160°C.[42]

Niobium oxide catalysts have been disclosed in the patent literature for the commercial production of MIBK from acetone. Higashio and Nakayama[44] disclosed a process for MIBK synthesis involving a $Pd/Nb_2O_5$ catalyst as well as some general details regarding the catalyst but did not disclose any catalyst preparative methods. The process patent is very broad in scope and encompasses a variety of possibilities regarding the catalyst formulation. For example, the patent suggests Pd being either dispersed directly onto the niobic acid or provided in a mixture with Pd being dispersed onto another distinct oxide support, with a loading which may range from 0.02 to 5 wt%. Additionally, it is suggested that the Pd may be deposited on a "mixed carrier" consisting of niobia combined with a second metal oxide support such as $Al_2O_3$ or $SiO_2$. However, the inventors do not explicitly state whether this "mixed carrier" is in fact a mixed oxide or is comprised of niobia dispersed onto the other oxide support. The process patent is sufficiently broad in scope to include most of the conceivable embodiments of the process at that time including carrying out the reaction in a slurry reactor in either batch or continuous mode or in a fixed bed flow reactor in either the gas or liquid phase, or in a trickle bed reactor.[44]

However, the inventors did disclose that in the fixed bed reactor embodiment, the catalyst preferentially consists of Pd dispersed onto niobic acid while in the slurry reactor embodiment, a mixture of niobic acid and a separate Pd catalyst is preferred.[44] In the comparative examples provided in the patent, the reactions were all carried out in the liquid phase between 140 and 160°C and pressures ranging from 2 to 4 MPa.[44] Only two catalysts were reported in the comparative examples; one consisting of 0.1 wt% $Pd/Nb_2O_5$ and the other a physical mixture of niobic acid with a 5 wt% Pd/C catalyst in a mass ratio of 2:1 niobic acid to hydrogenation catalyst.[44] When these catalysts were used for MIBK synthesis at 160°C and 2 MPa, the multifunctional catalyst gave the greatest acetone conversion and selectivity to MIBK.[44]

Maki et al.[94-96] disclosed several patents in the Japanese patent literature describing niobium oxide and other catalysts for the catalytic conversion of acetone to MIBK. The abstracts of these patents translated to English reveal in that in one patent, a $Pd/Nb_2O_5$ catalyst is reported whereby the Pd loading ranges (preferably) from 0.01 to 5 wt% and the niobium (V) oxide is calcined at 400 to 550°C.[94] In a second embodiment disclosed in a separate patent, the (hydrated) niobium (V) oxide catalyst is first treated with and acid such as oxalic acid, and then impregnated with a noble metal such as Pt or preferably Pd from 0.01 to 10 wt% or more preferably from 0.01 to 5 wt%.[95] In a third patent, an oxide support other than niobia is reported whereby the support consists of an oxide or hydroxide containing at least one of the following elements: Ce, Hf, or Ta and Pd is recommended as the hydrogenation metal but is supported on a separate catalyst, preferably as Pd/C.[96]

## 2.2 Synthesis, Characterization and Catalytic Properties of Surface-phase Niobium Oxide Species

### *2.2.1 Nanostructures of Surface-phase Niobium Oxide Species*

Bulk niobium (V) oxide is a stable, insoluble white polymeric solid comprised of $NbO_6$ octahedral monomers shared at the corners and edges as illustrated in Figure 2-2. The octahedral structure consists of a $Nb^{+5}$ cation surrounded by oxygen $O^{-2}$ anions. The $Nb^{+5}$ cation is too small to form a regular octahedral structure resulting the generation of distorted $Nb0_6$, $NbO_7$ and $NbO_8$ species (Figure 2-3) via the edge sharing and corner sharing of octahedra.[97] In the case of hydrated niobium (V) oxide, which contains an indeterminate amount of water, highly distorted $NbO_6$ species that are characterized by a terminal mono-oxo Nb=O bond, are the predominant structure. The Nb=O group found in the highly distorted $NbO_6$ octahedra accounts for the Lewis acid sites while the slightly distorted polyhedra ($NbO_6$, $NbO_7$ and $NbO_8$) have Nb-O-Nb bonds that are associated with Bronsted acid sites.[87,90] Bronsted acidity arises from the acidic protons of bridging hydroxyl groups. For a catalyst with niobia dispersed

onto an oxide support, the proton of a bridged hydroxyl group is particularly acidic if the terminal oxygen is linked to the support oxide (eg. Nb-OH-Si) thus allowing charge delocalization over the support.[90] Lewis acidity may also arise from the strong interaction between the surface-phase oxide and the support resulting in coordinative unsaturation about the Nb cation.[69,91]

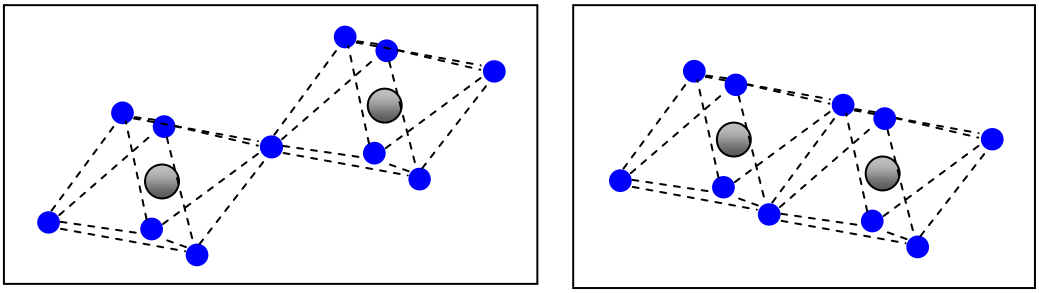

**Figure 2-2** Corner sharing (left) and edge sharing (right) of niobia octahedral monomers. *The grey sphere represents a $Nb^{+5}$ cation and the blue spheres represent $O^{-2}$ anions.*

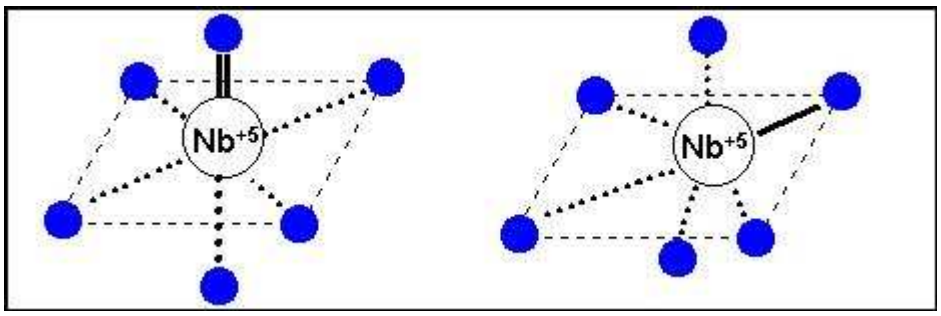


**Figure 2-3** (left) highly distorted $NbO_6$ octahedral structure with mono-oxo terminal Nb=O bond (right) slightly distorted $NbO_6$ octahedral structure (blue spheres denote $O^{-2}$ anions).

The supported niobia catalysts consist of a surface-phase niobium oxide, with a molecular structure distinct from bulk niobia, dispersed onto the outer most layer of another metal oxide which acts as a support. This configuration is distinct from mixed metal oxides, that may be prepared by co-precipitation and are comprised of a heterogeneous solid having two distinct solid oxide phases. It is well known and generally accepted that up to monolayer coverage, the surface-phase niobium oxide exists as a two dimensional "overlayer" rather than forming agglomerated 3 dimensional crystallites, as a consequence of the

preferential titration of the surface hydroxyls of the support oxide.[68,98] More generally, acidic metal oxides, such as $Nb_2O_5$, coordinate with the support via the preferential titration of the surface hydroxyls of the metal oxide support, whereas basic metal oxides such as the oxides of Fe, Ni and Co, coordinate with the support oxide via surface Lewis acid sites.[98] Direct empirical evidence of the preferential titration of the support oxide hydroxyls by niobia has been obtained via *in situ* FTIR spectroscopy.[99] $Nb_2O_5$ crystallites are observed above monolayer coverage and at elevated temperatures.[100] $TiO_2$, $ZrO_2$ and $Al_2O_3$ exhibit high surface concentrations of hydroxyl groups resulting in a close packed monolayer while $SiO_2$ has a lower concentration of surface hydroxyls and does not form a close packed monolayer.[68] The surface concentration of hydroxyls can be influenced by thermal pretreatment of the support.

When niobia is dispersed onto a metal oxide support, the physico-chemical interaction between the surface-phase oxide and the support gives rise to a diversity of niobium oxide species. Fortunately, the surface science of niobium compounds has been an area of intensive scientific investigation over the past two decades. A well established science now exists which allows the molecular engineering of the catalytic sites of the surface-phase niobium oxide from the careful control of the synthesis parameters and the judicious selection of catalytic materials.[68-70,73,74] The nanostructures of these unique niobium oxide species may be readily identified by Raman spectroscopy, Extended X-Ray Absorption Fine Structure spectroscopy (EXAFS) and X-Ray Adsorption Near Edge Spectroscopy (XANES).

The resultant structure of the surface-phase niobium oxide species is strongly dependent on the nature of the support material and is also influenced by the degree of hydration from adsorbed water.[87,100] Jehng and Wachs [68,87,97,100] elucidated the molecular structure of niobium oxide species dispersed onto various oxide supports. They found that basic supports lead to

the formation of highly distorted $NbO_6$ species while acidic supports resulted in the formation of slightly distorted polyhedra ($NbO_6$, $NbO_7$ and $NbO_8$). Lewis acid sites are present in all supported niobium oxide catalysts but Bronsted sites appear to be limited to the $Nb_2O_5/Al_2O_3$ and $Nb_2O_5/SiO_2$ systems.[73,87,91]

Bronsted acidity appears only at higher niobia loadings; above around 1/3 monolayer coverage, and increase with increasing niobia concentration.[87,91] Turek et al.[99] proposed the Bronsted acidity was related to the increase in surface concentration of the dispersed niobia species and in particular that a crowding effect is needed for the creation of Bronsted acidity. They proposed that the Bronsted acid sites consist of a proton being shared between oxygen atoms of adjacent (Nb-O-Al) linkages.[99] (However, the model could be applied generally to supports other than alumina.) Thus, the Bronsted acidity increases with niobia loading and a critical surface niobia concentration is required for the creation of Bronsted acidity. Since the proposed theory implies that Bronsted acidity exists primarily at adlineation sites, it also explains the observation by Datka et al.[91], who found the Bronsted acidity diminished for niobia loading exceeding monolayer coverage.

The surface niobium oxide nanostructure is also dependent on the niobia loading. For example, Jehng and Wachs[100] found that all niobia catalysts investigated having a niobia loading less than one half monolayer coverage, exhibited highly distorted $NbO_6$ octahedra with a terminal Nb=O bond length of 0.171 nm, regardless of the oxide support. Below a half monolayer coverage an $Nb_2O_5/Al_2O_3$ catalyst exhibited two $NbO_6$ species described as highly distorted and moderately distorted with Nb=O bond lengths of 0.171 and 0.176 nm respectively.[100] However, as the niobia loading increased approaching monolayer coverage, polymeric octahedral structures emerged resulting in a combination of highly distorted $NbO_6$ octahedra with a Nb=O bond length of 0.173 nm as well as slightly distorted $NbO_6$ species with Nb-O-Nb linkages having a Nb-O bond length of 0.192 nm.[100]

Although Wachs et al. originally reported that only highly distorted $NbO_6$ species were observed for $Nb_2O_5/SiO_2$ catalysts, many subsequent studies have demonstrated that in the case of niobia overlayers dispersed on silica, the predominant surface-phase niobium oxide species consist of $NbO_4$ tetrahedra.[69,90,93,101-103] Other structures for the surface-phase niobium oxide near monolayer coverage on silica have been proposed.[70] The $NbO_4$ tetrahedra often combine to form dimers and other polymeric structures (Figure 2-4). Incidentally, monomeric tetrahedral $NbO_4$ structures have recently been proposed to exist on $Al_2O_3$, $ZrO_2$ and $TiO_2$ for low niobia loading.[103]

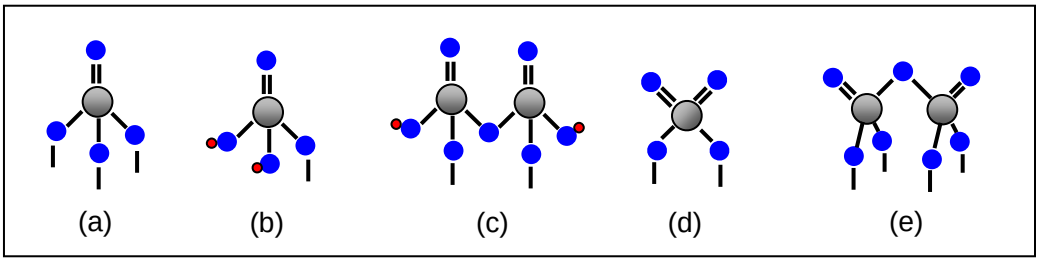


**Figure 2-4** Niobium Oxide Tetrahedral Monomers and Dimers on $SiO_2$
*Grey denotes $Nb^{+5}$, blue denotes $O^{-2}$ cations, red denotes $H^+$. Monomers and dimers bound to $SiO_2$ via Nb-O-Si linkages. (a) monomer[90] (b) monomer with OH groups[90] (c) dimer with OH groups[90], (d) monomer with di-oxo moities[69,93,101] e) dimer with mono-oxo moities [69,93,101]*

The Nb=O bonds of the $NbO_4$ tetrahedral species have shorter bond lengths than the terminal oxo group of highly distorted $NbO_6$ species. Consequently, the tetrahedral niobium species generally exhibit greater Lewis acidity than the highly distorted octahedral species, which have only moderate Lewis acidity.[69,90] In addition, niobia tetrahedra may exhibit Bronsted acidity due to Nb-O-Si bridging linkages. For example, the monomeric and polymeric tetrahedral structures proposed by Burke and Ko[90] and outlined in Figure 2-4 (b) and (c) have hydroxyl groups which serve as Bronsted acid sites. Ichikuni et al.[68,101] reported a unique monomeric $NbO_4$ species having di-oxo Nb=O bonds (Figure 2-4 (d)). They suggested that this unique nanostructure may be obtained through careful control of the synthesis route (which is outlined in section 2.2.2) and selection of catalytic materials.

It is important to note that the surface-phase niobium oxide nanostructures outlined thus far have been ascertained via Raman and EXAFS spectroscopy under conditions for which the catalyst has been activated at elevated temperature and therefore under dehydrated conditions. Under ambient conditions, the catalysts are hydrated by the adsorption of around 20 to 40 monolayers of water resulting in a significant solvation, and possibly the dissolution of the oxide species at the interfacial region.[104] Generally, the niobium oxide overlayer is very stable due to the strong interaction between the niobium oxide and the support (SOSI).[73] However, the presence of water is known to modify the structure of the surface oxide phase.

When hydrated, the structure of the surface-phase niobium oxide species is governed by the surface pH and its aqueous solution chemistry.[100] More specifically, it has been established that the molecular structures of a surface-phase oxide is governed by the net pH at the point of zero charge.[104,105] The point of zero charge corresponds to the condition where the solid is in equilibrium with the aqueous thin film at which point there is no net charge on the solid. According to Jehng and Wachs[100] the net surface pH is determined by contributions from both the niobium oxide (eg. $Nb_2O_5$ ~ pH 0.5) and the oxide support whereby the decrease in pH relative to the oxide support is proportional to the fractional surface coverage of niobia. Acidic supports such as $TiO_2$ and $ZrO_2$ may yield structures similar to niobic acid with slightly distorted $NbO_6$, $NbO_7$ and $NbO_8$ species while basic supports such as $Al_2O_3$ may yield dissolved hexanobiate species.[100] The various niobiate species that may be produced from the dissolution of niobic acid depend on the pH and are summarized in the literature.[73,87]

Jehng and Wachs[100] have elucidated the structure of several dispersed niobium compounds under hydrated conditions and found that the removal of chemisorbed water resulted in an increased distortion of $NbO_6$ species, and thus a further increase in its Lewis acidity, but does not appreciably affect the

slightly distorted $NbO_6$, $NbO_7$ and $NbO_8$ species. The length of the Nb=O bond is affected by the presence of adsorbed water due to hydrogen bonding.[105] As mentioned previously, niobia compounds exhibit excellent moisture tolerance and even an increase in activity when exposed to water. When calcined at moderate temperatures (100 to 300°C), resulting in a significant amount of chemisorbed water, niobic acid has a very strong Bronsted acidity. In fact, Iizuka et al.[88] have suggested that niobic acid exhibits the strongest Bronsted acidity of all metal oxides calcined at 100°C. The dispersion of niobia onto a metal oxide support will modify its catalytic properties compared to bulk niobia as well as improve its thermal stability. It is known that the Bronsted acidity of the surface-phase niobium oxide is maximized at 100°C and diminishes with increasing calcination temperature as protonic sites are replaced with Lewis acid sites while the Lewis acidity increases with calcination temperature until the onset of crystallization.[73]

### *2.2.2 Synthesis Methods*

A two dimensional surface-phase niobium oxide overlayer is usually achieved with 100% dispersion, when dispersed on another metal oxide below monolayer coverage via the reaction of a niobium precursor with the surface hydroxyls of the support.[98,104] In the case of $SiO_2$ supports, less than 100% dispersion is often realized due to the relatively acidic character and low reactivity of the hydroxyl groups.[98] The most common precursors used is niobium (V) ethoxide, which is diluted in an organic solvent such as hexane. The procedure involves four general steps. First the catalyst support is activated by thermal treatment, which also controls the surface hydroxyl concentration via dehydroxylation. Second, the catalyst is contacted with the precursor solution whereby the niobium ethoxide coordinates with the surface hydroxyls of the support in an attaching reaction. Third, after the supernatant liquid is separated from the solvent the catalyst is heated in inert environment to thermally decompose the organic ligands of the precursor. Finally, the catalyst is calcined

in air to complete the attaching reaction and generate the niobium oxide overlayer.

The approach by which the surface attaching reaction is carried out is the major distinction between the various synthesis methods. Ko et al.[89,90] carried out the surface attaching reaction at room temperature followed by thermal decomposition in nitrogen at 400°C then calcination in air at 500°C. Asakura and Iwasawa[70] activated the $SiO_2$ support at 200°C and carried out the attaching reaction under reflux conditions. The thermal decomposition was carried out in vacuum at 200°C and the calcination was carried out in oxygen at 500°C. This procedure was repeated twice. Ichikuni et al.[69,93,101] disclosed several synthesis methods for producing unique niobia tetrahedral monomers and dimers on silica. They developed a series of $Nb_2O_5/SiO_2$ catalysts for which the support was activated at 400°C and the attaching reaction was carried out under various conditions (room temperature, reflux conditions, in vacuum at 400°C and subzero temperatures of -40°C) using multiple niobium precursors with different Nb oxidation states and various ligands. The synthesis was completed by exposure to hydrogen at 600°C or 400°C followed by calcination in oxygen at 400 or 500°C. As an example, their technique to synthesize the tetrahedral niobia monomer with di-oxo Nb=O structure [Fig 2-4 (d) ] is illustrated schematically in Figure 2- 5.

An aqueous incipient wetness impregnation technique may also be used to produce dispersed niobium oxide catalysts. Niobium oxalate which can generate niobiate ions when dissolved in aqueous solution and can be used as the precursor. The resultant niobium oxide structure is believed to be dependent on the nature of the niobiate species in solution.[106] Niobium pentachloride may also be used as a precursor in aqueous medium. However, it is not recommended since the dissolution of niobium pentachloride liberates chloride ions, which are Lewis bases and may diminish the acidity of the catalyst.[106] Other synthesis techniques have been reported. For example, a

procedure has been disclosed for the synthesis of niobium oxide aerogels via sol gel technique, which could be utilized in thin films and wash coatings for catalytic reactors.[107] More recently, niobium oxide nanocrystals with diameters ranging from 2 to 4.5 nm have been synthesized from peroxo niobic acid sol.[107]

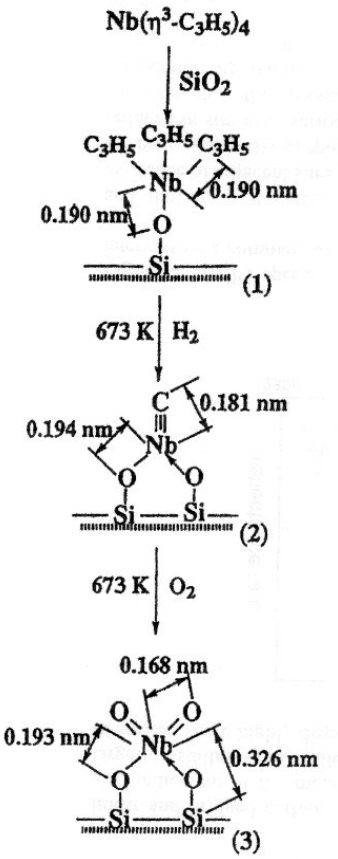


**Figure 2-5** Synthesis of tetrahedral $NbO_4$ monomers with di-oxo moiety on silica from N. Ichikuni et al.[69]♣

Evidently, there is currently a lack of consensus in the catalysis community regarding the importance of the synthesis method on the resultant molecular structure of the surface-phase niobium oxide. For example, Ichikuni et al.[69] have suggested that for $Nb_2O_5/SiO_2$ catalysts, the choice of precursor as well as synthesis conditions are critical and have advised that various designed

♣ Figure 2-5 was reprinted with permission from Elsevier Science from N. Ichikuni, M. Shirai and Y. Iwasawa, "Surface Structures and Catalytic Properties of Supported Niobium Oxides", *Catalysis Today*, **28**, (1996), pp. 49-58. © (1996) Elsevier Science

surface structures including monomers, dimers, layered structure and agglomerated clusters may be obtained by careful control of the synthesis technique and selection of precursors. In addition, they observed that these distinct surface species exhibit unique catalytic properties and markedly different activities and selectivities for ethanol dehydrogenation.[69,93,101] Jehng and Wachs[68] investigated the effect of niobium precursor and preparation technique on the catalytic performances of niobium oxide dispersed on $SiO_2$, $Al_2O_3$, MgO, $ZrO_2$ and $TiO_2$. The catalysts were prepared by nonaqueous impregnation using niobium (V) ethoxide, by aqueous impregnation using niobium oxalate and by surface reaction with $Nb(\eta^3\text{-}C_3H_5)_4$. They concluded that the choice of precursor and synthesis parameter did not affect the resultant niobium oxide structure or the reactivity. Wachs et al.[103] attributed this apparent discrepancy to the complicated curve fitting analysis required by EXAFS techniques. However, the nature of the oxide support, the calcination temperature and the niobia loading are undoubtedly important catalyst parameters affecting both structure and reactivity.[68]

Wachs[98] has explained that the niobium oxide nanostructure is self assembling and that the most thermodynamically stable structure is always attained regardless of the choice of precursor or synthesis technique. However, this argument seems over simplified and neglects the potential for metastable states for which the Gibbs free energy is a local minimum. Metastability is ubiquitous in nature, particularly in solid state chemistry. It is quite plausible and reasonable that locally stable surface structures may be obtained depending on the approach to the final state of the system. The empirical fact that the tetrahedral $NbO_4$ monomers and dimers prepared by Ichikuni et al.[69,93,101] exhibited distinct catalytic behaviour for ethanol dehydrogenation is indirect evidence that the molecular structures of the catalyst active sites were in fact modified through the synthesis technique. In addition, Jehng and Wachs[68] did not follow a synthesis technique disclosed by Ichikuni et al.[69,93,101] but rather used an incipient wetness impregnation. The agglomerated structures reported

by Jehng and Wachs[68] are, in fact, expected from an incipient impregnation technique.[69] It seems reasonable to conclude that the synthesis method does affect the molecular structure of the surface-phase niobium oxide, at least in the case of $Nb_2O_5/SiO_2$ catalysts.

## 2.3 Kinetic Studies on MIBK Synthesis

### *2.3.1 Fundamental Reaction Mechanism*

The synthesis of MIBK from acetone has been of industrial significance since the early to mid 20$^{th}$ century. Consequently this organic synthesis has been studied extensively in both the liquid and gas phases over both acidic and basic catalysts as well as catalysts exhibiting both acidic and basic sites. This review will focus on the mechanism of acid catalyzed MIBK synthesis.

The selective hydrogenation of MO to MIBK has been studied previously.[109-115] Quite recently, the author and co-workers[18] have proposed a novel theory for the selective, catalytic hydrogenation of MO for which MO diadsorbed as an $\eta_4$ species is postulated. The proposed mechanism and fundamental kinetic model have been outlined previously in section 1.2. The kinetics of the acid catalyzed aldol condensation of acetone as well as DAA dehydration have also been studied rather thoroughly using cation exchange resin catalysts and other polymeric catalytic materials[10,116-118], zirconium phosphate,[115] dimethyl sulfoxide[119] and various acidic aqueous media.[11,120-122] The fundamental reaction mechanism is considered to be well known.[50] The kinetics of the acid catalyzed aldol condensation of acetone and DAA dehydration are described by Melo et al.[50] and summarized here in equations 2-4 through 2-9.

First, an acetone molecule is activated either by coordination with a Lewis acid site via the carbonyl group or by protonation of the carbonyl group involving a Bronsted acid site, thus withdrawing electron density from the secondary carbon atom. Second, the enol tautomer of acetone with electron

density about the C=C bond undergoes nucleophillic attack of the secondary carbon of the activated acetone molecule to form a reactive intermediate. This step is known to be the rate determining step.[50,121] Third, proton abstraction from the reactive intermediate or desorption of the intermediate from the Lewis acid site yields DAA.

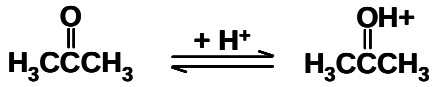

(2-4)

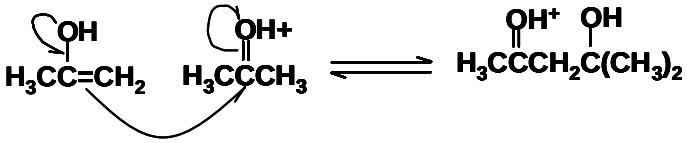

(2-5)

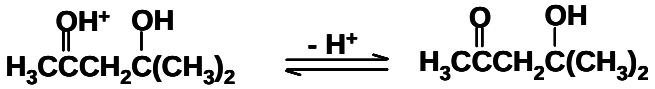

(2-6)

Melo et al.[50] has suggested that the acid catalyzed dehydration of DAA to produce MO also involves three steps. First, DAA is protonated at the hydroxyl group to form a reactive intermediate. Second, this intermediate liberates a molecule of water to form a carbenium ion. Finally, the carbenium ion is deprotonated to give MO. The protonation-deprotonation steps are known to be relatively rapid while the formation of the carbenium ion intermediate is likely the rate determining step.[50]

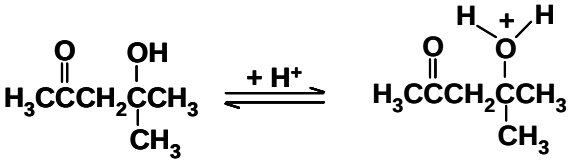

(2-7)

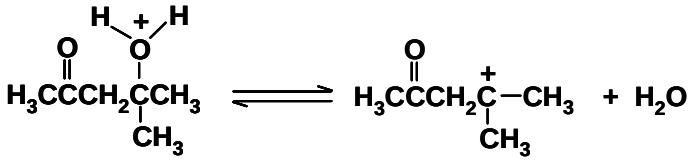

(2-8)

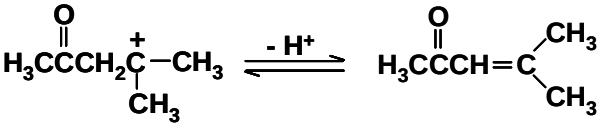

(2-9)

Although it is generally accepted that the dehydration of DAA follows three general stages, which include a protonation step, a second stage involving the creation of a carbenium ion and the liberation of water followed by a deprotonation step, the consensus in the literature is that it is in fact the carbonyl group that is protonated rather than the hydroxyl group.[11,121-123] Jensen and Carre[121] studied the kinetics of the hydration of various α,β-unsaturated ketones in acidic aqueous media utilizing radioactive isotopic labeling. They confirmed the acid catalyzed mechanism of the aldol condensation of acetone outlined in equations (2-4) through (2-6) and proposed a general mechanism for the dehydration/hydration of α,β-unsaturated ketones outlined in Scheme 2-1.

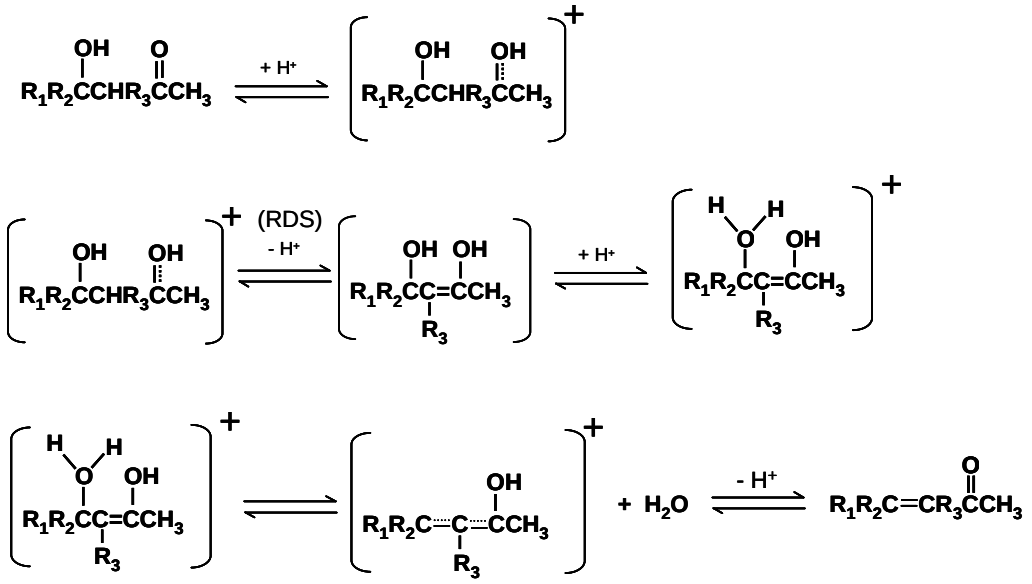


**Scheme 2-1** Mechanism of the Hydration-Dehydration of α,β-unsaturated ketones proposed by Jensen and Carre[122]

*2.3.2 Kinetic Modelling of the Overall MIBK Synthesis*

The well established mechanisms of acetone condensation and DAA dehydration presented in the previous section lead to the universally accepted conclusion that aldol condensation of acetone is a bimolecular reaction and is therefore second order with respect to acetone and is first order with respect to DAA in the reverse aldol condensation. Similarly, the DAA dehydration-MO

hydration reaction is first order with respect to the substrates in both directions. In the case of heterogeneously catalyzed reactions, a term expressing the fraction of available sites is usually included for which adsorption terms are present in the denominator of the rate expression, collectively raised to the second power as a consequence of the bimolecular nature of the reaction.

Of the three major reaction steps to produce MIBK from acetone, the aldol condensation of acetone to produce DAA is frequently reported and perhaps generally accepted to be the rate determining step.[23,42,47,50,116] In the case of gas phase MIBK synthesis, DAA is rapidly converted to MO such that DAA is never observed in the product mixture for the gas phase reaction conditions.[23] DAA is often not observed in the product mixture for the conditions in liquid phase reactions as well.[19,47,115] Consequently, DAA is frequently neglected from the kinetic analysis. In addition, since the aldol condensation steps are frequently controlling, pseudo zero order kinetics with respect to hydrogen partial pressure may be observed, particularly for gas phase reaction conditions.[19,115] For the case of the overall MIBK synthesis, the irreversible hydrogenation shifts the reaction in favour of product formation and thus the reverse reactions are often neglected. Therefore, the distinguishing features between the various kinetic rate expressions for MIBK synthesis available in the literature tends to be whether or not DAA is included in the model, whether or not reverse reactions are included and which adsorbed species are considered to be kinetically relevant and included in the rate law.

For example, Thotla et al.[124] quite recently proposed that the coproduction of MO and diacetone alcohol over Amberlyst 15 cation exchange resin via reactive distillation could be adequately modelled using the two kinetic rate expressions in equations (2-10) and (2-11) which assumes that the reverse reaction of MO and water to produce DAA is negligible and that water is the only kinetically relevant adsorbed species. In this model, activities rather than concentrations of species are used in the model.

$$\frac{dn_{DAA}}{dt} = W\left(k_f a_{Ac}{}^2 - k_b a_{DAA}\right) - r_{MO} \qquad (2\text{-}10)$$

$$r_{MO} = \frac{dn_{MO}}{dt} = \frac{Wk_{MO}a_{DAA}}{\left(1+K_W a_W\right)^2} \qquad (2\text{-}11)$$

Similarly Watanabe et al.[115] proposed a model consisting of 2 rate equations to describe the overall MIBK synthesis over a zirconium phosphate catalyst. One equation (2-12) predicts the rate of production of MO and water from acetone while the other (2-13) predicts the rate of MIBK production. In this model, the adsorption of acetone (A), MO (MO) and MIBK (I) are considered kinetically relevant. DAA is neglected entirely; as are the reverse reactions. The reaction is pseudo zero order with respect to hydrogen partial pressure.

$$-\frac{dC_A}{dt} = 2\frac{dC_{MO}}{dt} = \frac{28.48C_A{}^2}{[1+33.9C_A]^2} \qquad (2\text{-}12)$$

$$\frac{dC_I}{dt} = \frac{17.8C_{MO}}{[1+4.75C_{MO}+0.686C_A+19.65C_I]^2} \qquad (2\text{-}13)$$

As a final example, a novel kinetic model for the overall MIBK synthesis was recently proposed by Mahajani et al.[19] who, citing this author and co-workers' theory on the catalytic hydrogenation of MO[18], proposed that the inhibition term for the overall MIBK synthesis should be raised to the fourth power, suggesting that DAA might also be diadsorbed. The rate expression for the overall MIBK synthesis is given in equation (2-14). The reaction is pseudo zero order with respect to hydrogen and the adsorption of acetone and water are considered to be kinetically relevant. Again, activities were used in place of concentrations.

$$r = \frac{k a_{Ac}^{\ 2}}{\left(1 + K_W a_w + K_{Ac} a_{Ac}\right)^4} \qquad (2\text{-}14)$$

*2.3.3 Water and the Pseudo-Equilibrium Phenomenon*

In section 2.1.4 it was reported that Chen et al.[42] had found that the accumulation of water in a batch autoclave significantly inhibited the synthesis of MIBK and that the acetone conversion after a pre-determined time at 160°C decreased linearly with the amount of water added initially to the reactant mixture. The inhibiting effect of water when heterogeneous catalysts are used has been known for decades. However, this inhibition is not well understood. It is largely due to interfacial phenomena due to the presence of a solid phase and is not a consequence of material equilibrium.

When acetone is heated in the presence of an acidic catalyst in the absence of hydrogen, a mixture of acetone, DAA and MO results since the aldol condensation of acetone and DAA dehydration are equilibrium limited. The material equilibrium of the acetone-DAA-MO system have been thoroughly investigated in homogenous liquid phase.[10,11,120,121,125,126] At elevated temperature, the amount of DAA in the system is negligible and acetone is transformed to MO. Equation (2-15) is an expression for the equilibrium constant as a function of temperature based on experiments carried out in homogeneous systems.[10] However, when the synthesis of MO is carried out using a solid acid catalyst, the equilibrium conversion obtained is typically lower than the theoretical equilibrium conversion. du Toit et al.[127] have coined this as "*the pseudo equilibrium phenomenon*".

$$K_c = \left[\frac{C_{MO} C_W}{C_{Ac}^{\ 2}}\right] = 6.2\, x10^{-3} \exp\left(\frac{347}{T}\right) \qquad (2\text{-}15)$$

du Toit et al.[127] calculated the equilibrium constant from the Gibbs Free Energies of formation of the reactants and products and found that the theoretical value was in very good agreement with that predicted by equation

(2-15) proposed by Klein and Banchero[10] over the temperature range of interest (20 to 160°C). However, the experimentally measured equilibrium MO concentration differed significantly from the predicted value. For example, at 100°C the theoretical equilibrium concentration of MO is around 1.19 M but the actual value obtained using Amberlyst 16 cation exchange resin catalyst was around 0.7 M.[127]

du Toit et al.[127] confirmed that the experimentally observed equilibrium was in fact a pseudo equilibrium due to deactivation rather than material equilibrium by carrying out an experiment whereby water was added to an FBR reactor feed stream for conditions of maximum (equilibrium) conversion. If the experimentally observed equilibrium was the true material equilibrium, then the introduction of water would shift the equilibrium in favour of DAA formation (i.e MO hydration) and the equilibrium MO concentration should decrease. In fact, the MO concentration was observed to increase slightly.[127] Although this increase was slight, the fact that the MO concentration did not decrease confirms that the "equilibrium" conversion was a pseudo equilibrium and not a true material equilibrium.[127] A similar experiment was conducted by Klein and Banchero[10] over 50 years ago. They found that the addition of MO to a PFR feed stream had a slight inhibiting effect on the synthesis of MO using a cation exchange resin, but the addition of water had a far more profound inhibiting effect than MO. Thus, the inhibiting effect of water is due to interfacial phenomenon and not material equilibrium.

du Toit et al.[127] also ruled out the notion that activities must be used instead of actual concentrations to accurately predict the equilibrium and concluded that the pseudo equilibrium phenomenon must be due to a form of reversible catalyst deactivation.[127] du Toit et al.[127] could explain the reversible deactivation for conditions of low conversion in a batch autoclave as due to the adsorption of water. They could successfully model the autoclave data using a Freundlich adsorption isotherm however, the model apparently

breaks down for higher conversion and cannot account for the above observation for which the MO conversion increased when water was added to the FBR feed stream. It is well known that cation exchange resins are deactivated by water due to its strong affinity for acid sites.[19,33,66,116] Consequently, water is usually attributed to the pseudo equilibrium.[19,33] However, this phenomenon is not fully understood.

The material equilibrium for the acetone-DAA-MO system is known to be affected by acidity. Studies in homogenous systems found that the equilibrium constant remains invariant over a broad range of dilute acid concentrations, however at higher concentrations, the equilibrium constant increases markedly in favour of DAA dehydration to produce MO, possibly due to complex formation.[11,121] The rate of dehydration of DAA increases with increasing acidity and the equilibrium shifts markedly for $[H_3O]^+$ beyond around 6M, while no hydration of MO to produce DAA occurs for 8M $[H_3O]^+$.[121]

*2.3.4 The Role of Bronsted and Lewis Acidity*

Chen et al.[42] suggested that a combination of both Bronsted and Lewis acid sites might be beneficial for MIBK synthesis utilizing niobia catalysts, since they assert that Lewis sites are needed for the activation of acetone to produce the enol tautomer. However, the roles and relative importance of Bronsted and Lewis acidity for MIBK synthesis over niobium compounds is currently not clear. The niobia catalysts reported previously in the scientific literature for MO and MIBK syntheses were calcined at 400°C or higher, except that of Higashio and Nakayama[43], and likely did not exhibit significant Bronsted acidity. (Perhaps the intention in some cases was to maximize Lewis acidity.) However, fundamental studies on acetone condensation over other acidic materials have been carried out and may provide some insight.[127,128]

Pavnov and Fripiat[128] carried out an in situ FTIR investigation of the acetone aldol condensation reaction over alumina and acidic zeolites (HZSM-5

and USY). Their results support the notion that Lewis acid sites are responsible for the activation of acetone over both zeolites and alumina. They concluded that although acetone is less strongly bound to Lewis sites compared to the Bronsted sites of the materials investigated, that the Lewis acid sites are responsible for activation of the acetone molecule.[128] In addition, they found that in the case of alumina catalyst, the reaction occurs between adjacent acetone molecules adsorbed on Lewis acid sites whereas in the case of the zeolites, the reaction occurs between a molecule of acetone adsorbed on a Bronsted acid site and a molecule of acetone in the gas phase.[128] Evidently, the reaction mechanism and role of the acid sites is dependent on the catalytic material. Incidentally, the alumina catalyst was more active than the zeolites investigated.[128]

Flego and Perego[129] studied the aldol condensation of acetone over various molecular sieves with varying pore size distributions. They found that the catalyst activity for the aldol condensation of acetone increased linearly with increasing density of Bronsted acid sites.[129] The catalysts investigated exhibited both Bronsted and Lewis acidity. The fact that the activity increases linearly with acid site density is not surprising, but the importance of Bronsted acid sites seems to contradict the results of Pavnov and Fripiat[128] who concluded that Lewis sites are responsible for the activation of acetone. Perhaps more importantly, their investigation found that the product distribution, including the production of isophorone and other higher molecular weight species is strongly dependent on the pore size distribution of the catalysts.[129]

## 2.4 MIBK Production Technology

As introduced in chapter one, MIBK has been produced historically in a 3-stage process whereby the aldol condensation of acetone, DAA dehydration and the selective hydrogenation of MO are carried out in separate reactors. The product from the reactor effluents are further refined with distillation units and unreacted material is recycled to previous stages. Homogeneous catalysts are used for the acetone aldol condensation and DAA dehydration steps. In the final stage, a feed consisting of 98 to 99% MO is hydrogenated via catalytic distillation at 110°C and atmospheric pressure resulting in MIBK yields in excess of 96%.[1,20] This process has the advantage that DAA, which is a valuable high boiling solvent with excellent moisture tolerance, may be recovered as a by-product. Consequently, this 3-stage process is apparently still in use at Shell's Deer Park facility in Texas.[1] However, the process is very energy intensive and inherently inefficient. Consequently, one-step processes for MIBK production have been used commercially since the late 1960's.[1] However, little information is publicly available regarding the current state-of-the-art of this reactor technology. Here, that information which has been publicly disclosed, particularly in the patent literature, is reviewed.

### *2.4.1 Trickle Bed and Multi-Tubular Reactors*

The reader should note that "one-step" MIBK processes refer to processes whereby all three major reaction steps are facilitated in a single chemical reactor. In fact, currently the MIBK concentration in the reactor effluent for state-of-the-art commercial one step processes is typically less than 30 wt% resulting in the need for additional unit operations for downstream refining.[24] One step MIBK synthesis is carried out in the liquid phase in trickle bed (TBR) or multi-tubular reactors at temperatures from 120 to 160°C and pressures ranging from 1 to 10 MPa with an MIBK selectivity of around 90%.[23,24] Aside from the low efficiency of the current one-step process technology, relatively high operating pressures are needed, which increase operating costs.[23-25] MIBK synthesis may be carried out in the gas phase at atmospheric pressure. However

to date, no atmospheric gas phase process for MIBK synthesis has yet been successfully commercialized due to relatively low selectivity and particularly due to very poor catalyst stability despite extensive research in this area.[24,42] In fact, the development of an improved catalyst for the one-step synthesis of MIBK in either the liquid or gas phase has been described recently as "a priority concern".[42] Catalyst systems previously investigated for one-step MIBK synthesis have been summarized in section 1.3.

One of the first patents for a one-step process for MIBK synthesis was filed in 1948 by E.F. Smith.[130] This process involved a mixture of aqueous NaOH catalyst and a Pd/C hydrogenation catalyst used in either an autoclave, FBR or slurry column. Aside from being of historical significance, the inventor reported some insightful observations. First, the inventor noted that the addition of water to the reactant mixture was unexpectedly advantageous and explained that the presence of water prevented over condensation and aided in the mixing of the homogenous catalyst. Second, the inventor noted that inert gases such as nitrogen should be minimized or avoided all together since it resulted in the need to increase the total system pressure in order to maintain the required partial pressure of hydrogen to sustain the hydrogenation. Lastly, this patent is perhaps the first to report that carrying out the hydrogenation in the same unit operation as the condensation steps resulted in an enhanced yield.

Several patents followed throughout the 1960's as catalysis and reactor technology for one step MIBK synthesis progressed.[131-138] Robbins et al.[131] advocated the use of an adiabatic reactor rather than a multitubular FBR reactor and recommended the use of excess hydrogen since it resulted in enhanced catalyst life and enhanced conversion for the condensation step to produce MO. A similar observation was reported by Wollner et al.[132] who found that when using cation exchange resins as catalysts in the absence of hydrogen, the undesirable byproducts referred to as "acetone oil" from the consecutive

condensation reactions could be significantly mitigated in a single stage process with hydrogen.

Perhaps the most notable and insightful patent of this era was by Wollner et al.[133] who reported a novel one-step process for MIBK synthesis involving a trickle bed reactor at 120 to 140 °C and 2.5 to 3.5 MPa utilizing a novel multifunctional catalyst consisting of a noble metal dispersed on a strongly acidic resin. They outlined the deficiencies of the existing technology at that time, which included the deactivation of ion exchange resins from heavy metals dissolved from steel reactor components as well as the fragmentation of catalysts and wearing of agitators and other reactor internals in fluidized beds and other slurry reactors. Aside from enhanced selectivity, another advantage of a multifunctional catalyst over mixtures of acidic resins and a separate hydrogenation catalyst is the aversion of the fusing of the catalyst particles from the formation of undesirable byproducts from the production of phorones and other high molecular weight species, which often necessitates reactor shut down to remedy.[133] The most important advantage of the TBR process is that the TBR gives much higher conversion than fluidized bed and other backmix reactors since the accumulation of MIBK, water and other products reduce the acetone concentration and lower the reaction rate.[133] In the comparative examples, Wollner et al.[133] reported MIBK productivities ranging from 0.44 to 0.59 [$g_{MIBK}$/hr*$mL_{cat}$] with MIBK mass fractions in the effluent ranging from 34.5 to 44.5 wt%.

The one-step processes for MIBK production first commercialized in the late 1960's and early 1970's by Veba Chemie and Deutsche Texaco apparently remain the state-of-the-art for MIBK technology.[1] The Veba Chemie process[1,134] involves a strongly acidic cation exchange resin containing 0.05 to 0.08 wt% Pd and immobilized in a fixed bed within a trickle bed reactor with hydrogen flowing in a co-current fashion. Subsequent to the reactor is a phase splitter to recover unreacted hydrogen and 4 distillation units for product

refinement. The reactor is operated at 135°C and 6 MPa giving an acetone conversion of 35% with 96% selectivity to MIBK.[1] The Deutsche Texaco process flowsheet described in Muthusamy and Fischer[1], is essentially identical and also has a single reactor using a Pd/cation exchange resin catalyst, followed by phase separators and 4 distillation units. The reactor is operated at a similar temperature (130 to 140°C) but lower pressure 3 MPa and gives a comparable performance. Other processes have been patented and are summarized in Muthusamy and Fischer[1]. However, the Veba Chemie process appears to represent the performance benchmark.

More recently published patents[139-148] provide some insight into the advancement of MIBK production technology. Nissen et al.[139] reported a relatively inexpensive ZnO catalyst utilizing either Ni or Co as hydrogenation catalysts. Gefri et al.[140] of Allied Corporation addressed the high cost of the conventional Pd/cation exchange resin catalyst by proposing a novel mixed ketones process for which a relatively inexpensive Cu oxide catalyst converts the reactants, at least one of which is a ketone and the others are either ketones, alcohols or aldehydes to produce MIBK. Evidently, mixed ketone processes are still used for the commercial production of MIBK by some manufacturers including BASF, Union Carbide and Shell.[1] Di Cosimo et al.[24] have recently disclosed a one step process whereby IPA is dehydrogenated to produce acetone over a Cu-Mg-Al mixed oxide catalyst and the hydrogen generated *in situ* is used to convert MO to MIBK with 27% yield. One-step MIBK processes involving the dehydrogenation of IPA to generate *in situ* hydrogen for the hydrogenation of MO utilizing a mixed oxide catalyst containing oxides of copper and magnesium have been studied previously; however their MIBK yields have been unsatisfactory.[134]

The conventional Pd/cation exchange resin catalyst exhibits poor thermal stability, which is a detriment to DAA dehydration and deactivates in the presence of water. Many recent patents have proposed novel alternatives and

solutions. Huang and Haag[141] of Mobil Oil disclosed a process utilizing a 0.5 wt% Pd/ZSM-5 catalyst which enabled a higher reaction temperature of 180°C. When the reactor was pressurized to 600 psig and acetone was fed with a WHSV of 3.8 $hr^{-1}$ and hydrogen in 20% stoichiometric excess, MIBK was produced with 98% selectivity and the effluent had 28.5 wt% MIBK.[141] However, Olsen[142] of Union Carbide has argued that this result is not repeatable and these catalytic materials would yield a larger amount DIBK for the process conditions reported by Huang and Haag[141]. However, Olsen has pointed out that DIBK is also a useful product and that the product distribution can be tailored by exploiting the shape selectivity of molecular sieves as well as the starting reactants in a mixed ketones process.[142] Isogai et al.[143] patented a one step process whereby MIBK is produced from acetone in a carbon monoxide environment over a catalyst consisting of a group VIII metal, a halogen and phosphorous compound.

Chen et al.[54,144] have also disclosed single step MIBK processes involving zeolite catalysts carried out in either the vapour or liquid phase in an FBR. The results disclosed in their first patent[144] were poor. Although acetone conversions as high as 40% could be achieved, the MIBK selectivity was typically 30 to at most 60%.[144] However, in a more recent disclosure, it is claimed that MIBK can be produced with an acetone conversion of 72% and a selectivity of 94% using a 0.5 wt% Pd/HZSM-5 catalyst in a PFR at 160°C with acetone fed at WHSV =0.6 $hr^{-1}$.[54] This outstanding result seems singular in the literature.

Rohm and Haas quite recently sought patent protection for a new polysulfonated styrene/DVB cation exchange resin catalyst for MIBK synthesis.[145] The new cation exchange resin is purported to improve MIBK yield and productivity by about 20% compared to the state-of-the-art cation exchange resin as well as apparently improved thermal stability allowing temperatures as high as 150°C.[145] Previously, Brandes et al.[146] (Deutsche

Texaco) reported MIBK productivities as high as 0.654 g/hr*mL and MIBK selectivity as high as 93% when MIBK was produced in a 3 m tall, 26 mm diameter TBR at 125°C and 3 MPa using a 1.9 wt% Pd on strongly acidic sulfonated styrene DVB copolymer resin and an acetone feed of 3.2 L/hr.

Some of the most recent patents give insight into the state-of-the-art. In 2004, Johnson Matthey patented a catalyst consisting of a basic alkali metal dispersed onto an inert support such as silica for gas phase synthesis at 175°C of saturated ketones including MIBK as well as other products of aldol condensation processes.[147] In 2005, Eastman Chemical Co., one of the largest MIBK producers, received a patent for a mixed ketones process utilizing both homogeneous and heterogeneous catalysts. Higher molecular weight ketones such as MIBK and methyl amyl ketone are produced from the combination of aldehyde and ketone reactants fed along with hydrogen to one or more fixed bed reactors containing hydrogenation catalyst while a homogeneous catalyst for aldol condensation is also fed to the reactor.[148] The inventors claim that conventional mixed ketone processes are impractical and that since enolate formation is the controlling step that homogenous catalyst will achieve higher yields. In addition, it is suggested that higher selectivities and suppression of undesirable consecutive condensation reactions may be achieved.[148]

In 1996, Shell Oil, the world's largest producer of MIBK, patented a process for the co production of MIBK and methyl n-amyl ketone (MNAK) which is based on the modification of existing three stage MIBK production process.[144] MNAK is an environmentally friendly alternative to MIBK and MNAK demand is expected to increase. The inventors point out that processes involving the coproduction of high value ketones from existing process equipment, is of interest to manufacturers since it would increase their flexibility and responsiveness to market demand in a cyclical industry and also maximizes the utility of existing infrastructure. Thus, this invention is in direct

response to a growing industry need. The inventors also point out that the MIBK/MNAK separation is more facile than some of the more complex refining required of one step MIBK production processes.[144]

*2.4.2 MIBK Production via Catalytic Distillation*

To the best of this author's knowledge, no scientific studies regarding MIBK synthesis via catalytic distillation have been published aside from those stemming from this research project.[63-65] However, at the time this manuscript was being prepared, Thotla et al.[124,149] published the results of an experimental study and theoretical modelling of the co-production of MO and diacetone alcohol via reactive distillation. In addition, CD technology has been applied commercially for MIBK synthesis and has appeared in the patent literature.

Catalytic distillation technology has been utilized in the three-stage Hibernia Schloven process for the commercial production of MIBK.[1,13] The CD reactor is used to carry out the selective hydrogenation of a feed stream of 98 to 99% MO to MIBK at atmospheric pressure and 110°C over a $Pd/Al_2O_3$ catalyst. Typically greater than 96% yield is obtained. The original patent by Schmitt[13] described a CD column 8 meters in height and 10 cm in diameter with two reaction zones located 1 m and 2.5 m above the reboiler sump with both reaction zones containing catalyst consisting of 0.2 wt% Pd dispersed on 6 mm alumina rings. The upper zone contained 3 litres of catalyst while the lower zone contained 5 litres of catalyst. Hydrogen was fed to the bottom of the column at 4000 L/hr. MO was fed to a location between the reaction zones at 2 kg/hr. The reaction zone temperature was 91°C. The column was operated at 75% reflux with 99.6 wt% MIBK in the overhead distillate. No reboiler product (bottoms) stream was drawn from the reactor. Assuming steady state operation, this data suggests an MIBK productivity of around 0.18 [$g_{MIBK}$/hr*mL] and a hydrogen uptake efficiency of 13%.

More recently, a one-step process for the production of MIBK utilizing a CD column operating in batch mode utilizing a commercial catalyst consisting of Pd on strongly acidic cation exchange resin was reported.[32] This process is discussed in sections 1.4 and 1.5.1. The column was operated in batch mode with 1 litre of acetone charged to the reboiler initially and hydrogen fed to the column at 7 to 55 L/ hr. The reactor was operated with 100% reflux and the product was recovered in the reboiler after pre-determined batch times. However, the selectivity was poor, 33 to 68 wt% MIBK in the product, and gave a MIBK productivity (based on the time of the batch) of around 0.08 to 0.12 [$g_{MIBK}$/hr*mL] . The hydrogen uptake efficiency ranged from 4.5 to 34.8%.

Other multi stage process patents for MIBK synthesis involving CD have recently appeared.[60,61] These patents describe the same 3 embodiments of a "two stage" approach whereby a CD reactor is used to synthesize MO at around 120°C (0.2 to 0.7 MPa) using a cation exchange resin catalyst, followed by refinement of the MO stream prior to being fed to a second reactor where MO is converted to MIBK, followed by additional product refinement. The second reactor may be a CD reactor or a conventional FBR. The preferred embodiment (the third embodiment) suggests a conventional FBR should be used with a 0.5 wt% Pd/$Al_2O_3$ catalyst operating at 1.5 MPa and 150°C.[60,61] It is also suggested that additional polishing reactors may be needed. The inventors claim this process improves catalyst lifetime, increased yield and has fewer process units (a CD column, hydrogenation reactor and 3 distillation columns and 3 phase separators) than the state-of-the-art and represents a better return on investment.[60,61] However, it appears the CD processes disclosed in the preferred embodiment of these patents are more simplified than the Hibernia-Schloven 3 stage process but in fact have the same number of process units as the Veba Chemie and Deutsche Texaco processes. The other embodiments are even more convoluted.

Although no empirical data is presented in these most recent CD patents, expected conditions are outlined. Also, the patents provide some insight into the particular challenges of MIBK production. Specifically, MIBK losses are often due to the separation of MIBC from MIBK, which is extremely difficult. In addition, the build up of IPA in recycle streams is problematic. IPA can not be easily separated and is typically incinerated. Evidently, the largest problem is that MO can not be produced selectively resulting in numerous undesirable byproducts such as DAA, phorone, isophorone, mesitylene and other higher molecular weight species as well as water that must be removed from the product. The inability to produce MIBK selectively is also a major challenge for one-stage processes for MIBK production.[1]

## 2.5 Conclusions

Although $Pd/Nb_2O_5$ and $Pd/Nb_2O_5/SiO_2$ have been demonstrated to be promising catalysts for MIBK synthesis, little is known about the relationships between their structural properties and catalytic performance. To the best of this author's knowledge, scientific investigation of the application of dispersed niobia compounds on metal oxide supports towards MIBK synthesis is constrained to a single study by Chen et al.[42] The most important catalyst parameters that govern the molecular structure of the surface-phase niobium oxide species, including the nature of the oxide support, niobia loading and calcination temperature, remain largely unexplored for this organic synthesis. Further scientific investigation is needed, particularly for niobia loading below monolayer coverage, which gives rise to the unique structural and catalytic properties of highly dispersed niobia. Moreover, an investigation of the catalyst performance for this organic synthesis, prepared from low to moderate calcination temperatures, which creates Bronsted acidity is also lacking in the literature. The relative importance of Bronsted and Lewis acidity for MIBK synthesis using niobium compounds as catalyst is currently not known since all of the niobia catalysts for MIBK synthesis reported in the literature were

calcined at 400°C or greater and likely did not exhibit significant Bronsted acidity.

Although the kinetics of the acid catalyzed aldol condensation of acetone and MIBK synthesis have been extensively studied and are relatively well understood, to the best of this author's knowledge, a kinetic model for MIBK synthesis over a niobia catalyst has not been reported previously. Similarly, no scientific studies on the synthesis of MIBK via catalytic distillation, except those studies stemming from this research project[63-65] have been published. The state-of-the-art one step processes for MIBK synthesis currently produce MIBK in low yield with MIBK mass fractions less than 30 wt% in the product, necessitating further costly downstream refining. Consequently, there remains great incentive for the development of novel catalysts and catalytic reactor technologies for MIBK synthesis.

# Chapter Three

## Experimental Methods and Apparatus

### 3.0 Synopsis

In this chapter, the development and validation of analytical methods routinely employed in this work are outlined including the quantitative chemical analysis of liquid samples by gas chromatography (GC) and the quantification of the niobia loading (wt%) of catalysts by Energy Dispersive X-Ray Fluorescence (EDXRF) Spectroscopy. The bench scale reactor autoclave apparatus and the validation of the liquid sampling technique from the reactor are outlined. The catalyst preparation method and apparatus are explained. The fixed bed flow reactor as well as the pilot scale CD reactor methods and apparatus are described separately in Chapters Six through Eight. Detailed catalyst characterization utilized for the elucidation of the nature of the active sites, including Raman and FTIR Spectroscopy as well as Temperature Program Desorption (TPD) analysis are discussed separately in Chapter Five. The thermogravimetric analysis (TGA), BET surface area and other non-routine analyses of catalysts and supports are discussed with their respective results reported in subsequent chapters.

### 3.1 **Moisture Analysis of Oxygenated Solvents via Gas Chromatography**

#### *3.1.1 GC/TCD Method for the Analysis of Water Concentration*

Water is co-produced with MO in an equimolar amount and consequently, at least one mole of water is produced per mole of MIBK synthesized from acetone. In addition, water is usually present in the acetone feedstock and is also produced from many other possible condensation reactions including the consecutive reactions which produce phorone, mesitylene, DIBK, DMHA, propene and DIPE to name a few. It is well known that the presence of water can have a significant effect on the reaction kinetics since water is known to

inhibit MO formation and may lead to catalyst deactivation. Although many researchers investigating MIBK synthesis proceed under the assumption that the water concentration in the bulk may be accurately inferred from the material balance, a direct measurement is preferred over this inferential method. The inferential approach does not account for the amount of water inherent in the solvent and reactor system. Moreover, water produced by the competing condensation reactions may collectively lead to a significant contribution to the total water content. To complete the mass balance, the reactants involved in these condensation reactions must all be identified and accurately measured. Uncertainty in their quantification will introduce uncertainty in the estimate of the water concentration.

The author and co-workers[150] have developed and rigorously validated a gas chromatographic (GC) method to directly quantify the moisture content of oxygenated solvents. The GC method utilizes the external standard technique and is based on the method disclosed previously by Podrebarac[55] with some modifications. An Agilent Technologies 6890N gas chromatograph equipped with a HAYSEP-P packed column (8ft x 1/8" O.D.) connected to an EPC purge-packed inlet on one end and a thermal conductivity detector (TCD) on the other end was used. The GC was also equipped with an Agilent 7863 Series autosampler. It was determined that a 10 μL Agilent syringe (P/N 5181-3361) with a non-standard Teflon tip plunger gave excellent performance and is recommended for the GC/TCD and GC/FID methods described herein. The Agilent Technologies "Chemstation" software (Rev. A.09.03 [1417]) was used to control the operation of the GC as well as for data acquisition and analysis of the chromatograms for both the GC/TCD and GC/FID methods. The oven profile and GC parameters for the GC/TCD method are outlined in Table A1-1 (Appendix A) and a typical chromatogram is illustrated in Figure 3-1.

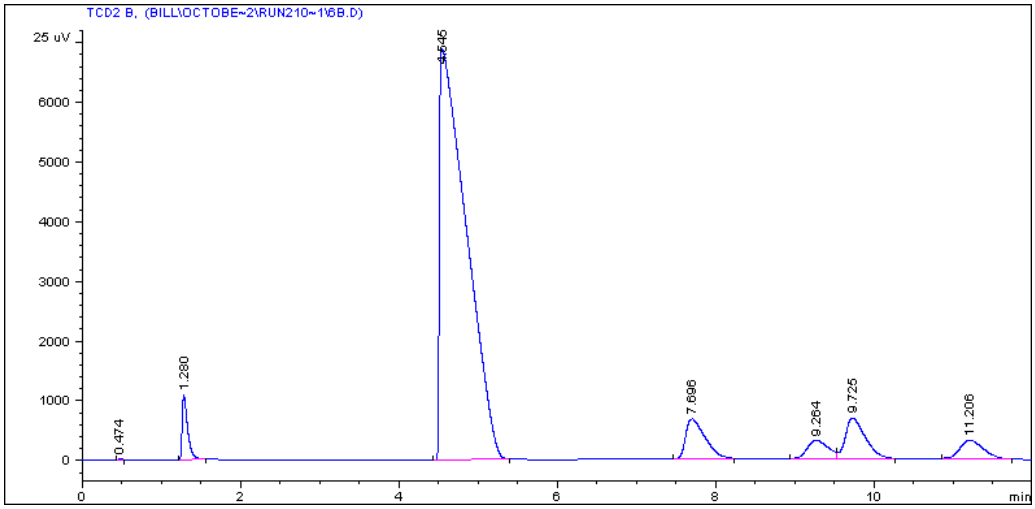


**Figure 3-1** A typical chromatogram for water analysis via GC/TCD *[Experiment 210 sample 6b; 04.10.2006] [Air: 0.474 min, $H_2O$: 1.280 min, Acetone: 4.545 min; MIBK 7.696; IMO: 9.264 min; MO: 9.725; DIBK: 11.206 min]:*

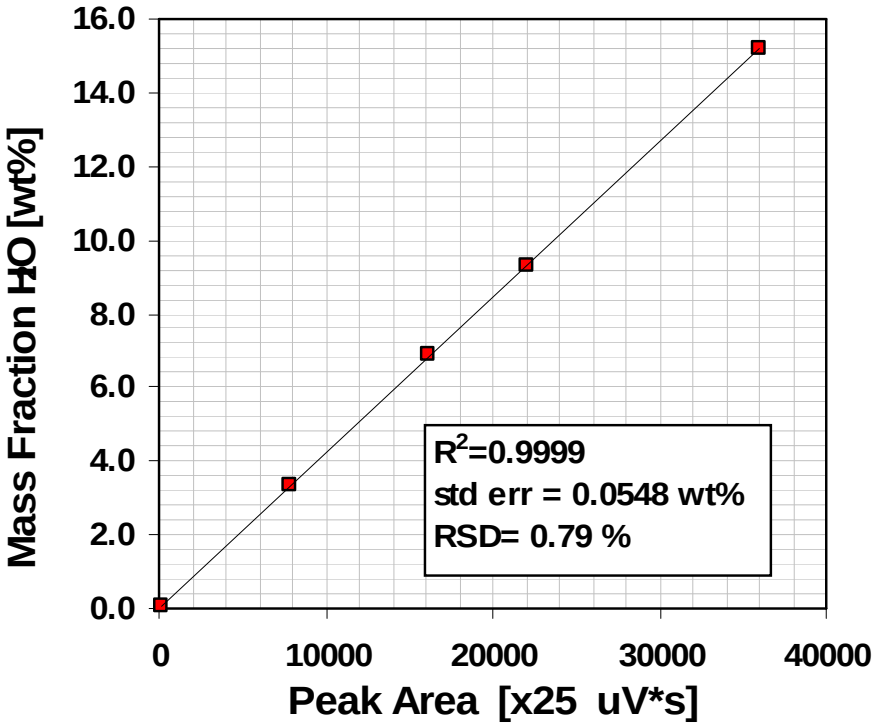


**Figure 3-2** A typical calibration curve for water analysis via GC/TCD *[Experiment 205; 21.09. 2006]*

The chromatogram in Figure 3-1 demonstrates excellent specificity with water eluting early in the analysis corresponding to the sharp peak observed around 1.28 minutes, followed by the organic species which elute in broad convoluted peaks several minutes later. The first minor peak, which elutes at around 0.47 min corresponds to air. Since the organic peaks are broad, convoluted and lack symmetry, this technique is not recommended to quantify the organic species. However, the mass fraction of water may be calculated from the water peak area with excellent accuracy using a correlation (Figure 3-2) obtained from the analysis of external GC standards of known moisture content in HPLC grade acetone, even though the water peak does not exhibit excellent symmetry.

The calibration standards were prepared by combining pre-determined amounts of acetone and water and accurately quantifying their amounts using a balance. 4 litres of HPLC grade acetone (Aldrich 179124-4L, Batch 00351LB, 99.98%) was dried using 32.6 g of 5A molecular sieves (Aldrich 208620-1KG) activated at 350°C in air for about 3 hours then cooled to ambient temperature under vacuum and transferred directly to the acetone solvent bottle and retained there during storage and use. 250 mL amber glass bottles were pre-dried in an oven at about 80°C overnight then sealed with screw caps and allowed to cool to ambient temperature before use. The dried acetone was refrigerated in an explosion proof freezer at temperature less than -20°C. Predetermined amounts of acetone ranging from 140 to 165 g were added to the five empty glass bottles. The mass of the bottle empty and with acetone were measured precisely to ± 0.005 g. Pre-determined amounts of purified water (Millipore) was subsequently added drop wise using Pasteur pipettes to the amber bottles containing the acetone and the masses before and after addition of water were recorded. The pipettes were dried in an oven at 80°C prior to their use. The mass fraction of water in the calibration standards were calculated from the recorded masses of the bottles empty, after the addition of acetone and after the

addition of water. The glass bottles were sealed and stored in an explosion proof freezer at temperatures less than -20°C until needed.

The GC was typically calibrated on a daily basis for experiments requiring water analysis and the samples were analyzed in duplicate with the average value being reported. A drawback of the external standard technique is that the result is strongly influenced by the injection volume. Although the use of an automated GC autosampler minimizes this due to its high degree of precision and repeatability, occasionally outliers are obtained due to gas bubbles in the syringe and other anomalies. Duplicate analysis not only allows an improved estimate of the water concentration but also provides opportunity to identify and reject outliers. Sample data for the moisture analysis for samples obtained in an autoclave experiment are illustrated in Figure 3-3. The duplicate analysis is included in the figure but is difficult to discern due to the high repeatability of the measurements. The standard error of estimate predicted by the regression model fit to the data of Figure 3-3 implies a high degree of accuracy.

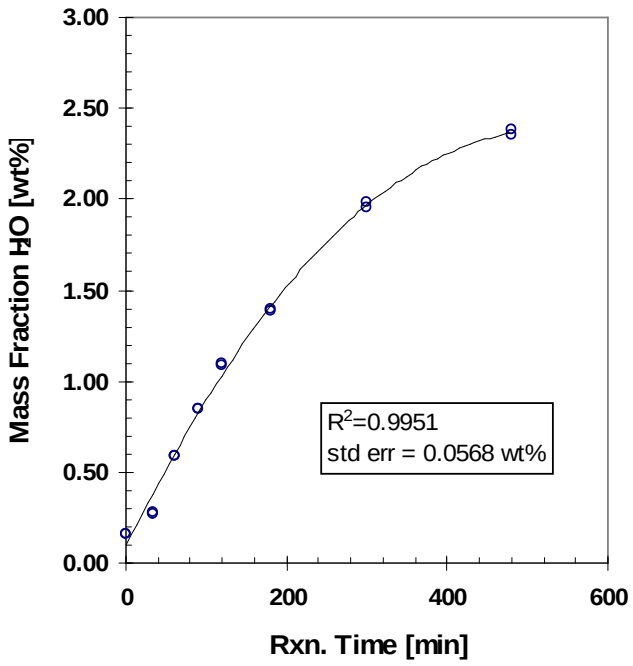


**Figure 3-3** Sample data illustrating a typical water analysis for an autoclave experiment *[Experiment 208; 28.09.2006]*

### *3.1.2 GC/TCD Method Validation*

Since this method of water analysis is not commonly used and has not been validated previously, the author has rigorously validated this technique following accepted scientific protocols and guidelines published by the US Food and Drug Administration (US FDA) for the validation of analytical methods used primarily in pharmaceutical research.[151-155] The characteristics of an analytical method or procedure which must be tested to demonstrate the validity of the technique include:

1. Accuracy
2. Precision (repeatability and intermediate precision)
3. Specificity
4. Linearity
5. Range
6. Robustness
7. Detection Limit
8. Quantitation Limit

Specificity and Linearity

Some of these characteristics have already been demonstrated in the previous figures. *Specificity* refers to resolution of the chromatogram. In particular, the peak corresponding to the analyte of interest must be "baseline resolved", meaning the peak of interest must be completely separated from other peaks and the signal return completely to the baseline before and after the peak. In contrast, convolution due to interference from other peaks would lead to a "valley" in the chromatogram. Specificity is clearly demonstrated in the chromatogram of Figure 3-1 where the water peak at 1.28 min clearly returns to the baseline and several minutes pass before the organic analytes are eluted from the column. Moreover, the Agilent "Chemstation" GC software confirms specificity by reporting the water peak classification as "BB" in the

Chemstation GC report, meaning "baseline to baseline". Excellent *linearity* ($R^2$=0.9999) is clearly demonstrated in the calibration curve of Figure 3-2 over a broad range of water concentrations from 0.04 to 15.2 wt%. This exceeds the US FDA requirement which stipulates that the coefficient of correlation should be greater than or equal to 0.999 over a minimum of 5 observations.[151-153]

Detection Limit

The Detection Limit (DL) is defined as the lowest concentration of an analyte that can be identified with 99% confidence by an analytic technique without necessarily quantifying the amount of analyte present.[151] In this study, the peak area rejection limit of the GC was set to 100 [x 25 μV*s] which corresponds to a water concentration of 0.021 wt%. Consequently all samples with water peak areas below the peak area rejection limit were ignored in the chromatographic analysis. However, the DL can be estimated from the statistical analysis of the background noise and the calibration curve (Figure 3-2) using equation (3-1).[152,153]

$$DL = \frac{3.3\sigma}{S} \qquad (3\text{-}1)$$

S in equation 3-1 denotes the slope of the calibration curve with mass fraction on the abscissa and peak area on the ordinate. σ in equation (3-1) represents the "standard deviation of the analytical background response". An estimate of σ is obtained by taking the standard deviation of multiple measurements of the magnitude of the instrument background noise.[152,153] The magnitude of the background noise was measured for the retention time interval from 0.7 to 1.2 min, (i.e. between the elution of the air and water peaks), for the five calibration standards used in Figure 3-2, using the Agilent Technologies Chemstation "Noise Determination" feature and was found to be 0.0094449 [x 25 μV*s]. The magnitude of the background noise represents six times the standard error associated with a regression line through the GC data

over the specified interval. The detailed results of the assessment of the background noise in the chromatograms are available in Table A2-1, (Appendix A).

If the data in Figure 3-2 were plotted with the mass fraction (wt%) on the abscissa and peak area on the ordinate, a slope of S=2368.89 [x 25 μV*s/wt%] is obtained. Substituting this value for S, along with the estimate of the standard deviation of the background noise, σ=0.0094449 [x 25 μV*s], as an estimate of the standard deviation of the analytical background response into equation (3-1) gives a detection limit of 13 ppm.

$$DL = \frac{3.3\sigma}{S} = \frac{3.3 * 0.009445}{2368.89} = 0.000013157x10^{-5}\ (wt\%) = \underline{13\ ppm} \leftarrow \text{Detection limit} \qquad (3\text{-}2)$$

Quantitation Limit

The Quantitation Limit (QL) is defined as the lowest concentration of an analyte in a sample that can be can be estimated with acceptable accuracy and precision under the specified experimental conditions.[151] The quantitation limit meeting US FDA standards can be calculated from the slope (S) of the calibration curve and the standard deviation of responses (σ) as outlined in equation (3-3).[152,153] The standard deviation of responses is simply the standard deviation of the y-intercepts obtained from a series of calibration curves.[152,153] From the results of the linear regression for the calibration curve of Figure 3-2, and using σ=0.034152 wt% calculated from the y intercepts of 10 arbitrarily selected calibration curves between 10 September, 2006 through 5 October, 2006 (Table A2-2, Appendix A), the Quantitation Limit is 0.346 wt%.

$$QL = \frac{10\sigma}{S} = \frac{10 * 0.034152(wt\%)}{0.000422\left(wt\%/\mu V * s\right)} = 809.07\ \mu V * s \quad = \quad \underline{0.346\ wt\%} \leftarrow \text{Quantitation Limit} \qquad (3\text{-}3)$$

Accuracy

The US FDA protocols suggest three acceptable means of confirming the accuracy of an analytical technique. First, by the application of the analytical procedure to an analyte of known purity.[149-152] Second, by the direct comparison of the results of the analytical method to a second method of known accuracy.[151,152] Third, accuracy may be inferred once linearity, range and specificity have been established.[151,152] Accuracy should be determined over a minimum of three levels and 9 observations.[149-151] In this case, the GC/TCD technique for water analysis was validated against a Coulometric Karl Fischer Titration (KFT) method using 26 observations over 9 levels. (A 27$^{th}$ observation was rejected as an outlier of the KFT analysis). The KFT method is known to be highly accurate, it does not require calibration and is considered to give the accepted true value of water concentration.

9 stock solutions of water in HPLC grade acetone solvent were prepared in the same manner as the calibration standards by adding predetermined amounts of purified water (Millipore) to HPLC grade acetone that had been dried previously with 5A molecular sieves that had been activated at 350°C for 3 hours. However, smaller vials (ca. 20 mL) were used instead of bottles. All glassware including pipettes and GC vials had been pre-dried in an oven overnight at about 80°C. 3 samples were extracted from each of the stock solutions and transferred to pre-dried GC vials. The moisture content of the 27 control samples were ascertained by the KFT method using a Mitsubishi CA-06 Moisture Meter with 50 μL and 100 μL injections depending on the nominal water concentration. The control samples were then analyzed using the GC/TCD method for comparison. An obvious outlier in a single KFT measurement was observed and was rejected from the analysis. The analysis of the remaining 26 control samples are illustrated in Figure 3-4. The figure shows excellent agreement between these two techniques. The average relative error for samples above the quantitation limit was only 3.49% . There was some disagreement between these techniques as the water concentration became

very low. GC/TCD analysis of the control sample No. 1 prepared at the lowest concentration (ca. 0.26 wt%) had an average relative error of 10.96%. However, excellent agreement is observed over the range of 3 to 15 wt% with a relative error of the 2.12% of the GC/TCD method with respect to the KFT method.

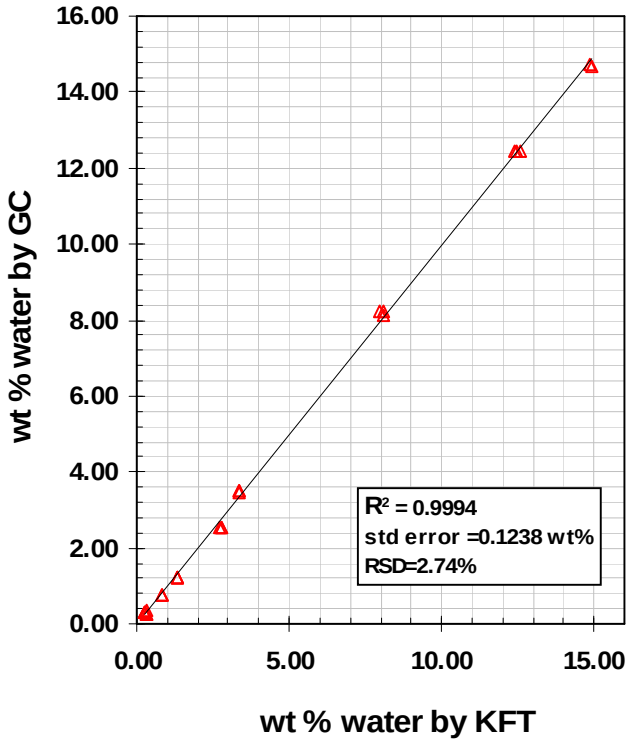


**Figure 3-4** Validation of the GC/TCD method of water analysis against the Karl Fischer Titration (KFT) Method (26 control samples)

Precision (Repeatability)

The precision of the instrument analysis was determined by repeated sample injections at concentrations spanning three locations over the established range of the moisture analysis including the highest and lowest concentrations of the calibration standards and a stock solution of intermediate concentration. The results illustrated in Table 3-1 show that the analysis is highly repeatable and exhibits excellent precision. The relative standard deviation (RSD) is typically less than 1%. In the worst case scenario, the calibration standard of the lowest water concentration on the calibration curve (ca. 0.04 wt% $H_2O$) shows good

precision with an RSD of 1.1% and a 95% confidence bounds, expressed as a relative error, of ± 0.69% .

**Table 3-1** Repeatability: Precision of the GC/TCD method of water analysis

| | Peak Area [x25 uV*s] | | |
|---|---|---|---|
| Inj No. | Control 3 | Std. 1 | Std. 5 |
| 1 | 18497 | 219 | 37306 |
| 2 | 18582 | 218 | 37450 |
| 3 | 18524 | 224 | 37418 |
| 4 | 18506 | 222 | 37591 |
| 5 | 18402 | 224 | 37524 |
| 6 | 18295 | 223 | 37313 |
| 7 | 18232 | 219 | 37017 |
| 8 | 18318 | 217 | 37184 |
| 9 | 18181 | 220 | 37848 |
| 10 | 18202 | 221 | 37371 |
| **average** | 18374 | 221 | 37402 |
| **stdev** | 147.35 | 2.45 | 227.71 |
| **RSD (%)** | 0.80 | 1.11 | 0.61 |
| **95% Confidence Bounds on average** | | | |
| **+/-** | 91.3 | 1.5 | 141.1 |
| **+/- (%)** | 0.50 | 0.69 | 0.38 |

Intermediate Precision (Reproducibility)

The reproducibility of the GC/TCD analysis on a separate instrument (i.e. *intermediate precision*) was demonstrated by analyzing the moisture content of 15 control samples via GC/TCD using a separate GC located in the UW Department of Chemical Engineering Analytical Laboratory using the same Hayesep P column. Intermediate precision is demonstrated in Figure 3-5, which illustrates excellent agreement between the measurements obtained on the two separate GCs. The standard error was 0.083 wt% and the average relative error of the department GC relative to the principal GC used in this research, denoted "GC-1" in Figure 3-5, was 0.85 % for samples with water concentrations above the quantitation limit. However as expected, there was some disagreement for the three samples obtained from the stock solution having a water concentration below the quantitation limit (ca. 0.3 wt%) as evidenced by a relative error of

15.1% . It can be concluded that the GC/TCD technique is highly reproducible for samples having a water concentrations above the quantitation limit.

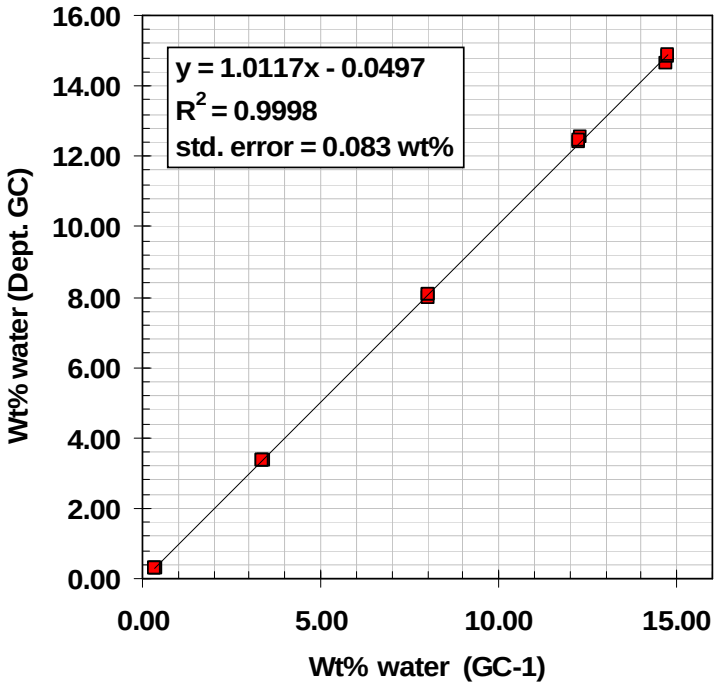


**Figure 3-5** Reliability and Reproducibility: (Intermediate Precision) *Comparison of the results obtained from the GC/TCD moisture analysis of 15 sample analyses obtained from two separate gas chromatographs*

Robustness

Robustness refers to an analytical method's ability to provide accurate results when finite errors are deliberately introduced to GC parameters of the analytical method.[151-153] Demonstration of robustness is not usually required by regulatory agencies but is recommended at the method development phase.[151-153] A pre-cautionary disclaimer should accompany the standard operating procedure if the method is found to be susceptible to uncertainty introduced by a specific GC parameter.[152,153] Here, the effect of carrier gas flow rate and GC oven temperature profile were assessed. In addition, samples were re-analyzed after 3 days in order to study the effect of sample retention prior to analysis on the resulting moisture content.

Table 3-2 shows that reducing the initial temperature of the oven profile by 5°C did not have a significant effect on the result of the analysis. However, reducing the carrier gas flow rate by 10% did have a significant effect. This tests the solution stability and is also an assessment of the robustness of the analytical technique. The results of this experiment (Table 3-3) for water concentrations above the quantitation limit, confirm that the delay in analysis does not significantly affect the result as evidenced by an RSD of 1.1%, which is within the level of accuracy of the instrument over this range of water concentration.

**Table 3-2** Test for Robustness of GC/TCD method of water analysis.

| DESCRIPTION | PEAK AREA [X25 UV*S] | WATER [WT%] | AVERAGE [WT%] | CHANGE [%] |
|---|---|---|---|---|
| Benchmark, control sample 3 with no changes to GC/TCD method | 17844 | 8.038 | | |
| | 17903 | 5.064 | 8.053 | |
| | 17890 | 8.058 | | |
| Initial isothermal plateau lowered from 140°C to 135°C | 17834 | 8.033 | | |
| | 17924 | 8.073 | 8.056 | + 0.034 |
| | 17898 | 8.062 | | |
| Carrier gas flow rate reduced by 10% from 20 to 18 [mL/min] | 19467 | 8.759 | | |
| | 19557 | 8.798 | 8.804 | + 9.31 |
| | 19678 | 8.853 | | |

*Control sample 3 was analyzed in triplicate for each condition*

**Table 3-3** Reproducibility of the GC/TCD water analysis after 3 days for control samples with water concentrations above the Quantitation Limit

| 14-Jan-05 | 17-Jan-05 | change (%) |
|---|---|---|
| 3.36 | 3.46 | 3.02 |
| 7.98 | 8.22 | 3.05 |
| 12.39 | 12.55 | 1.28 |
| 14.63 | 14.94 | 2.11 |
| 3.36 | 3.42 | 1.76 |
| 8.07 | 8.15 | 1.07 |
| 12.56 | 12.51 | -0.36 |
| 14.83 | 14.93 | 0.65 |
| 14.90 | 14.84 | -0.39 |
| 12.43 | 12.53 | 0.79 |
| 8.07 | 8.10 | 0.30 |
| 3.37 | 3.42 | 1.37 |
| | **avg** | **1.22** |

| | |
|---|---|
| std err | 0.110707 |
| avg | 9.71 |
| RSD | 1.14 |

Range

The range of the analytical method is bounded on the low end of concentration by the Quantitation Limit, which by definition is the lowest concentration that can be measured with acceptable accuracy, and bounded on the high end of concentration by the concentration of the calibration standard having the highest water concentration, since extrapolation is not recommended. Thus, the range of the GC/TCD method demonstrated in this study is from 0.346 to 15.2 wt%. Linearity, accuracy, precision and reproducibility have been demonstrated over this range.

Conclusions of the GC/TCD Method Validation

The accuracy, reproducibility, precision and linearity of the GC/TCD method have been demonstrated. It can be concluded that this technique is highly accurate, precise, and reproducible for water concentrations ranging from about 0.35 to about 15.2 wt%. For water concentrations above the Quantitation Limit, this technique is accurate to within 3.49 % and repeatable to within a relative error of ± 0.69 %. From 3 to 15 wt% water, the method is accurate to within 2.12%. However, if a project requires routine analysis of water with concentrations less than 0.35 wt%, then the KFT method is recommended.

### 3.2 Quantification of Organic Species via Gas Chromatography (GC/FID)

An Agilent Technologies 6890N Gas Chromatograph equipped with a J&W Scientific DB-WAX megabore capillary column (30m x 0.53 mm I.D. x 1.0 μm film thickness) connected to a split-splitless inlet on one end and a flame ionization detector (FID) on the other was used to measure the concentrations of organic species present in liquid product samples. The samples were provided in autosampler GC vials with septum caps and processed automatically by an Agilent Technologies 7863 Series autoinjector with a 10 μL Agilent syringe. Samples were analyzed in duplicate with the average value being reported. The GC was typically calibrated on a daily basis.

The GC method outlined in NIOSH 1300-1301, the international scientific protocol for the quantification of ketones via GC/FID, with some slight modifications. Specifically, the final temperature used in the oven thermal profile was 160°C instead of 170°C. It was found that the species of interest elute from the column at temperatures below 160°C. Consequently, 160°C was selected as the final temperature of the oven profile in order to mitigate thermo-oxidative degradation of the stationary phase of the DB WAX column. The other deviation from the protocol was that $CS_2$ was not used to dilute the samples as indicated in the test method. In this work, it is of interest to quantify the minor products in the reaction mixture such as phorones and mesitylene. The dilution of the samples is undesirable since it may lower the concentrations of some species of interest below the peak area rejection limit of the GC method (100 pA*s). Similarly, external GC standards were used rather than an internal standard in order to prevent the dilution of the samples.

Calibration curves were prepared from the GC/FID analysis of the external standards, which allowed calculation of the analyte mass fraction (wt%) in the sample from its peak area. The external standards were prepared from high purity stock solutions of the analytes for which their assays were accurately and precisely reported on certificates of analyses provided by the supplier. The GC method parameters are outlined in Table A1-2 (Appendix A). A typical chromatogram of a calibration standard is illustrated in Figure 3-6 and the analysis of the chromatogram and identification of peaks are outlined in Table 3-4. Acetone was always the solvent in the experiments reported in this work. Consequently the acetone peaks observed in the chromatograms were not ideal. Rather than quantify the acetone from its peak area, the acetone concentration was calculated from the mass balance by quantifying all of the organic species present other than acetone and subsequently calculating the number of moles of acetone converted from the known stoichiometric relationships.

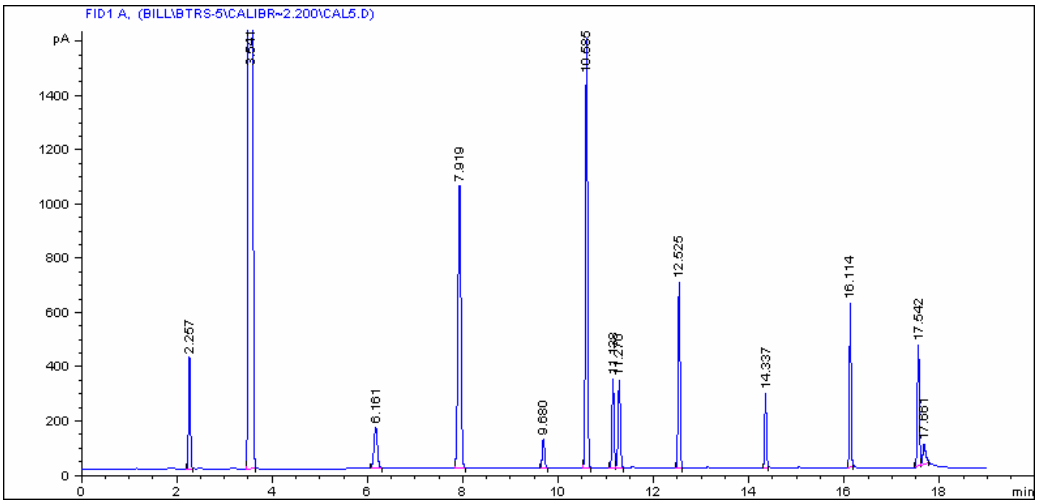


**Figure 3-6** A typical chromatogram of a GC/FID calibration standard [Calibration Standard #5, 09.02.2007]

**Table 3-4** Analysis of chromatographic performance of the chromatogram of Figure 3.6

| RETENTION TIME [MIN] | SPECIES | SYMM FACTOR | CAPACITY RATIO (K') | THEORETICAL PLATES (N) | RESOLUTION | TYPE | SELECTIVITY |
|---|---|---|---|---|---|---|---|
| 2.257 | DIPE | 0.95 | 0.60 | 16583 | n/a | BB | - |
| 3.341 | Acetone | 1.03 | 1.51 | 20704 | 15.21 | BB S | 2.51 |
| 6.161 | IPA | 0.96 | 3.37 | 35015 | 22.74 | BB | 2.23 |
| 7.919 | MIBK | 1.04 | 4.62 | 74409 | 14.16 | BB | 1.37 |
| 9.680 | IMO | 0.97 | 5.87 | 191377 | 17.18 | BB | 1.27 |
| 10.585 | MO | 1.05 | 6.51 | 275114 | 10.68 | BB | 1.11 |
| 11.138 | MIBC | 0.91 | 6.90 | 333205 | 6.99 | BV | 1.06 |
| 11.270 | DIBK | 0.99 | 7.00 | 272309 | 1.61 | VB | 1.01 |
| 12.525 | TMB | 0.99 | 7.89 | 445540 | 15.52 | BB | 1.13 |
| 14.337 | DAA | 0.90 | 9.17 | 669255 | 24.93 | BB | 1.16 |
| 16.114 | PHO | 0.95 | 10.43 | 1000568 | 26.37 | BB | 1.14 |
| 17.542 | IPO | 0.96 | 11.45 | 782796 | 19.84 | BV | 1.10 |
| 17.661 | HG | 0.60 | 11.53 | 388776 | 1.23 | VB | 1.01 |

*BB denotes baseline to baseline; BV denotes baseline to valley; VB denotes valley to baseline; BBS denotes baseline to baseline solvent peak.*

Peak Symmetry

The peak symmetry is calculated by the Agilent Chemstation software using moment equations based on the height of the peak and the height of the inflection points located on either side of the peak.[156] A peak symmetry of unity denotes a perfectly symmetrical peak. It is evident from the data in Table 3-4 and from visual inspection of the chromatogram of Figure 3-6 that the peaks exhibit excellent symmetry with the exception of the peak corresponding to hexelene glycol, which incidentally was not observed in this research study.

Specificity and Resolution

The chromatogram in Figure 3-6 also demonstrates excellent specificity for most of the analytes with the exception of the MIBC and DIBK peaks, which appear to be convoluted. However Figure 3-7, which shows more closely the overlap between these peaks, illustrates that the valley between these peaks almost reaches the baseline. The difference between the peak areas obtained by integrating to the halfway point in the valley between these convoluted peaks and the area that would be obtained from the fully deconvoluted peaks is very small. Consequently the uncertainty in the quantification of these peaks due to convolution is negligible considering the precision and accuracy of the instrument. Similarly, the isophorone peak is convoluted with the hexelene glycol peak.

Resolution in Table 3-4, refers to how well separated a peak is from the peak which preceded it. The Resolution is calculated from an ASTM formula that considers the retention times of the peaks as well as the widths of each peak measured at the baseline.[156] A Resolution greater than 2 is recommended.[151] Excellent resolution is observed for all peaks with the exceptions of the MIBC/DIBK and hexelene glycol/isophorone peaks whose resolution although not ideal do not lead to significant experimental error. Hexelene glycol was not observed in this work.

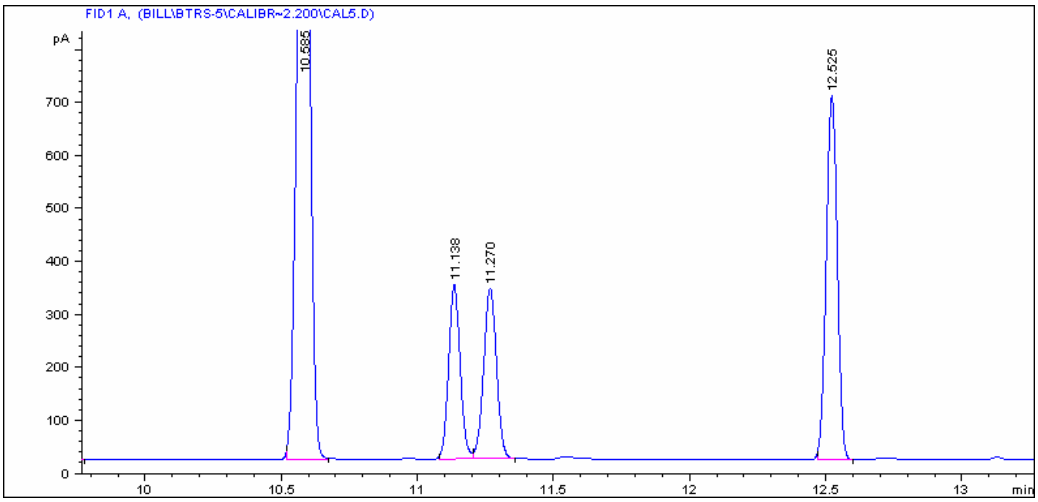


**Figure 3-7** Convoluted MIBC and DIBK GC peaks *[Calibration Standard #5, 09.02.2007]MIBC elutes at 11.138 min. DIBK elutes at 11.270 min*

Evaluation of System Suitability

The Agilent Chemstation software performs various system suitability tests to evaluate analytical performance. Some of these performance indicators for the Chromatogram of Figure 3-6 are included in Table 3-4 including the Capacity Ratio (k'), Selectivity and the number of theoretical plates (N). The Capacity Ratio is a measure of where the peak of interest is in relation to the elution time of non-retained compounds. The Chemstation software calculates k' following the ASTM definition and formula.[151,156] A capacity ratio of k'>2 is recommended.[151] All of the analytes quantified in this method except DIPE, which elutes the earliest, meet this specification. The theoretical plate number (N), (i.e. the number of theoretical plates per column) is a measure of the efficiency of the column separation calculated from the retention time and peak width of the analyte using the ASTM half width method equation outlined in the Chemstation manual.[156] The higher the value of N, the more efficient the column separation. N typically decreases with the life of the column and is tracked as a performance indicator. The theoretical plate number (N) should exceed 2000.[151] This specification is met for all analytes. The Selectivity in Table 3-4, also known as the relative retention, is a measure of the relative

location of a peak to the peak that preceded it and is calculated from the ratio of the capacity factor of the peak to the capacity factor of the preceding peak.[151] There is no specification for "selectivity" as long as the resolution is specified.[151]

Precision

In order to evaluate the precision of the GC/FID technique, two calibration standards representing the highest and lowest concentrations on the calibration curves were subjected to 10 repeated analyses each. The 95% confidence intervals for the estimates of the average peak area, expressed as a percentage, are outlined in Table 3.5. Additional results are available in Appendix A. The results demonstrate that the GC/FID technique has very good precision for the quantification of all species, typically from about ± 1 to 3%, with the exception of hexelene glycol, which may be quantified with marginally acceptable precision, considering that hexelene glycol is a minor product that was not observed in this work.

Since the external standard method is utilized in this technique, the results are strongly dependent on the injection volume. The instrument precision is governed by the repeatability of the injection volume and is dependent on the quality of the septum and the syringe. It is recommended that the septum be changed frequently (ca. every 50 injections or as needed if damage is evident) and that the syringe be routinely inspected for leaks, burrs or other damage. A 10 μL Agilent syringe (P/N 5181-3361) with a non-standard Teflon tip plunger gave excellent performance and is recommended for this technique. A 5 μL syringe would be preferred due to the smaller injection volume. However an Agilent 5 μL syringe, that also had a Teflon plunger, was not available for purchase.

**Table 3-5** Precision of the GC/FID technique for quantification of organic species

| species | 95 % CONFIDENCE INTERVAL CALIBRATION STD. 1 | 95 % CONFIDENCE INTERVAL CALIBRATION STD. 7 |
|---|---|---|
| DIPE | ± 2.45 % | ± 2.62 % |
| Acetone | ± 3.05 % | ± 2.82 % |
| 2- propanol (IPA) | N/A | ± 3.01 % |
| MIBK | ± 2.23 % | ± 2.70 % |
| IMO (IMO) | N/A | ± 2.73 % |
| MO (MO) | ± 1.94 % | ± 2.61 % |
| MIBC | N/A | ± 2.68 % |
| DIBK | ± 1.27 % | ± 2.08 % |
| Mesitylene (TMB) | ± 1.48 % | ± 2.15 % |
| Diacetone Alcohol (DAA) | N/A | ± 2.81 % |
| Phorone | ± 1.11 % | ± 1.68 % |
| Isophorone | N/A | ± 1.68 % |
| Hexelene Glycol | N/A | ± 6.06 % |

*(Some species below GC peak rejection limit for Std. 1 denoted " N/A")*

Accuracy , Linearity and Range

Rather than validate the accuracy of this technique against another analytical method, accuracy is inferred from the analysis of analytes of known composition and from the demonstration of linearity, specificity and range as deemed acceptable by the US FDA protocols.[152,153] Note that NIOSH 1300-1301 is the recommended international scientific standard for the quantification of ketones and alcohols and has been previously validated. The calibration curves illustrated in Figures 3-8 through 3-12 were prepared from the analysis calibration standards of known composition using high purity stock solutions whose precise assays (Table A3-1, Appendix A) were provided by certificate of analyses from the supplier. The standard error of estimate of the regression models for the following calibration curves and their relative standard deviations (RSD) are indicative of the accuracy. The following figures demonstrate that the GC/FID exhibits good accuracy and excellent linearity over a broad range of concentrations for the various species investigated.

Accuracy and repeatability have been demonstrated over the range defined by the calibration curves.

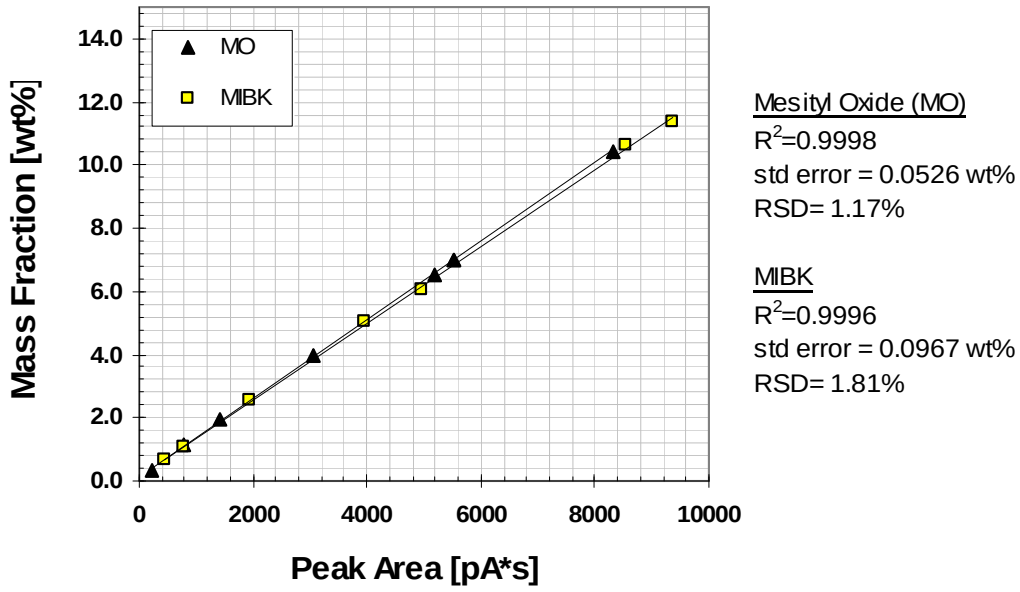


**Figure 3-8** GC/FID Calibration curves for MO and MIBK (09.02.2007) *The MO calibration curve was also used to calculate the IMO mass fraction since both isomers are assumed to have the same response to the GC/FID detector*

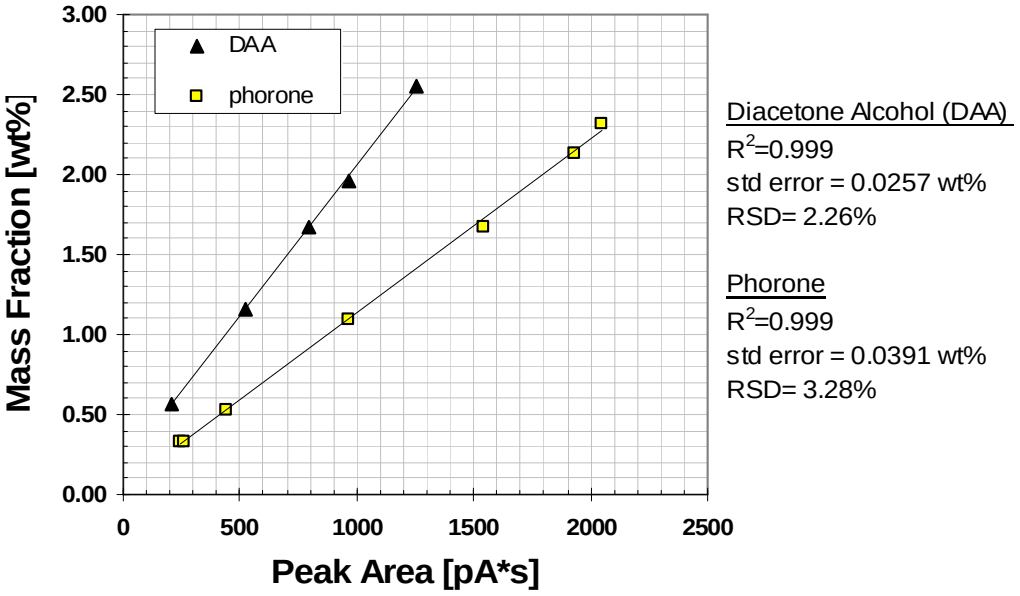


**Figure 3-9** GC/FID calibration curves for DAA and Phorone (22.02.2007)
*The technical grade MO stock solution contained DAA. The concentration of calibration standards were corrected to account for DAA introduced in the MO stock solution*

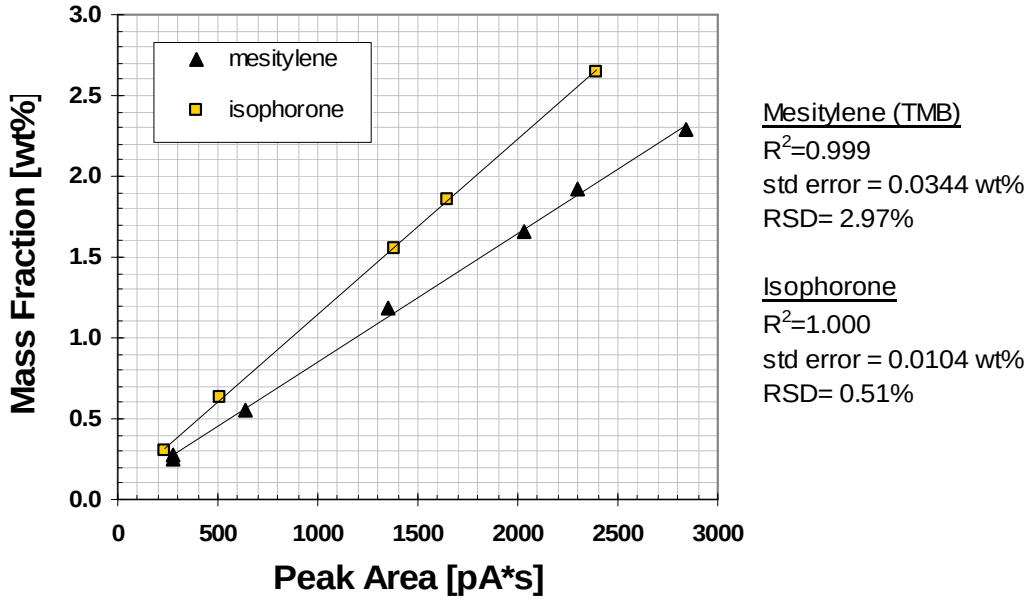


Mesitylene (TMB)
$R^2$=0.999
std error = 0.0344 wt%
RSD= 2.97%

Isophorone
$R^2$=1.000
std error = 0.0104 wt%
RSD= 0.51%

**Figure 3-10** GC/FID calibration curves for Mesitylene and Isophorone (09.02.2007)

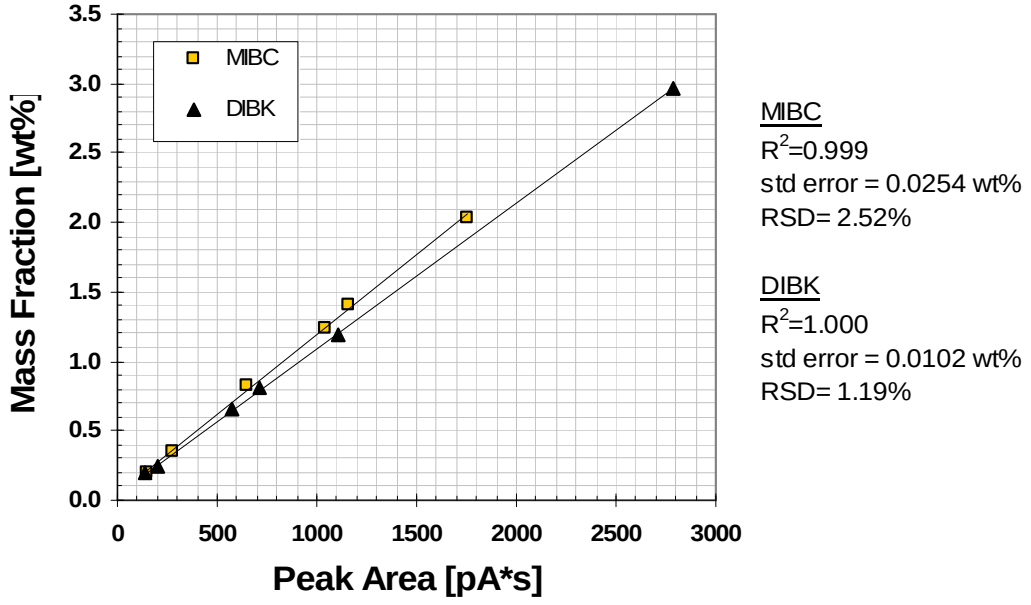


MIBC
$R^2$=0.999
std error = 0.0254 wt%
RSD= 2.52%

DIBK
$R^2$=1.000
std error = 0.0102 wt%
RSD= 1.19%

**Figure 3-11** GC/FID calibration curves for MIBC and DIBK (09.02.2007)

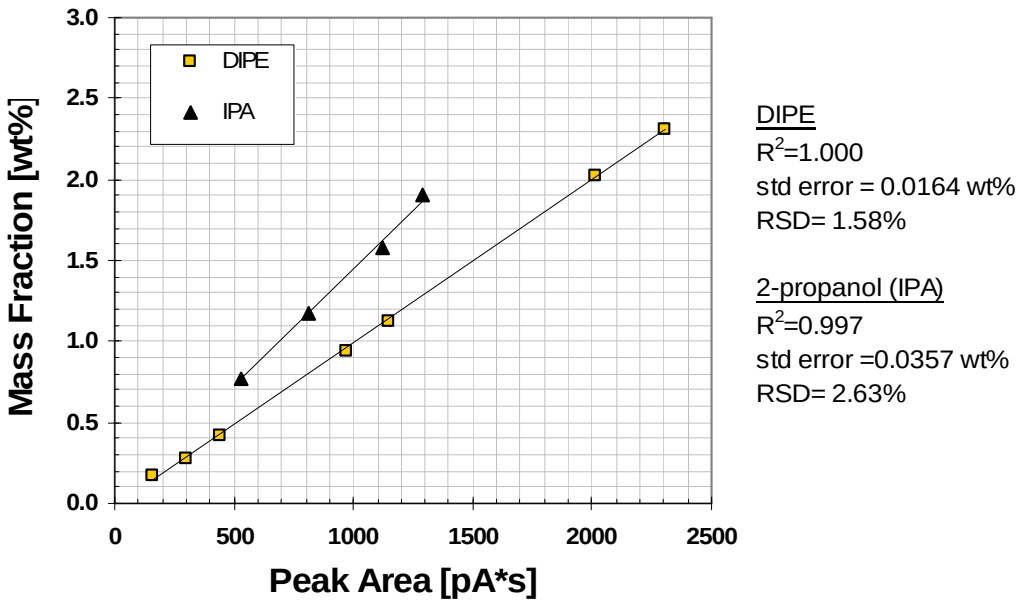


**Figure 3-12** GC/FID calibration curves for IPA and DIPE (09.02.2007)

### 3.3 Conversion of Mass Fraction (wt%) to Concentration [mol/L]

The mass fractions (wt%) of species quantified via the GC/TCD and GC/FID techniques were converted to concentration (mol/L) by assuming that the density of the solution is invariant and has the value of the density of acetone, $0.7899^{(20/4)}$, using equation (3-4) where $C_i$ is the concentration of species "i" (mol/L), $X_i$ is the mass fraction (wt%) of species "i", ρ is the solution density (g/mL) and $M_i$ is the molecular mass of species "i".

$$C_i = 10 * \frac{X_i \rho}{M_i} \qquad (3\text{-}4)$$

This approximation is reasonable since acetone is necessarily the solvent in the one-step MIBK synthesis and is typically in great excess. The density of MIBK, $0.7978^{(20)}$, is comparable to the density of acetone (ca. 1% difference). Therefore, the change in solution density due to the production of MIBK from acetone is negligible. MO, the other major product investigated in this work,

has a slightly higher density [$0.8653^{(20/4)}$ ] than acetone. However, MO is an reactive intermediate for the one step synthesis of MIBK that is often found trace amounts. The autoclave experiments investigating MO synthesis represent a greater test of this assumption. For MO synthesis in a closed system, the acetone conversion is low with a mass fraction of MO typically less than 13 wt% after 8 hours. Water is denser than acetone and does not mix ideally with the products of MIBK synthesis. However, the sample data in Figure 3-3 shows that the water mass fraction is typically less than 2.5 wt%. Consequently, the relative error introduced by the assumption of invariant density is usually less than 1%, which is within the limits of precision and accuracy of the analysis. Indeed, the assumption of constant mixture density is reasonable and has been routinely employed by researchers investigating MIBK synthesis including du Toit et al.[127]

## 3.4 Autoclave Experimental Methods and Apparatus

### *3.4.1 Autoclave Reactor Apparatus*

A 300 mL Parr Instruments Co. 4560 Series microreactor, illustrated schematically in Figure 3-13, was used for the catalyst screening, catalyst activity testing and the kinetic study reported in this work. The autoclave was constructed of 316 stainless steel with a Teflon o-ring seal on the bomb head. The reactor was rated to a maximum of 350°C and a maximum operating pressure of 20.7 MPa (3000 psig). The reactor was equipped with an axial flow impeller (4 pitched blades) powered by a 1/12 hp motor. The drive shaft was coupled to the impeller via a magnetic drive system. Over-pressure protection was provided by an Inconel rupture disk rated to fail at 2000 psi. PID temperature control was provided by a Parr 4842 controller which received analog inputs from a J-type thermocouple. The reactor was heated by a 400W heating mantle. A cooling coil inside the reactor provided a means to remove energy from the reactor when the temperature exceeded the desired set-point. A

solenoid valve on the cooling water supply line served as a control element to enable reactor cooling. The 4842 controller also received an input from a sensor monitoring the impeller agitation rate. However, the agitation rate was controlled manually by varying the voltage of the impeller motor. The pressure within the reactor was measured using an Omega pressure transducer (PX302-1.5KGV) and was displayed on an Omega DP-350 pressure indicator. The pressure was controlled manually by controlling the delivery pressure on the two-stage regulator for the gas cylinder. A purge line connected to the gas feed line provided a means to reduce the pressure in the reactor.

Since powdered catalysts were used extensively in this study, a Swagelok 0.5 μm in line particulate filter (SS-2F-05), the smallest size available, was installed on the end of the dip tube inside the reactor in order to prevent the loss of catalyst material from the reactor from convection through the dip tube and to ensure the samples collected were free of catalytic material. The product line external to the reactor had a custom made heat exchanger to prevent flashing by cooling the liquid samples below the bubble point of the mixture. The reactor was also equipped with a catalyst addition device used in previous studies. However, this device was not used in this study since preliminary experiments suggested that some powdered catalyst may remain within the apparatus or be dispersed onto the reactor walls in the headspace rather than enter the liquid when using this technique. The specific details of the autoclave experimental procedures depended on the objectives of the experiments and are outlined in Chapters Four and Six.

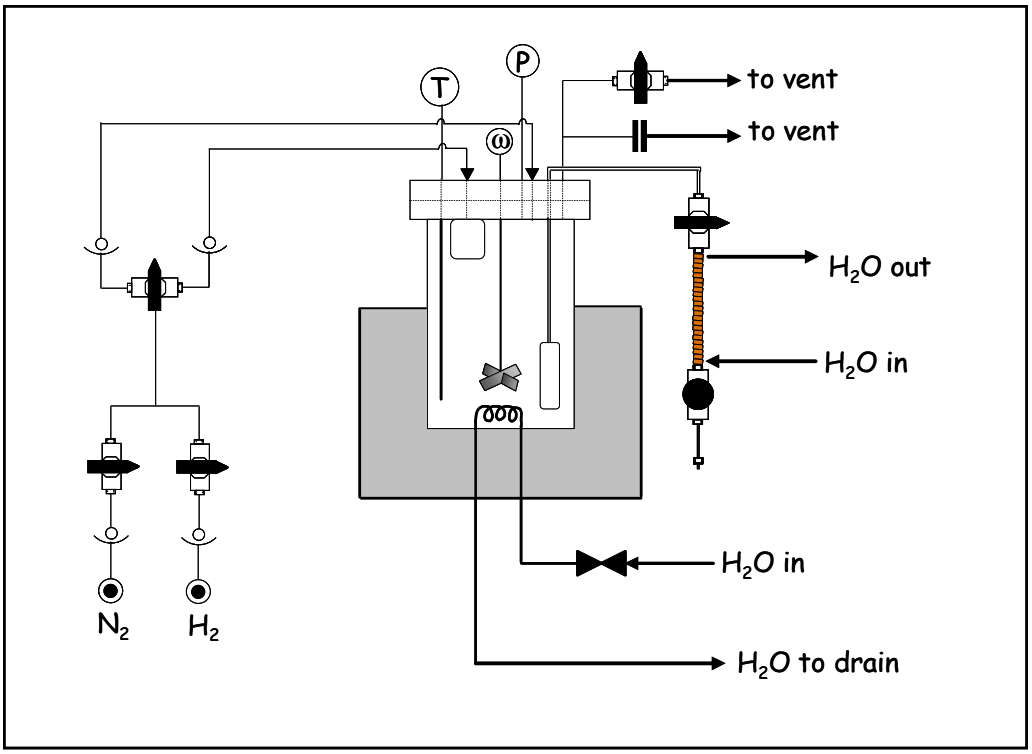


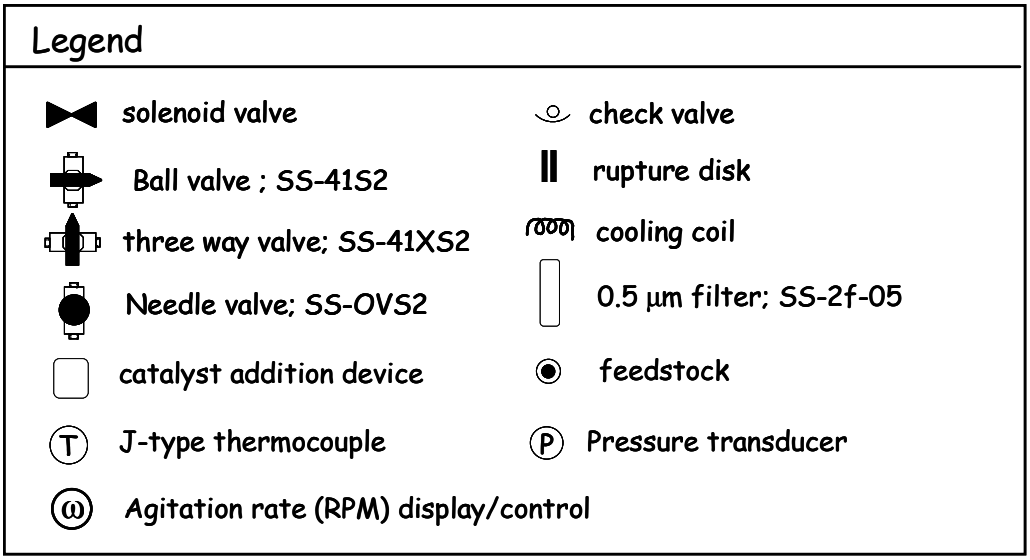


**Figure 3-13** Schematic Representation of the Autoclave Reactor Apparatus

### *3.4.2 Validation of the Liquid Sampling Technique*

The autoclave used in bench scale experiments was equipped with a custom made cooling coil to ensure that the liquid samples extracted from the autoclave were subcooled below the bubble point of the mixture in order to prevent flashing of the liquid sample. Flashing would result in phase separation and the subsequent acquisition of erroneous data. The cooling coil consisted of a 1/8" copper tube wrapped about a section of the product line isolated between a needle valve upstream and a metering valve downstream. The liquid samples obtained from the autoclave were typically retained within the cooling coil for residence times of 5 to 10 seconds before being transferred to GC autosampler vials. In order to validate the liquid sampling technique, two sets of experiments were conducted. The first set of experiments investigated the effect of the residence time in the heat exchanger on the sample temperature exiting the cooling coil in order to ascertain the residence time needed to ensure the liquid was subcooled. The second set of experiments explored the effect of residence time in the heat exchanger on the resultant GC analysis.

Validation by Direct Measurement of Effluent Temperature

In the first set of experiments, the temperature inside the heat exchanger was measured directly as liquid samples were extracted from the autoclave in order to ascertain the effect of residence time in the heat exchanger on the temperature of the reactor effluent. To achieve this, the metering valve and the tubing below it were removed and replaced with the fittings illustrated in Figure 3-14 to accommodate a K-type thermocouple probe (Omega POF26 84K4FB), which was inserted directly into the cooling coil assembly. The autoclave was charged with 200 mL of wash grade acetone, heated to 160°C and pressurized with nitrogen (ca. 2.45 MPa) to ensure the acetone remained in the liquid phase. Cooling water was fed through the cooling coil at a mass flow rate of 600 g/min, which is representative of normal operation.

The needle valve illustrated in Figure 3.14 was opened briefly to draw acetone from the autoclave through the dip tube to the cooling coil sample chamber. The valve (SS-42TF2-10147) beneath the cooling coil was always open allowing liquid to contact the thermocouple probe. The time that the needle valve remained open was the only variable in these experiments (Table 3-6). The temperature inside the cooling coil was obtained from the Omega HH501DK display and was recorded manually as a function of time. The outlet of the heat exchanger assembly was sealed by the fittings for the thermocouple port. Thus, the liquid sample was quiescent within the heat exchanger during these experiments rather than in a continuous flow mode. The heat exchanger was disassembled between tests to purge its contents.

**Table 3-6** Experiments to study the effect of residence time in the HEX on reactor effluent temperature

| Test | Description | INITIAL TEMP OF HEX [°C] |
|---|---|---|
| 1 | Immediately close toggle valve after opening | 21 |
| 2 | Close toggle valve after 1 second | n/a |
| 3 | Immediately close toggle valve after opening | 22 |
| 4 | Toggle valve remained open for experiment | 22 |
| 5 | Toggle valve remained open for experiment | 21 |
| 6 | Toggle valve remained open for experiment | 22 |
| 7 | Immediately close toggle valve after opening | 21 |
| 8 | Immediately close toggle valve after opening | 22 |

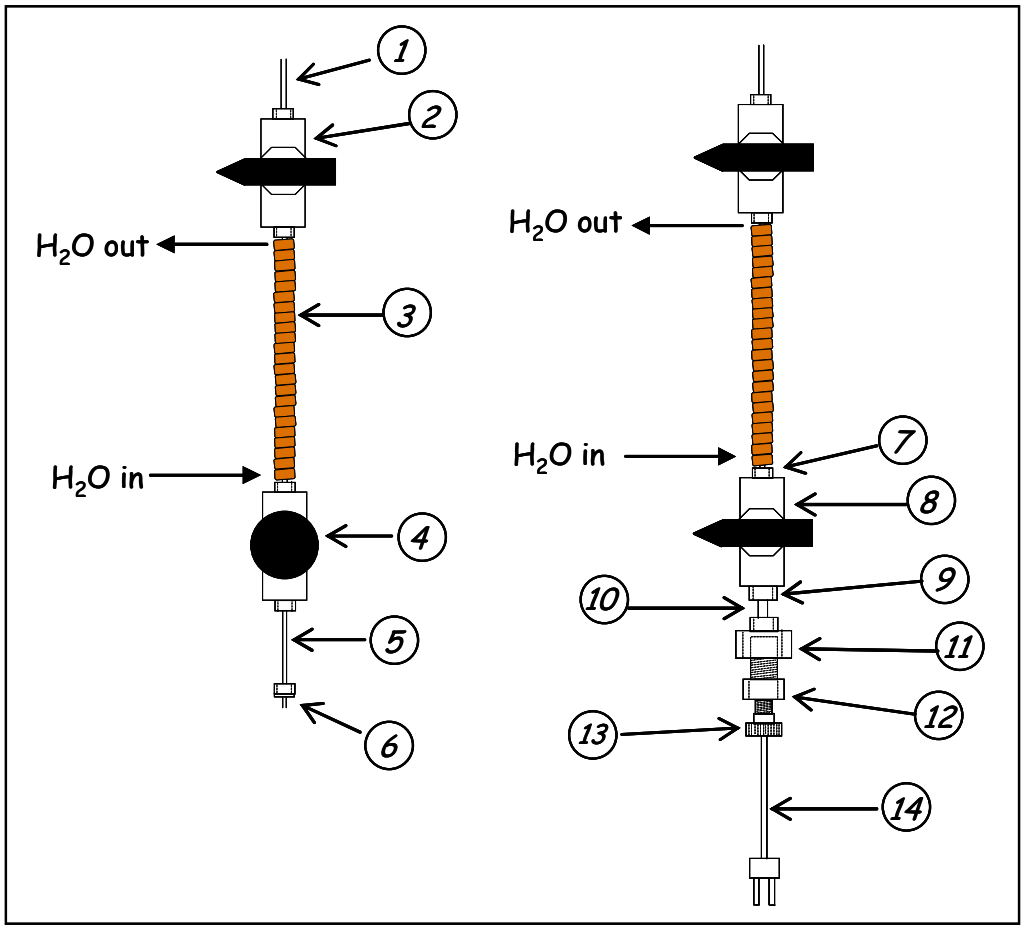


**Figure 3-14** Schematic representation of custom made heat exchanger for autoclave sampling port (left) normal configuration (right) modified to accommodate thermocouple probe for validation experiments

1. 1/8 inch SS tubing with 1/8" Swagelok tube fitting
2. Swagelok Ball Valve; SS-41XS2
3. 1/8 inch copper tubing coiled around 1/8 inch product line
4. Whitey SS-OVS2 Integral Bonnet Needle Valve
5. 1/8 inch stainless steel tubing
6. Sample port, (Swagelok) connects 1/8 inch tube fitting, reduces to 1/16 inch nozzle
7. SS Union, connects 1/8" female tube fitting to ¼" female NPT
8. Swagelok Ball Valve; SS-4T2F2-10147; two female ¼ inch NPT
9. SS Union, connects 1/4" female tube fitting to ¼" female NPT
10. ¼ inch SS tubing
11. Swagelok SS-200-7-4 Union; connects 1/8 inch female to ¼ inch male NPT
12. Swagelok reducing union; connects ¼ inch female NPT to 1/8" tube fitting
13. Swagelok SS-2-UT-1-2; Ultra Torr vacuum fitting, male connector 1/8" x 1/8" male NPT
14. Omega K type thermocouple

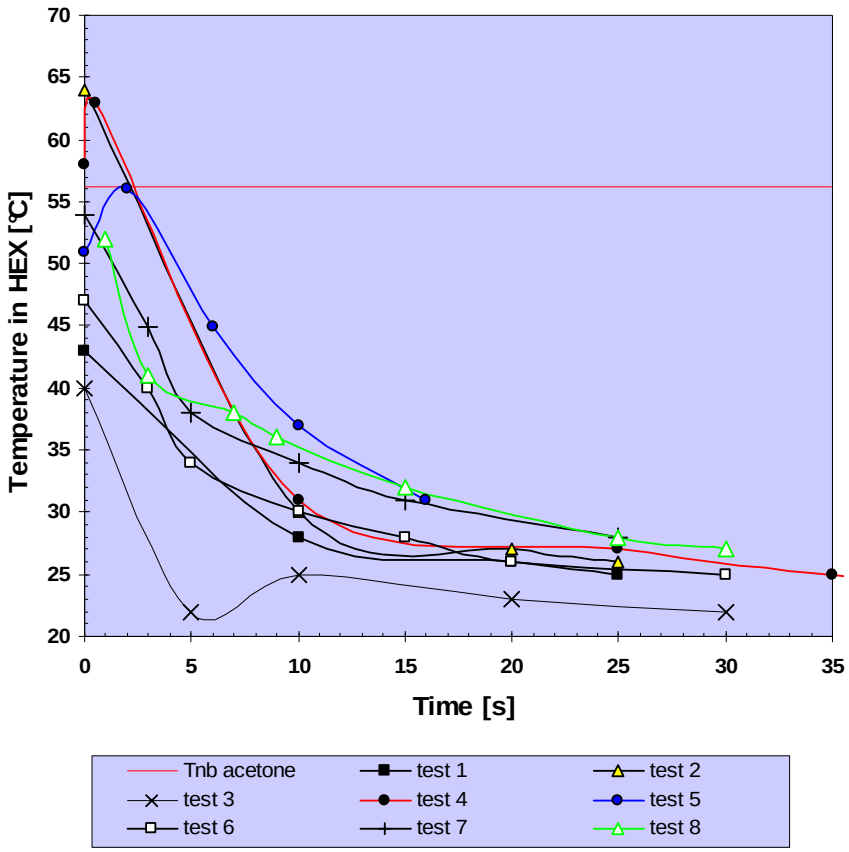


**Figure 3-15** Reactor effluent temperature as a function or residence time in the heat exchanger *The normal boiling point of acetone is indicated by the horizontal red line. All observations below this line represent subcooled liquid samples at atmospheric pressure.*

The results of these experiments illustrated in Figure 3-15 show that the temperature inside the cooling coil was below the normal boiling point of acetone for all but three observations in two experiments (Test 2 and Test 4). In these experiments, the toggle valve was allowed to remain open for some time resulting in heat transfer with the contents of the autoclave by conduction. Temperatures exceeding the normal boiling point of acetone were observed only for residence times of one second or less in the heat exchanger. The experiments with the toggle valve open were repeated two additional times. However in the repeated experiments, all temperature measurements were below the normal boiling point of acetone. In addition, the reactor effluent temperature was below the normal boiling point of acetone for each observation

for experiments for which the toggle valve was closed immediately after sample collection. Since acetone is the most volatile of species being quantified in this work, it can be concluded that the liquid samples extracted from the autoclave are subcooled for all finite residence times in the cooling coil provided the toggle valve is closed immediately. Moreover, the samples are likely subcooled even if this valve is left open, if the samples are retained in the heat exchanger for a few seconds.

Validation by Direct Measurement of Effluent Concentration

A second set of experiments was conducted to study the effect, if any, of the residence time of samples in the heat exchanger on the chemical composition ascertained via GC/FID analysis. For this experiment, the thermocouple probe was removed and the heat exchanger assembly was restored to its normal configuration. The autoclave was charged with a mixture consisting of 1.22 g of technical grade MO mixed with 200 mL of HPLC grade acetone and subsequently heated to 160°C and pressurized with nitrogen (> 3.8 MPa) to ensure the reactants remained in the liquid phase. Liquid samples were extracted from the autoclave and isolated in the sample chamber of the heat exchanger for residence times of 0, 5, 10, 30 and 60 seconds before transferring to GC autosampler vials and subsequent analysis of the MO concentration by GC/FID.

Three samples were collected for each of the 5 residence times investigated. The collection order and order of GC analysis were randomized (Table A3-1, Appendix A). The results illustrated in Figure 3-16 shows that the MO concentration in the effluent was not correlated with the residence time in the heat exchanger. If flashing had occurred, the liquid phase would become enriched with MO. One would expect that flashing would be more prominent for lower residence times in the heat exchanger and accordingly, one would expect the MO concentration to decrease with increasing residence time. This trend is not evident in Figure 3-16.

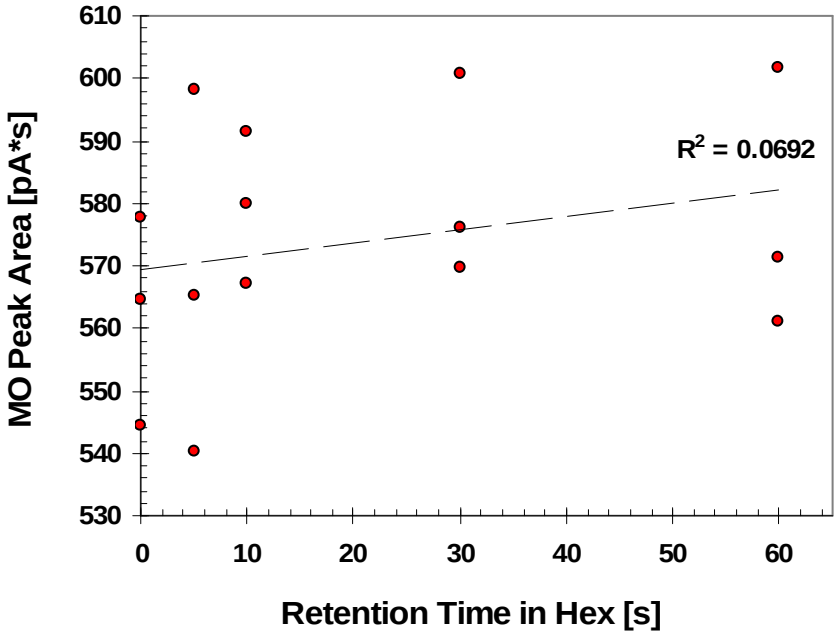


**Figure 3-16** Effect of residence time in the heat exchanger on the MO peak area obtained from GC/FID analysis

Conclusions of Liquid Sampling Technique Validation

The results of the two sets of experiments independently confirm the validity of the liquid sampling technique employed in this work. The data indicates that the temperature of the reactor effluent is below the normal boiling point of acetone for all residence times in the heat exchanger provided that the needle valve is closed immediately after sample collection. Further, there is no correlation between the residence time in the heat exchanger and the effluent concentration. For the experiments reported in Chapters Four and Six, the needle valve was closed immediately after sample collection and a residence time of 5 to 10 seconds in the heat exchanger was used as standard operating procedure.

## 3.5 Energy Dispersive X-Ray Fluorescence (EDXRF) Spectroscopy

### *3.5.1 Theory of Operation*

An Oxford Lab-X 3000 energy dispersive X-ray Fluorescence (EDXRF) analyzer was used to quantify the niobia loading (wt% $Nb_2O_5$) of catalysts. The XRF instrument is capable of quantifying the concentration minor elemental constituents in a solid matrix and has an elemental range from magnesium to uranium. The technique involves bombarding the catalyst sample with X-rays causing the sample to fluoresce and subsequently measuring and analyzing the resultant secondary radiation. Specifically, X-rays are produced from an X-ray source. The photons of the incident X-rays are annihilated upon absorption by atoms belonging to the catalyst, resulting in the ejection of electrons from the K, L, M and O shells of the atom. Electrons from higher energy levels drop down to occupy the vacant levels, losing energy in the process. The differences in energy are made up by the emission of photons of secondary X-rays, whose wavelengths (energy) are characteristic of the element.

Several characteristic "elemental lines" are produced from the allowable energy transitions. The most useful are the $K_\alpha$ and $L_\alpha$ lines, which correspond to the transitions of electrons from the L-shell to the K-shell and from the M-shell to the L-shell respectively. The $K_\alpha$ and $K_\beta$ lines are useful since they are the most energetic of these transitions, thus giving greater signal to background noise ratio. The energy of the K lines increase with increasing atomic number. The $K_\alpha$ and $L_\alpha$ lines are also quite sensitive as elemental indicators due to the large differences in the energy of these transitions between elements. $L_\beta$ and $M_\alpha$ transitions are also used.

The secondary X-rays are all detected simultaneously and the intensities (counts per second) of the X-rays of interest, which are proportional to the amounts of the elements present, are recorded. In order to minimize the

secondary background radiation generated by elements in the matrix that are not of interest, selective excitation and filters are employed. Selective excitation refers to the manipulation of the X-ray source such that the incident X-rays assume wavelengths sufficient to cause fluorescence in the element(s) of interest while minimizing background fluorescence. This is achieved by selecting the minimum tube voltage required to cause excitation at the highest energy line of interest but not higher. A primary filter located between the X-ray source and the sample constrains the spectral distribution of X-rays which impinge upon the sample in a manner which favours good excitation at the elemental line of interest and mitigates background fluorescence.

The Lab-X 3000 used in this work was equipped with an X-Ray tube with variable voltage (8 to 25 kV) as well as a fixed primary beam filter and multiple interchangeable secondary beam filters. The instrument has a "high range" and "low range" excitation condition. The high range excitation condition allows the measurement of the K lines of potassium through zirconium as well as the L lines for rhodium through americium. The low range of excitation condition allows the detection of the $K_\alpha$ and $K_\beta$ for aluminum through chromium and the L lines for strontium through cerium. For the quantification of niobium, the detection of the $L_\alpha$ line for voltages ranging from 8 to 25 kV is recommended and was used in this work. For the low energy range of excitation, the $L_\alpha$ line of niobium is observed at channel 96 of the Lab-X 3000. The XRF method developed and used in this work is outlined in Table B1-1 (Appendix B).

### *3.5.2 Sample Preparation and Analysis*

Catalyst samples were prepared for analysis by grinding them for 1 hour in a Fisher Mortar-Grinder stopping periodically to manually mix the contents of the mortar with a spoonula. A particle size of 95% passing 200 mesh (74 μm) is recommended.[157,158] This grinding process not only ensured that the samples were reduced to a fine powder necessary for analysis but also, and perhaps more importantly, that the specimens were well mixed. This was particularly

important in the preparation of calibration standards, which consisted of a physical mixture of niobium (V) oxide (Aldrich, >99.9%) combined with the appropriate support material.

Matrix effects can cause large changes in absorption and background radiation, leading to significant interference and experimental error. Therefore, XRF standards spanning a broad range of niobia loading were prepared for all of the catalyst supports used in this work. For example, in the case of alumina catalysts, separate XRF calibration standards were created from α-alumina, γ-alumina (weakly basic support), γ-alumina (weakly acidic support) and for high surface area γ-alumina Norpro raschig rings. Ground samples were loaded into the XRF in sample cell holders that had a Mylar or "Poly-S" plastic film base separating the sample from the X-ray beam. The instrument was calibrated on a daily basis and the niobia loading (wt% $Nb_2O_5$) was correlated to the intensity of the secondary X-rays corresponding to the $K_\alpha$ line of niobium. Note that the convention in the literature is to report the catalyst loading in terms of wt% $Nb_2O_5$ rather than wt% Nb. For the multifunctional catalysts investigated, the niobia loading was ascertained prior to impregnation with a palladium precursor. This averted the potential for spectral interference from the fluorescence of palladium.

A typical calibration curve is given in Figure 3-16. The calibration curve exhibits excellent linearity ($R^2$=0.999) with very little variance in the data (RSD= 1.95%). Since the distribution of niobia may not be perfectly homogeneous about the surface of the catalyst samples, the samples were analyzed 10 to 15 times each, agitating the mixture in the sample cell between each measurement. This allowed a more precise estimate of the niobia loading by narrowing the 95% confidence bounds on the estimate. A typical sample analysis is outlined in Table 3-6.

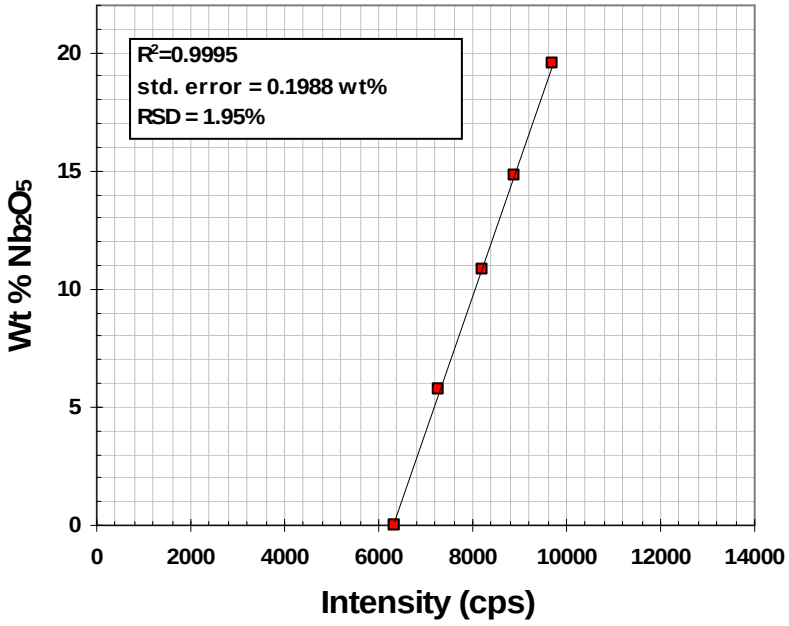


**Figure 3-17** EDXRF calibration curve for $Nb_2O_5/SiO_2$ catalysts (19.08.2006)

**Table 3-7** Sample EDXRF analysis to determine the niobia loading (wt% $Nb_2O_5$) of CAT 052 [19.08.2006]

| Analysis | wt% |
|---|---|
| 1 | 13.9827 |
| 2 | 13.7894 |
| 3 | 14.0477 |
| 4 | 14.1370 |
| 5 | 14.0993 |
| 6 | 13.6671 |
| 7 | 14.0281 |
| 8 | 14.0260 |
| 9 | 13.8702 |
| 10 | 13.9577 |

**Results**

| | | |
|---|---|---|
| average | **13.9605** | **(wt%)** |
| stdev | 0.1456 | (wt%) |
| 95% confidence bounds +/- | 0.0903 | (wt%) |
| relative precision (+/-) | **0.65** | **(%)** |
| relative standard deviation (RSD) | 1.04 | (%) |

**13.96 ± 0.09 (wt% $Nb_2O_5$)** ← *Result CAT 052*

EDXRF Precision

The 95% confidence bounds on the niobia loading (wt% $Nb_2O_5$) represent the precision of the elemental analysis via EDXRF. The precision for the vast majority of the analyses of the niobia catalysts in this work typically ranged from ± 0.06 to 0.16 wt% (i.e. a relative uncertainty of ± 1 to 2% of the estimated niobia loading). The most precise estimate was ± 0.026 wt% and the least precise measurement observed was ± 0.55 wt%. Only 3 of 63 analyses of powdered catalysts gave an uncertainty of ± 0.25 wt% or greater. Although this precision is quite good for the analysis of niobia catalysts, for which the niobia loading ranges from around 5 to 40 wt%, this technique was found to be not sufficiently precise for the elemental analysis of the Pd loading of multifunctional catalysts (Chapters Six through Eight). Consequently the Pd loading of multifunctional catalysts were ascertained via Inductively Coupled Plasma (ICP) by an external laboratory (Galbraith Laboratories, Knoxville, TN, USA.)

EDXRF Accuracy

The excellent linearity and minimal variance exhibited by the calibration curve in Figure 3-16 as well as the good precision of this technique, suggests that this method is quite accurate for the quantification of niobium in catalysts consisting of niobia dispersed onto metal oxide supports. The accuracy of this technique was further validated against Nb elemental analysis via ICP by an external laboratory (Galbraith Laboratories, Knoxville, TN, USA). Table 3-7 shows the results of the niobia analysis via EDXRF and ICP for two $Pd/Nb_2O_5/SiO_2$ catalysts (066 and 067). For these catalysts, niobia was dispersed on a high surface area silica support (Norpro SS65137, S/N 2006910020) in the shape of a Raschig ring. However, the catalysts were ground to a fine powder prior to analysis.

The results show that the niobia loading for catalyst 067 determined by ICP is in excellent agreement with the EDXRF analysis. The result of the ICP

analysis falls within the 95% confidence bounds of the EDXRF. The EDXRF analysis has a relative error (i.e. % recovery) of 2.2% with respect to the ICP analysis, which is assumed to give the accepted true value. In the second analysis there is a larger discrepancy with the EDXRF analysis having a relative error of 13% with respect to the ICP analysis. However, this does represent a relatively good agreement between these two techniques. Relative errors of ± 10% are not unusual for the elemental analysis of metal oxides via XRF.[157] Since no systematic bias is evident, the accuracy of this technique is perhaps best inferred from the variance inherent in the calibration curves. In this work, the RSD of the calibration curves, which may be considered a measure of the accuracy of the analysis, ranged from 0.53% to as high as 11%, but was more typically between 3 to 7%. Thus, this EDXRF technique can be considered a reliable method of niobium elemental analysis for the catalysts prepared in this work.

**Table 3-8** Validation of EDXRF against ICP Elemental Analysis

| CATALYST ID | NB (WT%) I.C.P | $NB_2O_5$ (WT%) I.C.P. | $NB_2O_5$ (WT%) EDXRF | RECOVERY (%) |
|---|---|---|---|---|
| 067 | 4.11 | 5.88 | 5.75 ± 0.16 | 2.21 |
| 065 | 3.76 | 5.38 | 6.09 ± 0.25 | 13.2 |

Conclusions of EDXRF Method Development and Validation

The accuracy and precision of this EDXRF technique is governed by the ability to produce high quality calibration standards, which consist of a physical mixture of the catalytic materials present in the catalyst samples. The calibration standard mixtures used are inherently heterogeneous; the analyte of interest is present in a separate solid oxide phase from the matrix. The EDXRF technique gives good accuracy and precision for the analysis of niobia loading on transition metal oxides for niobia loading ranging from 5 to 25 wt%. However, given the estimated precision of the instrumental analysis, the use of this technique for the quantification of trace palladium (0.05 to 0.1 wt%) is questionable. Consequently, the palladium loading of multifunctional catalysts

(Chapters Six through Eight) was determined by ICP analysis by an external laboratory. The EDXRF data and analyses are available in Appendix B.

## 3.6 Catalyst Preparation

### *3.6.1 Synthesis of Niobium Oxide Catalysts*

General Procedure

Catalysts consisting of a highly dispersed niobium oxide overlayer on various metal oxide supports were prepared based on the non-aqueous synthesis technique disclosed by Ko et al.[89,90] This preparative technique consists of six stages of preparation. First the catalyst support was activated by drying at elevated temperature in a calcinator (Figure 3-17) in moisture free air (Praxair, zero gas) at a flow rate of 3.8 mL/min, in order to control the surface hydroxyl concentration and remove adsorbed species from the support. This activation temperature was an experimental variable which ranged from 100 to 400°C. The dried support was transferred from the calcinator to a 250 mL vacuum flask sealed with a screw cap and by a stopcock valve on the vacuum line.

Second, niobium (V) ethoxide (Aldrich 339202, >99.95%) diluted in HPLC grade n-hexane solvent, was introduced to the vacuum flask and contacted with the metal oxide support at ambient temperature for 2 hours. Note that the precursor is not a dissolved ionic species that interacts with another charged surface species as in conventional impregnation techniques, but rather the precursor is known to preferentially titrate the surface hydroxyls of the metal oxide support. Since niobium ethoxide decomposes readily in the presence of water to give niobic acid and ethanol, all glassware including the calcinator was pre-dried in an oven prior to use. The n-hexane solvent was also pre-dried with 5A molecular sieves that had been activated at 350°C for 3 hours and allowed to cool to ambient temperature under vacuum before being transferred to the n-hexane stock bottle. Steps 2 through 5 (until the catalyst is

calcined) must be carried out in moisture free environment. The preparative steps are carried out in a glove bag filled with a moisture free gas such as argon or nitrogen. Third, the supernatant liquid was separated from the powder catalyst by applying a vacuum while using a liquid nitrogen trap to recover the solvent. In the case of large catalyst particles, the solid was separated from the supernatant by decantation while in inert environment within a glove bag. Fourth, the sample was retained under vacuum for 24 hours to dry the catalyst before thermal treatment.

Fifth, the catalyst was transferred into the calcinator while protected in moisture free environment in a glove bag. A thermal attaching reaction was carried out at elevated temperature in nitrogen environment with a flow rate of 4.0 mL/min. The thermal attaching/thermal decomposition reaction results in the cracking of the organic ligands and the destruction of the precursor. The reaction temperature was an experimental variable in this study and was either 200 or 400°C. Sixth, the niobium oxide overlayer was established by calcination in moisture free air (Praxair, zero gas) at a flow rate of 3.8 mL/min air at elevated temperature. The calcination temperature was also a variable in this study and ranged from 100 to 500°C. Once the catalyst has been calcined, the catalyst is moisture tolerant and can be exposed to the ambient without loss of catalytic performance.

Glove Bag

A glove bag (Cole Parmer, 04408-38) was used to provide an inert and moisture free environment to carry out the catalyst preparation steps. Moisture and air sensitive catalysts and materials were stored permanently inside the glove bag within a sealed dessicator along with adsorbent. A second dessicator containing adsorbent and activated 5A molecular sieves was kept inside the glove bag and left open to further dry the contents of the glove bag. The glove bag was kept sealed when not in use. Once the materials needed for the synthesis were transferred to the glove bag, the bag was sealed and then evacuated using a

vacuum pump. The bag was then filled with pre-purified nitrogen (Praxair, 4.8 grade). The glove bag was purged by repeating the evacuation and filling cycle three additional times with the fourth volume of nitrogen being the working volume.

Preparation of Niobium Ethoxide Solutions

The dried catalyst support was transferred from the calcinator to a 250 mL vacuum flask while in inert environment within the glove bag. A predetermined amount of pre-dried HPLC grade n-hexane was stored in sealed 20 mL vials that had been pre-dried in an oven at about 80°C. The amount of n-hexane solvent used depended on the type and amount of support used. The minimum amount of solvent needed to completely fill the pores and fully wet the supports was estimated experimentally and was used as a basis for the amount of precursor solution used to wet the support. Niobium (V) ethoxide (Aldrich 339202; 99.95%) was added to the hexane solvent using a glass 1 mL Hamilton syringe that had been dried and stored in an oven at about 80°C prior to being transferred to the glove bag. The impregnation solution was mixed by sealing the vial and agitating the mixture, prior to transferring the impregnation solution to the vacuum flask containing the support. The amount of niobium (V) ethoxide precursor needed to give a certain loading was determined through the course of experimentation. Once the impregnation solution was transferred to the vacuum flask, the flask was sealed with a screw cap and the stop-cock on the vacuum line was closed. The flask was agitated manually periodically throughout the 2 hour impregnation period.

Calcinator

The calcinator illustrated in Figure 3-17 was used to activate catalyst supports, conduct the thermal attaching/thermal decomposition reactions as well as catalyst calcination and the reduction of hydrogenation catalysts. The calcinator is equipped with a frit, upon which the catalytic materials were positioned. After the catalytic material is loaded into the calcinator, the two halves of the

calcinator were sealed by a tapered fitting coated with a thin layer of either vacuum grease or Teflon tape. In contrast to conventional calcinator design, the calcinator was modified to have a tapered seal, which prevents gyrational motion of the upper half of the calcinator relative to the bottom. This prevents potential damage to the calcinator since the glass internals are very delicate. In addition, the tapered design provides a greater sealing surface. A gas sparger connected to the top of the calcinator passes down the centre line of the calcinator, through the frit to the bottom of the calcinator where its outlet is located. The sparger directs a gas stream to the bottom of the calcinator. Due to the pressure drop across the calcinator, the gas stream flows upwards through the frit and the bed of catalytic materials, to the top of the calcinator where the gas outlet is located. The gas flow rates were controlled using a rotameter (Matheson model E1-1A101). The flow rates used in this study were measured using an Agilent Technologies Optiflow 650 digital flow meter. A Swagelok cross fitting was located immediately upstream from the rotameter, to which three gas supply lines (air, hydrogen and nitrogen) were connected. Needle valves installed on the supply lines allowed rapid switching between supply gases.

The top section of the calcinator was filled with inert glass wool in order to prevent loss of materials by entrainment. The gas inlet and outlet ports were equipped with stopcocks, which allow the calcinator contents to be sealed from the environment during transport of the apparatus or when not in operation. A thermocouple probe inserted into a thermowell running from the top of the calcinator down to the frit, allowed direct measurement of the temperature inside the catalyst bed. The catalyst bed temperature was controlled by an Omega CN 8200 series PID temperature controller with an Omega temperature display. The calcinator was heated by a 960W Applied Test Systems (ATS) Ltd. 3110 Series heating mantle. The heating mantle was equipped with a cooling line through which compressed plant air was passed manually to facilitate the cooling of the heating mantle and calcinator. This cooling feature

was not part of the temperature control strategy but was used for cooling the apparatus at the end of an experiment or when the process temperature needed to be lowered to a new set-point. For example if the catalyst was exposed to nitrogen at 200°C for the thermal decomposition reaction followed by calcination at 100°C.

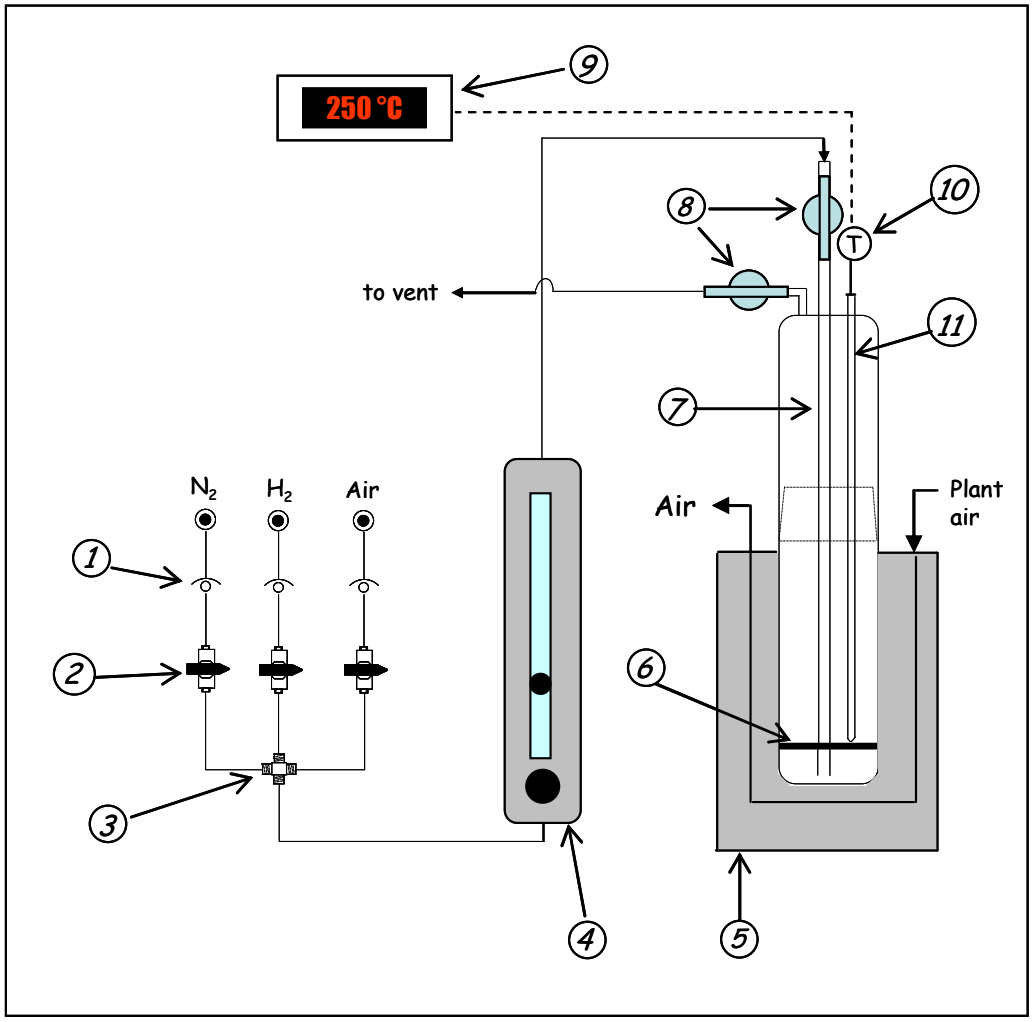


**Figure 3-18** Schematic representation of the calcinator apparatus

1. check valve
2. ball valve
3. Swagelok Union Cross ; 1/8" tube fittings
4. Rotameter; Matheson Gas model E1-1A101
5. 960 Watt Heating Mantle, Applied Test Systems (ATS) Ltd. 3110 Series
6. gas permeable frit
7. gas sparger
8. stopcock
9. Omega CN 8200 series PID temperature controller
10. Thermocouple probe
11. Thermowell

Sample Calculation of Fractional Monolayer Coverage

The synthesis technique described in Section 3.6.1 will yield a two dimensional surface-phase of niobia, typically one molecular layer thick, dispersed onto the transition metal oxide support. The fractional monolayer coverage (φ) may be calculated from the niobia loading and the BET surface area of the support prior to impregnation, based on the assumption that a $NbO_{2.5}$ unit of the 2D monolayer occupies 16 $Å^2$.[89]

*Eg. Sample calculation of the fractional monolayer coverage of a 15.8 wt% $Nb_2O_5/SiO_2$ catalyst. The silica support has $S_a$= 294 $m^2/g$. This data was reported by Chen et al. [42] for a catalyst with 0.5 monolayer coverage.*

Basis: 1g of support ($SiO_2$)

Let n represent the number of moles of ($NbO_{2.5}$) units in the monolayer
$N_A$ = Avogadro's number = 6.022 x $10^{23}$ $mol^{-1}$

1g $SiO_2$ and catalyst is 15.8 wt% niobia $\Rightarrow$ Mass of niobia ($Nb_2O_5$) = 0.18765 g
There are two moles of $NbO_{2.5}$ per mole of $Nb_2O_5$

$$\therefore\ n = \frac{0.18765g * 2}{265.8098\,{}^{g}\!/_{mol}} = 1.4119\,x10^{-3}\ mol\ NbO_{2.5}$$

$$\varphi = (nN_A)(16\dot{A}^2)\left(\frac{1x10^{-10}m}{1\dot{A}}\right)^2\left(\frac{g\ SiO_2}{294m^2}\right)\left(\frac{1}{1g\ SiO_2}\right) = 0.463 \approx 0.5$$

*3.6.2 Preparation of Multifunctional Catalysts*

Multifunctional catalysts used in this study for the one-step synthesis of MIBK were created by integrating palladium into the architecture of existing niobia catalysts developed from the synthesis method outlined in section 3.6.1. Palladium (II) acetate (Aldrich 205869, Lot 08126PB) was used as a precursor.[♣] Palladium chloride is not recommended for impregnating niobia catalysts with palladium since the chloride ion is a Lewis base and its interaction with the niobia may lead to a significant diminution of the catalyst's acidity.[106] Since

[♣] Assay 100% ± 2.5% (i.e. 47.4 ± 1.2 % Pd) reported on certificate of analysis

acetone will react in the presence of the niobia catalyst, an alternative organic solvent is needed to dissolve the precursor. Glacial acetic acid (HAc) was used for this purpose based on the technique disclosed by Wirtz et al. [159].

Procedure

1. The niobia catalyst to be impregnated was accurately and precisely weighed. Small batches (ca. 2 to 5 g) were placed in a 50 mL glass beaker and weighed on a Sartorius balance to ± 0.00005 g. Larger batches of catalysts (e.g. 10 grams HSA silica rings) were placed in a 250 mL beaker and weighed out on a different scale precisely to 4 significant figures.

2. The weighed out niobia catalyst was transferred to an oven and pre-heated at about 80°C for about 1 hour.

3. The amount of Pd(II) acetate required to give a maximum pre-determined Pd loading was calculated, precisely weighed out (± 0.00005 g) and transferred into a 10 mL beaker.

4. 35.5 mL of ACS reagent grade glacial acetic acid (Fisher UN279, Lot 505216) per gram of niobia catalyst was transferred to a beaker.

5. The Pd(II) acetate was transferred from the 10 mL beaker to the beaker containing the glacial acetic acid. Glacial HAc was used to rinse out the 10 mL beaker, using a Pasteur pipette, into the beaker containing the Pd acetate / HAc solution. The beaker containing the impregnation solution was sealed with Parrafilm and transferred to the oven to preheat at about 80°C for 1 hour.

6. The contents of the beaker containing the niobia catalyst were transferred into the beaker containing the impregnation solution. The beaker containing the catalyst and impregnation solution was re-sealed with Parrafilm and the impregnation was carried out for 2 hours at 80°C.

7. After two hours of impregnation, the catalyst was separated from the supernatant liquid by vacuum filtration.

8. The catalyst was returned to the oven and dried for 24 hours at about 80°C.

**9.** The catalyst was transferred to a calcinator (Figure 3-18) and reduced in ultra-high purity (UHP) or pre-purified (PP) hydrogen at a flow rate of about 6.4 mL/min, typically for 2 hours at 100°C. After the reduction was complete, the calcinator stopcocks were sealed and the calcinator was transferred to the glove bag where the catalyst was placed into a pre-dried vial and stored in the dessicator until needed.

ICP analysis of catalysts prepared by this technique (Chapters Six through Eight) suggest that about 40% of the Pd was integrated into the niobia catalyst while the difference remained in the impregnation solution.

# Chapter Four

## Study on the Effects of Niobia Catalyst Properties on the Activity, Selectivity and Stability for MO Synthesis

### 4.0 Synopsis

Niobia compounds have gained much attention in recent years due to their striking and unusual properties as catalysts and promoters as well as their synergistic effects as catalyst supports.[67] The physico-chemical interaction of the surface-phase niobium oxide with a strongly interacting metal oxide support leads to the self assembly of niobium oxide species with electronic and geometric characteristics distinct from the bulk oxide, thus having unique catalytic properties. Although niobic acid has been identified as a promising catalyst for MIBK synthesis, very little investigation into the use of supported niobia compounds as catalysts for this application has been done. The influence of the three most important niobia catalyst parameters, which according to Jehng and Wachs[68] include the niobia loading, the calcination temperature and the nature of the oxide support, remain largely unexplored for this organic synthesis. The scientific investigation of dispersed niobia catalysts for MIBK synthesis appears to be constrained to a single study.[42] An improved understanding of the association between the niobia catalyst properties and catalytic performance for MIBK synthesis is needed, particularly for catalysts consisting of highly dispersed niobia less than monolayer coverage and for those calcined at low to moderate temperatures exhibiting significant Bronsted acidity.

In this chapter, the results of catalyst screening studies investigating the effects of the nature of the oxide support on the activity and selectivity for MO synthesis are reported. $SiO_2$ and γ-alumina were identified as promising supports for this application and were subjected to more detailed experimentation whereby the effects of calcination temperature, support

activation temperature and niobia loading were investigated. The results presented in this chapter demonstrate that each of the major catalyst parameters investigated had a significant influence on the resultant catalytic performance for MO synthesis. An unexpected and significant finding was that the catalysts calcined at 100°C exhibited superior catalytic performance compared to those calcined at 500°C, suggesting that Bronsted acidity plays an important role in this organic synthesis, particularly with regard to catalyst stability.

## 4.1 Properties of the Metal Oxide Supports

Niobic acid ($Nb_2O_5 \cdot nH_2O$)) has a very high acidity and excellent stability for reactions in which water is either liberated or produced. It is not surprising therefore, that niobic acid has been identified as a promising catalytically active support for a multifunctional catalyst to facilitate MIBK synthesis.[43] However, it is of interest to study catalysts for which the niobium oxide phase is highly dispersed about the surface of another metal oxide with which it will strongly interact in order to generate unique niobia structures with catalytic properties that are distinct from, and potentially more beneficial than, bulk niobic acid.

Indeed, various catalysts consisting of a niobia surface oxide phase coated onto a transition metal oxide support have been investigated for many reactions. However, to the best of this author's knowledge, scientific investigation of the application of niobium compounds, other than niobic acid, towards the one-step synthesis of MIBK is constrained to a single study by Chen et al.[42] who explored the use of a $Pd/SiO_2/Nb_2O_5$ catalyst. Jehng and Wachs[68] have advised that "the specific oxide support is a critical parameter since it dramatically affects the reactivity of the surface niobium oxide species and determines if the surface niobium oxide site is active for redox or acid catalysis." Evidently, the single most important catalyst property for dispersed niobia catalysts has not been studied to determine its influence on either the synthesis of MO or MIBK.

The catalyst supports outlined in Table 4-1 were selected for investigation as potential supports for niobia catalysts for MO and MIBK syntheses. Alumina, titania, silica and magnesia have all been previously investigated as supports for niobium oxide catalysts for applications other than MIBK synthesis. Aside from their bulk chemical composition, the supports were intentionally selected for this screening study such that they differ in their inherent acidity/basicity and electronic properties, their surface area and other morphological and crystallographic properties. The intriguing results of Paulis et al.[14] as well as Flego and Perego[129] suggest that the morphological and topological properties of the catalyst might affect the product distribution for MO and MIBK syntheses.

**Table 4-1** Bulk Properties of Metal oxides investigated as catalyst supports

| Support | Crystal Structure | Space Group | Lattice Parameters | Band Gap (eV) | Acidity | BET Area [$m^2/g$] |
|---|---|---|---|---|---|---|
| (acidic) $\gamma$-$Al_2O_3$ | **Spinel** fcc | $Fd\bar{3}m$ ($O_h^7$) | a=0.79 nm $\alpha$=90° Ref. [160] | 7.0 Ref [166] | Weakly acidic (pH 6.0) [a] | 150 |
| (basic) $\gamma$-$Al_2O_3$ | **Spinel** fcc | $Fd\bar{3}m$ ($O_h^7$) | a=0.79 nm $\alpha$=90° Ref. [160] | 7.0 Ref [166] | Basic (pH 9.5) [a] | 150 |
| $\alpha$-$Al_2O_3$ | **Corundum** Rhombohedral (i.e. Trigonal) | $R\bar{3}c$ ($D_{3d}^6$) | a =0.5136 nm $\alpha$= 55.28° Ref. [163] | 8.3 Ref [163] 8.8 Ref [167] 9.0 Ref [168] 8.8 Ref [166] | basic (pH ~ 9) [b] | 14.1 |
| fumed $SiO_2$ | **Amorphous** | N/A | N/A | 8.9 Ref [169] | acidic (pH~2) [b] | 254 |
| $TiO_2$ | **Anatase** Tetragonal | $I4_1/amd$ ($D_{4h}^{19}$) | a=0.37845 nm c=0.9514 nm $\alpha$=90°C Ref. [164] | 3.23 Ref [170 ] | weakly Acidic (pH 5-6) [b] | 9.28 |
| MgO | **Isometric** (fcc) | Fm3m ($Oh^5$) | a=0.4213 nm $\alpha$=90°C Ref. [165] | 6.8 Ref [171] 7.2 Ref [168] | Strongly basic (pH ~12) [b] | 5.77 |

*The space groups in Table 4-1 are indicated in the Hermann-Mauguin notation used by crystallographers and by the equivalent Schonflies notation, used by chemists and surface scientists beneath in brackets*

*[a] pH of isoelectric point obtained from certificate of analysis; [b] pH of isoelectric point of materials compiled by Jehng and Wachs[87]*

*4.1.1 Molecular Symmetry and Crystallographic Structure*

The electronic and geometrical properties of the support oxide will govern the physico-chemical interaction between the support and the surface-phase niobium oxide. The crystallographic structures of the support oxides are of interest since the interatomic bond lengths and bond angles, coordination numbers and the densities of atomic packing determine the long range electrostatic interactions as well as the nearest neighbour interactions between atoms, which govern the electronic and physical properties of the solids. The structures of each of the supports selected, with the exception of fumed silica which is amorphous, exhibit distinct crystal structures characterized by structural periodicity and molecular order.

Each of the crystalline supports can be classified into one of seven crystal systems. The crystal structures can be further characterized by their molecular symmetry. Each may be classified into one of 32 mutually exclusive point groups. The point group outlines the complete set of symmetry operations, such as rotation, inversion and reflection which can be applied to the basis unit cell of the crystal with respect to a distinct point in space. Additionally, if one also considers translational symmetry operations applied to the unit cell as well as the point symmetry operations, every crystal structure can be classified into one of 230 mutually exclusive space groups. The space groups of the supports investigated are summarized in Table 4-1.

Two polymorphs of alumina, the metastable $\gamma$-$Al_2O_3$ (Aldrich 267740 batch 11111AA) and the thermodynamically stable $\alpha$-$Al_2O_3$ (Aldrich 23,474-5 Lot No. 09214TZ), having the same bulk chemical composition but differing in their crystallographic structures were investigated as potential supports for a niobia catalyst for MO synthesis. $\gamma$-$Al_2O_3$ has a relatively complex structure, best described as a "defect spinel structure", which is based on a face centred cubic (fcc) close packing. In the spinel structure, the planes of close packed oxygen anions form a repeating ABCABC sequence characteristic of the fcc structure.

As with most metal oxides, the aluminum cations are smaller than the oxygen anions and as a result form close packed layers occupying the interstitial spaces. The close packed aluminum cations form two distinct alternating layers: one layer having only octahedrally co-ordinated alumina cations and a second layer containing a mixture of both octahedral and tetrahedrally co-ordinated aluminum cations with both upward directed and inverted tetrahedra.[160] More specifically, it is generally accepted that the oxygen atoms are located at the 38e *Wyckoff positions*♠ in fully occupied and approximately close packed layers while the cations are located at the 8a, 8b, 16c, 16d and 48f Wyckoff positions; however the precise distribution of cations is not known.[160] Roughly two thirds of aluminum cations are octahedrally co-ordinated while around one third are tetrahedrally coordinated.[160,161] The spinel structure of γ-$Al_2O_3$ is distorted compared to the ideal spinel structure due to the presence of vacancies randomly distributed about the tetrahedral sites of the aluminum cation layers.[160] In addition, hydroxyl ions are also present within the defect spinel structure of γ-$Al_2O_3$. It has been suggested that the number of hydroxyl ions are equivalent to the number of interstitial vacancies.[162]

The spinel structure of γ-$Al_2O_3$ is relatively complex with 32 oxygen anions and 64/3 aluminum cations in the unit cell.[160] In contrast, the corundum structure of α-$Al_2O_3$ is based on a simple rhombohedral (i.e. trigonal) crystal structure with only 10 atoms in the unit cell.[161,163] Four aluminum cations are located at the Wyckoff positions c (0.352, 0.352, 0.352) and six oxygen anions are located at positions e(0.556, 0.994,1/4).[163] Both polymorphs of alumina are insulators, as indicated by the high band gaps in Table 4-1. γ-$Al_2O_3$ has a lower band gap due to its increased level of structural disorder in comparison to the crystal structure of α-$Al_2O_3$.[166] γ-$Al_2O_3$ also has a much higher surface area than α-$Al_2O_3$.

---

♠ *The Wyckoff positions are defined with respect to the specific space group. A discussion on group theory is outside the scope of this thesis. The reader is referred to Janner et al.[172] regarding Wyckoff positions and Hall[173] for a further discussion on symmetry operations and a complete list of the 230 crystallographic space groups*

The fumed silica (Aldrich 381276 batch 07519BC) is also an insulator having the highest band gap of the supports investigated. The fumed silica support consists of nanospheres 11 nm in diameter fused together into highly branched chains 100 to 200 nm long.[174] The morphology of fumed silica is amorphous, which is confirmed by the absence of lines in its XRD analysis.[174] Consequently, fumed silica represents one extreme of molecular disorder of the supports investigated, while MgO exhibits the greatest molecular symmetry. The fumed silica support also exhibits the highest surface area of the supports investigated (255 $m^2/g$) and has a relatively high concentration of surface hydroxyls available for reaction with niobium ethoxide. It is estimated that the fumed silica procured for this study had 4.0 ± 0.5 $OH^-$ groups per square nanometre prior to thermal treatment.[174]

The basic building blocks of the MgO, $TiO_2$ and $\alpha$-$Al_2O_3$ structures may be viewed as octahedra consisting of a metal cation surrounded six oxygen anions. The differences between the various structures are in the way in which the octahedra are connected, the degree of distortion of the octahedra and the resultant bond lengths. The MgO support (Alfa Aesar 35442, Lot E22N04) is a low surface area insulator having an isometric "rock salt" structure. The octahedra are connected via edge sharing. In contrast, the corundum structure involves a more complicated network involving face sharing, edge sharing and corner sharing of octahedra.[175] The anatase structure consists of chains of edge-sharing octahedra that "zig-zag" to form a three-dimensional network of edge-shared octahedra.[176,177]

Of the two main polymorphs of $TiO_2$ (anatase and rutile), anatase was selected for investigation. Rutile and anatase exhibit very similar tetragonal structures but different in the bond lengths and degree of distortion of the octahedral structure.[164,176] The four planar M-O bond lengths of the octahedra of rutile are 0.195 nm whereas in anatase the same bond lengths are 0.194 nm; the two azimuthal M-O bond lengths in rutile are 0.198 nm and are 0.196 nm

for anatase.[176] Anatase is less dense and has a slightly higher band gap (3.23 eV) than rutile (3.00 eV).[164,177] These polymorphs also exhibit different symmetry with anatase belonging to the point group $D_{2h}$ and rutile $D_{2d}$.[176,177] $TiO_2$ has been used as both a catalyst and support. Due to its low band gap, $TiO_2$ is a semiconductor and is known to be active as a photocatalyst for water decomposition, the partial oxidation of hydrocarbons and the reduction of nitrogen to produce ammonia.[176] As a support for dispersed metal catalysts, a strong metal support interaction enhances the activity and selectivity for hydrogenation and dehydrogenation reactions.[176]

*4.1.2 Acidity and Basicity*

It is known that the acidity or basicity of the support oxide will influence the physico-chemical interaction between the surface-phase oxide and the support and thus affect the resultant niobia structure. Jehng and Wachs[68,87] have reported that niobia dispersed onto basic surfaces lead to the formation of highly distorted niobia octahedra whereas acidic supports lead to weakly distorted niobia octahedra. The highly distorted octahedra exhibit mono-oxo (Nb=O) terminal bonds, which are associated with Lewis acidity whereas the weakly distorted octahedra exhibit (Nb-O) bonds, which are associated with Bronsted acidity.[87] Consequently, the metal oxides selected for this study represent a broad range of acidity including strongly basic MgO, basic $Al_2O_3$, $SiO_2$ has slightly acidic silanol groups and $TiO_2$ which is also acidic.

Two $\gamma$-$Al_2O_3$ supports, one basic (Aldrich 199443, Batch 12312CB) and the other weakly acidic (Aldrich 267740 batch 11111AA) were selected to directly investigate the effect of the support acidity while ensuring that the supports do not have a markedly different crystallographic structure. The $\gamma$-$Al_2O_3$ supports have the same bulk chemical composition and very similar local surface structures since they share the same defect spinel crystal structure. These materials also have the same particle size distribution with a mean size of 150 mesh, the same BET surface area (155 $m^2/g$) and the same mean pore diameter

of 58 Å. The pH of a slurry of the basic $\gamma$-$Al_2O_3$ is $9.5 \pm 0.5$ and that of the weakly acidic $\gamma$-$Al_2O_3$ is $6.0 \pm 0.5$.

*4.1.3 Thermogravimetric Analysis (TGA) of Metal Oxide Supports*

The thermal pre-treatment of the metal oxide support is known to be an important parameter for catalysts consisting of a highly dispersed surface-phase oxide supported on a second metal oxide. Generally, acidic surface-phase oxides, such as $NbO_x$, form chemisorptive linkages to the surface hydroxyls while basic surface-phase oxides attach to the Lewis acid sites of the metal oxide support.[103] The synthesis technique followed in this work (Chapter Three), involves the generation of unique niobia structures via the preferential titration of the surface hydroxyl groups of the support with niobium (V) ethoxide precursor, followed by thermal treatment to remove the organic ligands and subsequent calcination to generate the niobia overlayer. The surface-phase niobia consists of a one molecular layer thick, 2-dimensional "overlayer" at the external surface of the catalyst. The geometrical and electronic properties of the niobia structures are believed to be influenced by the surface hydroxyl chemistry of the metal oxide support.[68]

The generation of surface hydroxyls on metal oxides is due to the dissociative adsorption of water. The reverse reaction at elevated temperatures leads to dehydroxylation. Thus, the thermal pre-treatment of the support will influence surface concentration of hydroxyls on the metal oxide. The surface hydroxyl chemistry also depends on the type of oxide support. Coordinative unsaturation at the surface, results in surface ions which have a lower coordination number than those in the bulk oxide. At ambient conditions, these vacancies are occupied by surface hydroxyls or coordinated water in order to restore the coordination number of these ions. The nature of the surface coordinative unsaturation and the catalytic activity of coordinativley unsaturated ions are dependent on the crystal planes exposed and therefore is dependent on the nature of the oxide.[175] Alumina for example, has no less than 5 distinct

forms of surface hydroxyls.[178] Silica on the other hand exhibits two kinds of surface hydroxyls, the silanol (Si-OH) and geminal ($SiOH_2$) groups. Incidentally, the silanol groups are more reactive with niobium precursors to form niobia species while the geminal hydroxyls are relatively unreactive.[103] Busca et al.[179] have demonstrated that anatase $TiO_2$, such as is used in this work, exhibits a single hydroxyl species (TiOH). MgO exhibits at least two kinds of surface hydroxyls.[180]

The metal oxides supports investigated in this work were subjected to thermogravimetric analysis using a TA Instruments Thermal Analyst 2100 in order to ascertain the effect of temperature on solid state transitions. The samples were allowed to equilibrate at 50°C within the sample cell and were then heated from 50 to 700°C at 20°C/min in helium environment. The results are illustrated in the Figures 4-1 through 4-7, which show the sample masses as functions of temperature.

The $\gamma$-$Al_2O_3$ supports exhibited similar TGA scans. About 1% of the mass was lost at a relatively low temperature (less than 200°C) due to the desorption of physically adsorbed water. Roughly another 1% of the original sample mass is lost very gradually as the sample is heated from 200 to 500°C by the removal of chemisorbed water (dehydroxylation). The abrupt loss of mass beyond 500°C is observed only in the $\gamma$-$Al_2O_3$ TGA scan. The corundum and anatase $TiO_2$ lost a very small percentage of their total mass, 0.80 and 0.35% respectively, in a gradual manner presumably due to dehydroxylation, as the samples were heated from 50 to 700°C. No discrete structural changes were evident in their TGA scans.

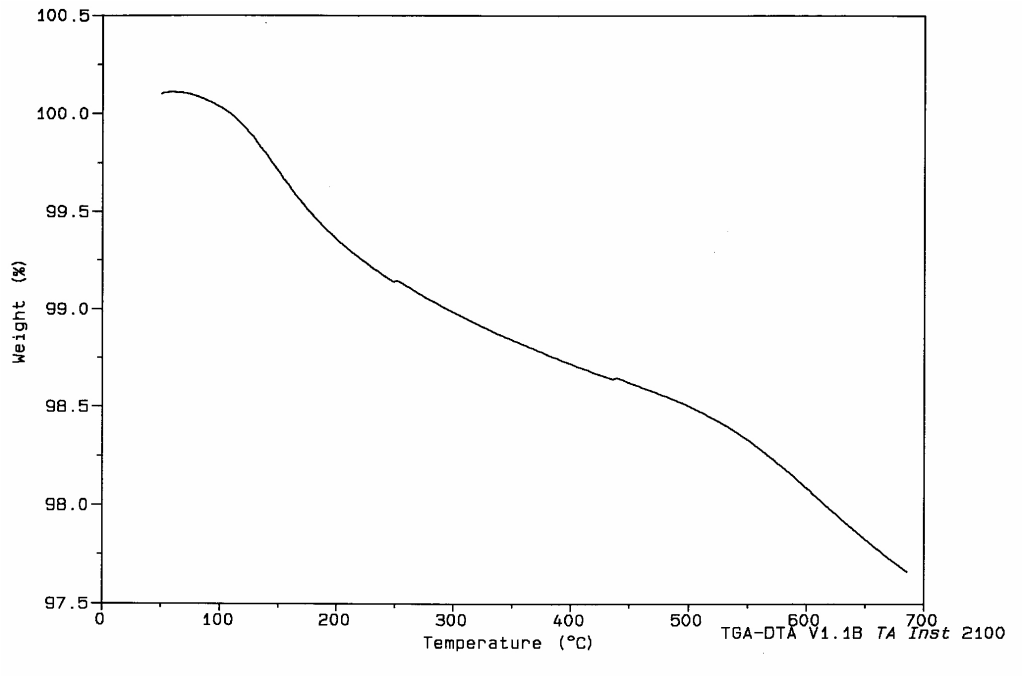


**Figure 4-1** TGA analysis of $\gamma$-$Al_2O_3$ (weakly acidic) support

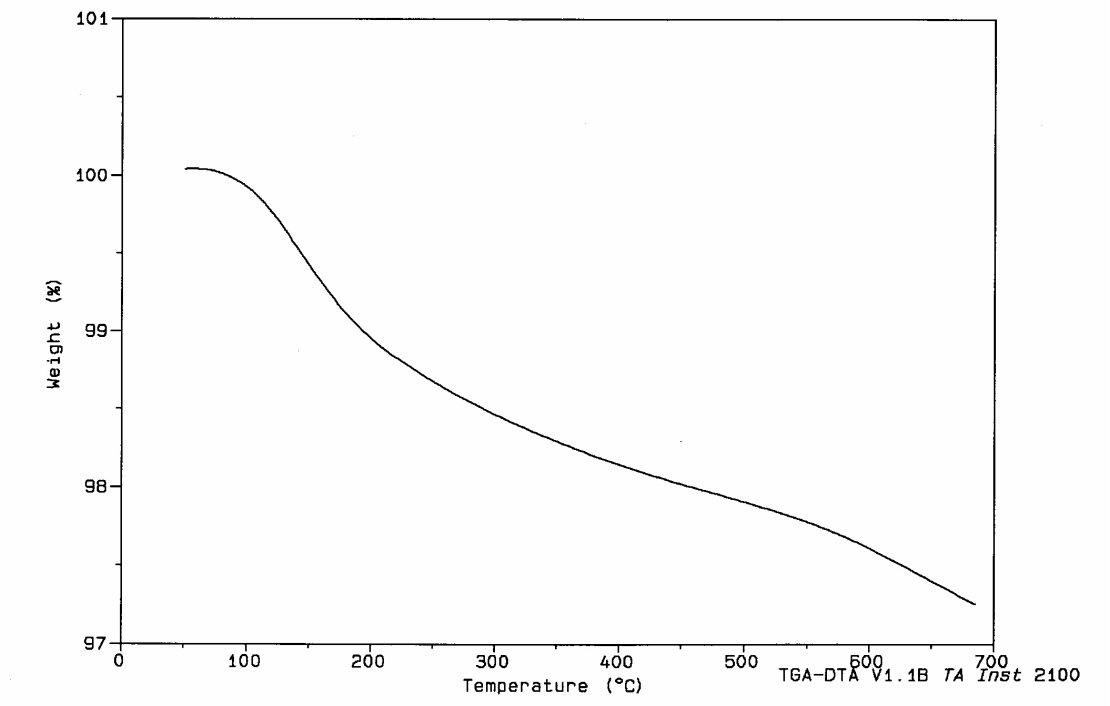


**Figure 4-2** TGA analysis of $\gamma$-$Al_2O_3$ (basic) support

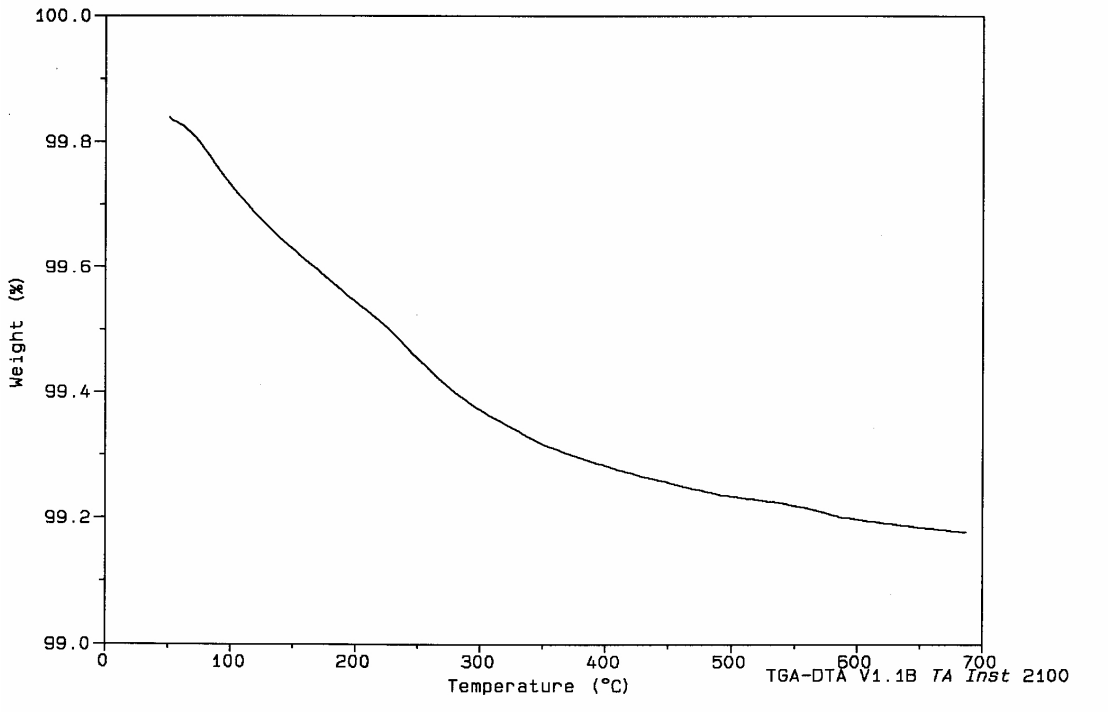


**Figure 4-3** TGA Analysis of corundum support

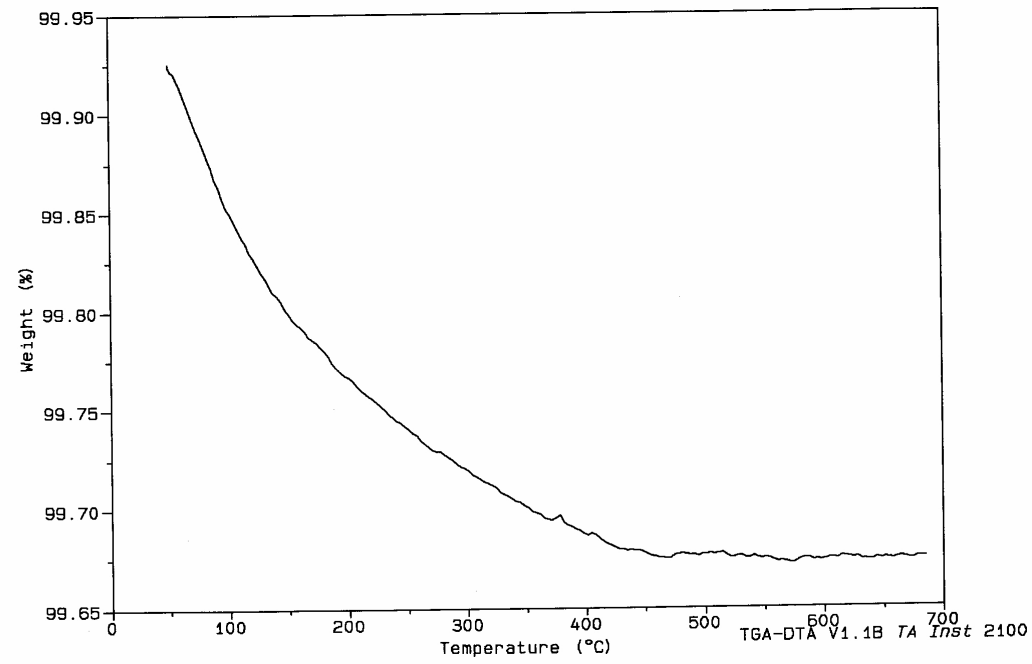


**Figure 4-4** TGA Analysis of the Anatase $TiO_2$ support

In contrast the fumed $SiO_2$ and MgO TGA scans revealed marked changes in the sample mass within specific temperature ranges. In both cases, significant losses in the sample masses at around 100°C were observed, which were due to the desorption of physisorbed water. The sample masses also dropped abruptly between 200 and 350°C. This structural change is attributed to the desorption of chemisorbed water (i.e. dehydroxylation). In the case of $SiO_2$, no other significant structural change was observed beyond this transition as evidenced by a negligible loss of sample mass beyond 350°C. In the case of MgO, the sample mass continued to decrease gradually as the temperature was increased.

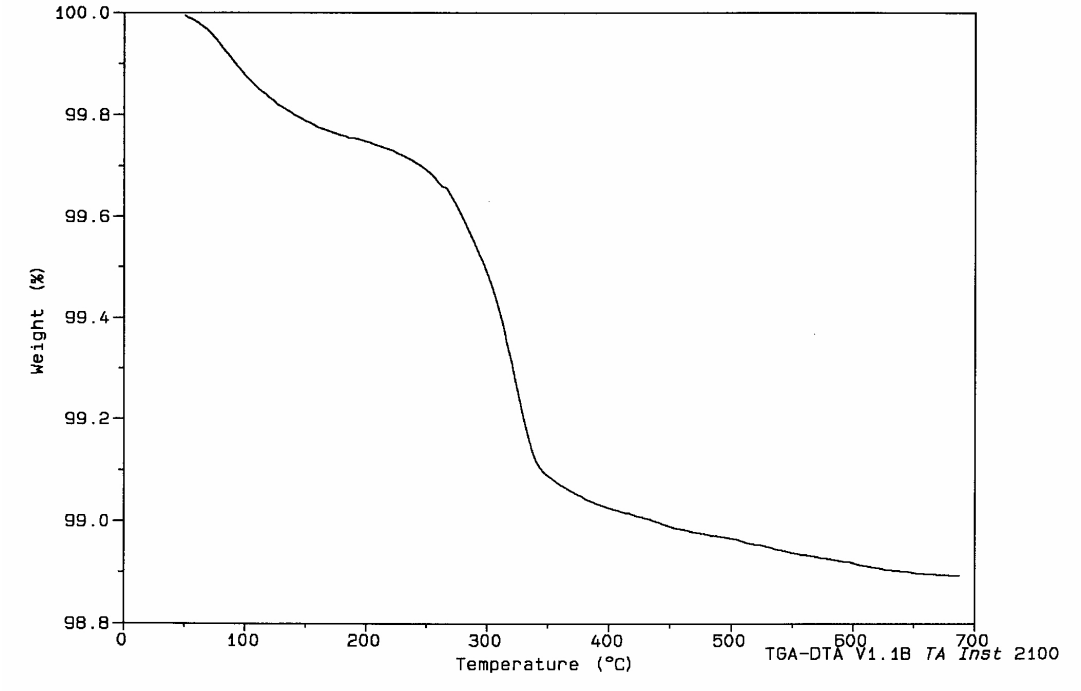


**Figure 4-5** TGA Analysis of the MgO Support

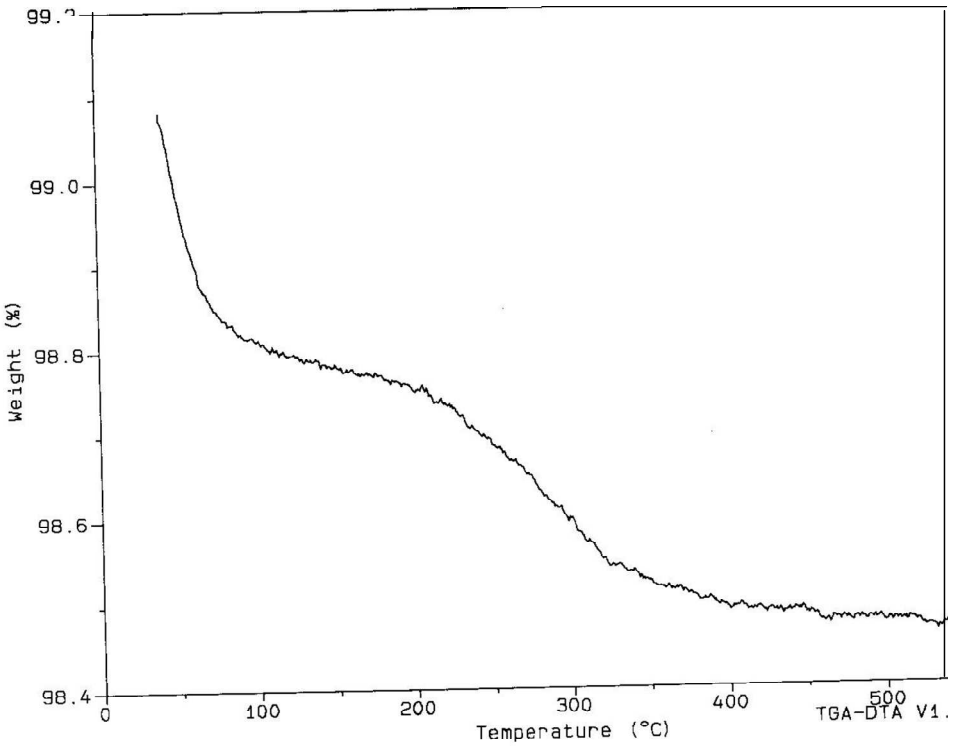


**Figure 4-6** TGA analysis of the fumed silica support

A few conclusions may be drawn from the TGA scans presented in the previous figures. First, the total loss of mass from the thermal treatment is small, even for $\gamma$-$Al_2O_3$, which exhibited the greatest reduction by about 2% of its total mass due to water. $TiO_2$ exhibited the least reduction in mass; about 0.35 wt%. Since the loss in sample mass is largely due to adsorbed water, one may infer that the corundum and Anatase $TiO_2$ supports exhibit significantly lower surface hydroxyl concentrations. It appears that with the exception of $SiO_2$ and MgO, dehydroxylation appears to be a gradual structural transition that occurs over a broad range of temperature. In alumina this may be due to the many forms of surface hydroxyls within the surface structure, which may exhibit various activation energies for dehydroxylation.

## 4.2 Sample Autoclave Data and Analysis

### *4.2.1 Sample Product Distribution*

The experiments discussed in this chapter involve the synthesis of MO from acetone at 160°C. Representative product distributions for this reaction, which are dependent on the catalyst formulation and the reaction temperature, are illustrated in Figures 4-7 and 4-8. As expected, water and MO are the major products and their concentrations are plotted on the primary y axis of Figures 4-7 and 4-8. The other products are minor constituents and their concentration profiles are plotted on the secondary y axes of Figures 4-7 and 4-8 with a different concentration scale. The steady state DAA concentration establishes rapidly (Figure 4-7), typically by the time the first sample is obtained. However the overall reaction to produce MO is slow and takes several hours to reach the equilibrium conversion.

Other minor products due to consecutive reactions involving MO become evident after some time. The most abundant of the minor products is IMO. However, the author and coworkers[18] have demonstrated that IMO is equally valuable as MO as a precursor for MIBK and is therefore a desirable product. Phorone, which is co-produced with water from the condensation reaction of MO with acetone, is the most dominant of the undesirable products at 160°C. In the experimental results outlined in Figure 4-8, the steady state DAA concentration is below the peak area rejection limit of the GC. In this case, DAA is rapidly converted to MO and may be considered a short-lived intermediate. The experimental results of Figure 4-8 also indicate the presence of mesitylene, also known as trimethyl benzene (TMB), which is co-produced with water from the internal 2-7 aldol condensation of phorone.

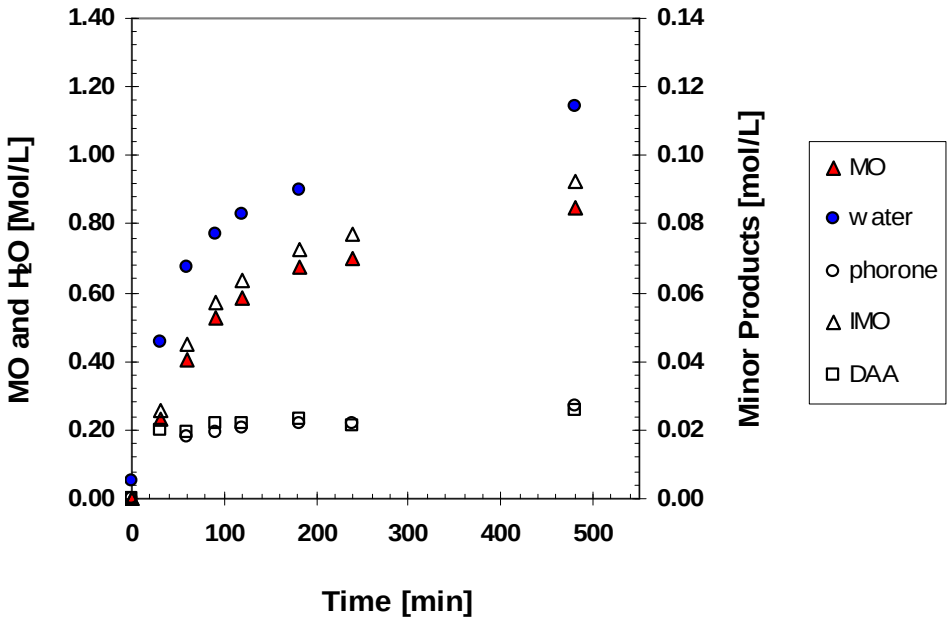


**Figure 4-7** Sample product distribution from the synthesis of MO from acetone [Experiment 141; T=160°C, P≥400 psig ($N_2$), ω= 700RPM, W=1.0084 g, CAT 015, 18.8 wt% $Nb_2O_5/\gamma$-$Al_2O_3$ (basic)] *Outlier in water concentration profile at t=240 minutes removed from plot. The minor products in Figures 4-7 and 4-8 include phorone, TMB and IMO*

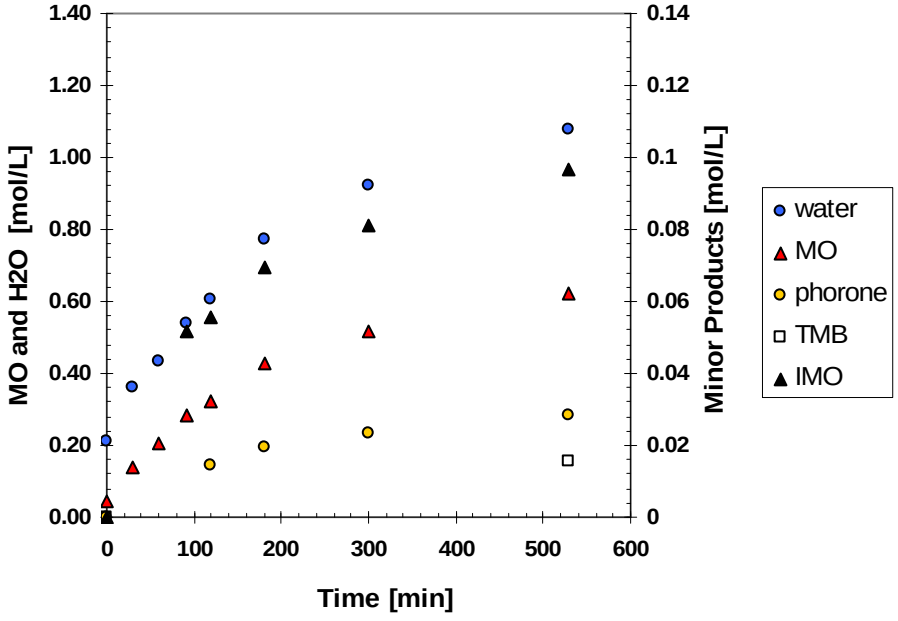


**Figure 4-8** Sample product distribution from the synthesis of MO from acetone [Experiment 184; T=160°C, P≥ 360 psig ($N_2$), ω= 700RPM, W=1.0042 g, CAT 044: 7.63 wt% $Nb_2O_5$/ $SiO_2$]

Phorone appears to have reached its steady state concentration at the time that mesitylene appears in the product mixture. An interesting observation is that isophorone, the cyclic isomer of phorone, was not observed in any of the autoclave experiments for which niobia catalysts were used. However, isophorone was observed at comparable acetone conversions for autoclave experiments in which Amberlyst-15 was used as a catalyst even though the reaction temperature was much lower. In the case of the niobia catalysts investigated in this work, the aldol condensation of phorone to produce mesitylene appears to be the dominant reaction pathway. Perhaps this is related to the pore size distributions and other morphological properties of the catalysts as suggested by Flego and Perego.[129] That is, constraining the substrates within the pore channels of the ion exchange resin may promote the synthesis of isophorone. The nature and strength of the acid sites likely affects the selectivity of this reaction.

The theoretical equilibrium conversion can be estimated from the relation in Equation (2-15) published by Klein and Banchero,[10] which relates the equilibrium constant ($K_c$) to the concentrations of water ($C_W$), MO ($C_{MO}$) and acetone $C_{AC}$. At 160°C this relation predicts an equilibrium MO concentration of 1.29 M, which corresponds to an acetone conversion of 19.0%. Projections of the MO concentration versus time profiles in the sample data of Figures 4-7 and 4-8 suggest that pseudo equilibria (section 2.3.4) are obtained. The MO concentration versus time profile presented in Figures 4-7 and 4-8 suggests an equilibrium concentration much lower than the theoretical equilibrium conversion.

In this work, the final pseudo equilibrium achieved based on the MO concentration profile was found to be dependent on the catalyst formulation, which supports the notion that the pseudo equilibrium is due to deactivation. Note the MO concentration versus time profiles in Figures 4-7 and 4-8 exhibit different final “equilibrium” MO concentrations for these two experiments.

However, the projection of the water concentration versus time profiles in Figures 4-7 and 4-8 suggest that the water concentration profiles do appear to approach the expected values. The rate of water production appears to exceed the rate of MO production as expected since consecutive aldol condensation reactions involving higher molecular weight species are significant and contributing to the total rate of water production.

A mass balance on the data in Figures 4-7 and 4-8 after 8 hours of operation suggests, that if one considers all of the reactions which produce water not only DAA dehydration and also consider the amount of residual water present in the solvent, that the number of moles of water observed was in reasonably good agreement with the amount of water predicted from the stoichiometry. In experiment #141 the average relative error between the predicted and observed was about 7%. The amount of water present after 8 hours of operation was slightly less than the amount predicted by 5.2 % after 8 hours. In experiment #184, there was initially a significant disagreement by about 30% between the amount of water predicted versus the amount observed within the first two hours of operation. However, after two hours of experiment, higher molecular weight species appeared above the peak area rejection limit of the GC and consequently, the amount of water predicted fell into good agreement with that observed, once the contributions of these reactions to the total water concentration was accounted for. After 8 hours of operation, the amount of water present exceeded the amount expected by only 7.5%. The average relative error was only 8.6% between the predicted versus observed water concentration for the data after two hours of operation in experiment 184.

### *4.2.2 Identification of Unknowns via GC/MS*

Some minor unknown compounds were frequently observed in the product distributions for MO and MIBK syntheses experiments. The overhead distillate samples from a CD experiment (Chapter Eight) provided an opportunity to

precisely ascertain the constituents two frequently observed unidentified peaks in the GC/FID analysis corresponding to retention times of 1.93 and 2.25 minutes. Although the retention time of 2.25 minutes is very close to that assigned to DIPE, the chemistry and process conditions for which this compound was detected suggested that the compound was not DIPE. DIPE is produced from the condensation of IPA, which is a secondary hydrogenation product. However, the impurity at 2.25 min was observed frequently in experiments in the absence of hydrogen and was also observed in the absence of the precursor IPA. These unknowns were believed to be non-polar and or volatile compounds such as coke precursors (Fig 1-1), as evidenced by their relatively short retention times within the highly polar DB-WAX column.

These unknowns were fortuitously isolated in several overhead distillate samples along with acetone and water. For example, an overhead distillate sample (sample 047D) obtained at 47 hours time on stream (TOS) in the fifth CD experiment of this study, contained the unknown observed at 2.25 minutes and the remainder was acetone and water. Similarly, a sample from the same experiment obtained at 119 hrs TOS (sample 119D) contained the unknown at 1.93 minutes and the bulk consisted of acetone and water. Other overhead distillate samples (eg. 085D) contained both unknowns.

The three overhead distillate samples mentioned above were analyzed by GC/MS in order to identify these unknowns using a Varian CP-3800 GC equipped with an HP-5 capillary column coupled with a Saturn 2000 Mass Spectrometer. The carrier gas (He) was passed through the column at 1.5 mL/min and the sample was injected with a split ratio of 100:1. Since the samples being analyzed were likely volatile, the oven profile consisted of an isothermal plateau of 40°C maintained for 20 minutes. The mass spectrometer was operated in electron impact (EI) mode with the trap set to 150°C, the manifold heated to 100°C and the transfer line heated to 170°C. Acetone was

determined to elute around 1.4 minutes. A three second interval from 1.38 to 1.43 minutes was cut from the MS analysis to prevent saturating the detector. The chromatographic separation of sample 119D resulted in a single GC peak. However, sample 047D revealed three distinct peaks which suggest the single peak observed in the GC/FID analysis at 2.25 minutes actually corresponds to multiple products. The 7 point average mass spectrum of the constituents of each chromatographic peak were obtained and cross referenced with the NIST library of mass spectra. The results in Table 4-2 suggest the most likely identities of these species. The results also include a "RSIM" value, which is a measure of how well the obtained spectrum matches the referenced spectrum with 999 being a perfect match. Adachour et al.[181] have advised that a similarity greater than 800 or a reverse similarity greater than 900 indicates a good match to the NIST library. Also included in Table 4-2 are probability values, which are also indicators of the quality of spectral matches. A more comprehensive set of the GC/MS results is included in Appendix C.

The results of sample 119D, which contained a single peak corresponding to the unknown observed at 1.93 min in the GC/FID analysis suggests the unknown is 2,4 dimethyl heptane ($C_9$). This result appears to be a good spectral match and is also reasonable from the process chemistry (Fig 1-1). $C_9$ hydrocarbons are coking compounds which produced from the consecutive reactions involving mesitylene and isophorone. Sample 085 D contained both impurities at 1.93 and 2.25 minutes. GC/MS analysis of this sample (Appendix C) confirmed that the impurity at 1.93 is likely a $C_9$ hydrocarbon. However in this case, the mass spectra of the largest peak most closely matched an isomer of 2,4-dimethyl heptane, namely 2,3,3-trimethly hexane. Incidentally, the precise identification of hydrocarbons via GC/MS is quite difficult, in part due to the possibility of numerous isomers associated with branching. Low probability values are frequently associated with the mass spectra of alkanes and alkenes since there are many spectra in the NIST library similar to any given spectrum for an alkane or alkene.[181] Therefore, the low probability

values observed in the results of Table 4-2 are not unexpected. Sample 047D contained a single unknown peak in the GC/FID analysis at 2.25 minutes and yielded 3 distinct peaks using the HP-5 column. The major peak showed a very good spectral match with a $C_9$ alkene, 2,3,3-trimethyl-1-hexene, which is also quite reasonable from the process chemistry. One minor peaks suggests the presence of 2-cyclopropyl-pentane ($C_8H_{16}$) and the other minor peak gives a very good match with the isomer (1,2-dimethylpropyl) cyclopropane ($C_8H_{16}$).

The product identification results of the GC/MS analysis consistently point to $C_9$ alkenes and alkanes, which is quite reasonable from the process chemistry. Although the assignments of these unknowns may be considered a "best guess", it can be concluded with great certainty that the unknown peak at 1.93 minutes in the GC/FID analysis is associated with a $C_9$ hydrocarbon, probably an alkane and the peak at 2.25 minutes is associated with $C_8$ hydrocarbons and predominantly a $C_9$ alkene . Consequently, the GC peaks at 1.93 and 2.25 will be henceforth lumped together and reported as $C_7^+$. As a first approximation, the response factor for phorone ($C_9H_{14}O$) was used for the quantification of these minor products via GC/FID.

**Table 4-2 (a)** Results of GC/MS analysis of sample 119D (one peak)

| **119D** | one major peak | | |
|---|---|---|---|
| **Rank** | **Species** | **RSIM** | **Prob** |
| 1 | 2,4-dimethyl heptane | 867 | 47.66 |
| 2 | 3-ethyl hexane | 807 | 10.15 |
| 3 | 2,3,5-trimethyl hexane | 760 | 8.18 |
| 4 | 4,4-dimethyl heptane | 814 | 3.45 |
| 5 | 2,3-dimethyl heptane | 747 | 2.78 |

**Table 4-2 (b)** Results of GC/MS analysis of Sample 047D (major peak)

| **47D** | peak (3/3) major peak | | |
|---|---|---|---|
| **Rank** | **Species** | **RSIM** | **Prob** |
| 1 | 2,3,3-trimethyl-1-hexene | 802 | 22.29 |
| 2 | 1,2,3,4,5-pentamethyl cyclopentane | 727 | 17.97 |
| 3 | 1,1'bicyclopentyl-2-one | 711 | 14.48 |
| 4 | 1,2-dimethyl propyl cyclopropane | 719 | 8.77 |

*4.2.3 Calculation of the Initial Rate of Reaction*

The initial specific rates or reaction (mol/L*min*$g_{cat}$), corresponding to acetone conversions of X=0, were measured and used to contrast the nominal activities of the various catalysts investigated in this study. The GC data for the MO concentration (C) [mol/L], not including the isomer MO, as a function of time (t) were fit to a second order polynomial expression (Eqn. 4-2) for the first 120 minutes of reaction as illustrated in Figure 4-4. The parameters were estimated via non-linear regression using NLREG v5.4 (Sherrod Software). The rate of reaction as a function of time is obtained from the first derivative (Eqn 4-2) of the concentration versus time profile. The specific reaction rate was calculated by dividing the reaction rate by the catalyst mass. The initial rate is calculated from equation (4-3) by setting t equal to the time at which the acetone conversion was zero.

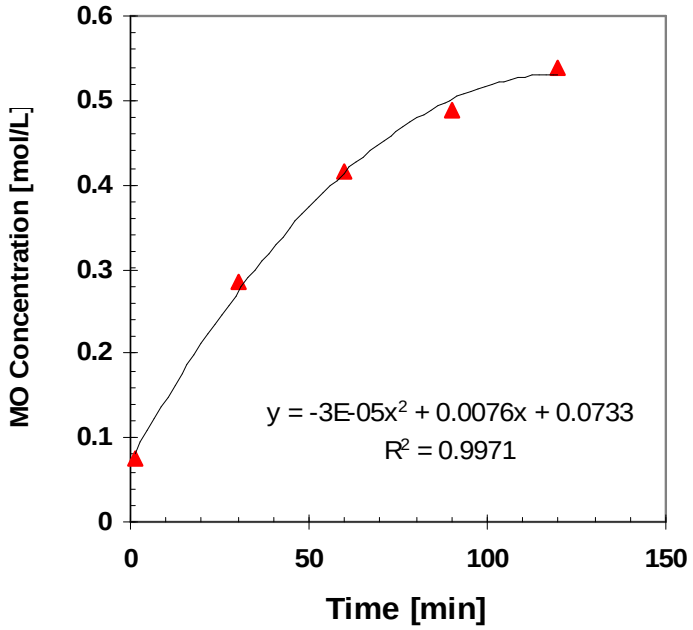


**Figure 4-9** Sample data: MO concentration modelled by a second order polynomial function of time [Experiment 162; T=160°C, P≥350 psig ($N_2$), ω=700 RPM, Catalyst 030: W=0.9979 g]

$$C(t) = k_0 + k_1 t + k_2 t^2 \quad (4\text{-}2)$$

$$\frac{dC}{dt} = k_1 + 2k_2 t \quad (4\text{-}3)$$

Initial Rate Data Reconciliation

Each autoclave experiment began with a brief period of unsteady operation during which, acetone was being converted to MO. The catalyst was mixed with acetone, the reactor was sealed and pressurized and then heated to the desired reaction temperature. The time at which the reactor reached the reaction temperature was denoted time zero. The first liquid sample was obtained at this time. For many experiments, including the ones illustrated in Figures 4-7 and 4-8, some MO was observed in the sample obtained at time zero and thus, the acetone conversion was non-zero. In order to obtain a meaningful comparison of the nominal activities of the catalysts investigated, the initial rates were calculated for a common acetone conversion of $X_{Ac}$=0.

For those experiments for which product was evident at time zero, the regression model fit to the steady state kinetic data obtained over the first 120 minutes was extrapolated back to the time at which the MO concentration would be zero if the reactor was operating at steady state prior to time zero. The root was determined iteratively using Newton's method (Table 4-3) and the initial rate of reaction was calculated from the derivative of the concentration profile that point using Eqn. (4-3). For those experiments for which MO was not observed at time zero, (i.e. MO was below the peak area rejection limit of the GC) the acetone conversion and the MO concentration were assumed to be zero at time zero.

The calculation in Table 4-3 illustrates that Newton's method rapidly converges to the root within a few iterations. The data in Table 4-2 is for a highly active catalyst and consequently represents a more extreme case in that X=0 corresponds to about 9 minutes prior to time zero. In most experiments,

X=0 was found within 5 minutes of time zero. The data in Table 4-2 also shows that the activity at time zero for experiment 162 was about 93% of the initial activity estimated at X=0. Thus if the rate of reaction at time zero were reported as the initial rate of reaction, the initial activity of the catalyst would have been underestimated by about 7%.

**Table 4-3** Sample data: Determination of the initial rate of reaction, $C'(t_{|X=0})$, using Newton's Method [Experiment 162, T=160°C, P≥350 psig ($N_2$),ω=700 RPM, Catalyst 030, W=0.9979 g]

| $t_{\|X=0}$ [min] | $C(t_{\|X=0})$ [mol/L] | $C'(t_{\|X=0})$ [mol/L*min] | next guess $t_0$ [min] | error [min] |
|---|---|---|---|---|
| 0 | 7.33E-02 | 0.00755910 | -9.69243 | 9.69243 |
| -9.6924 | -2.93E-03 | 0.00816357 | -9.33360 | -0.35884 |
| -9.3336 | -4.02E-06 | 0.00814119 | -9.33310 | -0.00049 |
| -9.3331 | -7.59E-12 | 0.00814116 | -9.33310 | -9.3E-10 |
| -9.3331 | 8.67E-19 | 0.00814116 | -9.33310 | 0 |
| -9.3331 | 8.67E-19 | 0.00814116 | -9.33310 | 0 |

Inflection Points and Higher Order Polynomials

Some authors have fit concentration versus time profiles to third order polynomials. Although this will invariably lead to higher coefficients of correlation, it does not necessarily improve the accuracy of the estimate of the initial rate of reaction. In fact, there is a danger in this approach. For a meaningful result, the product concentration versus time profile must be concave down in the absence of an autocatalytic reaction or induction period. When fitting the MO concentration versus time data to a second order polynomial, the curve is necessarily concave down. However, if a third order polynomial is used, the additional degree of freedom enables the possibility of an inflection point in the regression model within the region of interest, which could cause the curve to be concave up at the initial condition. As a result, the initial rate of reaction may be significantly underestimated.

In this study, the MO concentration versus time profiles was fit to both second and third order polynomials. In most experiments, an inflection point was not observed and very good agreement was found between the initial rates

of reaction predicted by the second and third order polynomials. However in a few experiments, slight variation in the data, due to uncertainty in measurement, yielded an inflection point within the region of interest, which caused the initial rate of reaction to be underestimated. Therefore, to ensure accuracy and consistency, the initial rates of reaction reported herein were calculated from concentration versus time data modelled to second order polynomials only.

Assessment of Outliers

Variance is inherent in all experimental data and with any analytical method, anomalous results are periodically obtained. The estimate of the initial rate of reaction obtained from nonlinear regression analysis can be significantly affected by outliers that are not representative of the kinetics being measured. In this work, an objective and strictly mathematical criterion was used to identify and reject outliers from the data set prior to the estimate of the initial rate of reaction. Only those observations which could be rejected as outliers at the 99% confidence interval were removed from the data set prior to the calculation of the initial rate of reaction.

If a set of data is normally distributed, then 95% of the data will fall within ± 2 standard deviation of the mean and 99% of the data will fall within ± 3 standard deviation of the mean. Therefore, an observation found more than 2 standard deviation from the mean can be rejected at the 95% confidence level as an outlier (i.e. it does not belong to the sample population). Similarly, if an observation is found more than 3 standard error from the mean, it can be rejected as an outlier at the 99% confidence level. Cobb[182] has advised that if the residuals for a regression model are normally distributed, then an observation should be rejected as an outlier if its residual is more than 3 times the standard deviation from zero. Consequently, in this work, those observations whose residual error were greater than 3 times the standard error of estimate for the regression model (developed excluding the questionable observation) were rejected as outliers. Outliers meeting this strict objective

criterion were rare. For example, in the catalyst screening study reported in section 4.4 (Tables 4-5 and 4-6) only one outlier was rejected from the calculation of the specific initial rate of reaction from over 100 observations used in the calculation of initial rate of reaction based on this criterion.

Residual plots and normal probability plots of the residuals were created in order to aid in the identification and assessment of outliers. A normal probability plot is a graph of the observed residual versus the expected residual assuming a Gaussian distribution. If the data is normally distributed, the expected versus observed residuals will follow a linear trend (y=x). The normal probability plot of the residuals (Figure 4-10) for the second order polynomial fit to the MO concentration versus time profile of Figure 4-9 confirms that the residuals are normally distributed.

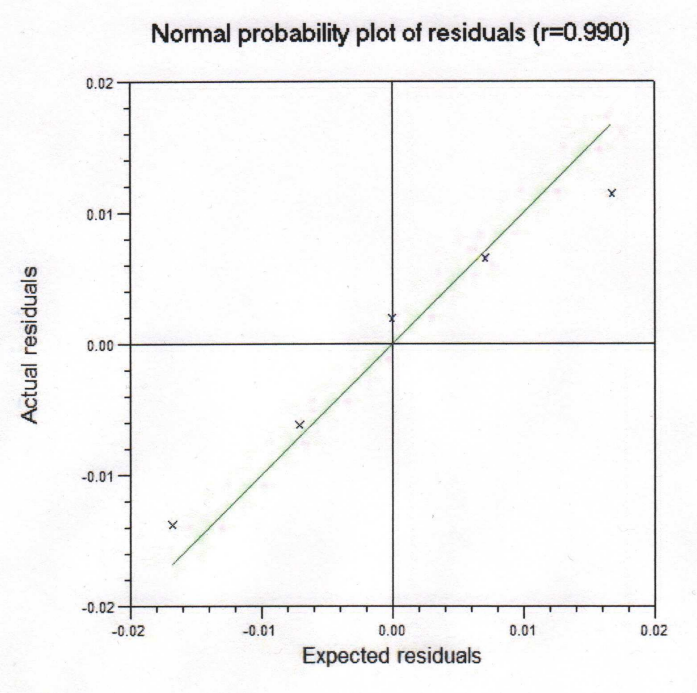


**Figure 4-10** Sample Data: Normal probability plot of the residuals generated by NLREG v. 5.4 (Sherrod Software) [Experiment 162]

Calculation of Acetone Conversion and Selectivity to MO

Acetone is necessarily the solvent in the one step synthesis of MIBK as well as for the synthesis of MO. Consequently, the GC peak corresponding to acetone is a solvent peak whose area is typically several orders of magnitude larger than the products. Rather than quantify the acetone from the integration of the solvent peak in the GC chromatogram, the acetone conversion was inferred from the mass balance of organic products evident in the GC analysis. The acetone conversions (%) for autoclave experiments were calculated from equation (4-4) where $N_{A0}$ denotes the number of moles of acetone initially charged to the reactor, $\nu_i$ denotes the stoichiometric coefficient of species "i" and $n_i$ denotes the number of moles of species "i" in the product.

$$X_{Ac} = 100\% \left( \frac{\Delta N_A}{N_{A0}} \right) = 100\% \left( \frac{\sum_i n_i / \nu_i}{N_{A0}} \right) \qquad (4\text{-}4)$$

The author and co-workers[18] have shown that IMO is equally valuable as MO as a precursor for MIBK, showing identical kinetic behaviour. Therefore, since IMO is also a desirable product, the isomers were lumped together when calculating the selectivity of the synthesis of MO. The selectivity to MO is defined in equation (4-5) where $n_{MO}$ and $n_{IMO}$ denote the number of moles of MO and IMO respectively in the product and $n_i$ denotes the number of moles an organic product, species "i", in the reactor product. Water was ignored in the calculation of selectivity as is the convention among researchers investigating MIBK synthesis.

$$S = 100\% \left( \frac{n_{MO} + n_{IMO}}{\sum_i n_i} \right) \qquad (4\text{-}5)$$

In some experiments unknown minor products were detected in the product in very low concentrations. In these cases, the mass fraction (wt%) of the unknown species were calculated by assuming that they exhibit the same GC response as phorone. Since the unknown compounds were typically at very low concentrations near the peak area rejection limit of the GC, this assumption did not introduce a significant relative error with respect to the quantification of the total product distribution. Therefore, in some cases, it was convenient to report the selectivity and acetone conversion based on mass fraction (wt%) rather than mol percent.

### 4.3 Preliminary Benchmarking of Supports and Amberlyst 15

Acidic cation exchange resins doped with Pd represent the state-of-the-art of catalysts for the one-step synthesis of MIBK since the early 1970's. However, cationic exchange resins deactivate rapidly at elevated reaction temperatures and are known to deactivate when exposed to water. A motivation for the use of metal oxides for MIBK synthesis is that these refractory materials provide improved thermal stability, which may enable a chemistry that is more favourable for the synthesis of the precursor MO.

Amberlyst 15 is strongly acidic macroreticular cation exchange resin commercially available from Rohm and Haas and has a maximum recommended operating temperature of 120°C. The activity and selectivity of Amberlyst 15 for MO synthesis was investigated in an autoclave at 120°C. Since this experimental condition represents the performance of a state-of-the art catalyst at its maximum operating temperature, the results of this experiment will serve as a benchmark against which the performance of catalysts investigated in this work will be gauged.

The concentration versus time profiles for the major and minor products are illustrated in Figures 4-11 and 4-12 respectively. The major organic products are MO and DAA. The DAA concentration in the product is

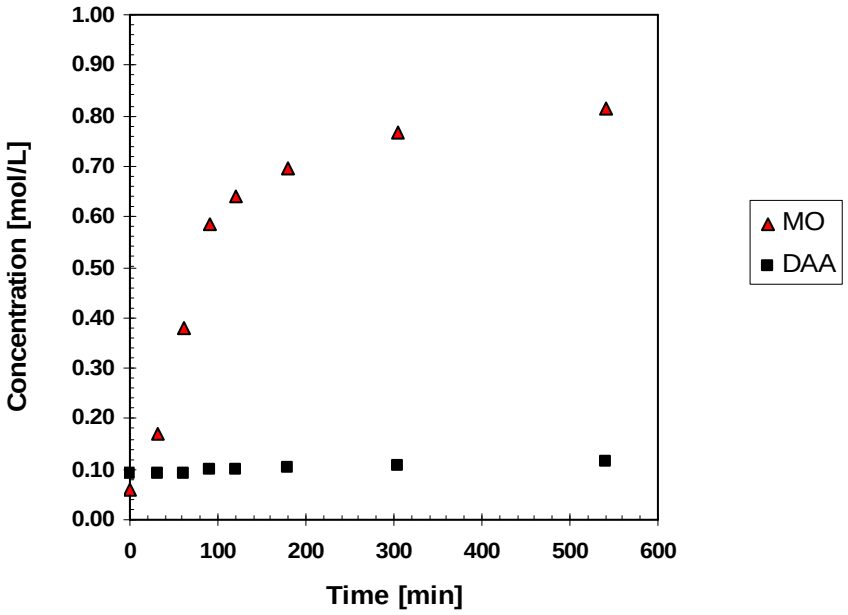


**Figure 4-11** MO and DAA concentration versus time profiles for Experiment #170 using Amberlyst 15 [Expt. 170, T=120°C, P≥ 320 psig ($N_2$), ω=700 RPM, W=1.12 g Amberlyst 15]

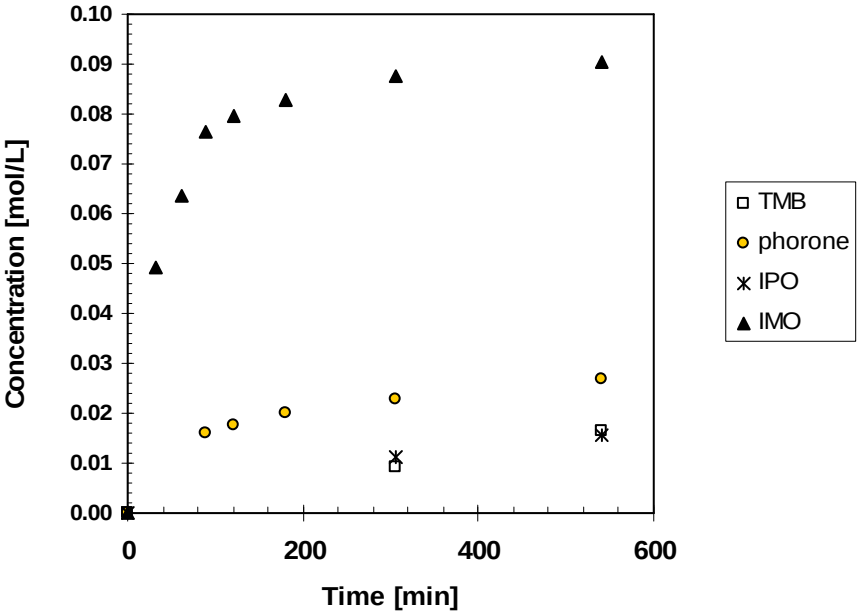


**Figure 4-12** Concentration versus time profiles for the minor products of Experiment #170 using Amberlyst 15 [Expt. 170, T=120°C, P≥ 320 psig ($N_2$), ω=700 RPM, W=1.12 g Amberlyst 15]

significant in this case because of the relatively low reaction temperature. The phorone and mesitylene concentration versus time profile for the minor products (Figure 4-12) are similar to the results in Figure 4-8. However, isophorone is present in the last two samples for the experiment in which Amberlyst 15 was used. In contrast, isophorone was notably absent in the product for all autoclave experiments in which niobia compounds were studied in this work. The MO concentration in Figure 4-12 increased rapidly over the first two hours of operation, after which the rate of reaction decreased significantly as the equilibrium was approached.

The initial rate of reaction for the synthesis of MO from acetone using Amberlyst 15 at 120°C is given in Table 4-4 along with the nominal activities of some other metal oxides used in this study as supports. The strongly basic γ-$Al_2O_3$ support showed a catalytic performance at 160°C (Figure 4-13) comparable to that of the commercial catalyst Amberlyst 15 at its maximum temperature. The weakly acidic alumina support also showed a significant catalytic activity for MO synthesis. Consequently, γ-$Al_2O_3$ must be regarded as a co-catalyst rather than strictly as a support in this investigation. Fumed $SiO_2$ was completely inert for MO synthesis. With $SiO_2$ as a catalyst, no MO was detected although some DAA was observed and appeared to remain constant at about 0.005 M. Bulk niobium (V) oxide showed negligible activity. Some MO was observed when the niobia was exposed to air prior to its use. However, the niobia appears to have lost its activity shortly after the reaction began. No products were observed for the reaction in which niobia calcined at 500°C was used as a catalyst.

The initial specific reaction rate (X=0) for MO synthesis at 160°C using the basic γ-$Al_2O_3$ support was 1.5 times that of Amberlyst 15 at its maximum operating temperature. However, the activity of the alumina support seemed to deactivate slightly whereas the Amberlyst 15 maintained a very high activity until the MO concentration approached its pseudo equilibrium value.

**Table 4-4** Nominal activities of some metal oxides and Amberlyst 15 for the synthesis of MO at 160°C

| Expt. I.D. | Description | Rxn. Temp. [°C] | Initial Rate [mol/L*min*$g_{cat}$] | Observations |
|---|---|---|---|---|
| 170 | Amberlyst-15 | 120 | 0.00575 | Isophorone in product |
| 167 | Fumed $SiO_2$ | 160 | 0 | Inert; No MO detected, some DAA present |
| 142 | γ-$Al_2O_3$ (basic) | 160 | 0.00871 | Active for MO synthesis |
| 168 | γ-$Al_2O_3$ (weakly acidic) | 160 | 0.00395 | Active for MO synthesis |
| 165 | Nb(V) Oxide not calcined | 160 | 0.000038 | Some MO present but catalyst appears to have deactivated rapidly |
| 166 | Nb(V) Oxide Calcined at 500°C for 2 hours | 160 | 0 | No product observed |

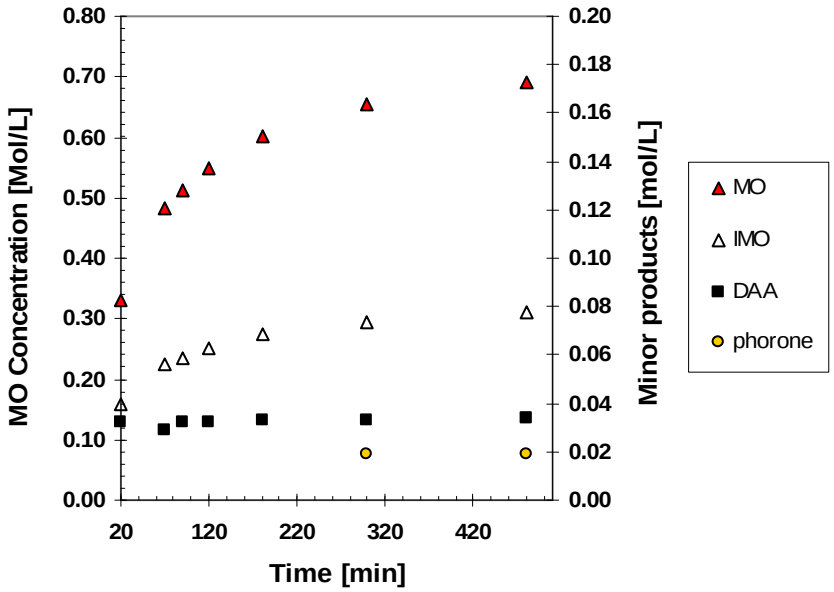


**Figure 4-13** Product distribution for MO synthesis at 160°C using strongly basic γ-$Al_2O_3$ as a catalyst [Experiment 142, T=160°C, W=0.98g, P≥400 psig ($N_2$), ω=700 RPM]

The basic $\gamma$-$Al_2O_3$ support was more selective for MO synthesis compared to Amberlyst 15. At an acetone conversion of 10%, the $\gamma$-$Al_2O_3$ support gave a selectivity to MO (and IMO) of 95.1 mol% while Amberlyst 15 gave a selectivity of 86.4 mol%. No isophorone or mesitylene was observed in the reaction mixture when the basic $\gamma$-$Al_2O_3$ support was used. In contrast, both of these undesirable higher molecular weight cyclic compounds were observed in significant amounts when Amberlyst 15 was used, even though the reaction temperature was much lower. Phorone was produced in a comparable amount for each experiment, however in a slightly greater rate when Amberlyst 15 was used. The relatively poor selectivity of Amberlyst 15 was largely due to the amount of DAA present in the product when carrying out MO synthesis at 120°C. The steady state DAA concentration for the experiment using the alumina support was about 1/3 of that for the experiment using Amberlyst 15. It is therefore evident that the higher reaction temperature is more favourable for DAA dehydration and enhances the selectivity to MO.

## 4.4 DoE #1: Catalyst Screening and Study on the Effect of the Nature of the Metal Oxide Support

### *4.4.1 Design of Experiment and Results*

A catalyst screening study was carried out in order to study the effects of the nature of the metal oxide support on the catalyst's nominal activity and selectivity for MO synthesis as well as the efficiency of utilization of the niobia. Promising catalyst supports identified in this screening experiment were investigated in greater detail in subsequent experiments. Since this was a screening study, many of the important catalyst parameters were kept constant as *noise variables*. Specifically, each catalyst was calcined for 2 hours at 500°C in air (Praxair, zero gas) at 3.8 mL/min and each support was impregnated with the same amount of Niobium (V) ethoxide precursor ($0.533 \pm 0.048$ mL-precursor/g-support). The niobia loading of the catalysts was determined by EDXRF spectroscopy. The impregnation time for each experiment was 2 hours

and was carried out at ambient temperature. The thermal decomposition reaction was carried out at 400°C for 2 hours in flowing nitrogen (Praxair, pre-purified) at 4.0 mL/min prior to calcination.

A calcination temperature of 500°C represents the maximum calcination temperature investigated in this work. 500°C was selected since it is known that Lewis acidity is maximized with increasing calcination temperature until the onset of crystallization above 500°C whereas Bronsted acidity, which represents a small fraction of the total acid sites, diminishes significantly at elevated calcination temperatures.[73] All niobia catalysts exhibit Lewis acidity but only alumina and silica supported niobia catalysts are known to exhibit Bronsted acidity.[91] A calcination temperature of 500°C was selected as a baseline since many authors investigating dispersed niobia catalyst have reported calcination temperatures of 500°C in their synthesis method.[42,69,70,87,89,90,91,93,99,100-103,107]

The two experimental variables investigated were the type of oxide support and the thermal pre-treatment temperature. In this screening experiment, the thermal pre-treatment temperatures for the $\gamma$ and $\alpha$ aluminas as well as magnesia supports were investigated at two levels. The effect of pre-treatment temperature on the silica support was investigated in a separate experiment (DoE #4 in section 4.7). The pre-treatment temperatures were selected based on the analyses of the TGA scans of Figures 4-1 through 4-6. The high level of pre-treatment temperature corresponded to a sufficiently high temperature to ensure the complete removal of chemisorbed water. In this condition, the surface coordinative unsaturation of the metal oxide support was maximized from the dehydroxylation of the surface. The high pre-treatment temperature also ensured activation of the support by the removal of strongly adsorbed species from oxide support prior to impregnation. The low pre-treatment temperature was determined from the TGA scans such that the support was activated at the minimum temperature necessary for the removal of

weakly adsorbed compounds without achieving a sufficiently high temperature that would result in the removal of chemisorbed water.

Approximately 1 gram of catalyst was accurately measured and charged to the autoclave reactor along with 100 mL of acetone. The synthesis of MO was carried out at 160°C for 8 hours with liquid samples being extracted periodically from the autoclave. The resultant MO concentration versus time profiles are outlined in two figures for clarity, Figures 4-14 and 4-15. The catalyst parameters for the experiment are outlined in Table 4-5. The response variables investigated in this experiment included the specific initial rate of reaction, the acetone conversion after 2 and 8 hours as well as the selectivity to MO and IMO at acetone conversions of 8 and 13%. The initial rate of reaction per gram of niobia is also given in Table 4-6. However, this value is not reported in the case of the $\gamma$-$Al_2O_3$ catalysts since the $\gamma$-$Al_2O_3$ support was shown to exhibit significant catalytic activity for MO synthesis and is therefore a co-catalyst.

Three experiments were repeated to confirm their results. Experiment 151 was a repeat of experiment 143 with a weakly acidic $\gamma$-$Al_2O_3$ supported catalyst. In this case, the initial rate of reaction for experiment 151 was within 6.0% of the initial rate for experiment 143. In addition, the MO concentration versus time profiles (Figure 4-15) showed good agreement. Experiment 137 was a repeat of experiment 136 involving a MgO supported niobia catalyst. The results of these experiments showed good agreement as well. However experiment 156, which is a repeat of experiment 138 involving a $TiO_2$ supported catalyst, was not in close agreement with the result of experiment 138. However, it did reveal a consistent trend in terms of catalytic activity and acetone conversion relative to other supports.

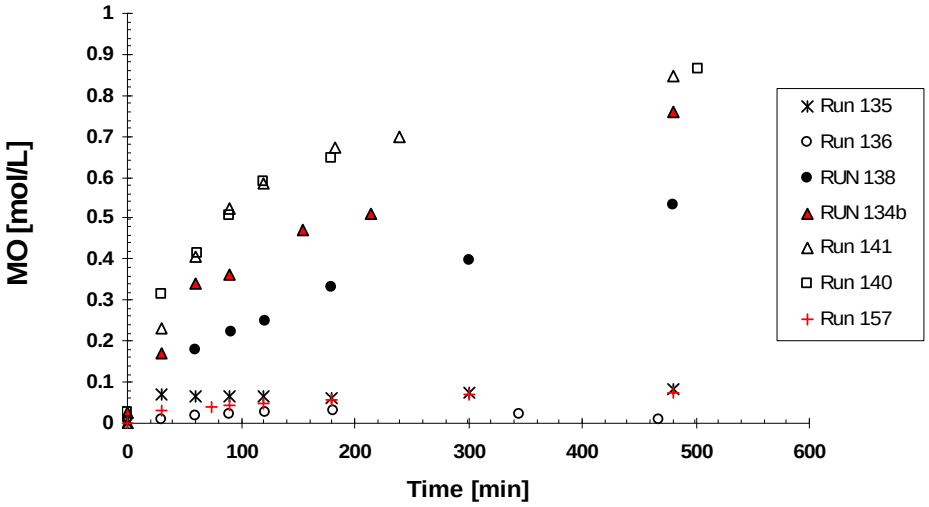


**Figure 4-14** MO concentration versus time profiles for experiments 135, 136, 138, 134b, 141, 140 and 157 *An outlier observed in RUN 140 at t=327 min was removed from the Figure*

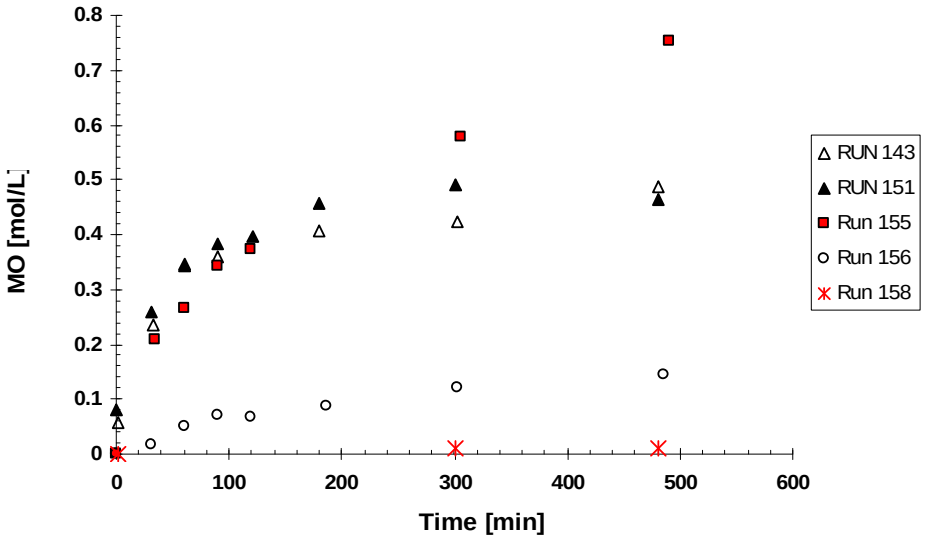


**Figure 4-15** MO concentration versus time profiles for experiments 143, 151, 155, 156 and 158 *An outlier observed in Run 155at t=180 minutes was removed from the Figure*

**Table 4-5** Catalyst parameters of the Catalyst screening investigation (DoE #1)

| Expt. ID | Catalyst ID | Support | Thermal Treatment [℃] | Precursor Amount [mL/g] | XRF $Nb_2O_5$ wt% |
|---|---|---|---|---|---|
| 135 | 010 | $\alpha$-$Al_2O_3$ | 450 | 0.503 | 4.2 |
| 157 | 024 | $\alpha$-$Al_2O_3$ | 250 | 0.542 | 4.3 |
| 155 | 021 | fumed $SiO_2$ | 250 | 0.548 | 26.5 |
| 140 | 014 | $\gamma$-$Al_2O_3$ (acidic) | 400 | 0.493 | 14.6 |
| 143 | 016 | $\gamma$-$Al_2O_3$ (acidic) | 250 | 0.555 | 12.0 |
| 151 | 018 | $\gamma$-$Al_2O_3$ (acidic) | 250 | 0.521 | 17.1 |
| 134b | 009 | $\gamma$-$Al_2O_3$ (basic) | 250 | 0.568 | 17.1 |
| 141 | 015 | $\gamma$-$Al_2O_3$ (basic) | 400 | 0.499 | 17.3 |
| 136 | 012 | MgO | 400 | 0.540 | 12.9 |
| 137 | 011 | MgO | 400 | 0.588 | 6.2 |
| 158 | 022 | MgO | 250 | 0.571 | 5.4 |
| 138 | 013 | $TiO_2$ | 400 | 0.504 | 11.8 |
| 156 | 023 | $TiO_2$ | 400 | 0.502 | 14.8 |

**Table 4-6** Results of the Catalyst Screening Experiment (DoE #1)

| Expt. ID | CAT ID | Initial Rate (MO synthesis) [mol/(L*min*$g_{cat}$)] | Initial Rate (MO synthesis) [mol/(L*min*g $Nb_2O_5$)] | Conversion (X) [%] | | Selectivity [mol %] | |
|---|---|---|---|---|---|---|---|
| | | | | 120 min | 480 min | X=8% | X=13% |
| 135 | 010 | n/a | n/a | 1.82 | 2.08 | | |
| 157 | 024 | 0.000777 | 0.0179 | 0.90 | 1.33 | | |
| 155 | 021 | 0.00615 | 0.0232 | 5.14 | 10.83 | 92.9 | |
| 140 | 014 | 0.00864 | n/a | 10.21 | 14.61 | 93.6 | 95.0 |
| 143 | 016 | 0.00642 | n/a | 7.34 | 8.23 | 96.5 | |
| 151 | 018 | 0.00681 | n/a | 7.15 | 8.54 | 95.7 | |
| 134b | 009 | 0.00617 | n/a | 7.52 | 13.61 | 91.8 | 93.8 |
| 141 | 015 | 0.00865 | n/a | 10.40 | 14.80 | 92.8 | 94.7 |
| 136 | 012 | 0.000639 | 0.00496 | 0.81 | 0.32 | | |
| 137 | 011 | 0.00000 | 0.00000 | 0.00 | 0.00 | | |
| 158 | 022 | 0.000047 | 0.000875 | 0.39 | 0.49 | | |
| 138 | 013 | 0.00369 | 0.0311 | 4.85 | 9.74 | 93.4 | |
| 156 | 023 | 0.00109 | 0.00735 | 1.34 | 2.56 | | |

*4.4.2 Effect of the Nature of the Oxide Support*

The results show that the nature of the oxide support for supported niobia catalysts calcined at 500°C had a significant effect on the catalytic activity. For example, a 12 wt% $Nb_2O_5/TiO_2$ catalyst (CAT 013 experiment 138) had six times the activity for MO synthesis and 6 times the acetone conversion after two hours compared to a 13 wt% $Nb_2O_5$/MgO catalyst (CAT 012 experiment 136),

which showed a very low activity and deactivated rapidly. The general trend of relative catalytic activity observed for MO synthesis by supported niobia catalysts was as follows $MgO << \alpha\text{-}Al_2O_3 < TiO_2 << SiO_2 \approx \gamma\text{-}Al_2O_3$.

The 17 wt% $Nb_2O_5/\gamma\text{-}Al_2O_3$ catalyst (CAT 015, experiment 141) whose basic support was calcined at 400°C showed essentially an identical MO concentration versus time profile as a 15 wt% $Nb_2O_5/\gamma\text{-}Al_2O_3$ (CAT 014, experiment 140) catalyst whose weakly acidic support was also calcined at 400°C. These catalysts gave essentially the same initial rate of reaction to within 1%. Thus, the acidity or basicity of the $\gamma\text{-}Al_2O_3$ support did not appreciably affect the catalytic activity. However, the surface area and morphological characteristics of the alumina support did have a significant effect on the resultant catalytic behaviour. The $Nb_2O_5/\alpha\text{-}Al_2O_3$ catalysts (experiments 135 and 157) showed very low activities for MO synthesis and deactivated rapidly after acetone conversions of only 1 and 2%. Both experiments with the corundum support achieved the same final MO concentration. The conversion was slightly higher in experiment 135 due to a larger quantity of unreacted DAA. The initial activity in experiment 135 could not be accurately measured since the reaction had already reached its final steady state concentration by the time the second sample was collected after 30 minutes of reaction.

The significant effect of the oxide support on the catalyst activity appears to be largely due to the capacity of the support to coordinate with the niobium ethoxide precursor and establish a highly dispersed monolayer of niobia. Each of the supports in the screening experiment outlined in Table 4-4 were impregnated with the same amount of precursor. However, the resultant niobia loading ranged from only 4.2% for $\alpha\text{-}Al_2O_3$ to 26.5% for fumed $SiO_2$. The niobia loadings for the 26.5 wt% $SiO_2$ (Sa=255 $m^2/g$) and 17.1 wt%. $\gamma\text{-}Al_2O_3$ ($S_a$=150 $m^2/g$) catalysts correspond to exactly 1.0 monolayer coverage in each case. Evidently, the amount of precursor was sufficient to saturate the support

with an adsorbed monolayer of niobium ethoxide, while the additional monolayers of physisorbed precursor were largely removed during the vacuum drying and the thermal treatment steps of the catalyst preparation. However, the titania, magnesia and corundum supports, which have an order of magnitude lower nominal surface areas, appear to have yielded niobia loadings which exceeded monolayer coverage. Thus, the acidic properties of the surface-phase oxide for these catalysts diminished as the morphology approached that of bulk niobium oxide.

The corundum, fumed silica and titania supported catalysts showed comparable specific initial reaction rates when normalized by the amount of dispersed niobia rather than by the total catalyst mass. However, the corundum catalysts deactivated rapidly after achieving acetone conversions of only around 1 to 2%. A comparison of the catalytic performances of theses supported niobia catalysts in Figure 4-14 and the BET surface area data in Table 4-7 demonstrate that surface area alone is not the sole factor which determines catalytic performance. Note that the 14.8 wt% $Nb_2O_5/TiO_2$ catalyst in Table 4-7 had a lower surface area (13 $m^2/g$) than the 4.3 wt% $Nb_2O_5/\alpha$-$Al_2O_3$ support ($S_a$=18 $m^2/g$) and a much lower surface area than the 16.7 wt% $Nb_2O_5/SiO_2$ catalyst ( $S_a$=190 $m^2/g$) and yet an 11.8 wt% $Nb_2O_5/TiO_2$ catalyst (013) , which would have a similar surface area, showed an activity comparable to a 26.5 wt% $SiO_2$ catalyst having a surface area an order of magnitude greater!

The $TiO_2$ (anatase) and $\alpha$-$Al_2O_3$ (corundum) supports had very similar surface areas. However, the $TiO_2$ support resulted in an uptake of about 3 times the amount of niobia compared to the $\alpha$-$Al_2O_3$ support. Moreover, the $TiO_2$ catalyst (013) in experiment 158 actually exhibited the most efficient use of niobia of all of the catalysts studied in Table 4-6 (with the exception of the gamma alumina co-catalysts for which this parameter is not meaningful) as evidenced by the greatest initial specific rate of reaction for MO production when normalized by the amount of niobia. This suggests the acid sites on the

anatase catalyst were more reactive or in a greater density than the other catalysts. This experiment also resulted in a relatively high acetone conversion (9.74 % after 8 hours) with excellent selectivity (93.4 mol % at X=8%). The relatively high activity, selectivity and stability of this catalyst are attributed to a strong metal support interaction due to the semiconductive properties of $TiO_2$ arising from its low band gap. It is interesting to note that the repeated experiment using the $TiO_2$ catalyst, which had a higher loading of niobia, resulted in a lower catalyst activity. This observation is consistent with the notion that unique acid sites are generated from dispersed niobia species and are diminished with increasing loading beyond monolayer coverage. Therefore, it would be of interest to investigate this $TiO_2$ catalyst at a lower niobia loading.

$Nb_2O_5$/MgO catalysts have been studied previously for the partial oxidation of methanol and were found to exhibit highly distorted $NbO_6$ structures with mono-oxo Nb=O bonds associated with Lewis acidity.[87] However, the MgO catalysts investigated in this work showed the lowest activity of the catalysts investigated and deactivated rapidly. In experiment 137, no product was observed using a 6.2 wt% $Nb_2O_5$/MgO catalyst. In experiment 136 the 13 wt% $Nb_2O_5$/MgO catalyst not only deactivated, but the reaction appears to have reversed after deactivation as evidenced by a decrease in the MO concentration to about 0.01 M after first reaching a maximum of about only 0.03 M (Appendix C). Clearly, $Nb_2O_5$/MgO is not suitable as a niobia catalyst support for the synthesis of MO. This result is consistent with the findings of Jehng and Wachs[87] who found that the Lewis acid sites of the niobia were more active when dispersed onto alumina and silica supports than on MgO. They suggested that the very strong acid-base interaction between the MgO and niobia might result in the incorporation of $Nb^{+5}$ into the lattice.[87]

*4.4.3 BET Surface Area Analysis of Select Catalysts*

The BET surface areas of some select catalysts were obtained using a Micromeritics Gemeni 2375 and are outlined in Table 4-7. The catalysts calcined at 100°C were de-gassed at 100°C in flowing nitrogen for 1 hour prior to analysis while the catalysts calcined at 500°C were de-gassed at 250°C for 1 hour prior to analysis. The BET measurements were repeated in triplicate for catalysts 029 and 031 in order to obtain an estimate of the instrument precision. The 95% confidence bounds on their estimates are given in Table 4-7. The results in Table 4-7 compared to the BET data for the supports in Table 4-1 show that the deposition of niobia onto the oxide support resulted in a slight loss of surface area for the high surface area $\gamma$-$Al_2O_3$ and particularly the fumed $SiO_2$ supports but resulted in a net increase in surface areas of the corundum, anatase and MgO supported catalysts. The calcination temperature did not appreciably affect the surface area of the catalysts with crystalline supports. However, the high calcination temperature (500°C) did appear to result in some loss of surface area in the amorphous $SiO_2$ catalysts, which did remain the highest surface area catalysts.

**Table 4-7** BET surface areas of select catalysts

| CATLAYST ID | DESCRIPTION | BET SURFACE AREA [$m^2/g$] |
|---|---|---|
| 029 | 16.7 wt% $Nb_2O_5/SiO_2$ calcined at 100°C | 197 $\pm$ 2 |
| 031 | 6.3 wt% $Nb_2O_5/\gamma$-$Al_2O_3$ calcined at 100°C | 111 $\pm$ 6 |
| 026 | 2.65 wt% $Nb_2O_5/\gamma$-$Al_2O_3$ calcined at 500°C | 143 |
| 028 | 5.82 wt% $Nb_2O_5/SiO_2$ calcined at 500°C | 153 |
| 022 | 5.41 wt% $Nb_2O_5$/MgO calcined at 500°C | 10 |
| 023 | 14.8 wt% $Nb_2O_5/TiO_2$ calcined at 500°C | 13 |
| 024 | 4.34 wt% $Nb_2O_5/\alpha$-$Al_2O_3$ calcined at 500°C | 19 |

*4.4.4 Effect of Thermal Pre-Treatment Temperature*

It is known that two-dimensional surface-phase niobium oxide monolayer may be synthesized on the outer most surface of a metal oxide support via the coordination of the niobium precursor with surface hydroxyl groups. The preferential titration of surface hydroxyl groups has been confirmed

experimentally by IR spectroscopic measurements.[91,103] Therefore the surface hydroxyl chemistry is an important factor which influences the assembly of niobium oxide surface structures.[68] The results of this experiment (DoE #1) suggest that the catalyst performance for MO synthesis benefited from activation of the support at high temperature, for which the surface coordinative unsaturation was maximized and the surface hydroxyl concentration was minimized.

A comparison of the initial rates of reaction obtained using catalysts consisting of niobia supported on basic $\gamma$-$Al_2O_3$ pre-treated at 250°C and 400°C (experiments 134b and 141 respectively) shows that the increase in thermal pre-treatment temperature of the support resulted in a 40% increase in the initial rate of reaction. A similar result was realized for the niobia supported on weakly acidic $\gamma$-$Al_2O_3$. The niobia catalyst supported on weakly acidic $\gamma$-$Al_2O_3$ pre-treated at 400°C had an initial rate of reaction about 30% higher than the average result for the niobia catalysts supported on weakly acidic $\gamma$-$Al_2O_3$ pre-treated at 250°C. The acetone conversion after 2 hours was consistently higher for those catalysts whose supports were pre-treated at 400°C (or 450°C in the case of $\alpha$-$Al_2O_3$) than the corresponding catalysts whose supports were activated at 250°C. The acetone conversion after 2 hours was about 40% higher for the $\gamma$-$Al_2O_3$ catalysts pre-treated at 400°C compared to the $\gamma$-$Al_2O_3$ pre-treated at 250°C.

The magnesia experiments were less conclusive due to the very low reaction rates and lack of repeatability between experiments 136 and 137. However, the preliminary results of the effect of thermal pre-treatment of the MgO support are consistent with the alumina catalysts in that the best result obtained involved an MgO catalyst whose support was pre-treated at the higher pre-treatment temperature (400°C). The MgO support pre-treated at 400°C (Cat 012) resulted in over double the uptake of niobia compared to the support activated at 250°C (Cat 011). The initial rate of reaction for the MgO catalyst

pre-treated at 400°C (experiment 136) was an order of magnitude greater than the rate of reaction for the MgO catalyst pre-treated at 250°C (experiment 158). The acetone conversion after two hours was about double for the MgO catalyst pre-treated at 400°C compared to the catalyst pre-treated at 250°C.

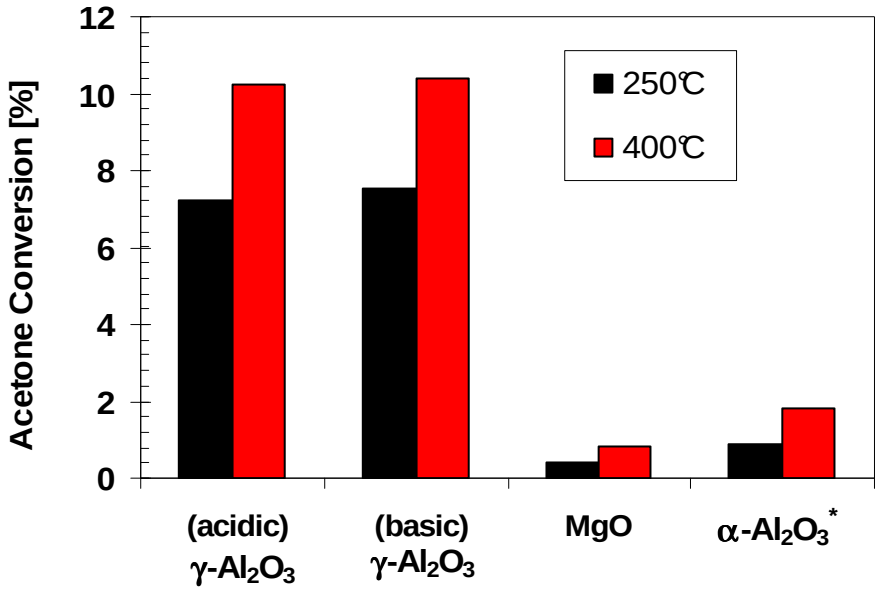


**Figure 4-16** Effect of thermal pre-treatment temperature of alumina and magnesia supports on the acetone conversion (%) after two hours *( *The α-$Al_2O_3$ support high pre-treatment temperature was 450°C instead of 400°C. The average conversion is reported for the repeated experiments for the acidic γ-$Al_2O_3$ support activated at 250°C )*

EDXRF analysis of the MgO catalysts indicates that the niobia uptake was almost double for the catalyst pre-treated at 400 °C compared to the catalyst pre-treated at 250°C. However, the thermal pre-treatment temperature did not appear to have a significant effect on the niobia uptake of the alumina catalysts. A comparison of the initial rates of reaction per gram niobia for the MgO catalysts 012 and 022 (Table 4-6) shows that the niobia was utilized more efficiently by a factor of 5.7 for the catalyst whose MgO support was pre-treated at 400°C compared to 250°C). The results suggest that higher thermal pre-treatment temperature not only resulted in an increased uptake of niobia but also yielded a more active form of niobia.

Since all of the catalysts were calcined at 500°C, any effect of the thermal pre-treatment temperature on the catalytic behaviour must be related to the interaction of the surface oxide phase with the activated support and can not be due to the generation of acid sites on the metal oxide support from the thermal pre-treatment (with the exception of $\gamma$-$Al_2O_3$ which exhibits Lewis acid and base sites). The results suggest that a higher thermal pre-treatment temperature resulted in a more active form of niobia and in the case of MgO, an increased niobia uptake by the support.

A possible explanation for this is that the increased support thermal pre-treatment temperature resulted in an increased level of surface coordinative unsaturation of the metal oxide support and thus affected the strength of the interaction between the niobia surface-phase and the metal oxide support. The increased thermal pre-treatment temperature increased the strength and number of basic sites ($O^{2-}$ anions) active for bonding with adsorbates. Alternatively, a reduction in the surface hydroxyl concentration may have resulted in the assembly of more highly dispersed niobia species having superior geometrical and electronic properties. In the case of the $\gamma$-$Al_2O_3$ supported catalysts, the support should be considered a co-catalyst. It is not surprising therefore that an increase in the surface coordinative unsaturation of the support would result in an increased catalytic activity since the Lewis acidity of the support would increase along with its activity for MO synthesis. The basic $\gamma$-$Al_2O_3$ support was found to be highly active for MO synthesis (Table 4-4). In this case, the oxygen anions likely play an important role in the catalytic cycle by generating enolate ions via the heterolytic dissociative adsorption of acetone.

*4.4.5 MO Selectivity*

The acidic $\gamma$-$Al_2O_3$ supported catalyst consistently gave higher selectivity to MO, than the basic $\gamma$-$Al_2O_3$ supported catalyst, albeit a marginal improvement (Table 4-6). The average MO selectivity was 95.3 mol% for the acidic $\gamma$-$Al_2O_3$ supported catalyst compared to 92.3 mol% for the basic $\gamma$-$Al_2O_3$ supported

catalyst at an acetone conversion of 8%. The $TiO_2$ and $SiO_2$ catalysts calcined at 500°C gave comparable MO selectivities around 93 mol% at an acetone conversion of 8%. However, all of the catalysts which achieved acetone conversions of at least 8% showed much higher selectivity to MO than Amberlyst 15, which gave 84.9 mol% selectivity to MO at 120°C an acetone conversion of 8%. In fact, the selectivity was slightly lower since a very minor unknown compound observed in the experiment with Amberlyst 15 (RT=1.8 min) was neglected from the calculation of selectivity (mol%).

The benchmark catalyst Amberlyst 15 also resulted in the production of cyclic compounds such as mesitylene and isophorone. In contrast, isophorone was never observed in any autoclave experiments using the niobia catalysts reported herein. For example, in experiment 140, the $Nb_2O_5/\gamma\text{-}Al_2O_3$ catalyst had 1.5 times the initial rate of reaction for MO synthesis at 160°C than that of Amberlyst 15 at 120°C and yet did not produce any mesitylene, isophorone or any unidentified higher molecular weight species during the 8 hour experiment and achieved a MO selectivity of 95.0 mol% at an acetone conversion of 13%. The selectivity of Amberlyst 15 was relatively low compared to the niobia catalysts in Table 4-6, largely due to the presence of unreacted acetone (Figure 4-12). The results clearly demonstrate that the higher reaction temperature afforded by the refractory niobia catalysts has enabled chemistry more favourable for DAA dehydration and MO synthesis.

The general trend of MO selectivity as a function of acetone conversion is illustrated in Figure 4-17 (a) for an experiment from DoE #2 (section 4.5) which achieved a relatively high conversion. The acetone conversion as a function of time is illustrated in Figure 4-17(b) for this experiment. Initially, the selectivity to MO is quite low due to a relatively high ratio of DAA to MO. The selectivity increases with acetone conversion since the equilibrium concentration of DAA is rapidly established, whereas the concentration of MO continues to increase with acetone conversion. A discontinuity appears in the

selectivity versus concentration plot after an acetone conversion of around 7% as minor products appear above the peak area rejection limit of the GC analysis. In this case, phorone is evident. The selectivity continues to improve since the rate of MO formation exceeds the rate of phorone formation. Another discontinuity is evident at an acetone conversion of around 13 % as new minor products become apparent in the GC analysis. In this case, mesitylene appears in the product mixture.

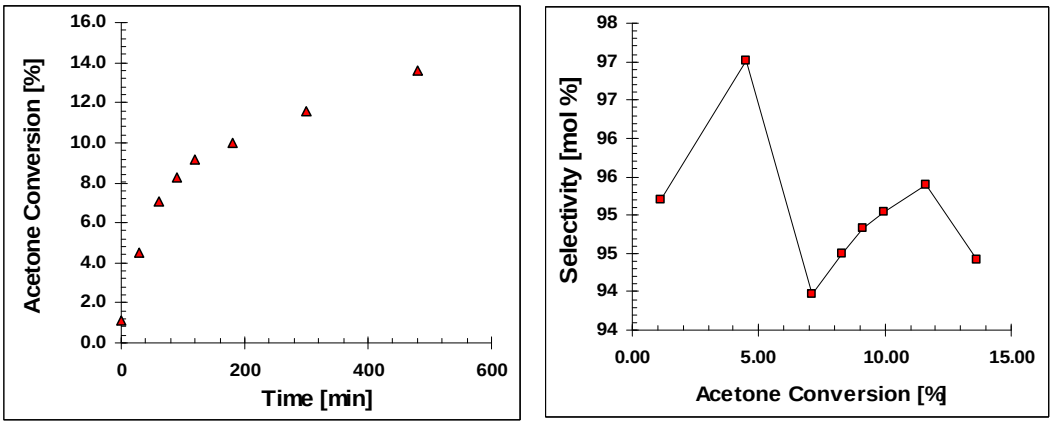


**Figure 4-17 (a)** left; acetone conversion as a function of time
**Figure 4-17 (b)** right; MO selectivity (mol %) as a function of acetone conversion [Experiment 162, T=160°C, Cat 030 (12.3 wt% $Nb_2O_5/SiO_2$) W=1.00g, ω≥ 700 RPM, P≥ 350 psig ($N_2$)]

## 4.5 DoE #2: Effect of Calcination Temperature on Alumina and Silica Supported Catalysts

Only silica and alumina supported niobia catalysts are known to exhibit both Bronsted and Lewis acidity whereas niobia supported on other metal oxides exhibit only Lewis acidity.[73,91] The Bronsted acidity arises due to the presence of acidic hydroxyls associated with Nb-O bonds in weakly distorted $NbO_6$, as well as $NbO_7$ and $NbO_8$ species, whereas strong Lewis acidity arises due to the presence of mono-oxo (Nb=O) and di-oxo (O=Nb=O) structures in highly distorted $NbO_6$ octahedra as well as in $NbO_4$ tetrahedral monomers and dimers.[68,87,90,91] Lewis acidity is also generated in silica supported catalysts from the coordinative unsaturation of the Nb sites and the associated formation of (Nb-O-Si) bonds.[69]

The calcination temperature affects the surface concentration of acidic hydroxyls. Dehydroxylation of the catalyst, which becomes more pronounced with increasing calcination temperature, results in a decrease in Bronsted acidity. In addition, the loss of chemisorbed water from the catalyst surface leads to an increased distortion of the highly distorted octahedral structures of the niobium oxide, thus resulting in an increase in their Lewis acidity. Furthermore, the dehydroxylation leads to an increase in surface coordinative unsaturation, which also increases the Lewis acidity. Iizuka et al.[88] found that for bulk niobic acid, the Bronsted acidity is maximized after calcination at 100°C and is non-existent after calcination at 500°C. The Lewis acidity of niobic acid is maximized at around 500°C since bulk niobia crystallizes at 527°C and consequently loses its acidity and catalytic properties.[73]

It is of great interest to determine the effect of the nature of the acidity, Bronsted versus Lewis, on the catalytic performance of supported niobia catalysts for the synthesis of MO and MIBK. Although niobic acid and supported niobia compounds have long been identified as a promising catalyst for MIBK synthesis, remarkably, to the best of this author's knowledge, no study has been carried out on the effect of calcination temperature on the product distribution of niobia supported catalysts for MO or MIBK synthesis. The supported niobia and niobic acid catalysts previously disclosed in the literature for MO and or MIBK synthesis have been calcined at 500°C, which necessarily precludes the possibility of the existence of Bronsted acidity.[42,43]

The objective of the second experiment (DoE #2) was to obtain a cursory assessment of the effect of calcination temperature on the performance of $Nb_2O_5/\gamma\text{-}Al_2O_3$ and $Nb_2O_5/SiO_2$ catalysts (Table 4-8). The weakly acidic $\gamma\text{-}Al_2O_3$ support was used rather than the strongly basic support since Jehng and Wachs[87] found that basic supports give rise to highly distorted $NbO_6$ structures, which are associated with Lewis acidity while acidic surfaces give rise to weakly distorted $NbO_6$, $NbO_7$ and $NbO_8$ structures associated with

Bronsted acidity. Therefore, the weakly acidic support was selected in order to promote the generation of Bronsted acidity. The effect of calcination temperature on the synthesis of MO was studied at two levels of calcination temperature (100°C and 500°C) for two levels of nominal niobia loading for the $\gamma$-$Al_2O_3$ and the $Nb_2O_5/SiO_2$ catalysts (Table 4-8).

The results in Table 4-9 and Figures 4-18 and 4-19 demonstrate that the calcination temperature had a substantial effect on the catalytic performance for MO synthesis for the catalysts investigated. Most notably, the acetone conversion after 8 hours for those catalysts calcined at 100°C is essentially 3 times greater than those calcined at 500°C for the silica supported catalysts and double in the case of alumina supported catalysts. The catalysts calcined at 500°C appear to deactivate and reach a pseudo equilibrium MO concentration while those catalysts calcined at 100°C appear to maintain a high activity even after 8 hours of reaction and acetone conversions in excess of 13% regardless of the niobia loading. A comparison of experiments 159 and 162 using 12 wt% $Nb_2O_5/SiO_2$ catalysts shows that the initial rate of reaction for MO synthesis was 2.6 times greater for the catalyst calcined at 100°C than the catalyst calcined at 500°C with the same niobia loading. This result implies that a far more active form of niobia exists on the catalysts calcined at 100°C.

**Table 4-8** Catalyst parameters for the investigation of the effect of calcination temperature on the synthesis of MO (DoE #2)

| Expt. ID | Catalyst ID | Support | $Nb_2O_5$ [wt %] | Support Activation [℃] | Pretreatment (N2) [℃] | Calcination Temp [℃] |
|---|---|---|---|---|---|---|
| 153 | 025 | $\gamma$-$Al_2O_3$ | 7.05 | 250 | 400 | 500 |
| 154 | 026 | $\gamma$-$Al_2O_3$ | 2.65 | 250 | 400 | 500 |
| 163 | 031 | $\gamma$-$Al_2O_3$ | 6.29 | 250 | 200 | 100 |
| 164 | 032 | $\gamma$-$Al_2O_3$ | 3.79 | 250 | 200 | 100 |
| 159 | 027 | $SiO_2$ | 12.5 | 250 | 400 | 500 |
| 160 | 028 | $SiO_2$ | 5.82 | 250 | 400 | 500 |
| 161 | 029 | $SiO_2$ | 16.7 | 250 | 200 | 100 |
| 162 | 030 | $SiO_2$ | 12.3 | 250 | 200 | 100 |

**Table 4-9** Effect of calcination temperature on catalyst performance for the synthesis of MO (Results of DoE #2)

| Expt. ID | CAT ID | Initial Rate (MO synthesis) [mol/(L*min*$g_{cat}$)] | Initial Rate (MO synthesis) [mol/(L*min*g $Nb_2O_5$)] | Conversion (X) [%] 120 min | 480 min | Selectivity [mol %] X=8% | X=13% |
|---|---|---|---|---|---|---|---|
| 153 | 025 | 0.00506 | n/a | 5.62 | 8.06 | 96.3 | |
| 154 | 026 | 0.00684 | n/a | 6.09 | 8.23 | 95.6 | |
| 163 | 031 | 0.00750 | n/a | 8.35 | 15.32 | 97.1 | 95.8 |
| 164 | 032 | 0.00935 | n/a | 8.41 | 13.72 | 94.8 | 95.9 |
| 159 | 027 | 0.00320 | 0.0256 | 3.46 | 5.36 | | |
| 160 | 028 | 0.00101 | 0.017 | 1.30 | 2.52 | | |
| 161 | 029 | 0.0106 | 0.0636 | 9.93 | 13.57 | 90.9 | 92.7 |
| 162 | 030 | 0.00816 | 0.0663 | 9.14 | 13.67 | 94.4 | 94.7 |

"*n/a" means activity normalized by amount of niobia is not meaningful for alumina catalysts since the support is a co-catalyst*

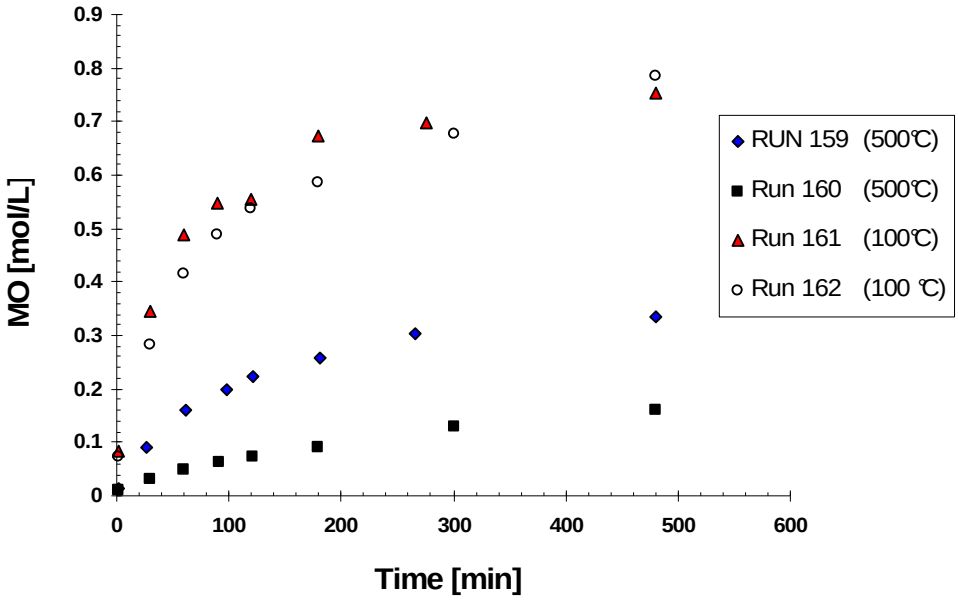


**Figure 4-18** Effect of the calcination temperature on the synthesis of MO at 160°C using $Nb_2O_5/SiO_2$ catalysts

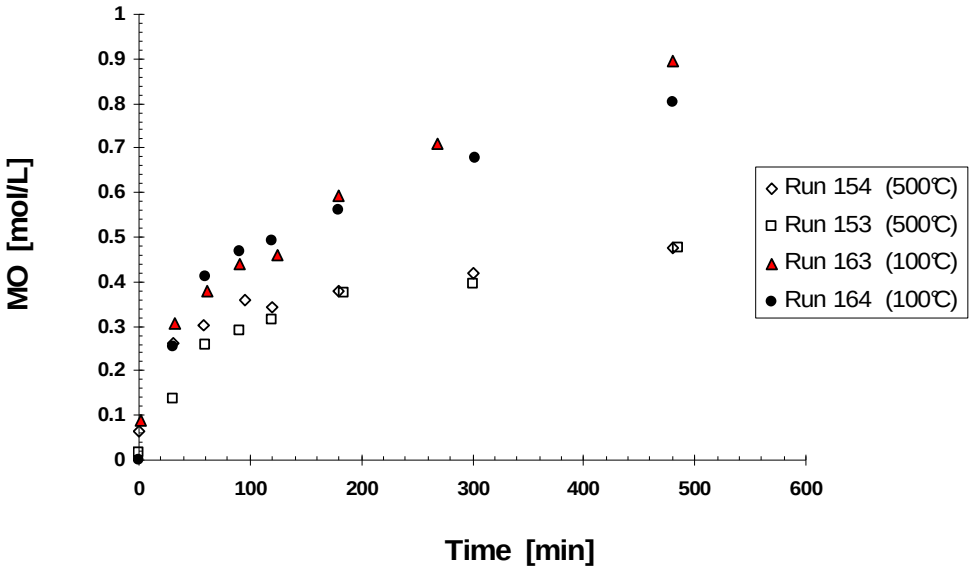


**Figure 4-19** Effect of the calcination temperature on the synthesis of MO at 160°C using $Nb_2O_5/\gamma\text{-}Al_2O_3$ catalysts

The effect of calcination temperature was significant but less pronounced on the $Nb_2O_5/\gamma\text{-}Al_2O_3$ catalysts. This is likely due to the significant intrinsic activity of the $\gamma\text{-}Al_2O_3$ support which compensates for the low activity of the niobia when calcined at 500°C. (i.e. there are a greater number of acid sites to deactivate) Note that the in the case of $Nb_2O_5/\gamma\text{-}Al_2O_3$ catalysts calcined at 500°C, the initial rate of reaction is the same order of magnitude as those calcined at 100°C. However, when calcined at 100°C the silica catalysts give a comparable performance, with in fact higher initial reaction rates for MO synthesis than the alumina supported catalysts. The alumina catalysts calcined at 500°C also appear to approach a relatively low pseudo equilibrium concentration of MO, whereas those calcined at 100°C maintain a high activity for MO synthesis after 8 hours of operation. Evidently, the catalysts calcined at 100°C exhibit enhanced stability compared to those calcined at 500°C, all of which invariably deactivate.

## 4.6 DoE #3: Effect of Niobia Loading on the Catalytic Performance of $Nb_2O_5$/ γ-$Al_2O_3$ catalysts

The $SiO_2$ and γ-$Al_2O_3$ supports have demonstrated promise as supports for niobia catalysts for MO synthesis, particularly considering the performance of the catalysts calcined at 100°C and the apparent importance of Bronsted acidity for this organic synthesis. Consequently, the $SiO_2$ and the acidic γ-$Al_2O_3$ supported catalysts were selected for further investigation while the other supports were abandoned. In this experiment, the effect of the niobia loading on the resultant catalyst performance for MO synthesis was investigated. Autoclave experiments were carried out at 160°C using $Nb_2O_5$/γ-$Al_2O_3$ catalysts with a broad range of niobia loading (Table 4-9). The calcination temperature was kept fixed at 500°C.

**Table 4-10** $Nb_2O_5$/γ-$Al_2O_3$ catalysts used in DoE #3

| Expt. ID | Catalyst ID | Thermal Treatment [℃] | Calcination Temp [℃] | Precursor Amount [mL/g] | XRF $Nb_2O_5$ wt% |
|---|---|---|---|---|---|
| 130 | 005 | 400 | 500 | 1.29 | 41.3 |
| 151 | 018 | 250 | 500 | 0.521 | 17.1 |
| 143 | 016 | 250 | 500 | 0.555 | 12.0 |
| 152 | 019 | 250 | 500 | 0.088 | 6.7 |
| 154 | 026 | 250 | 500 | 0.036 | 2.6 |
| 168 | support | 250 | n/a | 0 | 0 |
| 139 | support | n/a | n/a | 0 | 0 |

The results in Figure 4-20 reveal some interesting trends. For the catalysts calcined at 500°C, the initial specific rate of reaction is relatively insensitive to the niobia loading. In fact, with the exception of the last observation at 17 wt% $Nb_2O_5$, the activity for MO synthesis appears to diminish with niobia loading. The effect of niobia loading on the initial rate of reaction appears to be more pronounced for the catalysts calcined at 100°C. It can be concluded from Figure 4-20 that the addition of a small amount of niobia had a beneficial effect on the catalyst activity for MO synthesis. However, the further addition of niobia to the γ-$Al_2O_3$ catalyst had an adverse effect on the activity

and selectivity to MO synthesis. The optimal loading can not be precisely determined from the data in Figure 4-20 but is evidently between 0 and 6 wt% (i.e. less than 1/3 monolayer coverage).

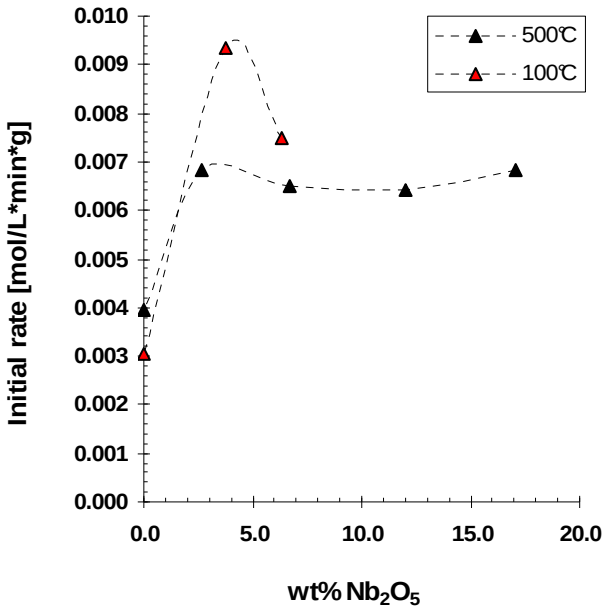


**Figure 4-20** Effect of niobia loading on the activity of $Nb_2O_5/\gamma\text{-}Al_2O_3$ catalysts calcined at 100 and 500°C for the synthesis of MO at 160°C *The data point with 0 wt% niobia for data set calcined at 500°C represents the nominal activity of the support when activated at 250°C for 2 hours in moisture free air. Data from experiment #153 (outlier) was omitted from Figure but is available in Appendix C.*

These observations are consistent with the IR spectroscopic results reported by Datka et al.[91] who found that in the case of a $Nb_2O_5/Al_2O_3$ catalyst, the concentration of Lewis acid sites increased with niobia loading for very low niobia concentration up to about 5 wt% after which the concentration of Lewis acid sites decreased. Datka et al.[91] attribute this to a competing process whereby Lewis acid sites associated with the surface oxide phase increase with increasing niobia loading at the expense of stronger Lewis acid sites associated with coordinativley unsaturated aluminum cations inherent in the metal oxide surface. Initially there is an increase in net acidity for low niobia loading. However, at higher niobia concentrations, more Lewis acid sites disappear than are created by the addition of niobia.[91] Thus, the results in Figure 4-20 can be

adequately explained by the above model. The diminution of catalytic activity observed with increasing niobia loading in Figure 4-20 is due to a net loss of acidity. The results seem to suggest that for the case of $\gamma$-$Al_2O_3$ supported catalysts, the niobia acts more like a promoter than a catalyst.

The nominal activity of the $\gamma$-$Al_2O_3$ support activated at 250°C for two hours in moisture free air for MO synthesis at 160°C (experiment 168) was found to be 0.00395 (mol/L*min*g), about half of the activity for the $Nb_2O_5$/$\gamma$-$Al_2O_3$ catalysts calcined at 500°C. In a separate experiment (139), the $\gamma$-$Al_2O_3$ support was not activated by thermal pre-treatment and was used "off the shelf" in the hydrated state. Its nominal activity was slightly lower (0.00303 mol/L*min*g) The untreated support was included with the plot of catalysts calcined at 100°C. Since the TGA scan of the acidic $\gamma$-$Al_2O_3$ support revealed that most of the water is removed from the support by heating to 250°C, the data for the sample treated at 250°C was included with the plot of the catalysts calcined at 500°C, as a first approximation.

The data for experiment 130 was omitted from Figure 4-20 since it was a preliminary experiment for which an accurate estimate of the initial rate of reaction could not be reliably obtained because the acetone conversion was already 8.8% at the time the first sample was obtained (t=80 min). However, from the data obtained from experiment 130, the initial specific rate of reaction was estimated to be 0.0028 [mol/(L*min*$g_{cat}$)], which is reasonable and comparable to the nominal activity of the weakly acidic $\gamma$-$Al_2O_3$ support. It is also consistent with the general trend of decreasing activity with increasing niobia loading. The amount of niobia deposited was sufficient for 2 monolayers for experiment 130. Consequently, the activity will approach that of bulk niobia, which is less active.

The MO selectivity at an acetone conversion of X=13% as a function of niobia loading is illustrated in Figure 4-21 for five experiments (130,140,131,163 and 164) for which a substantial acetone conversion could be achieved using $Nb_2O_5/\gamma\text{-}Al_2O_3$ (acidic support). Experiment 130 was a preliminary experiment (Appendix C) for which 2g of catalyst was used and a very high conversion was achieved. Experiments 163 and 164 correspond to the experiments for which the catalysts were calcined at 100°C and achieved very high acetone conversions. Experiment 140 was the only acidic $\gamma\text{-}Al_2O_3$ catalyst from the screening study in Section 4.4.1. which achieved greater than 13% acetone conversion. Experiment 130 was a preliminary experiment with very high niobia loading (41.3 wt%) which exceeded two monolayers coverage.

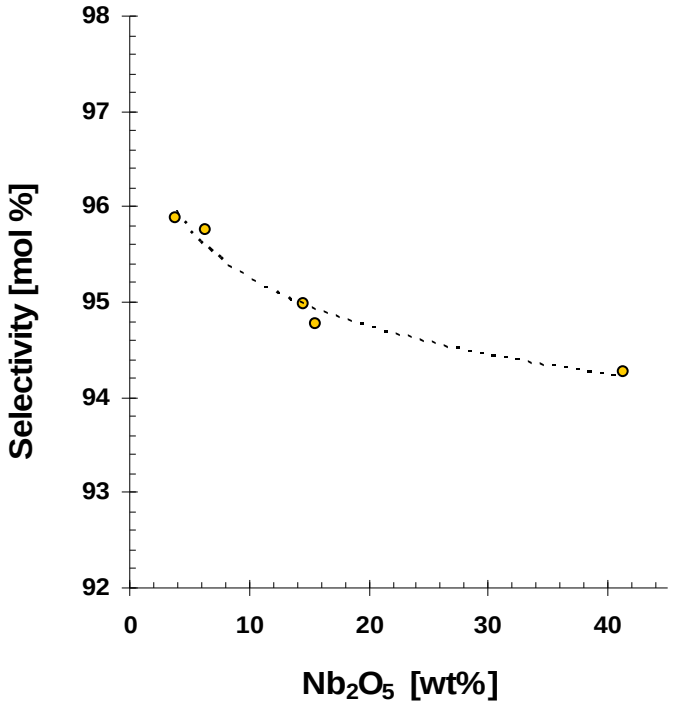


**Figure 4-21** Effect of niobia loading on the MO selectivity (mol%) at an acetone conversion of 13% for $Nb_2O_5/\gamma\text{-}Al_2O_3$ (acidic) catalysts

The results of Figure 4-21 demonstrate that the selectivity decreases with increasing niobia loading. This suggests that either the more highly dispersed niobia are more selective for MO synthesis due to their geometrical or

electronic properties or that the Lewis acid sites of the alumina support are more selective for MO as a consequence of their relative adsorption strengths. The two catalysts in Figure 4-21 having about 5 wt% $Nb_2O_5$ which achieved the highest selectivity were calcined at 100°C. The other data points were calcined at 500°C. Therefore, the enhanced selectivity at low niobia loading might be due to the contribution of Bronsted acidity. Lastly, it should be noted that although the niobia loading has a statistically significant effect on the selectivity to MO, the magnitude of this effect does not appear to be sufficient to exploit for engineering purposes.

## 4.7 DoE #4: Effects of Catalyst Loading, Support Activation Temperature and Calcination Temperature on $Nb_2O_5/SiO_2$ catalysts

The data obtained from previous experiments involving $Nb_2O_5/SiO_2$ catalysts in DoE #1 and #2, presented here in Figure 4-22 show that the initial specific rate of reaction for MO synthesis at 160°C increases roughly linearly with niobia loading. This dependence on the activity for MO synthesis on the niobia loading is reasonable and expected. Although the silanol groups of the silica support are weakly acidic, the data in Table 4-4 shows that the fumed silica support is inert for MO synthesis. Ammonia TPD analysis of the fumed silica support presented in Chapter Five confirms a negligible surface acidity. Thus, the number of acid sites on a $Nb_2O_5/SiO_2$ catalyst, and hence its catalytic activity for acid catalyzed reactions, increases with increasing niobia loading; at least for less than monolayer coverage. As with the alumina supported catalysts, the effect of niobia loading on the catalyst activity appears to be more pronounced for the catalysts calcined at 100°C. The fact that the catalysts calcined at 100°C are significantly more active than those calcined at 500°C, as well as the fact that their activity for MO synthesis is more strongly dependent on the niobia loading, suggests that the active form of niobia is different for the catalysts calcined at 100°C compared to those calcined at 500°C. This will be further investigated by spectroscopic methods and ammonia TPD analysis in Chapter Five.

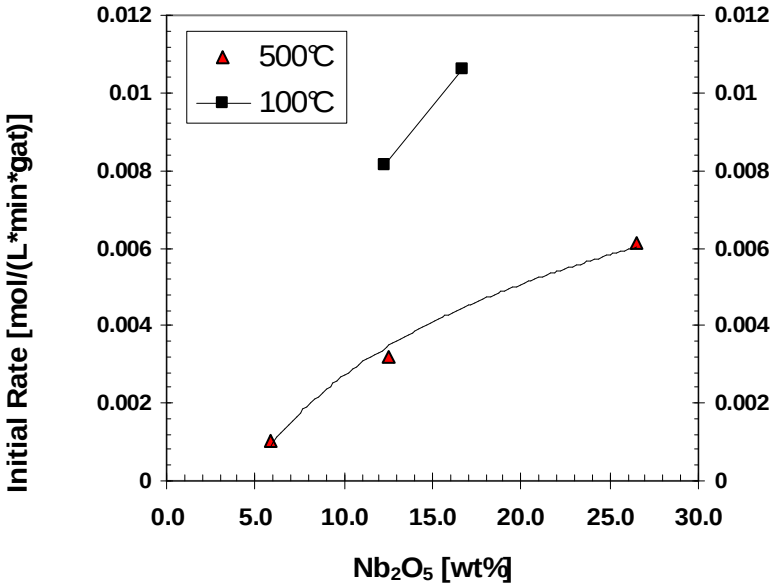


**Figure 4-22** Effect of niobia loading on the activity for MO synthesis at 160°C for $Nb_2O_5/SiO_2$ catalysts calcined at 100 and 500°C. *(All catalysts were pre-treated at 250°C, T= 160°C, W=1 g, ω=700 RPM)*

A 2X2 factorial designed experiment with centre-points (table 4-11) was carried out in order to further explore the effects the calcination temperature, support thermal pre-treatment temperature and niobia loading on the performance of $Nb_2O_5/SiO_2$ catalysts for MO synthesis at 160°C with an emphasis on highly dispersed niobia below about 1/3 fractional monolayer coverage. The inclusion of centre points within the experimental matrix allows the study of three experimental variables over three levels. The niobia loading was varied from around 3 to 9 wt% (0.1 to 0.35 monolayer). Calcination temperatures of 100, 300 and 500°C and support thermal pre-treatment temperatures of 100, 250 and 400°C were investigated.

The results of the multivariable regression analysis using NLREG v.5.4 (Sherrod Software) reveals, when applied to the entire data set, that for highly dispersed $Nb_2O_5/SiO_2$ catalysts for niobia loading less than 1/3 monolayer

coverage, the thermal pre-treatment temperature did not have a significant effect on the observed initial specific rate of reaction for MO synthesis. The Pearson coefficients of correlation were R= -0.107 for the main effect of thermal pre-treatment.

**Table 4-11** 2x2 Factorial designed experiment with centre points (DoE #4)

| Trial | Expt. ID | CAT ID | $Nb_2O_5$ [wt%] | Dry T [K] | Calcine T [K] | Monolayer |
|---|---|---|---|---|---|---|
| 1 | 173 | 036 | 4.52 | 373 | 373 | 0.17 |
| 2 | 187 | 047 | 3.94 | 673 | 373 | 0.15 |
| 3 | *175* | *038* | *9.06* | *373* | *373* | *0.35* |
| 4 | 184 | 044 | 7.63 | 673 | 373 | 0.29 |
| 5 | 190 | 050 | 2.80 | 373 | 773 | 0.11 |
| 6 | 188 | 048 | 3.40 | 673 | 773 | 0.13 |
| 7 | 189 | 049 | 7.96 | 373 | 773 | 0.31 |
| 8 | 218 | 059 | 8.79 | 673 | 773 | 0.34 |
| 9 | 174 | 037 | 6.82 | 523 | 573 | 0.26 |
| 10 | 186 | 045 | 5.55 | 523 | 573 | 0.21 |
| 1 (rpt) | 183 | 039 | 5.11 | 373 | 373 | 0.20 |

The fact that the thermal pre-treatment temperature did not have a significant effect on the catalyst performance is perhaps not surprising since the niobia loading in these experiments were so low (less than 1/3 monolayer coverage) that there was likely a surplus of surface hydroxyl groups for the niobium ethoxide precursor to coordinate with regardless of the thermal pre-treatment temperature. Shirai et al.[93] have reported that Aerosil 200, which is also an amorphous fumed $SiO_2$ with similar surface area as the fumed $SiO_2$ investigated in this work, has surface hydroxyl concentrations of 2 and 5 $OH/nm^2$ after thermal pre-treatment temperatures of 400 and 200°C respectively. Asakura and Iwasawa[70] and Shirai et al.[93] have also pointed out that a surface hydroxyl concentration of 5 $OH/nm^2$ is sufficient to generate a single monolayer of niobia on silica. It follows then that 2 $OH/nm^2$ should be more than sufficient to generate 1/3 monolayer coverage. Therefore, it seems reasonable that there might be an excess of surface hydroxyls even after thermal pre-treatment at 400°C for the fumed silica support used in these experiments.

The results also seem to suggest that the calcination temperature did not have a significant effect on the initial specific rate of reaction. The initial rate data obtained from this experiment, when added to the previously collected data is in good agreement for the catalysts calcined at 100°C (Figure 4-23). However, the catalysts calcined at 500°C have unexpectedly high initial activity compared to the data collected previously for higher niobia loading.

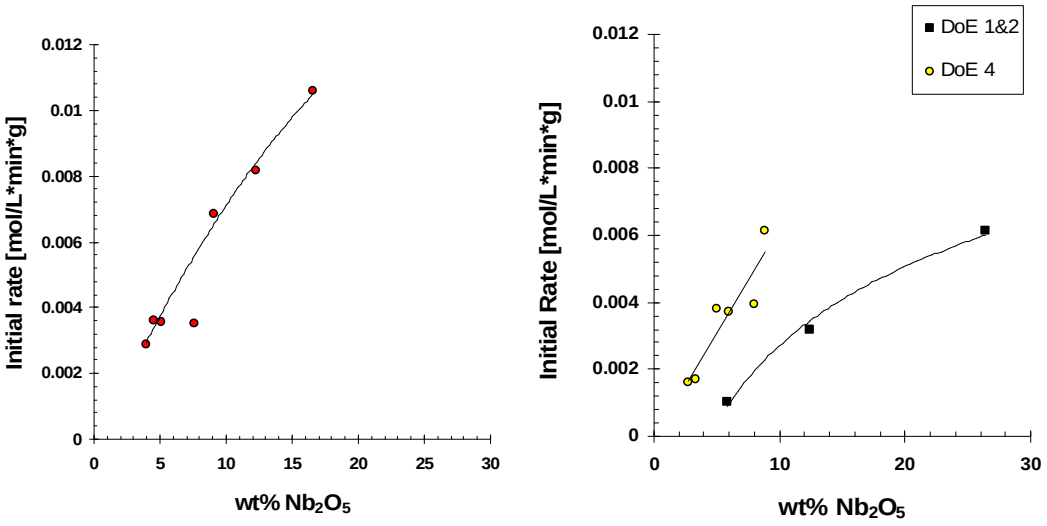


**Figure 4-23** Effect of niobia loading and calcination temperature on the initial specific rate of reaction for $Nb_2O_5/SiO_2$ catalysts (Left) catalysts calcined at 100°C (Right) catalysts calcined at 500°C

Their initial activity is comparable to those catalysts calcined at 500 and 300°C. This discrepancy is difficult to explain but may mean that the niobia catalysts exhibiting Lewis acidity have greater initial activity when highly dispersed below 1/3 monolayer coverage. Perhaps the apparent lack of an effect of calcination temperature for low niobia loading might be expected if a critical niobia loading of around 1/3 monolayer coverage is required to generated Bronsted acidity as suggested by Wachs et al.[87,91] Note that all of the catalysts calcined at 100°C and having at least 0.3 monolayer of niobia achieved initial rates of reaction in excess of 0.068 [mol/L*min*g] whereas the maximum initial rate of reaction of catalysts calcined at 500°C for the 9 experiments presented in

Figure 4-23 was only 0.0062 for the catalyst with 26 wt% (1.0 monolayer) niobia.

The acetone conversion after three hours (Figure 4-24) clearly confirms the effect of calcination temperature on the long term stability of the catalyst. The catalysts calcined at 300°C showed comparable results to those calcined at 100°C. However, the catalysts calcined at 500°C showed consistently lower acetone conversion after three hours.

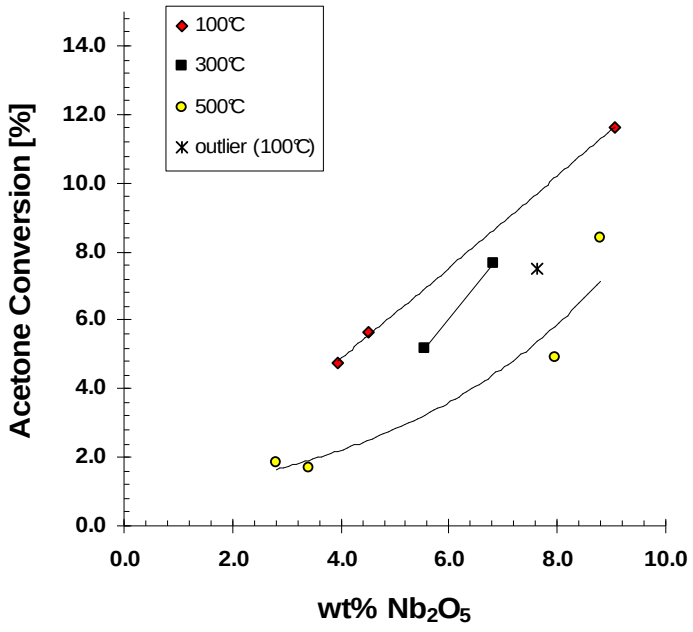


**Figure 4-24** Effect of calcination temperature on acetone conversion after three hours for $Nb_2O_5/SiO_2$ catalysts (DoE #4)

One experiment in the test matrix (DoE #4), gave a particularly surprising result and is possibly an outlier. The catalyst which had the condition of high niobia loading, low calcination temperature and high support activation temperature (Cat 044, Run 184) was expected to give the highest initial rate of reaction, comparable to experiment 175 for which the niobia loading was also maximized and the calcination temperature minimized, and a similarly high acetone conversion after three hours was expected. Although it did achieve a relatively high acetone conversion it was much lower than expected (outlier in

Figure 4-24), and its initial rate of reaction was the second lowest of the 4 catalysts calcined at 100°C. This result might be due to the effect of thermal pre-treatment temperature of the support. Perhaps for catalysts calcined at 100°C, the surface hydroxyl concentration is important in order to generate bridging hydroxyls associated with Bronsted acidity.

The process interaction graph in Figure 4-25 in fact strongly suggests that for catalysts calcined at 100°C, the supports activated at low drying temperature (100°C) produce catalysts which exhibit higher initial specific rates of reaction for MO synthesis. Moreover, for the supports activated at 100°C, the effect of the niobia loading on the resultant initial specific activity becomes far more pronounced. The data in Figure 4-25 implies that a high surface concentration of hydroxyls is favourable for the generation of highly active $Nb_2O_5/SiO_2$ catalysts when calcined at 100°C, which presumably exhibit significant Bronsted acidity.

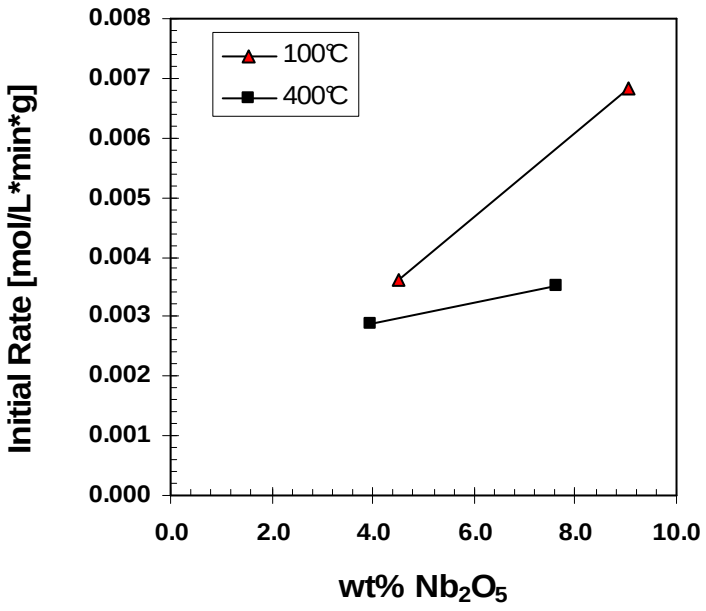


**Figure 4-25** Process interaction graph illustrating the effects of thermal pre-treatment temperature and niobia loading on the initial activity of $Nb_2O_5/SiO_2$ catalysts calcined at 100°C for MO synthesis at 160°C

The process interaction graph in Figure 4-26 for the catalysts calcined at 500°C seems to suggest a reverse, yet less pronounced effect of support thermal pre-treatment temperature. At low niobia loading, the pre-treatment temperature does not appear to have a significant effect. The catalyst activity is very low for these experiments. However, at higher niobia loading for which the catalytic activity becomes significant, the catalyst with the support activated at the higher pre-treatment temperature produced the catalyst with greater initial activity. However, the effect is far less pronounced compared to the effect of the support thermal pre-treatment on the catalysts calcined 100°C. For the condition of high niobia loading and low calcination temperature, the initial activity essentially doubles for the catalyst with support treated at 100°C compared to the catalyst with the support treated at 400°C (Figure 4-25).

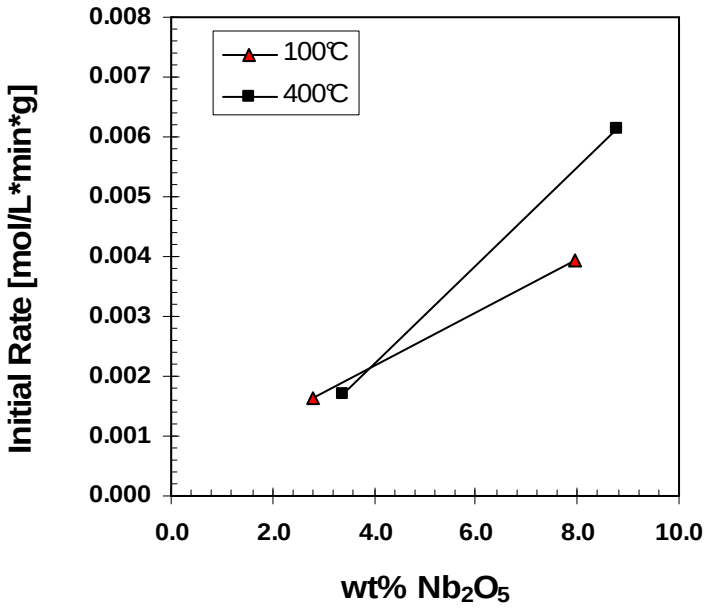


**Figure 4-26** Process interaction graph showing the effects of niobia loading and support activation temperature on the initial activity of $Nb_2O_5/SiO_2$ catalysts calcined at 500°C

The effect of thermal pre-treatment of the support on the initial activity of the catalysts illustrated in Figure 4-26 is perhaps expected for catalyst calcined at 500°C, since these catalysts only exhibit Lewis acidity which is maximized with increased surface coordinative unsaturation and diminishes with adsorbed

moisture. Pre-treating the oxide support at elevated temperature has been shown in general (Figure 4-16) to increase the catalyst activity for those catalysts calcined at 500°C. This is attributed to an increased interaction strength between the metal oxide support and surface oxide phase, due to increased surface coordinative unsaturation, which enhances the strengths of acid sites.

## 4.8 Conclusions

Catalysts consisting of a surface-phase niobium oxide dispersed onto various metal oxides were developed and tested in an autoclave reactor for their activity and selectivity for MO synthesis at 160°C. The three most important catalyst parameters for a dispersed niobia catalyst, including the nature of the oxide support, the calcination temperature and the niobia loading were investigated. In addition, the effect of the support thermal pre-treatment temperature, which governs the surface hydroxyl chemistry and the degree of surface coordinative unsaturation was studied. The results demonstrate that each of these parameters had significant effects on the resulting catalyst performance.

Refractory metal oxides exhibiting a broad range of acidity/basicity, morphological and electronic properties and exhibiting unique symmetries were screened to identify promising catalyst formulations for the synthesis of MO from acetone at 160°C including (anatase) $TiO_2$, MgO, $\alpha$-$Al_2O_3$ (corundum), and an acidic $\gamma$-$Al_2O_3$ and a basic $\gamma$-$Al_2O_3$ as well as amorphous fumed $SiO_2$. The general trend of activity for MO synthesis per gram of catalyst is as follows: $MgO < \alpha\text{-}Al_2O_3 << TiO_2 < SiO_2 \approx \gamma\text{-}Al_2O_3$. Gamma alumina exhibited significant catalytic activity for MO synthesis at 160°C and consequently must be regarded as a co-catalyst rather than strictly a support.

The suitability of these supports is largely governed by their capacity to interact with the niobia precursor and establish a dispersed monolayer of niobia.

When impregnated with the same amount of precursor, the niobia loading ranged from around 4 wt% for corundum and 26.5 wt% for fumed $SiO_2$. The high surface area supports ($SiO_2$ and $\gamma$-$Al_2O_3$) resulted in the establishment of 1.0 monolayer coverage while the low surface area supports exceeded monolayer coverage and consequently, a diminution of acidic properties. However, the results clearly demonstrate that the specific surface area is not the sole factor which governs the catalyst activity. The electronic properties are important as well.

The anatase $TiO_2$ produced the most active form of niobia of all of the catalysts investigated in the initial screening study. This is attributed to a strong metal support interaction arising from the semiconductive nature of $TiO_2$ ($E_g$=3.23 eV). The catalyst activities generally were found to increase with increasing support thermal pre-treatment temperature. This suggests that a higher degree of surface coordinative unsaturation results in a stronger interaction between the support and surface-phase oxide giving rise to a more active form of niobia. In the case of MgO, the increased thermal pre-treatment temperature also resulted in an increased uptake of the niobium ethoxide precursor. The two $\gamma$-$Al_2O_3$ supports, one basic (pH 9.5) and the other acidic (pH 6.0) with roughly monolayer coverage of niobia, when calcined at 500°C exhibited essentially identical kinetic behaviour. This suggests the support acidity/basicity did not appreciably affect the surface oxide phase structure and properties. However, the strongly basic MgO catalyst showed the lowest activity and rapidly deactivated.

The fumed silica support is inert for MO synthesis. Not surprisingly the activity of the silica catalyst was found to increase with increasing niobia loading. However, the role of niobia in the $\gamma$-$Al_2O_3$ catalysts is more comparable to a promoter effect than that of an active catalytic material. The addition of a small amount of niobia to the weakly acidic $\gamma$-$Al_2O_3$ support

resulted in a marked increase in the initial rate of MO synthesis at 160 °C, by a factor of roughly 2 and 3 for catalysts calcined at 500°C and 100°Crespectively. However, the further addition of niobia resulted in a decrease in catalytic activity. The optimal loading can not be precisely determined from the data obtained, however it is between 0 and 6 wt%. The loss of activity with increasing niobia loading is attributed to the loss of strong Lewis acid sites from the $\gamma$-$Al_2O_3$ support in favour of weaker Lewis acid sites from the surface oxide phase niobia.

A significant finding was that the calcination temperature had a profound effect on the performance of $Nb_2O_5/SiO_2$ and $Nb_2O_5/\gamma$-$Al_2O_3$ catalysts for MO synthesis. Catalysts calcined at 100°C exhibited superior catalyst performance compared to those calcined at higher temperature. Not only were the catalyst calcined at 100°C more active, but more importantly it was observed that the catalysts calcined at low temperature obtained far greater acetone conversion than those calcined at 500°C and maintained their activity throughout the course of an 8 hour experiment. In stark contrast, the catalysts calcined at 500°C achieved lower acetone conversions and approached a final "pseudo equilibrium" MO concentration much lower than its theoretical equilibrium concentration. The final pseudo equilibrium MO concentration achieved was dependent on the catalyst formulation, which suggests that the pseudo equilibrium phenomenon is due to catalyst deactivation. The results suggest that Bronsted acidity plays an important role, not only in the catalyst's activity but also its long term stability for MO synthesis. This result is perhaps unexpected since niobia catalysts for MIBK synthesis disclosed previously in the literature were all calcined at elevated temperature, which implies an intention to maximize Lewis acidity.

The effect of the thermal pre-treatment of the fumed $SiO_2$ support on the initial activity of the catalyst for MO synthesis depends on the calcination temperature. For catalysts calcined at 500°C, an increased thermal pre-

treatment temperature resulted in an increased catalyst activity. This is consistent with the results obtained for other oxide supports investigated and is attributed to an increased interaction between the support and surface-phase oxide due to enhanced surface coordinative unsaturation of the support. In the case of $Nb_2O_5/SiO_2$ catalysts calcined at 100°C, the effect of support thermal pre-treatment is more pronounced. The supports activated at 100°C, for which the surface hydroxyl concentration is maximized, not only gives far more active catalysts, but also show a much stronger effect of niobia loading on the initial activity. This implies that the surface hydroxyl chemistry of the support is important in establishing the active sites for $Nb_2O_5/SiO_2$ catalysts calcined at 100°C. It is postulated that the active centres for MO synthesis are protonic sites associated with bridging hydroxyls (i.e. adlineation sites) created by (Si-O-Nb) linkages. This hypothesis and the results of this chapter will be revisited in Chapter Five as the nature of the acidity of these catalysts are elucidated and the strengths of the acid sites quantified.

# Chapter Five

## Detailed Catalyst Characterization and the Elucidation of the Nature of the Acid Sites

---

### 5.0 Synopsis

The acidity of the niobia catalysts used in autoclave experiments in Chapter Four were ascertained via the temperature programmed desorption (TPD) of ammonia probe molecules. The nature of the acidity was elucidated via *in situ* DRIFT adsorption spectra of pyridine probe molecules. The results demonstrate that catalyst calcined at 100°C exhibited unique and very strong acid sites not present in the catalysts calcined at 500°C while catalysts calcined at 300°C exhibited an intermediate acidity. Bronsted acid sites were evident only on catalysts calcined at 100°C but were not present for those catalyst calcined at 500°C.

The activity for MO synthesis is correlated with the acid site density as well as the acid strength. The stability of the catalyst for MO synthesis is clearly linked to the nature of the acidity. Catalysts exhibiting only Lewis acidity deactivate resulting in a "pseudo equilibrium" whereas catalysts exhibiting Bronsted acidity exhibit superior catalytic activity and stability. Once calcined at 500°C, the annihilated Bronsted acidity is not regenerated upon rehydration. This indicates that niobia structure obtained from the high temperature calcination is thermodynamically stable. Raman spectroscopic analysis suggests the transformation involves a change from slightly distorted octahedra to highly distorted octahedra upon calcination. This implies that the Nb-OH-Nb bridging hydroxyls are responsible for the Bronsted acidity rather than the Nb-OH-Si bridging hydroxyls. Catalyst characterization via XRD and Raman spectroscopy confirm the absence of crystallites. Thus, the loss of catalyst activity and stability from high temperature calcination is not due to a

polymorphic phase change resulting in the formation of crystallites but rather is associated with the nature and strength of the acidity.

An interesting finding was that a strong interaction between the Norpro $SiO_2$ catalyst carrier support and the niobium oxide phase resulted in the generation of unique and very strong Bronsted acid sites in the catalyst when calcined at 100°C. FTIR analysis showed that the proportion of Lewis acidity in this catalyst formulation was significantly diminished compared to the catalysts consisting of niobia dispersed on fumed silica calcined at 100°C. This implies that the niobium oxide structure on the Norpro silica carrier was distinct from the niobia structure on the fumed silica.

## 5.1 Temperature Programmed Desorption (TPD)

Information regarding the strength and nature of the acidity of niobium oxide catalysts was obtained via the quantitative and qualitative analysis of the temperature programmed desorption (TPD) of ammonia. The catalyst specimens were activated *in situ* by prolonged thermal treatment while exposed to carrier gas and were subsequently saturated with ammonia. The physisorbed ammonia was removed by thermal treatment and the specimen was then heated according to a predetermined thermal profile. The signal peaks resulting from the desorption of ammonia as a function of temperature provided information regarding the number of types of acid sites as well as their relative acid strengths. Deconvolution of the peaks and the numerical integration to determine the peak areas provided a quantitative measure of the number of acid sites. However, this technique does not reveal the nature of the acidity since $NH_3$ will adsorb indiscriminately on both Lewis and Bronsted acid sites. Consequently, the nature of the acidity was determined independently by FTIR spectroscopic techniques (Section 5.2).

### *5.1.1 TPD Method and Apparatus*

Preparation of Catalyst Samples

The catalyst samples were ground with a mortar and pestle (if not already in a powder form) and subsequently pressed into thin wafers. The wafers were then broken down and sieved through sizing screens. Catalyst particles between 250 and 500 μm were collected for TPD analysis. Typically, about 0.06 to 0.12 g of catalyst meeting this size specification, precisely weighed using a Sartorius balance (± 0.00005 g), were fixed in place within a quartz U-tube reactor utilizing a small amount of glass wool (Perkin Elmer N610-2354) on both ends of the catalyst sample. The U-tube was then secured to the sample station of an Altamira AMI-200 Catalyst Characterization System using ultra-torr fittings with o-ring seals[♣] provided by Altamira Instruments.

Altamira AMI-200 Catalyst Characterization System

Once the U-tube was inserted into the sample station of the Altamira AMI-200 and sealed, an 800 W heating mantle was raised into position to surround the U-tube. The U-tube was enclosed at the top of the mantle with ceramic insulation and insulating tape. The AMI-200 is equipped with multiple gas input ports capable of accommodating up to 4 carrier gases, 4 treatment gases and 4 blend gases. The volumetric flow rates of the carrier, treatment and blend gas streams are controlled by three Brooks mass flow controllers within the AMI-200 apparatus. UHP 5.0 Argon was used as a carrier gas and anhydrous ammonia was connected to a treatment gas inlet. No blend gases were used in these experiments. Both the anhydrous ammonia and argon were procured from Praxair (Kitchener, ON).

The direction of gas flow within the apparatus was controlled by two multi-port sampling valves as illustrated in the schematic representation of the

[♣] The reader is advised that general purpose Viton o-rings routinely used in laboratory applications are severely incompatible with ammonia and are not recommended. Neoprene and Buna-N o-rings give acceptable compatibility for use with hot ammonia gas.

Altamira AMI-200 (Figure 5-1). The AMI-200 was equipped with a thermal conductivity detector (TCD) downstream of the analytical vent enabling the quantification of ammonia desorbing from the specimen.

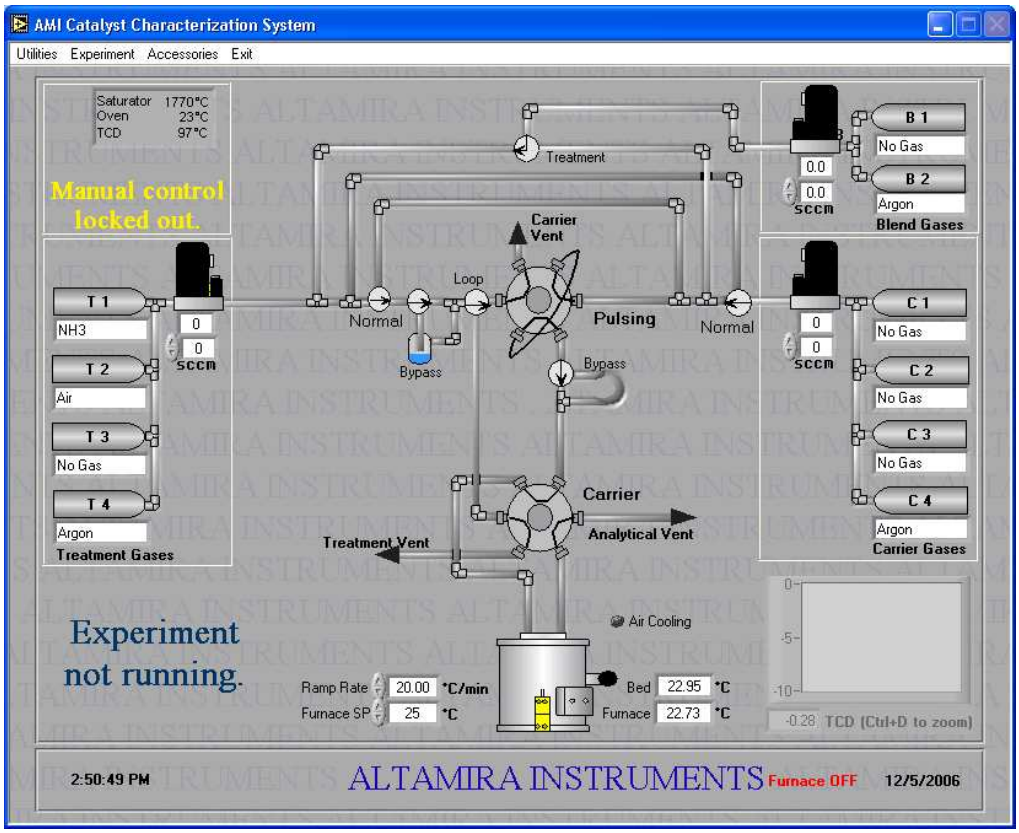


**Figure 5-1** Schematic representation of the Altamira AMI-200 Catalyst Characterization System (Screen print out from AMI-200 Human-Machine Interface)

The AMI-200 was also integrated with a mass spectrometer located downstream from the TCD analytical vent line, thus enabling the identification of species passing through the analytical vent from the sample specimen. This was achieved by the connection of a heated capillary tube to the outlet of the sample U-tube. Samples could be extracted periodically from the U-tube through the capillary tube to the mass spectrometer for analysis. However the mass spectrometer was not used for the $NH_3$/TPD experiments reported in this chapter.

Thermal Treatment

The catalyst samples were activated *in situ* by heating the samples in inert environment at 120°C for 10 hours. Either UHP 5.0 or pre-purified 4.8 argon (Praxair, Kitchener, ON.) was passed over the sample during this time at a volumetric flow rate of 30 sccm. The samples were heated from ambient temperature to 120°C at a relatively slow heating rate of 2°C/min to ensure that the samples did not significantly overshoot the desired temperature set-point. Prolonged thermal treatment for a period of 10 hours at 120°C was found to be sufficient to activate the catalyst by removing physisorbed material without inducing structural modification of the catalyst from thermal treatment. This is particularly important for the catalysts prepared from low temperature calcination since thermal treatment at elevated temperatures will significantly modify the catalyst structure and acidic properties prior to TPD analysis.

Pulse Chemisorption and Temperature Programmed Desorption

After the 10 hour thermal treatment step was completed, the catalysts were saturated with 10 consecutive pulses of ammonia at 30 sccm with each pulse lasting for 120 seconds. The volume of ammonia injected was the same for each injection and is governed by the instrument's sample loop volume, which in this case was 524.0 μL. Argon flowing at 20 sccm was used as a carrier gas. For most of the experiments reported, the pulse chemisorption step was carried out with a bed temperature around 130 to 135°C. Therefore it is likely that only chemisorbed ammonia was present on the catalyst surface of these catalysts. However, for some earlier experiments, the pulse chemisorption step was carried out at room temperature followed by an isothermal treatment at 120°C for 1 hour prior to the TPD step to ensure removal of physisorbed ammonia. Since ammonia is a very strong base, ammonia would likely displace any chemisorbed species such as carbon dioxide interacting with acid sites.

The pulse chemisorption of ammonia onto a 7 wt% $Nb_2O_5/\gamma Al_2O_3$ catalyst is illustrated in Figure 5-2. Each peak labelled in Figure 5-2 corresponds to the

injection of 524.0 μL of ammonia. The first peak is relatively small, which indicates that a significant proportion of the ammonia injected became adsorbed on the catalyst. In subsequent injections, the peak area becomes increasingly larger and the signal strength intensifies as an increasingly greater proportion of ammonia bypasses the catalyst with each injection and is detected by the TCD. By the sixth injection, the catalyst is fully saturated with ammonia and all of the ammonia injected bypasses the catalyst resulting in the same peak sizes in subsequent injections. From the first injection onwards, the signal intensity does not return to the original baseline since ammonia is still eluting as the next injection occurs.

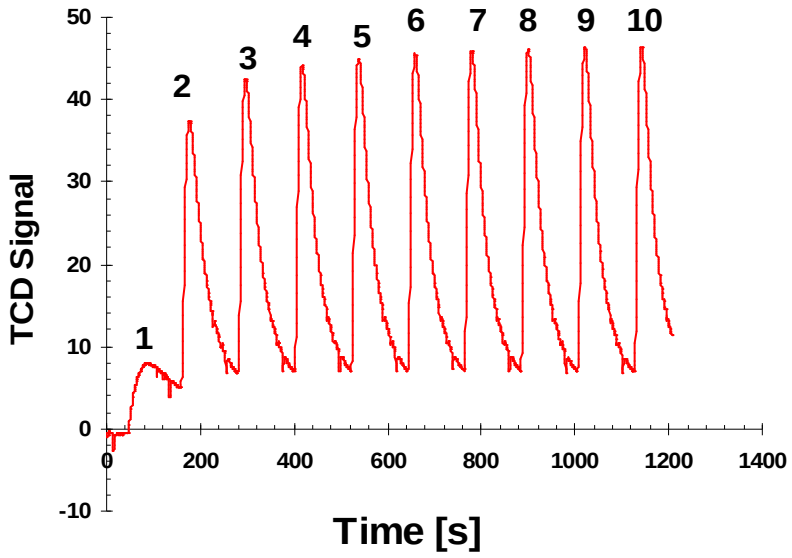


**Figure 5-2** Pulse chemisorption of $NH_3$ on a 7.1 wt% $Nb_2O_5/\gamma$-$Al_2O_3$ catalyst (CAT 025; 28.06.2007) [TCD gain 5, TCD current 85 mA, data acquisition rate 2 Hz]

After the pulse chemisorption step was completed, the specimen was heated from 120°C to 500°C at a heating rate of 10°C/min. In a few select experiments, the final temperature set-point was as high as 700°C. During the period in which the sample was heated, argon was flowing through the U-tube at a rate of 30 sccm. As the specimen temperature increased, the ammonia desorbed from the catalyst, passed through the analytical vent and was detected

by the TCD. The TCD was operated at a gain of 20, a current intensity of 85 mA and acquired data at a sampling period of 5.0 sec/pt (0.2 Hz).

Calibration

The Altamira calibration procedure consists of multiple injections of a known volume (i.e. the sample loop volume of 524.0 μL) of pure ammonia directly into the analytical line of the instrument for detection and quantification by the TCD. Linearity is assumed and the calibration curve is assumed to pass through the origin (i.e. no signal offset). Ammonia was injected directly to the TCD via the multi-port valves without passing through the U-tube. The pressure in the sample loop was atmospheric pressure and the temperature was data-logged by the instrument. Therefore, the number of moles of ammonia injected can be calculated from the ideal gas law. The area under the TCD signal versus time curve resulting from the pulse injection of ammonia was integrated numerically using OriginPro 7.5.

The peak area per number of moles of ammonia injected for each of the 10 injections was determined from the ideal gas law assuming the pressure was 1 atm and using the known injection volume and the measured null station temperature, which was found to increase slightly throughout the course of the pulse calibration experiment. The average peak area per number of moles of ammonia injected for the 10 pulse injections (i.e. the absolute response factor for $NH_3$) was used to relate the TCD peak area to the amount of ammonia eluted in TPD experiments.

It is important to note that the TCD current intensity affects the sensitivity of the TCD and significantly affects the results. Therefore, the current intensity must have the same value for the calibration as for the TPD method. In contrast, the gain is a signal amplifier. One may use a different gain for the calibration if needed and correct the signal prior to integration. In these experiments, a TCD gain of 20 was found to give good resolution in the TPD

profiles. However, a gain of 20 resulted in the saturation of the detector signal during the calibration step. Consequently, a gain of 1 was used for the calibration step and the TCD signal for the TPD step was corrected by multiplying the data by a factor of (1/20). Users of the Altamira AMI-200 should note that the TCD gain indicated in the data files are encoded and are not the actual gain. For example an encoded value of 1 corresponds to an actual gain of 2; an encoded value of 2 corresponds to an actual gain of 5, etc. The details and calculations of the instrument calibration are available in Appendix D.

The accuracy of the TPD analysis technique is limited by the fact that the TPD peaks require deconvolution. Thus, the uncertainty introduced in the analysis due to detector drift over time and uncertainty introduced in the calibration curve is small compared to uncertainty introduced from the data reconciliation step involving the deconvolution of the peaks. In this work, the precision of the instrument is perhaps more important than the accuracy since a comparison of the relative acidity of catalyst samples is more meaningful than an absolute measure of the total number of acid sites. Although the Gaussian model fit to the TCD signal for the 10 pulse injections of ammonia resulted in good repeatability of the peak areas (RSD= 4.5%) and a good fit to the data as evidenced by an average coefficient of correlation of $R^2$=0.98, the data acquisition rate for the pulse calibration was poor. A higher sampling rate of 2.0 Hz is recommended for the calibration and pulse chemisorption steps in future work. However, for the TPD step a lower sampling frequency of 0.2 Hz is recommended, otherwise very large data files will be created.

Deconvolution of TPD Peaks

As ammonia desorbs from the catalyst, it is detected by the TCD detector. The plots of the TCD signal versus bed temperature do not reveal a single peak. Rather, the TCD profiles indicate the presence of multiple peaks corresponding to distinct acid sites. However, these peaks are convoluted. The summation of

these peaks give the characteristic $NH_3$/TPD profiles whereby the signal intensity generally increases initially with temperature and then decreases near the end of the thermal profile as the ammonia is completely desorbed.

In order to reveal the contribution of the individual acid sites to the resultant TPD profile, the TPD peaks were deconvoluted and the resultant peaks numerically integrated using OriginPro 7.5. A minimum number of peaks were used to fit the data. For example, for the typical TPD profile is illustrated in Figure 5-3. An obvious peak is observed around 160°C corresponding to weakly adsorbed ammonia. However, the subsequent peak, which shows a plateau from around 290 to 400°C can not be fit by a single peak and is more realistically described by two overlapping peaks.

Only the data up to 500°C was analyzed, as was done by da Silva et al.[92] who investigated the acidic properties of niobia-aluminas via $NH_3$/TPD. Although some very strong Lewis acid sites may be observed at desorption temperatures higher than 500°C such as in the case of alumina, these sites are unlikely to participate in the chemical reaction due to the strong adsorption strengths. Consequently, the end point of the TPD profile was considered an artefact and deconvoluted from the data by assigning a "background" peak to it as illustrated in Figure 5-3. Figure 5-3 also illustrates a minor peak eluting around 120 to 150°C. This peak corresponds to physisorbed ammonia and was present in the samples for which the pulse adsorption steps were carried out at ambient temperature. The peak areas corresponding to physisorbed ammonia were not included in the calculation of total acidity.

Once the number of peaks have been specified and an initial guess as to the size and location of the peaks has been provided, the OriginPro algorithm determines the statistically optimum parameters for the peak distribution functions. Either Gaussian or Lorenzian distributions may be used for the deconvolution of peaks using OriginPro 7.5. In this work, Gaussian

deconvolution was found to give more appropriate data fit, which implies the data is normally distributed. The data in Figure 5-3 shows that the deconvoluted peaks adequately explain the variation in the resultant TPD profile ($R^2$=0.998).

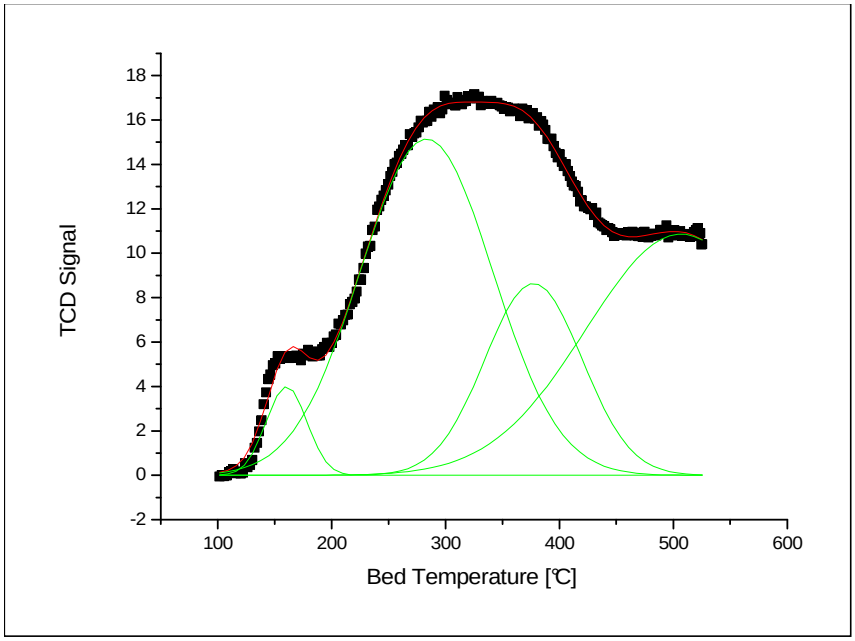


**Figure 5-3** Deconvolution of an $NH_3$/TPD profile [CAT 044, 7.6 wt% $Nb_2O_5/SiO_2$, calcined at 100°C, W=0.0816 g] $R^2$=0.998

Much like adding additional polynomial terms to a regression model, the addition of peaks to fit the TPD profiles generally results in improved coefficients of correlation. However, the addition of a peak may not be statistically significant or physically meaningful. Therefore, one must be cautious when making inferences on TPD data. In addition, the number of peaks selected can also affect the estimate of total acidity, since the proportion of the total area assigned to an artefact will change. In analyzing the data, the minimum number of peaks necessary to fit the data was used. In most cases in this work, only two peaks were required (neglecting the physisorbed $NH_3$ peak observed in some analyses). No more than three peaks plus the background peak were necessary to fit the data. This is consistent with the approach of Arena et al.[183] who used three Gaussian peaks, corresponding to weak, medium

and strong sites to deconvolute their TPD profiles. The deconvolution of the TPD profiles obtain in this work are outlined in Appendix D.

### *5.1.2 TPD Analysis*

Inherent acidity of $\gamma$-$Al_2O_3$

The TPD profile of the weakly acidic $\gamma$-$Al_2O_3$ support (Figure 5-4) provides the explanation for its catalytic activity for MO synthesis. The TPD profile reveals that the $\gamma$-$Al_2O_3$ support has a significant population of medium strength acid sites as evidenced by the desorption of a large peak of ammonia at around 240°C as well as very strong acid sites, probably Lewis sites, as indicated by the desorption of ammonia at around 660°C. In fact, the $\gamma$-$Al_2O_3$ supported catalysts had the greatest total acidity of the catalysts tested. The gamma alumina support with no niobia in Figure 5.4 also had a very high inherent total number of acid sites (164 μmol/g) corresponding to peaks eluting before 500°C. However, since the $\gamma$-$Al_2O_3$ support alone exhibits a relatively low catalytic activity and generally poor catalytic performance compared to those catalysts containing niobia, it is evident that the nature and strength of the acidity are likely important factors that affect the catalyst activity and stability.

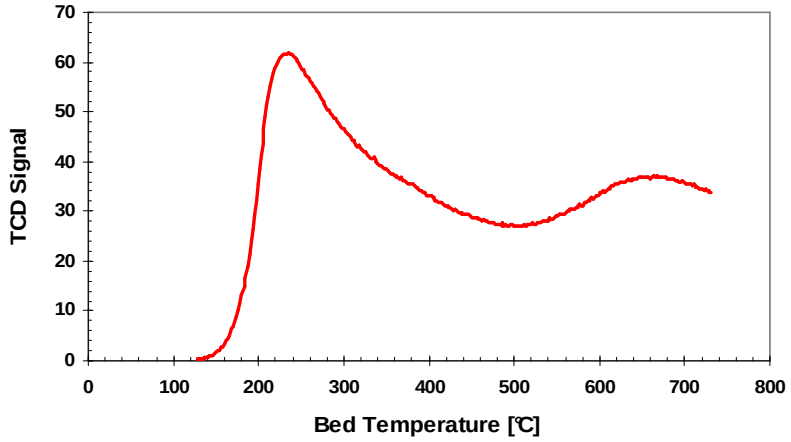


**Figure 5-4** $NH_3$/TPD profile of ammonia desorption from $\gamma$-$Al_2O_3$ (Aldrich 267740) (W=0.1261 g)

DoE #2 (Section 4.5) revisited

The autoclave experiments of DoE #2 in section 4.5 investigated the effects of calcination temperature on the activity and stability of $Nb_2O_5/\gamma\text{-}Al_2O_3$ and $Nb_2O_5/SiO_2$ catalysts. Figure 4-19 (Chapter Four) illustrates the kinetic performance for MO synthesis for $Nb_2O_5/\gamma\text{-}Al_2O_3$ catalysts CAT 026 and CAT 032, which were calcined at 500 and 100°C respectively. CAT 026 had a niobia loading of 2.65 wt% and CAT 032 had a niobia loading of 3.79 wt%. The catalyst calcined at 100°C (CAT 032, Expt. 164) had an initial activity for MO 37% greater than the catalyst calcined at 500°C (CAT 026, Exp. 154). In addition, the acetone conversions after 2 hours of operation were 6.1 and 8.4 % for the catalysts calcined at 500 and 100°C respectively.

$NH_3$/TPD analysis of these catalysts demonstrate that the marked difference in catalytic performance observed in Figure 4-19 arises as a consequence the disparity in the strength and number of acid sites, which are more prevalent in the catalyst calcined at 100°C. Figures 5-5 and 5-6 illustrate the $NH_3$/TPD profiles for catalysts 026 and 032 respectively. The $NH_3$/TPD data were deconvoluted into three peaks corresponding to weak, medium and strong sites as was done by Arena et al.[183] The analysis is summarized in Table 5-1. The catalyst calcined at 100°C had over twice the total acidity as the catalyst calcined at 500°C. In addition, the maximum desorption temperatures ($T_M$) associated with these peaks occurred at higher temperatures for the catalyst calcined at 100°C indicating that the acid sites were stronger for the catalyst calcined at 100°C. This shift in desorption temperature is most pronounced for the strong acid sites. Incidentally, these 2 catalysts exhibited the highest total acidity of the catalysts investigated. The gamma alumina support in the hydrated state also exhibited a very high total acidity. However, the biggest difference between the TPD results of catalyst 026 and 032 is the strength and number of strong acid sites, particularly the strong acid sites. The $NH_3$/TPD profiles appear similar, but twice as much catalyst was used for the TPD analysis of CAT 026 calcined at 500°C. Regardless, the peak corresponding to

the strongest acid sites is far more pronounced for catalyst 032 in Figure 5-6 than catalyst 026 in Figure 5-5.

**Table 5-1** Effect of calcination temperature on acidity of $Nb_2O_5/\gamma\text{-}Al_2O_3$ catalysts

| CAT ID (calc. T) | TM1 [°C] | TM2 [°C] | TM3 [°C] | Acidity Weak [µmol/g] | Medium [µmol/g] | Strong [µmol/g] | Total Acidity [µmol/g] |
|---|---|---|---|---|---|---|---|
| 026 (500°C) | 253 | 296 | 368 | 16.7 | 31.6 | 44.3 | 92.6 |
| 032 (100°C) | 262 | 308 | 397 | 30.2 | 64.3 | 99.5 | 193.9 |

*$TM_1$, $TM_2$ and $TM_3$ denote the temperatures associated with the $NH_3$ desorption peak maxima in Figures 5-5 and 5-6*

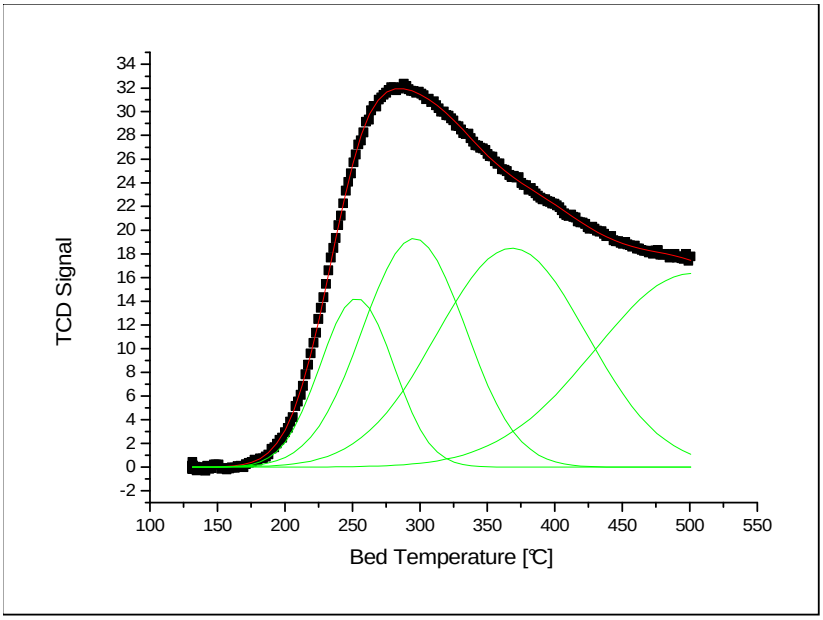


**Figure 5-5** $NH_3$/TPD profile of CAT 026, 2.65 wt% $Nb_2O_5/\gamma\text{-}Al_2O_3$, calcined at 500°C, (W= 0.122 g, $R^2$= 0.9998)

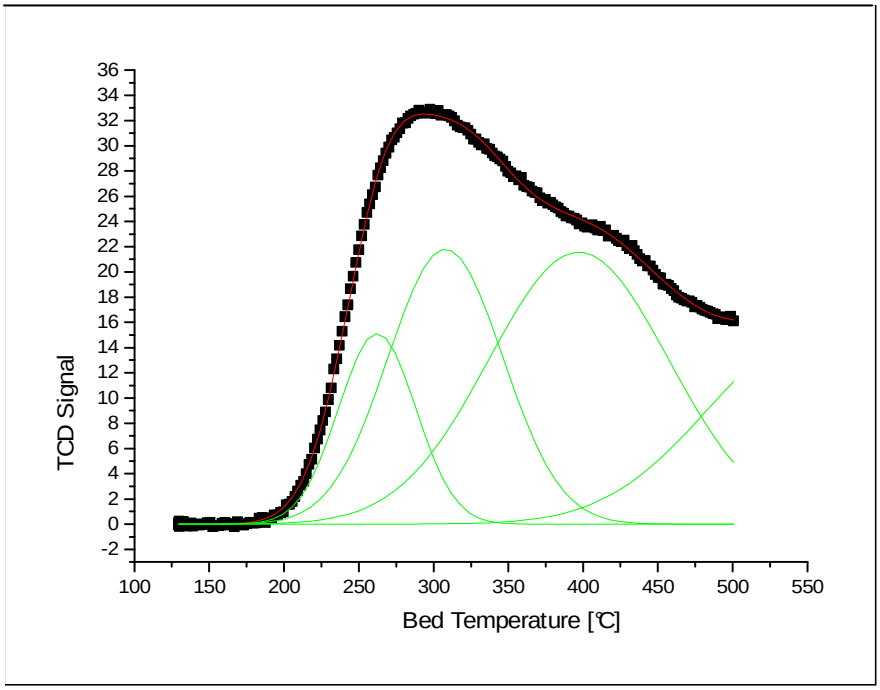


**Figure 5-6** $NH_3$/TPD profile of CAT 032, 3.79 wt% $Nb_2O_5/\gamma$-$Al_2O_3$ , calcined at 100°C, (W=0.068 g, $R^2$=0.9998)

The effect of the calcination temperature of the $Nb_2O_5/SiO_2$ catalysts on their catalytic performance for MO synthesis was investigated in DoE #2 (Section 4.5) and over three levels in the autoclave experiments of DoE #3 outlined in section 4.7. The TPD analysis of the acidity of these catalysts is very insightful. The results clearly demonstrate that the calcination temperature affects the acid strength. Specifically, the $Nb_2O_5/SiO_2$ catalysts with fumed silica supports calcined at 100°C exhibit very strong acid sites relative to those calcined at 500°C.

In Figures 5-7 through 5-9, the TPD profiles were deconvoluted using only two peaks to describe the data, neglecting the background peak and the peak associated with physisorbed species observed in some figures. CAT 029 (Fig 5-7) was one of the most active catalyst produced in this work (Fig 4-18). The strong acid site in Figure 5-7 is centred about an average desorption temperature of 389°C. For the fumed silica catalysts calcined at 100°C, the

desorption of the last ammonia peak prior to the artefact is observed on average around 370°C when deconvoluted with only two peaks. This peak corresponding to the strong acid sites is observed on average around 320°C for the catalysts calcined at 500°C (Figure 5-8). The catalysts calcined at 300°C showed an intermediate acid strength as evidenced by the desorption of the last ammonia peak prior to the artefact on average at around 340°C (Figure 5-9).

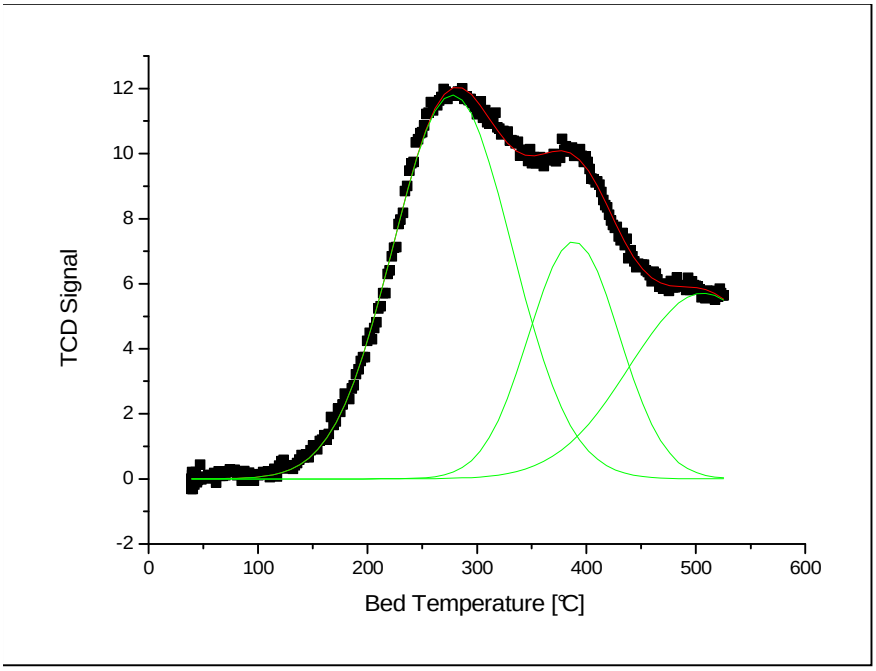


**Figure 5-7** $NH_3$/TPD profile of a $Nb_2O_5/SiO_2$ catalyst calcined at 100°C exhibiting very strong acid sites (CAT 029, W=0.0331 g, $R^2$=0.998) *The strong acid sites have Tm=368°C*

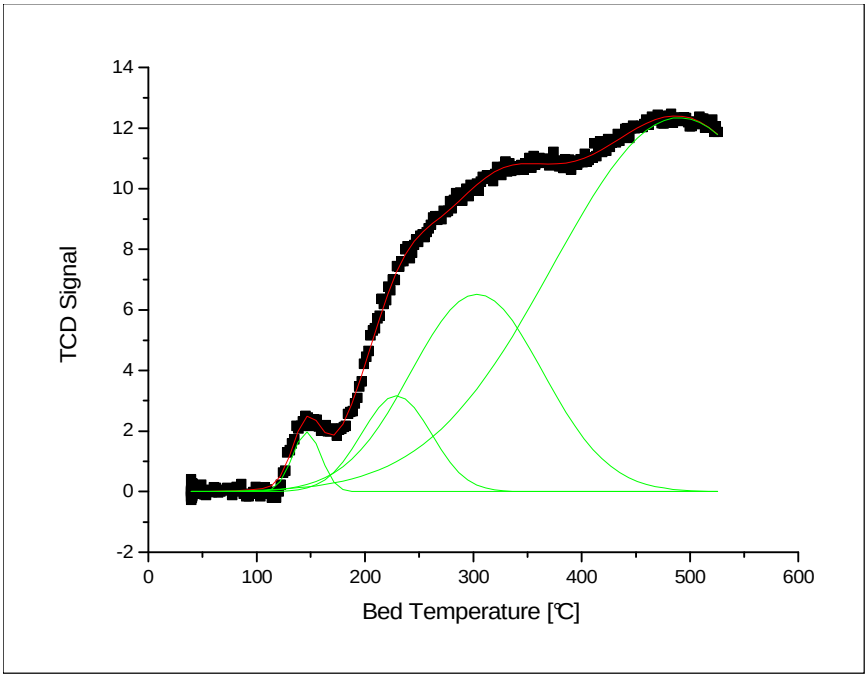


**Figure 5-8** $NH_3$/TPD profile of a $Nb_2O_5/SiO_2$ catalyst calcined at 500°C (CAT 048, W=0.0999 g, $R^2$=.999) *The strong acid sites have $T_m$=315°C.*

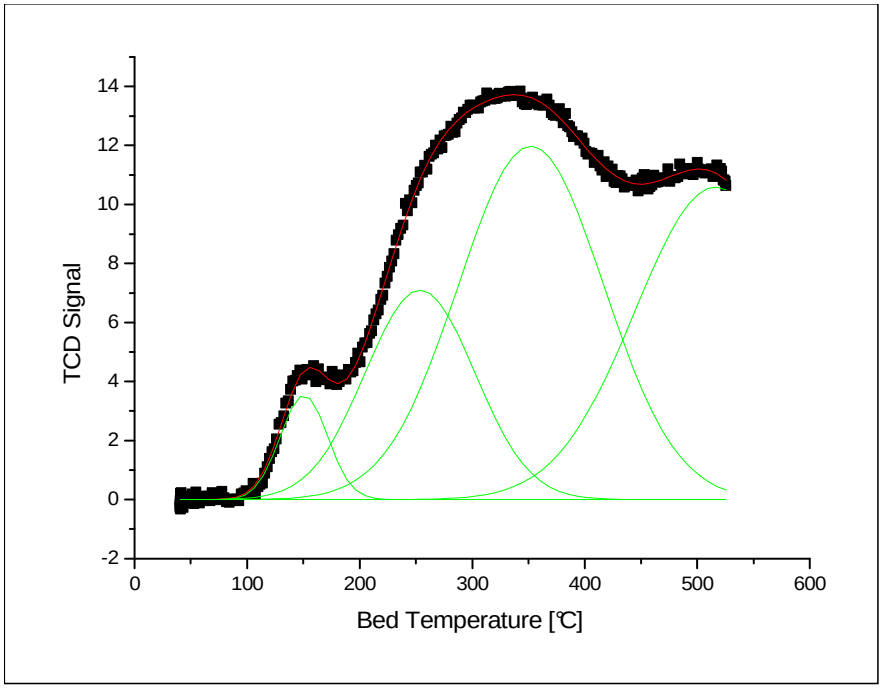


**Figure 5-9** $NH_3$/TPD profile of a $Nb_2O_5/SiO_2$ catalyst calcined at 300°C (CAT 045, W=0.0899 g, $R^2$=.999) *Catalyst 045 has intermediate acidity; the strong acid sites have $T_m$=352℃.*

For the fumed $SiO_2$ catalysts calcined at 500°C in this work, the highest desorption temperature of ammonia observed over the range of 120 to 520°C was 338°C (CAT 049; 7.96 wt% $Nb_2O_5$) when using only two peaks to characterize the acidity. This catalyst had a high level of niobia loading in DoE #4 (Chapter Four). The most active $SiO_2$ catalysts for MO synthesis were calcined at 100°C. For the most active catalysts, the ammonia desorption peak around 370°C were more pronounced, which suggests that these strong acid sites are primarily responsible for the catalytic activity. Catalyst 040 (10.2 wt% $Nb_2O_5/SiO_2$ calcined at 100°C) was found to exhibit a relatively high activity for MO synthesis (experiment 176). The initial rate of MO production found in experiment 176 was 0.00996 mol/(L*min*$g_{cat}$) or in terms of niobia, 0.0980 mol/(L*min*g$Nb_2O_5$).

Both the autoclave experiment and the TPD experiment were repeated to confirm this result. Experiment 179 was a replicate of autoclave experiment 176. The initial rate of reaction for MO synthesis at 160°C estimated in experiment 176 was within 2% of that of determined in experiment 179. The TPD profile was also highly repeatable (Appendix D). When using two peaks to characterize the acidity, the total acidity was repeatable to within 3%. The TPD analysis of catalyst 040 in Figure 5-10 reveals a large proportion of relatively strong acid sites as evidenced by the elution of ammonia centred about a desorption peak maximum temperature of 375°C.

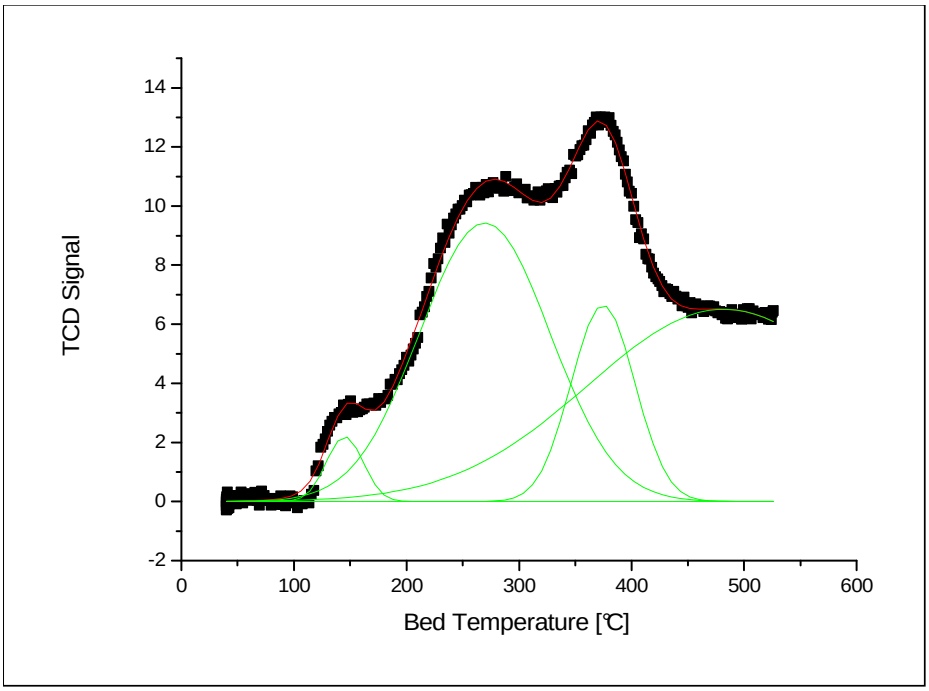


**Figure 5-10** $NH_3$/TPD profile of a highly active $Nb_2O_5/SiO_2$ catalyst for MO synthesis (CAT 040, 10.2 wt% $Nb_2O_5/SiO_2$, calcined at 100°C)

*Strong acid sites with 360<Tm< 400°C when using two peaks to characterize the acidity, are only observed for catalysts calcined at 100°C. This peak becomes more pronounced with higher catalyst loading and appears to be correlated with catalyst activity.*

The effect of calcination temperature on the desorption peak maximum temperature ($T_M$) associated with the most strongly adsorbed $NH_3$ for $Nb_2O_5/SiO_2$ catalysts is illustrated in Figure 5-11. The results clearly demonstrate that the $SiO_2$ catalysts calcined at low temperature give rise to very strong acid sites, presumably Bronsted acid sites. The relative strength of the strongest acid sites present in each specimen, diminish with increasing calcination temperature. The broad 95% confidence bounds illustrated in the Figure arise as a consequence of the variation in the niobia loading for the specimens, which was an experimental variable. The niobia loading also affected the strength of the acid sites present. The maximum ammonia desorption temperature associated with the strongest acid sites increased slightly with increasing niobia loading.

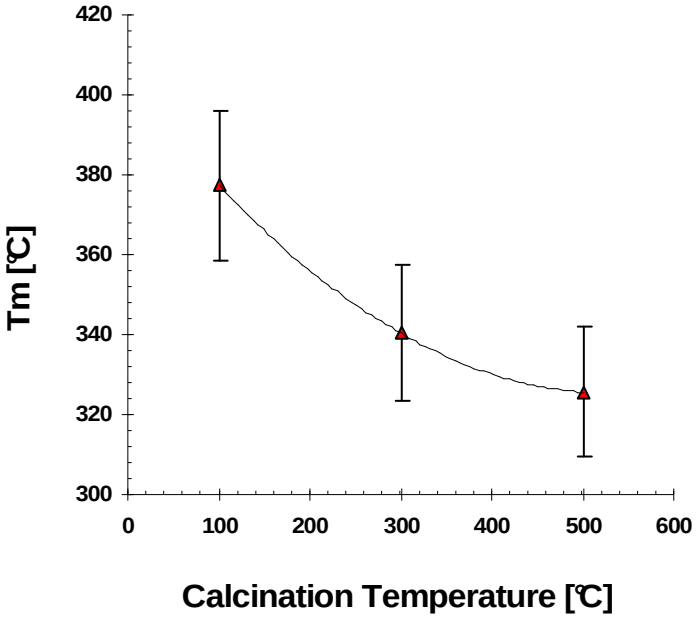


**Figure 5-11** Effect of calcination temperature on the average desorption temperature ($T_m$) associated with the strongest acid sites observed in the TPD profiles below 500°C for the $Nb_2O_5/SiO_2$ catalysts investigated (17 specimens, 95% confidence bounds indicated on average $T_m$)

The strong acid sites characterized by high desorption maximum temperature in excess of 360°C appear to be the signature of a niobia catalyst exhibiting excellent catalytic performance for MO synthesis. Note that although catalyst 040 was more active for MO synthesis than CAT 032, (3.79 wt% $Nb_2O_5/\gamma$-$Al_2O_3$ calcined at 100°C), the more active catalyst had much lower total acidity (55.3 μmol/g averaged over two measurements) compared to CAT 032 (194 μmol/g). It is evident that the total number of acid sites alone does not determine the overall activity and that the nature and strength of the acidity must also be important.

In the final catalyst formulation used in the catalytic distillation experiments of Chapter Eight, a commercial silica catalyst carrier (Norpro SS 65137, ca. 155 $m^2/g$) was used. Figure 5-12 is the $NH_3$/TPD profile of a catalyst consisting of niobia dispersed onto the commercial silica catalyst carrier for use in a flow reactor experiment (Chapter Six). This catalyst (CAT 057)

was calcined at 100°C and exhibited excellent performance for MO synthesis. The TPD profile shows that the strong acid sites observed in previous catalysts calcined at 100°C are present. However, this peak is very pronounced and corresponds to a higher ammonia desorption maximum temperature (396°C) which indicates a much larger population of these acid sites as well as a greater acid strength associated with these sites. In addition, Figure 5-12 reveals that a new and very strong acid site is present corresponding to the desorption of ammonia around 460°C, which was not previously observed in these TPD experiments. TPD analysis of the support without niobia (Appendix D) confirms that the Norpro HSA silica support does not exhibit any inherent acidity. The fumed silica support also was found to exhibit negligible acidity.

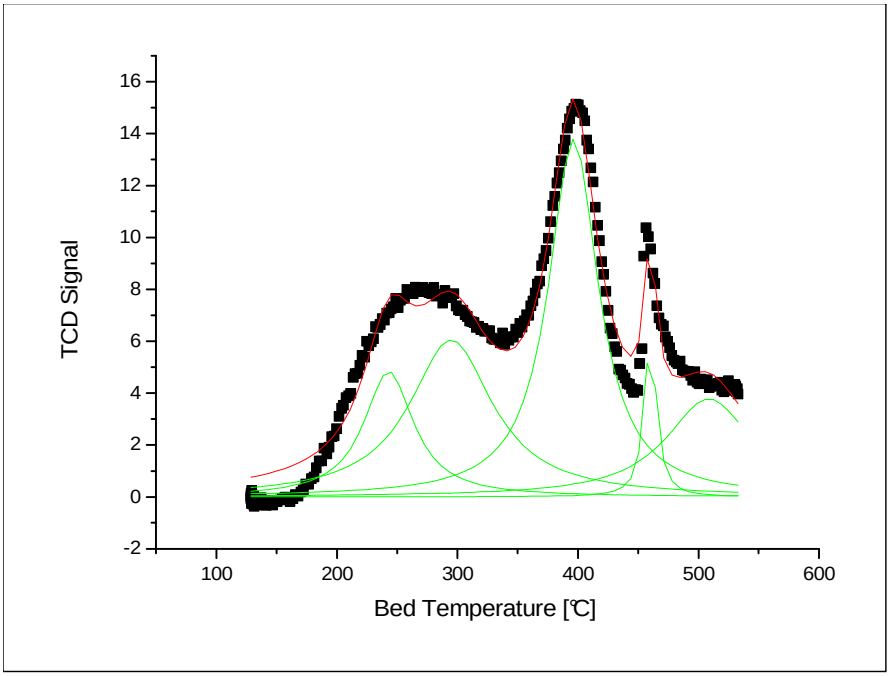


**Figure 5-12** $NH_3$/TPD profile of catalyst 057 5.30 wt% $Nb_2O_5$/ Norpro HSA $SiO_2$ (W=0.126 g) *A new and very strong acid site, not observed in previous experiments, is evident in the TPD profile of catalyst 057 from $NH_3$ desorption at 460°C. A very large population of strong acid sites is also evident from the desorption of ammonia at 396°C.*

It is interesting to note that this catalyst with very strong surface acidity had a relatively low niobia loading, 5.30 wt% (XRF) which corresponds to about ¼ monolayer coverage. Evidently, the niobia was more efficiently utilized on this lower surface area silica support, which also resulted in

numerous unique and very strong acid sites. In addition, the total acidity of this catalyst, was only 41.2 μmol/g. However, about half of the acid sites (49.4%) are very strong acid sites ($T_m \geq 360°C$). This suggests that the activity for MO synthesis increases with increasing acid strength.

During catalyst preparation of CAT 057, sufficient precursor was used to achieve monolayer coverage on the higher surface area fumed silica support (255 $m^2/g$). However, in the case of the Norpro catalyst carrier, a smaller fraction of the precursor was integrated into the catalyst during the thermal attaching reactions responsible for the generation of the overlayer, which resulted in a much lower surface coverage (1/4 monolayer). XRD analysis (section 5.3) of similar catalysts with the same catalyst formulation as CAT 057, suggests that the niobia overlayer is highly dispersed with no evidence of $Nb_2O_5$ crystallites.

**T**he peak associated with strong acid sites increase in area and increase slightly in desorption temperature with increasing niobia loading. In addition, ammonia desorption peaks with maxima in excess of around 360°C associated with the relatively strong acid sites were not present in any $Nb_2O_5/SiO_2$ catalysts calcined at 500°C, regardless of their niobia loading when using two peaks to characterize the acidity. This indicates that these strong acid sites are unique to low temperature calcination, which strongly suggests that these acid sites are Bronsted acid sites. This $NH_3$/TPD data, coupled with *in situ* DRIFT spectra of the adsorption of pyridine probe molecules on the catalysts (Section 5.2) confirm that these sites are indeed Bronsted acid sites.

The $NH_3$/TPD profile of CAT 066, a 6.09 wt% $Nb_2O_5/SiO_2$ catalyst is given in Figure 5-13. This catalyst also had a Norpro silica catalyst carrier as a support and represents the final catalyst formulation of this work. This catalyst was used in a catalytic distillation pilot plant experiment (CD 003, Chapter Eight). The niobia loading of this catalyst corresponds to only 30% monolayer

coverage (~1/3 monolayer). However, the results in Figure 5-13 illustrate the presence of a large population of very strong acid sites centred about a desorption maximum temperature of 485°C. The TPD scan was carried out to as high as 800°C to elucidate other strong acid sites centred about a desorption maxima at 626°C. Niobia catalysts with other supports including fumed silica, when scanned to elevated temperatures, exhibited a "flat line" like artefact and did not reveal acid sites beyond 500°C (Appendix D). The TPD results of the analysis of catalyst 066 reveals significant total acidity (115 μmol/g) with a substantial proportion of strong acid sites (83.2% Tm ≥ 360) considering only the first 4 peaks in Figure 5-13.

It is interesting that such a significant increase in the acidity (CAT 066 vs CAT 057) occurred due to a subtle increase in niobia loading from 5.3 to 6.1 wt%. In addition, the fact that very strong and unique acid sites are created when niobia is dispersed onto the Norpro silica catalyst carrier, compared to niobia dispersed onto fumed silica is striking evidence of the important influence of the surface oxide support interaction (SOSI) on the resultant niobia structure and properties. Yet these very strong acid sites are achieved only on the catalyst carrier and at relatively low niobia loading.

The details of the TPD analyses of all catalysts, including the temperatures associated with the peak maxima, the peak areas, the acidity associated with the peaks and the total catalyst acidity is given in Table D2-1 (Appendix D).

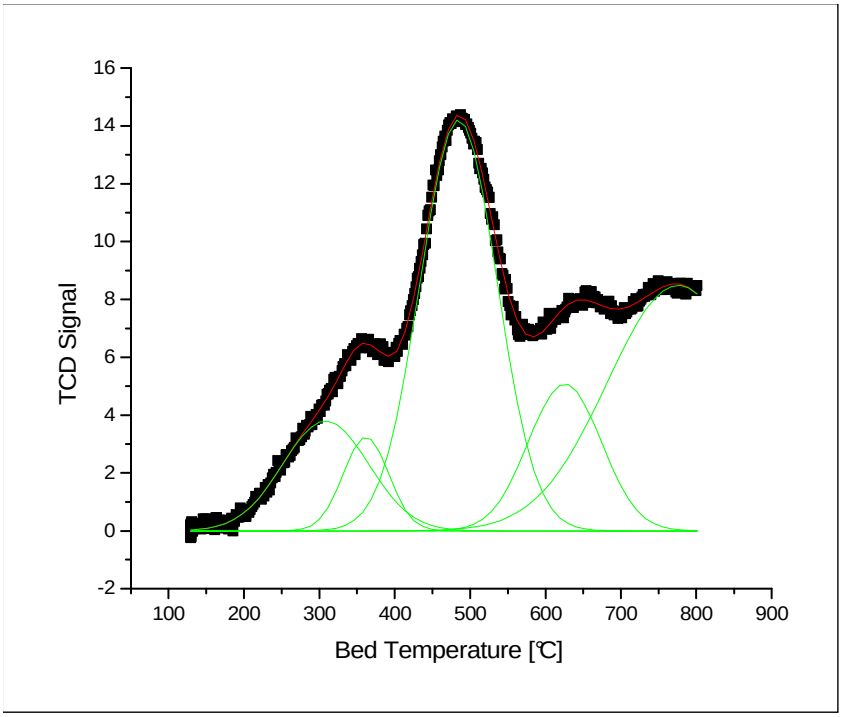


**Figure 5-13** $NH_3$/TPD profile of CAT 066, 6.09 wt% $Nb_2O_5$/ Norpro HSA $SiO_2$ (W=0.0585 g)

*5.1.3 Regression Analysis*

The $NH_3$/TPD profiles of fumed silica catalysts used in DoE #2 and DoE #4 for which the niobia loading, support activation temperature and calcination temperature were varied were analyzed to determine if any associations existed between the catalyst acidity and resultant kinetic behaviour established in the previous experiments. Not surprisingly, when the total acidity of the catalysts were ascertained by TPD data using two peaks to characterize the acidity, the niobia loading was found to be correlated with the acid site density (Figure 5-14). With the exception of a couple of outliers, the acid site density was also weakly correlated to the initial rate of reaction for MO synthesis.

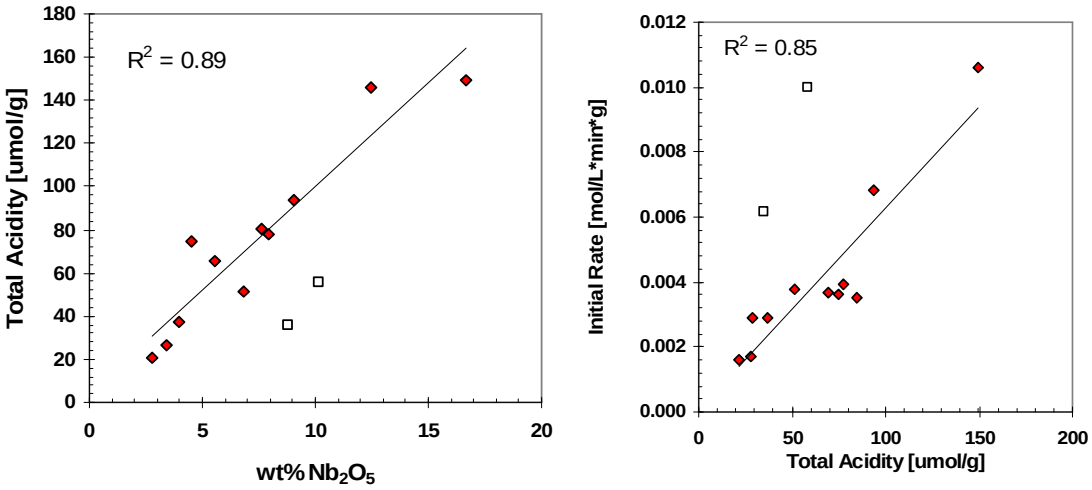


**Figure 5-14** (a) (left) Effect of niobia loading on the acid site density (b) (right) Effect of the acid site density on the initial rate of reaction for MO synthesis *Data obtained from fumed silica catalysts used in DoE #2 and DoE #4. Apparent outliers are indicated by open squares. The TPD profiles were deconvoluted using two peaks to characterize the acidity.*

The fact that the catalyst activity correlates with the acid site density suggests that both Lewis and Bronsted acid sites are active for MO synthesis. For example, if only Bronsted acid sites were active, then those catalysts exhibiting only strong Lewis acid sites (eg. calcined at 500°C) would exhibit strong acidity but would not correlate well with the activity for MO synthesis. This conclusion is supported by the autoclave experiments in chapter Four whereby some catalysts calcined at 500°C, which deactivated rapidly to a "pseudo equilibrium" conversion, exhibited good initial activity. Considering the relatively good repeatability of the TPD experiments, and the relatively low coefficients of correlation, the results suggest that there are factors other than the total number of acid sites which also affect the initial rate of reaction for MO synthesis. Similarly, the generation of acid sites likely depends on factors in addition to the niobia loading, such as, possibly, the thermal treatment including support activation temperature.

Indeed, the outlier in the plot of total acidity vs activity for MO synthesis, for which a very high activity was observed (~ .010 mol/L*min*$g_{cat}$) for a

relatively low total acidity (58.4 μmol/g), corresponds to CAT 040 (Figure 5-10), which was calcined at 100°C and exhibited a large proportion of very strong acid sites. The second outlier at the lower total acid strength also exhibited a higher than expected activity. This data point corresponds to CAT 059, which was also calcined at 100°C. Similarly, some catalysts which exhibited very high total acid site density showed low activity for MO synthesis. For example, the γ-$Al_2O_3$ support exhibited significant total acidity (164 μmol/g) but low activity (0.003 mol/L*min*g). Evidently, the total acid site density is not the sole factor which determines catalytic activity.

Figure 5-15 shows that the activity for MO synthesis is also related to the acid strength. In Figure 5-15 the initial rate of reaction for MO synthesis is plotted against the temperature associated with the desorption peak maximum ($T_m$) of the peak corresponding to the strongest acid sites. The temperature associated with the desorption peak maximum is a measure of the strength of the acid sites associated with the peak. For example, empirical correlations of the form of equation (5-1), where a and b are material specific constants, allow prediction of the Hammet acidity as a function of the desorption temperature.[184] With the exception of a couple of outliers in Figure 5-15, the initial rate of reaction for MO synthesis appears to correlate well with the acidity of the strongest acid sites.

$$H_0 = a + \frac{b}{T_m} \qquad \textbf{(5-1)}$$

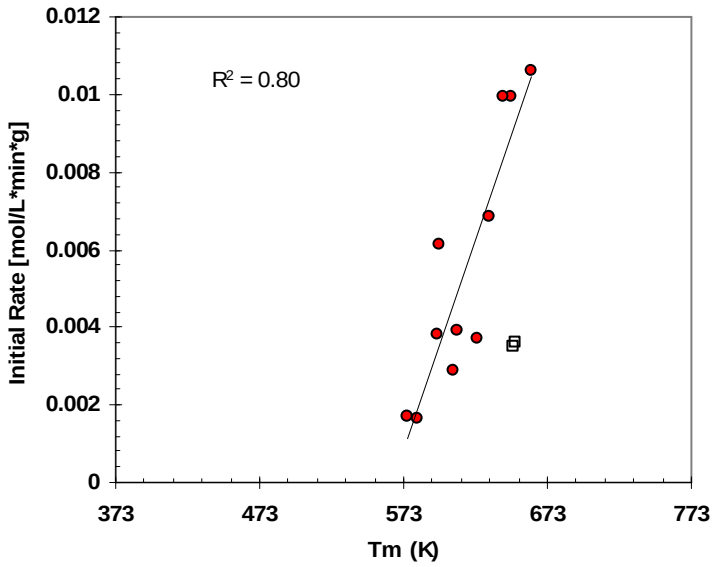


**Figure 5-15** Effect of the acid strength of $Nb_2O_5/SiO_2$ catalysts on the initial rate of reaction of MO synthesis at 160°C. (*Catalysts used in DoE #2 and DoE #4. Apparent outliers identified by hollow circles.)*

## 5.2 Diffuse Reflectance Infrared Fourier Transform Spectroscopy

### *5.2.1 in situ DRIFT Adsorption Spectra of Pyridine Probe Molecules*

IR spectroscopic investigation of the physicochemical interaction of basic probe molecules with the niobia catalysts were employed in order to ascertain the nature of the acidity. Pyridine (Caledon, Reagent Grade, 8700-1, Lot 48178, ≥99.0%) was used as the probe molecule since it is a strong base which can selectively detect both Lewis and Bronsted acidity.[184] Moreover, *in situ* IR study of pyridine adsorption has been used extensively by previous investigators to elucidate the nature of the acidity of niobic acid and niobia supported on various metal oxides.[68,87,88,91-93,97,99,100,103,105] Consequently, the IR vibrations of pyridine adsorbed on niobia compounds are well known.

The interaction of pyridine with Bronsted acid sites results in the formation of pyridinium ions whereas the interaction of pyridine with Lewis acid sites results in one of several possible coordinativley bonded adsorbed species. Pyridine may also form hydrogen bonds with an acidic surface. The

characteristic IR skeletal vibrations of pyridine associated with these unique adsorption modes on acidic surfaces are summarized in Table 5-2.

**Table 5-2** Assignment of IR skeletal vibrations of pyridine adsorbed on solid acid catalysts

| Interaction | Assignment IR Wavenumber [$cm^{-1}$] | References |
|---|---|---|
| Pyridinium ion (Bronsted) | 1540<br>1580<br>(1485-1500)<br>1640 | 88, 91, 99, 184<br>92<br>184<br>184 |
| Coordinative Bond (Lewis) | 1450, (1447-1460),<br>(1488-1503), 1490<br>1575<br>1580<br>(1600-1633)<br>1620<br>1610, 1480, 1440 | 99, 92, 184<br>92, 184<br>92, 184<br>184<br>184<br>92<br>88 |
| Hydrogen Bond | (1400-1477)<br>(1485-1490)<br>(1580-1600) | 184<br>184<br>184 |
| Iminium ion (Bronsted-Lewis pair) | 1462 | 184 |

A Bio-Rad Spectrometer (Excalibur-Super) equipped with a MCT detector was used to obtain *in situ* measurements of Diffuse Reflectance Infrared Fourier Transform (DRIFT) spectra of pyridine probe molecules interacting with the acidic catalyst surfaces. The IR sample cell was filled to about 2/3 of its capacity with silicon carbide. The remaining volume of the cell was then filled with the catalyst sample. The specimen was then compressed into a disk and its external surface smoothed. The sample cell was sealed and installed into the FTIR. The catalyst was subjected to a pre-determined thermal treatment under high vacuum in order to activate the specimen. The sample was then cooled to a predetermined temperature and isolated from the vacuum system. The background scan was obtained prior to pulse adsorption of pyridine and was subtracted from the DRIFT spectra obtained so that only vibrations associated with the adsorption of pyridine would be visible in the DRIFT spectra. The catalyst was then saturated with pyridine by a succession

of 30 second pulses. The pulse adsorption of pyridine was monitored by collecting DRIFT spectra after each successive pulse. Once saturated, the cell was reconnected to the vacuum system and the in situ DRIFT spectra were obtained periodically.

To obtain the spectra, the samples were irradiated with a 600 μW monochromatic laser source with a wavelength of 632.8 nm. The resultant spectra consisted of time-averaged results of 25 scans with a resolution of 4 $cm^{-1}$ and a data acquisition frequency of 10 kHz. Other Bio-Rad FTIR parameters were sensitivity=1, Filter=1.2 and UDR=2. The custom made vacuum system was equipped with a primary BOC Edwards vacuum pump and a secondary diffusion pump to enable high vacuum. The pressure was monitored with a BOC Edwards Wide Range Gauge (WRG-5) and a BOC Edwards Active Pirani Gauge and Active Gauge controller (APGX-M-15MM ST/ST). The MCT detector of the FTIR cell was cooled to cryogenic temperature (ca. 77 K) using liquid nitrogen in order to minimize radiation from the ambient.

In preliminary experiments, the DRIFT spectroscopic analysis procedure was based on the procedure disclosed by Datka et al.[91] who investigated the acidic properties of surface-phase niobia dispersed onto various transition metal supports. The IR cell was evacuated to about $10^{-2}$ torr, heated to 100°C and held there for 30 minutes. The sample was then heated to 220°C and held there for 10 minutes. Finally, the sample was heated to the pre-treatment temperature of 425°C. The secondary diffusion pump was then enabled which reduced the vacuum in the IR cell to about $10^{-5}$ torr. Once high vacuum was achieved, the sample was retained at 425°C for 2 hours. After thermal treatment, the IR cell was then cooled to 200°C, isolated from the vacuum system and a background scan of the catalyst was obtained. Pyridine was then pulse adsorbed onto the catalyst and the DRIFT spectra were obtained as described previously.

Although activation of the material at elevated temperature is useful for investigating the acidic properties of the catalysts which had been calcined at 500°C, for samples calcined at low temperature, a thermal treatment at 425°C under high vacuum for 2 hours would be sufficient to appreciably modify the catalyst's acidic properties. That is, one would be modifying the very structure one is trying to measure. The thermal treatment would destroy the Bronsted acidity due to dehydroxylation making it less likely to elucidate the Bronsted nature of the acid sites. In fact, the IR spectra presented by Datka et al.[91] for niobia aluminas calcined at 500°C for which very slight Bronsted acidity was claimed was questioned by da Silva et al.[92] who argued that Datka et al's spectra did not conclusively show the presence of Bronsted acidity. da Silva et al.[92] reported that no Bronsted acidity was present in their own niobia-alumina specimens that were calcined at 450°C and activated in the IR cell at 480°C. Consequently, in later experiments in this work, the catalysts were activated *in situ* in the IR cell at low temperatures and high vacuum for prolonged periods of time. For example, catalysts were typically activated at 120°C for 10 hours at a pressure of about 1 x $10^{-5}$ torr. Pulse adsorption of pyridine would be carried out at the same temperature.

The DRIFT spectra of a 17.1 wt% $Nb_2O_5/\gamma$-$Al_2O_3$ catalyst (CAT 018) calcined at 500°C is given in Figure 5-16. The figure reveals four characteristic peaks at ~ 1450 $cm^{-1}$, 1490 $cm^{-1}$, 1577 $cm^{-1}$ and a broad feature at around 1610 $cm^{-1}$. Each of these vibrations corresponds to coordinativley adsorbed pyridine, which is indicative of Lewis acid sites. These vibrations were observed in most specimens. The spectra in Figures 5-16 and 5-17 are characteristic of other $Nb_2O_5/\gamma$-$Al_2O_3$ and $Nb_2O_5/SiO_2$ catalysts calcined at 500°C in that the spectra for these catalysts reveal significant Lewis acidity and no evidence of Bronsted acidity. Figure 5-17 illustrates an example of an *in situ* DRIFT spectrum for a $Nb_2O_5/SiO_2$ catalyst calcined at 500°C. The same peaks corresponding to coordinativley bonded pyridine on Lewis acid sites are present.

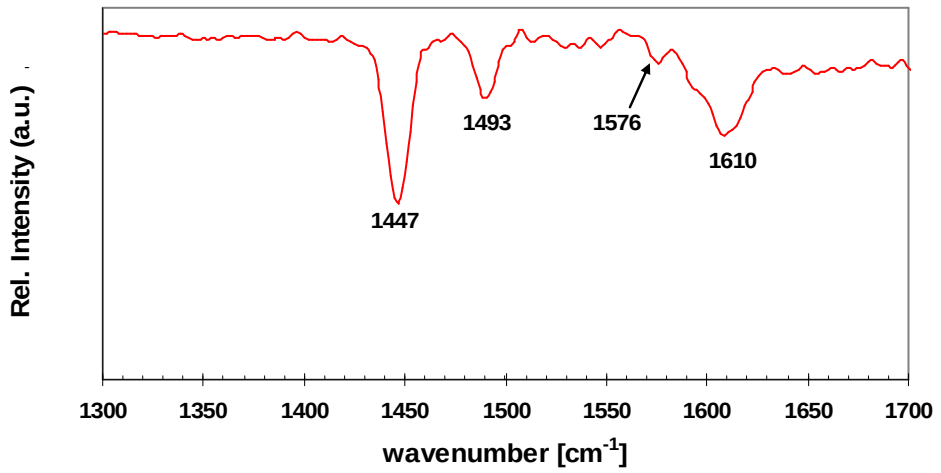


**Figure 5-16** *in situ* DRIFT spectrum of pyridine adsorption on a 17.1 wt% $Nb_2O_5/\gamma$-$Al_2O_3$ catalyst (CAT 018) calcined at 500°C after 2.5 hours *in vacuo*. *The specimen in Figure 5-14 was activated in situ at 425°C for 2 hours at P=1.5 x $10^{-4}$ torr. The pulse adsorption of pyridine and the resultant DRIFT spectra were obtained at 200°C.*

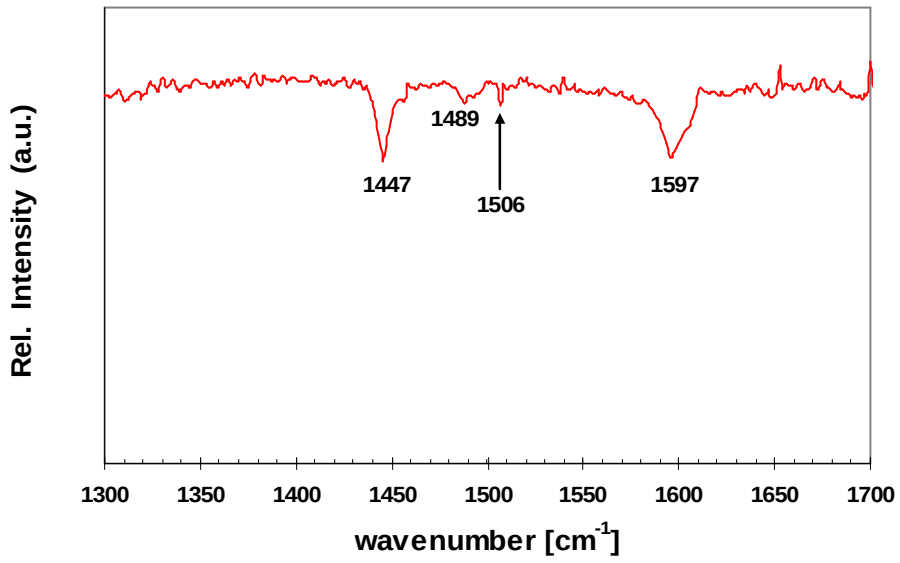


**Figure 5-17** *in situ* DRIFT spectrum after 15 minutes *in vacuo* ( of pyridine adsorption on a 12.5 wt% $Nb_2O_5/SiO_2$ catalyst (CAT 027) calcined at 500°C *The specimen in Figure 5-15 was activated in situ at 120°C for 2 hours at P=9.5 x $10^{-6}$ torr. The pulse adsorption of pyridine and subsequent spectra were obtained at 120°C.*

Some of the peaks in the $Nb_2O_5//\gamma$-$Al_2O_3$ catalyst are shifted to slightly higher frequencies, suggesting those sites are more acidic. The signal intensity is weaker for the silica catalysts since they typically have about one third to one

half the total acid site density as the alumina catalysts. The baseline tends to be noisier for specimens activated at low temperature such as the case in Figure 5-17.

The TPD results of the previous section demonstrate that the catalysts calcined at 100°C exhibit very strong and unique acid sites not observed in those catalysts calcined at 500°C. From the TPD results in the previous section, combined with the FTIR results presented in this section, it is reasonable to conclude that the very strong acid sites are in fact Bronsted acid sites. Figure 5-18 shows the DRIFT spectra for catalyst 040, which is a $Nb_2O_5/SiO_2$ catalyst with a similar loading to catalyst 027, whose spectra is shown in the previous figure (5-14). The $NH_3$/TPD profile of catalyst 040 is given in Figure 5-10, which reveals a significant proportion of very strong acid sites. The DRIFT spectra in Figure 5-18 reveals peaks at associated with Lewis acidity also observed in previous specimen including those calcined at 500°C, at 1447, 1409, 1506 and 1598 $cm^{-1}$. However, two new peaks are evident at 1539 $cm^{-1}$ and 1560 $cm^{-1}$. These vibrations were only observed in catalysts calcined at 100°C. The vibration at ca 1540 $cm^{-1}$ is known to be associated with the pyridinium ion and is direct evidence of Bronsted acidity. The vibration at 1560 $cm^{-1}$ is unknown but is present in all of the catalysts calcined at 100°C and appears to be associated with Bronsted acidity.

Figure 5-19 is an example of the DRIFT spectrum of another catalyst calcined at 100°C. The scale is adjusted to better illustrate the peaks. The baseline for this spectrum is also noisy due to the low temperature activation temperature. This figure also reveals vibrations at 1540 $cm^{-1}$ and 1560 $cm^{-1}$ associated with Bronsted acidity. Additional higher frequency vibrations are evident beyond 1600 $cm^{-1}$ at about 1635 and 1653 $cm^{-1}$. A comparison of Figure 5-19 to 5-17 suggests that these high frequency vibrations are also associated with catalysts calcined at 100°C.

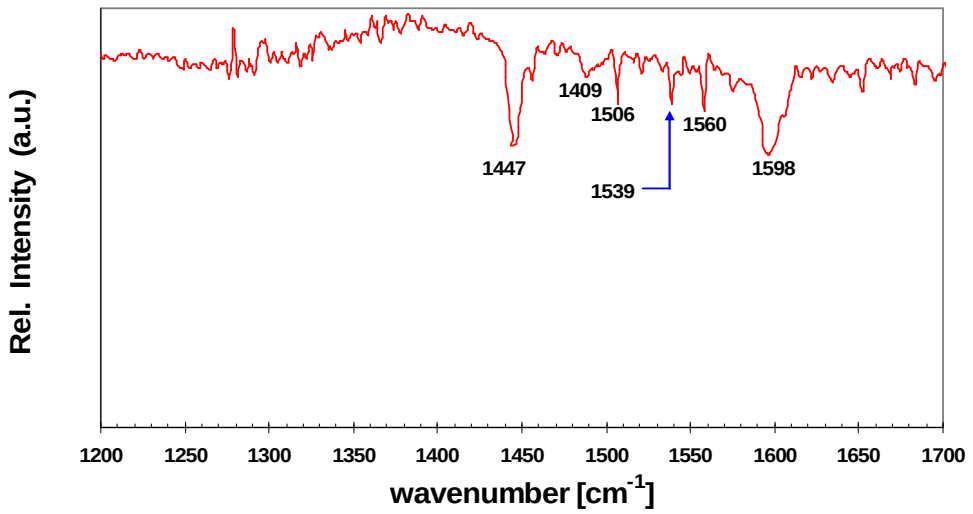


**Figure 5-18** *in situ* DRIFT spectrum of pyridine adsorption after 15 minutes *in vacuo* (1.6 x $10^{-5}$ torr)on a 10.2 wt% $Nb_2O_5/SiO_2$ catalyst (CAT 040) calcined at 100°C. *The catalyst was activated in situ at 120°C for 10 hours at P=~ 9 x $10^{-6}$ torr; pyridine adsorption and spectra obtained at 120°C*

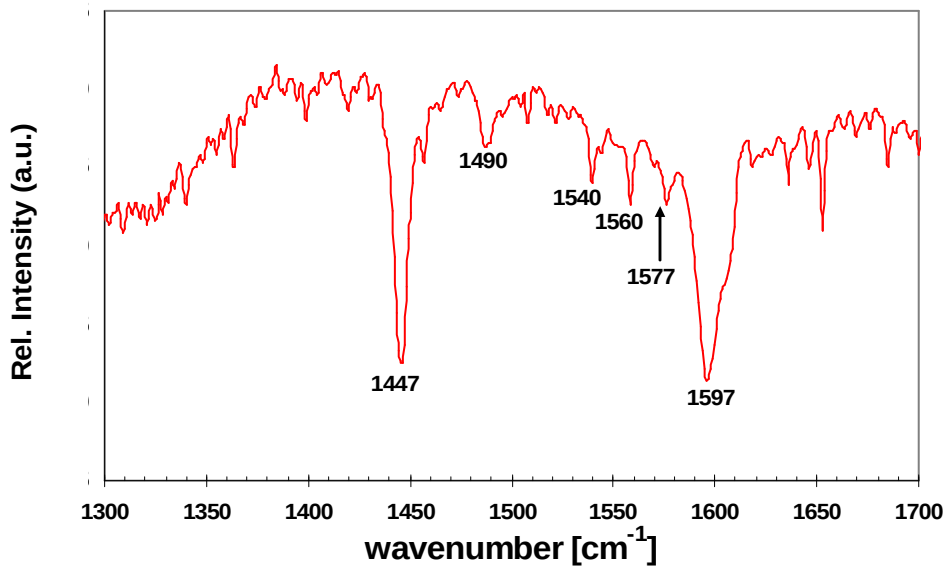


**Figure 5-19** *in situ* DRIFT spectrum after 15 minutes *in vacuo* of pyridine adsorption on a 12.3 wt% $Nb_2O_5/SiO_2$ catalyst (CAT 030) calcined at 100°C (1.7 x $10^{-5}$ torr) *Catalyst activated in situ at 120°C for 10 hours at P ~ 9 x $10^{-6}$ torr. Pyridine adsorption and spectrum obtained at 120°C. Intensity axis scale adjusted to better illustrate peaks.*

The FTIR results for catalyst 065 a $Pd/Nb_2O_5/SiO_2$ catalyst of the formulation used in the final catalytic distillation experiments is illustrated in Figure 5-20. The baseline is not flat in this region due to strong IR reflectance in the region from around 1270 to 1770 $cm^{-1}$ for this multifunctional catalyst as illustrated in Figure 5-21. The result is interesting in that not only are the vibrations associated with Bronsted acidity present at ca. 1540 $cm^{-1}$ and 1560 $cm^{-1}$ as expected due to the low temperature calcination, but interestingly, the major peaks at 1450, 1490 and 1600 $cm^{-1}$ associated with Lewis acidity are significantly diminished in the DRIFT spectra. Since the peak intensity in the IR spectrum is proportional to the surface concentration of sites, this result suggests that the acid sites are predominantly Bronsted in character for this catalyst. This conclusion seems supported by the $NH_3$/TPD profile of Figure 5-13 for catalyst 066, which had the same formulation. The TPD profile suggest that the majority of acid sites belong to a population of very strong acid sites, which appear to be Bronsted acid sites based on the IR results.

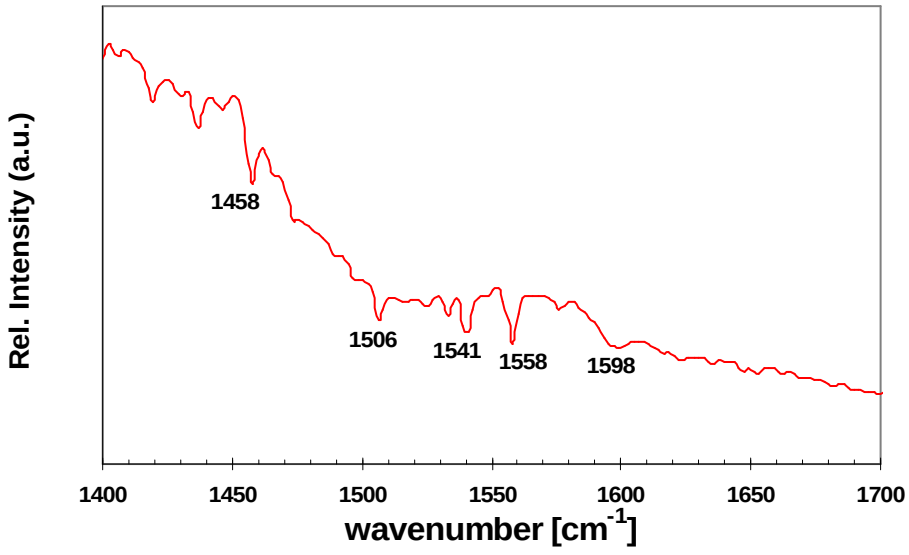


**Figure 5-20** *in situ* DRIFT spectrum after 15 minutes *in vacuo* of pyridine adsorbed on a $Nb_2O_5$/Norpro SS 65137 $SiO_2$ catalyst (CAT 065) (1.9 x $10^{-5}$ torr). *The catalyst was activated in situ at 120°C for 10 hours at P ~ 1 x $10^{-5}$ torr. Pulse adsorption of pyridine and sample scan obtained at 120°C.*

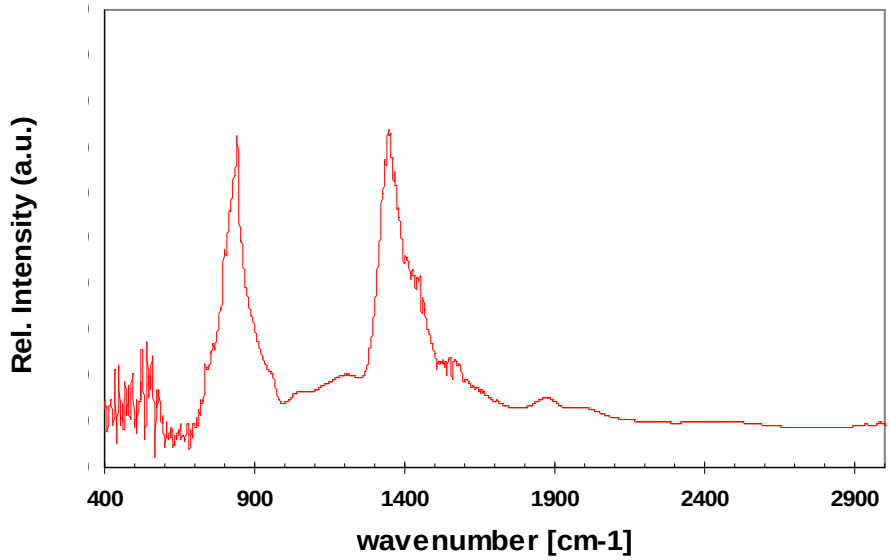


**Figure 5-21** DRIFT spectrum of Figure 5-20 expanded to show a broader range of wavenumbers (pyridine adsorption on CAT 065 after 15 minutes in vacuum)

It is possible that the treatment of the catalyst with glacial acetic acid during the palladium impregnation stage may have enhanced the population of Bronsted acidity. However, the $NH_3$/TPD profile for CAT 057 (Figure 5-10), which had the same formulation with the exception that it was not impregnated with palladium, showed a similar TPD profile with the majority of sites belonging to a population of very strong acid sites.

### *5.2.2 Catalyst Characterization via Carbon Monoxide Probe Molecules*

The final catalyst formulation used in this work for the CD experiments in Chapter Eight involve palladium and niobium oxide dispersed onto a silica commercial catalyst carrier. The *in situ* DRIFT adsorption spectra of carbon monoxide probe molecules on the catalyst were ascertained in order to characterize the catalyst surface morphology and oxidation state of the palladium. A few pellets of catalyst 065 (6.09 wt% $Nb_2O_5$, 0.04 wt% Pd on Norpro $SiO_2$) was crushed with a mortar and pestle and loaded into the IR cell. The specimen was dried in situ at 100°C for 17 hours in helium flowing

continuously through the IR cell at 20 mL/min, controlled by a Brooks mass flow controller. After 17 hours, the catalyst was reduced *in situ* at 100°C with hydrogen flowing at 20 mL/min. The IR cell was cooled to 25°C, after which, a background scan was obtained. The catalyst was probed with 5 consecutive 60 second pulses of carbon monoxide (CO) via a stream of 10% Co/He mixture. DRIFT spectra were obtained after each pulse.

The results (Figure 5-22) reveal a band at 2185 $cm^{-1}$ which is ascribed to gaseous CO. Two additional bands are evident at ca. 2092 and 1940 $cm^{-1}$ which are ascribed to linearly adsorbed CO. Notably absent from the DRIFT spectra are bands in the region from 1200 to 1700 $cm^{-1}$ corresponding to Pd carbonate, which suggests that the catalyst is completely reduced (i.e. $Pd^0$). However, there is some noise in this region.

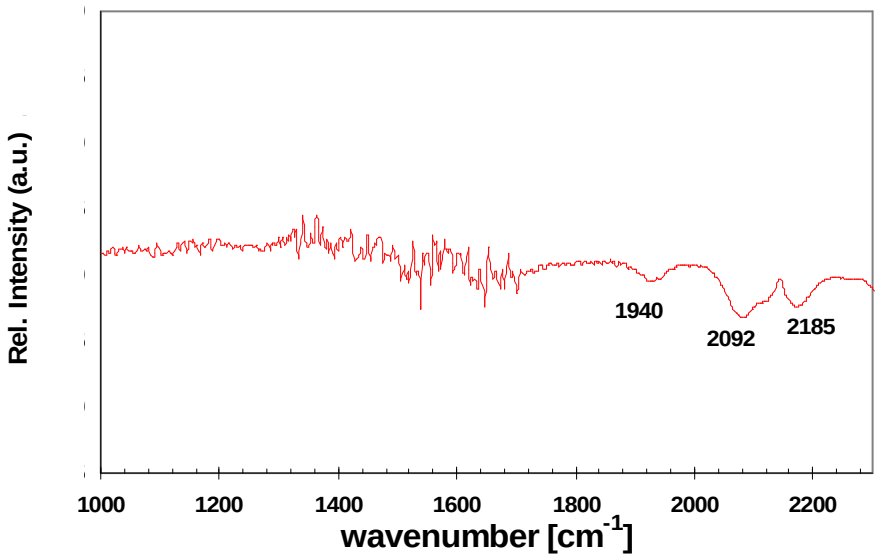


**Figure 5-22** *in situ* DRIFT spectra of carbon monoxide adsorption on a $Pd/Nb_2O_5/SiO_2$ catalyst (CAT 065) at 25°C, *The catalyst was reduced in situ with hydrogen for 2 hours at 100°C and dried in situ at 100°C in flowing He for 17 hours. The catalyst was probed with 5 consecutive 60 second pulses of carbon monoxide.*

The author and co workers have previously characterized the adsorption properties of various organic substrates including carbon monoxide on a commercial 0.52 wt% $Pd/Al_2O_3$ catalyst used in the preliminary pilot plant

catalytic distillation experiments of Chapter Seven and used in a previous kinetic study on the selective hydrogenation of MO.[18,64] In contrast to the DRIFT spectra obtained for the $Pd/Al_2O_3$ catalyst, the niobia catalyst appears to have essentially linearly adsorbed CO, which implies a relatively high degree of Pd dispersion, whereas the DRIFT spectra of CO adsorption on the commercial catalyst (Figure 5-21) revealed a significant proportion of bridged and multi-bridged CO as evidenced by vibrations at 1980 and 1920 $cm^{-1}$ respectively, suggesting a greater degree of agglomeration of Pd crystallites in the Aldrich catalyst. The commercial catalyst was found to become increasingly agglomerated with reduction temperature up to 250°C, beyond which no morphological changes were observed.[64]

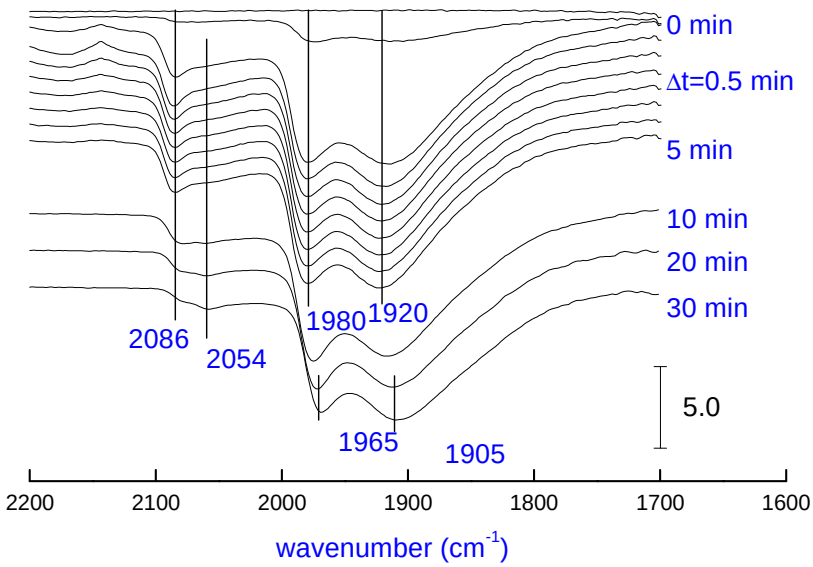


**Figure 5-23** *in situ* DRIFT spectra of carbon monoxide adsorption at 25°C on a commercial $Pd/Al_2O_3$ catalyst (Aldrich 20,574-5) pre-reduced at 100°C.♣

The vibrations associated with linearly adsorbed carbon monoxide are observed at higher frequencies for the niobia catalyst than the commercial catalyst. Since the stretching frequency is associated with the degree of agglomeration, it can be concluded that the sites for linearly adsorbed CO are

♣ DRIFT spectra obtained by and Figure prepared by Dr. Ming Jiang, unpublished data.

more agglomerated for the niobia catalyst than the alumina catalyst. However, in general the palladium crystallites are more agglomerated for the commercial catalyst as evidenced by the significant relative intensities of the peaks associated with the bridged and multibridged species. The Pd is likely more dispersed on the niobia catalyst due to the much lower palladium loading. Also, due to the low reduction temperature (100°C), it is possible that the organic ligands of the palladium acetate precursor may have remained intact and stabilized the Pd. Intact organic ligands may inhibit sintering of the palladium at low to moderate temperatures (< 200°C).

### 5.3 X-Ray Diffraction (XRD)

One of the most important insights of this work is the profound influence of the calcination temperature on the resultant activity and particularly the catalyst stability for MO synthesis as well as its effect on the strength and nature of the acid sites. The results in the previous sections in this chapter show that the catalysts calcined at 100°C exhibit very strong acid sites not present in the catalysts calcined at 500°C. Catalysts calcined at 300°C exhibit intermediate acid strength. Characterization of the nature of the acid sites via in situ DRIFT spectroscopy shows that these very strong acid sites are Bronsted sites. Bronsted acidity was not observed in catalysts calcined at 500°C. However, it is known that bulk niobic acid ($Nb_2O_5 \cdot nH_2O$) crystallizes at around 523°C transforming to the hexagonal TT or T form.[73] Moreover, it well known that a significant loss of acidity and loss of catalytic activity is accompanies this phase change.[73,75,78]

Although the FTIR results of the previous section demonstrate that the catalyst calcined at 500°C exhibit significant Lewis acidity, it is possible that a loss of acidity may have occurred due to the onset of crystallization in the surface oxide phase. In addition to thermally induced phase change, niobia crystallites may form due to poor precursor distribution on the support surface,

due to weak interaction with between the surface-phase and the support oxides and if monolayer coverage is exceeded.[104] Therefore, select $Nb_2O_5/SiO_2$ and $Nb_2O_5/\gamma\text{-}Al_2O_3$ catalysts were characterized by X-Ray diffraction (XRD) in order to ascertain whether any niobia crystallites formed in these catalysts. The XRD analysis confirms that the niobia overlayer of all of the specimens were amorphous. No crystallites were evident in any of the specimen.

Catalysts used in DoE #2 (Section 4.5), which investigated the effect of calcination temperature on the activity for MO synthesis as well as their fumed silica and gamma alumina supports, were analyzed via XRD. XRD patterns were obtained using a Bruker-D8 x-ray diffractometer which bombarded the specimens with monochromatic $CuK_\alpha$ radiation. The vacuum tube parameters were set to 40 kV potential and 30 mA current intensity. The intensities of scattered x-rays for diffraction angles ($2\theta$) ranging from 10 to 40° were obtained as was done by Chen et al.[42] It is known that the first principal diffraction peak for the hexagonal T polymorph ($\gamma$-phase), if present, would be observed at a diffraction angle of 22°C.[14] Numerous other diffraction peaks for this and other polymorphs would be observed over the interval from 10 to 40° if crystallites had formed. The scans were obtained at a step rate of 0.050° per second.

The XRD pattern of the fumed silica support (Figure 5-24) exhibits a very broad peak characteristic of an amorphous specimen. In contrast, a crystalline specimen would exhibit very sharp and pronounced peaks clearly emerging from the background at a very precise diffraction angles. An example of this is the sharp peak observed at precisely 38.2° in Figure 5-24 for the $SiO_2$ support and CAT 030. It is well known from experience in the XRD laboratory that this peak is due to the metal tray that the specimen were held in and was not due to the structural properties of the specimen. This peak was observed in some analyses if the amount of specimen in the tray was small. The $Nb_2O_5/SiO_2$ catalysts investigated all exhibited the broad feature observed in figure 5-24

associated with the fumed silica support. The broad feature associated with the fumed silica support appears to diminish with increasing niobia loading. However, the XRD patterns show no evidence of niobia crystallites present in the specimens. The XRD spectra are similar for each specimen.

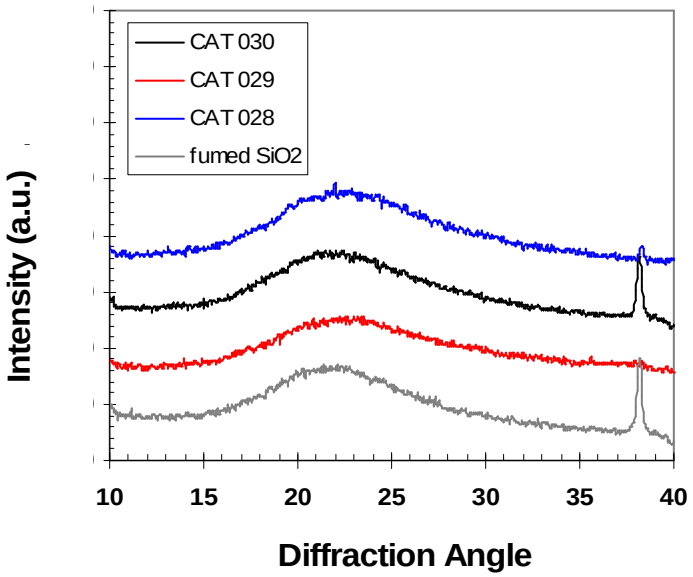


**Figure 5-24** (left) XRD patterns of $Nb_2O_5/SiO_2$ catalysts; CAT 029 (16.9 wt% $Nb_2O_5/SiO_2$, calcined at 100°C) and CAT 030 (12.3 wt% $Nb_2O_5/SiO_2$, calcined at 100°C) CAT 028 (5.82 wt%, calcined at 500°C) and fumed silica support (untreated). *XRD patterns offset for clarity. The peak at 38.2° is due to the metallic sample holder.*

The XRD patterns for two $Nb_2O_5/\gamma\text{-}Al_2O_3$ catalysts used in DoE #2 as well as the $\gamma\text{-}Al_2O_3$ support are given in Figure 5-25. These XRD patterns show that the $Nb_2O_5/\gamma\text{-}Al_2O_3$ catalysts used in the experiment investigating the effect of calcination temperature were all amorphous. The XRD patterns for the catalysts are quite similar to the support due to the low niobia loading. Unfortunately, at the time the XRD experiments were carried out, there were insufficient amounts of catalysts 025, 027 and 031 for analysis. However, the results presented here seem sufficient to confirm that the niobia of the catalysts used in DoE #2 did not lose catalytic activity as a result of crystallization. CAT

025 and CAT 031 were alumina catalysts with only slightly higher loading than catalysts 026 and 032. CAT 027 had a loading comparable to CAT 029 but was calcined at 500°C.

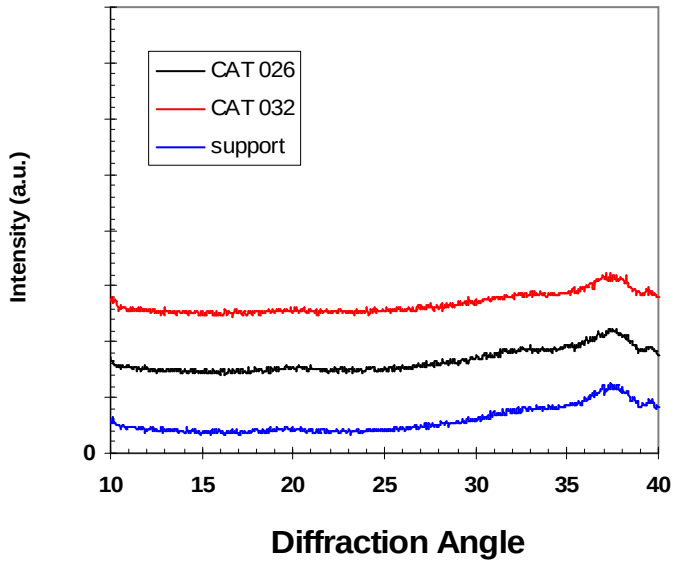


**Figure 5-25** XRD patterns of Nb2O5/γ-$Al_2O_3$ catalysts (intensities were offset for clarity) CAT 026: 2.65 wt% $Nb_2O_5$/γ-$Al_2O_3$ calcined at 500°C; CAT 032: 3.79 wt% $Nb_2O_5$/γ-$Al_2O_3$ calcined at 100°C; γ-$Al_2O_3$ support (untreated)

The XRD patterns for the $Nb_2O_5$/Norpro $SiO_2$ catalysts used in the final pilot scale catalytic distillation experiments outlined in Chapter Eight are given in Figure 5-26. These specimens also exhibit the broad feature characteristic of amorphous silica. No crystallites are evident in these XRD patterns as well.

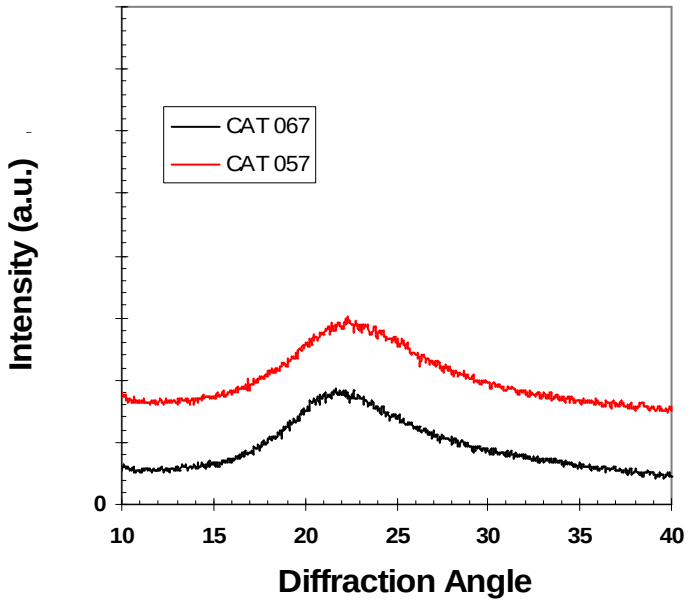


**Figure 5-26** XRD patterns of $Nb_2O_5$/Norpro SS 65137 $SiO_2$ catalysts used in pilot plant experiments (CD 003, CD 004 and CD 005)

### 5.4 Raman Spectroscopy

A principal objective of this work is the elucidation of the structure-activity relationships for supported niobia catalysts for the synthesis of MO. Raman spectroscopy is a powerful characterization technique which provides molecular level information regarding the structures of catalytic materials. Raman spectroscopy has particular utility in the characterization of supported metal oxides since the catalytically active material exists as a highly dispersed two-dimensional overlayer below monolayer coverage which give rise to strong Raman signals that are not complicated due to the co-existence of mixed oxide phases.[104] Below monolayer coverage, the oxide support may give a Raman signal. However, the Raman signal associated with the support tends to be weak.[104] Raman and IR spectroscopy are complementary techniques in that those vibrations which are IR active tend to be Raman inactive and vice versa. Bonds with significant polar character give rise to strong IR signals while those bonds with significant covalent character give rise to strong Raman signals.[105]

Alumina, and silica exhibit significant polar character in the anion cation pair and typically do not exhibit Raman signals or if so, exhibit only very weak Raman signals in the range of 100 to 1100 $cm^{-1}$ where Raman vibrations of M-O and M-O-M bonds of supported metal oxides are observed.[105] Therefore, Raman spectroscopy is ideal for the elucidation of the structure of many dispersed metal oxides on these supports.

The Raman spectra of select catalyst specimen were obtained using a Renishaw RM 1000 Ramanscope equipped with a surface sensitive 488 nm Argon ion laser, dielectric edge filter and an Olympus BHZ-UMA microscope with a Peltier cooled (-50°C) CCD. The spectrometer was operated in non-confocal mode with a slit width of 50 μm and a focal area of 5 μm. The laser power measured at the objective lense (50 X) was 2.6 mW. The spectra were obtained in extended mode (10 x 30 accumulations) and processed with Grams/32 software.

The Raman spectrum of catalyst 065 (0.04 wt% Pd, 6.09 wt% $Nb_2O_5$/ Norpro $SiO_2$ catalyst carrier) is illustrated in Figure 5-27. The catalyst was in the hydrated state when the measurement was taken since it was exposed to the ambient during the measurement and was exposed to the ambient for a prolonged period of time prior to Raman analysis. The resultant spectrum is excellent with very strong Raman vibrations evident at 142, 400, 520, and 641 $cm^{-1}$ and a broad feature evident around 835 $cm^{-1}$. Note that a correction factor of +1.8 $cm^{-1}$ should be added to these wavenumber values obtained in extended mode. A comparison of this spectrum to the Raman spectrum of the Norpro $SiO_2$ support in Figure 5-28 conclusively demonstrates that the Raman vibrations observed in Figure 5-27 are due to surface species in the niobia overlayer. However, the support does exhibit a broad feature around 840 $cm^{-1}$ as did catalyst 067. The $SiO_2$ support, being a commercial catalyst carrier, likely contains binders and other additives which may give rise to Raman vibrations.

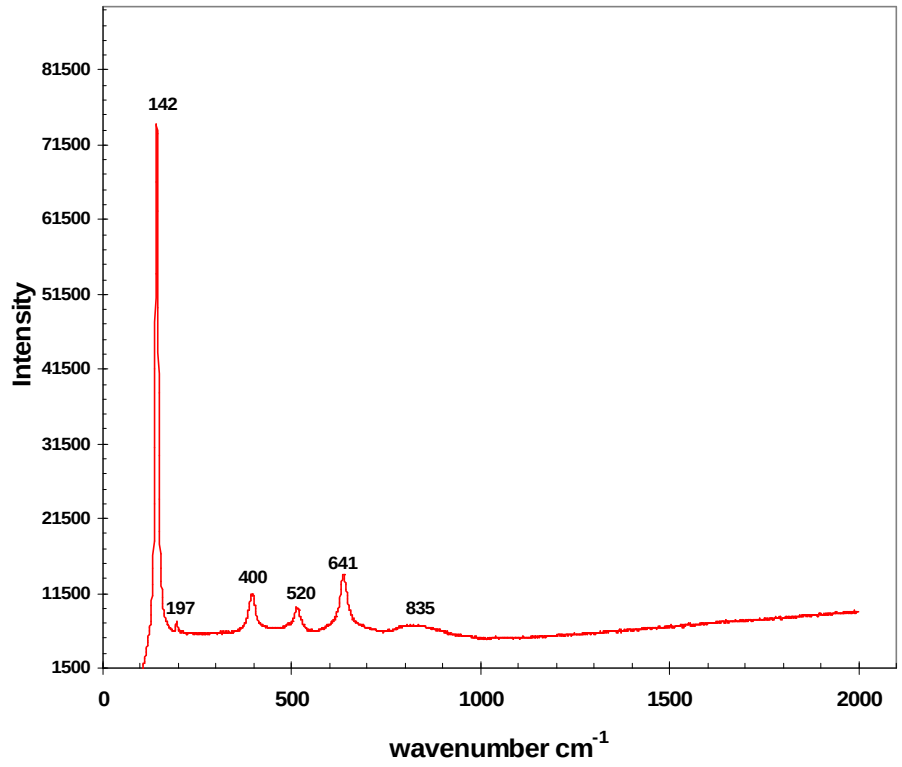


**Figure 5-27** Raman spectrum of catalyst 065 $Pd/Nb_2O_5$/Norpro SS 65137 $SiO_2$ catalyst under hydrated (ambient) conditions, catalyst originally calcined at 100°C♠

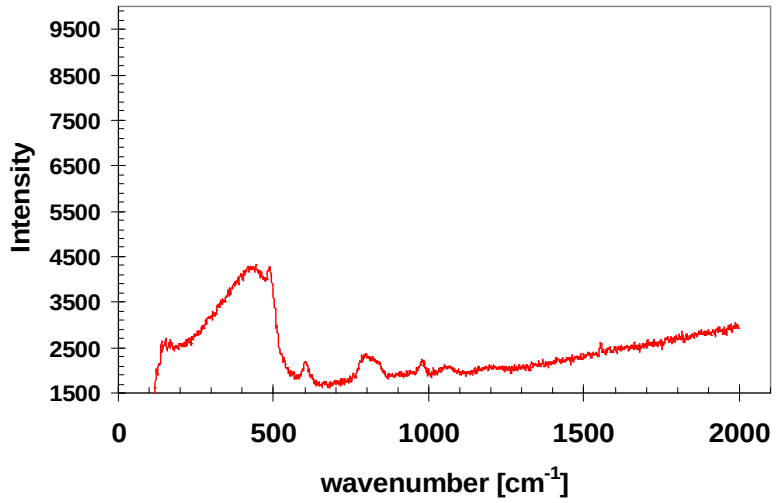


**Figure 5-28** Raman spectra of Norpro SS 65137 $SiO_2$ support in hydrated state

♠ Raman spectra obtained in extended mode. A correction of +1.8 wavenumbers should be added to the results obtained in extended mode.

The investigation of the niobia catalysts dispersed onto fumed silica support were inconclusive due to excessive background fluorescence, probably arising due to elemental impurities in the silica. The gamma alumina supported catalysts also resulted in significant background fluorescence. However, one specimen, catalyst 026 (2.65 wt% $Nb_2O_5/\gamma$-$Al_2O_3$ calcined at 500°C) which, although exhibited significant background fluorescence, also revealed the strong Raman vibration at 143 $cm^{-1}$ as well as a peak at 418 $cm^{-1}$ and possible a broad feature at around 640 $cm^{-1}$ . Although the quality of this spectrum is poor, it can be concluded that the vibration at 143 $cm^{-1}$, which dominates the spectrum of CAT 065 (Figure 5-27), is related to a structural feature of the surface oxide niobia phase that is common to both specimens. Low frequency vibrations are often attributed to the support, however, the vibration at 143 $cm^{-1}$ is observed in two catalysts with different supports and is not observed in the Raman spectrum of the Norpro $SiO_2$ support (Figure 5-28). The low frequency of vibration implies a very long bond length, associated with a partial bond. Raman bands below 200 $cm^{-1}$ have been previously ascribed to lattice vibrations.[97]

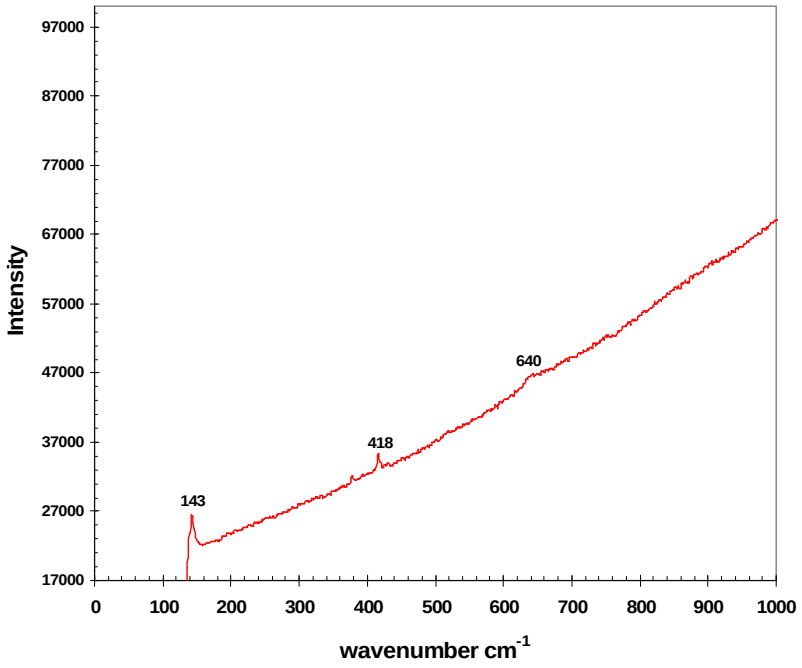


**Figure 5-29** Raman spectra of a 2.65 wt% $Nb_2O_5/\gamma$-$Al_2O_3$ catalyst (CAT 026) calcined at 500°C under hydrated conditions.

The Raman vibrations in the spectrum of CAT 065, which had the same catalyst formulation as the catalysts used in the pilot plant experiments of chapter Eight, are clearly revealed in Figure 5-25. The peak at 643 $cm^{-1}$ (641 + 1.8 $cm^{-1}$) is ascribed to Nb-O-Nb symmetric stretching vibrations which are known to occur at around 647 $cm^{-1}$.[100,103] The Nb-O-Nb bond is characteristic of a slightly distorted octahedral structure ($NbO_6$) and is associated with Bronsted acidity in niobia compounds. Therefore, the prevalence of the Nb-O-Nb linkages is perhaps expected for catalysts calcined at 100°C. The lower frequency vibrations in Figure 5-25 at 520, 400 $cm^{-1}$ are unknown but likely correspond to various Nb-O stretching vibrations. These low frequency vibrations are similar but not identical to those observed in various compounds by Jehng and Wachs.[97]

A broad feature around 840 $cm^{-1}$ is observed in the Raman spectrum of the Norpro support, which is also observed around 835 $cm^{-1}$ in the $Nb_2O_5/SiO_2$ catalyst. This band may possibly be due to the terminal Nb=O bond, which is longer in the slightly distorted octahedra than in the strongly distorted octahedral or tetrahedral structures, particularly in the hydrated condition and would consequently have a lower frequency of vibration. Bands ranging from 825 to 883 $cm^{-1}$ have been previously assigned to the Nb=O terminal bond for niobia dispersed on alumina and zirconia for low loading.[103] It is common for the Nb=O peak to be broad and lack intensity for a specimen in the hydrated state. This band typically becomes sharper after calcination.

However, Jehng and Wachs[100] reported Raman spectra for 2 and 4 wt% $Nb_2O_5/SiO_2$ catalysts calcined at 400°C which also showed this broad feature around 812 $cm^{-1}$ in addition to a band around 960 to 980 $cm^{-1}$ corresponding to the Nb=O stretching vibration. The band at 812 $cm^{-1}$ was ascribed to the Si-O-Si stretching vibration. Considering that this feature is also observed in the Norpro $SiO_2$ support, it is reasonable to conclude that this broad feature is due to Si-O-Si stretching. This implies a unique result in that the strong band for the

Nb=O stretching vibration is apparently absent in the spectrum of Figure 5-25 which suggests negligible Lewis acidity. This observation is consistent with the DRIFT spectrum for this catalyst (Figure 5-18), as well as the TPD data for this catalyst formulation, which suggests the acid sites are predominantly Bronsted and that the population of Lewis acid sites is relatively small.

Many authors have reported niobia tetrahedra with strong Lewis acidity on silica supported catalysts. However, the Raman vibrations associated with niobia tetrahedra are found in the range of 790 to 830 $cm^{-1}$.[97] The Raman vibrations observed in Figure 5-27 seem consistent with a slightly distorted octahedral structure for which the major peaks are observed over the range of 500-700 $cm^{-1}$.[97] Indeed, the slightly distorted amorphous $Nb_2O_5$ are expected to exhibit a strong band around 650 $cm^{-1}$ and a weak Raman band associated with the Nb=O bond around 900 $cm^{-1}$.[87] However, the Raman spectrum presented in figure 5-27 seems quite unique and is distinct from the Raman spectra for $Nb_2O_5/SiO_2$ catalysts presented previously by Jehng and Wachs.[87,97,100] Most notably is the fact that the band around 900 $cm^{-1}$ for the Nb=O symmetric stretching vibration is absent in Figure 5-27. Another interesting result is that the Nb-O-Nb vibration at 647 $cm^{-1}$ is normally associated with polymeric niobia structures created at higher niobia loading but XRF analysis of catalyst 065 shows the niobia loading was relatively low, only 6.09 wt% corresponding to roughly 1/3 monolayer coverage. However, when preparing the catalyst it was intended to generate single monolayer coverage but the niobia uptake was low. Perhaps there was localized crowding of niobia octahedra at certain points on the surface of the final catalyst.

The Raman spectrum of Figure 5-27 also provides information regarding the catalyst morphology which supports the results of the XRD analysis. Specifically, the conclusion that the niobium oxide overlayer in the final catalyst formulation used in this work was free of niobia crystallites. A Raman band at 690 $cm^{-1}$, which is associated with the TT-$Nb_2O_5$ crystalline polymorph,

is absent in Figure 5-25 which provides further evidence that niobium oxide crystallites did not form.[97]

The Raman spectrum in Figure 5-30 of a preliminary experiments on a 12.0 wt% $Nb_2O_5/\gamma$-$Al_2O_3$ catalyst (CAT 016) with about 0.6 monolayer coverage in the hydrated state reveals a broad feature at around 900 $cm^{-1}$ which corresponds to the Nb=O stretching vibration. This spectrum suggests a highly distorted octahedral structure that is perhaps expected considering the relatively high niobia loading and the high calcination temperature, which serves to further distort the octahedra. The prevalence of the mono-oxo Nb=O moiety is consistent with the strong Lewis acidity in the niobia overlayer from calcination at 500°C. In this Raman experiment, a 632.8 nm laser was used to obtain the spectrum. Again, this spectrum should be considered a preliminary result due to the excessive fluorescence.

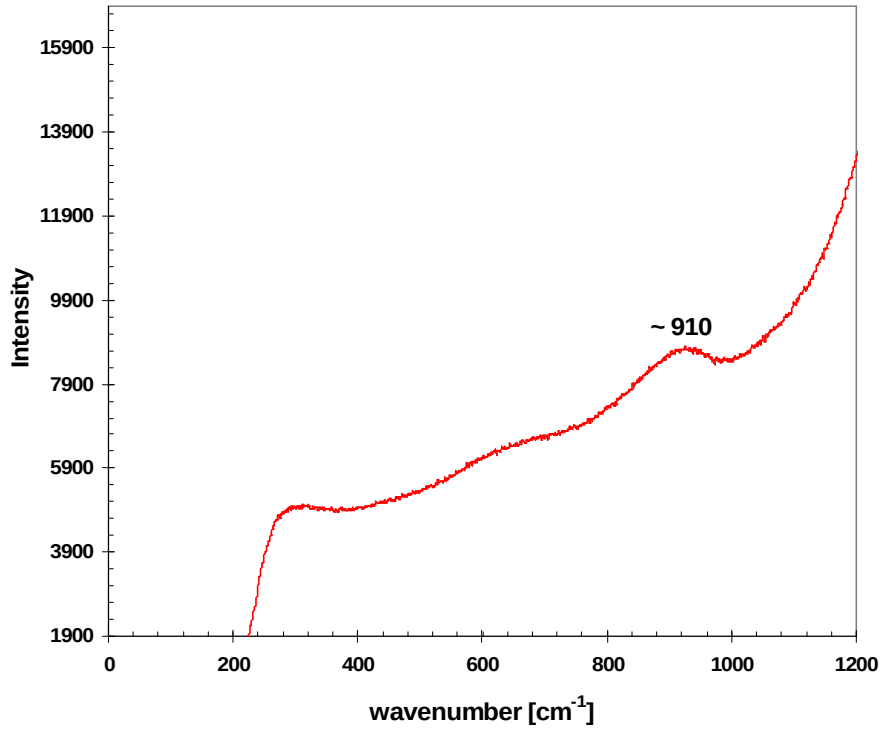


**Figure 5-30** Raman spectrum of a 12.0 wt% $Nb_2O_5/\gamma$-$Al_2O_3$ catalyst (CAT 016) calcined at 500°C measured under hydrated conditions using a 632.8 nm laser

## 5.5 Discussion on the Role of Acidity in MO Synthesis

The results demonstrate that Bronsted acidity plays an important role in both the activity and stability of niobia catalysts for MO synthesis. The Bronsted acid sites are the strongest acid sites these catalyst specimen and as a consequence significantly contribute to the overall activity of the catalyst, particularly for silica supported catalysts. Bronsted acid sites apparently do not deactivate during MO synthesis, whereas those catalysts calcined at 500°C which exhibit predominantly Lewis acid sites deactivate resulting in a "pseudo equilibrium" conversion.

Banares and Wachs[104] have pointed out that in the hydrated condition, there is "extensive solvation" of the surface oxide phase due to the adsorption of around 20-40 monolayers of water. In the reaction environment for MO synthesis, water is produced in a stoichiometric equivalent amount as the product. It is reasonable to assume therefore, that the surface oxide phase is also extensively solvated due to water as well as the organic solvent during MO and MIBK syntheses. It is proposed that the stability of Bronsted acid sites is due to the facile proton exchange between the active sites (bridging hydroxyls) in the surface oxide phase and Bronsted bases in the liquid phase at the interface. It is postulated that the extensive solvation of the surface oxide phase gives rise to a "pseudo-homogeneous" liquid phase reaction at the interface (Figure 5-31a), which results in the regeneration of the active site rather than deactivation due to strong adsorption. Lewis acid centres on the other hand deactivate due to strong adsorption of water and other substrates (Figure 5-31b).

Once calcined at 500°C, the destruction of the Bronsted acid sites by dehydroxylation to produce Lewis acid sites is irreversible. The FTIR and TPD results show that the catalysts calcined at 500°C, when hydrated to not result in a restoration of the Bronsted acidity. In addition, autoclave experiments in Chapter Four support this conclusion as evidenced by the deactivation of

catalysts calcined at 500°C when hydrated during MO synthesis. This implies that the niobia structures obtained from high temperature calcination are thermodynamically stable. Moreover, the loss of Bronsted acidity with this structural transformation, presumably from distorted octahedral to highly distorted octahedral structure, suggests that the (Bronsted) active sites for MO synthesis are predominantly associated with Nb-O-Nb bridging hydroxyls rather than Nb-O-Si bridging hydroxyls.

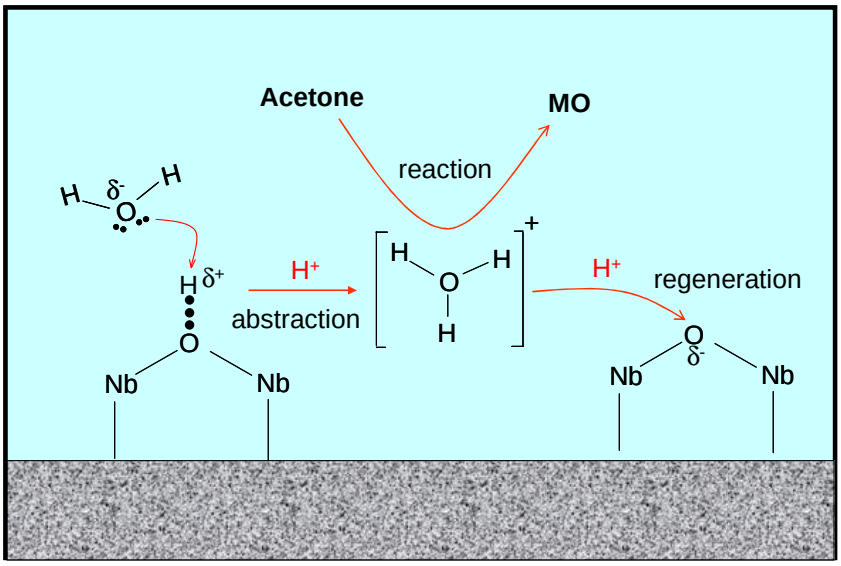


**Figure 5-31** (a) (above) Representation of "pseudo homogeneous" chemical reactions occurring in the liquid boundary layer at the solid-liquid interface enabled by facile proton exchange between solvated niobium oxide surface-phase and basic species (eg. water) in the liquid phase. (b) (below) Schematic representation of catalyst deactivation resulting from the irreversible adsorption of water and ketones on Lewis acid sites of the surface oxide phase

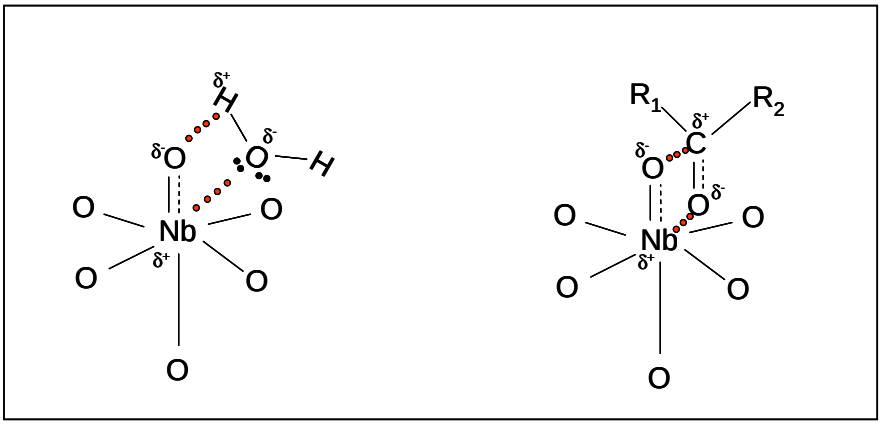

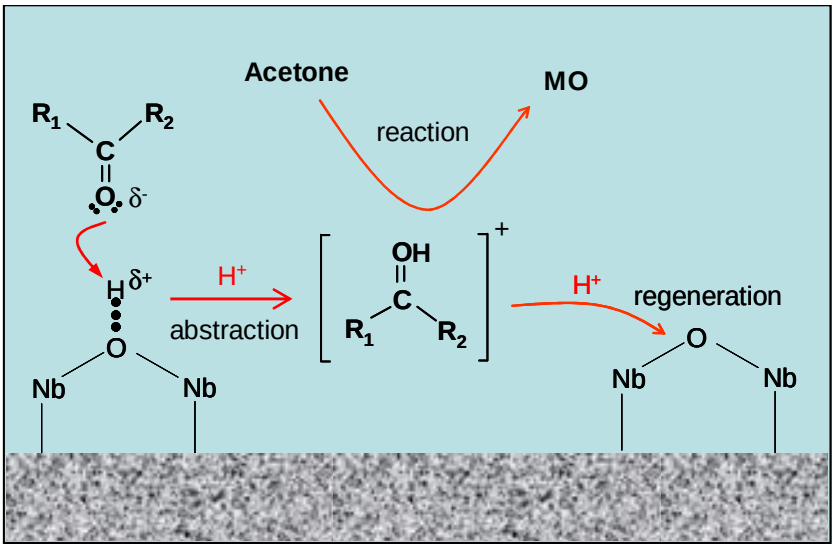


**Figure 5-31 (c)** Representation of pseudohomogeneous reaction occurring in the liquid phase at the interfacial region due to abstraction of proton by ketones and facile proton exchange between species in the liquid phase

Figure 5-31 (c) presents an alternative mechanism by which the proton is abstracted by acetone or another ketone. In the case of acetone, the proton abstraction from the niobia resulting in the protonation acetone is the first elementary step in the known reaction mechanism. In the case of DAA dehydration, protonation of the ketone group of DAA is also the first step in the known reaction mechanism. The protonation of DAA may occur from proton abstraction from a Bronsted acid site in the niobia overlayer or may occur due facile proton exchange in the bulk. The intermediate created from the protonation of acetone has a pKa of -7.3 whereas hydronium ($H_3O^+$) has a pKa of -1.7.[185] Thus water, the conjugate base of hydronium, is more basic than acetone. In the presence of a very strong Bronsted acid such as hydrated niobia, water and other ketones may readily abstract the proton from the surface-oxide phase. What is conceptually important is that the reaction occurs in the liquid phase, affording the advantages of homogeneous reaction and that many catalytic turnovers may occur before the active site is regenerated. Furthermore, of the active site may occur on a different (Nb-O-Nb) linkage. Thus, the catalyst exhibits long term stability due to facile proton exchange.

Lewis acid sites are localized in space in the solid and foul readily due to strong adsorption of substrates.

## 5.6 Conclusions

The activity for MO synthesis was found to be correlated with the acid site density as well as the acid strength ($T_m$). TPD analysis of the fumed silica supported catalysts shows that a main effect of reducing the calcination temperature is to increase the strength of the acid sites. The TPD results also show that new and very strong acid sites appear for the catalysts calcined at 100°C, which increase in density with increasing niobia loading. *in situ* DRIFT adsorption spectra of pyridine probe molecules on the surface of these niobia compound show that these very strong acid sites are Bronsted acid sites. No Bronsted acidity was detected for catalysts calcined at 500°C. Thus the calcination temperature also affects the nature of the acidity.

The experiments in Chapter Four demonstrate that those catalyst calcined at 100°C exhibit enhanced catalytic activity and particularly enhanced stability for MO synthesis whereas those catalysts calcined at 500°C may show good initial activity but ultimately deactivate at a "pseudo equilibrium" acetone conversion. This pseudo equilibrium arises due to the strong adsorption of water and or organic substrates on the Lewis acid sites. It is postulated that the catalysts calcined at 100°C do not deactivate due to the facile proton exchange between Bronsted sites and species in the liquid phase. It is proposed that the solvation or hydration of the surface oxide phase results in a pseudo-homogeneous reaction in the liquid boundary layer in the interfacial region.

The effect of calcination temperature on the activity and stability for MO synthesis is irreversible. TPD and FTIR analysis of catalysts calcined at 500°C show that the Bronsted acidity is not restored in the hydrated state after exposure to the ambient. This conclusion is also supported by the autoclave

experiments of chapter Four, for which the catalysts calcined at 500°C showed lower activity and particularly lower catalyst stability for MO synthesis when in the hydrated state due to the generation of water from DAA dehydration. Thus, the niobia species in the surface oxide phase are thermodynamically stable after calcination at 500°C. Preliminary Raman analysis of a $Nb_2O_5/SiO_2$ catalyst calcined at 500°C at moderately high niobia loading suggest the structure is predominantly highly distorted niobia octahedra. Raman analysis of the final catalyst formulation used in the CD pilot plant calcined at 100°C reveals slightly distorted octahedra with an absence of the band associated with the Nb=O moiety responsible for Lewis acidity. The Nb-O-Nb vibration associated with Bronsted acidity is the most significant vibration in the Raman spectrum of Figure 5-27.

The final catalyst formulation in this work used in the catalytic distillation pilot plant experiments of Chapter Eight involved niobia dispersed onto a Norpro silica catalyst carrier and calcined at 100°C. TPD analysis of the resultant catalyst revealed a significant proportion of unique and very strong acid sites. FTIR analysis showed that the acid sites of the catalyst were predominantly Bronsted sites whereas the Lewis acidity was significantly diminished in contrast to other catalysts for which niobia was dispersed onto fumed silica. These very strong and unique acid sites were due to the strong interaction between the surface oxide phase and the silica support (SOSI). The Norpro support exhibited negligible acidity. This result also suggests that the niobium oxide structure on the Norpro support was distinct from the niobia structure on the fumed silica support.

Characterization of the final catalyst formulation ($Pd/Nb_2O_5$/ Norpro $SiO_2$ calcined at 100°C) by *in situ* DRIFT adsorption spectra of carbon monoxide probe molecules shows that the palladium is highly dispersed in contrast to the commercial $Pd/Al_2O_3$ catalyst used in the preliminary CD experiments of Chapter Seven. The niobia catalyst exhibited only linearly adsorbed carbon

monoxide whereas the commercial catalyst exhibited linear, branched and multibranched carbon monoxide indicative of agglomerated palladium crystallites. XRD and Raman analysis confirm that the surface oxide phase is free of crystallites in the niobia catalysts.

# Chapter Six

## Catalyst Development and Kinetics of the One-Step Synthesis of MIBK over a Multifunctional $Pd/Nb_2O_5/SiO_2$ Catalyst

---

### 6.0 Synopsis

$SiO_2$ and $\gamma$-$Al_2O_3$ were identified as promising materials as supports for dispersed niobia and $Pd/Nb_2O_5$ catalysts for MO and MIBK syntheses respectively. In this chapter, experiments investigating the one-step synthesis of MIBK over multifunctional $SiO_2$ and $\gamma$-$Al_2O_3$ supported catalysts were investigated. Commercially available $SiO_2$ and $\gamma$-$Al_2O_3$ raschig ring catalyst carriers were investigated for scale-up of the catalyst to the reactor scale. The $Nb_2O_5/\gamma$-$Al_2O_3$ raschig ring catalyst revealed a significant internal mass transfer resistance as evidenced by an effectiveness factor of only 1.6%. In contrast the $Nb_2O_5/SiO_2$ catalyst exhibited an effectiveness factor of 66% and showed good activity for MO synthesis. Consequently, the $SiO_2$ carrier was selected for further investigation.

The macrokinetics of the syntheses of MO and MIBK were investigated in a fixed bed flow (FBR) reactor. The final catalyst formulation showed excellent activity for MIBK synthesis, as high as 1.3 [g/hr*$g_{cat}$] at 160°C. However, the selectivity typically ranged from 82 to 85 wt% due to the co-production of IPA and DIBK. The results confirm the claims of other authors[23,26,48,50] that a careful balance of sites for responsible for MO synthesis and MO hydrogenation must be achieved to attain good activity and selectivity. In the final catalyst formulation, the Pd loading was about 0.04 wt%, which appears to be at or near the optimal loading for this niobia catalyst formulation. A synergistic effect was observed, whereby the catalyst activity increased by 22% at 160°C and WHSV of 8.6 $hr^{-1}$ when hydrogen was introduced into the reactor compared to the condition in the absence of hydrogen. It is postulated that fraction of

available sites is increased due to a reduction in the surface concentration of MO and its derivatives due to the hydrogenation of MO.

The intrinsic kinetics of the one-step synthesis of MIBK over a $Pd/Nb_2O_5$/fumed $SiO_2$ catalyst were investigated in an autoclave reactor. Evaluation of the Weisz-Prater and Mears criteria confirm the absence of mass transfer effects. A kinetic model is proposed which is valid at hydrogenation total pressure of 500 psia and greater. The kinetic model gives excellent prediction of acetone with a relative standard error of estimate (RSEE) of 1.07%. Good predictions of water (RSEE=12.8%) and fair predictions of MIBK (19.7%) were realized. The predicted and observed MO concentrations were relatively low, near the GC peak area rejection limit. The model MO predictions were not reliable due to the low accuracy of the quantification of MO in this range.

### 6.1 Catalyst Development: Integration of Palladium into the $Nb_2O_5/SiO_2$ Architecture

A major objective of this Ph.D. research project was the development of a robust multifunctional catalyst for the one step synthesis of MIBK via catalytic distillation.[65] Silica and gamma alumina were selected as potential catalysts supports based on the results of the investigations outlined in Chapter Four. Palladium was selected as the hydrogenation catalyst, since as mentioned in Chapter One, it has been demonstrated experimentally that palladium, rhodium and nickel consistently give the highest selectivity to olefin group hydrogenation in $\alpha,\beta$-unsaturated compounds.[16] Palladium has been proven to be more robust for the one-step synthesis of MIBK and represents the state-of-the-art for hydrogenation catalysts for commercial MIBK production. Furthermore, the author and co-workers[18] have characterized the kinetics of the selective hydrogenation of MO utilizing a palladium catalyst and have gained insight into the catalytic reaction mechanism. In this section, the results of preliminary experiments investigating the effects of the palladium impregnatio

method parameters on the activity, selectivity and stability for MIBK synthesis are reported.

### *6.1.1 Effect of Acetic Acid Treatment on Niobia Catalyst Activity*

Although palladium chloride ($PdCl_2$) is commonly used as a precursor for the aqueous impregnation of catalysts with palladium, it is known that the chloride ions may have an adverse effect on the niobia catalyst by the diminution of its acidity.[106] For this reason, niobium pentachloride was not used as a precursor for generating the surface oxide phase nor was palladium chloride used for the hydrogenation metal precursor. Palladium (II) acetate was selected as the precursor and acetic acid was chosen as the solvent based on the synthesis technique disclosed by Wirtz et al.[159] for the development of a novel catalyst for the synthesis of vinyl acetate.

Considering that the niobium oxide phase exists as a dispersed phase rather than as a mixed-oxide phase, there are two possible approaches to preparing the multifunctional catalyst, both involving two general steps. In the first approach, one may first disperse the hydrogenation metal onto the support and then in the second stage deposit the niobium oxide. Alternatively, one may first deposit the niobium oxide onto the support and then impregnate the niobia catalyst with the hydrogenation metal. In this work, only the latter approach was followed as reported by Chen et al.[42] who investigated MIBK synthesis and as reported by Ko et al.[89] who investigated strong metal support interactions in $Ni/Nb_2O_5/SiO_2$ catalysts. It seems intuitive that the latter approach would be superior since the niobia exists as a 2 dimensional overlayer. Dispersing the metal onto the niobia, rather than adjacent to it, would minimize the separation distance between hydrogenation and acid sites. The final impregnation procedure has been described previously in Chapter Three.

Prior to impregnation of catalysts with palladium, a set of preliminary experiments were carried out in order to assess the affect of treatment in acetic acid on the resultant niobia catalyst activity for MO synthesis. It was of interest to determine if the acidic solvent would leach niobium from the catalyst in a manner which adversely affects the catalyst activity. Three experiments were carried out. A batch of 10.2 wt% $Nb_2O_5/SiO_2$ catalyst calcined at 100°C (CAT 040) was prepared and subdivided into three sets. The first catalyst (CAT 040) was left untreated and used as a control. The second catalyst (CAT 040-A) was made by taking approximately 0.5 g of the original catalyst and immersing it in 17 mL of glacial acetic acid at 80°C for 2 hours prior to vacuum separation followed by drying in an oven overnight at 80°C. The third catalyst (CAT 040-B) was prepared by taking approximately 0.5 g of the original catalyst (CAT 040) and immersing in 17 mL of 1.0 M aqueous acetic acid for two hours prior to separation by vacuum filtration followed by drying overnight in an oven at 80°C. The resultant catalysts were tested for their activities for MO synthesis at 160 °C in an autoclave reactor. A fourth experiment was carried out in which some of the untreated catalyst (control) was re-examined.

The results in Figure 6-1 suggest that the acidic treatment did not appear to appreciably affect the catalyst activity. The MO concentration versus time profiles for the two experiments for the treated catalysts are bounded by the profiles of the two experiments of the untreated catalysts. Relatively low MO conversions were achieved in these experiments due to the relatively small amounts of catalysts used in these experiments (ca. 0.3 g) compared to about 1 g used in the autoclave experiments of Chapter Four. Due to the relatively low concentrations of MO, the relative variation in the data was more significant. Consequently, the estimates of the initial rates of reaction were subjected to greater uncertainties. It is worth noting however, that the two experiments involving the untreated catalyst gave initial specific rates of reaction, as determined by the method described in section 4.2.3, repeatable to ± 3%. The small amount of catalyst used in these preliminary experiments also contributed

to the variation and poor repeatability since catalyst sticking to the reactor wall in the headspace, which did not participate in the reaction, would become significant compared to the total catalyst mass.

Compared to experiment 179 (untreated catalyst) the treated catalyst appear to produce less MO. The catalyst treated in glacial acetic acid had an initial activity for MO synthesis of 0.76 relative to the untreated catalyst used in experiment 179 (a ≡1.00). However, compared to the repeated experiment with untreated catalyst (experiment 176), the results are relatively consistent with the catalyst treated with glacial acetic acid giving a slightly greater amount of MO produced after 2 hours. Considering the variation in the data and the lack of repeatability of the experiment with the untreated catalyst, the results do not conclusively indicate any significant effect, positive or adverse, of the acid treatment of $Nb_2O_5/SiO_2$ catalysts on their activity for MO synthesis that would justify abandoning the use of acetic acid as a solvent. Indeed, the data presented in the next section shows the multifunctional catalyst is extremely active for MIBK synthesis.

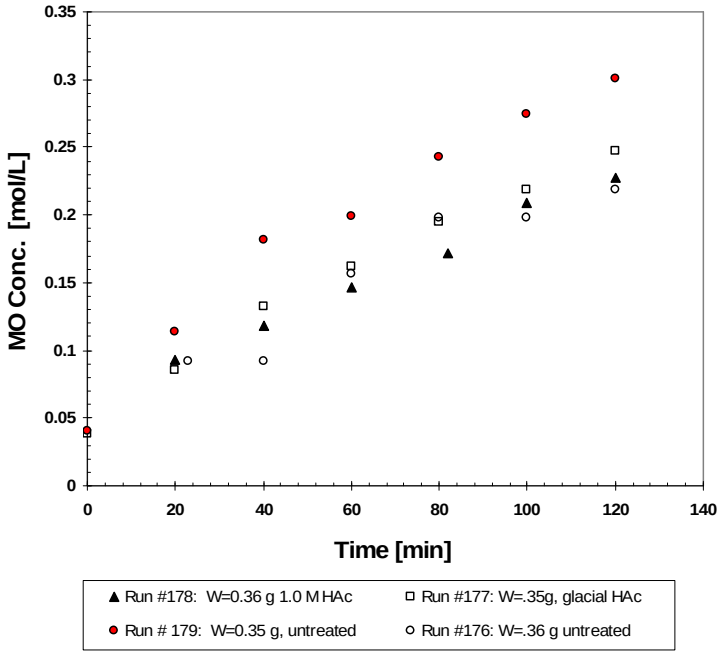


**Figure 6-1** Effect of the exposure of a 10.2 wt% $Nb_2O_5/SiO_2$ catalyst to acetic acid solution for 2 hours at 80°C on the synthesis of MO at 160°C.

*6.1.2 One-Step MIBK Synthesis using $Pd/Nb_2O_5/SiO_2$ catalysts*

A multifunctional $Pd/Nb_2O_5/SiO_2$ catalyst (CAT 042) was prepared following the procedure outlined in Chapter Three with the specific details outlined in Appendix B. While under inert environment in the glove bag, 0.597 g of the catalyst was charged to the autoclave reactor described in Chapter Three along with 100 mL of acetone and sealed. This was designated as time zero for the reaction. The autoclave was quickly transferred to the bench top reactor assembly and pressurized to 600 psig with UHP hydrogen. The temperature controller was enabled and set to 160°C. The chemical composition in the reactor was monitored for 10 hours by obtaining liquid samples periodically, which were analyzed by both GC/FID and GC/TCD. The results in Figure 6-2 illustrate that the catalyst was extremely active for MIBK synthesis as evidenced by a significant yield of MIBK utilizing only a small amount of catalyst 0.6 g. The initial rate of reaction at 160°C was determined to be 0.00952 [mol/L*min*$g_{cat}$]; an activity of 1.67 relative to the benchmark activity of Amberlyst 15 for MO synthesis at its maximum operating temperature of 120°C (Section 4.3).

In this experiment (#180), the MO was rapidly converted to MIBK. The initial rate of reaction for MIBK synthesis for experiment #180 was the same as the initial rate of reaction for MO synthesis for experiment #179, for which the same niobia catalyst (without Pd impregnation) was used for MO synthesis, to within 2.6%, which is within the bounds of experimental error. This suggests that the acid catalyzed steps to produce MO are slow and rate determining whereas the hydrogenation of MO is rapid under these conditions. The product is also produced with very high selectivity, essentially 100% selectivity up to an acetone conversion of around 8% (3 hours) where the products of undesirable competing reactions, specifically IPA and DIBK appear. Not shown in Figure 6-2, mesitylene was observed after 10 hours (0.007 M) and DAA was observed

in two observations at 120 and 180 minutes having concentration of 0.014 and 0.015 M respectively.

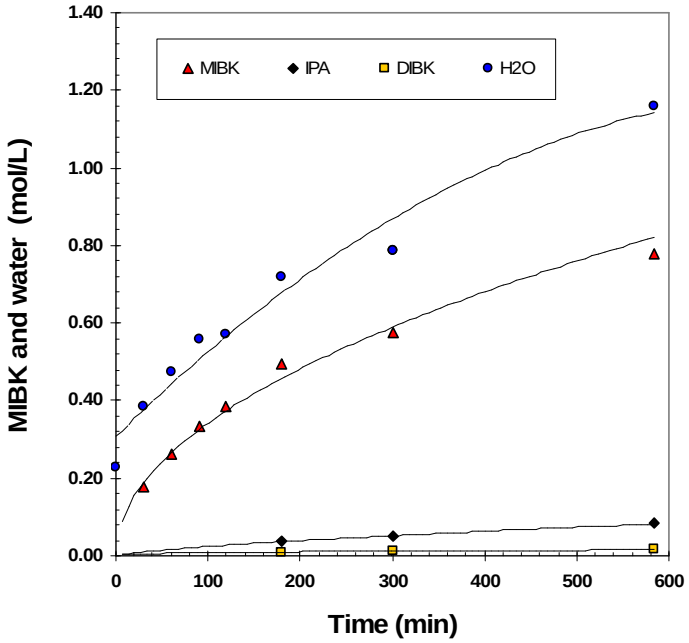


**Figure 6-2** One-Step Synthesis of MIBK in an autoclave reactor using a $Pd/Nb_2O_5/SiO_2$ catalyst [Expt. 180; CAT 042, T=160°C, ω=700 RPM, P=600 psig (H2), W=0.5974 g]

To confirm this result, the experiment was repeated. A new catalyst was prepared (CAT 046) following the same procedure. However, the timing device malfunctioned and an impregnation of about 2.5 hours occurred. The results of the activity test in the autoclave (Figure 6-3) demonstrates that the product distribution for MIBK synthesis for the experiment with catalyst 046 was markedly different than that for catalyst 042, perhaps due to the additional half hour of impregnation time. The results in Figure 6-3 show that the catalyst had poor initial activity for MIBK synthesis [0.056 mol/L*min*$g_{cat}$] and had essentially deactivated after three hours of reaction. However, the hydrogenation sites remained active resulting in a substantial increase in the rate of IPA production. It is likely that the additional impregnation time resulted in a significantly higher surface concentration of palladium acetate (which likely remained intact due to the low reduction temperature) at the expense of acid

sites, which diminished the catalyst's activity for MO and MIBK syntheses and contributed to the catalyst deactivation for MIBK production. The fact that the IPA production rate increased as the MIBK production rate decreased is evidence of the competition between MO and acetone for hydrogenation active sites. Note the MIBK concentration profile is concave down whereas the IPA concentration versus time profile is concave up. The results in Figure 6-3 also demonstrate that acetone is hydrogenated preferentially over MIBK. No MIBC is evident in the product mixture.

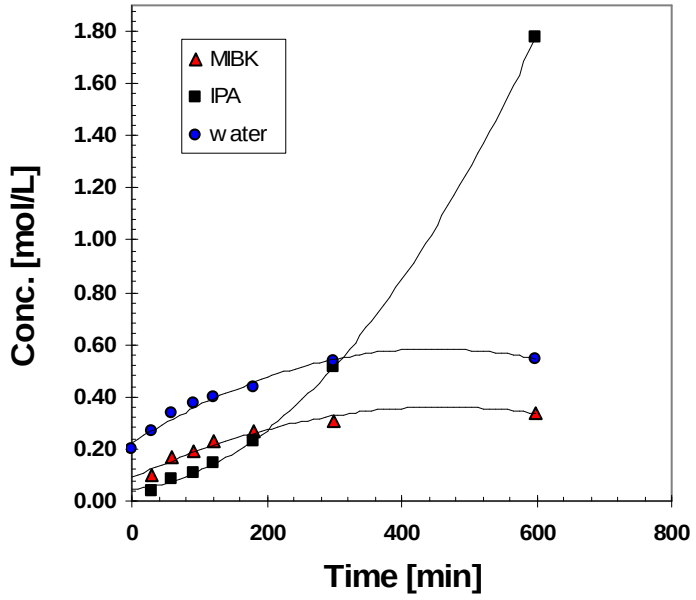


**Figure 6-3** One-Step synthesis of MIBK using a $Pd/Nb_2O_5/SiO_2$ catalyst after 2.5 hours of impregnation with palladium acetate/acetic acid solution [Expt #185, CAT 046, T=160°C, P=600 psig ($H_2$), ω=700 RPM, W=0.6183 g]

The experiment was repeated again using a new catalyst (CAT 051) prepared by the same method, the details of the preparation are also in Appendix B. The results of the activity test of the catalyst in the autoclave reactor (Expt. # 191, Figure 6-4) show a result similar to experiment # 185 (Figure 6-3) except the catalyst did not deactivate. The rate of IPA production was comparable to the rate of MIBK production, with an essential equimolar amount of hydrogenation products present in the reaction mixture after 8 hours

of reaction. Although the hydrogenation selectivity is poor, the catalyst activity for MIBK synthesis at 160°C is good 0.00751 [mol/L*min*$g_{cat}$]; an activity of 1.31 relative to the benchmark activity of Amberlyst 15 for MO synthesis at 120°C.

Although the palladium impregnation experimental variables were kept constant for these three experiments, with the exception of a slightly longer impregnation time in experiment #185, the resultant catalysts gave distinct product distributions, which implies that each of these catalysts had a unique palladium loading. The results suggest that in the presence of excess palladium (II) acetate, the adsorption of the precursor is dependent on the acidic properties of the $Nb_2O_5/SiO_2$ catalyst. Indeed, the UV-Vis analysis (Appendix B) suggest the palladium loading of the catalyst was an order of magnitude higher in experiment #191 compared to experiment #180 (Table 6-1).

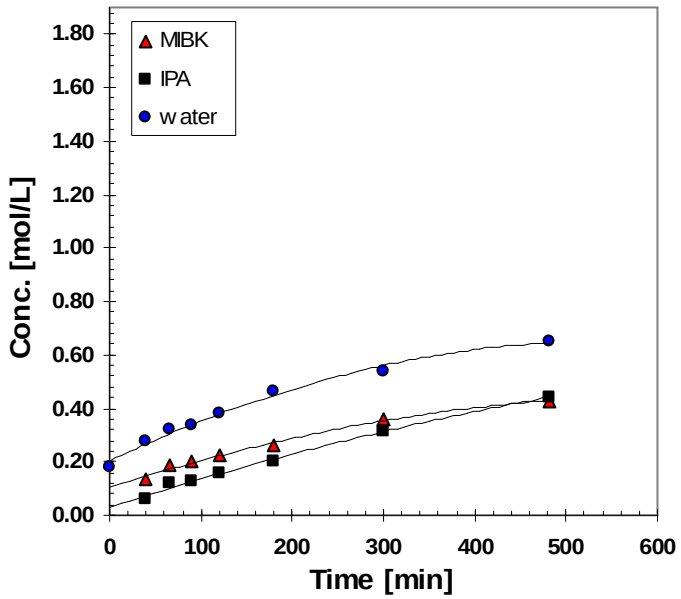


**Figure 6-4** One-Step Synthesis of MIBK in an autoclave reactor
[Expt. 191, CAT 051, T=160°C, P=600 psig ($H_2$), ω=700 RPM, W=0.5106 g]

**Table 6-1** $Pd/Nb_2O_5/SiO_2$ catalyst composition for preliminary experiments for one-step MIBK synthesis in an autoclave reactor

| Autoclave Expt | Catalyst I.D. | Wt% $Nb_2O_5$ (EDXRF) | Wt% Pd (UV-Vis) | Results in Figure |
|---|---|---|---|---|
| 180 | 042 | 10.2 | 0.15 | 6-2 |
| 185 | 046 | 12.3 | 1.06 | 6-3 |
| 191 | 051 | 13.6 | n/a* | 6-4 |

** UV-Vis measurement inconclusive for CAT 051. Based on observed experimental results in autoclave, the Pd loading is likely in excess of 1 wt% and is comparable to CAT 046,*

It can be concluded from these experiments that the palladium loading should be minimized for two reasons. First, the direct hydrogenation of acetone to produce IPA is a significant competing reaction with MO being hydrogenated preferentially. Thus, a reduction in the palladium loading will shift the selectivity in favour of MIBK production. Second, the results demonstrate that an excessive amount of palladium (II) acetate adsorbed on the catalyst will adversely affect the catalyst activity for MIBK synthesis and may result in catalyst deactivation. It also seems reasonable to conclude that when excess palladium acetate is used in the impregnation solution, the uptake of palladium acetate depends on the acidic properties of the $Nb_2O_5/SiO_2$ catalyst. The results also confirm previous findings for which it was concluded that the rate of IPA production will increase as the rate of MIBK production decreases, due to competition for the same kind of active sites.[18]

### *6.1.3 Preliminary Experiments with $Pd/Nb_2O_5/SiO_2$ catalysts (low Pd loading)*

Based on the UV-Vis results, an experiment was carried out for which a substantially lower amount of palladium (II) acetate precursor was used, which ensured a maximum possible palladium loading of 0.107 wt%. The resultant catalyst (CAT 053) and acetone were charged to the autoclave reactor in inert environment within a glove bag as described previously and the activity for MIBK synthesis at 160°C and 600 psig hydrogen pressure was assessed. The results of the autoclave experiment (#195) are interesting and worth reporting

for a couple of reasons. First, due to the very high activity of the acid function of the catalyst, the rate of MO synthesis exceeds the rate of its hydrogenation to produce MIBK for the first 2 hours of reaction. Thus, this experiment demonstrates the importance of obtaining a proper balance between the active sites for the aldol condensation/DAA dehydration steps and the hydrogenation step. The niobia loading corresponded to roughly 0.5 monolayer coverage while the Pd loading was at most 0.1 wt%, but likely much less. The data in Figure 6-5 also demonstrates that the production of IPA was essentially fully suppressed due to the relatively high concentration of MO. A small amount of IPA (ca. 0.09 mol/L) was observed after 8 hours along with a lesser amount of DIBK (ca. 0.03 mol/L).

Second, the overall catalyst activity is phenomenal compared to the benchmark. Although a small amount of catalyst was used (0.6 g compared to 1g normally used), an acetone conversion of 21.2 % was achieved after 8 hours, which incidentally exceeds the theoretical equilibrium conversion of acetone at 160°C predicted by the relation (Equation 2-15) for MO and acetone equilibria reported by Klein and Banchero.[10] The initial rate of reaction for MIBK synthesis at 160°C was 0.00738 [mol/L*min*$g_{cat}$]. However, a significant amount of MO was also co-produced with an initial rate of reaction of 0.0100 [mol/L*min*$g_{cat}$]. The total combined initial rate of reaction corresponding to the production of organics at 160°C was therefore 0.01738 [mol/L*min*$g_{cat}$], which is more than 3 times greater than the benchmark (i.e. the rate of MO synthesis using Amberlyst 15 at its maximum operating temperature 120°C). This calculation neglected the amount if IMO present, which would have resulted in a slightly higher value.

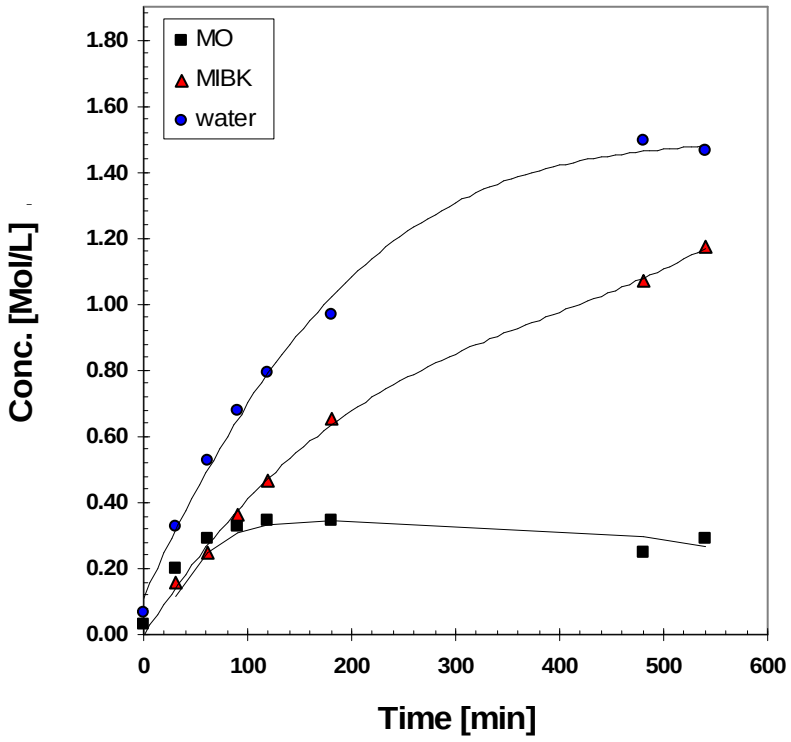


**Figure 6-5** One step synthesis of MIBK in an autoclave reactor with a $Pd/Nb_2O_5/SiO_2$ catalyst (Pd ≤0.1 wt%, $Nb_2O_5$=14.0 wt%) [Expt. 195: CAT 053, T=160°C, P= 600 psig (H2), ω=700 RPM, W=0.6156 g]

Figure 6-6 demonstrates that the overall selectivity of the reaction increased with time as the unreacted MO that had accumulated in the system was eventually converted to MIBK as the rate of MO synthesis diminished with time. This raises the point that in a flow system in contrast to a static system, unreacted MO will be removed from the reaction zone by convection. Therefore, it is more critical in the case of flow reactors to achieve a proper balance between acid sites and hydrogenation sites in order to achieve high selectivity. In the case of this experiment in a semi-batch microreactor, the hydrogenation was carried out with essentially 100% selectivity up to an acetone conversion of around 20% due to the high MO concentration. However, the overall selectivity was only around 74 mol% at an acetone conversion of 23%.

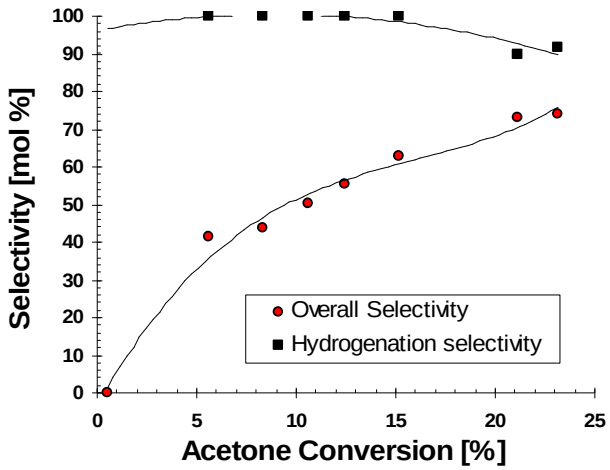


**Figure 6-6** Overall selectivity (mol%) and hydrogenation selectivity (mol%) in equation as a function of acetone conversion [Expt. 195: CAT 053, T=160°C, P= 600 psig (H2), ω=700 RPM, W=0.6156 g]

*The hydrogenation selectivity $S_H$ (mol%) and the overall selectivity S (mol%) are defined in Equations (6-1) and (6-2) respectively*

$$S_H = 100\% \left[ \frac{n_{MIBK}}{n_{MIBK} + n_{IPA} + n_{DIBK} + n_{MIBC}} \right] \qquad (6\text{-}1)$$

$$S = 100\% \left[ \frac{n_{MIBK}}{\sum_i n_i} \right] \qquad (6\text{-}2)$$

Some additional preliminary experiments were carried out using catalyst 051 (1.06 wt% Pd, 13.6 wt% $Nb_2O_5$). The details of these experiments are in Appendix C but are briefly summarized here. In experiment #193, the multifunctional catalyst was used to carry out the synthesis of MO at 160°C in inert environment ($N_2$). The catalyst showed excellent activity 0.010 [mol/L*min*$g_{cat}$] and achieved an acetone conversion of 12.8 % after 8 hours. Phorone was evident in the product mixture. This experiment showed that the palladium (II) acetate did not significantly interfere with the function of the acid sites.

In experiment #194, catalyst 051 was used to carry out the one step synthesis of MIBK in hydrogen environment (600 psig). However, the initial

reactant mixture consisted of a 50% (v/v) acetone-MO mixture. The results demonstrated that essentially all of the MO initially present was converted to MIBK within 1.5 hours after which, the catalyst remained active for MIBK synthesis. The MIBK concentration was 4.3 mol/L and 4.6 mol/L after 90 minutes and 8 hours respectively. A reverse reaction to produce DAA was not observed. DAA was at all times below the peak area rejection limit of the GC. This experiment also demonstrated that the catalyst remained highly active in the presence of significant concentrations of organic substrates. With the palladium loading (1.06 wt%) at least an order of magnitude greater than in experiment 195 (Fig 6-6), and with MO in excess, the rate of MIBK production was an order of magnitude higher than observed in previous experiments [0.120 mol/L*min*$g_{cat}$]

*6.1.4 MIBK Synthesis utilizing a Pd/$Nb_2O_5$/γ-$Al_2O_3$ Catalyst*

The results of the experiments in Chapter Four suggested that γ-$Al_2O_3$ would be a promising catalyst support for the dispersion and generation of a surface oxide phase niobia for MO synthesis. A preliminary experiment was carried out in order to assess the performance of a Pd/$Nb_2O_5$/γ-$Al_2O_3$ catalyst for the one-step synthesis of MIBK. 0.9954 g of catalyst 032 (3.79 wt% $Nb_2O_5$/γ-$Al_2O_3$ calcined at 100°C) was impregnated for 2 hours at 81°C with a solution of 0.1202 g of Pd (II) acetate dissolved in 35.5 mL of glacial acetic acid. The amount of palladium precursor relative to the niobia catalyst was ca. 0.12 g/g which was the same as that used in the preliminary experiments for the silica based catalysts in Section 6.1.2 since this preliminary experiment was carried out around the same time. After impregnation, the catalyst was recovered by vacuum filtration and dried overnight in an oven at around 81°C. The catalyst was reduced with flowing hydrogen in a calcinator as described in Chapter Three, at 100°C for 2 hours and 15 minutes.

The activity test for MIBK synthesis in an autoclave reactor at 160°C and 600 psig ($H_2$) (Figure 6-7) shows that the activity of the catalyst was quite low

0.00447 [mol/L*min*$g_{cat}$]. Incidentally, this activity only 48% of the activity of the $Nb_2O_5/\gamma$-Al2O3 support, catalyst 032 (3.79 wt% $Nb_2O_5/\gamma$-$Al_2O_3$ calcined at 100°C) for MO synthesis at 160°C. After 8 hours of reaction, the catalyst had only achieved an acetone conversion of around 4.6%. This result seems comparable to experiment #185 (Figure 6-3) with the significant distinction that the IPA production was minimal in experiment #181, while the IPA was the major product in experiment #185. This implies a low surface concentration of active palladium sites for catalyst 043. However, it is quite evident that the presence of the palladium (II) acetate adversely and significantly affected the acid function of the catalyst. Perhaps the palladium acetate interacts preferentially or differently with the niobium oxide phase, which is presumably primarily responsible for catalytic activity. A low palladium acetate adsorption, or low surface concentration of active palladium sites may have occurred due to a relatively low niobia loading (3.79 wt%; 18% monolayer coverage).

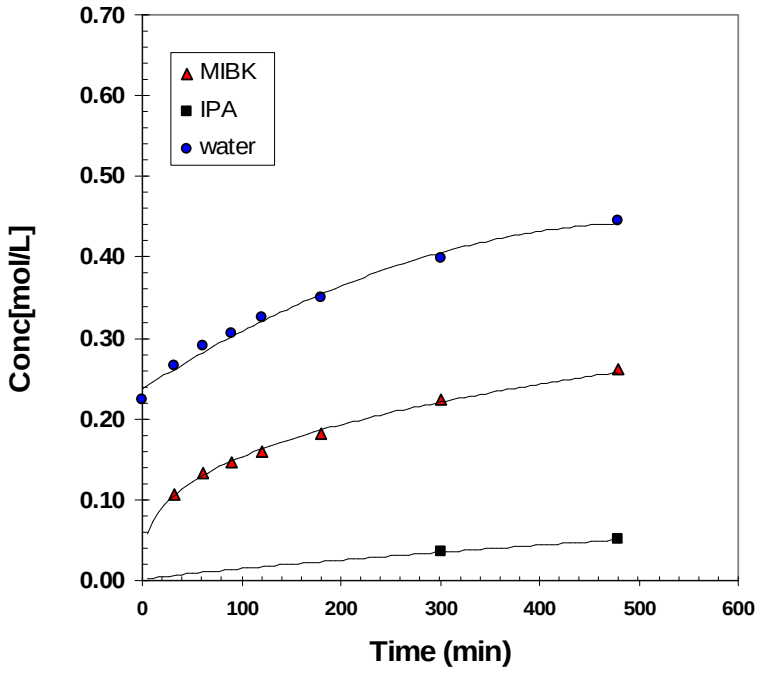


**Figure 6-7** MIBK synthesis using a $Pd/Nb_2O_5/\gamma$-$Al_2O_3$ catalyst. [Expt. #181: CAT 043; T=160°C, P=600 psig (H2), ω=700 RPM, W=0.7009 g cat]

## 6.2 Scale-up of Catalyst to Pellet Scale

### *6.2.1 Commercially Available Catalyst Carriers*

The catalysts used for the preliminary screening of catalytic materials (Chapter Four) and to investigate the structure-activity relationships for MO synthesis (Chapters Four and Five) as well as to investigate the kinetics of the one-step synthesis of MIBK in an autoclave reactor (Chapter Six), were in powder form. Minimization of particle size mitigates the potential for thermal and chemical gradients within the catalyst pore structure, which may falsify the intrinsic kinetics. In addition, having the catalyst in powder form is convenient for materials characterization and averts potential complications that may arise from the comminution of egg-shell catalysts (eg. heterogeneity in samples).

However, a major objective of this Ph.D. research project is the development of a practical catalyst that can be utilized in a pilot scale reactor. As mentioned previously in Chapter One, in a catalytic distillation reactor, a minimum void fraction of at least 0.5 is required in order to prevent an excessive pressure drop which could lead to flooding of the CD column.[56] Since most commercial catalysts range in size from 1 to 3 mm in characteristic dimension, the catalysts are contained within or dispersed onto engineered structures which immobilize the catalyst within the reactive section while ensuring sufficient void volume to enable counter current flow.[57] Aside from the issue of pressure drop, the catalyst must also exhibit sufficient mechanical strength to withstand the stresses due to applied loads from the weight of catalyst loaded above it and other compressive stresses. Various designs for loading the catalyst into the reactive sections have been summarized in Chapter One and have been reviewed previously by Taylor and Krishna.[57]

A popular technique included among these designs is the concept of dispersing a catalytically active material onto a support that has the shape of a distillation packing such as a Raschig Ring.[57,186-189] Alternatively, the catalyst

material itself may be shaped into a distillation packing.[57] Catalysts moulded into the shape of distillation packings have been utilized since the 1960's.[187] According to Sundmacher and Hoffman[187,188], the advantages of using a catalytically active Raschig ring for catalytic distillation includes: i) the rings act simultaneously as a catalyst and distillation packing, ii) a high ratio of catalyst active sites per volume can be achieved iii) the rings afford a low pressure drop iv) the large external surface of the catalyst facilitates liquid-vapour contacting v) ease of catalyst handling vi) low catalyst manufacturing cost and vii) a rapid response to CD process perturbations is realized due to low liquid holdup.

Two lots of silica catalyst carrier in the shape of Raschig rings were procured from Saint-Gobain Norpro (Stow, OH). A batch of Norton SRK 13650 silica rings (S/N 9516511) was used in preliminary experiments. This batch of discontinued product was used in some preliminary experiments. A second batch with comparable specifications (Saint-Gobain Norpro SS 65137; S/N 2006910020) with a characteristic dimension of 5 mm and specific surface area of 160 $m^2/g$ was subsequently procured for use in the catalytic distillation experiments (Chapter Eight) and experiments in a fixed bed reactor (Chapter Six). Additionally, high surface area (ca 200 $m^2/g$) ¼ inch gamma alumina catalyst carriers in the shape of Raschig Rings (Saint-Gobain Norpro SA6573, Lot # 2004670154) was procured.

### *6.2.2 Catalytic Performance of $Nb_2O_5/\gamma$-$Al_2O_3$ Raschig Ring Catalysts in a Batch Autoclave Microreactor*

The first preliminary experiments were carried out using the Norpro gamma alumina Raschig ring support. Since it is known that catalyst particles larger than 3 mm in their characteristic dimension typically exhibit internal mass transfer limitations, the objective of first two experiments (Expt. #148 and #149) were to ascertain the catalyst effectiveness factor for a $Nb_2O_5/\gamma$-$Al_2O_3$ Raschig ring catalyst for MO synthesis at 160°C in the batch autoclave reactor

described in Chapter Three. A third experiment (#150) was carried out to assess the nominal activity of the Norpro alumina support for MO synthesis at 160°C.

A batch of catalyst (CAT 017) was prepared following the synthesis technique described in Chapter Three. The details are in Appendix B. The catalyst was calcined at 500°C since these preliminary experiments were carried out prior to the experiments in Section 4-5 which revealed the effects of calcination temperature on the catalytic properties of niobia-silica and niobia-alumina compounds. Some of the catalyst batch was ground to a powder and characterized by EDXRF, which revealed a niobia loading of 22.3 wt% corresponding to 1.0 monolayer coverage.

In the first experiment (#148), 3 pellets of the $Nb_2O_5/\gamma\text{-}Al_2O_3$ Raschig ring catalyst (0.9937 g) were used to carry out the synthesis of MO in acetone (l) at 160°C with the autoclave headspace pressurized to around 400 psig ($N_2$) to maintain the liquid phase. The pellets were slurried in the liquid with the agitation rate maximized at 700 RPM. Despite this high agitation rate, the pellets were found to be intact at the end of the experiment. In the second experiment (#149) 0.9635 g of catalyst 017 that had been ground to a fine powder was slurried in acetone in the autoclave reactor and the synthesis of MO was similarly carried out at 160°C in the liquid phase with the agitation rate maximized at 700 RPM.

The results in Figure 6-8 show that the powdered catalyst was highly active for MO synthesis at 160°C with an initial rate of 0.00930 [mol/L*min*$g_{cat}$], which corresponds to an activity of 1.62 relative to the benchmark activity of Amberlyst 15 for MO synthesis at 120°C, whereas the catalyst in pellet form showed negligible activity for MO synthesis. In fact, the activity of the Raschig Ring catalyst was less than the nominal activity of the gamma alumina support with no niobia. This unexpected result clearly demonstrates a substantial internal mass transfer limitation present in the

$Nb_2O_5/\gamma\text{-}Al_2O_3$ Raschig ring catalyst. The catalyst effectiveness factor was estimated to be 1.64% based on the initial rates of reaction. The rate of reaction for experiment #148, was estimated by modelling the data as a linear function based on the three observations above the GC peak area rejection limit. The initial rate of reaction for experiment # 149 was carried out as described in Chapter Four by fitting the data obtained during the first 2 hours of reaction to a second order polynomial.

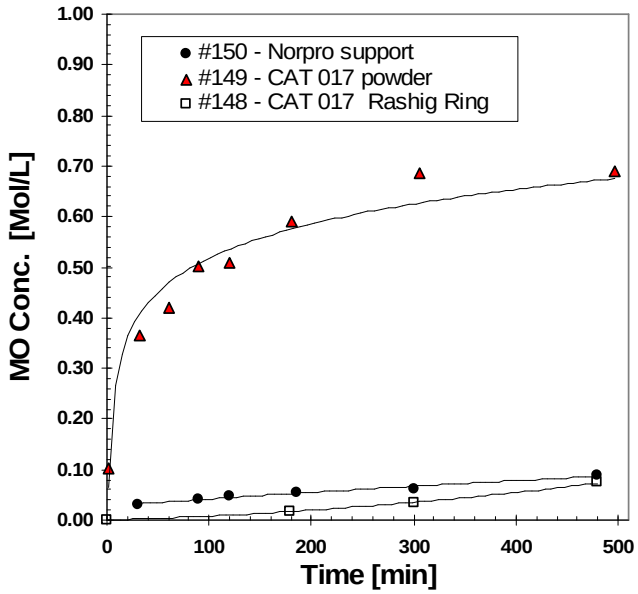


**Figure 6-8** Effect of particle size on the activity of a $Nb_2O_5/\gamma\text{-}Al_2O_3$ Norpro SA 6573 Raschig Ring catalyst carrier on the catalyst activity for MO synthesis at 160°C

### *6.2.3 Catalytic Performance of $Nb_2O_5/SiO_2$ Raschig Ring Catalysts in a Batch Autoclave Microreactor*

Experiments were carried out to assess the catalyst effectiveness factor for the $Nb_2O_5/SiO_2$ Raschig ring catalysts for MO synthesis at 160°C in an autoclave reactor. A batch of 14 catalyst pellets (CAT 055) was prepared following the procedure outlined in Chapter Three, using Norton SRK 13560 silica raschig rings as supports. The preparation details are available in Appendix B. Some of the catalyst pellets were crushed into a powder and used for EDXRF analysis

as well as for use in an autoclave experiment (#213) to obtain the catalyst activity for MO synthesis in the absence of internal mass transfer limitations.

The autoclave experiment with crushed catalyst (#213, Appendix C) revealed a rate of reaction of [0.00824 mol/L*min*gcat] for MO synthesis at 160°C, which represents an activity of 1.14 relative to the benchmark rate of reaction for MO synthesis using Amberlyst 15 at 120°C. The autoclave experiment with the intact Raschig ring catalysts (#212) however was inconclusive since the catalyst particles fragmented from contact with the impeller blades within the reactor during operation. A new batch of catalyst (CAT 057) was prepared with the exact same preparative steps. However, for some unknown reason, EDXRF analysis of catalysts 055 and 057 gave different results for niobia loading. The surface concentration of niobia for CAT 055 and CAT 057 were 10.4 wt% (0.56 monolayer) and 5.30 wt% (0.27 monolayer) respectively. The activity of catalyst 057 for MO synthesis at 160°C was ascertained in an autoclave reactor experiment (#215, Appendix C) at a reduced agitation rate of 100 RPM which resulted in the catalyst particles remaining intact. When the initial rates of reaction for MO synthesis for the powdered catalyst 055 and the ring catalyst 057 were normalized by the mass of niobia in each catalyst, the reaction rates suggest a catalyst effectiveness factor of 66%. The crushed catalyst 055 had an activity for MO synthesis at 160°C of 1.43 relative to the benchmark activity Amberlyst 15 for MO synthesis at 120°C. With the rings intact, the activity of the niobia catalyst for MO synthesis at 160°C is comparable to the activity of Amberlyst 15 for MO synthesis at 120°C with a relative activity of 0.94. When normalized by the amount of niobia, the ground silica raschig ring catalyst 055 was more active for MO synthesis at 160°C by a factor of 1.19 compared to CAT 030, the fumed silica catalyst with the highest nominal activity for MO synthesis observed in DoE #2 (Chapter Four).

Autoclave experiment #149 utilizing the alumina raschig ring ground to a powder confirmed that a catalyst with monolayer coverage of $Nb_2O_5/\gamma$-$Al_2O_3$ has good activity for MO synthesis, as observed in various experiments in Chapter Four (i.e. #140, #143, #151). The silica and alumina catalysts had different morphological characteristics. Most notably, the surface area of the alumina support was much greater (200 $m^2/g$) compared to the silica rings (Norton SRK 13650, 150 $m^2/g$). In addition, according to the Saint-Gobain Norpro product literature, the mean pore size for the alumina rings was 7 nm whereas the Norpro SS 65137 silica, which has the same morphological characteristics of the Norton SRK 13650, had a mean pore size of 11 nm. Thus the silica support had a lower surface area and larger pores than the alumina. Perhaps a lower surface area alumina catalyst might give an improved result.

Another major distinction between the silica and alumina raschig ring carriers is their surface reactivity to the niobium (V) ethoxide precursor. Although it was intended to prepare these raschig ring catalysts to have one complete monolayer of coverage, the niobia uptake of Norpro silica rings was much less. In this research project, the niobia raschig ring catalysts typically had less than 1/3 monolayer coverage at most with the exception of one batch of catalyst (CAT 055) that had roughly ½ monolayer coverage. This suggests a low surface concentration of hydroxyl groups to interact with the niobium ethoxide precursor. Regardless, the silica raschig rings catalysts have shown good activity for MO synthesis. More importantly, the results of Chapter Five demonstrate that the interaction of the niobia with the silica raschig ring support gives rise to unique acid sites with very strong acidity not observed in other catalysts including the niobia-fumed silica catalysts. The activity for mesityl oxide synthesis is correlated with the acid strength (Figure 5-15). The TPD profile for catalyst 057 is given in Figure 5-10.

Although mass transfer effects are evident in the silica based raschig ring catalyst, the reasonably high overall catalyst effectiveness factor of 66%

observed in the autoclave experiments suggests that the Norpro silica raschig ring catalyst carrier would be an effective support for application towards MIBK synthesis via CD. In contrast, the results in Figure 6-8 reveals substantial mass transfer effects that resulted in a very low catalyst activity for the alumina raschig ring catalyst. Given this result, and also considering the results of preliminary pilot scale CD experiments (Chapter Seven), which suggest the interaction of the organic substrates with the alumina catalysts affected the residence time distribution in the reaction zone (Figure 7-7) and considering our spectroscopic investigations[63,64] which show that the organic substrates strongly interact with the Lewis acid sites of the alumina support, which is undesirable and may lead to coke formation and catalyst deactivation, the alumina raschig ring support was abandoned in favour of the silica based raschig ring support.

A preliminary autoclave experiment was carried out to investigate the one-step synthesis of MIBK utilizing a $Pd/Nb_2O_5$/Norpro SS 65137 $SiO_2$ raschig ring support. Approximately 10 grams of catalyst were prepared following the technique outlined in Chapter Three. The preparation details are available in Appendix B. An autoclave experiment (#219) was carried out to investigate the activity of catalyst 060 for MIBK synthesis. The catalyst was charged to the reactor along with acetone in the glove bag as described previously and then transferred to the bench where the reactor was pressurized to 600 psig ($H_2$) and the temperature controller set to 160°C. The agitation rate was set to 100 RPM to ensure the catalyst did not fragment. Samples were obtained periodically from the reactor and analyzed by GC/FID and GC/TCD. The results in Figure 6-9 show that the catalyst has very good initial activity for MIBK synthesis [0.00688 mol/L*min*$g_{cat}$] at 160°C, which represents an activity of 1.16 relative to the benchmark activity of Amberlyst 15 for MO synthesis at 120°C. The acetone conversion after 8 hours (14.8 %) was very high, especially considering the small amount of catalyst used (0.38 g) compared to the usual 1g.

This excellent result also shows that essentially 100% of the MO was converted to MIBK as evidenced by no DAA or MO present in the product mixture. In addition, the MIBK concentration versus time profile very closely mirrors the water concentration versus time profile, which implies these species were produced in stoichiometric equivalent amounts. However, at higher acetone conversions (ca. 11.7 %), the secondary hydrogenation products appear in the product mixture. DIBK is produced from the reaction of MIBK and acetone on the acid sites. However, the dominant impurity is IPA, which is produced from the direct hydrogenation of acetone and remains a significant competing reaction.

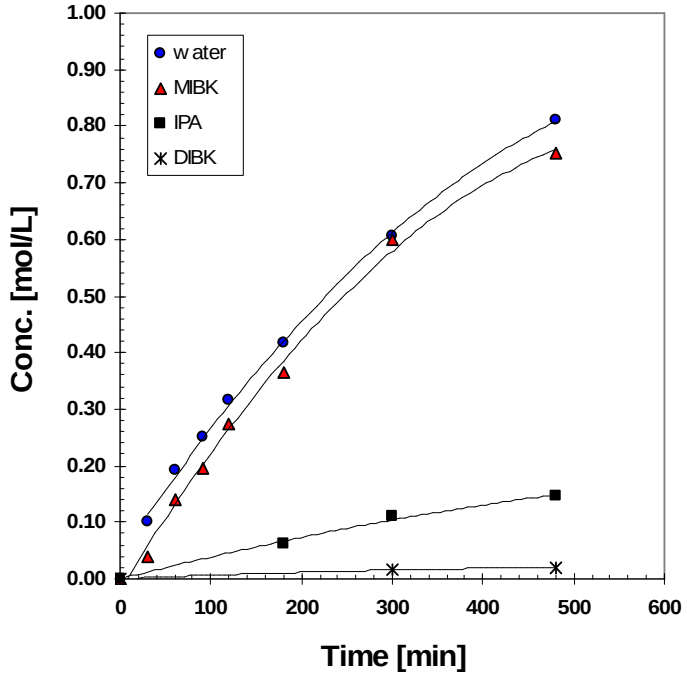


**Figure 6-9** Product distribution as a function of time for the one-step synthesis of MIBK from acetone in an autoclave reactor utilizing a $Pd/Nb_2O_5$/Norpro SS 65137 catalyst (CAT 060). [Expt. #219, T=160°C, P=600 psig ($H_2$), ω=100 RPM, W=0.3758 g]

## 6.3 Macro-Kinetic Measurements in a Fixed Bed Flow Reactor (FBR)

### *6.3.1 Bench-top Fixed bed Micro-reactor Apparatus*

Clearly, the catalysts consisting of palladium and niobia dispersed onto a silica raschig ring carrier are promising catalysts for application for MIBK synthesis in a commercial scale reactor. Consequently, the macro-kinetics of these niobia catalysts were investigated in greater detail using a bench scale fixed bed flow reactor (FBR). The reactor apparatus is a custom designed Autoclave Engineers (a division of Snap-Tite Inc, Erie, PA) BTRS-Jr/PC® Micro-scale Benchtop Reaction System procured in 1996 (S/N 96200924).

The reactor is a vertically mounted tubular reactor constructed of 316 stainless steel 16 inches in length and 0.44 inch I.D with an internal volume is 23 mL.[189] The reactor is encompassed by a removable heater band which acts as a single zone furnace. A thermowell running inside the reactor allows measurement of temperature at three locations by three K-type thermocouple probes. These thermocouple probes are for monitoring the process and can enable alarms. However, their signals are not used for process control. A K-type thermocouple inserted within a furnace wall sleeve thermowell allows measurement of the reactor external wall temperature at the mid-point of the reactor major axis. The feedback signal from this thermocouple probe is used to control the reaction temperature. The tubular reactor engages to the benchtop reactor module with custom threaded fittings. Once installed, the entire reactor is enclosed within an insulated, temperature controlled heated oven rated to a maximum temperature 280°C.

The benchtop reactor module accepts 4 feed streams; two liquid and two gaseous. The liquid streams are fed by high pressure precise fluid metering pumps and the gaseous streams are controlled by Brooks mass flow controllers. Flow rates are governed by the BTRS-Jr flow control module and are set directly at the computer. Two computers are involved in the operation of the

reactor system. One computer is responsible for the programmable logic control (PLC) modules which includes proportional integral derivative (PID) process control and governance of the failsafe interlocks while the other computer (the PC) serves as the human machine interface and allows data processing by running a control application program on Wonderware Software. The pressure in the reactor was controlled manually by a backpressure regulator on the reactor product line. However, precise pressure measurement is reported at the human machine interface. In this work, a Swagelok backpressure regulator (KPB1A1D3PP40) rated to 3000 psig and equipped with PEEK and PCTFE polymer seals, which are compatible with acetone was used.

A multi-port "Reactor Status Valve" causes the feed streams to bypass the reactor when the reactor status is "offline" and enables flow through the reactor when the reactor status is "on-line". Although the BTRS-Jr system was fully integrated to a GC with on-line sampling and analysis capability, in this work, liquid samples were obtained directly from the reactor effluent by collection in GC autosampler vials and analyzed off line by GC/FID. A custom made heat exchanger, similar to the one used on the autoclave reactor described in Chapter Three, which consisted of a copper cooling coil in intimate contact with the product line, was installed at the end of the reactor product line to ensure the reactor effluent was sub-cooled. HPLC grade acetone feedstock was loaded into a feed tank consisting of a 2L Parr autoclave reactor, rated to 3600 psig. The feedstock was degassed by repeatedly pressurizing and depressurizing the headspace with UHP nitrogen.

### *6.3.2 MO Synthesis in a Tubular Fixed Bed Reactor*

An experiment was carried out in order to assess the effects of the reaction temperature and the flow rate on the synthesis of MO from acetone in the liquid phase utilizing a $Nb_2O_5$/Norpro SS 65137 silica raschig ring catalyst. A batch of approximately 10 g of catalyst was prepared following the procedure outlined

in sections 3.6.1 and 3.6.2. The details of the preparation are available in Appendix B. The niobia loading of the catalyst (CAT 061) was ascertained via Inductively Coupled Plasma (ICP) by an external laboratory (Galbraith Laboratories, Knoxville, TN) and was found to be 5.58 wt% $Nb_2O_5$, which corresponds to 0.27 monolayer. 3.01 g of this catalyst was loaded into the mid region of tubular reactor with the remaining space filled with 3.5 mm diameter glass beads (Canadawide Scientific, 40410-03, #3000).

19 steady state conditions including 3 repeated conditions were investigated over a 10 day period. The reactor was operated intermittently with the reactor being shut down overnight. At the end of the day, the heating elements were disabled; however the pump was left pumping overnight to prevent products from accumulating in the catalyst bed during cool-down. At the beginning of the day, the reactor was brought on-line with acetone flowing at the desired flow rate and the reactor pressurized at the desired set point. The reactor temperature was slowly increased to the desired set point over a period of about an hour. Steady state was achieved rapidly due to the small liquid hold-up. In this experiment, the pressure was not critical and was not controlled precisely but was maintained at 350 ± 50 psig to ensure the reactant mixture remained in the liquid phase. The acetone feed rate was varied from 0.25 to 1.84 mL/min for reaction temperatures of 140, 160 and 180°C. The effects of the acetone flow rate and reaction temperature on the steady state MO (and IMO) productivity are illustrated in Figure 6-10.

The repeated conditions (with the exception of condition #3) are not indicated in Figure 6-10. Condition #3 (WHSV = 16.6 $hr^{-1}$) was a repeat of condition #1 to assess repeatability of process. The activity in condition #3 was 1.03 [$g/hr*g_{cat}$] whereas in condition #1 it was 0.981 [$g/hr*g_{cat}$]. (i.e. repeatable to within 5% relative error) The other repeated conditions give an assessment of catalyst deactivation and are discussed separately here. The data at 160°C were obtained first, followed by experiments at 140°C. The experiments carried

out at 180°C were performed last. Condition #12 was a repeat of the initial condition after the data for the experiments at 160°C and 140°C were obtained. A comparison of the steady state MO productivity for condition #12 to the initial catalyst activity indicates that the catalyst had deactivated very slightly losing 9.0% of its initial activity. The results suggest that the catalyst deactivation became significant after the reaction temperature was increased to 180°C. On the seventh day of the experiment, after the first condition at 180°C was investigated, the initial condition was repeated at 160°C. The result suggests the catalyst had deactivated slightly. Additional conditions were investigated at 180°C on the 8$^{th}$ and 9$^{th}$ days of the experiment. The last condition (319) was a repeat of condition #15 (day 7). This result suggested the catalyst lost an additional 9.2% of its activity while investigating the reaction at 180°C. The two data points obtained on the last day particularly seem to not be in agreement with the trend of the first four data points obtained at 180°C and were neglected from the Figure. These data along with the repeated conditions are available in Appendix E.

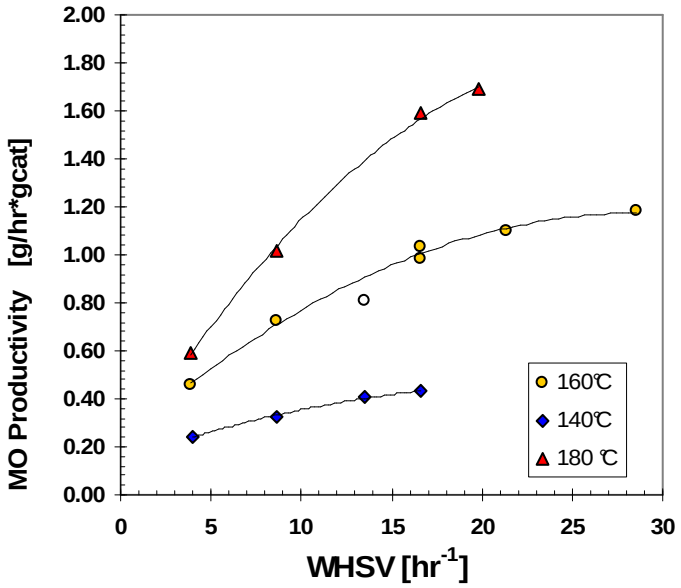


**Figure 6-10** Effect of the weight hourly space velocity (WHSV) and reaction temperature on the steady state MO productivity using a 5.58 wt% $Nb_2O_5$/Norpro SS 65137 catalyst (CAT 061) in a Fixed Bed Flow Reactor *The hollow sphere denotes an apparent outlier (Condition #2)*

The results in Figure 6-10 shows that the catalyst has a significant activity for MO synthesis with about half of the observations in excess of 1 [g/hr*$g_{cat}$]. It is evident from Figure 6-10 that the space velocity has a substantial effect on the MO productivity and its influence becomes more pronounced with increasing reaction temperature. At 140°C, the MO productivity becomes relatively insensitive to the space velocity at a relatively low value of around 15 $hr^{-1}$. At 160°C, the trend suggests the reaction rate becomes independent of space velocity at around 30 $hr^{-1}$. The reaction rate at 180°C is strongly dependent on the space velocity, increasing nearly linearly throughout the entire range investigated. The results clearly demonstrate that the increase in residence time, and hence increase in conversion, is accompanied by a reduction in the reaction rate due to a decrease in reactant concentration within the reactor as well as the suppression of catalytic activity due to product inhibition. The catalyst activity was maximized where the acetone flow rate was maximized resulting in a rapid removal of product from the reaction zone and a maximum mean acetone concentration in the reactor. These results are also consistent with an external mass transfer limitation, whereby the reaction rate increases with the flow rate. However, the synthesis of MO is known to be a slow reaction and the loss of activity with increasing residence time may be due to product inhibition.

Although the catalyst activity was relatively high, the acetone conversion was typically quite low for the range of space velocities investigated. Three of four conditions investigated at 140°C had acetone conversions ranging from 2.4 to 3.6%. The fourth condition at the lowest space velocity had a conversion of 6.4%. As the reaction temperature was increased, the acetone conversions increased. The acetone conversion ranged from 4.1 to 12.2 % for the experimental conditions investigated at 160°C and ranged from 8.8 to 16.4% for the conditions investigated at 180°C.

The major products were MO and IMO. The concentration of MO in the effluent ranged from 0.19 to 1.10 mol/L. The IMO concentration was approximately $1/10^{th}$ the value of the MO concentration. Phorone became evident in the GC analysis of the reactor effluent for acetone conversions above 6%. Mesitylene was observed only in experimental conditions where the acetone conversion was in excess of 10.5% and the reaction temperature was 180°C. Incidentally, the theoretical equilibrium concentration of MO at 140°C, 160°C and 180°C predicted by the model of Klein and Banchero[10] (i.e. Eqn. 2-15) were 1.31, 1.29 and 1.28 M respectively, which assuming a density of 0.7899 g/cc corresponds to MO mass fractions of 16.3, 16.1 and 15.9 wt% at 140°C, 160°C and 180°C. The MO concentration observed in these experiments (Appendix E2) were well below the theoretical equilibrium concentration of MO with the exception of condition #13 where the reactor was operated at maximum temperature and residence time (180°C and WHSV=3.8 $hr^{-1}$) where the MO concentration was 13.7 wt%. For experiments at 140 and 160°C, the MO concentration in the effluent ranged from roughly 2 to 10 wt% for the flow rates investigated.

It is interesting to note that du Toit et al.[127] were constrained to MO concentrations of less than 0.8 M when investigating MO synthesis in a FBR at 100 to 120°C using Amberlyst 16 regardless of residence time due to a pseudo equilibrium phenomenon. Considering that the reaction is endothermic, the high MO concentration observed in condition #13 (1.10 mol/L) suggests the pseudo equilibrium phenomenon described by du Toit et al.[127] may be specific to the cation exchange resin catalyst Amberlyst 16.

The data in Figure 6-10 provides a benchmark against which the catalyst utilization in the catalytic distillation reactor may be measured. In the CD experiments, the reflux flow rate typically varied from around 5 to 50 g/min with about 78 grams of catalyst loaded in the reactive section. This implies a liquid WHSV ranging from about 4 to 40 $hr^{-1}$. If the catalyst utilization in the

CD reactor is comparable, then from Figure 6-10, one would expect the MO (or MIBK) productivity at 160°C to range from roughly 0.45 to 1.2 [g/hr*gcat].

*6.3.3 Macrokinetic Model of MO Synthesis*

The data obtained in the experiment illustrated in Figure 6-10 provides an opportunity to model the macrokinetics of MO synthesis over a $Nb_2O_5$/Norpro SS 65137 catalyst. A simple two-parameter empirical kinetic model (Eqn. 6-3) for MO synthesis, was used to model the production rate of MO over a $Nb_2O_5$/Norpro SS 65137 catalyst, where $-r_{A'}$ denotes the specific rate of acetone conversion (mol/hr*$g_{cat}$) and $C_{A,}$ $C_W$ and $C_{MO}$ denote the concentrations in (mol/L) of acetone, water and MO respectively. $k_1$ and $k_2$ denote empirically determined model parameters. The reaction is modelled as second order with respect to acetone due to the bimolecular nature of the aldol condensation reaction and first order in the reverse direction with respect to MO and water. The third term of the expression accounts for mesityl oxide conversion to phorone. The water concentration was inferred from the product distribution.

$$-r_A = k_1 C_A^{\,2} - k_2 C_{MO} C_w - k_3 C_{MO} C_{AC} \qquad (6\text{-}3)$$

Since the acetone conversion was low in these experiments, the reactor was modelled as a differential reactor. The reaction rate data obtained for each of the conditions investigated in Figure 6-10 (with the exception of the outlier) were used to estimate the model parameters for the rate expression in equation (6-3) following a simplifying assumption. The concentrations of species in the reactor bed were estimated as the arithmetic mean of the inlet and outlet concentrations. Thus the reaction rate was related to the average concentration in the reactor bed, based on a first approximation of a linear concentration profile within the reactor. This approximation is valid for low conversions and is a particularly good assumption for acetone, which was the solvent whose concentration did not change appreciably through the reactor. A second

assumption was that the reactor operated isothermally. Although, this may be a questionable assumption in some FBR experiments, in this case, it is a good assumption since the reaction heat for the aldol condensation of acetone, which is exothermic, essentially cancels out the heat effect for the endothermic DAA dehydration step. The net heat effect is about -2 kJ/mol.[1] Moreover the heat effects were small due to the low chemical conversions which ranged from 2.4 to 16.4 %.

The regression was carried out in two stages. First the parameter $k_3$ was determined at 160 and 180°C by nonlinear regression analysis relating the rate of phorone production to the MO and acetone concentration with the empirical kinetic equation 6-4. The rate of phorone production at 140°C was negligible at 140°C. The regression results are in Table 6-2. The phorone production rate for the 6 observations at 160°C, not including the condition producing the outlier in Figure 6-10, correlated very well ($R^2$=0.99) for the fit to equation (6-4). However, the 4 observations for 180°C showed a weaker correlation ($R^2$=0.93). From these two estimates of $k_3$, assuming Arrhenius behaviour of the reaction rate constant, the apparent activation energy for phorone production was estimated to be 7.71 kJ/mol. This very low value implies a significant mass transfer limitation associated with phorone production and a weak temperature dependence of $k_3$.

$$r_{pho}=k_3 C_A C_{MO} \qquad (6\text{-}4)$$

**Table 6-2** Regression results for data fit to the empirical model of Eqn. 6-3

| **Temp [°C]** | **$k_3$ [L$^2$/(mol*hr*gcat)]** | **$R^2$** |
|---|---|---|
| 160 | 4.444 x $10^{-5}$ | 0.99 |
| 180 | 4.885 x $10^{-5}$ | 0.93 |

In the second stage, the values of $k_3$ in Table 6-2 were substituted into Equation (6-3). The remaining two model parameters were estimated by nonlinear regression analysis at 140, 160 and 180°C. The rate of phorone production was neglected at 140°C. The results are in Table 6-3. The data fit to the model at 160°C showed good agreement ($R^2$=0.97). However, residual plots for the regression results at 140°C and 180°C revealed an outlier in the data set at 140°C corresponding to condition #11 and an outlier in the data set at 180°C corresponding to condition #17. With these outliers removed, along with the outlier in Figure 6-10 (condition #2) removed, the model showed excellent agreement with the data. The regression analysis was repeated neglecting the third term in equation (6-2) corresponding to the rate of phorone production. The results showed that this term did not appreciably contribute to the acetone conversion rate and could be neglected. If so, the estimates of $k_1$ and $k_2$ would be within 2% of those reported in Table 6-4. An Arrhenius plot of the natural log of the forward rate constant ($k_1$) versus (1/T) (Figure 6-11) reveals an apparent activation energy of 65.9 kJ/mol.

**Table 6-3** Results of nonlinear regression analysis of data fit to the empirical kinetic model of equation (6-2)

| **Temperature [°C]** | **$k_1$ [$L^2$/(mol*g*hr)]** | **$k_2$ [$L^2$/(mol*g*hr)]** | **prob($T_1$)** | **prob($T_2$)** | **$R^2$** |
|---|---|---|---|---|---|
| 140 | $4.038 \times 10^{-5}$ | 0.04247 | 0.00040 | 0.001740 | (n/a)* |
| 160 | $1.202 \times 10^{-4}$ | 0.05229 | 0.00001 | 0.00043 | 0.9726 |
| 180 | $2.177 \times 10^{-4}$ | 0.05447 | 0.00516 | 0.01241 | 0.9997 |

* *$R^2$ not meaningful for 140°C since only 3 observations;*

*Conditions # 2, #11 and #17 were neglected from the analysis. Repeated experiments at 180°C on Day #9 (conditions #18 and 19) which show deactivation of catalyst were neglected from analysis but the data is available in Appendix E2.*

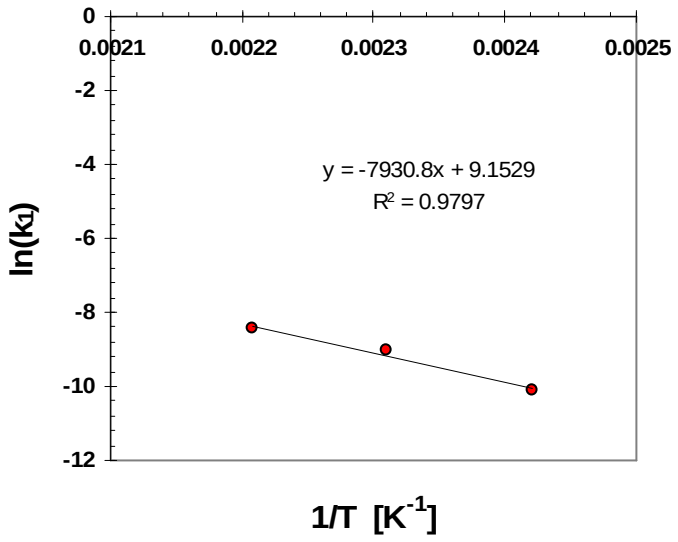


**Figure 6-11** Arrhenius plot of $\ln(k_1)$ versus (1/T).

*6.3.4 MIBK Synthesis in a Fixed Bed Flow Reactor (FBR)*

A preliminary experiment was carried out in the fixed bed flow reactor in order to study the performance of a multifunctional $Pd/Nb_2O_5$/Norpro SS 65137 catalyst (CAT 062) for MIBK and MO syntheses. The catalyst had a niobia loading of 5.97 wt% (0.29 monolayer coverage) and a maximum palladium loading of 0.1 wt% based on the amount of precursor used. The niobia catalyst was calcined at 100°C and the multifunctional catalyst was reduced at 100°C for 3 hours in the calcinator as described in Chapter Three. 2.58 grams of the multifunctional catalyst was charged to the BTRS-Jr/PC® tubular microreactor in between two fixed beds of glass beads. Once the reactor was installed into the BTRS-Jr benchtop reactor module, the catalyst was reduced again in situ at ambient temperature for one hour and then for 2 hours at 100°C with hydrogen flowing at 147 sccm. The hydrogen mass flow controller was calibrated for methane. The actual hydrogen volumetric flow rate is obtained by multiplication by a conversion factor of 1.403.

The flow reactor experiment investigated three conditions over a three day period. In the first day, the synthesis of MIBK was investigated at 160°C and at about 555 psig with acetone flowing at 1.05 ml/min (WHSV=19.3 $hr^{-1}$). This condition was maintained for 9 hours and then the reactor was shut down. On the second day, the reactor operated briefly for about 2 hours and shut down due to a PLC control problem. On the third day, the reactor was started up and the synthesis of MO was investigated at 160°C also at 555 psig with acetone flowing at 1.05 ml/min. The process was monitored for four hours after which, the hydrogen flow was enabled at 147 sccm and the process was monitored for another 4 hours. The results are illustrated in Figure 6-12.

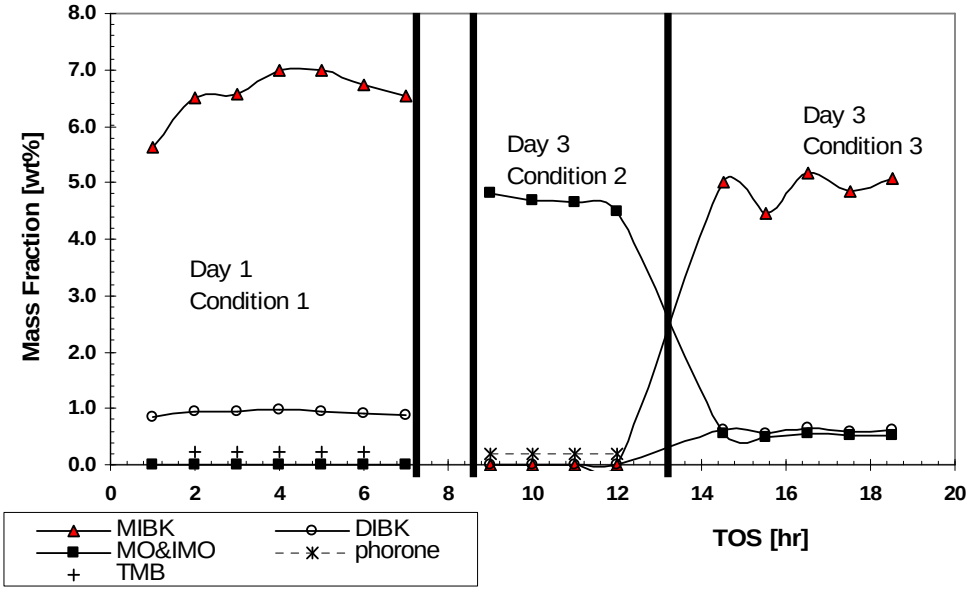


**Figure 6-12** Reactor effluent concentration as a function of time on stream for the investigation of MIBK and MO syntheses at 160°C in a FBR (Expt. I.D. "BTRS-5", T=160°C, $F_A$=1.05 mL/min; W=2.58 g (CAT 062); *The reactor was operated briefly on the second day with no samples collected. The reactor was shut down due to a PLC problem.*

During the first condition, essentially all of the MO was converted to MIBK and no IPA was evident in the product. However, DIBK produced from the reaction of MIBK and acetone was evident. Mesitylene (TMB) was observed in a significant amount. In addition, trace amounts of a hydrocarbon

(ca. 0.15 wt%) was detected. This compound had a retention time of 1.9 min and was previously determined by GC/MS (Section 4.2.2) to most likely be a saturated $C_9$ hydrocarbon. In the second condition where the reactor was operated without a hydrogen feed stream, MO became the dominant product along with IMO and phorone. After the hydrogen feed stream was enabled, MIBK appeared as the major product. However, this time, not all of the MO was converted to MIBK. This suggests the hydrogenation catalyst had lost activity for MIBK synthesis, perhaps due to exposure to phorones and other compounds during MO synthesis.

The productivity data presented in Table 6-4 suggests the catalyst deactivated between condition #1 and condition #2. The activity for MIBK synthesis in the third condition was 0.73 relative to the fresh catalyst in condition #1. More interestingly, the data suggests a synergistic effect whereby the introduction of hydrogen in the third condition resulted in an increase in the overall catalyst activity. The total productivity of organics increased from .928 [g/hr*$g_{cat}$] in the second condition to 1.15 [g/hr*$g_{cat}$] in the third condition. This implies the rapid hydrogenation of MO to MIBK may reduce the inhibiting effect of organic substrates such as MO, phorones and so on. The reverse reaction to produce DAA does not appear to be significant since DAA was not observed in any of the flow reactor experiments. Consequently, DAA may be considered an reactive intermediate.

**Table 6-4** Productivity and Selectivity for the syntheses of MIBK and MO in an FBR (Expt: "BTRS-5") [T=160°C, $F_{Ac}$=1.05 mL/min, P=555 psig]

| No. | Hydrogen Feed rate [sccm] | MO or MIBK productivity [g/hr*$g_{cat}$] | Total Organics Productivity [g/hr*$g_{cat}$] | MIBK Selectivity [wt%] |
|---|---|---|---|---|
| 1 | 105 | 1.30 (MIBK) | 1.53 | 85.0 |
| 2 | 0 | 0.9042 (MO) | 0.928 | n/a |
| 3 | 105 | 0.945 (MIBK)<br>0.0934 (MO) | 1.15 | 82.0 |

A second flow reactor experiment was conducted ("BTRS-6") to confirm the apparent synergistic effect observed in the previous experiment. A new batch of catalyst (CAT 065) was prepared following the same procedure as the catalyst used in the previous experiment. The elemental analysis of the catalyst was determined by ICP by an external laboratory (Galbraith Laboratories, Knoxville, TN). The niobia loading was 5.38 wt% (0.27 monolayer coverage) and the palladium loading was 0.057 wt%. The niobia catalyst was first calcined at 100°C in zero gas air before impregnation with palladium (II) acetate. The catalyst was reduced in a calcinator in flowing hydrogen at 100°C for 3 hours. 2.99 g of the catalyst was loaded into the reactor in between two fixed beds of glass beads. The first bed (bottom of reactor when vertically installed) was 58 mm in depth. The catalyst bed was 212 mm in depth. The top bed of glass beads was 147 mm in depth.

Five conditions were investigated. In the first condition, the activity of the fresh catalyst (CAT 065) for MIBK was obtained at 160°C and 555 psig. The acetone feed rate was set to a nominal flow rate of 1 mL/min (WHSV=16.5 $hr^{-1}$) and the hydrogen flow rate was 147 sccm. This gave a molar ratio of acetone to hydrogen of 2:1. In the second condition, the hydrogen feed was disabled with all other process variables remaining constant. In the third condition, the hydrogen volumetric flow was enabled to restore the original condition. In the fourth condition, the acetone feed rate was reduced to 0.54 mL/min (WHSV = 8.6 $hr^{-1}$). In the fifth condition, the hydrogen feed was enabled with a volumetric flow rate of 74 sccm to maintain the same stoichiometric ratio of acetone to hydrogen of 2:1.

The results of this experiment confirm a synergistic effect as observed in the previous experiment at the condition of lower space velocity but not at the condition of higher space velocity. The results in Figure 6-13 show that the total productivity for all organic products was found to increase by 10% when the hydrogen feed was enabled from condition #2 to condition #3 and by 22%

when the hydrogen feed was enabled between condition #4 and #5. However, IPA was observed in the reactor effluent when hydrogen was fed to the reactor. The production of IPA is a parallel competing reaction that does not involve the acid sites and should be accounted for when considering a synergistic effect. At the high space velocity, the 10 % increase in organic products coincides with the production of IPA which made up 10% of the organic products. Thus at the conditions of high space velocity there is not a synergistic effect. However, at the condition of low space velocity, IPA made up only 3.6% of the total organic products, while the total productivity of organic species increased by 22%. In addition, the productivity of MIBK (mmol/hr*$g_{cat}$) in condition #5 was 22% greater than the productivity of MO and IMO (mmol/hr*gcat) in the previous condition. Thus a synergistic effect was observed for the condition of low space velocity.

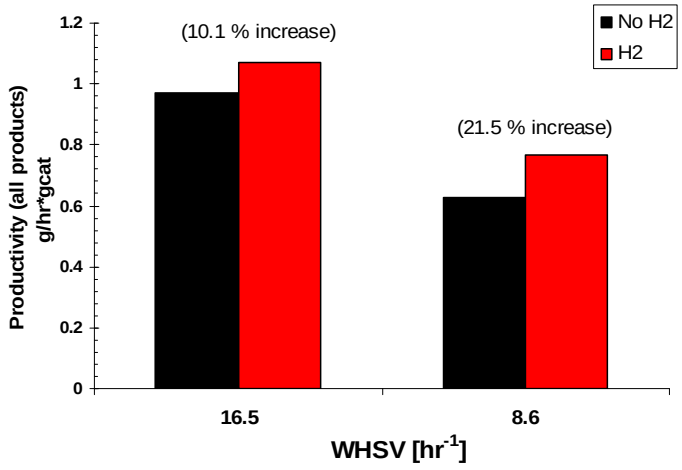


**Figure 6-13** Effect of hydrogen on the total productivity (all organic products) in a fixed bed reactor [Expt: "BTRS-6", T=160°C, P=555 psig, W=2.99 g (CAT 065)]

Low space velocities are associated with higher acetone conversions as well as greater concentrations and longer residence times of products in the reactor. It is not surprising from this data that no synergistic effect was observed for a WHSV of 16.5 $hr^{-1}$ at 160°C, since the data in Figure 6-10 indicates that the inhibiting effect of substrates is weak under these conditions. The reaction

rate is nearly independent of the flow rate at a WHSV of 16.5 $hr^{-1}$. In contrast, at WHSV of 8.6 $hr^{-1}$, the inhibiting effect of organic substrates is significant. These results suggest that the rapid hydrogenation of MO increases the fraction of available acid sites for catalytic reaction by reducing the surface concentration of MO and its derivatives (phorones etc.).

**Table 6-5** Composition of reactor effluent for process conditions investigated [Expt: "BTRS-6'; T=160°C, W=2.99g (CAT 065), P=555 psig]

| | Mass Fraction (wt%) | | | | | | | |
|---|---|---|---|---|---|---|---|---|
| No. | IPA | MIBK | MO | IMO | DIBK | phorone | TMB | C9 |
| 1 | 1.61 | 4.17 | | | 0.28 | | | |
| 2 | | | 5.03 | 0.63 | | 0.24 | | |
| 3 | 0.66 | 5.41 | | | 0.41 | | | |
| 4 | | | 6.17 | 0.75 | | 0.28 | | |
| 5 | 0.38 | 8.63 | | | 1.01 | | 0.26 | 0.18 |

**Table 6-6** MIBK productivity and selectivity and total organics productivity [Expt: "BTRS-6'; T=160°C, W=2.99g (CAT 065), P=555 psig]

| | Acetone | H2 | MIBK | | Total organics |
|---|---|---|---|---|---|
| | WHSV | Feed | Selectivity | Productivity | Productivity |
| No. | [$h^{r-1}$] | [sccm] | [wt%] | [g/hr*gcat] | [g/hr*$g_{cat}$] |
| 1 | 16.5 | 147 | 68.9 | 0.690 | 1.00 |
| 2 | 16.5 | 147 | - | - | 0.97 |
| 3 | 16.5 | 147 | 83.5 | 0.894 | 1.07 |
| 4 | 8.6 | 74 | - | - | 0.63 |
| 5 | 8.6 | 74 | 82.5 | 0.615 | 0.76 |

Mesitylene was observed in the reactor effluent in the fifth condition (No. 5 indicated in Tables 6-5 and 6-6) involving low space velocity in the presence of hydrogen. Again, the precursors to mesitylene including MO, IMO and phorone were not observed. Reactor effluent samples obtained from the last two flow reactor experiments were re-analyzed by GC/FID with the injection volume increased from 1 μL to 5 μL in order to reveal species which may have been present below the peak area rejection limit of the GC. The results (Table 6-7) confirm that in the presence of hydrogen, mesitylene is present while phorone is not observed in any of the specimen. MO is observed in a small proportion of the product in most specimens. The results also confirm that the

impurity observed with a retention time of 1.9 min in the GC/FID analysis is a hydrogenation product, which is not observed in the specimens produced in the absence of hydrogen.

**Table 6-7** GC/FID analyses of reactor effluent specimens with injection volume of 5 μL.

| Species | Retention Time [min] | BTRS-6 Condition #1 Area % | BTRS-6 Condition #3 Area % | BTRS-5 Condition #1 Area % | BTRS-5 Condition #3 Area % |
|---|---|---|---|---|---|
| C9 alkane | 1.93 | 0.04 | 0.07 | 0.11 | 0.05 |
| C7+ | 2.25 | | | | 0.03 |
| Acetone | 3.58 | 92.94 | 92.25 | 89.03 | 92.12 |
| IPA | 6.17 | 1.62 | 0.57 | | 6.03 |
| MIBK | 7.94 | 4.84 | 6.33 | 8.58 | 0.05 |
| MO | 10.60 | | 0.03 | 0.20 | 0.44 |
| MIBC | 11.14 | 0.11 | 0.05 | | |
| DIBK | 11.27 | 0.36 | 0.54 | 1.45 | 0.87 |
| TMB | 12.48 | 0.09 | 0.16 | 0.42 | 0.23 |
| u/k | 13.54 | | | | 0.04 |
| DAA | 14.71 | | | 0.22 | 0.13 |

*High injection volume analysis of condition #5, BTRS-5 not performed.*

Autoclave experiments as well as the flow reactor experiments demonstrate that MIBK can be produced in relatively high yield in the presence of excess hydrogen at elevated pressure since MO is rapidly converted to MIBK before it can react with acetone to produce phorones or other trimers. It is curious that in the presence of hydrogen, mesitylene is produced in significant amounts, particularly considering its precursors are not evident. The results of the autoclave experiments involving MO synthesis in the absence of hydrogen presented in Chapter Four show that mesitylene appears in the product mixture at 160°C at relatively high acetone conversion (ca. 10%) and always appears after phorone has accumulated in the reactor to an appreciable amount. In the flow reactor experiment presented in Section 6.3.2 involving MO synthesis using a $Nb_2O_5$/Norpro SS 65137 silica raschig ring catalyst, mesitylene was observed only in experiments at 180°C. In contrast, when hydrogen is present, mesitylene is routinely observed in FBR experiments at 160°C. Also, in the autoclave hydrogenation experiment #180 (Figure 6-2) discussed previously in

this chapter, mesitylene was observed after 8 hours but not phorone. In the successful catalytic distillation experiments (#004 and #005) presented in Chapter Eight, where hydrogen was effectively utilized in the CD reactor, mesitylene was observed in the reboiler product, but phorone was not.

These observations suggest that the presence of hydrogen promotes the synthesis of mesitylene from phorone. The synthesis of mesitylene involves the 1,6-internal aldol condensation of 2,4-dimethyl-hept-2,4-diene-6-one the isomer of phorone (Scheme 6-1).[1,12] Double bond migration, such as that depicted in Scheme 6-1, and dehydration reactions are known to occur on strongly acidic catalysts.[67,129] However, it is somewhat perplexing that the production of mesitylene is promoted by hydrogen since the synthesis of mesitylene from phorone does not involve hydrogenation. Perhaps the presence of adsorbed atomic hydrogen or palladium hydride somehow facilitates the acid catalyzed cyclization reaction in Scheme 6-1, possibly as a source of protons for Bronsted acidity. Another reason why phorone might not be observed is that it may be hydrogenated to produce DIBK, which is present in the reaction mixture. However, this does not explain the significant quantity of mesitylene produced.

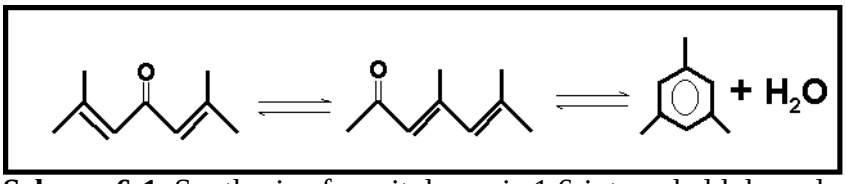


**Scheme 6-1** Synthesis of mesitylene via 1,6-internal aldol condensation[1,12]

## 6.4 Characterization of the Intrinsic Kinetics in a Semi-Batch Autoclave Reactor

### *6.4.1 Catalyst and Statistical Experimental Design*

The intrinsic kinetics of the overall one-step synthesis of MIBK from acetone in the liquid phase over a $Pd/Nb_2O_5/SiO_2$ catalyst was investigated in the batch autoclave reactor described previously in Chapter Three. A large batch of

catalyst (CAT 054) was prepared using fumed silica powder (Aldrich 38,127-6) as a support. The catalyst was prepared following the technique described in Chapter Three with the specific experimental details in Appendix E. The niobia catalyst was calcined at 100°C to maximize the Bronsted acidity. After impregnation with palladium (II) acetate, the catalyst was dried overnight and subsequently reduced in flowing hydrogen in a calcinator at 100°C for 2 hours and 15 minutes. The catalyst was protected in a dessicator under an inert environment within a glove bag until needed. The niobia loading of the catalyst was determined by EDXRF to be 15.2 wt% (0.51 monolayer). Elemental analysis via inductively coupled plasma (ICP) spectroscopy revealed a palladium loading of 0.047 wt%.[♣]

A central composite design is the most appropriate choice of statistical experimental design for modelling purposes, since it enables the development of a non-linear response surface. The design of a CCD may be either rotatable or orthogonal or both. If the purpose of experimentation is to establish cause and effect relationships, then an orthogonal design is appropriate; however, if the purpose is modelling, then a rotatable design is more appropriate since the model prediction errors will be equivalent in all dimensions.[191] Consequently, the rotatable central composite statistical experimental design (CCD), illustrated in Figure 6-14 and outlined in Table 6-8, was employed to investigate the intrinsic kinetics of the one step synthesis of MIBK from acetone.

The CCD is an efficient means of experimentation, which allowed investigation of the effects of hydrogenation pressure over 5 levels from 217 to 700 psia and temperatures over 5 levels from 127 to 183°C in only 9 experiments. However, the centre point was repeated to give a total of 10

[♣] ICP analysis was performed by Galbraith Laboratories (Knoxville, TN). Two specimens were analyzed. The first result gave 0.18 wt% Pd, which exceeded the maximum possible Pd loading (0.1 wt%) based on the amount of precursor used. However, the second measurement (466 ppm) was consistent with the analysis of the other specimen prepared with the same nominal Pd loading.

experiments. In addition, some experiments were also repeated to confirm their results. The order of the experimental runs was randomized using a random sequence generator.* About 0.5 g of catalyst was uses in each experiment. However, due to the repetition of some experiments and due to some unexpected material losses when working in a glove bag, there was insufficient catalyst to complete the experimental design. The star point at the extreme conditions of low pressure (Expt #209), which was considered to be the least critical of the experiments, was carried out using recycled and regenerated catalyst. The star point at the condition of high temperature was investigated with fresh catalyst (Expt 200) and investigated in a repeated experiment with regenerated catalyst (Expt. 211). The results showed that the acid function was unaffected giving highly repeatable water and acetone concentration versus time profiles. However the hydrogenation activity was significantly lower. Consequently, the MIBK concentration data in experiments 209 and 211 were not used in the kinetic model for MO hydrogenation. However, the data from these experiments were included in the model for MO synthesis.

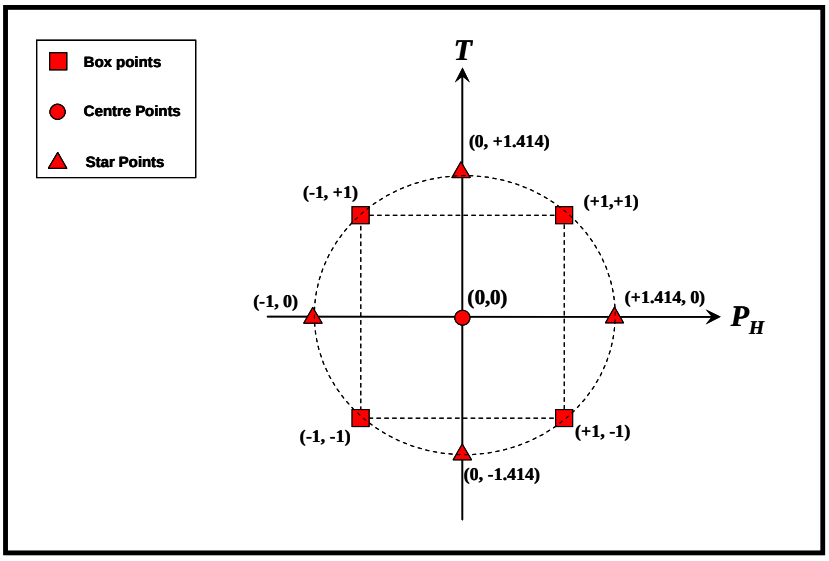


**Figure 6-14** Central composite design to investigate the effects of pressure ($P_H$) and temperature (T) on the kinetics of the MIBK synthesis. *The box point, star points and centre points indicate process conditions investigated (coded space).*

* An online random sequence generator was used. http://www.random.org/sform.html

**Table 6-8** CCD statistical experimental design used for the investigation of the liquid phase kinetics of the one-step synthesis of MIBK from acetone over a $Pd/Nb_2O_5/SiO_2$ catalyst.

| Expt I.D. | CODED SPACE Temp | CODED SPACE Press | Rxn T [℃] | Pressure [psia] |
|---|---|---|---|---|
| 199 | 0 | 0 | 155 | 500 |
| 200 | *+1.414* | 0 | *183* | *500* |
| 201 | -1 | +1 | 135 | 700 |
| 203 | -1 | +1 | 135 | 700 |
| 204 | -1 | -1 | 135 | 300 |
| 205 | +1 | +1 | 175 | 700 |
| 206 | 0 | 0 | 155 | 500 |
| 207 | -1.414 | 0 | 127 | 500 |
| 208 | 0 | -1.414 | 155 | 217 |
| 209 | 0 | +1.414 | 155 | 783 |
| 210 | +1 | -1 | 175 | 300 |
| 211 | +1.414 | 0 | 183 | 500 |

*Problem with reactor during experiment #202 (Appendix E); results not included in analysis.*

### *6.4.2 Results*

The results of the kinetic study indicate that when hydrogen is in excess at elevated pressure, the catalyst was highly active and selective for MIBK synthesis. The result of experiment 199 at 155°C and 500 psia total pressure (Figure 6-15) showed an extremely active and selective catalyst for MIBK synthesis. The initial MIBK activity was 0.0163 [mol/L*min*$g_{cat}$] at 155°C which was roughly 3 times the activity of Amberlyst 15 for MO synthesis at 120°C. It is interesting to note that the catalyst activity for MIBK synthesis in terms of moles of product per unit time compared to that of experiment #161 for MO synthesis using a 16 wt% $Nb_2O_5/SiO_2$ catalyst suggests the multifunctional catalyst for MIBK synthesis was 1.51 times more active, which supports the notion of a synergistic effect. MIBK was produced with 100 % selectivity up to an acetone conversion of 16.6% (after 8 hours) where some MO and DIBK was observed. The water and MIBK molar concentration versus time profiles in Figure 6-15 suggest these products are produced in stoichiometric amounts.

However in general, some unreacted MO was present in the system. Particularly when the reaction temperature was high (175 and 183°C) or the

system pressure was low (< 500 psia) such that the rate of MO synthesis initially exceeded the rate of MO hydrogenation. The results of experiment 208, for which the hydrogen pressure was minimized (star point) in Figure 6-16 show that for low pressure, a significant amount of unreacted MO remains in the product even after 8 hours of reaction.

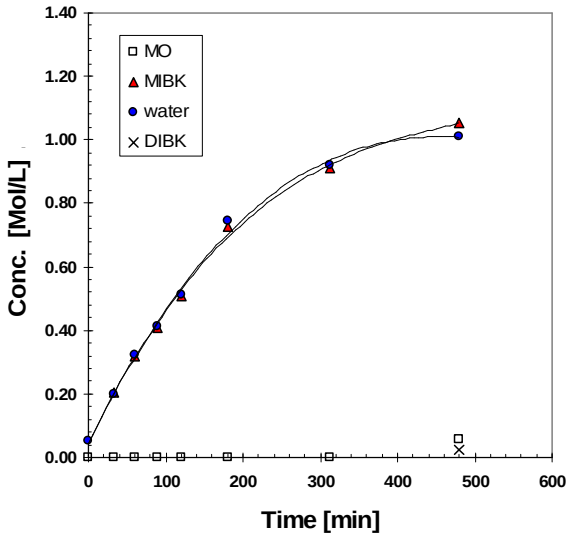


**Figure 6-15** Concentration versus time for MIBK synthesis in an autoclave reactor at 155°C and moderate pressure using a $Pd/Nb_2O_5/SiO_2$ catalyst [Expt. 199, CAT 054, W=0.4858 g, T=155 °C, P=500 psia, ω=700 RPM]

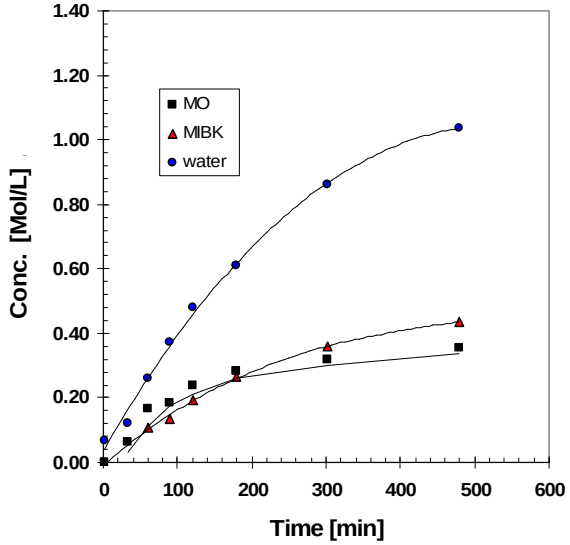


**Figure 6-16** Concentration versus time profile for MIBK synthesis in an autoclave reactor at 155°C and low pressure using a $Pd/Nb_2O_5/SiO_2$ catalyst [Expt. 208, CAT 054, W=0.4927 g, T=155 °C, P=217 psia, ω=700 RPM]

*6.4.3 Kinetic Modelling*

The results show that in general, unreacted MO is present in the product mixture. Consequently, a single rate expression for the conversion of acetone to MIBK is insufficient to fully describe the data. Two rate expressions in equations (6-5) and (6-6) were used to model the kinetics of the one step synthesis of MIBK from acetone. The first rate expression is second order with respect to acetone in the forward direction in accordance with the well known reaction mechanism and consistent with kinetic models published previously in the literature.[19,115,124] The term in the denominator of equation (6-5) that accounts for product inhibition considers water as the only kinetically relevant inhibiting substrate, consistent with the kinetic model published by Thotla et al.[124] (equation 2-12). The term is raised to the second power due to the bimolecular nature of the reaction and in accordance with kinetic models published in the literature.[115,124] The second rate expression (6-6) accounts for the rate of hydrogenation of MO to MIBK. MO is considered to be the only kinetically relevant adsorbed species consistent with kinetic models reported previously in the literature.[18,114,115] The term is raised to the fourth power due to the diadsorption of MO and consistent with kinetic models published in the literature.[18,19] The reaction velocities ($k_j$) in each rate expression exhibit Arrhenius behaviour as described in equation (6-7) where $A_j$ is the pre-exponential factor and $E_j$ is the activation energy for reaction "j". As a simplifying assumption, the temperature dependence of the equilibrium adsorption constants $K_w$ and $K_M$ were neglected. Thus, the kinetic model has 6 adjustable parameters rather than 8.

$$r_1 = \frac{k_1 C_A^{\,2}}{\left(1 + K_w C_w\right)^2} \qquad (6\text{-}5)$$

$$r_2 = \frac{k_2 C_{MO} C_H}{\left(1 + K_M C_{MO}\right)^4} \qquad (6\text{-}6)$$

$$k_j = A_j \exp\left\{ -E_j \middle/ RT \right\}; \quad j = 1,2 \qquad (6\text{-}7)$$

The rate of MO hydrogenation in equation (6-6) was related to the bulk liquid phase concentration of hydrogen ($C_H$) rather than the partial pressure of hydrogen. It was assumed that for each experiment, the acetone solvent was initially saturated with dissolved hydrogen and that the concentration of dissolved hydrogen in the liquid phase did not change appreciably during the course of the reaction. The concentration of dissolved hydrogen was calculated from the total system pressure using a pseudo Henry's law constant determined from vapour liquid equilibrium data published in the literature.[192]

Brunner[192] charged acetone to an autoclave reactor, purged the headspace and then pressurized the system with hydrogen. The system was allowed to reach material equilibrium for various pressures and the total system pressure was correlated to the measured dissolved hydrogen concentration. Thus the constant of proportionality is not truly the Henry's Law constant since the total pressure was used rather than the partial pressure of hydrogen. Brunner's estimates of the solubility of hydrogen in acetone are in very good agreement, to within a relative error of 2.4%, with the data of Purwanto et al.[193] Brunner's tabulated data is reproduced graphically in Figure 6-17. From this data, the constant ($K_H$) which relates the mole fraction of dissolved hydrogen to the total system pressure can be determined for each temperature. An empirical model was fitted to Brunner's data (Figure 6-18) to predict the pseudo Henry's Law constant at the temperatures investigated in this work.

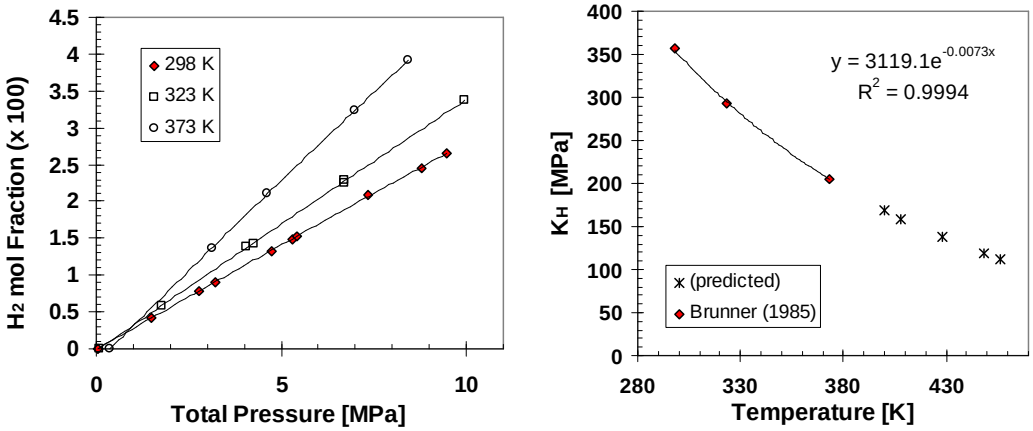


**Figure 6-17** (a) (left) Mole fraction of hydrogen as a function of total pressure (Data from Brunner[192]); (b) (right) $K_H$ as a function of temperature (◊) data from Brunner[192] and (*) predicted from empirical model

The statistically optimum values of the parameters of the kinetic model were estimated using the state-of-the-art parameter estimation feature of gPROMS (Process Systems Enterprise Ltd., London, UK). A process model was developed in gPROMS in order to carry out dynamic simulations of the batch autoclave reactor used in the kinetic study. The process model consists of four ordinary differential equations (ODE) (Eqn. 6-8) detailing the mole balances on the four major species monitored in these experiments: acetone, MO, water and MIBK, the kinetic model equations (6-5) through (6-7), as well as the liquid phase volume (6-9) and component concentrations (6-10). Ideal mixing was assumed as a first approximation. The four ODE's require specification of four initial conditions, specifically the initial holdup (moles) of each of the four species. In addition, the amount of catalyst ($W_{cat}$ ) and the initial volume of the reactant mixture (V), the reaction temperature and the dissolved hydrogen concentration must be specified for each experiment in the input files. $N_i$ denotes the number of moles of species "i", $\nu_{i,j}$ denotes the stoichiometric change in the number of moles of species "i" in reaction "j". $r'_j$ is the specific rate of reaction "j" in (mol/hr*$g_{cat}$) and $\rho_i$ is the density of species "i" in kmol/$m^3$. The reactor model in gProms language is available in Appendix E.

$$\frac{dN_i}{dt} = \sum_j \sum_i \nu_{i,j} r'_j VW_{cat} \qquad i = Ac, MO, MIBK, H_2O \tag{6-8}$$

$$V = \sum_i \frac{N_i}{\rho_i} \qquad i = Ac, MO, MIBK, H_2O \tag{6-9}$$

$$C_i = \frac{N_i}{V} \qquad i = Ac, MO, MIBK, H_2O \tag{6-10}$$

The MIBK, MO, water and acetone concentration versus time data obtained experimentally were entered into gPROMS as input files. Each experiment resulted in a unique input file. gPROMS attempts to maximize the likelihood that the model will predict the observed experimental values in the input files through maximizing the objective function in (6-11) where $z_{ijk}$ is the kth prediction of variable j in experiment i.[194] The z with the "~" above it denotes the predicted value. Similarly $\sigma^2_{ijk}$ denotes the variance of the kth measurement of the jth variable in experiment i. A statistical variance model is assigned to the input data, either constant variance, constant relative variance or heteroscedastic variance. Constant variance implies the measurement error has a constant standard deviation; constant relative variance implies the measurement error depends on the magnitude of the measurement and heteroscedastic variance implies a more general variance model whereby the variance has a nonlinear dependence on the measured value. In this work, the concentration versus time data was assigned a constant relative variance model, which is characteristic of GC and other instrumental analysis.

$$\Phi = \frac{N}{2}\ln(2\pi) + \frac{1}{2}\min_{\theta}\left\{\sum_{i=1}^{NE}\sum_{j=1}^{NV_i}\sum_{k=1}^{NM_{ij}}\left[\ln(\sigma_{ijk}{}^2) + \frac{(\tilde{z}_{ijk} - z_{ijk})^2}{\sigma^2_{ijk}}\right]\right\} \tag{6-11}$$

Parameter estimation using gProms proved to be problematic. A unified model which could adequately model the entire data set was not found. The kinetics seemed partitioned. The six experimental conditions at or above 500 psia could be fit well to the kinetic model. However the data from the three low pressure conditions could not be adequately modeled. Possibly the reaction mechanism had changed, mass transfer effects had become significant due to the low solubility of hydrogen at low hydrogen partial pressure or the catalyst performance had changed. The results in section 6.4.4 demonstrate the absence of mass transfer effects during this experiment. The results presented in section 6.4.3.3 suggest that significant catalyst deactivation had occurred in at least one of the three low pressure conditions.

6.4.3.1 Kinetic Model I

For hydrogenation pressure greater than or equal to 500 psia, the kinetic model of equations (6-5) through (6-7) adequately model the kinetic data. The model parameters are outlined in Table 6-9. The model provides an excellent prediction of the acetone concentration (Figure 6-18). The relative standard error of estimate, which is the standard error of estimate of the model prediction compared to the experimentally observed value normalized by the average value over the interval, was 1.07%. Similarly, the prediction of the water concentration was good as evidenced by a relative standard error of estimate of 12.8%. The model predictive capability for MIBK was fair with a relative standard error of estimate of 19.7%. The relative standard error of estimate of the model predictions for the MO concentrations were high since the MO concentration was very low for these process conditions. The predicted value was often below the peak area rejection limit of the GC (ca. 0.05 mol/L). However, the MO predicted concentrations are in relatively good agreement with the observed values in experiment #205, illustrated in Figure 6-19, which gives the product distribution as a function of time for a typical experiment. The parity diagrams of model prediction versus observed values for acetone, water and MIBK concentrations are given in Figures 6-20 through 6-22.

**Table 6-9** Parameters for Kinetic Model I (P ≥ 500 psia).

| EQUATION | PARAMETER | DESCRIPTION | VALUE |
|---|---|---|---|
| (6-10) | $E_{A1}$ | Activation energy in $r_1$ | 87.41 (kJ/mol) |
| (6-10) | $A_1$ | pre-exponential factor in $r_1$ | $5.002 \times 10^6$ (L/mol*min*$g_{cat}$) |
| (6-8) | $K_w$ | inhibition term for water in $r_1$ | 1.110 (L/mol) |
| (6-10) | $E_{A2}$ | Activation energy in $r_2$ | 61.48 (kJ/mol) |
| (6-10) | $A_2$ | pre-exponential factor in $r_2$ | $5.005 \times 10^6$ (L/mol*min*$g_{cat}$) |
| (6-9) | $K_M$ | inhibition term for MO in $r_2$ | 0 (L/mol) |

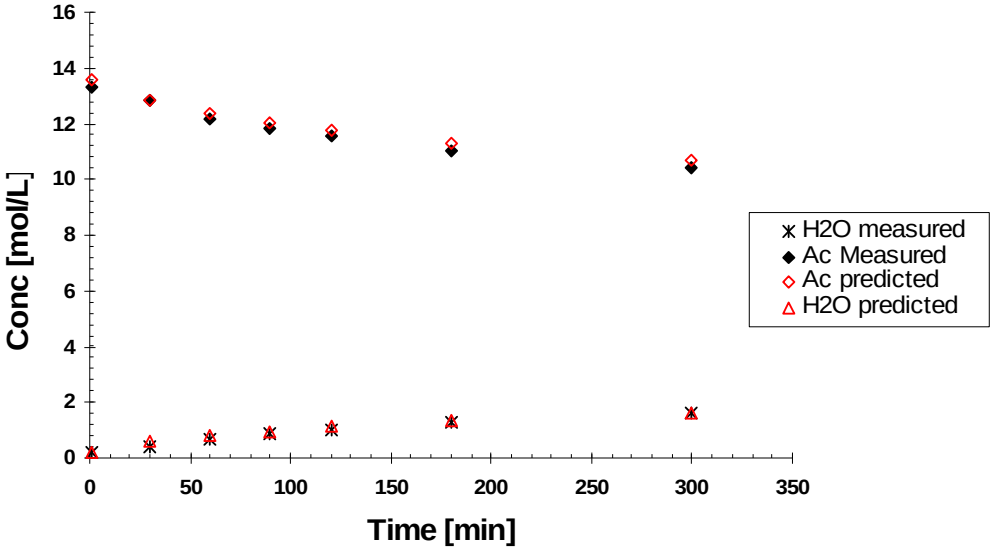


**Figure 6-18** Model prediction and experimentally observed acetone and water concentration versus time profiles for a typical autoclave experiment [Expt. 205, T=175°C, P=700 psia ($H_2$), ω=700 RPM, W=0.4688g (CAT 054)] *A GC/TCD outlier was observed for the measurement at 480 min (water). This observation is neglected from the figure. Data available in Appendix E.*

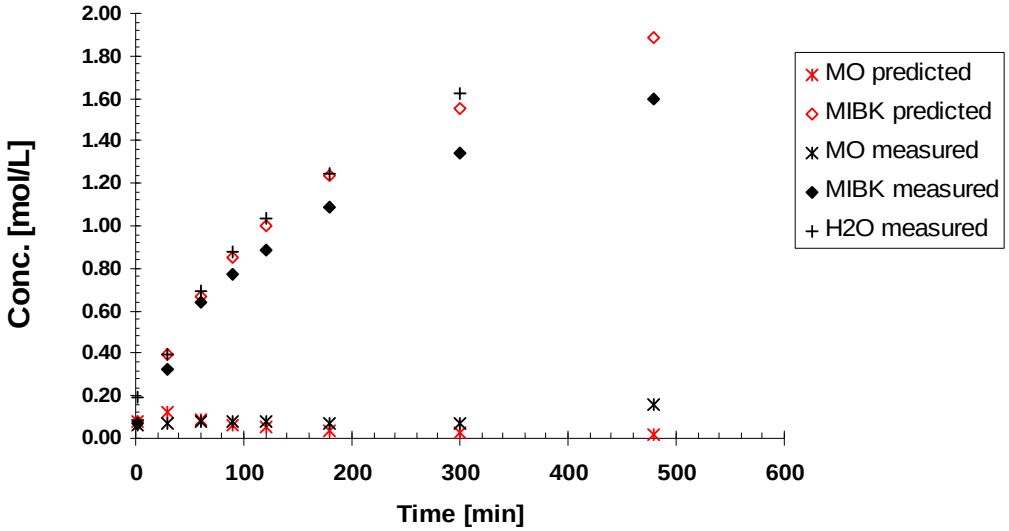


**Figure 6-19** Model prediction and experimentally observed MO, MIBK and water concentration versus time profiles for a typical autoclave experiment [Expt. 205, T=175°C, P=700 psia ($H_2$), ω=700 RPM, W=0.4688g (CAT 054)]

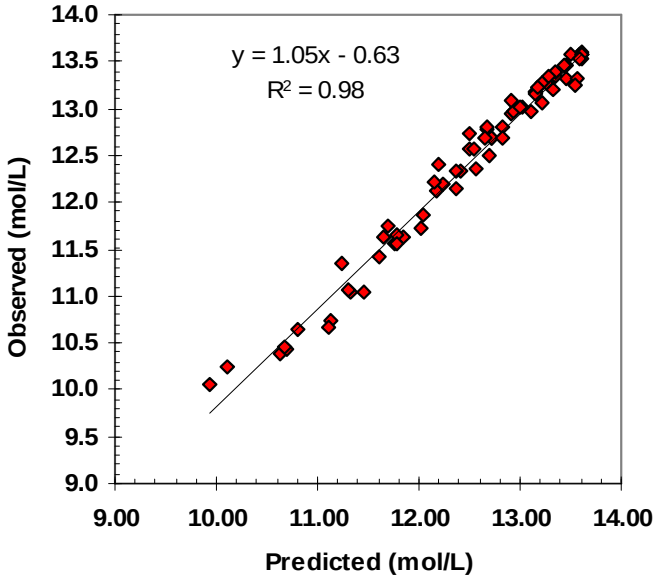


**Figure 6-20** Model prediction versus experimentally observed acetone concentration for kinetic experiments carried out at 500 psia and greater. [Experiments 197, 199, 200, 201, 203, 205, 206, 207, 209, 211]

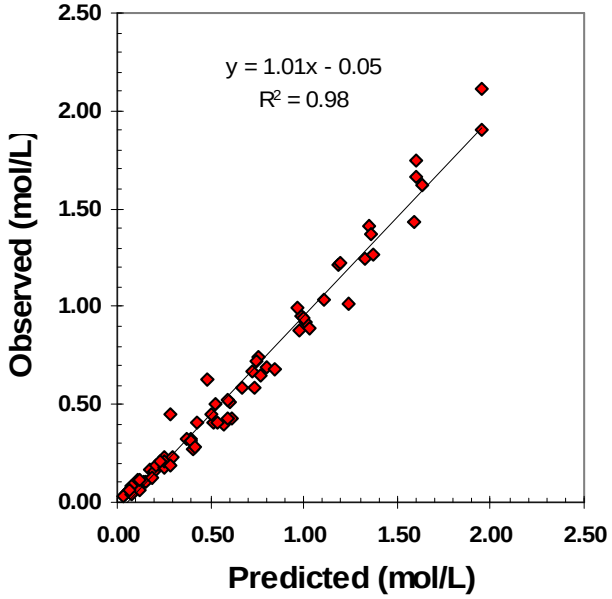


**Figure 6-21** Model predictions versus experimentally observed water concentration for kinetic experiments at 500 psia and greater system pressure. [Experiments 197, 199, 200, 201, 203, 205, 206, 207, 209, 211] ♣

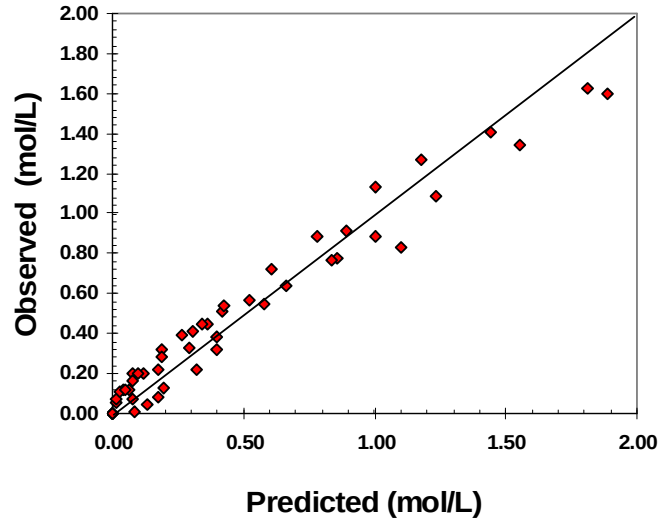


**Figure 6-22** Model predictions versus experimentally observed MIBK concentration [Experiments 197, 199, 200, 201, 203, 205, 206, 207]

---

♣ *Regarding Figures 6-20 through 6-22; The data from the star points with regenerated catalyst (Expt. 209 and 211)) were not included in the kinetic model for hydrogenation. However, the data was included for the model of MO synthesis. . Data from a preliminary experiment (#197, T=160°C, P=600 psia, CAT 054) was added to the data set. 5 observations were rejected from Figures 6-22 and 6-23 as outliers due to obvious error in GC/TCD moisture analysis (Data available in Appendix E).*

The predicted versus observed MIBK concentration in Figure 6-22 as well as the data in Figure 6-19 show that the model gives good estimates of the MIBK concentration up to MIBK concentrations of around 1.2 mol/L, which corresponds to an acetone conversion of roughly 20%. For higher conversions, the model prediction significantly diverges from the observed value and overestimates the MIBK concentration. This is due in part because the model does not account for the consecutive reaction of MIBK to produce DIBK and other undesirable reactions such as the production of mesitylene, which become significant at high acetone conversion. In addition, the catalyst may deactivate with time at high conversion. The proposed kinetic model gives excellent prediction of acetone and water profiles and can be used reliably for MIBK prediction for acetone conversions less than around 20%.

It is interesting to note that the numerical solution to the parameter estimation in gPROMS resulted in the inhibition term in the hydrogenation reaction being set to zero as the optimal solution, despite the observed diminution of MIBK productivity at high acetone conversions. Evidently, the diminution of MIBK production with acetone conversion appears to be primarily the result of the decrease in the rate of MO synthesis with acetone conversion, which is inhibited by water and or organic substrates. Modifying the rate expression to consider other inhibitors, such as water, acetone or MIBK also resulted in the inhibition term being set to zero. Modification of the exponent in the rate expression did not yield an improved result.

#### 6.4.3.2 Kinetic Model II – Neglecting MO

The parameter estimation for the second rate expression required fitting of MO concentration data obtained at low concentration near the peak area rejection limit of the GC using gPROMS. In addition, the very low MO concentration is used in the calculation of the MIBK reaction rate. These concentrations were well below the concentration of the least concentrated

calibration standard used for the GC/FID analysis. Consequently, the MO concentration data may not be highly accurate and may have adversely affected the model predictive capability.

Since the MO concentration is low in many of the experiments at high pressure (≥ 500 psia) a simplified kinetic model is proposed that neglects the MO and assumes that all of the MO is rapidly and completely converted to MIBK (Equation 6-12). Keeping the parameters for the first rate equation for MO synthesis, it was found that the model predictions for MIBK concentration improved slightly as evidenced by a relative standard error of estimate of 15.9%. The model prediction versus observed MIBK concentration is given in Figure 6-23. Although the residual errors are generally smaller for the model-II predictions compared to model-I predictions for MIBK concentration, the model-II predictions appears to frequently underestimate the observed value. This may reflect an instrumental bias since the predicted value is calculated from the water concentration measured by GC/TCD while MIBK is measured by GC/FID. Regardless, the model predictions diverge from the observed value at high acetone conversion although, perhaps, not as significantly as that observed in Figure 6-23.

$$\frac{dC_{MIBK}}{dt} = \frac{dC_w}{dt} \qquad (6\text{-}12)$$

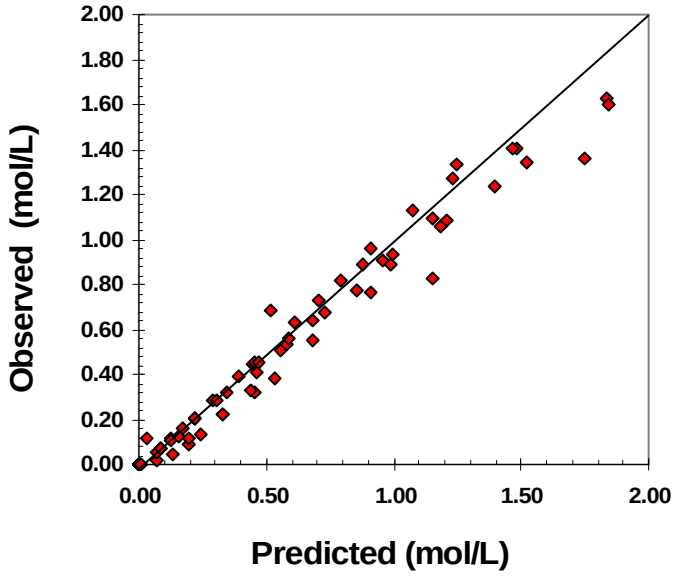


**Figure 6-23** Kinetic model II predicted versus observed MIBK concentration assuming MO is rapidly and completely converted to MIBK [Experiments 197, 199, 200, 201, 203, 205, 206, 207, 211]

6.4.3.3 Experiments at Low Pressure

The kinetic data for the experiments obtained at the three low pressure conditions in fact do not suggest that the kinetic model actually fails to predict the observed product distribution. Rather, the catalyst appears to have been adversely affected by the low hydrogenation pressure and resulting in deactivation. Figure 6-24 shows the MIBK concentration versus time profile for two experiments conducted at 175°C; one at 700 psia and the other at 300 psia. The experiment at 300 psia shows a lower initial activity for MIBK synthesis as expected due to the lower solubility of hydrogen. However, the hydrogenation activity clearly diminishes with almost complete deactivation after three hours of reaction. The MO concentration increases monotonically throughout this experiment. Given this, the rate of MIBK production should increase with MO concentration. The accumulation of MO is indicative of a loss of catalyst activity for hydrogenation.

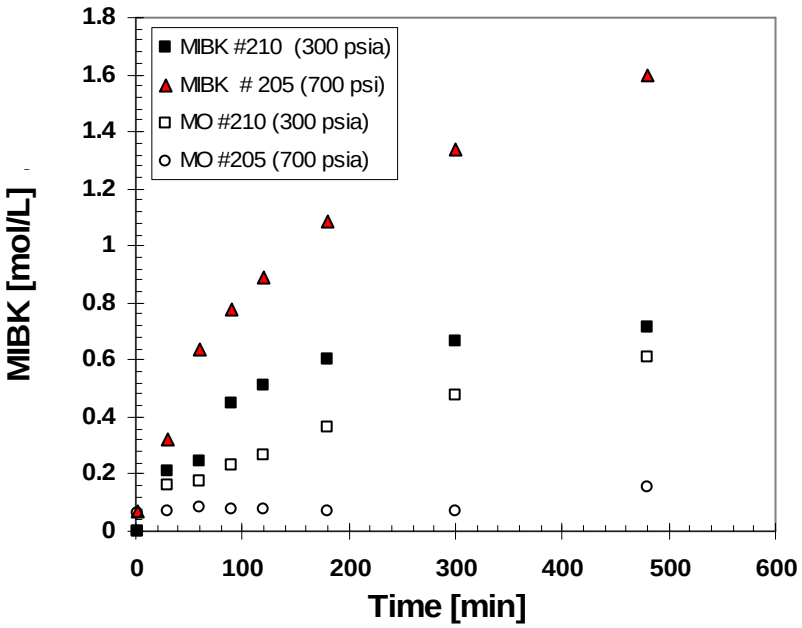


**Figure 6-24** Effect of (total) hydrogenation pressure on the synthesis of MIBK at 175°C over a $Pd/Nb_2O_5/SiO_2$ catalyst in an autoclave [Experiments 210 and 205]

The box point experiment conducted at the condition of low temperature and pressure (Experiment # 204) is actually in fair agreement with the kinetic model prediction (Figure 6-25). The predicted MIBK concentration is in relatively good agreement with the observed result for the first two hours of reaction but diverges after some time. In fact, there is more MIBK observed than predicted in this experiment. However, it is clear from the data that this experimental measurements exhibited significant variation. Consequently the experiment should be considered preliminary and should be repeated. More MIBK was produced than expected because in fact more acetone was converted to MO than predicted by the model (Appendix E), likely due to experimental error as evidenced by the variation in the measured data. However, the result suggests the kinetic model is valid. The low reaction temperature (135°C) appears to have mitigated the deactivation of the hydrogenation catalyst.

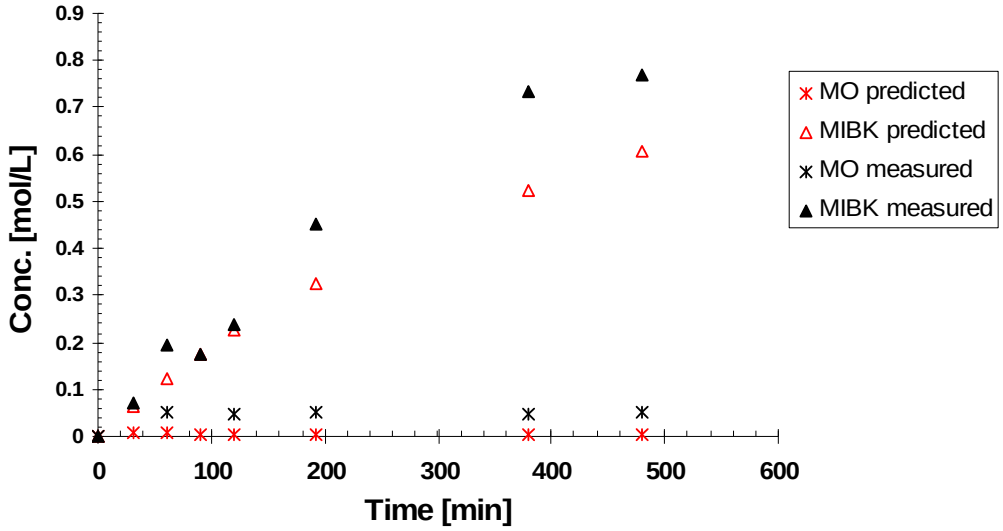


**Figure 6-25** MIBK and MO predicted and observed concentrations as a function of time on stream at 135°C and 300 psia. [Expt # 204, T=135°C, P=300 psia, ω=700 RPM, W=0.4692 g (CAT 054)]

The star point experiment at very low pressure (Experiment 208, Figure 6-16) is inconclusive since regenerated catalyst was used. This result was similar to that of Experiment #210 (Figure 6-24) in that less MIBK than predicted was observed and the MO concentration increased monotonically during the experiment. However, the hydrogenation catalyst remained active. A preliminary experiment (#196, Appendix E) conducted at 388 psia showed fair agreement with the kinetic model prediction with a relative standard error of estimate of 12.6% for the prediction of the MIBK concentration. However, the model consistently underestimated the amount of MIBK present and predicted a larger amount of MO present initially. In fact, MO was not observed and was converted to MIBK. Thus the model underestimated the initial rate of hydrogenation. The predicted and observed measurements were in good agreement after 6 hours of experiment (8% error).

6.4.4 Assessment of Mass Transfer Effects

The synthesis of MIBK is a relatively slow irreversible reaction. The acetone conversion was typically less than 20% after 8 hours of reaction. Consequently, mass transfer effects are not expected. To ensure absence of external heat and mass transfer effects, the kinetic experiments were carried out in a well mixed batch autoclave with the agitation rate maximized at 700 RPM. In addition, the catalyst consisted of a finely ground powder, which ensured negligible intraparticle heat and mass transfer effects. For these reasons, it is reasonable to consider thermal gradients within the catalyst and the bulk liquid phase to be negligible. However, the absence of mass transfer effects need be confirmed. Although experiments were not carried out to rigorously assess mass transfer effects, in this section the absence of mass transfer effects is demonstrated by the evaluation of accepted scientific criteria for the assessment of interparticle and intraparticle transport phenomena in a chemical reactor.

To evaluate the effects of mass transfer, consider the diffusion of acetone from the bulk liquid. MO is created *in situ* at the active sites within the pore structure and may be viewed as an intermediate. In the kinetic study, the condition most likely to exhibit internal and external mass transfer effects would be the star point at the condition of extreme high temperature (Exp. 200) since the reaction rate is more sensitive to temperature than the diffusion rates. The maximum rate of reaction occurred at the initial condition (X=0). The Mears criterion was evaluated in order to confirm the absence of external mass transfer effects. It has been demonstrated that if the inequality of equation 6-13 is valid, then external mass transfer effects are negligible.[195]

$$\frac{r_A \rho_b R n}{k_c C_A} < 0.15 \qquad (6\text{-}13)$$

In this expression, ($r'_A$) denotes the observed specific reaction rate ($kmol/kg_{cat}*s$), $\rho_B$ is the catalyst bed bulk density ($kg/m^3$), R is the particle

diameter (m), n is the order of reaction, $C_A$ is the bulk liquid phase concentration of the reactant (kmol/$m^3$) and $k_c$ is an appropriate mass transfer coefficient (m/s). The initial acetone concentration was 13.60 (mol/L) or 13.6 (kmol/$m^3$). The initial rate of acetone conversion was estimated from computer simulation using the kinetic model of equations (6-6) through (6-11) with "E-Z Solve" v. 1.0 (Intellipro, Inc.). The initial rate of reaction was estimated to be 2.25 x $10^{-4}$ (mol/s*$g_{cat}$). The catalyst was ground to a fine powder and its particle size distribution was not measured. However, as a conservative estimate, a mean particle size of 100 μm (1 x $10^{-4}$ m) is assumed. Although the catalyst was dispersed into a slurry, as a conservative estimate, the bulk density of fumed silica was used (72.08 kg/$m^3$). The reaction is second order with respect to acetone. However, due to substrate inhibition, the apparent order is between 1 and 2. As a conservative estimate, the reaction was considered second order.

To estimate the mass transfer coefficient for mass transfer to suspended solids in a highly turbulent mixer, the correlation in equation (6-14) was used where $k'_L$ is the appropriate mass transfer coefficient, Sc is the Schmidt number (Eqn 6-15), $\mu_c$ is the dynamic viscosity of the continuous phase (kg/ms), $\rho_c$ is the density of the continuous phase (kg/$m^3$) and (P/V) is the power consumption per unit volume in the mixer (kW/$m^3$).[195]

$$k'_L Sc^{2/3} = 0.13\left(\frac{(P/V)\mu_c}{\rho_c^{\,2}}\right)^{1/4} \qquad (6\text{-}14)$$

$$Sc = \frac{\mu_c}{\rho_c D_{AB}} \qquad (6\text{-}15)$$

The self diffusivity of acetone ($D_{AA}$) was calculated using the correlation of Sitaraman et al.[197] in equation (6-16) where $V_A$ is the molar volume at the normal boiling point ($m^3$/kg), ΔH is the latent heat of vapourization at the normal boiling point (J/kg), μ is the dynamic viscosity (cP), T is the absolute

temperature (K) and M is the molecular mass (kg/kgmol). The molar volume of acetone at 303.2 K (0.056 m3/kgmol) was used.[198] Viscosity and densities at room temperature were used, which lead to conservative estimates since reduction in these parameters with temperatures enhance mass transfer. Neglecting the effect of fumed silica catalyst on the viscosity and assuming a viscosity of acetone of 0.32 cP, given a molecular mass of 58.08 kg/kgmol, an absolute temperature of 456 K and a heat of vapourization of 519970 J/kg gives a self-diffusivity of acetone of 5.47x $10^{-9}$ $m^2/s$. Substitution of this value into equation (6-15) gave a Schmidt number of 74.1.

$$D_{AB} = (16.79x10^{-14})\left(\frac{M_B^{1/2}\Delta H_B^{1/3}T}{\mu_B V_A^{1/2}\Delta H_A^{0.3}}\right)^{0.93} \qquad (6\text{-}16)$$

To determine the power consumption per unit volume, the impeller Reynolds number was calculated from equation (6-17) where $D_a$ denotes the impeller diameter (m), N denotes the agitation rate (rev/sec), ρ is the liquid phase density ($kg/m^3$) and μ is the dynamic viscosity (kg/ms).[196] Neglecting the effect of the fumed silica on the viscosity and assuming a viscosity of acetone (3.2 x $10^{-3}$ kg/ms), a density of acetone (789.9 $kg/m^3$), an impeller diameter of 1 inch (0.0254 m) and considering the agitation rate of 700 RPM (11.67 rev/s), the impeller Reynolds number was found to be 18580, which is in the turbulent regime.

$$\mathrm{Re} = \frac{D_a^{\,2} N\rho}{\mu} \qquad (6\text{-}17)$$

The power consumption by the impeller (P) can be calculated from the power number ($N_P$) which is related to the mixer parameters in Equation (6-18). The power number can be obtained from agitator performance curves which consist of a log-log plot of the impeller Reynolds number versus the power number. In the turbulent regime, the power number becomes independent of the Reynolds number. For turbine agitators of various geometries, the power

number corresponding to an impeller Reynolds number of 20 000 range from 0.4 to 4.[197] It has been reported that a 4 pitched blade axial flow impeller, such as the one used in these experiments, has a turbulent power number of 1.27.[199] Using this value, an acetone density of 789.9 kg/m$^3$, an agitation rate of 11.67 rev/s and an impeller diameter of 0.0254 m gives a power consumption of 1.68 x $10^{-5}$ kW. Considering the reactant volume of 100 mL gives a power per unit volume of 0.168 kW/m$^3$.

$$Np = \frac{P}{\rho N^3 D_a{}^5} \qquad (6\text{-}18)$$

Substitution of the power per unit volume, the diffusivity of acetone, the Schmidt number and the density and viscosity of acetone into equation (6-14) allowed calculation of the mass transfer coefficient $k_L$ which was found to be 2.25 x $10^{-5}$ m/s. Substitution of the mass transfer coefficient into equation (6-13) along with observed specific reaction rate, the catalyst bed density, the reaction order and the acetone concentration allowed calculation of the Mears parameter, which was found to be 0.011, an order of magnitude lower than the critical value. Thus the inequality (6-13) is valid.

External mass transfer effects are frequently observed for hydrogen transport in multiphase reactions due to the low solubility of hydrogen in organic solvents. Liquid phase catalytic hydrogenation requires the absorption of hydrogen into the bulk, which could be the limiting step. However, if the rate of reaction is very slow, the gas phase resistance can be neglected. The Hatta number (Ha) is a dimensionless number which represents the relative magnitudes of chemical reaction and mass transfer.[200] The accepted criterion for which the gas phase resistance may considered to be negligible is that the Hatta number is less than or equal 0.3 as outlined in equation (6-19) where $k_L$ is the liquid mass transfer coefficient (m/s), k is the bimolecular reaction rate constant (m$^3$/kmol*s) and D is the diffusivity of the solute in the liquid solvent.[201]

$$Ha = \frac{\sqrt{kD}}{k_L} \leq 0.3 \qquad (6\text{-}19)$$

The correlation of equation (6-14) was used to calculate the liquid mass transfer coefficient. The rate constant from the kinetic model (Equation 6-5) expressed in ($m^3$/kmol*s) by multiplying the specific rate by the catalyst mass was calculated for each experiment. The molecular diffusivity is a strong function of concentration. Consequently, the Wilke-Chang correlation (6-20), intended for dilute solutions of non-electrolyte solutes, was used to calculate the diffusivity of hydrogen in acetone using an association factor ($\xi_B$) of 1, which is recommended for non-polar solutes, and a molar volume of hydrogen at its normal boiling point of 0.0143 ($m^3$/kgmol).[202] The viscosity of acetone at room temperature (0.32 cP) was assumed.

$$D_{AB} = \frac{\left(1.17x10^{-13}\right)\left(\xi_B M_B\right)^{1/2} T}{V_A^{0.6}\,\mu} \qquad (6\text{-}20)$$

The hydrogen diffusivity, liquid mass transfer coefficient, rate constant, Hatta number and Mears parameter were calculated for each experiment in the kinetic study (Appendix E4). The hydrogen diffusivities ranged from $1.43 \times 10^{-8}$ $m^2$/s to $1.62 \times 10^{-8}$ $m^2$/s. The Hatta numbers ranged from 0.055 to 0.170, which clearly satisfies the criterion of equation (6-19). Assuming the liquid phase was saturated with hydrogen, the Mears parameter ranged from 0.002 to 0.022 which satisfies the criterion of equation (6-13). Thus it can be concluded that the reactions investigated in the kinetic study were free of external mass transfer effects.

To assess the effects of internal mass transfer, the Weisz-Prater criterion was evaluated. First proposed by Weisz and Prater[203] for positive finite reaction orders up to 2 and later generalized by Hudgins[204] to include all finite reaction orders, including those reactions exhibiting product inhibition, it has

been demonstrated that if the inequality in equation (6-21) is valid, then one may conclude that internal mass transfer effects are negligible. (i.e. $\eta \geq 0.95$).

The term on the left hand side of the inequality, referred to as the Weisz-Prater parameter, is essentially the ratio of a reaction rate to a diffusion rate. $r_{obs}$ is the experimentally observed rate of reaction per unit particle volume (~mol/s*$m^3$), $r_p$ is the pellet diameter (m), De is the effective diffusivity ($m^2$/s), $C_{AS}$ is the concentration of the diffusing reactant at the catalyst surface, which in the absence of external mass transfer limitations is equivalent to the bulk liquid phase concentration (mol/L) and n is the order of the reaction.[205] To calculate the observed reaction rate per unit particle volume, the specific reaction rate is multiplied by the density of the catalyst as in equation (6-22). As a first approximation, the bulk density of the fumed silica (72 080 g/$m^3$) was used.

$$\frac{r_{obs} r_p^{\,2}}{D_e C_A} < \frac{1}{|n|} \qquad (6\text{-}21)$$

$$r_{obs}\left(\frac{mol}{s*m^3}\right) = r'_{obs}\left(\frac{mol}{s*g_{cat}}\right) * \rho\left(\frac{g_{cat}}{m^3}\right) \qquad (6\text{-}22)$$

Diffusion through a solid may occur through three distinct modes of diffusion including ordinary diffusion, Knudsen diffusion and surface diffusion. Surface diffusion does not contribute significantly to the overall transport and may be neglected. Knudsen diffusion is assumed to be the principal mode of transport. The Knudsen diffusivity of acetone was calculated from equation (6-23) where r is the mean pore diameter. The catalyst pore diameter was not obtained in the BET experiments of Chapter Four. However, since the catalyst preparation method is loosely based on that of Chen et al.[42] and since their 0.5 monolayer niobia catalyst was supported on silica with a similar surface area, their mean pore diameter (17.2 nm or 1.72 x $10^{-8}$ m) and pore volume (1.51 $cm^3$/g) was used in these calculations. The effective diffusivity ($D_e$) is

calculated giving consideration to the catalyst porosity (ε), constriction factor (σ) and tortuosity (τ). Values of the constriction factor and tortuosity (0.8 and 3 respectively), which are typical of catalysts, were used.[195]

$$D_{A,K} = 97.0r\left(\frac{T}{M_A}\right)^{1/2} \tag{6-23}$$

$$D_e = D_{A,K}\left(\frac{\sigma\varepsilon}{\tau}\right) \tag{6-24}$$

Based on the pore volume observed by Chen et al.[42] and assuming a density of non-porous silica of 2.2 g/cm$^3$, a porosity of 76.8% was estimated and used in the calculation of $D_e$. From equations (6-23) and (6-24) an effective diffusivity of 9.57 x $10^{-7}$ (m$^2$/s) for acetone at 183°C was estimated. From this value, along with the other parameters, the Weisz-Prater parameter was found to be exceedingly small (3.8 x $10^{-4}$), considerably smaller than the critical value of 0.5. The diffusivity for hydrogen will be greater as a result of its very low molecular mass, resulting in a lower value of the Weisz-Prater parameter. Therefore, the criterion of equation (6-21) is satisfied.

Thus, both internal and external mass transfer effects are negligible and the observed kinetics correspond to the intrinsic kinetics of the overall synthesis of MIBK from acetone and hydrogen. Due to the very low value of the Weisz-Prater parameter observed for these experiments, the assumptions inherent in the calculation such as catalyst porosity, particle size and density could be relaxed to extreme conditions without affecting the conclusion of this calculation. Similarly, the Mears parameter was typically one to two orders of magnitude below the critical value.

## 6.5 Conclusions

Preliminary experiments investigating the one-step synthesis of MIBK using a multifunctional catalyst in a batch reactor highlight the importance of obtaining a balance between the acid sites and hydrogenation sites as suggested by other authors.[23,26,48,50] At very low Pd loading (<< 0.1 wt%), unreacted MO was observed in the product. In contrast, for palladium loading around 1 wt%, the rate of IPA production from direct hydrogenation of acetone become comparable to the MIBK productivity from MO hydrogenation. These observations support our previous findings that MO and acetone compete for the same active sites for hydrogenation.[18] In the final catalyst formulation, a palladium loading of around 0.04 wt% was used, which is at or near the optimum loading. An excessive amount of palladium (II) acetate precursor (eg. 1 wt% Pd loading) not only resulted in a reduction in the hydrogenation selectivity but also significantly reduced the overall catalyst activity and in some cases contributed to complete catalyst deactivation due to the interaction of the palladium acetate with the acid sites. This effect was more pronounced on the gamma alumina supported catalysts. When excessive palladium acetate is used during impregnation, the uptake of the precursor appears to depend on the acidic properties of the niobia catalyst.

Two commercial catalysts carriers, one silica and one gamma alumina, were evaluated for use as a catalyst support for a multifunctional catalyst for pilot scale catalytic distillation experiments. When these supports were used to disperse a surface niobium oxide phase and carry out the synthesis of MO from acetone at 160°C in an autoclave, the alumina catalyst was found to present a substantial internal mass transfer resistance yielding a catalyst effectiveness factor of only 1.64%. In contrast, the silica carrier showed an effectiveness factor of 66%. This disparity in catalyst performance is attributed to the morphological characteristics of the supports. The silica catalyst carrier had a lower surface area and larger mean pore diameter than the alumina. The silica

multifunctional catalyst also exhibited an activity for MIBK synthesis of 1.16 relative to the activity of Amberlyst 15 for MO at its maximum operating temperature.

Experiments in Chapter Five demonstrate that the interaction of the niobia with the silica catalyst carrier generates unique and very strong acid sites not observed in other supported niobia catalysts in including fumed silica. Consequently, the silica carrier was selected for further catalyst development. The silica raschig ring catalysts showed excellent activity for MO and MIBK synthesis in a FBR, typically in excess of 1 [g/hr*$g_{cat}$] and as high as 1.3 [g/hr*gcat] MIBK productivity at 160°C. However, the MIBK selectivity typically ranged from 82 to 85 (wt %) under the reaction conditions investigated, primarily due to the co-production of DIBK and IPA.

Experiments involving the syntheses of MO and MIBK in a fixed bed flow reactor revealed a synergistic effect whereby the catalyst activity increased in the presence of hydrogen by 22% at a space velocity of 8.6 $hr^{-1}$. It is postulated that the rapid hydrogenation of MO to MIBK increases the fraction of available surface sites for chemical reaction by reducing the surface concentration of MO and its derivatives which may inhibit the global reaction rate. The synergistic effect becomes more pronounced for low space velocity where the inhibiting effects of substrates become increasingly significant and are less pronounced for conditions of high space velocity where the inhibiting effects of organic substrates is less significant. Another curious observation is that the presence of hydrogen appears to facilitate the synthesis of mesitylene from phorone, which does not involve hydrogenation. Moreover, the precursors of mesitylene, including phorone and MO, are typically not observed in the reactor effluent. In contrast in the absence of hydrogen in the FBR, mesitylene was only observed at 180°C and was co-produced with significant amounts of its precursors phorone and MO.

The intrinsic kinetics of the overall one-step synthesis of MIBK was investigated in an autoclave reactor over a broad range of temperatures and hydrogenation pressures over a $Pd/Nb_2O_5/SiO_2$ catalyst with 0.51 monolayer niobia coverage and a palladium loading of 0.047 wt%. Evaluation of the Mears and Weisz-Prater criteria confirm the absence of mass transfer effects for this investigation. Activities for MIBK synthesis as high as 6.5 times that of MO production using Amberlyst 15 at its maximum operating temperature were observed. At high moderate to high pressure, MIBK can be produced in essentially 100% selectivity up to acetone conversions around 20%, after which, mesitylene, DIBK and IPA were observed. The hydrogenation pressure had a significant effect on the selectivity. At lower hydrogenation pressures, the initial rate of MO synthesis exceeded the rate of its hydrogenation resulting in a significant amount of unreacted MO which accumulated in the reactor, in some cases resulting in catalyst deactivation.

A kinetic model was developed which gives excellent prediction of the acetone concentration as evidenced by a relative standard error of estimate (RSEE) of 1.07% over the interval investigated. The kinetic model gives good predictions of the water concentration (RSEE = 12.8%) and fair estimates of the MIBK concentration (RSEE = 19.7%). MO prediction was poor. High relative errors were observed in the prediction of MO due to the relatively low observed and expected concentrations, which were near the GC peak area rejection limit. The kinetic model is valid for system pressures of 500 psia and greater. However, the model predictions become unreliable at lower pressure.

# Chapter Seven

## Preliminary Pilot Scale Experimental Studies on the Syntheses of MO and MIBK via Catalytic Distillation

---

### 7.0 Synopsis

This chapter outlines the results of two preliminary pilot scale experiments, which were conducted using commercially available catalysts in order to obtain process benchmarks for the syntheses of MO and MIBK via catalytic distillation. These experiments were carried out in the first year of this research project in order to aid in the development of the problem definition. The results of these experiments provided a cursory assessment of these CD processes and identified their limitations and the immediate challenges for further CD process development. Specifically, the results demonstrate that the hydrogenation step was limiting the CD process for the one step synthesis of MIBK. The results indicate that significant hydrogenation catalyst deactivation had occurred during the CD experiment. The nature of the deactivation was unclear and warrants further investigation. However, DRIFT spectroscopic evidence suggests that MIBK interacts strongly with the Lewis acid sites of the alumina support.

### 7.1 Introduction

The one-step synthesis of MIBK from acetone has been carried out previously in a CD column operating in batch mode utilizing a multifunctional catalyst.[32] However, no results have been reported in the scientific literature for any CD process for MIBK synthesis operating in either continuous or batch mode. Moreover, the potential advantages of a one zone approach versus a two zone mode of CD operation have not been investigated for this application. Although the results reported by Lawson and Nkosi[32] have demonstrated the technical feasibility of a one-step CD process for MIBK, the results were poor (Table 1-1). The average MIBK productivity for the best operating condition was only about 0.10 $g_{MIBK/}(hr*mL_{cat})$ and the selectivity to MIBK ranged from only 33 to

68% (wt%). Consequently, a major objective of this research is the development of an improved CD process for MIBK synthesis. More generally however, the principal objective is to gain insight into the potential advantages and limitations of CD technology through the application of CD towards a complex organic synthesis.

Two pilot scale experiments were carried out to investigate the syntheses of MO and MIBK from acetone. Commercially available catalysts, which represent the state-of-the-art for MIBK synthesis, were used in two separate reaction zones in order to obtain a cursory assessment of these CD processes and to acquire a process benchmark against which further process improvement may be gauged.

## 7.2 CD Pilot Plant Apparatus

CD Column

Pilot scale catalytic distillation (CD) experiments were conducted utilizing the CD reactor apparatus whose schematic is outlined in Figure 7-1. The reactor is constructed from 5 segments of 316 stainless steel (SS) schedule 40 pipe with 1 inch nominal inside diameter connected by 600 psi class flanges (ANSI B.15) fixed in place with butt-weld joints. The CD reactor has a total height of 23 ft (7m) with a total packing height of 16 ft (4.9 m). ¼ inch ceramic Intalox saddles (Norton) were used as a distillation packing and loaded into the column in a random manner. Heterogeneous catalyst was immobilized within discrete reactive sections of the CD column.

Each segment of the column contained multiple sample ports constructed of 316 SS schedule 80 pipe (1/4 inch ID X 5 ¾ in. long) welded to the reactor major axis spaced out in 6 inch and 12 inch intervals. Thermocouple probes were inserted into these ports and sealed with Swagelok tube fittings in order to obtain direct measurements of temperature within the reactor. These access

ports, if appropriately modified, could also be used to obtain liquid samples from the reactor along its major axis.[206] A 1000 W variable output explosion proof immersion heater inserted into the bottom of the CD column and sealed with a flanged joint served as the reboiler for the CD column. Variable power output explosion proof heating elements (1000 W) running up the major axis of the column were used to make up for heat losses from the column. The CD column was enclosed with high temperature ceramic insulation and aluminum sheeting.

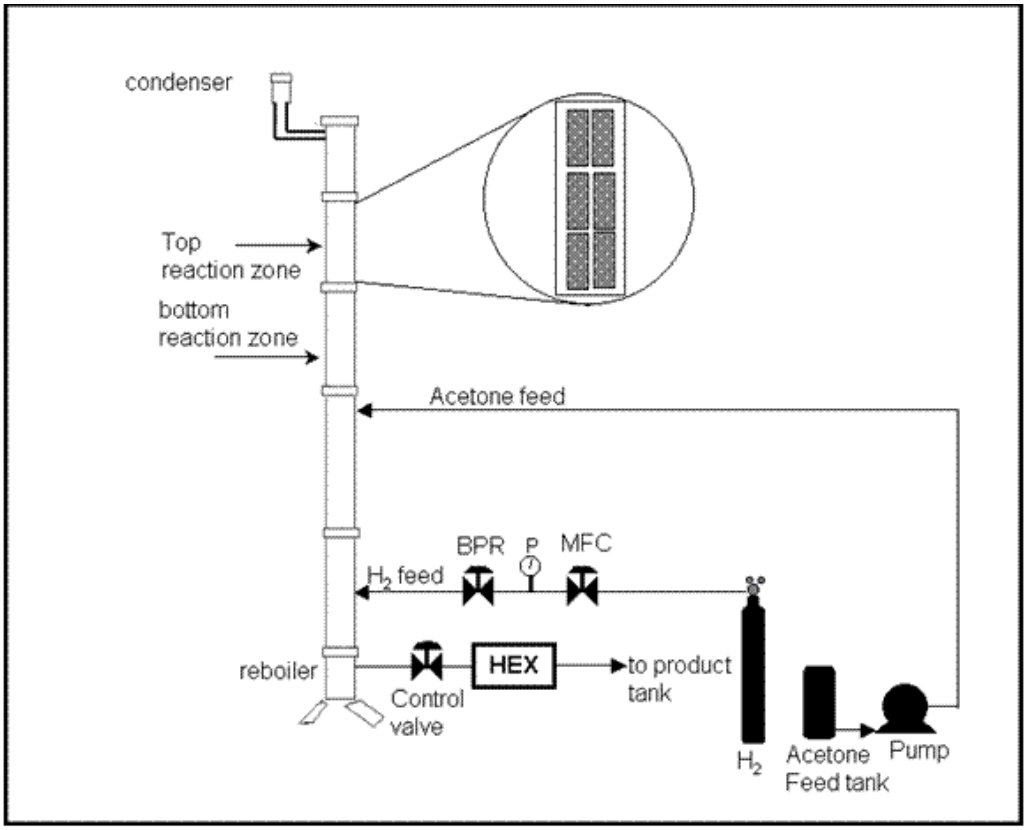


**Figure 7-1** Schematic Representation of the pilot scale CD Reactor and ancillary equipment; reprinted from O'Keefe et al.[63]♣

♣ Reprinted with permission from W.K. O'Keefe, F.T.T. Ng and G.L. Rempel (2007), *Ind. Eng. Chem. Res.*, **46(3)**, pp. 716-725. © 2007 American Chemical Society

Durlon 9000 Blue (PTFE with inorganic filler) ring gaskets were selected for this work due to their excellent chemical resistance even to the most aggressive chemicals and particularly for their superior sealing characteristics. Durlon 9000 has been used extensively in the pharmaceutical, pulp and paper and food and beverage industries.[207] Typical applications of Durlon 9000 Blue gaskets include operations involving gaseous or liquid oxygen, nitrogen or chlorine as well as caustics and high purity applications in the pharmaceutical industries such as blood components manufacturing.[207]

Although the Durlon 9000 Blue gaskets have excellent chemical resistance for the oxygenated solvents investigated in this work, for this CD application, the sealing characteristics of the gasket are of paramount importance. An excellent seal is required in order to minimize the potential for leakage and the possible ignition of flammable vapours, particularly when hydrogen is being used. However, the reader is advised that the optimal performance of the gaskets and indeed the safe operation of the CD column are dependent on proper gasket installation. Specifically, the bolts at the flanges must be torqued to meet the specification outlined in Table 7-1 in no less than three stages of successively increasing torque following the crossing pattern outlined in the Durlon Technical Handbook.[207] In addition, the bolts should be re-torqued to the required torque specification in a circular pattern 24 to 72 hours after installation to account for bolt relaxation.[207]

The author recommends that the bolts should be tightened to the maximum recommended torque in anticipation of torque loss throughout the course of experimentation due to bolt relaxation as well as thermal cycling of the apparatus between experiments. It is also important to note that to achieve the proper compression of the gaskets, the bolts must be clean such that they may be installed finger tight by hand without any unintended resistance from debris such as fragments of insulation. Also, it is important to note that the

torque specification provided by the gasket manufacturer assumes that the bolts have been lubricated with an anti-seize compound.

**Table7-1** Torque specifications for 1/16 inch thick DURLON 9000 Blue ring gaskets for raised face flanges[207]

| Gasket Diameter (inches) | Bolts | Minimum Torque (ft-lbf) @ P=100 psi | Minimum Torque (ft-lbf) @ P=300 psi | Maximum Torque ($ft\text{-}lb_f$) |
|---|---|---|---|---|
| 1 | 4 @ 5/8” | 13 | 18 | 36 |
| 1.5 | 4 @ 3/4” | 31 | 45 | 92 |
| 2 | 8 @ 5/8” | 21 | 30 | 62 |

Threaded pipe fittings that were permanently sealed were sealed with Loctite 567 high temperature sealant in order to minimize the potential for leakage. However, some pipe thread on the sample ports of the reaction zones were sealed with Teflon tape after installation of the catalyst since a 72 hour cure period is required for the Loctite sealant to be effective. After installation of the catalyst, the reactor was pressurized with argon and leak tested. After major leaks had been corrected, the column was pressurized to 350 psig and isolated. Its pressure loss was monitored overnight and was typically around 3 psi per hour or less at 200 psig when sealed properly.

ACS reagent grade acetone (Aldrich 67-64-1, >99.5% ) was fed continuously to the CD column at a location 6 inches (15 cm) below the reactive sections illustrated in Figure 8-1 using a Milton Roy LCD mini-pump to precisely control the mass flow rate. In accordance with the Ontario Fire Code[208] the acetone feed tank and CD column were grounded to a copper cooling water drain pipe using an AWG copper braid conductor cable and code approved grounding connectors following the guideline provided by the Industrial Accident Prevention Association.[209]

A condenser located at the top of the CD column condenses the vapours into a liquid stream (distillate). Some or all of the overhead distillate may be

refluxed to the CD column or recovered as an overhead product and transferred to a product reservoir. The reflux ratio is controlled using a solenoid valve. The Keithly process control software allows control of the period of time that the solenoid valve is open to collect overhead distillate product and the time period for which the solenoid valve is closed whereby liquid is refluxed to the CD column throughout a predetermined cycle time.

Cooling water was fed to the condenser using a rotameter to control the volumetric flow rate of water. Thermocouple probes were inserted at the cooling water inlet and outlet and these temperatures were continuously monitored. For the first two CD experiments outlined in this chapter, the condenser cooling water temperatures were recorded manually once per hour during operation. However, for the subsequent CD experiments outlined in Chapter Eight, the condenser cooling water temperatures at the inlet and outlet were continuously monitored, filtered and datalogged at one minute intervals using LabView 7.1 in order to obtain more accurate estimates of the condenser duty.

The condenser duty was calculated from the measured temperature change of the cooling water passing through the condenser and the known cooling water mass flow rate. First, the volumetric flow rate of water was converted to a mass flow rate using the known density of water at the measured inlet temperature from tabulated data in Weast.[210] Second, the heat capacity ($C_p$) of water was determined at the condenser water inlet temperature from tabulated data in Weast.[210] The temperature dependence of the heat capacity was neglected for the small changes in cooling water temperatures observed across the condenser since it affects the result in the fourth significant figure. The heat capacity of water differs by a maximum of 0.1% between 18 and 40°C. The condenser duty was then calculated using equation (7-1). The Watson correlation (Eqn 7-2) was used to calculate the latent heat of vapourization of acetone at the measured reflux temperature from the latent heat of vapourization

of acetone at its normal boiling point (30.2 kJ/mol at 1 atm, 329 K) and the critical temperature of acetone (508.0 K).[211] The reflux flow rate was subsequently calculated from the energy balance about the condenser using equation (7-3) assuming that the reflux stream consisted entirely of saturated liquid acetone.

$$\dot{Q} = \dot{m}_w \overline{C}_p \Delta T \tag{7-1}$$

$$\Delta H_v(T_2) = \Delta H_v(T_1)\left(\frac{T_c - T_2}{T_c - T_1}\right)^{0.38} \tag{7-2}$$

$$\dot{Q} = \dot{m}_{Ac} \Delta H_v(T_2) \Rightarrow \dot{m}_{Ac} = \frac{\dot{Q}}{\Delta H_v(T_2)} \tag{7-3}$$

Liquid product was continuously withdrawn from the reboiler through a Badger Research control valve in a manner to maintain a constant liquid level of 55% (± 5%) capacity in the reboiler. The control valve was operated manually by controlling the valve percentage output on the Keithly human-machine interface screen. The liquid level in the reboiler was measured by visual inspection through a sight glass by the operator. Liquid product recovered from the reboiler was passed through a double pipe heat exchanger in a U-tube bundle configuration with the product running shell side and cooling water running tube side prior to collection within a product reservoir. The product was drained periodically from the reservoir into glass bottles. A separate bottle was used for each hour of CD operation or every two hours when the CD column was operating at very low flow rates. The amount of material recovered was determined by weighing the bottle before and after sample collection using a balance precise to ±0.005 g. The liquid samples were subsequently analyzed by GC/FID to ascertain their chemical composition and in some cases GC/TCD to determine the moisture content using the gas chromatograph and GC techniques described in Chapter Three. However, for the first two CD experiments, an

internal standard (1-propanol Fisher A414-500, >99.8%) was used instead of external calibration standards.

For the CD experiments involving MO hydrogenation, UHP hydrogen (Praxair, >99.995%) was fed to the CD column at a point about 1m from the bottom of the column. The hydrogen flow rate was controlled by a Brooks 5850E mass flow controller (MFC). The MFC was calibrated by Trillium Measurement and Control Ltd. (Markham, Ontario, Canada) following NIST traceable standards. The delivery pressure to the MFC was 1.03 MPa and a back pressure regulator (BPR) ensured a constant pressure drop of 0.34 MPa across the control valve. Hydrogen was not used for the first CD experiment. Instead nitrogen was fed to the CD column at a relatively small mass flow rate in order to promote thermal mixing through the forced convection of matter and energy up the CD column from entrainment. The same gas feed port was used as that for the hydrogen feed in other experiments. The flow rate of nitrogen was regulated using a Whitey SS-22RS4 fine metering valve.

The pressure within the column was measured at two locations, the top and bottom of the column, which allowed a measurement of the pressure drop across the column as well as the average column pressure. These measurements were obtained using pressure transducers. The analog signals from the pressure transducers as well as the 23 thermocouples were transmitted to an “AD interface”, which converted the analog signals to digital signals prior to processing by the Keithly control software running on a personal computer. The pressure within the CD column was controlled using proportional-integral (PI) control. The control elements consisted of two pneumatically actuated Badger Research valves operating on a split range. One “inlet” valve when open and the other “outlet” valve closed allowed nitrogen to be fed to the reactor to increase the system pressure. Conversely, with this inlet valve closed and the outlet valve open, the pressure within the reactor was decreased as gas was vented.

The reboiler level control valve was also pneumatically actuated. It had a P1 trim set for the first two CD experiments. However, this valve was known to be over-sized ($C_V$=0.004) for the CD work being undertaken and consequently, the trim set was replaced with a P7 trim set ($C_V$=0.00018) after the first two experiments.[206] The P7 trim set was not optimal but did result in significantly improved reboiler level control.

The pilot plant was equipped with "GAT-WD" combustible gas sensors (BW Technologies), one located at the top of the column and the other at the bottom, which continuously monitored the level of flammable compounds in the ambient including hydrocarbons such as acetone and MIBK as well as hydrogen. These gas sensors transmitted the data to a 4 channel controller-monitor which displayed the gas concentration as a percentage of the lower explosive limit (LEL). The sensors were calibrated to give a response with respect to methane. However, a correction factor of 1.93 was used to express the % LEL in terms of the lower explosive limit of acetone. A warning alarm would sound at 10% LEL and a high alarm would result at 20% LEL. The controller-monitor was interlocked with the CD process control. In the event of a high level alarm, the power supply to the CD process including power to the computer, heating elements and pumps, would be disabled and all control valves would be rendered to their fail-safe positions. A low level alarm resulted in an audible warning to take corrective action.

### 7.3 Catalyst Selection for Preliminary CD Experiments

In order to obtain meaningful process benchmarks for MO and MIBK synthesis, commercially available catalysts which represent the state-of-the-art for MIBK synthesis were selected. The one-step synthesis of MIBK requires a multifunctional catalyst to facilitate the three major reaction steps. The most commonly employed multifunctional catalyst for the commercial production of MIBK in a single stage comprises a strongly acidic cation exchange resin

containing 0.05 wt% palladium. The strongly acidic support catalyses the synthesis of MO from acetone. Palladium is used as the hydrogenation catalyst since is known to give consistently high selectivity to the hydrogenation of the olefin group of $\alpha,\beta$-unsaturated ketones.

The first one-step processes for MIBK synthesis commercialized by Veba- Chemie specified such a catalyst.[1] This catalyst formulation remains the most commonly used for MIBK synthesis. Today, Rohm and Haas markets Amberlyst CH28, which consists of 0.05 wt% Pd dispersed onto a strongly acidic macroreticular resin, for the commercial manufacture of MIBK. Unfortunately, Amberlyst CH28 was not commercially available in North America at the time of this study. Instead Amberlyst 15 (Aldrich 21638-0), a strongly acidic macroreticular cation exchange resin, was procured for the investigation of the synthesis of MO from acetone. Incidentally, Lawson and Nkosi[32] used a 0.05 wt% Pd/Amberlyst 15 catalyst in their investigation of MIBK synthesis via CD.

Rather than use a multifunctional catalyst, the one-step synthesis of MIBK via CD was benchmarked using two separate catalysts in two discrete reaction zones. Amberlyst 15 was utilized in one reaction zone for the synthesis of MO while a 0.52 wt% $Pd/Al_2O_3$ catalyst (Aldrich 20,574-5) was used in a separate reaction zone to facilitate the hydrogenation of MO. Schmitt et al.[20] have demonstrated that MIBK can be produced with 96% yield from the hydrogenation of MO in a CD reactor using a 0.2 wt% $Pd/Al_2O_3$ catalyst. This catalytic distillation process was integrated into the Hibernia-Schloven three stage process for the commercial production of MIBK. Aside from the successful commercial use of $Pd/Al_2O_3$ as a catalyst for MO hydrogenation, the 0.52 wt% $Pd/Al_2O_3$ catalyst (Aldrich 20,574-5) was selected specifically since the author and co-workers[18] have previously characterized the intrinsic kinetics of the liquid phase MO hydrogenation over this catalyst.

## 7.4 The Synthesis of MO via Catalytic Distillation (CD 001)

Design of Experiment and Overview of Results

In the first CD experiment, MO was synthesized from acetone using Amberlyst 15 as a catalyst. 135.5 mL of Amberlyst 15 that had been swollen in 2-propanol for 24 hours was loaded into 13 wire mesh bundles. The bundles were constructed of 304 SS (Ferrier, Toronto Canada) and had a mesh count of 150 X 150, a wire gauge of 0.0026 inches, a clear opening of 0.041 inches and having 37.8% open area. These bundles were approximately 5 inches (13 cm) in length and were loaded in pairs into the reactive sections of the CD column illustrated in Figure 7-1 with a 9 ft (2.7 m) stripping section located below the reaction zones and a 3 ft (0.9 m) rectification section located above the reactive sections. Both non-reactive sections were filled with ¼ inch Intalox saddles. The catalyst bundles were evenly spaced within the reactive sections with demister wire filling the void space. Six bundles were loaded in the top reactive section and seven bundles loaded into the bottom reactive section. The unpaired catalyst bundle in the bottom reaction zone was centred within the CD column by wrapping it with demister wire.

The objective of the experiment was to ascertain the main effects and interactions of the major process parameters on the MO productivity and the product distribution including the reaction temperature, the acetone feed rate and the reboiler duty as well as to obtain a process benchmark for the CD process utilizing Amberlyst 15 as a catalyst. Since there are an insufficient number of degrees of freedom to independently specify the system pressure and reaction temperature for a given feed composition, the reaction temperature was controlled via control of the total system pressure. The reboiler duty is a measure of the energy imparted to the system, which governs the liquid and vapour flow rates within the CD column. The acetone feed rate affects the residence time in the CD reactor and the chemical conversion for the unit operation.

The design of experiment is outlined in Table 7-2. Experimental conditions 2 through 5 constitute a 2X2 full factorial experiment with the reaction temperature and reboiler duty as control factors (experimental variables) and the external heater duty and nitrogen flow rate as noise factors. The effect of the acetone feed rate on the MO productivity and product distribution are investigated in conditions 4, 6 and 7. However, the results of condition 7 are preliminary since steady state was not fully achieved by the time the experiment was terminated after 120.5 hours. Condition 1 is the same as condition 5 with the exception of the value of the external heater duty which was 500 W in condition 1 and 800W for all subsequent experimental conditions. In addition, nitrogen was not fed to the column for condition 1.

For each experimental condition, the CD reactor was maintained at steady state for 5 to 10 hours depending on the process stability in order to acquire a sufficient number of experimental observations to obtain accurate and precise estimates of the reboiler composition at the 95% confidence level. Steady state was defined as the condition whereby the temperature was invariant to within ± 0.5°C at all locations along the major axis of the CD reactor and the GC peak areas for all species were invariant to within a relative standard deviation of 5% with respect to the mean value obtained over the interval. For example, six reboiler samples were collected over a five hour period for steady state condition number 5. The average MO concentration for condition number 5 was 18.50 ± 0.11 wt%.

**Table 7-2** Design of Experiment (DoE) for the first CD experiment[♣]

| Trial | Ac Feed Rate [mL/hr] | Rxn. Zone Temp [°C] | Reboiler Duty [W] | Ext. Heater Duty [W] | $N_2$ Feed Enabled ? | Avg. System Pressure [MPa] | Avg. Reflux Rate [g/min] |
|---|---|---|---|---|---|---|---|
| 1 | 152 | 101 | 300 | 500 | No | 0.32 | 7.25 |
| 2 | 152 | 114 | 300 | 800 | Yes | 0.46 | 3.64 |
| 3 | 152 | 114 | 350 | 800 | Yes | 0.46 | 8.57 |
| 4 | 152 | 101 | 350 | 800 | Yes | 0.32 | 27.9 |
| 5 | 152 | 101 | 300 | 800 | Yes | 0.32 | 24.1 |
| 6 | 91.6 | 100 | 350 | 800 | Yes | 0.33 | 30.6 |
| 7 | 37.3 | 99 | 350 | 800 | Yes | 0.33 | 24.3 |

The reboiler composition as a function of time-on-stream (TOS) for this CD experiment is illustrated in Figure 7-2. The steady state conditions are bounded by vertical bars within the figure. The high molecular weight species produced from the consecutive reactions of MO were lumped together and labelled as "TMB and phorones" in Figure 7-2. The steady state reboiler product composition is summarized in Table 7-3 and the MO productivity and selectivity are summarized in Table 7-4. The acetone conversion for the unit operation and MO selectivity were defined by equations 7-4 and 7-5 respectively. The selectivity to MO was calculated on a mass basis rather than a molar basis since some unidentified species were present in the product mixture. The author and co-workers[18] have shown previously that IMO is equally valuable as MO as a precursor to MIBK, exhibiting identical kinetic behaviour. Consequently, the IMO concentration was lumped with the MO concentration for the calculations of selectivity to MO and MO productivity.

$$X_{Ac} = 100\% * \left[ \frac{F_{AO} - F_A}{F_{AO}} \right] \qquad (7\text{-}4)$$

[♣] Reprinted in part with permission from W.K. O'Keefe, F.T.T. Ng and G.L. Rempel (2007), *Ind. Eng. Chem. Res*., 46(3), pp.716-725. © 2007 American Chemical Society

$$S = 100\% * \left[ \frac{X_{MO} + X_{IMO}}{\sum_i X_i} \right] \qquad (7\text{-}5)$$

**Table 7-3** Steady state concentrations of organic species in the reboiler product stream (acetone solvent neglected) Data reproduced from O'Keefe et al.[63]♣

| Trial | MO [wt%] | IMO [wt%] | MO / IMO | DAA [wt%] | TMB [wt%] | IPO [wt%] | Other $C_6^+$ [wt%] |
|---|---|---|---|---|---|---|---|
| 1 | 12.9 | 0.69 | 18.7 | 1.42 | 0.03 | 0.01 | 0.23 |
| 2 | 19.0 | 1.20 | 15.8 | 1.31 | 0.22 | 0.11 | 0.53 |
| 3 | 18.6 | 1.17 | 15.9 | 1.81 | 0.12 | 0.04 | 0.34 |
| 4 | 19.5 | 1.05 | 18.6 | 3.73 | 0.02 | 0.00 | 0.22 |
| 5 | 18.5 | 0.99 | 18.6 | 3.38 | 0.01 | 0.00 | 0.20 |
| 6 | 33.7 | 1.85 | 19.3 | 6.91 | 0.03 | 0.00 | 0.37 |
| 7[a] | 78.2 | 2.69 | 29.1 | 14.2 | 0.07 | 0.01 | 0.85 |

[a]*Trial number 7 is a preliminary result since the process had not fully achieved steady state*

**Table 7-4** Effect of CD process on MO productivity and selectivity Data reproduced from O'Keefe et al.[63]♣

| Trial | Acetone Conversion X [%] | Productivity MO [g/(hr*mL$_{cat}$)] | Productivity MO & IMO [g/(hr*mL$_{cat}$)] | Selectivity MO & IMO [wt%] |
|---|---|---|---|---|
| 1 | 19 | 0.119 | 0.126 | 88.9 |
| 2 | 26 | 0.142 | 0.151 | 90.3 |
| 3 | 27 | 0.160 | 0.170 | 89.5 |
| 4 | 29 | 0.179 | 0.188 | 83.8 |
| 5 | 27 | 0.171 | 0.172 | 84.4 |
| 6 | 50 | 0.181 | 0.190 | 82.9 |
| 7[a] | > 99.9 | 0.141 | 0.146 | 84.2 |

[a]*Trial number 7 is a preliminary result since the process had not fully achieved steady state*

♣ Reprinted in part with permission from W.K. O'Keefe, F.T.T. Ng and G.L. Rempel (2007), *Ind. Eng. Chem. Res.*, **43(6),** pp.716-725 © 2007 American Chemical Society.

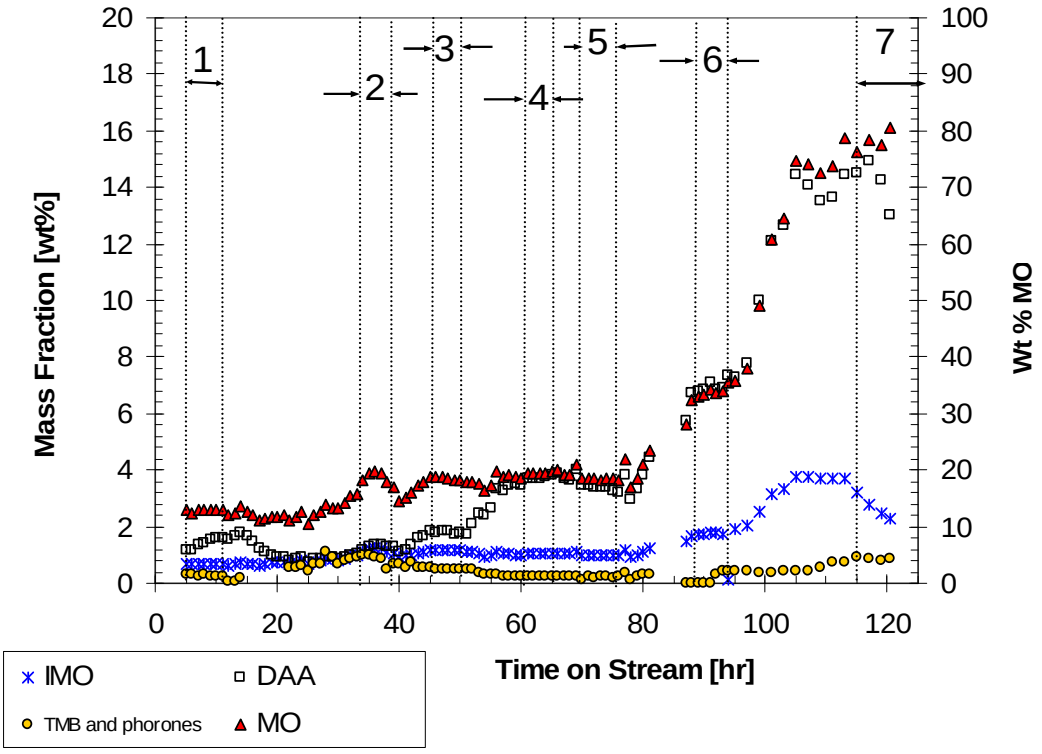


**Figure 7-2** Mass fraction of organics in the reboiler product as a function of TOS for MO synthesis via CD. Reprinted from O'Keefe et al.[63]♣ *MO mass fraction on separate ordinate. All other species have mass fraction indicated on principal y-axis.*

Effect of Reflux Flow Rate

The data in Figure 7-3 clearly demonstrates that the synthesis of MO via CD utilizing cationic exchange resins in wire mesh bundles is a *liquid limited* reaction. The MO productivity is highly correlated and increases non-linearly with the reflux flow rate in the CD column. In addition, the steady-state DAA mass fraction in the reboiler product stream, and thus the DAA productivity is also highly correlated with the reflux flow rate ($R^2$=0.9998). This suggests that the overall reaction rate is controlled by the rate of external mass transfer of acetone.

---

♣ Reprinted in part with permission from W.K. O'Keefe, F.T.T. Ng and G.L. Rempel (2007), *Ind. Eng. Chem. Res.*, 43(6), pp.716-725 © 2007 American Chemical Society.

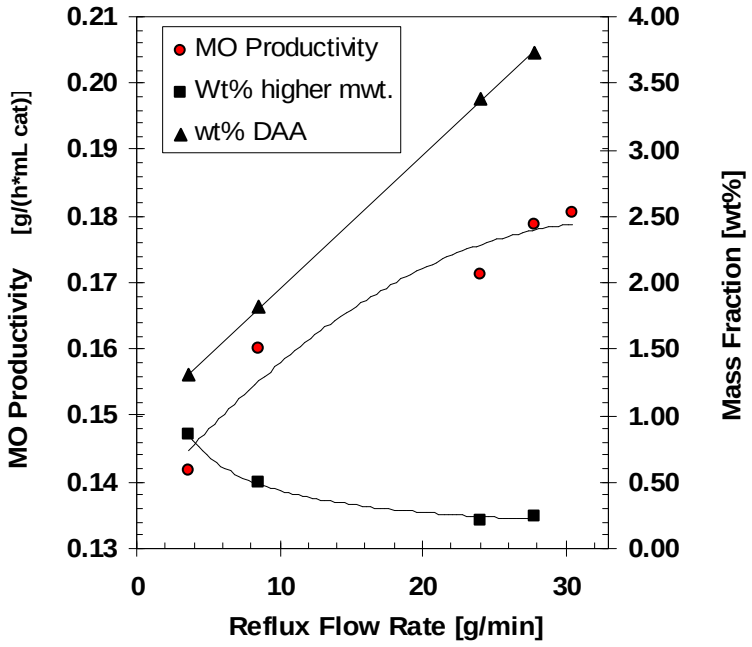


**Figure 7-3** Effect of reflux flow rate on MO productivity and the mass fractions of DAA and higher molecular weight species in the reboiler product (Q=800 W) Figure reprinted from O'Keefe et al.[63]♣

*The data in Figure 7-3 for MO productivity includes all 5 steady state observations for an external heater duty of Q=800W. However, the data for the plots of mass fraction of DAA and higher molecular weight species contain only the four observations corresponding to an acetone feed rate of 152 mL/min since the acetone feed rate, which is different in condition 6, affects the reboiler composition.*

An enhancement of the catalyst utilization as a consequence of improved external catalyst wetting efficiency ($\eta_{CE}$) with increasing reflux flow rate may have also been a contributing factor to the results illustrated in Figure 7-3. In fact, the validation of plug flow models for trickle bed reactors has shown that both external mass transfer effects as well as external catalyst wetting efficiency must be accounted for in the model.[212,213] In general, for conditions of trickle flow, the catalyst is only partially wetted both externally and internally.[212-216] Consequently, only a fraction of the total population of active sites is wetted and accessible to reactants in the liquid phase. The catalyst external wetting efficiency only approaches unity for relatively high liquid flow rates, high

♣ reprinted with permission from W.K. O'Keefe, F.T.T. Ng and G.L. Rempel (2007), *Ind. Eng. Chem. Res*. 43(6), pp. 716-725. © 2007 American Chemical Society

pressure and high superficial gas velocities. In the case of a liquid-limited reaction, the limiting reagent is transported primarily within the liquid phase to the active sites of the catalyst. Therefore, an increase in the wetting efficiency will increase the global rate of reaction since more catalyst sites will become available. Indeed, the catalyst wetting efficiency is known to be an important design and scale-up parameter which determines the degree of catalyst utilization under conditions of trickle flow in a multiphase reactor.[107]

Al-Dahhan and Dudukovic[214] have developed a phenomenological hydrodynamic model which allows the prediction of the catalyst wetting efficiency from the pressure gradient ($\Delta P/Z$) and the dimensionless modified Reynolds (Re) and Galileo ($Ga_L$) numbers which characterize the liquid phase trickle flow through the porous media. This model is given by equation (7-6) and is known to be valid for pressures ranging from 0.31 to 5 MPa.

$$\eta_{CE} = 1.104\,\mathrm{Re}^{1/3}\left(\frac{1+\Delta P/\rho_L g Z}{Ga_L}\right)^{1/9} \tag{7-6}$$

Where

$$\mathrm{Re} = \frac{\rho U d_p}{\mu(1-\varepsilon)} \quad \text{and} \quad Ga_L = \frac{d_p{}^3 \rho^2 g \varepsilon^3}{\mu^2 (1-\varepsilon)^3}$$

Equation (7-6) was used to calculate the wetting efficiency of the catalyst with the following assumptions. As a first approximation, it was assumed that the reaction zone had the same void fraction and wetting characteristics as the distillation packing. ¼ inch Intalox saddles have a characteristic diameter of 6 mm and yield a bed porosity of $\varepsilon$=0.75.[200] The density of the mixture was assumed to be the density of acetone 789.9 kg/m$^3$. The viscosity was assumed to be that of acetone at its normal boiling point. The viscosity at 56°C was estimated from equation (7-7) which is known to be accurate for reduced temperatures reduced temperatures ($T_r$) below 0.75.[200] The empirical

parameters for equation 7-7 (A, B and C) were determined from nonlinear regression analysis of viscosity data for acetone tabulated in Weast.[210] The density of acetone was estimated to be 0.24 cP at 56°C.

$$\ln \eta = A + \frac{B}{C + T} \qquad (7\text{-}7)$$

The pressure gradient was calculated from the known packing bed height of 16 ft (4.88 m) and the experimentally measured pressure drop across the bed. The average steady state pressure drop ranged from 0.57 to 0.82 psi for this experiment. Since the pressure drop in a CD column is greatly minimized to prevent flooding, the pressure gradient term could be omitted from equation (7-6) without introducing a significant error to the calculation. Inclusion of this term in the calculations was found to not significantly affect the results. The superficial liquid velocity was calculated from the measured reflux flow rate, the known cross sectional area of the CD column and the density of acetone. The results of the calculations (Figure 7-4) predict wetting efficiencies ranging from 27 to 54%.

It should be noted however, that the results of Figure 7-4 represent the wetting efficiency over the 6 mm Intalox saddles. The assumption that the reaction zone exhibited comparable wetting characteristics as the distillation packing is questionable. However, the results clearly demonstrate that for this CD process the wetting efficiency of the catalyst was likely far from unity for this experiment and was a strong function of the reflux flow rate. This also explains the relatively low MO productivity in contrast to the productivity observed for the synthesis of MO with a fully wetted Amberlyst 15 catalyst in an autoclave reactor at 120°C (Experiment 170). The initial rate of reaction of MO synthesis of experiment 170 gave a MO productivity two orders of magnitude greater than that observed in this CD experiment.

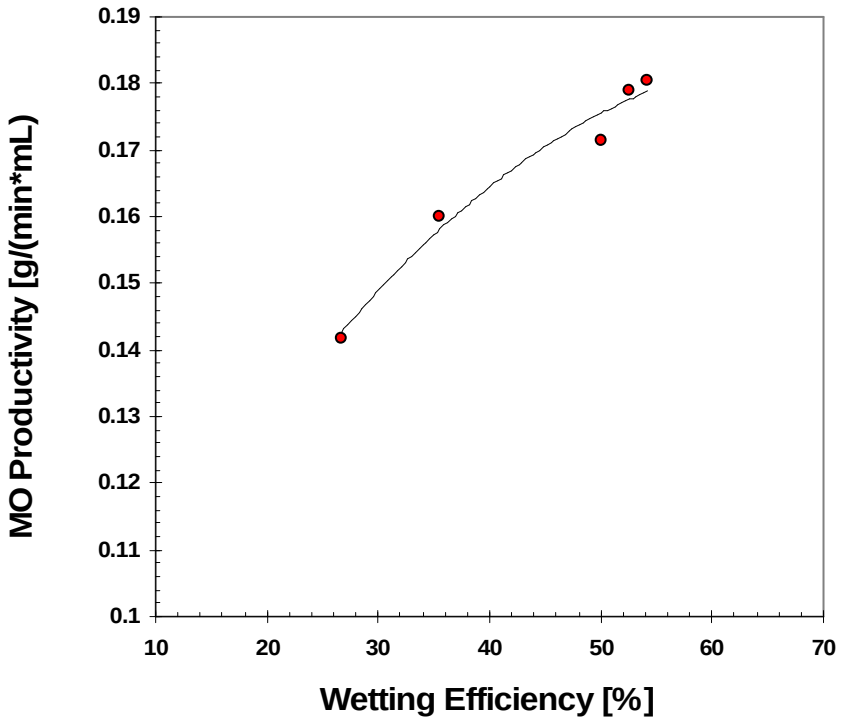


**Figure 7-4** External wetting efficiency predicted by equation (7-6) from the experimentally measured reflux flow rate for conditions 2-6 (CD 001)

However, the application of CD technology may lead to enhanced catalyst utilization for *gas limited* reactions if in fact the catalyst wetting efficiencies of Figure 7-4 are representative of most CD processes. For a gas limited reaction, the global rate of reaction is governed by the rate of mass transfer of gaseous reactant to the active sites. Non-condensable gases such as hydrogen or oxygen are only sparingly soluble in liquids. For example, the Henry's law constant for hydrogen dissolved in acetone at 323K, is only 292 (MPa).[193] Consequently, hydrogen is usually the limiting reagent in a solid-liquid-gas contactor since the concentration of dissolved hydrogen in the solvent is typically a few orders of magnitude lower than that of the reactant to be hydrogenated. To compensate for this, trickle bed reactors are operated at relatively high pressure, often as high as 30 MPa, to enhance mass transfer rates.[212]

Dry regions on a partially wetted catalyst provide a means for hydrogen or other gaseous reactants to adsorb directly onto the active sites of the solid from the gas phase without having to dissolve into and diffuse through the liquid. The gas-liquid-solid transport route represents a substantial mass transfer resistance whereas the gas-solid route is facile and presents a negligible mass transfer resistance.[215] The diffusion rate of a gas through a porous solid is approximately 10000 times greater than the diffusion rate of the gas through a liquid.[216] Consequently, the concentration of the gaseous reactant on the catalyst surface can be substantially increased and significant kinetic enhancement may be realized as a result of the enhanced mass transfer due to the partial wetting of the catalyst.

Effect of the Process Parameters on the Product Distribution

The data in Table 7-4 corresponding to the 2x2 factorial experiment investigating the effects of the reaction temperature and reboiler duty give the apparently paradoxical result that the experimental conditions carried out at the lower reaction temperature (101°C in conditions 4 and 5) resulted in greater MO productivities than the higher reaction temperatures (114°C conditions 2 and 3). However, this result is reasonable and expected considering that the reaction is liquid limited. Since there are an insufficient number of degrees of freedom to independently specify the temperature and pressure in a CD process, the pressure was used to control the reaction temperature. Therefore, the effects of temperature and pressure on the process are *convoluted*. It is in fact the effect of the system pressure not the temperature that is influencing the global rate of reaction over the range of temperature and pressure investigated.

Figure 7-5 shows the effects of the system pressure and reboiler duty on the reflux flow rate. As expected, an increase in the reboiler duty resulted in an increase in the reflux flow rate. However, the system pressure has a more significant effect on the reflux flow rate. The reflux flow rate was much higher for the condition corresponding to the lower system pressure. This is due to the

inverse pressure dependence of the equilibrium distribution coefficients, which reflect the propensity of species to remain in the condensed matter phase at elevated pressure. Therefore, lower vapour flow rates and hence lower reflux flow rates are observed for conditions of high system pressure (and temperature) while high vapour and liquid flow rates within the CD column are observed for conditions of low system pressure (and temperature).

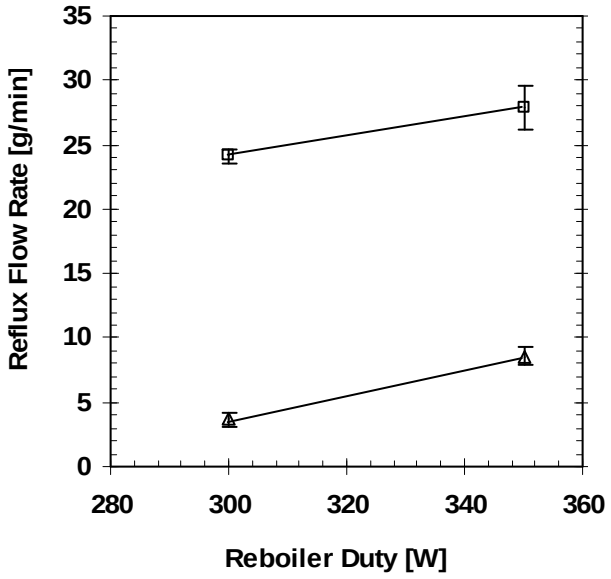


**Figure 7-5** ($Q_R$ x P) Two factor interaction plot showing the effects of pressure (P) and reboiler duty ($Q_R$) on the reflux flow rate: [(□) = 0.32 MPa, 101°C; (△)=0.46 MPa 114 °C] Reprinted from O'Keefe et al.[63]♠ *The 95% confidence bounds on the reflux flow rate are indicated by vertical bars.*

A process interaction is also evident from the data of Figure 7-5, whereby the effect of the reboiler duty on the reflux flow rate is dependent on the system pressure. A step change in the reboiler duty from 300 to 350 W at a system pressure of 0.46 MPa (condition 2 vs. 3) resulted in a relative increase in the reflux flow rate by 135% and the MO productivity by 13%. However, a step change in the reboiler duty from 300 to 350 W at a system pressure of 0.32

♠ Figure 7-5 is reprinted with permission from W.K. O'Keefe, F.T.T. Ng and G.L. Rempel (2007), *Ind. Eng. Chem. Res.*, **46(3)**, pp. 716-725. © 2007 American Chemical Society

(condition 5 vs. 4) resulted in a marginal increase in the reflux flow rate by 16% along with a slight increase in the MO productivity by less than 5%.

The data presented in Table 7-4 shows that the selectivity to MO (and IMO) was constrained to a narrow window from about 83 to 90% (wt%) for this CD process using Amberlyst 15 as a catalyst. This is due to a balance between competing reactions. When the CD process was operated at the low temperature (101°C) and low system pressure (0.32 MPa), relatively high reflux flow rates were achieved. Consequently, the MO productivity was maximized. In addition, the high reflux flow rate reduced the residence time of MO in the reaction zone. A combination of a low residence time and low reaction temperature mitigated the formation of phorone, isophorone, mesitylene and other higher molecular weight products from the consecutive reactions involving MO. However, the low reaction temperature and high liquid flow rates in the CD column resulted in the production of a large amount of unreacted DAA in the reboiler product stream. For conditions of high reaction temperature (114°C) and high system pressure (0.46 MPa) relatively low reflux flow rates were achieved. Consequently, the rate of MO production was diminished. Further, the relatively low liquid reflux resulted in increased residence times within the reactive section at a relatively higher reaction temperature. As a result, the consecutive reactions involving the production of phorones and mesitylene from MO became more prominent. However, the higher reaction temperature and longer residence time resulted in less unreacted DAA within the reboiler product.

The data in Table 7-4 show that the MO productivity was maximized for conditions of low reaction temperature and high reflux flow rate. However, the selectivity was maximized in condition #2 for which the reaction temperature (114°C) and residence time were maximized and the reflux flow rate was minimized (3.64 g/min). This result suggests that higher reaction temperatures would be more favourable for highly efficient MO synthesis. This is not

surprising since the dehydration of DAA is an endothermic reaction. Autoclave experiments using Amberlyst 15, presented in Chapter Four, show that although the equilibrium concentration of DAA is very low, the equilibrium establishes rapidly. In contrast the DAA dehydration reaction is slow relative to the acetone dimerization and takes several hours to reach equilibrium.

Probably the most interesting observation of this experiment is revealed in Figure 7-3, in which there is clear and direct evidence which demonstrates that in general, by using CD technology, the productivity of a desired intermediate may be enhanced while simultaneously minimizing the rate of undesirable consecutive reactions. In this case the productivity of MO was maximized while simultaneously minimizing the production of phorone, mesitylene and isophorone produced from the consecutive reactions involving MO by exploitation of the transport phenomena in the CD process.

The change in the acetone feed rate did not have a significant effect on the MO productivity or selectivity. This is expected since the global reaction rate was found to be governed by the liquid flow rate in the column. The acetone feed rate was negligible in comparison to the internal liquid flow rate within the CD column and thus did not significantly affect the reaction rate. In order to maintain steady state operation, the rate of removal of product from the reboiler must be equivalent to the acetone mass flow rate. Therefore, an increase in the acetone feed rate simply resulted in an increase in the concentration of unreacted acetone in the reboiler product stream. Thus, the acetone feed rate affects the concentration of MO and other species in the reboiler product and therefore governs the chemical conversion of the unit operation.

This pilot scale experiment highlights a unique advantage of CD technology from which it gains its greatest utility. The continuous removal of product from the reactive section shifts the equilibrium in favour of product formation in accordance with Le Chatelier's principle. As a result, conversions

much higher than the theoretical equilibrium conversion may be achieved. The synthesis of MO from acetone is an equilibrium limited reaction. Klein and Banchero[10] developed a relation which affords the calculation of the equilibrium constant ($K_c$) as a function of temperature and acetone and MO concentration. This relation predicts an equilibrium MO concentration of 1.36 M at 100°C. Assuming a mixture density of acetone (0.79 g/cc), this implies an equilibrium conversion of 20 %. The data in Table 7-4 shows that the theoretical equilibrium conversion was exceeded in every experimental condition except the first condition (19 %). Although steady state was not fully achieved in condition number 7, this result demonstrates that a reboiler product essentially free of acetone ( < 0.001 wt%) could be achieved. In other words, the results demonstrate that essentially 100 % conversion could be achieved for an equilibrium limited reaction.

Empirical Process Model

The data acquired in this CD experiment can be conveniently reduced into empirical equations which accurately represent the data sets. These models provide insight into the main effects and interactions of the CD process parameters on the global reaction rate and product distribution. The maximum likelihood estimates of the model parameters were obtained via non-linear regression analysis of the steady state data obtained from conditions 2 through 6 (Q=800 W) using NLREG v.5.4 (Sherrod Software). One obvious outlier in the measurement of the reflux flow rate was rejected out of 27 observations. The parameter estimates, their 95% confidence intervals, their corresponding t statistics are outlined in Table 7-5. The regression statistics are summarized in Table 7-6.

Knowledge of the liquid reflux flow rate is necessary and sufficient to accurately predict the product distribution and reaction rates over the range of reaction conditions investigated and for the reactor configuration, dimensions and catalyst specified in this experiment. The data in Figure 7-5 shows that the

reflux flow rate is dependent on the system pressure as well as the reboiler duty and reveals a process interaction between these variables. The process interaction manifests mathematically as a non-linear term involving the product of the pressure (P) and reboiler duty ($Q_R$) in the non-linear regression model is given by equation (7-8). The author and co-workers[63] have previously disclosed this model (Eqn. 7-8), which was developed from the analysis of the 2x2 factorial design experiments of conditions 2 through 5 which was designed specifically for the investigation of the main effects and interactions of the system pressure and reboiler duty on the CD process. However, it was found that inclusion of the data of condition 6 in the regression analysis improves the significance of the regression and increases the utility of the model since the acetone feed rate span a greater range. Consequently, the parameter estimates and regression statistics for the model of equation (7-8) reported in Table 7-5 and 7-6 are based on all 31 steady state data observations from conditions 2 through 6 for which the external heater duty was 800W with the one obvious outlier in the measurement of reflux flow rate being rejected from the analysis. The t-statistic (t= -10.62, prob(t) < 0.00001) for the parameter $\beta_3$ in table 7-5 confirms that the process interaction between the system pressure and reboiler duty is statistically significant and that the interaction term should be retained in the model.

$$L = \beta_1 Q_R + \beta_2 P + \beta_3 Q_R P \qquad (7\text{-}8)$$

Equation (7-9) is an empirical model which accurately predicts the experimentally measured average steady state MO and IMO productivity as a function of the average steady state reflux flow rate. As illustrated in Figure 7-3, the MO productivity increases non-linearly with reflux flow rate for the conditions investigated. The average steady state DAA productivity increases linearly with the average reflux flow rate ($R^2$=0.999) as illustrated in Figure 7-3. The DAA productivity is given by equation (7-10). Higher molecular weight species produced from the consecutive reactions of MO were found to decrease

non-linearly with reflux flow rate as illustrated in Figure 7-3. These products, when lumped together, have a average steady state productivity given by equation 7-11.

$$\frac{d\hat{C}_{MO}}{dt} = \beta_4 L^{\beta_5} \qquad (7\text{-}9)$$

$$\frac{d\hat{C}_{DAA}}{dt} = \beta_6 + \beta_7 L \qquad (7\text{-}10)$$

$$\frac{d\hat{C}_{C6^+}}{dt} = \beta_8 + \beta_9 L + \beta_{10} L^2 \qquad (7\text{-}11)$$

**Table 7-5** Regression statistics for empirical models[♣]

| **Equation** | **$R^2$** | **Standard error of estimate [g/min][a] [g/(hr*mL$_{cat}$)][b]** | **F** | **Prob(F)** |
|---|---|---|---|---|
| (8-7)[a] | 0.9868 | 1.304 | 1045 | < 0.00001 |
| (8-8)[b] | .9720 | 0.003086 | 104.3 | 0.00200 |
| (8-9)[b] | 0.9986 | 0.0005139 | 2158 | 0.00002 |
| (8-10)[b] | 0.9931 | 0.0002170 | 144.0 | 0.00690 |

**Table 7-6** Parameter estimates and statistical significance for empirical models of the CD process for MO synthesis [♣]

| Parameter | Equation | Maximum Likelihood Estimate 95% confidence interval | T | Prob(t) |
|---|---|---|---|---|
| $\beta_1$ | (8-7) | 0.2314 ± 0.0084 | 56.45 | < 0.00001 |
| $\beta_2$ | (8-7) | -0.3337 ± 0.1206 | -5.67 | <0.00001 |
| $\beta_3$ | (8-7) | -0.002146 ±0.000413 | -10.62 | < 0.00001 |
| $\beta_4$ | (8-8) | 0.1252 ± 0.0124 | 32.02 | 0.00007 |
| $\beta_5$ | (8-8) | 0.1053 ± 0.0341 | 9.82 | 0.00224 |
| $\beta_6$ | (8-9) | 0.006568 ± 0.001477 | 14.15 | 0.00076 |
| $\beta_7$ | (8-9) | 0.0009891 ± 0.0000678 | 46.46 | 0.00002 |
| $\beta_8$ | (8-10) | 0.007736 ± 0.001543 | 21.58 | 0.00214 |
| $\beta_9$ | (8-10) | -0.0004854 ± 0.0002641 | -7.91 | 0.01562 |
| $\beta_{10}$ | (8-10) | $1.006 \times 10^{-5} \pm 5.865 \times 10^{-7}$ | 5.62 | 0.03020 |

## 7.5 MIBK Synthesis via CD Utilizing Commercially Available Catalysts (CD 002)

Design of Experiment and Overview of Results

The objective of the second CD experiment was to conduct the one-step synthesis MIBK from acetone in a single CD column using commercially available catalysts in order to obtain a process benchmark as well as to gain a cursory assessment of the main effects and process interactions on the product yield, the product distribution and catalyst activity under realistic conditions of space time yield in the low interaction regime of trickle flow for significant time on stream at the pilot plant scale.

Two reactive sections containing two distinct catalysts were used in this experiment. 135.0 mL of Amberlyst 15, which had been swelled for 24 hours in

[♣] Data in Tables 7-5 and 7-6 reprinted in part with permission from W.K. O'Keefe, F.T.T. Ng and G.L. Rempel, *Ind. Eng. Chem. Res.* **46(3)**, pp. 716-725, © 2007 The American Chemical Society

acetone, were loaded into 8 stainless steel wire mesh bundles as described previously. 6 catalyst bundles were loaded into the top reactive section (Figure 8-1). Two catalyst bundles were installed at the top of the bottom reaction section. Beneath these two catalyst bundles, 4 wire mesh bundles containing 50.1 g of a 0.52 wt% $Pd/Al_2O_3$ hydrogenation catalyst consisting of cylindrical extrudates 3.23 mm dia. x 3.27 mm in length. The hydrogenation catalyst was reduced *ex situ* in hydrogen at 350°C for 3 hours and transferred into the CD column while under a nitrogen blanket. The Amberlyst 15 was swelled in acetone rather than 2-propanol, since 2-propanol is an expected minor product of the MIBK synthesis and residual 2-propanol introduced with the catalyst may introduce uncertainty in the measurement of the 2-propanol.

The process conditions investigated in this experiment are outlined in Table 7-7. The process variables investigated included the volumetric flow rate of hydrogen; the acetone feed rate and the reaction zone temperature. The effect of temperature is convoluted with the effect of system pressure since these variables can not be independently specified. Since the synthesis of MO was shown in the previous experiment to be a liquid limited reaction, the reboiler duty and external heater duties were maximized at 350 and 800 W respectively and kept constant as noise variables in this experiment.

This experiment was carried out in order to obtain a cursory assessment of the effects of the major process parameters on the MIBK yield and to assess the catalyst performance under realistic conditions of trickle flow and space velocity for a substantial time on stream. Only a few select process conditions were investigated. The experiment consisted of select step changes in the major process parameters. Since this was the first time ever that a hydrogenation experiment was carried at the pilot scale in a catalytic distillation column at the University of Waterloo, the process was operated at a very low volumetric flow rate of hydrogen (3.6 L/h at STP) for the first 39 hours TOS (i.e. almost half of the experiment). The hydrogen flow rate was gradually increased only after

visual inspection and measurement of the ambient conditions using gas sensors confirmed that no hydrogen leaks were present and only after experience with the process had been obtained. The composition of the reboiler product stream as a function of time on stream is given in Figure 7-6. Within this figure, the periods of steady state operation are bounded by vertical lines and labelled accordingly. The steady state reboiler product compositions are summarized in Table 7-8. The acetone conversion, MIBK productivity, the MO conversion and the hydrogenation selectivity are summarized in Table 7-9.

**Table 7-7** Process conditions investigated in the second CD experiment [$Q_R$=350 W, Q=800 W]

| Trial | Rxn Temp [°C] | System Pressure [MPa] (abs) | Acetone Feed Rate [mL/h] | $H_2$ Feed Rate [L/h @STP] |
|---|---|---|---|---|
| 1 | 110 | 0.42 | 35 | 3.62 |
| 2 | 110 | 0.44 | 150 | 20.0 |
| 3 | 110 | 0.46 | 150 | 60.0 |
| 4 | 119 | 0.60 | 150 | 60.0 |

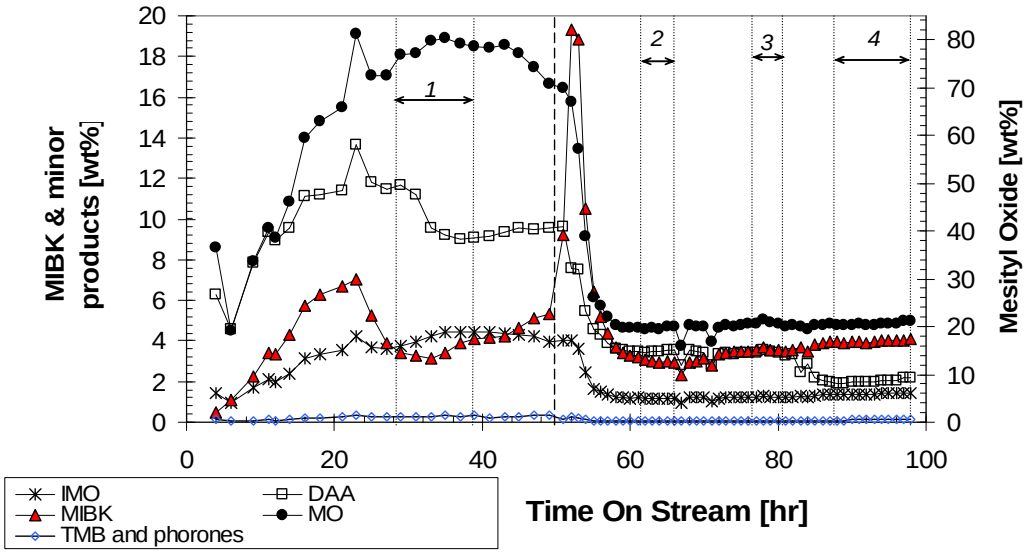


**Figure 7-6** Reboiler product composition as a function of time-on-stream Reprinted from O'Keefe et al.[63]♠

♠ Figure 7-6 rreprinted with permission from W.K. O'Keefe, F.T.T. Ng and G.L. Rempel (2007), *Ind. Eng. Chem. Res.*, **46(3)**, pp. 716-725. © 2007 American Chemical Society

**Table 7-8** Steady state concentration of organic species in the reboiler product

| Trial | MO [wt%] | IMO [wt%] | DAA [wt%] | TMB [wt%] | IPO [wt%] | Unknown $C_6^+$[wt%] | MIBK [wt%] | IPA [wt%] |
|---|---|---|---|---|---|---|---|---|
| 1 | 78.7 | 4.21 | 9.95 | 0.17 | 0.08 | 1.01 | 3.53 | 0.11 |
| 2 | 19.1 | 1.15 | 3.38 | 0.05 | 0.00 | 0.22 | 2.88 | 0.17 |
| 3 | 20.7 | 1.23 | 3.45 | 0.05 | 0.00 | 0.26 | 3.57 | 0.26 |
| 4 | 20.6 | 1.19 | 2.02 | 0.13 | 0.00 | 0.33 | 2.98 | 0.44 |

**Table 7-9** Steady state conversion, MIBK productivity and hydrogenation selectivity.

| Trial | Acetone Conversion $X_{Ac}$ [%] | MO Conversion $X_{MO}$ [%] | MIBK Productivity [g/(hr*$g_{cat}$)] | Hydrogenation Selectivity [mol%] |
|---|---|---|---|---|
| 1 | > 99 | 4.00 | 0.0199 | 94.9 |
| 2 | 30.4 | 12.2 | 0.0738 | 90.9 |
| 3 | 33.3 | 13.8 | 0.0820 | 89.2 |
| 4 | 32.8 | 15.1 | 0.0963 | 84.4 |

*The MO conversion is defined in Eqn. (7-12) and the hydrogenation selectivity is defined in equation (7-13) The Acetone conversion was defined in Eqn. (7-4)*

$$X_{MO} = 100\% \left( \frac{F_{MIBK}}{F_{MIBK} + F_{MO} + F_{IMO}} \right) \tag{7-12}$$

$$S = 100\% \left( \frac{F_{MIBK}}{F_{MIBK} + F_{IPA}} \right) \tag{7-13}$$

It is clear from the results in Figure 7-6 and Tables 7-8 and 7-9 that the hydrogenation step is currently limiting the CD process for MIBK synthesis. The proportion of MO which was successfully converted to MIBK ranged from only 4 to 15%. The MIBK productivity was relatively low ranging from 0.02 to 0.10 [g/hr*$g_{cat}$)]. The latter result seems comparable to the results obtained by Lawson and Nkosi[32] who achieved a maximum average MIBK productivity of 0.10 [g/(hr*$mL_{cat}$)] operating in batch mode with a multifunctional catalyst. No

higher molecular weight products from the hydrogenation of MIBK such as MIBC or from reaction of MIBK with acetone such as di-isobutyl ketone were observed in this experiment. However, the direct hydrogenation of acetone to produce 2-propanol (IPA) was found to be a significant competing reaction which greatly affected the hydrogenation selectivity. The 2-propanol concentration was relatively low and omitted from Figure 8-6 for clarity.

Initially, the CD reactor was operated under conditions which maximized the acetone conversion. The acetone feed rate was minimized at 35 mL/h and the reaction zone temperature was 110°C. The hydrogen flow rate was 3.6 L/hr (STP). 0 hr TOS corresponded to the time that the reboiler was first energized. Reflux within the CD column was established by 2 hrs TOS. This first condition resulted in a mass fraction of MO of about 78 wt% in the reboiler. During the initial transient start up period, the MIBK concentration in the product stream increased along with the MO concentration. However, after around 23 hr (TOS), the MIBK concentration began to decrease without any changes to the process being made. This appears to have occurred as a consequence of deactivation of the hydrogenation catalyst.

The MIBK and MO concentrations stabilized after about 29 hours and remained stable for the next 10 hours as the data from steady state condition number 1 was collected. However, this condition did not strictly meet our previous definition of steady state since the variation in the concentrations of minor compounds, particularly DAA were found to be in excess of 5% RSD. After the data from condition number 1 was collected, the volumetric flow rate of hydrogen was slowly increased from 3.6 to 20 L/hr (STP) over the period from 39.0 to 42.3 h (TOS). During this time there was no measurable effect on the MIBK productivity as a result of the increase in the hydrogen flow rate. At 45 hr TOS, the MIBK concentration in the reboiler product appears to begin to increase while the MO concentration appears to decrease. At 49 hrs TOS, the reboiler product had become cloudy. At 50 hr TOS, there was a two phase

mixture in the reboiler sample as an aqueous phase had separated from the organic phase.

At this point (50 h TOS) it was decided to explore a different process condition with a lower acetone conversion. The acetone feed rate was increased to 150 mL/hr. This change in the acetone feed rate is indicated in Figure 7-6 by a vertical dashed line. As a consequence of this process change, a single organic phase in the reboiler product was restored by the time steady state was achieved. Subsequent process changes had marginal effects on the product distribution. The most notable change occurred between condition 3 and 4 for which the reaction temperature and system pressure were increased from 110°C to 120°C and 0.46 to 0.60 MPa respectively. As a result, the MIBK productivity increased by 17% and the DAA concentration in the reboiler decreased by 41% due to the higher reaction temperature.

Catalyst Deactivation and the Apparent Effect of Acetone Feed Rate

The data in tables 7-7 and 7-9 suggest that the step change in the acetone feed rate from 35.0 to 150 mL/hr had the greatest effect on the MIBK productivity. The MIBK productivity increased by a factor of 3.7 after the acetone feed rate was increased by a factor of 4.3. This result was unexpected. The previous CD experiment had clearly demonstrated that changing the acetone feed rate did not appreciably affect the rate of production of the MO, since the acetone feed rate is small compared to the liquid reflux flow rate within the CD column. An increase in the acetone feed rate simply results in a greater amount of unreacted acetone in the reboiler product. Therefore, a change in the acetone feed rate should not affect the rate of MIBK production, since it is not affecting the productivity of the precursor, MO.

The apparent effect of the acetone feed rate on the MIBK productivity can be explained in terms of the catalyst activity and catalyst utilization before and after the step change in the acetone feed rate. Specifically, the experimental

evidence indicates that the hydrogenation catalyst had deactivated to some extent during the CD run. A change in the acetone feed rate appears to have coincided with a regeneration of the hydrogenation catalyst.

The data in Figure 7-6 shows that without any process changes being made, the MIBK concentration in the reboiler product dropped from around 7.1 to 3.3 wt% over the period from 23 to 29 h TOS during the transient start up. This suggests that the hydrogenation catalyst had deactivated by over 50% during the transient start up period. This is not surprising since the acetone conversion and residence time in the reactor were maximized under these conditions and the volumetric flow rate of hydrogen was minimal. The hydrogenation catalyst was exposed to very high concentrations of phorone, mesitylene and isophorone as well as water during this time.

Figure 7-7 shows the MIBK productivity and condenser duty as a function of time-on-stream. Immediately prior to the increase in the acetone feed rate, the MIBK productivity increased dramatically. About 1/3 of all of the MIBK produced in this 99 hour experiment was produced in a 7 hour period of unsteady operation from around 49 to 56 h TOS, corresponding to the large pulses in MIBK concentration and MIBK productivity in Figures 7-6 and 7-7 respectively. During this transient period that followed after the acetone feed rate was increased, the MO, IMO and DAA concentrations decrease monotonically to new steady state values, as expected, as the proportion of unreacted acetone in the reboiler product increased. However, instead of decreasing to a new steady state concentration, the MIBK concentration first increased to a maximum of 19.3 wt% at 52 h TOS before decreasing to a new steady state value. The trends of the minor products are less clear. However, the 2-propanol mass fraction was observed to increase from 0.11 wt% at 49 h TOS to 0.57 wt% at 53 h TOS before decreasing to its final steady state value. Isophorone was observed to increase from 0.09 wt% at 49 h TOS to 0.19 wt% at 53 h TOS before dropping to a new steady state concentration which was below

the peak area rejection limit of the GC. Mesitylene and other phorones did not show any evidence of increasing in concentration during this transient period.

A mass balance about the CD column indicates that a far greater number of moles of MIBK were produced during the transient interval from 49 to 56 h TOS than could be accounted for due to the decrease in the MO concentration. This suggests that the increase in MIBK concentration was not due to a rapid increase in the rate of hydrogenation. Rather, a large quantity of MIBK, which had been accumulating in the reactor, was eluted from the system during this transient interval.

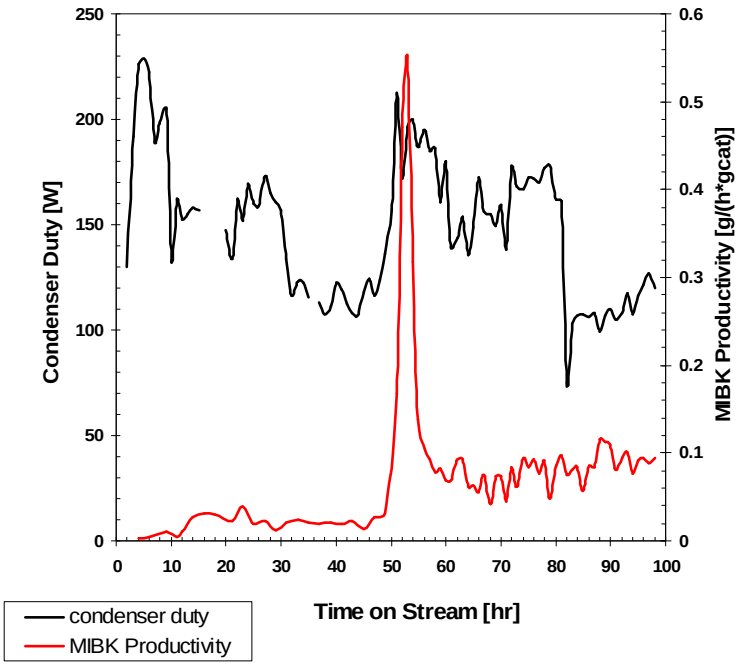


**Figure 7-7** MIBK productivity and condenser duty as a function of time on stream. Reproduced from O'Keefe et al.[63]♠

♠ Figure 7-7 reprinted with permission from W.K. O'Keefe, F.T.T. Ng and G.L. Rempel. (2007), *Ind. Eng. Chem. Res.*, **46(3)**, pp. 716-725. Used by permission of the American Chemical Society © 2007 American Chemical Society

Figure 7-7 reveals that the condenser duty increased dramatically at around 48 h TOS, immediately prior to the elution of the large pulse of MIBK the system, due to some unknown perturbation. This demonstrates that the liquid reflux flow rate increased dramatically, immediately prior to the elution of the large quantity of MIBK. It is likely that the significant increase in the liquid reflux flow rate resulted in the desorption and removal of MIBK and other species which had accumulated in the reactive section. The increased liquid flow rate would result in increased mass transfer rates, including the rate of removal of species from the catalyst to the bulk liquid. The results suggest a profound change in the column hydrodynamics occurred such as a change in the flow pattern or the extent of catalyst wetting. The data in Figure 7-7 shows that the catalyst activity remained elevated for the remainder of the experiment after the elution of the large pulse of MIBK as evidenced by MIBK productivities about 4 to 5 times greater than the MIBK productivity prior to the elution of MIBK. This suggests that the active sites of the hydrogenation catalyst were regenerated due to the change in the column hydrodynamics and or due to the rapid removal of higher molecular species from the system due to the increased space velocity.

Catalyst Activity Testing in an Autoclave Reactor

At the end of the CD experiment, the hydrogenation catalyst was recovered from the CD reactor under nitrogen blanket and transferred into acetone solvent so that the activity of the recovered catalyst could be ascertained. Approximately 1g of catalyst was transferred to a 300 mL Parr autoclave while in nitrogen environment in a glove bag. Approximately 120 g of CD product obtained from the first CD run consisting of 20.3 wt% MO was used as the reactant mixture. The autoclave was heated to 100°C and pressurized to a total system pressure of 4.13 MPa. The hydrogenation of the MO mixture was monitored with liquid samples being obtained periodically and analyzed by GC/FID. The experiment was repeated using fresh catalyst. Assuming the reaction was first order with respect to MO, the pseudo rate constants were

obtained from the analysis of the semi-log plots in Figure 7-8 and were normalized by the catalyst and reactant masses. The activity of the recovered catalyst is given by equation (7-14). The fresh catalyst has an activity of unity.

$$a(t) = \frac{k'_s C_{MO}(t)}{k'_0 C_{MO}(t)} = \frac{k'_s}{k'_0} \qquad (7\text{-}14)$$

An induction period over the first 60 to 80 minutes of reaction is evident in Figure 7-8 in the case of the hydrogenation of MO using spent catalyst. The catalyst activity obtained from the slope of the semi-log plots over the interval from 0 to 80 minutes was 0.302 relative to the fresh catalyst.

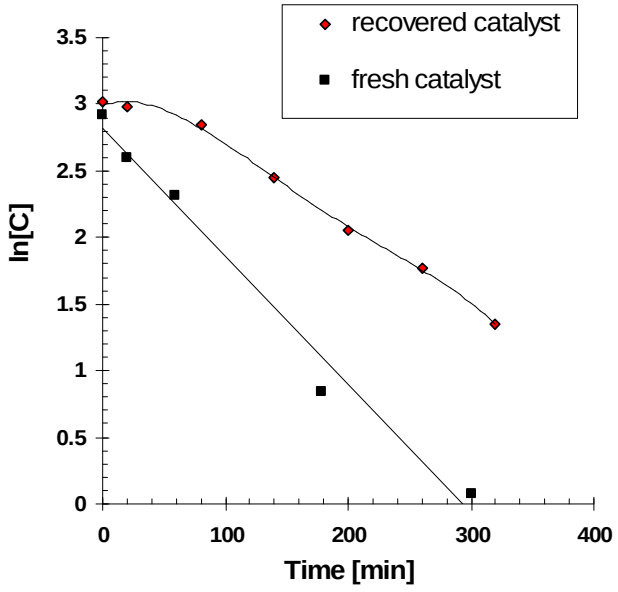


**Figure 7-8** Semi-log plot of the logarithm of the MO concentration [wt%] versus time for spent and fresh catalyst for MO hydrogenation [T=100°C, W= 1g, P=4.13 MPa]. Reprinted from O'Keefe et al.[63]♠

♠ Figure 7-8 and 7-9 reprinted with permission from W.K. O'Keefe, F.T.T. Ng and G.L. Rempel (2007), *Ind. Eng. Chem. Res.*, **46(3)**, pp. 716-725. Used by permission of the American Chemical Society © 2007 American Chemical Society

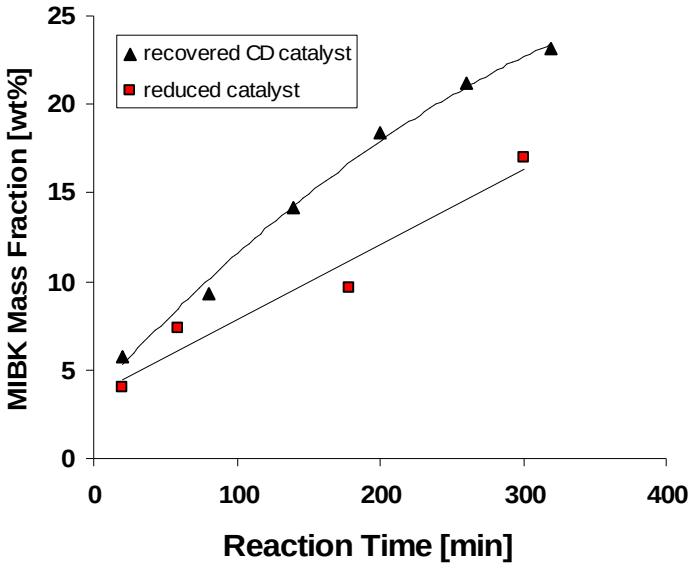


**Figure 7-9** MIBK mass fraction in the autoclave for the hydrogenation of MO in the CD product mixture [T=100°C, W=1g, P=4.13 MPa]

However, after the induction period, the catalyst activity was 0.826. Figure 7-8 shows that the hydrogenation of MO proceeded far more rapidly using the fresh catalyst, as expected. However, Figure 7-9 shows that a much greater amount of MIBK was present in the product mixture for the case in which the spent catalyst was used. In the case of the spent catalyst, a significant amount of the MIBK detected in the autoclave experiment was likely already adsorbed on the catalyst at the time it was recovered from the CD reactor and was introduced into the autoclave system along with the catalyst.

The results of the autoclave experiment suggest that the catalyst had lost up to 70% of its initial activity, probably due to poisoning from the adsorption of MIBK and other species. However, this deactivation appears to be partially reversible as evidenced by an activity of .826 observed after an induction period of about 1.5 hours in the autoclave.

DRIFT Spectroscopy

It is evident that the hydrogenation catalyst had deactivated to some extent due to poisoning from the strong adsorption of one or more products including possibly MIBK. The GC data from the CD run also shows that during the transient interval from 49 to 56 h TOS, the isophorone concentration also increased before decreasing to its final steady state value. It appears that ketones interact with the $Pd/Al_2O_3$ catalyst. The author and co-workers[64] have investigated the adsorption/desorption properties of MO, MIBK and acetone on the $Pd/Al_2O_3$ catalyst and have confirmed via spectroscopic methods that the ketones, acetone and MIBK interact very strongly with this catalyst.

The hydrogenation of MO was carried out in situ in the IR cell of a Bio-Rad Excalibur spectrometer and was found to be facile proceeding readily at ambient temperature.[64] The top half of Figure 7-10 shows the adsorption of MO onto fresh $Pd/Al_2O_3$ catalyst in a series of 10 s pulses at 25°C. The catalyst had been reduced in situ in hydrogen at 120°C for 1 hour. For the adsorbed MO, the bands at 1677 $cm^{-1}$ and 1610 $cm^{-1}$ represent the carbonyl and olefin groups respectively in the conjugated system adsorbed on the catalyst. These frequencies are notably shifted relative to that of gaseous MO (1690 $cm^{-1}$ and 1620 $cm^{-1}$) which indicates that MO is molecularly adsorbed on the catalyst. The bands at 2982 $cm^{-1}$ and 2920 $cm^{-1}$ correspond to asymmetric and symmetric $\nu(CH_3)$ stretching vibrations. The $\delta$(CH3) bending vibrations are observed over the range of 1350 to 1470 $cm^{-1}$. The frequencies of the CH stretching and bending vibrations are shifted for MIBK. The band at 1226 $cm^{-1}$ corresponds to the coupling of (CCC) stretching and bending vibrations.

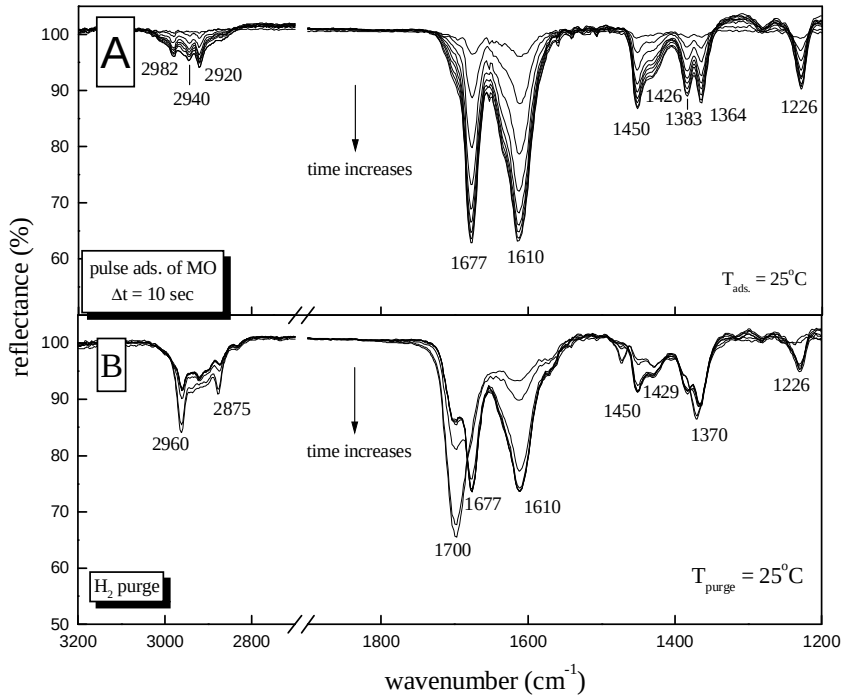


**Figure 7-10** DRIFT spectra of (A) MO adsorbed in 10 s pulses onto a 0.5 wt% $Pd/Al_2O_3$ followed by (B) *in situ* hydrogenation via successive pulses of hydrogen of 10 s duration at 25°C. Reprinted from M. Jiang and F.T.T. Ng[216] used by permission

Figure 7-10 shows that as hydrogen is introduced to the IR cell, the band at 1610 $cm^{-1}$ corresponding to the olefin group disappears while the band associated with the carbonyl group shifts from 1677 to 1700 $cm^{-1}$ which is characteristic of the carbonyl bond stretching of a ketone. Also, the CH stretching vibrations become more intense. It can be concluded from Figure 8-10 that the hydrogenation of MO is facile and proceeds readily, even at ambient temperatures.

Figure 7-11 illustrates the desorption characteristics of MIBK from the $Pd/Al_2O_3$ catalyst. Since the intensities of the in situ spectra are proportional to the amount of MIBK adsorbed on the catalyst, the desorption spectra of Figure 7-11 demonstrate that even at 200°C, MIBK remains strongly adsorbed on the catalyst. Similar spectra were obtained for acetone adsorbed on $Pd/Al_2O_3$.[64] In

addition, similar desorption spectra were obtained for MIBK on $\gamma$-$Al_2O_3$ without Pd. Therefore, it can be concluded that ketones strongly adsorb onto the $Pd/Al_2O_3$ catalyst, most likely as a consequence of the strong interaction of the ketone group with Lewis acid sites on the alumina support.

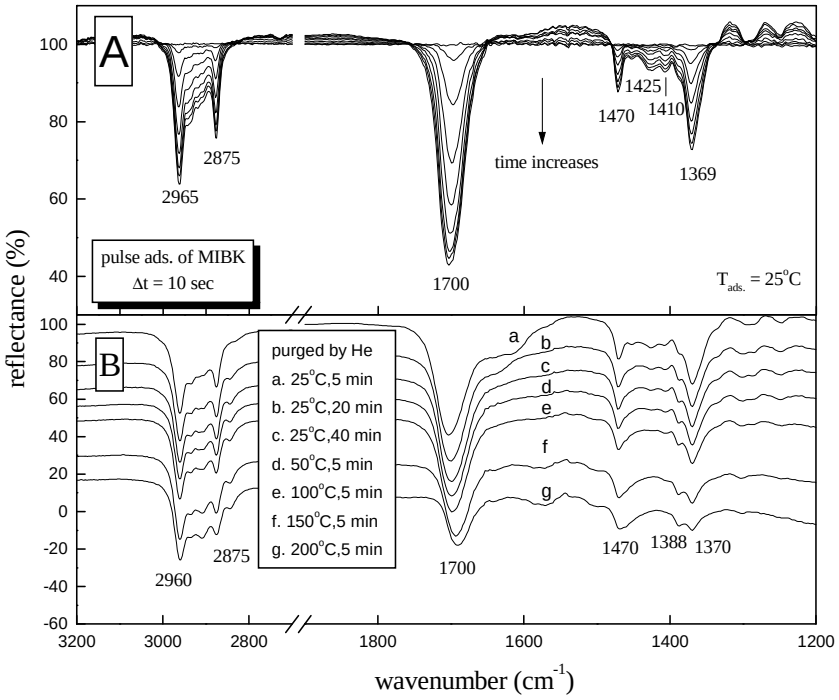


**Figure 7-11** (A) in situ DRIFT spectra of MIBK adsorbed onto a $Pd/Al_2O_3$ catalyst in successive pulses of 10 s duration at 25°C (B) in situ DRIFT spectra of MIBK desorption from a $Pd/Al_2O_3$ catalyst as the temperature is increased to 200°C. Reprinted from M. Jiang and F.T.T. Ng[216]; used by permission

Effect of Hydrogen Flow Rate and Reaction Temperature and Pressure

After the acetone feed rate had been increased and a single organic phase in the reboiler product had been restored, the effects of hydrogen feed rate and reaction temperature were investigated as outlined in Table 7-7. The hydrogen feed rate was increased from 20 to 60 L/hr (STP) between conditions 2 and 3 while the reaction temperature was increased from 110 to 119°C between conditions 3 and 4. The results in Tables 7-8 and 7-9 show that increases in these variables had weak positive effects on the MIBK productivity and had negative effects on the selectivity of the MO hydrogenation. An increase in

the hydrogen flow rate from 20 to 60 L/hr (STP) resulted in an 11.1% increase in the MIBK productivity while an increase in the reaction temperature from 110 to 119°C, as well as an increase in the total system pressure from 0.46 to 0.60 MPa (absolute) resulted in a 17.4 % increase in the MIBK productivity. The highest MIBK productivity obtained in this experiment 0.0963 [g/hr*$g_{cat}$] is comparable to the highest MIBK productivity obtained in the batch CD experiment of Lawson and Nkosi[32] 0.10 [g/hr*mL].

It is evident from the results in Tables 7-8 and 7-9 that the hydrogenation of MO was the controlling step in the CD process as evidenced by relatively low MO conversions ranging from 4 to 15 mol %. The fact that the MIBK productivity is a function of the hydrogen mass flow rate suggests an external mass transfer limitation with respect to hydrogen transport. The hydrogen uptake efficiency of this experiment was less than 2% for conditions 3 and 4 for which the hydrogen feed rate was maximized and was 6.6 % for condition 1, for which the hydrogen feed rate was minimized. For comparison, the hydrogen uptake efficiencies for the best experimental conditions for MIBK synthesis via CD outlined in the patents by Lawson and Nkosi[32] as well as Schmitt et al.[20] were 4.1 and 10.7 % respectively. The hydrogen uptake efficiency defined in equation 7-15 is the proportion of the number of moles of hydrogen fed to the reactor, expressed as a percentage, which participates in hydrogenation reactions. This proportion is calculated from the known hydrogen feed rate, the concentrations of hydrogenation products in the reactor effluent streams and the stoichiometric relationships.

$$\eta = 100\% \left[ \frac{\sum_i \alpha_i n_i}{n_{H_2}} \right] \qquad (7\text{-}15)$$

The results in tables 7-8 and 7-9 also show that the selectivity of the MO hydrogenation decreases as the conditions become more favourable for MIBK

synthesis. Previously, the author and co workers[18] have demonstrated that MO and acetone compete for the same hydrogenation sites and that for a given Pd loading, the MO hydrogenation selectivity decreases with decreasing MO concentration. Since a two reaction zone approach was utilized in this experiment, an increase in the rate of MIBK production from an increase in hydrogen feed rate, increased system pressure or increased reaction temperature would not result in a significant increase in the MO concentration at the hydrogenation catalyst active sites. Conversely, the increased conversion of MO would result in a decrease in the steady state MO concentration at the hydrogenation catalyst active sites. Thus, a decrease in the MO hydrogenation selectivity would be expected. From the results of experiments presented in Chapter Six, it is now known that the optimal Pd loading is about an order of magnitude, lower (ca. 0.04 wt% Pd) than the catalyst used in this experiment (0.5 wt%).

### 7.6 Conclusions and Recommendations

Two preliminary pilot scale CD experiments were carried out in order to obtain process benchmarks and cursory assessments of the syntheses of MO and MIBK from acetone. For the synthesis of MO via CD, the MO productivity and the product distribution were found to be governed by the liquid reflux flow rate, which suggests either an external mass transfer limitation or reflects a dependence on the external catalyst wetting efficiency or most likely a combination of both.

Using Amberlyst 15 as a catalyst, the selectivity to MO was constrained to a narrow range of 83 to 90 wt% due to an apparent balance between the rates of DAA dehydration and the consecutive reactions for which MO is a precursor for the reaction conditions investigated. The condition of high reflux flow rate and low system pressure and temperature resulted in the MO productivity being maximized and the rate of consecutive reactions to produce phorones and other

high molecular weight species being minimized. However, a greater proportion of unreacted DAA was present in the reboiler product stream for this condition. The condition of low reflux flow rate and high temperature and high system pressure resulted in much less unreacted DAA in the reboiler product. However, the MO productivity was minimized and the rate of undesirable consecutive reactions to produce higher molecular weight products was greater due to the higher temperatures and longer residence time in the reaction zone. For this condition, the MO selectivity was maximized.

The results demonstrate that in general, it is possible to enhance the productivity of a desired intermediate within a series of consecutive reactions by exploiting the transport phenomenon inherent in a CD reactor. In this case, increasing the reflux flow rate in the CD reactor resulted in an increase in the MO productivity while simultaneously reducing the concentration of phorone, isophorone, mesitylene and other undesirable high molecular weight species in the reboiler product stream. The MO productivity was maximized as the liquid reflux flow rate was maximized.

MIBK was successfully produced in a single unit operation via catalytic distillation. However, the MIBK yield was relatively low due to significant hydrogenation catalyst deactivation and exacerbated by the relatively low system pressures used to carry out the hydrogenation. The total system pressure ranged from 0.3 to 0.6 MPa absolute for this experiment. In contrast, MIBK synthesis is carried out industrially at 1 to 10 MPa. The results demonstrate that the hydrogenation of MO is currently limiting the CD process as evidenced by relatively low MO conversions from 4 to 15 mol % and suggest that the rate of transport of hydrogen to the catalyst active site is the limiting step. A weak dependence of the MIBK productivity on the hydrogen mass flow rate was observed and suggests an external mass transfer limitation with respect to hydrogen. The hydrogen uptake efficiency was less than 2% for the condition with the highest MIBK productivity.

The nature of the hydrogenation catalyst deactivation is unclear and warrants further investigation. However, spectroscopic evidence indicates that MIBK interacts strongly with the $Pd/Al_2O_3$ catalyst, likely via a strong interaction with the Lewis acid sites of the alumina support. This may lead to product inhibition and promote coke formation. The data obtained from the activity testing of the spent hydrogenation catalyst in an autoclave reactor suggest that MIBK had accumulated on the catalyst and may have lead to product inhibition. The catalyst activity was found to increase after an induction period during which time MIBK and other products desorbed from the catalyst. The pilot plant data also demonstrate that MIBK had accumulated in the reactive section throughout the course of the experiment. The hydrogenation catalyst activity was enhanced after the elution of a large transient pulse of MIBK from the reactive section during a change in the process conditions. This not only suggests product inhibition had occurred but also highlights the importance of CD reactor hydrodynamics on the process performance. Consequently an improved understanding of role of hydrodynamics on this CD process is needed.

It is evident that improved catalyst performance is needed. The thermal limitations of the commercial cation exchange resin constrains the CD system pressures to less than 0.6 MPa, which is unfavourable for catalytic hydrogenation in an industrial reactor. In addition, the relatively low reaction temperature of 120°C (the maximum recommended operating temperature of Amberlyst 15) is unfavourable for DAA dehydration as evidenced by a substantial amount of unreacted DAA in the reboiler product stream. Therefore a catalyst with improved thermal stability is needed. Moreover, the selectivity of Amberlyst 15 to the precursor MO was found to be relatively low (83 to 90 wt%). Since MIBK is a relatively low value commodity, a highly efficient process for MIBK is needed. High selectivity is critical in order to avoid costly downstream refining. Therefore a highly selective catalyst which enables a chemistry more favourable for DAA dehydration is needed.

A relatively high palladium loading (0.52 wt%) for the hydrogenation catalyst resulted in a relatively low MO hydrogenation selectivity. A lower Pd loading would increase competition for active sites and give improved hydrogenation selectivity. A less acidic catalyst support such as θ-$Al_2O_3$ or more preferably an inert neutral support such as $SiO_2$ is recommended for MIBK synthesis in order to avert undesirable interactions between the organic substrates and the catalyst which could lead to product inhibition, coking or enable other undesirable reaction pathways.

# Chapter Eight

## On the Role of Water and Reactor Hydrodynamics in the One-Step Synthesis of MIBK via Catalytic Distillation

---

### 8.0 Synopsis

Three pilot scale catalytic distillation experiments (CD) were carried out utilizing a novel $Pd/Nb_2O_5/SiO_2$ catalyst developed in the first two phases of this research project in order to assess the performance characteristics of the catalyst under pilot scale conditions of trickle flow and for substantial time on stream. In the first CD experiment, the MIBK productivity was found to decrease steadily over the first day of operation until a steady state value of 0.02 [$g/hr*g_{cat}$] was achieved. Analysis of the spent catalyst showed that although the catalyst lost some activity, the low activity observed in the CD experiment was due to the reaction environment in the CD reactor rather than due to an irreversible deactivation. The catalyst activity in the CD experiment was only 3% of that of the spent catalyst when tested in an FBR reactor at the same reaction temperature. The results suggest that the MO synthesis was inhibited, perhaps by insufficient contact time in the reactive section. To test this theory in the second CD experiment, a fresh batch of catalyst was crushed and loaded into wire mesh bundles. The reduction in particle size was intended to increase the dynamic liquid holdup in the reactive section and promote DAA dehydration. However, an essentially identical result was observed in the second CD experiment for the first condition. Evidently, the increased dynamic liquid holdup did not affect MO and MIBK synthesis.

Significantly, moisture analysis of liquid samples obtained from the reactive and rectification sections from the column in the second experiment revealed that water had accumulated in the top half of the CD column. Based on this insight, a process solution was developed, whereby water was separated *in situ* from the reactant mixture and removed from the reactor via the

utilization of an overhead distillate stream with a reflux ratio of around 83 to 92%. This novel embodiment of the CD process resulted in an increase in MIBK productivity by a factor of 21 compared to the previous CD experiment and an increase in hydrogen uptake efficiency by 2 orders of magnitude. In addition, the hydrogenation selectivity improved from 80.5% to values ranging from 93 to 100%. The results of this experiment clearly demonstrated that MO synthesis had been inhibited by the accumulation of water in the reactive section and that significantly enhanced MIBK productivity could be achieved by the continuous removal of water via the overhead distillate stream.

A moisture free reboiler product with MIBK in excess of 50 wt% was achieved. This is quite significant for a number of reasons. First, state-of-the art one-step processes for MIBK synthesis typically achieve less than 30 wt% MIBK in the product, which necessitates further downstream refining.[23,24] The required separations are significant. In particular, MIBK and water form azeotropic mixtures, which make separation by distillation problematic.[1,62] In the novel CD process developed in this work, not only is the product essentially moisture free, but the results demonstrate that MIBK may be produced with very high selectivity, greater than 90% in the bottoms product.

In the final CD run, a statistical experimental design was employed to investigate the effects of the hydrodynamic parameters; specifically the hydrogen feed rate and the reflux flow rate, on the MIBK productivity and selectivity as well as the hydrogen uptake efficiency. The experiment lasted 191 hours TOS and each of steady state process conditions were maintained for at least 6 hours and for as long as 12 hours, in order to obtain accurate estimates of the product distributions in the reboiler and distillate streams. The results show that the rate of hydrogen transport to the active sites controls the overall MIBK synthesis, with the MIBK productivity and selectivity being strongly dependent on the volumetric flow rate of hydrogen. A significant and curious finding is that the MO conversion to MIBK is inhibited by the liquid phase as

evidenced by a negative correlation with the reflux flow rate. Evidently, the liquid phase presents a barrier to hydrogen mass transport.

## 8.1 Pilot Plant Experiment CD 003

### *8.1.1 Experimental*

A pilot scale CD experiment was conducted to assess the performance of the multifunctional $Pd/Nb_2O_5/SiO_2$ catalyst developed in the first two phases of this research project. Niobia was dispersed onto a high surface area silica catalyst carrier in the shape of a Raschig ring (Saint Gobain Norpro; SS 65137; sample No 2006910020) with a characteristic dimension of 5 mm. The niobium oxide overlayer was established following the synthesis technique described in chapter three using 0.30 mL niobium (V) ethoxide per gram of support. The catalyst was calcined at 100°C in zero gas air flowing at 3.8 mL/min for two hours. The catalyst was subsequently impregnated for 2 hours at 80°C with a solution of Pd acetate in glacial acetic acid. After impregnation, the supernatant liquid was separated by vacuum separation and the catalyst was subsequently dried overnight in an oven at 80°C. The catalyst was then reduced at 100°C in hydrogen flowing at 6.2 mL/min for 2 hours. Catalyst was prepared in several batches with each batch producing about 15 g of catalyst.

The catalyst formulation was the same for all pilot scale CD experiments reported in this chapter as well as the flow reactor experiments reported in Chapter Six. Two catalysts were used in the three pilot scale experiments outlined in this chapter. Catalyst 066 was removed from the CD reactor after the first experiment and replaced with CAT 067, which was used for the two subsequent experiments. The surface area of the fresh catalyst (CAT 066) was obtained using a Micromeretics Gemini 2375 and was found to be 153.91 ± 1.34 $m^2/g$. The elemental compositions of the catalysts were ascertained via energy dispersive X-Ray fluorescence spectroscopy (EDXRF) and Inductively Coupled Plasma (ICP) spectroscopic analysis (Galbraith Laboratories, Knoxville, TN). The results are outlined in Table 8-1.

**Table 8-1** Elemental analysis via ICP and EDXRF of niobia catalysts used in CD experiments

| CD Run | Catalyst | wt% Nb2O5 ICP | wt% Nb2O5 EDXRF | Pd wt% |
|---|---|---|---|---|
| 003 | 066 | | 6.21 ± 0.21 | |
| 004 | 067 | 5.88 | 5.75 ± 0.16 | 0.041 |
| 005 | 067 | 5.88 | 5.75 ± 0.16 | 0.041 |

It is interesting to note that the niobia uptake onto the Norpro HSA silica rings was much less than that observed on the high surface area fumed silica support. However the niobia was utilized far more efficiently on the Raschig ring support and the surface oxide phase exhibited unique and very strong acid sites not present in other catalysts (Chapter Six). In addition, TPD analysis of the Norpro silica support showed that the support exhibited negligible acidity (Appendix D, Figure D2-2). Therefore the strong acidity is associated with the surface oxide phase (niobia). XRD and Raman analyses (Chapter Six) also revealed no evidence of crystallites. The niobia loading in the catalysts above corresponds to about 1/3 monolayer coverage.

For the first CD experiment, the catalyst was protected in an inert environment prior to use. 78.14 g of Raschig Ring catalyst diluted with Intalox saddles was loaded into the top two reaction zones of the CD column (Figure 7-1) while protected under a blanket of inert gas created from the flow of argon through the column. After the reactor was sealed, the CD column was pressurized to 350 psig with argon and leak tested over a 24 hour period as described in Chapter Seven. The catalyst was reduced *in situ* to ensure that any Pd oxidized during catalyst loading was reverted back to $Pd^0$. This was achieved by pressurizing the CD column to 300 psig with hydrogen while feeding hydrogen gas through the column at about 130 mL/min (STP). The external heating elements were enabled and the temperature inside the reactor increased from 22°C to about 72°C over 2 hours and 45 minutes. The reduction was continued for another 2 hours and 45 minutes at this temperature. The column was then depressurized and ACS reagent grade acetone was charged

into the reboiler. The headspace of the acetone feed tank was purged with pre-purified nitrogen to remove oxygen from the system.

The reboiler was then energized (TOS≡0) and the reactor was pressurized to 120 psig with hydrogen. The hydrogen feed rate was set to 54 L/hr (STP). The column pressure was gradually increased to 180 psig over the first four hours of operation, in order to increase the temperature in the reaction zone to 160°C. The CD column was operated at 100% reflux with the cooling water flow rate to the condenser set at 200 mL/min. Reflux was established at 3.3 hrs TOS and the acetone feed pump to the CD column was subsequently enabled at 4 hrs TOS at a flow rate of 155 g/hr. This was reduced to 126 g/hr after 5 hrs TOS. The reboiler level was controlled manually by the continuous removal of product through a Badger control valve to maintain a constant reboiler level of around 55%. The reboiler level was determined by visual measurement at a sight glass and recorded at 15 minute intervals. For this experiment, the reboiler level was maintained at an average level of 54.3 % with a relative standard deviation (RSD) of 8.8% over the course of the experiment from 5 hrs TOS onward. The reboiler product was drained from the product reservoir on an hourly basis and the product composition was ascertained via GC/FID. Unfortunately, the GC with the TCD detector for moisture analysis was not available for this experiment. The CD pilot plant was upgraded prior to the experiments reported in this chapter, in order to enhance the datalogging capability. Labview 7.1 was installed on one of the control computers and used to continuously monitor the cooling water temperature at the condenser inlet and outlet. This significantly improved the estimate of the reflux flow rate.

### *8.1.2 Results CD 003*

Prior to this CD experiment, the activity of the catalyst used (CAT 066) was determined for MIBK synthesis at 160°C and 550 psig in a fixed bed flow reactor (FBR) experiment (Chapter Six). Acetone was fed to the FBR with a WHSV of 0.39 $min^{-1}$ and hydrogen was fed to the reactor with a molar ratio of

$H_2$ to acetone of 2.17. The catalyst was found to be highly active for MIBK synthesis with an estimated MIBK productivity of 1.36 [g/hr*$g_{cat}$]. However, in this CD experiment, the reboiler composition and the MIBK productivity as functions of time on stream illustrated in Figures 8-1 and 8-2 respectively, show that the catalyst utilization with respect to the activity in the FBR was much lower than expected; by two orders of magnitude. The average catalyst utilization, which is calculated as the average MIBK productivity observed in this CD experiment from 30 hrs TOS to the end of the experiment divided by the nominal activity of the catalyst observed in the FBR at the same temperature, expressed as a percentage, was only 1.18%.

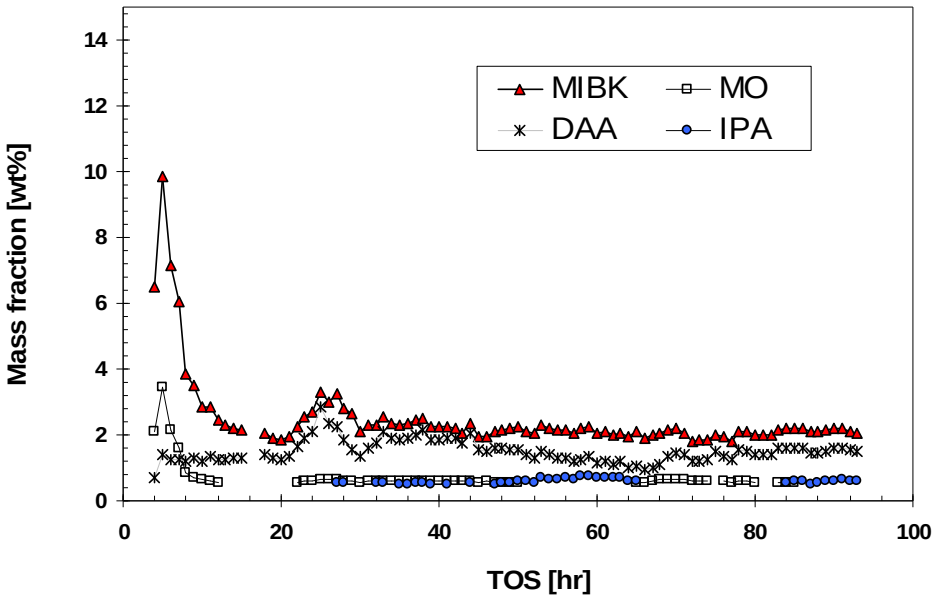


**Figure 8-1** Reboiler composition as a function of time on stream (CD 003)

*Water was not quantified by GC/TCD in this experiment. There is a gap in the data at 14 to 18 hrs TOS since samples were not analyzed. Some data points for IPA and MO are not reported where the concentration fell below the peak area rejection limit of the GC*

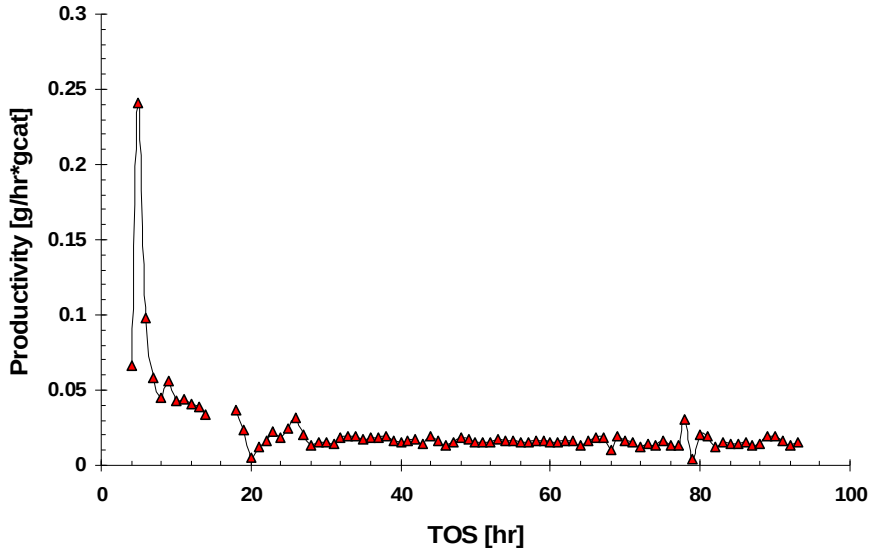


**Figure 8-2** MIBK productivity [g/hr*$g_{cat}$] as a function of time on stream (CD 003) *There is a gap in the data at 14 hrs TOS since samples were not analyzed*

The first unsteady state samples collected from the reboiler at 3 and 4 hours time on stream showed reasonably high MIBK concentrations with a maximum at 5 hours TOS (9.87 wt% MIBK, 0.24 g/hr*$g_{cat}$) From this point the catalyst appears to deactivate as evidenced by a continuous drop in the MIBK concentration in the reactor effluent. At about 20 hrs TOS, the concentrations of all species appear to increase. This was due to a process change. The acetone feed rate was reduced from 126 to 69.0 g/hr between 18 and 20 hours TOS in order to increase the conversion of the unit operation and gain a more accurate appraisal of the product distribution. By 30 hours TOS, the MIBK productivity was only about 0.02 g/hr*$g_{cat}$ and remained essentially invariant for the remainder of the experiment. This was the lowest steady state MIBK productivity observed in this research and was only one fifth of the MIBK productivity obtained in the previous CD experiment (Chapter Seven, CD 002 condition #4) for which a process benchmark was obtained using a commercially available catalyst.

The reboiler product distribution observed in this CD experiment was also unexpected. An unusually high proportion of DAA was observed whereby DAA was the second most abundant organic product observed in this experiment behind only MIBK. Previous experiments in the FBR (Chapter Six) and an autoclave reactor under conditions of kinetic control (Chapter Four) demonstrate that DAA is typically a short lived intermediate at this reaction temperature and is rapidly converted to MO. In the autoclave experiments, the steady state DAA concentration is near and often below the peak area rejection limit of the GC. The results of this CD experiment suggest that the DAA dehydration reaction was either significantly inhibited or the DAA conversion was low due to an insufficient retention time within the reactive section under the process conditions investigated. Considering the results of subsequent CD experiments outlined in this chapter, it is most likely that the DAA dehydration reaction was significantly inhibited under these process conditions.

Rather than terminate the experiment, it was decided to attempt to study the effects of reflux flow rate and the hydrogen feed rate on the product distribution at the relatively low acetone conversion of this experiment. In total, four steady state conditions were investigated and are summarized in Table 8-2. The first condition was a condition of relatively high reflux flow rate and high hydrogen feed rate. The second condition studied the effect of reducing the reflux flow rate while maintaining a relatively high hydrogen feed rate. In the third condition, the reflux flow rate was returned to a condition of relatively high reflux flow rate and the hydrogen feed rate was reduced to a relatively low level. In the fourth and final condition, the reaction temperature was increased from 160 to 169°C by increasing the system pressure from 1.34 to 1.65 MPa.

**Table 8-2** Experimental steady state conditions for the third CD experiment

| No. | Time Interval (TOS) | Rxn. Zone Temp [°C] | System Pressure [MPa] abs. | Reboiler Duty [W] | $H_2$ Feed [L/hr] STP | Condenser Duty [W] | Reflux Rate [g/min] |
|---|---|---|---|---|---|---|---|
| 1 | 32 to 42 | 160 | 1.43 | 720 | 58.0 | 322 | 51.7 |
| 2 | 56 to 61 | 159 | 1.41 | 450 | 57.7 | 83 | 13.0 |
| 3 | 70 to 74 | 161 | 1.34 | 500 | 10.8 | 122 | 19.7 |
| 4 | 83 to 93 | 169 | 1.65 | 750 | 59.0 | - | - |

*Acetone feed rate $F_{A0}$=69.0 g/hr; External heater duty Q=800 W; condenser cooling water mass flow rate = 200 cc/min; The condenser cooling water ΔT data was not saved for condition #4. Note that the condenser duty and reflux flow rate were estimated assuming the reflux consisted of essentially pure acetone.*

The reaction zone temperature reported in Table 8-2 is the average value over the steady state time interval of the hourly measurements obtained from three thermocouple probes located within the two reaction zones used in this experiment. The average value of the system pressure, recorded at 15 minute intervals over the interval is reported after conversion to absolute pressure using the local barometric pressure which was datalogged by the University of Waterloo weather station at 15 minute intervals.[♣] The average reboiler product composition as well as the MIBK productivity and selectivity are outlined in Table 8-3. The MIBK selectivity is expressed as the mass fraction of MIBK in the organic products (neglecting the solvent acetone) expressed as a percentage. Water is also neglected in the calculation of selectivity as is the convention among researchers investigating MIBK synthesis.

[♣] http://weather.uwaterloo.ca

**Table 8-3** Average steady state reboiler product composition and MIBK productivity [g/hr*$g_{cat}$] (CD 003)

| No. | MIBK (wt%) | MO (wt%) | DAA (wt%) | IPA (wt%) | MIBK Productivity [g/hr*gcat] | MIBK Selectivity (wt %) |
|---|---|---|---|---|---|---|
| 1 | 2.35 | 0.60 | 1.93 | 0.53 | 0.0178 | 44.7 |
| 2 | 2.14 | - | 1.30 | 0.67 | 0.0158 | 52.1 |
| 3 | 1.96 | 0.62 | 1.30 | - | 0.0142 | 43.8 |
| 4 | 2.15 | 0.56 | 1.56 | 0.58 | 0.0155 | 49.1 |

Generally, the changes in the process variables did not have significant effects on the product distribution. The amount of products created in this experiment was quite low and the variation inherent in the process data was large compared to the main effects due to changes in process variables under these conditions. In addition, the process conditions investigated in this experiment were not particularly stable. For example, the DAA concentration was monotonically decreasing during condition #2 and had an RSD of 7.5%. In condition #3, the MIBK and DAA concentrations had RSD of 8.3 and 9.2% respectively over the steady state interval. Consequently, the results of this experiment are preliminary and will be discussed qualitatively here. A more rigorous analysis is reserved for the results of the more robust experimental design outlined in section 8.4.

Some trends are evident. As expected, a reduction in the reflux flow rate between conditions 1 and 2 resulted in a decrease in the production of MO and DAA, which confirms the findings of the previous CD experiments which demonstrated that the aldol condensation and DAA dehydration steps are governed by the liquid flow rates in the reactor. For most of the CD experiment, the DAA concentration mirrored the MIBK concentration. However, the reduction in the reflux flow rate in the second steady state condition from 43 to 62 hours TOS resulted in a significant decrease in the DAA and MO concentrations. The MO concentration dropped below the peak area rejection limit of the GC. Consequently, the selectivity for this condition

is slightly inflated since MO was not quantified. The MIBK productivity decreased by about 11% due to the reduction in the productivity of its precursor, MO. The amount of IPA produced from the direct hydrogenation of acetone also increased as a consequence of the reduction in the production rate of MO, which competes with acetone for hydrogenation active sites.

In the third condition the effect of reducing the hydrogen flow rate from 58 to 11 L/hr (STP) at the condition of low reflux flow rate was investigated. However, the reflux flow rate was not kept constant as planned and increased by around 47%. Regardless, the results demonstrate that the reduction in the hydrogen feed rate resulted in a 10% reduction in the MIBK productivity and a greater proportion of unreacted MO in the reboiler product stream. The greater reflux flow rate undoubtedly contributed to the increase in the MO concentration. The IPA concentration also dropped below the peak area rejection limit of the GC as the MO concentration increased. Interestingly, the DAA concentration remained unchanged.

The fourth condition investigated the effect of increasing the reaction temperature from 160 to 169°C at conditions of high hydrogen feed rate, 59 L/hr (STP) and conditions of high reflux flow rate comparable to the first condition. The results of this test are inconclusive since unsaved condenser cooling water temperature data for this condition was lost due to a computer "crash". The results show that the MIBK productivity in condition #4 was less than condition #1. This is likely due to a lower reflux flow rate in condition #4 compared to condition #1. Although the reboiler duty was greater for condition #4, the system pressure in condition #4 was also greater in order to achieve the higher reaction temperature. The results of previous CD experiments clearly demonstrate that the reflux flow rate is more strongly dependent on the system pressure than the reboiler duty (Figure 7-5). A lower reflux flow rate would also explain the lower MO and DAA concentrations as well as the greater IPA

concentration in the reboiler product observed in condition #4 compared to condition #1.

*8.1.3 Root Cause Analysis*

The MIBK productivity observed in this CD experiment was 2 orders of magnitude lower than the activity observed with the same fresh catalyst when used to study MIBK synthesis in an FBR. A root cause analysis was carried out in order to ascertain the failure mode of this catalytic process. The spent catalyst (CAT 066) was recovered from the CD column and several experiments were carried out. In the first set of experiments, the activity of the spent catalyst for MIBK synthesis was measured at 160°C and 555 psig in the BTRS-Jr, fixed bed flow reactor described in Chapter Six. In one experiment, the activity of the spent catalyst was tested "as is" whereas in a second experiment, the spent catalyst was first reduced *in situ* in the flow reactor for 2 hours at 100°C with hydrogen flowing at 140 mL/min (STP). The results were contrasted to the activities of fresh catalyst from previous batches with the same catalyst formulation (CAT 064, 065 and 066). The results of these experiments are summarized in Table 8-4 and Figure 8-3.

**Table 8-4** Steady state catalyst activity for MIBK synthesis at 160°C and 555 psig in a FBR

| Experiment ID | Cat ID | Acetone [mL/min] | Catalyst [g] | WHSV $min^{-1}$ | MIBK Productivity [g/hr*gcat] |
|---|---|---|---|---|---|
| BTRS-9 | 066 fresh | 1.24 | 2.52 | 0.39 | *1.36* |
| BTRS-12 | 066 spent | 1.24 | 2.71 | 0.36 | 0.63 |
| BTRS-11 | 066 spent (reduced) | 1.24 | 2.00 | 0.49 | 0.62 |
| BTRS-6 | 065 | 1.04 | 2.99 | 0.27 | 0.89 |
| BTRS-5 | 064 | 1.05 | 2.58 | 0.32 | 0.94 |
| BTRS-5 | 064 | 1.05 | 2.58 | 0.32 | 1.30 |

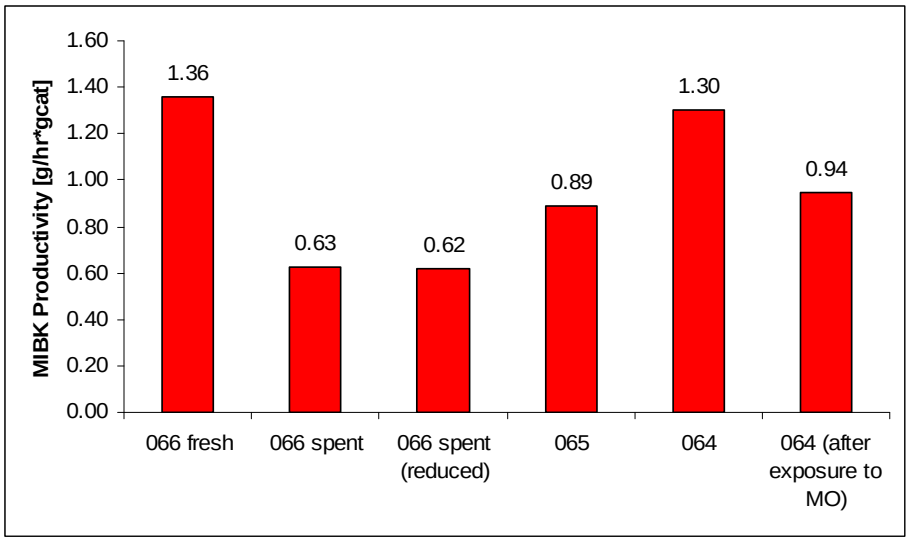


**Figure 8-3** Steady State activity for MIBK synthesis of various catalysts in a FBR at 160°C and 555 psig

The acidity of the spent catalyst (CAT 066) was ascertained by TPD. The results showed that the spent catalyst did in fact exhibit significant surface acidity. A soxhlet extraction was carried out on the spent catalyst in order to identify potential poisons. This experiment did not result in the conclusive identification of any particular poison and is summarized in Appendix E. The results of the PFR experiments confirm that the catalyst did lose some activity for MIBK synthesis during the CD experiment, perhaps as much as 50% of its initial activity. However, since the activity of the catalyst in the CD reactor was only about 3% of the activity of the spent catalyst when tested in the FBR, it can be concluded that the low activity observed in the CD reactor was not entirely due to irreversible catalyst deactivation but rather was predominantly the result of the reaction environment within the CD reactor.

A major difference between the reaction environment within a CD reactor and that of a PFR is the fact that in the PFR, the catalyst is fully wetted whereas in the CD reactor, the catalyst is only partially wetted when exposed to counter current liquid-vapour flow in the low interaction regime of trickle flow. It has been estimated that the wetting efficiency over ¼ inch Intalox saddles with a characteristic dimension of 6 mm and a bed porosity of $\varepsilon$=0.75 for the

conditions in the previous CD experiments, ranged from 16 to 33% (Figure 7-4). The Raschig rings catalysts used in the previous experiment had a characteristic dimension of 5 mm.

*8.1.4 Vapour Phase Reaction in a Fixed Bed Reactor (Expt. BTRS-10)*

An experiment (BTRS-10) was carried out in the FBR in order to determine the effects of catalyst dryout on the catalyst performance. 2.52 g of fresh catalyst (CAT 066) was loaded into the FBR. Four experimental conditions were investigated. Each condition was maintained for four hours of operation with the exception of the last condition, which is a preliminary result. The experiment was terminated prematurely due to equipment malfunction. The acetone and hydrogen flow rates were kept constant at 1.05 mL/min and 147 mL/min (STP) respectively. This corresponds to a hydrogen to acetone molar ratio of 2.866 (i.e. 43.3% stoichiometric excess hydrogen). The temperature was also constant at 160°C. In the first condition, the reactor was pressurized to 600 psig, which ensured that acetone remained in the liquid phase. Samples were collected at hourly intervals from the product line for GC/FID analysis. After four hours, the pressure was reduced to only 15 psig. Consequently, the reaction was conducted in the vapour phase. After four hours of operation, the pressure was increased to 120 psig. At this pressure, the boiling point of acetone, as predicted by the Antoine Equation, is 141°C. Consequently, the third condition was also a vapour phase reaction but at a higher partial pressure of hydrogen. Finally, after four hours, the pressure was increased to 600 psig, which repeated the initial condition and restored the liquid phase reaction.

The results (Tables 8-4 and 8-5) show that the productivity diminished and the product distribution changed when the process transitioned from liquid phase reaction to vapour phase reaction. Specifically, in the liquid phase reaction DIBK was the second most abundant species in the effluent (neglecting the solvent and water) behind MIBK. In contrast, MO became the most abundant species in condition number 2 and the second most abundant species

in condition number three. Evidently, a significant amount of unreacted MO was in the product stream due to the low hydrogenation pressure. The final condition is a preliminary result since the apparatus malfunctioned and the experiment was terminated after one hour at that condition (unsteady state).

When the process was restored to the initial condition of liquid phase reaction at 600 psig (condition #4), a large amount of MIBK and other products were present in the effluent. In fact, the productivity was much higher than the initial condition. The hydrogenation selectivity and overall selectivity were observed to approach that of the initial condition when the liquid phase reaction was restored. The increase in productivity compared to the initial baseline condition was likely due to the elution of organic products synthesized from the vapour phase reaction and retained in the catalyst bed by chemisorption. This is consistent with the results of the second CD experiment (CD 002, Chapter Seven) whereby a large pulse of MIBK and other products were eluted from the CD column after a change in the column hydrodynamics. This FBR experiment reproduces the result of the CD experiment (CD 002) and supports the notion that the liquid phase plays an important role in the removal of species from the reaction zone by convection.

**Table 8-5** Results of FBR Experiment BTRS-10 (condition #4 is preliminary)

| No | Description | Hydrogenation Selectivity [%] | Overall Selectivity [%] | MIBK [g/hr*g] | Total [g/hr*g] |
|---|---|---|---|---|---|
| 1 | 600 psig, liquid phase | 90.5 | 88.0 | 1.19 | 1.35 |
| 2 | 20 psig vapour phase | 82.4 | 43.3 | 0.34 | 0.70 |
| 3 | 120 psig vapour phase | 88.1 | 71.0 | 0.83 | 1.17 |
| 4 | 600 psig liquid phase | *88.7* | *82.8* | *1.72* | *2.13* |

**Table 8-6** Product distribution in PFR Effluent (BTRS-10)

| No. | MIBK [wt%] | MO [wt%] | TMB [wt%] | DIBK [wt%] | $C_9$* |
|---|---|---|---|---|---|
| 1 | 6.08 | | 0.19 | 0.64 | |
| 2 | 1.54 | 1.68 | | 0.33 | |
| 3 | 4.22 | 1.15 | | 0.57 | |
| 4 | *8.77* | | *0.28* | *1.11* | *0.43* |

** C9 corresponds to material eluting at 1.9 min, which was determined by GC/MS to be a hydrocarbon most likely 2,4-dimethyl heptane*

The results of the PFR experiment confirm that the gas phase reaction results in much lower selectivity to the desired product compared to the liquid phase reaction. The change from condition 1 (liquid phase 600 psig) to condition 2 (vapour phase 15 psig) resulted in a substantial decrease in MIBK selectivity from 88% to 43%. This is largely due to the presence of unreacted MO in the effluent, resulting from the low partial pressure of hydrogen. When the partial pressure of hydrogen was increased in the third condition, the overall selectivity increased from 43 to 71%. The concentrations of mesitylene (TMB) and DIBK in the effluent were greater for the conditions in the liquid phase at elevated pressure. This likely reflects the higher conversion achieved under these conditions. It is not surprising that undesirable higher molecular weight species would be observed at higher conversions.

Unfortunately, the apparatus malfunctioned and the experiment had to be terminated after 1 hour of operation in the last condition. Consequently the results of the last condition are preliminary and no definitive conclusions may be drawn about the long term effect of catalyst dryout on the performance of the catalyst. However, although the activity of the catalyst seemed unaffected after 8 hours of vapour phase reaction, BET analysis of the catalyst suggests a loss of surface area of 15.6% occurred due to exposure to the vapour phase reaction after only 8 hours on stream in the vapour phase (Table 8-7). In contrast, the spent catalyst recovered from the CD column after 98 hours TOS (CAT 066) did not show a significant difference in specific surface area compared to the

fresh catalyst. This result supports the notion that the presence of a liquid phase serves to enhance the stability of the catalyst. The loss of surface area is possibly due to coke formation, which may be mitigated by the liquid phase. Perhaps, hot spots in the catalyst bed of the CD column are diminished by the boiling medium.

**Table 8-7** BET surface areas of CAT 066 after experiments in flow reactors

| DESCRIPTION | BET AREA [$m^2/g$] | Total TOS [hr] |
|---|---|---|
| CAT 066 Fresh | 154 | 0 |
| CAT 066 spent (CD 003) | 157 | 93 |
| CAT 066 spent (BTRS-10) | 130 | 24* |

** 8 hours TOS in vapour phase, remainder in liquid phase. Catalyst also used for brief experiment BTRS-9 (8 hours TOS)*

### 8.2 Pilot Plant Experiment CD 004

The results of the root cause analysis in section 8.1 suggests that the low catalyst activity observed in the first CD experiment with a $Pd/Nb_2O_5/SiO_2$ catalyst (CD 003) was due to the reaction environment within the CD column. The data obtained from the CD run indicated that the DAA dehydration reaction was either inhibited by the chemical species present in the reaction zone or exhibited a low chemical conversion due to insufficient residence time in the reaction zone. To test the latter possibility, the CD experiment was repeated. The same catalyst formulation and preparation method was used. However, the catalyst rings were crushed into smaller fragments and loaded into 304 stainless steel wire mesh bundles whose specifications were described in Chapter Seven. The reduction in catalyst particle size allows for an increase in the dynamic liquid holdup in the reaction zone. If the low MIBK productivity was due to insufficient liquid contacting in the previous experiment, then a reduction in the catalyst size would result in an increase in MIBK productivity.

*8.2.1 Catalyst and Reactive Section*

Catalyst batch 067 was used for the last two CD experiments of this work. The rings were crushed and sieved to give particle sizes ranging from 500 to 1200 μm (Table 8-8). 77.7 g of catalyst 067 was loaded into nine wire mesh bags and installed into the top two reactive sections of the CD column indicated in Figure 7-1. The geometry of the reaction zones are represented schematically in Figure 8-4.

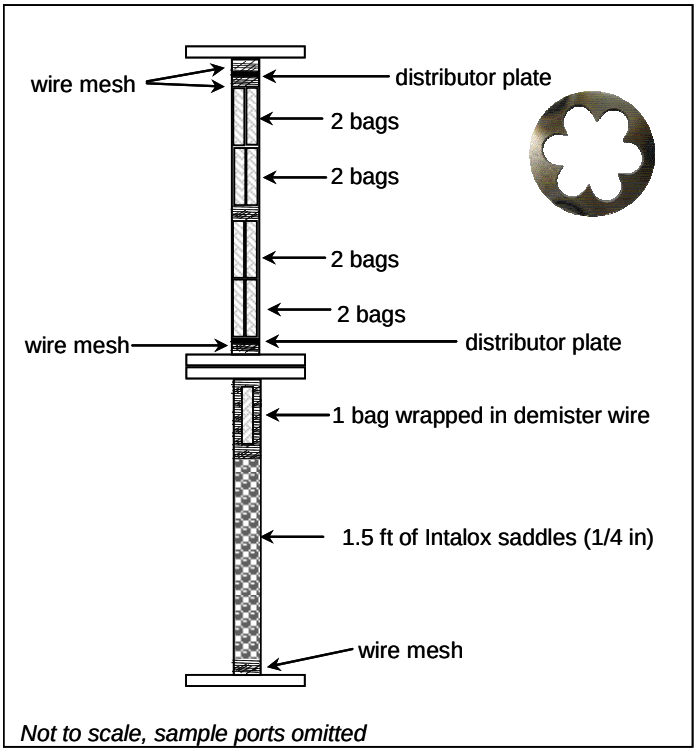


**Figure 8-4** Schematic representation of reaction zone for experiments CD 004 and CD 005

**Table 8-8** Particle size distribution of CAT 067 used in Experiments CD 004 and CD 005 (catalyst less than 500 μm was not used in CD experiments)

| **Particle Size ϕ (μm)** | **Amount (g)** |
|---|---|
| 700 < ϕ < 1200 | 69.62 |
| 500 < ϕ < 700 | 13.67 |
| ϕ < 500 | 27.28 |

*8.2.2 Extraction of Liquid Samples from CD Column*

For the last two CD experiments, liquid samples were extracted from the CD column at three sample ports located approximately 1.59, 3.36 and 4.95 m above the reboiler flange. These distances were determined by measurement with a meter stick with the insulation in place on the column. More accurate estimates of distances may be obtained from the mechanical drawings. The sample port at 1.59 m was in the rectification section, the sample port at 3.36 was at the lower most sample port in the bottom reactive section and the sample port at 4.95 m was in the rectification section. Samples were collected using a novel liquid sampling device, based on the design of Dooley et al.[206] which was developed and validated in our group by undergraduate students as an undergraduate senior chemical engineering design project under the supervision of W.K. O'Keefe and Professor F.T.T. Ng.

The design consists of a capillary tube made of stainless steel which extends beyond the dead zones created by the sample ports, into the CD column. On the end of the tube is a flared cup which facilitates the collection of liquid. Liquid is selectively extracted without flashing by controlling the flow rate. The flow rate is made sufficiently slow to prevent flashing by using a metering valve with a minimum valve flow coefficient (Cv) of 0.001. The design is illustrated in Figure 8-5. For the device used in these CD experiments, the quick-connect fitting was replaced with a coil of 1/16 in stainless steel tubing which allowed liquid to drain directly into GC vials. The liquid was found to be completely subcooled by the time it exited the sampling device and tubing. The sample lines were purged before sample collection.

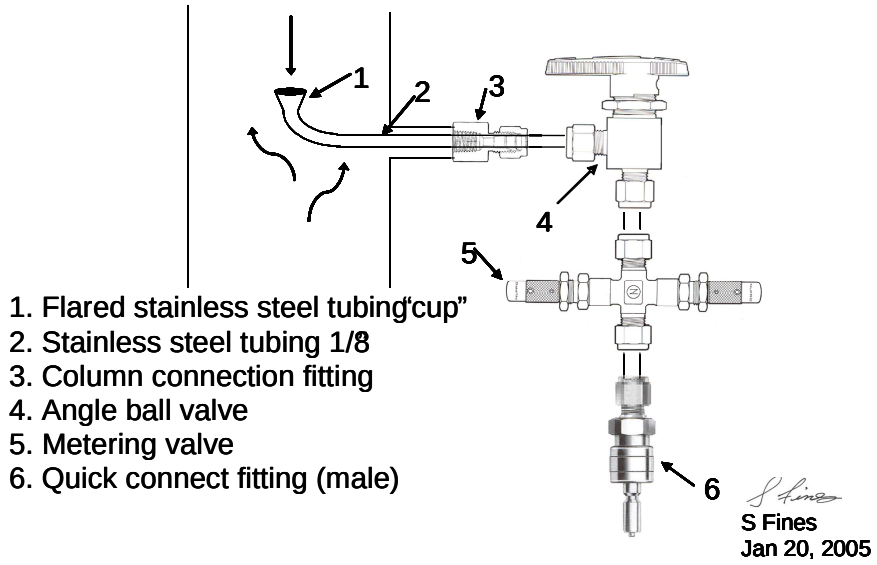


**Figure 8-5** Schematic representation of liquid sampling device designed by Dooley, Fines, Trebacz and Walker[206]. Drawing by S.K. Fines, (not to scale)

*8.2.3 Results CD 004*

For the first 40 hours TOS, the CD reactor was pressurized to 180 psig resulting in a reaction zone temperature of around 160°C. The external heater duty was set to 800 W. The reboiler duty was initially set to 800 W but was reduced and adjusted between 23 and 29 hrs TOS to its setpoint of 450 W. This first condition, was the same as condition #2 in the previous CD experiment for which the reflux flow rate was minimized. The hydrogen flow rate was maximized at 60 L/hr (STP). The MIBK productivity as a function of time on stream for the first 40 hours (Figure 8-6) demonstrates that the MIBK productivity diminished continuously for the first 20 hours TOS until it reached a final steady state value of 0.02 [g/hr*$g_{cat}$]. This result is essentially identical to that observed in the previous CD experiment. Note that reducing the reboiler duty between 23 and 29 hours TOS in an attempt to improve hydrogen mass transfer, by reducing the catalyst wetting efficiency, did not affect the MIBK productivity. Evidently, increasing the liquid holdup in the reaction zone by reducing the catalyst particle size did not affect the MIBK productivity.

During this initial condition, samples were obtained through the sample port located at the reaction zone at 23 and 24 hours TOS. When these samples were analyzed by GC/TCD, the results showed that the water concentration in the reaction zone was quite high, with values of 8.74 and 9.06 wt% for samples collected at 23 and 24 hrs TOS respectively. In contrast, the concentration of organic species obtained in the CD column, measured during this work typically varied from 0.5 to 1.4 wt%. The water concentration in the reboiler was only 0.45 wt% at that time. Considering the fact that water is produced in the same stoichiometric ratio as MO and that MO and MIBK have molecular masses approximately 5 times greater than water, the water concentration seemed unusually high.

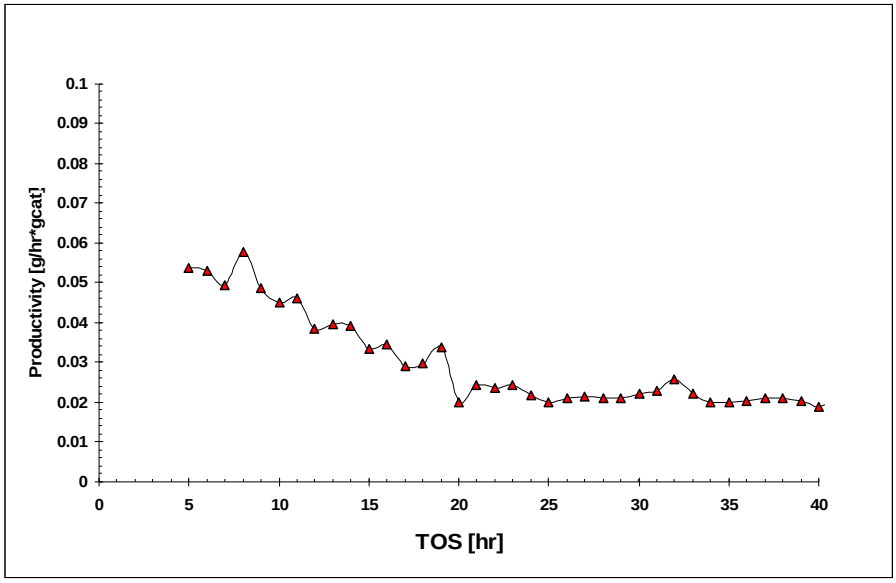


**Figure 8-6** MIBK productivity as a function of time on stream (TOS) for the first 40 hours TOS (CD 004)

The results obtained suggest that water had accumulated in the top half of the CD reactor. This result is unexpected based on previous CD process design data for MIBK synthesis disclosed in the literature.[32,60,61] Lawson and Nkosi[32] for example suggested that all of the by-products including water that have higher boiling points than acetone and would "not significantly vaporized by the reboiling" and should be removed from the system in the reboiler

product. Indeed, the expected conditions for MIBK synthesis via CD, presumably obtained via computer simulation, led to a CD process design for the two-stage MIBK CD process which stipulates a water recovery unit located downstream from the reboiler product of the first CD reactor for MO synthesis and 100% recycle of the acetone rich distillate stream.[60,61] In fact, water is expected to be recovered in the bottoms product of the CD column with an expected mass fraction of 14 wt% in the bottoms stream as designed.[61] At the time of this manuscript preparation, Thotla et al.[124] disclosed the results of theoretical modeling and experimental simulation of the aldol condensation of acetone via CD. They both predicted and measured a water concentration profile along the major axis of the CD reactor operating at 100% reflux for which the water concentration in the liquid phase was a minimum at the overhead condenser and increased monotonically towards the reboiler where the water concentration was a maximum.[124] However, the reaction temperature investigated was much lower. In this work, the opposite trend for water concentration was observed. Samples obtained at three sample ports along the CD column at around 47 hours TOS clearly shows that the water concentration increases towards the top of the CD column (Figure 8-7).

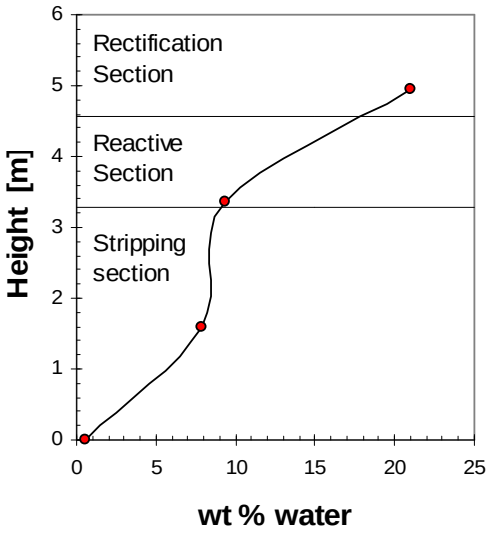


**Figure 8-7** Water concentration as a function of axial position in the CD column at around 47 hrs TOS (CD 004)

*The data point in Figure 8-7 corresponding to the reboiler was collected at 43 hrs TOS (steady state). The remaining three points were collected shortly afterwards prior to switching process conditions around 47 hours TOS. No water analysis of the reboiler stream is available during the interval 44-47 hrs TOS. The reactive section consists of two flanges sections. The majority of the catalyst was located in the top flanged section (Figure 8-5).*

Separation by distillation is based on relative volatility. The relative volatilities of acetone-water ($\alpha_{AW}$), acetone-MIBK ($\alpha_{AM}$) and water-MIBK ($\alpha_{WM}$) calculated from their vapour pressures at various temperatures are summarized in Table 8-9. The data in Table 8-9 shows that for temperatures up to 120°C, water and MIBK have comparable vapour pressures. Note the CD process designs proposed in the patent literature[32,61,62] involve MIBK synthesis or MO synthesis around 120°C. However at 160°C, water has an intermediate vapour pressure. Since water is highly miscible with acetone and is also relatively immiscible with MIBK, it seems reasonable that water would preferentially accumulate in the top half of the reactor under these conditions of elevated temperature.

**Table 8-9** Relative volatilities of acetone, water and MIBK at various temperatures

| Temp [°C] | $\alpha_{AM}$ | $\alpha_{AW}$ | $\alpha_{WM}$ |
|---|---|---|---|
| 25 | 11.95 | 9.92 | 1.20 |
| 120 | 5.39 | 3.05 | 1.77 |
| 160 | 4.62 | 2.25 | 2.05 |

The vapour pressure of water was obtained from tabulated data from Weast.[210] The vapour pressures (P*) of MIBK and acetone in Pascals (Pa) were calculated from the empirical correlation in equation 8-1. The empirical constants for acetone are A=70.72, B=-5685, C=-7.351, D=0.0000063 and E=2.[218] The empirical constants for MIBK are A=80.53, B=-7421.8, C=-8.379, D=1.81E-17 and E=6.[1] The correlations for acetone and MIBK are valid up to 235°C and 301°C respectively.[1,218]

$$P^* = \exp\left\{A + \left(\frac{B}{T}\right) + C\ln T + DT^E\right\} \qquad (8\text{-}1)$$

The high concentration of water in the reaction zone likely inhibited the DAA dehydration reaction. This also explains the transient behaviour in Figures 8-2 and 8-6 whereby the MIBK productivity was initially high and decreased with time until a steady state was achieved. In order to test this theory, the reactor was operated in a novel embodiment of the CD process for MIBK synthesis whereby an overhead distillate stream was drawn from the top of the reactor (Figure 8-8). This would enable the removal of water from the system by convection through the distillate stream. Around 47 hrs TOS, the removal of the overhead distillate stream was enabled. The first samples were collected from the product reservoir at 48 hrs TOS.

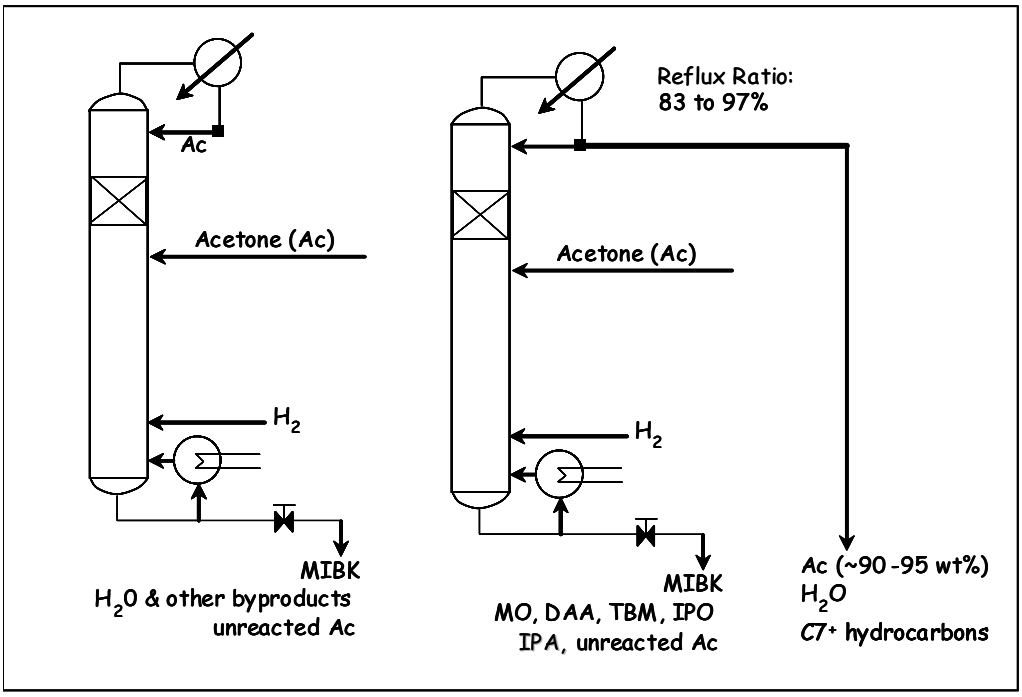


**Figure 8-8** (a) (left) One step MIBK synthesis via CD proposed by Lawson and Nkosi[32] (b) (right) A novel embodiment of the CD process for the one step synthesis of MIBK via CD with two product streams drawn: an acetone rich overhead distillate stream removing water and low boilers and a MIBK rich reboiler product stream

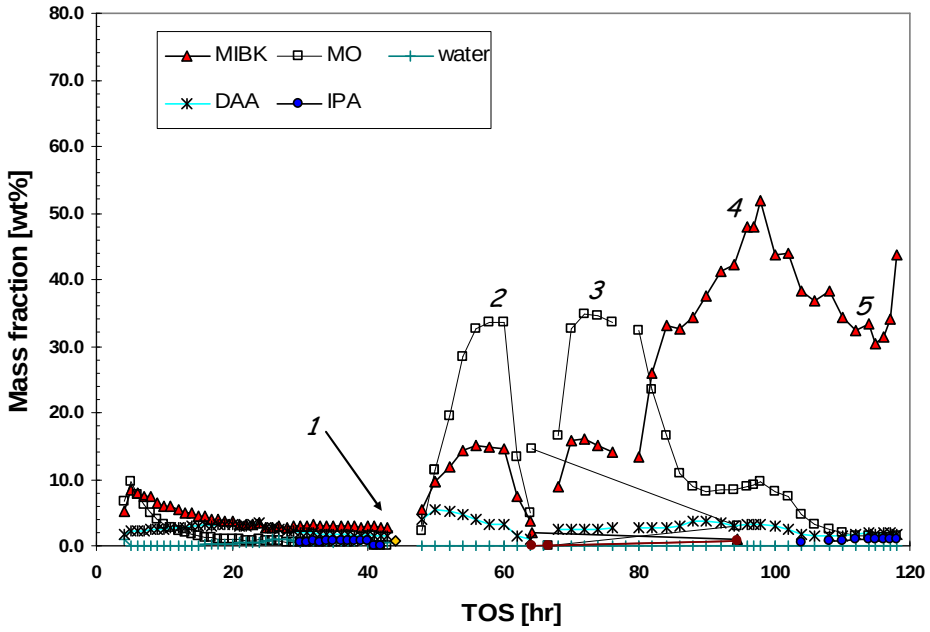


**Figure 8-9** Reboiler product composition vs time on stream (CD 004)

The reboiler composition versus time on stream data (Figure 8-9) demonstrates that the continuous removal of water from the system via an overhead distillate stream resulted in a dramatic increase in the MIBK productivity. The mass fraction of MIBK in the reboiler product stream increased from 2.6 wt% at 43 hrs TOS to 15.0 wt% at 56 hrs TOS while the MIBK productivity increased from around 0.02 to 0.10 [g/hr*gcat] during this interval. In addition, the amount of unreacted MO in the product stream increased dramatically as well. Also, the water in the reboiler product stream dropped below the peak area rejection limit of the GC (<< .1 wt%). Previously, it had ranged from around 0.5 to 1.0 wt%.

Interestingly, the solenoid valve stopped actuating at 60 hours TOS due to a computer glitch resulting in the restoration of 100% recycle of the overhead distillate. The plant operators did not detect this malfunction and continued to monitor the process. The data in Table 8-9 clearly shows that after the solenoid valve failed and the overhead distillate was completely recycled to the column,

the MIBK, MO and DAA concentrations dropped to their previous levels. However, the malfunction was corrected at the beginning of the night shift at 66 hrs TOS and the overhead distillate stream was restored. The data in Figure 8-9 shows that the process quickly re-established and the MIBK, MO and DAA concentrations in the reboiler stream were restored to the previous condition (#2). In fact, a comparison of condition #3 and #2 in Figure 8-10 suggests that the process is highly repeatable, although there appears to be some slight process drift in condition #3.

In condition #3, the hydrogen feed rate was at a relatively low level, 11 L/hr (STP). For the fourth condition the hydrogen feed rate was increased to 54 L/hr (STP) at 80 hrs TOS. The data in Figure 8-9 demonstrates that after this process change, the amount of unreacted MO decreased dramatically while the amount of MIBK in the reboiler product increased significantly. The MO concentration in the reboiler product stream dropped from around 33 wt% to 8.5 wt% while the MIBK concentration increased from around 15 or 16 wt% to as high as 52 wt% at 98 hours TOS. The average MIBK productivity from 96 to 98 hrs TOS was 0.42 [g/hr*gcat], which represents an increase in MIBK productivity by a factor of 21 compared to the best result in the previous CD experiment.

The high concentrations of MIBK and MO in the reboiler product resulted in reboiler temperatures in excess of 200°C. It is likely the MIBK concentration would have continued to increase beyond 52 wt% and as a result, the reboiler product temperature would increase as well. Consequently, at that point, the operator reduced the reflux flow rate by lowering the reboiler duty in order to reduce the catalytic activity until further discussions could take place with the CD team. This resulted in the decrease in MIBK and MO concentrations in the reboiler product after 98 hrs TOS observed in Figure 8-9.

A final steady state condition #5 was monitored at this lower reflux flow rate while maintaining a relatively high hydrogen feed rate. As a result, the amount of unreacted MO in the reboiler product decreased dramatically from 8.5 wt% to around 1.4 wt% as evident in Figure 8-10. As the MO concentration diminished, IPA produced from the direct hydrogenation of acetone became more prevalent. The IPA concentration in the reboiler product stream was below the peak area rejection limit of the GC at 104 hrs TOS but was around 1.0 wt% in the final steady state condition (#5). The final experimental condition supports previous findings of this work, which shows that the direct hydrogenation of acetone becomes significant when the concentration of MO becomes low since MO and acetone compete for the same active sites.[18]

The experiment was terminated after 118 hrs TOS, after clearly demonstrating that a significantly enhanced catalytic activity for MIBK synthesis may be achieved from the *in situ* removal of water from the reactive section via the utilization an overhead distillate stream. The results of this CD experiment demonstrate conclusively that water accumulating in the reaction zone inhibited the DAA dehydration reaction and demonstrated that an essentially moisture free reboiler product in excess of 52 wt% MIBK could be achieved in a single stage via CD. Incidentally, the state-of-the-art reactor technologies for MIBK synthesis typically result in less than 30 wt% MIBK in the product stream and require further complex downstream refining, since water forms azeotropic mixtures with MIBK.

The five process conditions investigated are summarized in Tables 8-10 and 8-11. The fourth condition being a preliminary result since steady state had not been fully achieved. The fifth condition is also a preliminary result since the "steady state" was maintained for only 3 hours. For these conditions, the MIBK concentrations were invariant to an RSD within 5% with the exception of the third condition, which exhibited slight process drift and an MIBK variance of 8% RSD. The reaction temperature was the weighted average of

observations made from thermocouples 13, 14 and 15 with each thermocouple weighted equally.

**Table 8-10** Steady state process conditions investigated (CD 004)

| | Period TOS | Reboiler Duty [W] | System Pressure [Mpa] (abs) | Reaction Temp [℃] | External Heater duty [Watts] | solenoid (SV-1) on/off |
|---|---|---|---|---|---|---|
| 1 | 35 to 40 | 450 | 1.45 | 160 | 800 | closed |
| 2 | 54 to 60 | 800 | 1.31 | 162 | 800 | 0.2 / 99.8 |
| 3 | 70 to 78 | 800 | 1.31 | 162 | 800 | 0.2 / 99.8 |
| 4 | 96 to 98 | 800 | 1.38 | 161 | 800 | 0.2 / 99.8 |
| 5 | 112 to 115 | 450 | 1.41 | 166 | 800 | 0.2 / 99.8 |

**Table 8-11** Steady state mass flow rates (CD 004)

| | Acetone Feed [g/hr] | Hydrogen [L/hr] (STP) | Bottoms (reboiler) [g/hr] | Condensate flow [g/min] | Distillate (D) [g/min] | Reflux Rate ($L_o$) [g/min] | Reflux Ratio (%) |
|---|---|---|---|---|---|---|---|
| 1 | 69.0 | 57.8 | 54.7 | 14.9 | 0.0 | 14.9 | 100.0 |
| 2 | 141 | 11 | 55.3 | 36.6 | 1.19 | 35.4 | 96.8 |
| 3 | 141 | 11.2 | 62.2 | 39.6 | 1.21 | 38.4 | 97.0 |
| 4 | 141 | 59.3 | 85.1 | 37.3 | 0.93 | 36.4 | 97.5 |
| 5 | 141 | 59.3 | 75.2 | 13.4 | 1.22 | 12.2 | 90.9 |

The condensate mass flow rate was calculated from the energy balance about the condenser as described previously in Chapter Seven. The latent heat of vapourization of acetone was calculated from the Watson correlation at the observed distillate temperature. Although the distillate stream was analyzed by GC/TCD and GC/FID, the impurities were neglected in the calculation. The condensate was assumed to be pure saturated acetone. Figure 8-10 illustrates the cooling water temperature difference across the condenser during this experiment. The steady state conditions are indicated on the figure. For the conditions in which an overhead distillate stream was drawn, the solenoid valve (SV-1) was opened for 0.2 seconds and closed for 99.8 seconds per cycle. This resulted in a constant distillate mass flow rate of around 1 g/min.

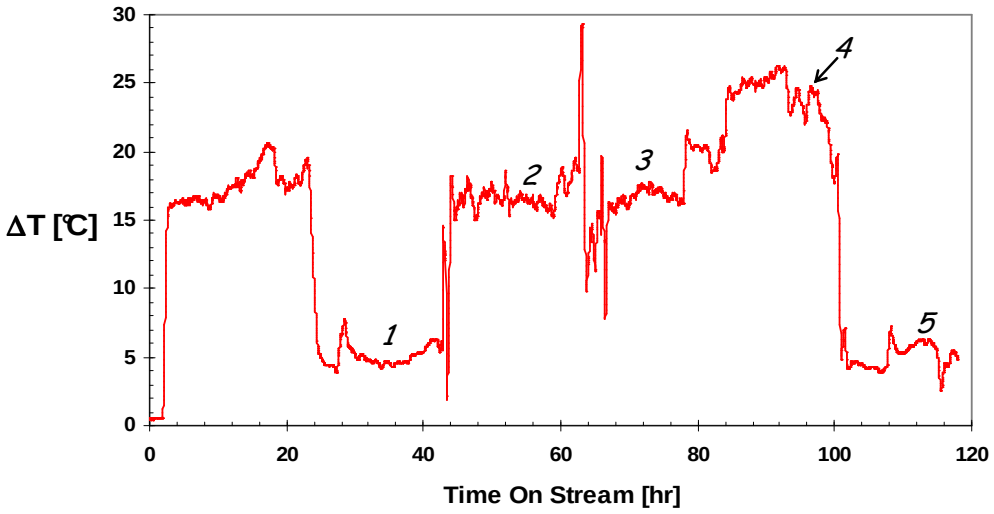


**Figure 8-10** Cooling water temperature difference across the condenser (CD 004). Cooling water flow rate 200 mL/min

The product distributions in the reboiler and overhead distillate streams for the steady state conditions are outlined in Table 8-12 and 8-13 respectively. The species labelled $C_9$ in the overhead distillate streams are labelled according to their retention times in the GC/FID analysis. These compounds were determined by GC/MS to be C9 hydrocarbons. The compound with retention time 1.9 minutes was determined to most likely be either 2,4-dimethyl heptane or 2,3,3-trimethyl heptane. The compound with retention time 2.2 minutes was determined to be, most likely, 2,3,3-trimethyl-1-hexene.

**Table 8-12** Reboiler product distribution (CD 004)

| | Reboiler Composition [wt%] | | | | | | | | |
|---|---|---|---|---|---|---|---|---|---|
| | MIBK | MO | IMO | DAA | IPA | DIBK | TMB | C6+ | water |
| 1 | 2.89 | 0.44 | 0.0 | 1.63 | 0.70 | 0.0 | 0.0 | 0.00 | 0.68 |
| 2 | 14.66 | 32.01 | 2.89 | 3.73 | 0.0 | 0.0 | 0.0 | 0.42 | 0.0 |
| 3 | 15.31 | 33.96 | 3.34 | 2.55 | 0.0 | 0.0 | 0.0 | 0.64 | 0.0 |
| 4 | 49.20 | 9.25 | 1.01 | 2.52 | 0.0 | 0.46 | 0.13 | 0.17 | 0.0 |
| 5 | 32.05 | 1.42 | 0.0 | 1.83 | 0.97 | 0.49 | 0.14 | 0.0 | 0.0 |

*The solvent, acetone, is neglected from the Table.*

**Table 8-13** Overhead distillate product distribution (CD 004)

| | Period TOS | Overhead Distillate: Mass Fraction (wt%) | | | | |
|---|---|---|---|---|---|---|
| | | | | $C_9$ | | |
| | | water | IPA | 1.9 min | 2.2 min | Acetone |
| 1 | 35 to 40 | n/a | n/a | n/a | n/a | n/a |
| 2 | 54 to 60 | 8.16 | 0 | 0 | 0.18 | 91.7 |
| 3 | 70 to 78 | 8.13 | 0 | 0 | 0.20 | 91.7 |
| 4 | 96 to 98 | 7.83 | 0 | 0.17 | 0.00 | 92.0 |
| 5 | 112 to 115 | 6.8 | 0.97 | 0 | 0.00 | 92.2 |

The MIBK productivity, selectivity and acetone conversion for the process conditions investigated are summarized in Table 8-14. The acetone conversion was calculated as defined in equation (8-2) which gives consideration to both acetone present in the reboiler product stream as well as in the overhead distillate stream. The selectivity for the overall reaction is expressed in wt% and gives consideration to undesired products in both the distillate and bottoms product streams. The selectivity of the process, i.e. the proportion of MIBK in the organic products in the bottoms product is indicated in Table 8-13 as "bottoms" selectivity. The selectivity of the hydrogenation reaction considers the production of secondary hydrogenation products such as MIBC, DIBK as well as IPA and MIBK production. Again, water is neglected in the calculation of selectivity as is the convention for researchers investigating MIBK synthesis.

$$X_{Ac} = 100\% \left[ \frac{F_{A0} - F_{A,B} - F_{A,D}}{F_{A0}} \right] \qquad (8\text{-}2)$$

**Table 8-14** MIBK productivity and Selectivity (CD 004)

| | Period TOS | Acetone Conversion X (%) | Productivity [g/hr*$g_{cat}$] MIBK | Total Organics | MIBK Selectivity Hydrogenation (wt%) | Overall Rxn (wt%) | Bottoms (wt%) |
|---|---|---|---|---|---|---|---|
| 1 | 35 to 40 | 6.2 | 0.020 | 0.040 | 80.5 | 51.1 | 51.1 |
| 2 | 54 to 60 | 35.3 | 0.104 | 0.384 | 100.0 | 27.2 | 27.3 |
| 3 | 70 to 78 | 33.2 | 0.124 | 0.448 | 100.0 | 27.3 | 27.4 |
| 4 | 96 to 98 | 46.3 | 0.418 | 0.688 | 99.1 | 78.3 | 78.4 |
| 5 | 112 to 115 | 16.6 | 0.312 | 0.366 | 93.0 | 84.7 | 86.9 |

*8.2.4 Hydrogen Utilization*

The amount of hydrogen needed for complete MO hydrogenation was calculated from the amount of MO and IMO to be hydrogenated as well as the number of moles of MIBK, DIBK and MIBC which were derivatives of MO hydrogenation. The MO conversion was calculated from the number of moles of MO and IMO produced and the number of moles of TMB, DIBK, MIBK, MIBC etc which are derivatives of MO. $C6^+$ unknowns, which were present in negligible amounts were not included in this calculation (molecular masses unknown). This did not affect the result in the number of significant figures reported.

The data in Table 8-15 demonstrates that hydrogen was fed in stoichiometric excess for each condition. The hydrogen uptake ranged from around 10 to 19% for the conditions for which water was removed from the reaction zone via a distillate stream. However, the hydrogen uptake efficiency was less than 1% for the condition of 100% reflux, as was also observed in the previous experiments CD 002 and CD 003. The data shows that the hydrogen uptake efficiency improved by two orders of magnitude while operating with an overhead distillate stream to remove water from the reaction zone.

**Table 8-15** Hydrogen utilization and stoichiometric excess (CD 004)

| | Hydrogen [L/hr] (STP) | Hydrogen [mol/hr] | MO & IMO [mol/hr] | MIBK [mol/hr] | $H_2$ required [mol/hr] | % Excess $H_2$ | $H_2$ uptake (%) | MO conversion X (%) |
|---|---|---|---|---|---|---|---|---|
| 1 | 57.8 | 2.579 | 0.0024 | 0.0158 | 0.0182 | 14077 | 0.9 | 86.6 |
| 2 | 11.0 | 0.491 | 0.1967 | 0.0810 | 0.2776 | 77 | 16.5 | 29.2 |
| 3 | 11.2 | 0.500 | 0.2363 | 0.0950 | 0.3313 | 51 | 19.0 | 28.7 |
| 4 | 59.3 | 2.646 | 0.0889 | 0.4177 | 0.5066 | 422 | 16.0 | 82.6 |
| 5 | 59.3 | 2.646 | 0.0108 | 0.2404 | 0.2513 | 953 | 9.7 | 95.7 |

Evidently, the majority of hydrogen fed to the reactor did not participate in chemical reaction. However, the results of the experiment demonstrate conclusively that the volumetric flow rate of hydrogen significantly affects the MIBK productivity and selectivity. Note that a step change in the hydrogen

volumetric flow rate from 11 to 59 L/hr between conditions 2 and 3, with other parameters held constant, resulted in an increase in MIBK by a factor of 3.4. In addition, the overall reaction selectivity increased from 27 to 78% as a large amount of unreacted MO was converted to MIBK due to the increase in hydrogen flow rate. The MO conversion increased from 29 to 83%. Although hydrogen was fed in stoichiometric excess, this result implies mass transfer limitations and hydrogen concentration gradients likely occurred for the conditions of high MIBK productivity. (i.e. hydrogen may not be in stoichiometric excess at the catalyst surface). In the fifth condition, at relatively low MO productivity (low reflux flow rate) 96% of the MO was converted to MIBK. However for the fourth condition for which the MIBK productivity was a maximum, the hydrogenation step was still controlling the overall synthesis with only 82% MO conversion.

The data in Table 8-15 also provides a comparison of the one zone versus two zone approach for MIBK synthesis via CD (CD 002 vs CD 004). Although different catalytic materials were used, the results suggest that the use of a multifunctional catalyst may be preferred for MIBK synthesis. The selectivity is largely governed by the presence of unreacted MO and to a lesser extent the reaction of MO to form higher molecular weight species. In addition, the production of MO appears to limit the overall productivity. A comparison of the first condition from CD 004 (100% recycle at .02 g/hr*g) to the results of CD 002 show a much higher MO conversion at a comparable MIBK productivity was achieved with the multifunctional catalyst. Using commercial catalyst in a two zone approach resulted in MO conversions ranging from 4 to 15%. In contrast, the MO conversion in condition 1 of CD 004 was much higher, 86.6%. Further, while the MIBK productivity was significantly enhanced utilizing the new CD process with the overhead distillate stream, MO conversions as high as 96% were achieved.

The relatively high MO conversion for the first condition, which also exhibited very low MIBK productivity and low hydrogen uptake efficiency, supports the notion that the production of MO was inhibited by water accumulation in the reactive section. The majority of the MO synthesized (86%) was converted to MIBK. Therefore, the MIBK productivity was low due to a low rate of MO synthesis.

### *8.2.5 CD Column Concentration Profiles (CD 004)*

Liquid samples were extracted from the CD column for both GC/TCD and GC/FID analyses at 75, 88 and 118 hrs TOS during steady state conditions 3, 4 and 5 respectively. GC/FID analyses of only the last samples collected at 118 hrs TOS revealed a significant amount of organic species. Trace denotes that peaks were observed in the GC/FID chromatogram but were rejected by the GC software due very low peak areas below the rejection limit (<< .1 wt%)) Moisture analysis via GC/TCD revealed significant quantities of water in all specimens. The results are summarized in Table 8-16.

**Table 8-16** Chemical compositions of samples obtained along the CD column (CD 004)

| No | TOS | Sample Port | Location (m) | Water (wt%) | Organics (wt%) |
|---|---|---|---|---|---|
| 3 | 75 | distillate | 7 | 8.21 | Distillate: 0.22 wt% C9 (avg. 74-76 TOS) |
| | | P1 | 4.95 | 5.72 | P1: Trace IPA, MIBK, MO, DAA and C9 |
| | | P2 | 3.36 | 3.96 | P2: Trace MO |
| | | P3 | 1.59 | 0.45 | P3: Trace MO and MIBK |
| | | reboiler | 0 | 0 | Bottoms: (avg 74-76 hrs TOS): 14.7 % MIBK, 34.1% MO, 2.59% DAA, 3.29% IMO, 0.59 wt% $C6^+$ |
| 4 | 88 | distillate | 7 | 7.77 | Distillate: 0.33 wt% C9 |
| | | P1 | 4.95 | 5.32 | P1: no organics detected |
| | | P2 | 3.36 | 0.32 | P2: Trace MO |
| | | P3 | 1.59 | 0 | P3: Trace MO and MIBK |
| | | reboiler | 0 | 0 | Bottoms: 34.4 wt% MIBK, 8.86 wt% MO, 3.63 wt% DAA, 0.35 wt% DIBK, 1.04 wt% IMO, 0.27 wt% C6+ |
| 5 | 118 | distillate | 7 | 7.05 | Distillate: 0.51 wt% C9, 0.97 wt% IPA |
| | | P1 | 4.95 | 3.79 | P1: 0.60 wt% IPa |
| | | P2 | 3.36 | 0.23 | P2: 0.60 wt% IPA, 0.84 wt% MIBK |
| | | P3 | 1.59 | 0.08 | P3: 0.53 wt% IPA, 0.94 wt% MIBK |
| | | reboiler | 0 | 0 | Bottoms: 1.07 wt% IPA, 43.8 wt% MIBK, 1.46 wt% MO, 0.67 wt% DIBK, 0.18 wt% TMB, 1.75 wt% DAA |

## 8.3 Pilot Plant Experiment CD 005

The previous CD experiment (CD 004) showed conclusively that the low MIBK activity occurred as a result of the inhibition of the DAA dehydration reaction as a consequence of the accumulation of water in the reactive section. More importantly, the previous CD experiment clearly demonstrated that a significantly enhanced MIBK productivity, selectivity and hydrogen uptake efficiency may be achieved from the *in situ* separation of water from the reactive section via the employment of an overhead distillate stream. In the last CD experiment, the MIBK productivity in the fourth condition was 21 times greater than the MIBK productivity observed when the reactor was operated without the overhead distillate stream. The previous CD experiment was an exploratory experiment and the results are preliminary since some steady states were maintained for brief periods and only three distinct process conditions were investigated for the new CD process. Consequently, a robust statistical experimental design was employed to obtain accurate steady state process data and to rigorously evaluate the effects of the process parameters on the resultant productivity and product distribution for one-step MIBK synthesis via CD.

### *8.3.1 Statistical Experimental Design*

A fifth CD experiment (CD 005) was carried out for the purpose of evaluating the catalyst performance characteristics for pilot scale conditions of trickle flow and for substantial time on stream as well as to obtain a fundamental understanding of this CD process by investigating the main effects and interactions of the major process variables. In particular, the effects of the column hydrodynamic parameters, specifically the reflux flow rate and hydrogen volumetric flow rate, on the MIBK productivity, selectivity and hydrogen utilization were investigated at a constant reaction temperature of 160°C. The acetone feed rate as well as the bottoms and distillate mass flow rates were kept constant. A robust statistical experimental design, outlined in Tables 8-17 and 8-18, was carried out. Each steady state condition was

maintained for at least 6 hours and for as long as 12 hours in order to obtain precise estimates of the steady state compositions of the product streams.

**Table 8-17** Process conditions investigated (CD 005)

| Run No. | Interval TOS | Reboiler Duty [Watts] | System Pressure [Mpa] (abs) | Press. Drop ΔP [kPa] | Rxn Temp [℃] | Ext. Heater Duty [Watts] | Solenoid (SV-1) on/off |
|---|---|---|---|---|---|---|---|
| 1 | 41 to 47 | 800 | 1.31 | 5.8 | 162 | 800 | .02 / 99.8 |
| 2 | 81 to 89 | 400 | 1.30 | 5.1 | 162 | 800 | .02 / 99.8 |
| 3 | 113 to 125 | 400 | 1.41 | 5.0 | 161 | 800 | .02 / 99.8 |
| 4 | 155 to 161 | 680 | 1.31 | 6.2 | 160 | 800 | .02 / 99.8 |
| 5 | 175 to 185 | 530 | 1.31 | 5.4 | 161 | 800 | .02 / 99.8 |

**Table 8-18** Steady State Mass flow rates (CD 005)

| | Acetone Feed [g/hr] | Hydrogen [L/hr] (STP) | Bottoms [g/hr] | Condensate [g/min] | Distillate [g/min] | Reflux Rate [g/min] | Reflux Ratio [%] |
|---|---|---|---|---|---|---|---|
| 1 | 141 | 10.8 | 58.6 | 41.3 | 1.19 | 40.1 | 97.1 |
| 2 | 141 | 10.9 | 58.9 | 7.11 | 1.23 | 5.9 | 82.7 |
| 3 | 141 | 60.0 | 58.1 | 9.89 | 1.13 | 8.8 | 88.5 |
| 4 | 141 | 60.0 | 55.4 | 44.3 | 1.12 | 43.2 | 97.5 |
| 5 | 141 | 35.9 | 54.0 | 25.4 | 1.17 | 24.2 | 95.4 |

The process conditions in Table 8-18 constitute a 2 X 2 full factorial experiment with a centre point in the variables reflux flow rate and hydrogen volumetric feed rate. The other process parameters are noise factors to be kept constant. The first condition represents a condition of high reflux flow rate and low hydrogen feed rate (+1,-1). The second condition is a condition of low reflux flow rate and low hydrogen feed rate (-1,-1). The third point is a condition of high hydrogen feed rate and low reflux flow rate (-1, +1). The fourth point is a condition of both high hydrogen feed rate and high reflux flow rate (+1,+1). The final condition is the centre point of intermediate reflux flow rate and hydrogen feed rate (0,0). The centre point allows for modelling of non-linear behaviour.

*8.3.2 Results (CD 005)*

The steady state reboiler composition as a function of time on stream is illustrated in Figure 8-11. The data shows that each steady state condition investigated resulted in a unique product distribution. The steady state MIBK productivity ranged from 0.10 to 0.37 [g/hr*$g_{cat}$] and the MIBK selectivity varied over a broad range from 22 to 89%. The first condition with high reflux flow rate and low hydrogen feed rate resulted in a large amount of unreacted MO. However, when the reflux flow rate was decreased in the second condition, a greater proportion of MO was converted to MIBK. In the third condition for which the reflux flow rate was minimized and the hydrogen flow rate was maximized, the vast majority of the MO synthesized was converted to MIBK. As expected, IPA production from the direct hydrogenation of acetone became significant for this process condition as the MO concentration was quite low. In addition, MIBC, which is produced from the hydrogenation of the carbonyl group of MIBK, appeared in the bottoms product.

In the fourth condition, where both the volumetric flow rate of hydrogen and reflux flow rate were maximized, the MIBK concentration in the reboiler product increased above 50 wt% to its maximum steady state value. However, a greater proportion of unreacted MO was present in the product compared to the previous condition. In the fifth condition, where both the reflux flow rate and hydrogen feed rate were at intermediate values (i.e. the centre point), the amount of MIBK and MO in the product also took on intermediate values. The product distributions in the bottoms product and the overhead distillate are summarized in Tables 8-19 and 8-20 respectively. The MIBK productivity and selectivity as well as the acetone conversion for the five steady state process conditions investigated are summarized in Table 8-21.

**Table 8-19** Steady state product distribution in the bottoms product (CD 005)

| | MIBK (wt%) | MO (wt%) | DAA (wt%) | IPA (wt%) | DIBK (wt%) | TMB (wt%) | IMO (wt%) | MIBC (wt%) | C6+ (wt%) |
|---|---|---|---|---|---|---|---|---|---|
| 1 | 12.70 | 36.75 | 4.10 | 0 | 0.00 | 0 | 3.50 | 0 | 0.49 |
| 2 | 30.21 | 18.41 | 1.60 | 0 | 0.47 | 0.19 | 2.03 | 0 | 0.48 |
| 3 | 44.61 | 1.38 | 1.61 | 0.98 | 0.64 | 0.00 | 0 | 0.28 | 0 |
| 4 | 52.27 | 7.01 | 3.63 | 0 | 0.45 | 0.19 | 0.96 | 0 | 0 |
| 5 | 41.48 | 6.96 | 2.78 | 0 | 0.41 | 0 | 0.96 | 0 | 0.20 |

*The water concentration in the reboiler product specimen were always below the peak area rejection limit of the GC analysis (<< 0.1 wt%) and is neglected from Table 8-19. The solvent, acetone, is neglected from the table.*

**Table 8-20** Steady state product distribution in the distillate (CD 005)

| | water [wt%] | IPA [wt%] | C9 (1.9 min) [wt%] | C9 (2.2 min) [wt%] | Acetone [wt%] |
|---|---|---|---|---|---|
| 1 | 8.13 | 0 | 0 | 0.24 | 91.6 |
| 2 | 7.49 | 0 | 0.36 | 0.41 | 91.7 |
| 3 | 6.80 | 0 | 0.48 | 0 | 92.7 |
| 4 | 8.06 | 0 | 0.48 | 0 | 91.5 |
| 5 | 7.86 | 0 | 0.66 | 0.21 | 91.3 |

**Table 8-21** MIBK productivity, selectivity and acetone conversion (CD 005)

| | Period TOS | Acetone Conversion X (%) | Productivity [g/hr*$g_{cat}$] MIBK | Productivity [g/hr*$g_{cat}$] Total Organics | MIBK Selectivity Hydrogenation (wt%) | MIBK Selectivity Overall Rxn (wt%) | MIBK Selectivity Bottoms (wt%) |
|---|---|---|---|---|---|---|---|
| 1 | 41 to 47 | 35.9 | 0.096 | 0.436 | 100.0 | 22.0 | 22.1 |
| 2 | 81 to 89 | 32.2 | 0.229 | 0.412 | 98.5 | 55.6 | 56.6 |
| 3 | 113 to 125 | 34.5 | 0.334 | 0.375 | 95.5 | 89.1 | 90.1 |
| 4 | 155 to 161 | 42.1 | 0.372 | 0.464 | 99.1 | 80.3 | 81.0 |
| 5 | 175 to 185 | 36.2 | 0.288 | 0.375 | 99.0 | 76.9 | 78.6 |

**Table 8-22** Hydrogen utilization and stoichiometric excess hydrogen (CD 005)

| | Hydrogen [L/hr] (STP) | Hydrogen [mol/hr] | MO & IMO [mol/hr] | MIBK [mol/hr] | $H_2$ required [mol/hr] | % Excess $H_2$ | $H_2$ uptake (%) | MO conversion X (%) |
|---|---|---|---|---|---|---|---|---|
| 1 | 10.8 | 0.482 | 0.240 | 0.0742 | 0.314 | 53 | 15.4 | 23.6 |
| 2 | 10.9 | 0.486 | 0.123 | 0.177 | 0.300 | 62 | 36.9 | 59.5 |
| 3 | 60.0 | 2.68 | 0.00820 | 0.259 | 0.267 | 902 | 10.2 | 97.0 |
| 4 | 60.0 | 2.68 | 0.0449 | 0.289 | 0.334 | 702 | 10.9 | 86.6 |
| 5 | 35.9 | 1.60 | 0.0435 | 0.223 | 0.267 | 500 | 14.0 | 83.8 |

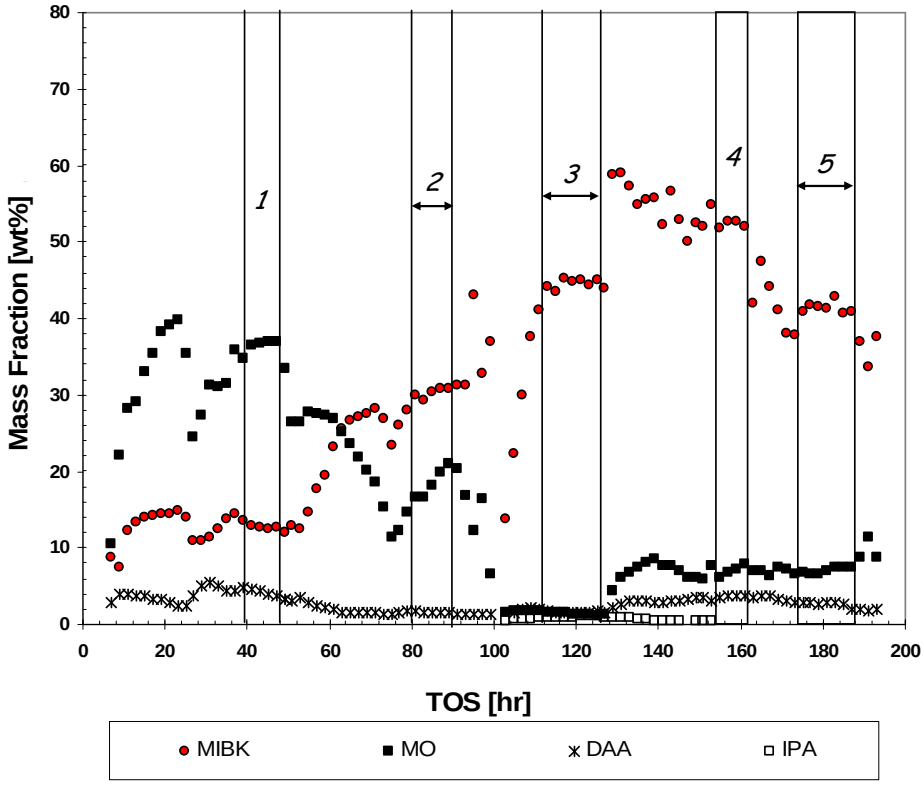


**Figure 8-11** Reboiler product composition as a function of TOS (CD 005)
*The concentrations of some minor constituents are neglected from the figure for clarity (MIBC, DIBK, $C6^+$, TMB, etc.)*

The chemical composition profiles along the major axis of the CD column were ascertained via collection of samples from the three sample ports at the end of each steady state process condition. The samples were analyzed by GC/FID and GC/TCD and are summarized in Table 8-23. As with the previous experiments, the organic species are present in relatively low concentrations, frequently falling below the peak area rejection limit of the GC. However, the major products MIBK and MO are frequently observed and were quantified. The organic species were more concentrated within the column for the conditions of low reflux flow rate (#2 and #3). IPA created from the direct hydrogenation of acetone was also most concentrated for these conditions where MO synthesis is at a minimum. This is expected since it is now well established within this work that acetone and MO compete for the same active sites.[18] The data in Table 8-23 suggests that the concentrations of the major products MO

and especially MIBK, which concentrate in the reboiler product are typically more concentrated at the reaction zone than in the stripping section. The results of condition #3 (Figure 8-12), shows that IPA, which is a relatively volatile compound, will concentrate in the reboiler product rather than the overhead distillate. Interestingly, IPA is more volatile than water, yet water becomes more concentrated in the acetone rich overhead distillate stream while IPA becomes more concentrated towards the reboiler. Water is not very miscible with MIBK but is highly miscible with acetone.

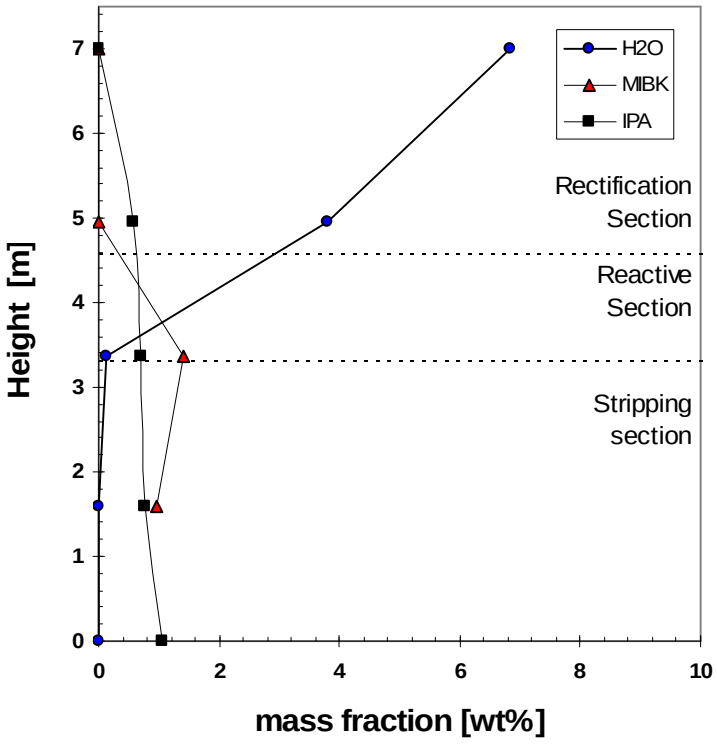


**Figure 8-12** Concentration of IPA, MIBK and water along the CD column at 125 hrs TOS (CD 005)

*The value at 7m is the distillate product analysis and the value at 0m is from the bottoms (reboiler) product analysis. MIBK had a value of 45 wt% in the reboiler product at 125 hrs TOS and is omitted from the figure for clarity.*

**Table 8-23** CD column concentration profiles (CD 005)

| No | TOS (hr) | Sample Port | Location (m) | Water (wt%) | Organics (wt%) |
|---|---|---|---|---|---|
| 1 | 47 | distillate | 7 | 8.17 | Distillate: 0.24 wt% C9 (2.2 min) |
| | | P1 | 4.95 | 5.18 | P1: n/a |
| | | P2 | 3.36 | 0.14 | P2: 0.70 wt% MO |
| | | P3 | 1.59 | 0 | P3: 0.69 wt% MO |
| | | reboiler | 0 | 0 | Bottoms: 12.7 wt% MIBK, 3.53 wt% IMO, 36.91 wt% MO, 3.66 wt% DAA, 0.49 wt% $C6^+$ |
| 2 | 89 | distillate | 7 | 7.57 | Dist: 0.34 wt% C9 (1.9 min), 0.37 wt% C9 (2.2 min) |
| | | P1 | 4.95 | 4.63 | P1: n/a |
| | | P2 | 3.36 | 0.33 | P2: 1.1 wt% MIBK, 0.97 wt% MO |
| | | P3 | 1.59 | 0 | P3: 0.66 wt% MIBK, 0.96 wt% MO |
| | | reboiler | 0 | 0 | Bottoms: 30.7 wt% MIBK, 2.25 wt% IMO, 20.91 wt% MO, 0.47 wt% DIBK, 0.19 wt% TMB, 1.50 wt% DAA |
| 3 | 125 | distillate | 7 | 6.83 | Dist: 0.48 wt% C9 (1.9 min) |
| | | P1 | 4.95 | 3.79 | P1: 0.57 wt% IPA |
| | | P2 | 3.36 | 0.12 | P2: 0.70 wt% IPA, 1.40 wt% MIBK |
| | | P3 | 1.59 | 0 | P3: 0.76 wt% IPA, 0.97 wt% MIBK |
| | | reboiler | 0 | 0 | Bottoms: 1.05 wt% IPA, 45.0 wt% MIBK, 0.47 wt% IMO, 1.36 wt% MO, 0.28 wt% DIBK, 0.23 wt% TMB, 1.64 wt% DAA, 0.07 wt% $C6^+$ |
| 4 | 163 | distillate | 7 | 8.19 | Dist: 0.48 wt% $C_9$ (1.9 min) |
| | | P1 | 4.95 | 5.12 | P1: n/a |
| | | P2 | 3.36 | 0.21 | P2: 0.92 wt% MIBK |
| | | P3 | 1.59 | 0 | P3: n/a |
| | | reboiler | 0 | 0 | Bottoms: 46.1 wt% MIBK, 0.96 wt% IMO, 7.07 wt% MO, 0.39 wt% DIBK, 3.67 wt% DAA |
| 5 | 185 | distillate | 7 | 7.84 | Dist: 0.34 wt% C9 (1.9 min) 0.37 wt% C9 (2.2 min) |
| | | P1 | 4.95 | 5.39 | P1: n/a |
| | | P2 | 3.36 | 0.25 | P2: 0.94 wt% MIBK |
| | | P3 | 1.59 | 0 | P3: 0.77 wt% MIBK |
| | | reboiler | 0 | 0 | Bottoms: 40.8 wt% MIBK, 0.99 wt% IMO, 0.42 wt% DIBK, 0.19 wt% TMB, 0.20 wt% $C6^+$ |

### *8.3.3 Mass Balance and Process Stability*

The mass balance about the CD column during the 5 steady state conditions investigated in this experiment are summarized in Table 8-24. The results demonstrate that the material losses from the column were not appreciable. The material losses were about 5.7 to 7.7% for the conditions of low hydrogen flow rate, which is comparable to the process variation, but were as high as 10.3 to 12.6% when the hydrogen volumetric flow rate was maximized at 60 L/hr (STP). The high volumetric flow rate of hydrogen may have lead to increased losses by entrainment. The mass flow rates of the two product streams were measured directly during the experiment. The acetone feed rate was inferred from the known calibration of the pump. Similarly the hydrogen feed rate was carefully controlled and accurately monitored using a Brooks 5850E mass flow controller, calibrated by Trillium Measurement and Control Ltd. (Markham,

ON). The controller is reported to be accurate to ± 1.0 % according to the published design specifications.

**Table 8-24** Mass balance about the CD column (CD 005)

| | Acetone Feed [g/hr] | Hydrogen Feed [L/hr] (STP) | [g/hr] | H2 uptake (%) | Hydrogen exhaust [g/hr] | Bottoms [g/hr] | Distillate [g/hr] | Losses (%) |
|---|---|---|---|---|---|---|---|---|
| 1 | 140.6 | 10.8 | 0.97 | 15.4 | 0.82 | 58.57 | 71.25 | 7.7 |
| 2 | 140.6 | 10.9 | 0.98 | 36.9 | 0.62 | 58.86 | 74.04 | 5.7 |
| 3 | 140.6 | 60.0 | 5.40 | 10.2 | 4.84 | 58.15 | 67.95 | 10.3 |
| 4 | 140.6 | 60.0 | 5.40 | 10.9 | 4.81 | 55.37 | 67.47 | 12.6 |
| 5 | 140.6 | 35.9 | 3.23 | 14.0 | 2.78 | 53.96 | 70.40 | 11.6 |

The process stability during the steady state conditions is characterized in Table 8-25 by the relative standard deviation (RSD) which is the standard deviation divided by the mean value over the interval, expressed as a percentage. The data in Table 8-25 shows that the MIBK concentration in the reboiler product was extremely stable during these steady states, with an average RSD of 1.5%. The other products exhibited a higher average RSD of 6.4%, with some individual observations as high as 14%. The MO concentration in particular showed significance variance in conditions #2 and #3. The data in Figure 8-11 suggests the MO concentration may have been drifting during condition #2. However, the variance in the products is quite acceptable with the exception of perhaps 3 observations (2 in condition #3 and 1 in condition #2) which exceeded 10% RSD.

To account for this process variation, the process was monitored for very long time periods in order to obtain a sufficient number of observations to minimize the 95% confidence bounds on the estimates of the concentrations of species in the products. For example, condition #3 which exhibited significant variance in the MO and DIBK measurements, was maintained for 12 hours. The 95% confidence bounds on the major products in the reboiler, expressed as a relative error are summarized in Table 8-26. The results show that the majority of observations are accurate to within ± 5% relative error. Only one

observation of MO concentration is as high as ± 10 %. However, the MO concentration for this condition is low. (i.e. Condition #3, [MO] =1.38 ± 0.146 wt%)

**Table 8-25** Relative standard deviation of concentrations of species in the reboiler product for the 5 steady state conditions (CD 005)

| | MIBK (%) | MO (%) | DAA (%) | DIBK (%) |
|---|---|---|---|---|
| 1 | 1.49 | 0.65 | 8.84 | n/a |
| 2 | 1.88 | 10.7 | 6.40 | 1.58 |
| 3 | 1.39 | 14.2 | 5.24 | 10.9 |
| 4 | 0.87 | 9.88 | 4.09 | 4.28 |
| 5 | 1.78 | 5.56 | 3.28 | 3.53 |

**Table 8-26** 95% confidence bounds on estimates of steady state concentrations of species in the reboiler product expressed as relative errors for the 5 steady state conditions investigated (CD 005)

| | MIBK (± %) | MO (± %) | DAA (± %) | IPA (± %) | DIBK (± %) |
|---|---|---|---|---|---|
| 1 | 1.46 | 0.63 | 8.66 | | |
| 2 | 1.65 | 9.40 | 5.61 | | 1.38 |
| 3 | 1.03 | 10.53 | 3.88 | 5.91 | 8.1 |
| 4 | 0.85 | 9.69 | 4.01 | | 4.20 |
| 5 | 1.42 | 4.45 | 2.62 | | 2.82 |

### *8.3.4 Analysis (CD 005)*

The analysis of the results of the last two pilot scale experiments, CD 004 and CD 005, demonstrate that the hydrogen volumetric flow rate and reflux flow rate have significant effects on the MIBK productivity and selectivity. The results presented in this section suggest that the MIBK productivity and overall reaction selectivity are limited by the rate of transport of hydrogen to the active sites. Low MIBK selectivity is largely due to unreacted MO in the reboiler product stream and to a much lesser extent due to the consecutive reactions of MO to produce phorones etc. and the consecutive reactions of MIBK to produce DIBK and MIBC.

The MIBK productivity and selectivity were observed to increase substantially with increased hydrogen volumetric flow rate (Figures 8-13 and 8-

14). Interestingly, the MO conversion to MIBK, i.e. the proportion of MO and isomer converted to MIBK, DIBK and MIBC, is not only dependent on the hydrogen flow rate but also appears to be affected by the reflux flow rate in the column. Evidently, the increased catalyst wetting efficiency due to increased reflux flow rate appears to have inhibited the hydrogenation of MO.

The MIBK productivity increased substantially with increasing hydrogen volumetric flow rate. The MIBK productivity was also affected by the reflux flow rate being over 2 times greater for the condition of low reflux flow rate compared to the condition of high reflux flow rate at a constant nominal hydrogen volumetric flow rate of 11 L/hr. The hydrogen uptake efficiency (Figure 8-15) suggests the hydrogen was more efficiently utilized for conditions of low reflux flow rate.

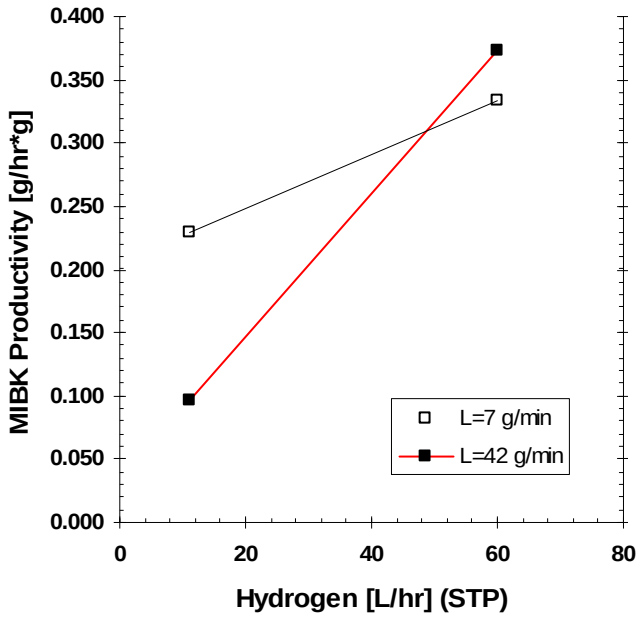


**Fig 8-13** The main effects of hydrogen flow rate ($V_H$) and reflux flow rate (L) on MIBK productivity (box points CD 005)

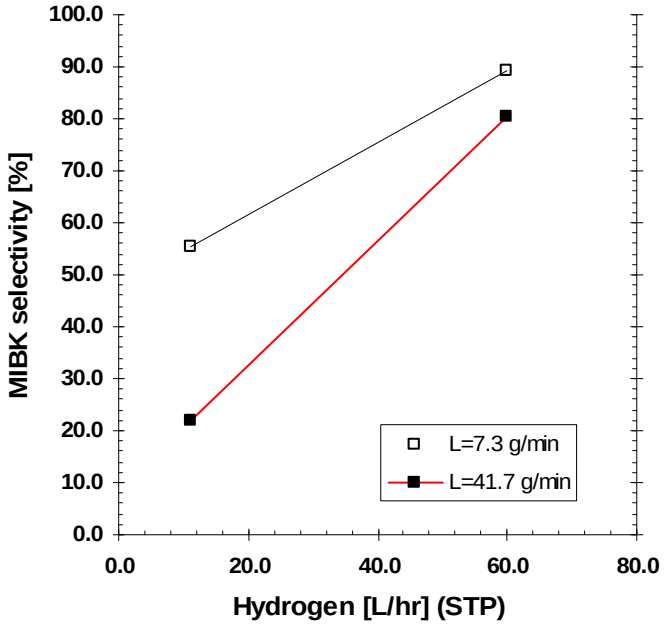


**Fig 8-14** The main effects of hydrogen flow rate ($V_H$) and reflux flow rate (L) on MIBK selectivity (box points CD 005)

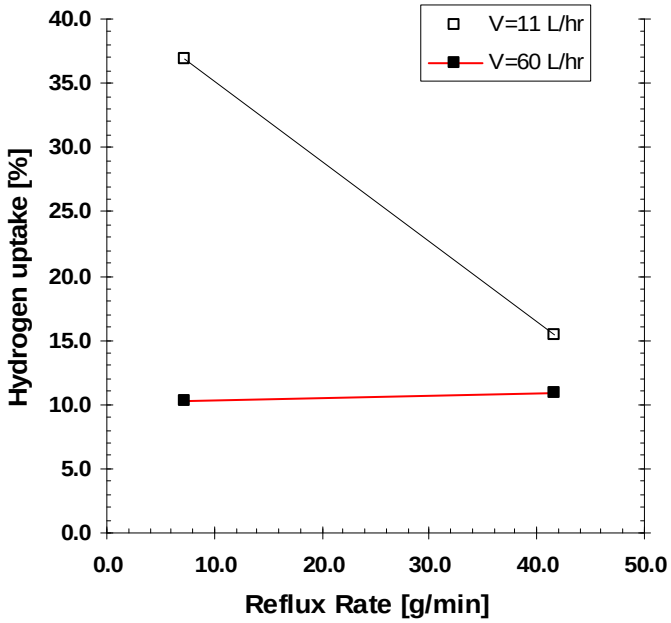


**Figure 8-15** Effect of reflux flow rate (L) and hydrogen volumetric flow rate ($V_H$) on the hydrogen uptake efficiency ($\eta$) (data from box points of CD 005)

Multivariable regression analysis of the data for CD 005 including the centre point for these steady state conditions using NLREG v.5.4 (Sherrod Software) shows that the hydrogen uptake efficiency is negatively correlated with hydrogen volumetric flow rate (R=-.705) That is, the greater the hydrogen flow rate, the less efficiently it is used, albeit the effect is weak. The results also show that the hydrogen uptake efficiency is negatively correlated with the reflux flow rate (R=-.527). The hydrogen utilization decreases with increasing reflux flow rate. This effect is also weak but appears to be significant. The low coefficients of multiple determination may reflect a non-linear dependence rather than lack of a cause-and-effect relationship.

The proportion of MO converted to MIBK (and derivatives of MIBK) as a function of reflux flow rate for all of the steady state conditions investigated in the last two CD experiments utilizing an overhead distillate stream is illustrated in Figure 8-16. This data supports the conclusion that the hydrogenation of MO is limited by the rate of hydrogen transport and provides more convincing evidence to support the conclusion that an increase in the reflux flow rate inhibits the transport of hydrogen to the active sites. The dependence of the MIBK productivity, selectivity and MO conversion on the volumetric flow rate of hydrogen is direct evidence of an external mass transfer limitation in the hydrogenation step. The effect of hydrogen flow rate clearly has a greater effect on the MO conversion than does the effect of reflux flow rate. However, the results in Figure 8-16 clearly shows that the MO conversion diminishes with increasing reflux flow rate, which suggests the liquid phase presents a barrier to mass transfer. In Figure 8-16, the MO conversion only considers the MO converted to MIBK and derivatives of MIBK via hydrogenation. (i.e. the conversion of MO to phorones and derivatives is not considered)

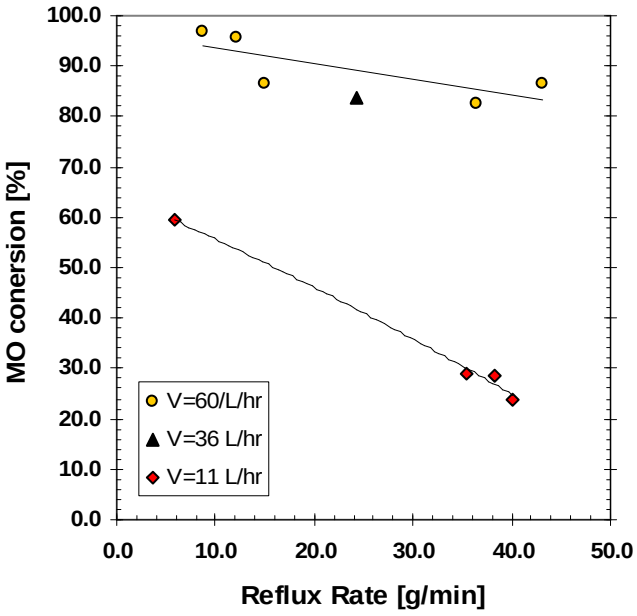


**Figure 8-16** Effects of hydrogen flow rate and reflux flow rate on the MO conversion to MIBK (CD 005) *Each data point in Figure 8-15 represents a value averaged over the steady state condition from experiments CD 004 and CD 005 utilizing an overhead distillate stream*

In contrast to the results of the preliminary CD experiments in Chapter Seven which showed that the synthesis of MO using Amberlyst 15 cation exchange resin is a liquid limited reaction for which the MO productivity increases with reflux flow rate, the results of CD 004 and CD 005 (Figures 8-17 and 8-19) indicate that the total productivity of the all organic species is only weakly dependent on the reflux flow rate for the catalyst and reaction conditions investigated for the CD process utilizing an overhead distillate stream. The average steady state total productivity of the collective of all organic products in the five process conditions of experiment CD 005 was 0.412 [g/hr*$g_{cat}$] with a maximum and minimum of .464 and .375 [g/hr*gcat] respectively. The main effects of reflux flow rate and hydrogen volumetric flow rate from CD 005 illustrated in Figure 8-17 suggest a very weak effect. For the condition of low hydrogen flow rate the total productivity only increased by 5.8% between the low and high reflux flow rate condition. In the case of the high hydrogen flow

rate condition, the increase in total productivity from the low to high reflux flow rate condition was more pronounced, 23.7%.

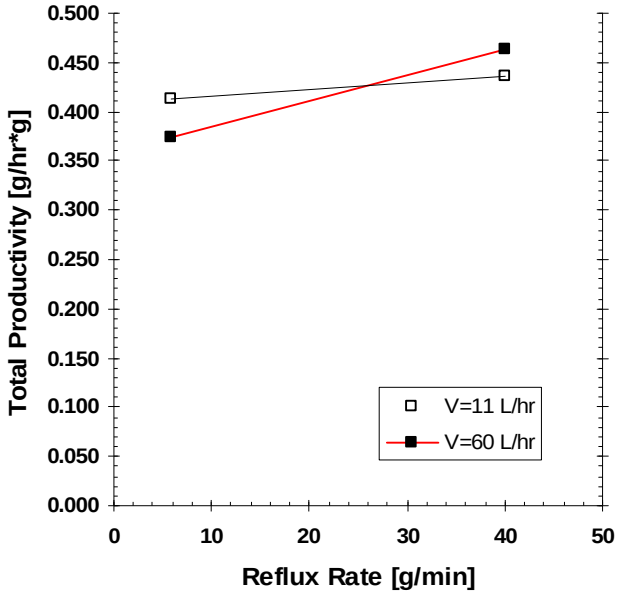


**Figure 8-17** Effects of reflux rate and hydrogen flow rate on total productivity (Box points CD 005)

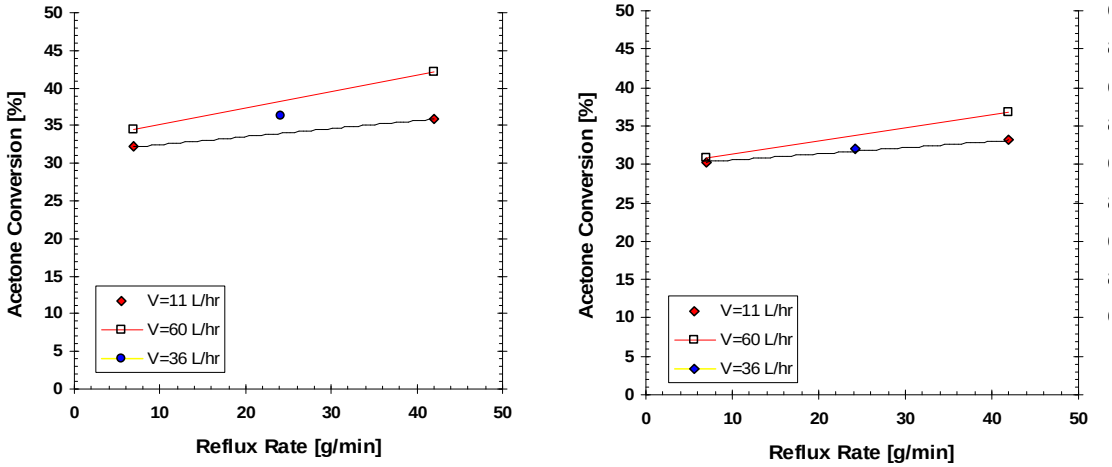


**Figure 8-18** Effects of hydrogen flow rate and reflux rate on acetone conversion (CD 005) (left) raw data (right) normalized to account for material losses

*The calculation of acetone conversion is based on the amount of acetone fed and the amounts in the reboiler and distillate streams and can be significantly affected by material loss. The figure in the right is normalized assuming the material losses from the column (Table 8-24) was entirely acetone. Material loss is through the pressure control outlet valve. The material has the composition of the distillate at this access point.*

The results in Figures 8-17 and 8-18 imply a process interaction, whereby the effects of the reflux flow rate on the total productivity and acetone conversion depends on the hydrogen volumetric flow rate. The hydrogen feed stream may result in improved turbulence and enhanced mass transfer. Alternatively, the enhanced productivity may be a kinetic phenomenon such as the synergistic effect observed in FBR experiments (Chapter Six). However, when also considering the preliminary data from CD 004 (Figure 8-19), the effect of hydrogen flow rate on the total productivity is not clear.

An outlier is reported in Figure 8-19 which corresponds to a condition from CD 004, which was only maintained for 2 hours and was not likely at steady state. All other observations were within ±13.8% of the average value regardless of the process conditions. However, with the exception of the first two data points in Figure 8-19 (and the outlier), the productivity increased monotonically with reflux flow rate during the interval from 12 to 43 [g/min]. The data in Figure 8-19 implies a minimum is observed. Perhaps the benefits of enhanced mass transfer may be offset by a reduction in contact time in the reaction zone at low reflux flow rate. An external mass transfer effect is evident; however, the CD process appears to be approaching the kinetic control regime for MO synthesis. The data reported previously shows that the hydrogenation of MO is clearly controlled by external mass transfer of hydrogen. The hydrogen feed rate does not have a large effect on the total productivity of organic species but does have a profound effect the proportion of MO that is converted to MIBK and hence the MIBK productivity and selectivity.

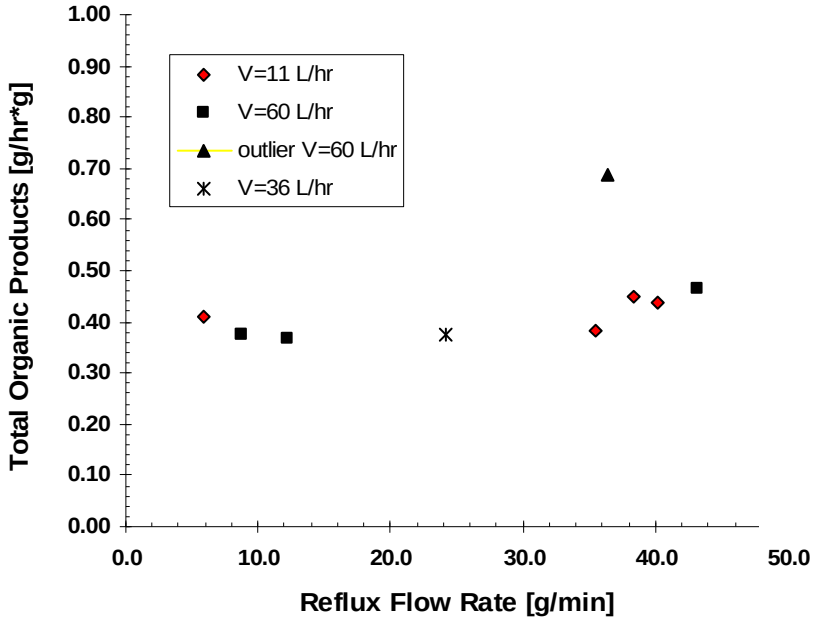


**Figure 8-18** Effect of Reflux flow rate on the steady state total productivity (all organic products [g/hr*$g_{cat}$]) (experiments CD 004 and CD 005 with overhead distillate stream) *The outlier corresponds to condition #4 of CD 004, which was maintained for only 2 hours and was not likely at steady state.*

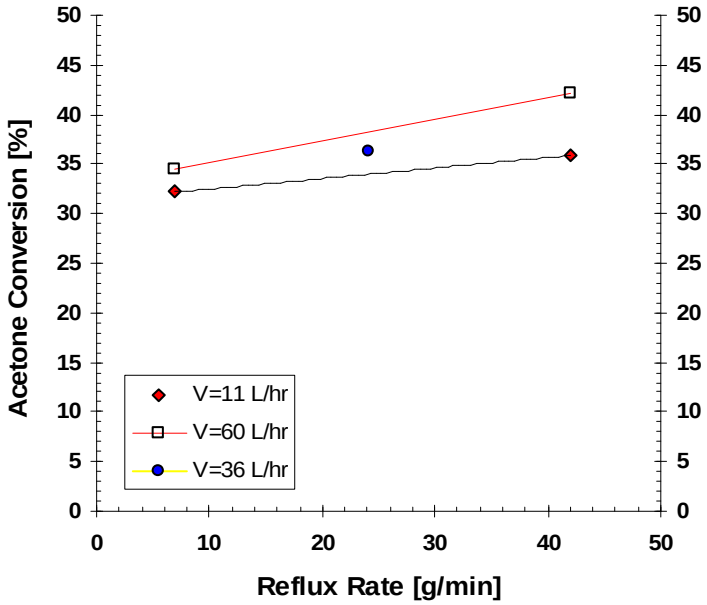


**Figure 8-19** Effect of reflux flow rate and hydrogen volumetric flow rate on acetone conversion (CD 005)

The total productivity is relatively insensitive to reflux flow rate. However the MIBK selectivity improves with lower reflux flow rate due to enhanced MO conversion. This is a promising result for the prospect of using CD technology for the commercial production of MIBK, since a lower reflux flow rate implies lower energy consumption necessary to drive the distillation process. A comparison of condition #3 to condition #4 for CD 005 shows that when the reflux flow rate was increased from 8.8 to 43.2 g/min at a nominal hydrogen volumetric flow rate of 60 L/hr (STP), the MIBK productivity increased by only 11%. However, to achieve the higher reflux flow rate, the reboiler duty was increased by 70% from 400 to 680 W. Condition #3 with the lower reflux flow rate had much lower power consumption, a slightly lower MIBK productivity but also had a higher MIBK selectivity in the reboiler product (90.1 wt% compared to 81.0 wt% neglecting solvent). Thus, operating at a lower reflux flow rate may lead to more economical and a highly selective process for one-step MIBK synthesis.

Condition #2 of the last CD experiment (CD 005) resulted in an unusually high hydrogen uptake efficiency (36.9%). Generally, over the 9 steady state conditions investigated in the last 2 CD experiments operating with an overhead distillate stream, the hydrogen uptake efficiency ranged from only 10 to 19%. For condition #2, the reflux flow rate and the hydrogen flow rate were minimized. Additionally, condition #2 had by far the lowest reflux ratio (82.7%). A lower reflux ratio implies a greater rate of removal of water from the system for a given reaction rate. However, the water concentration in the reactive section and the mass flow rate of water in the distillate stream did not correlate with either the hydrogen uptake efficiency or the MO conversion. Perhaps the unique combination of low reflux rate, low hydrogen feed rate and low reflux ratio for this specific condition resulted in a condition more favourable for efficient hydrogen utilization. It is tempting to suggest that higher hydrogen uptake efficiency may be achieved at lower reflux ratios below some critical value (Figure 8-20). However, this inference would be based on a

single observation. More experimentation is needed for conditions of low reflux ratio to confirm or refute this.

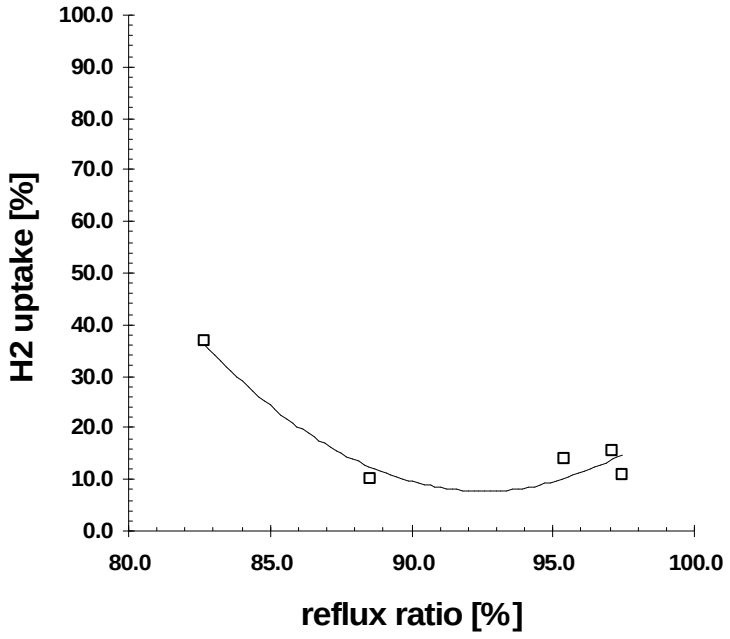


**Figure 8-20** Effect of reflux ratio on hydrogen uptake efficiency (CD 005)

*Note the hydrogen volumetric flow rate and reflux flow rate affect hydrogen uptake efficiency as well. These parameters were not kept constant for the experiments in Figure 8-16. However, the figure illustrates the unusually high value of hydrogen uptake efficiency for one observation at low reflux flow rate.*

The hydrogenation of MO was achieved with very high selectivity. In CD 005, the MO hydrogenation selectivity to MIBK was greater than or equal to 99 % (wt%) for four of the five conditions investigated. The lowest selectivity was 96 wt% (95.0 mol%), for condition #3 where the MO conversion was the greatest (97.0%). For this condition, the direct hydrogenation of acetone to produce IPA was significant due to the low MO concentration. In addition consecutive reactions involving MIBK also became significant for condition #3 due to the high MIBK concentration. The hydrogenation of MIBK to produce MIBC was observed as well as the reaction of MIBK with acetone to produce DIBK. Considering the results of experiments CD 004 and CD 005, the hydrogenation selectivity improved significantly when the CD process was operated with an overhead distillate stream to remove water from the reaction

zone. In the absence of a distillate stream, the suppression of DAA dehydration resulted in a greater rate of IPA production. The selectivity in condition #1 of CD 004 with 100% recycle was only 80%.

A comparison of the hydrogenation selectivity for CD 005 to that of the commercial 0.5 wt% $Pd/Al_2O_3$ catalyst investigated previously (CD 002), shows that significantly higher hydrogenation selectivity was achieved with the $Pd/Nb_2O_5/SiO_2$ catalyst. The 0.5 wt% $Pd/Al_2O_3$ catalyst, when used for MO hydrogenation under kinetic control in a moisture free environment resulted in MIBK selectivities ranging from 81.7 to 98.1 mol% and had an average value of 94.5 mol% at 100°C. Note that the hydrogenation of acetone has a higher activation energy than MO hydrogenation. Therefore, the selectivity in the autoclave using the $Pd/Al_2O_3$ catalyst would be worse at 160°C than the results reported at 100°C. In a previous CD experiment (CD 002), the MO hydrogenation selectivity using the commercial $Pd/Al_2O_3$ catalyst at ca 120°C and 100% recycle, ranged from 84.4 to 94.9 mol% but the MO conversion was very low (4 to 15%). In terms of mol percent, the MIBK selectivity for the hydrogenation reaction in the last CD experiment (CD 005) at 160°C and utilizing an overhead distillate stream ranged from 95.0 to 100 mol% with MO conversion as high as 97%. The higher hydrogenation selectivity observed with the $Pd/Nb_2O_5/SiO_2$ catalyst was largely due to a suppression of acetone hydrogenation as a consequence of the lower Pd loading (0.04 wt% Pd).

The use of the multifunctional $Pd/Nb_2O_5/SiO_2$ catalyst resulted in a significant improvement in the overall reaction selectivity. Condition #1 (100% reflux) from CD 004 resulted in over 50 % selectivity to MIBK. The commercial catalysts resulted in 3.6 to 13.8 (wt%) selectivity to MIBK at a comparable MIBK productivity (CD 002). The significant improvement in selectivity is a result of the rapid hydrogenation of MO to MIBK using the multifunctional catalyst. The proportion of isophorone, mesitylene and higher molecular mass species produced from consecutive reaction of MO was much

higher using Amberlyst 15 and a separate hydrogenation catalyst in a two zone approach (CD 002). In contrast, isophorone and phorone were never observed and mesitylene (TMB) was rarely observed using the multifunctional niobia catalyst.

The overall MIBK selectivity was significantly enhanced from the process engineering solution involving the use of an overhead distillate stream to remove water from the system. This significantly enhanced the hydrogen uptake efficiency resulting in MO conversions as high as 97% and MIBK selectivities as high as 90% in the reboiler product (neglecting solvent). In contrast, the one-step synthesis of MIBK via CD utilizing a state-of-the-art Pd/Amberlyst catalyst reported by Lawson and Nkosi[32] operating at 100% reflux resulted in MIBK selectivities which ranged from 54.1 to 67.6% (wt %). The maximum selectivity was achieved after 48 hours of semi-batch distillation using 100 mL of catalyst and 55 L/hr (STP) of hydrogen. After two days of semi-batch distillation, the MO conversion was only 71.7%.[32]

## 8.4 Conclusions

Moisture analysis of samples obtained from the reactive and rectification sections of the CD reactor operating at 100% reflux revealed that the accumulation of water in the CD column was responsible for the inhibition of MO synthesis, which resulted in the relatively low MIBK productivities observed in previous CD experiments. A novel CD process was developed, whereby an overhead distillate stream operating at a reflux ratio of 83 to 97% enabled the continuous removal of water from the system. As a direct result, the MIBK productivity increased by a factor of 21 times compared to the initial benchmark where the process was operating at 100% reflux. The hydrogen uptake efficiency increased by two orders of magnitude and MO conversions as high as 97% were achieved. The hydrogenation selectivity also increased from 81% to values ranging from 93 to 100 % (wt%). The results demonstrate that a

moisture free reboiler product with MIBK in excess of 50 wt% MIBK could be easily achieved using the new CD process. Higher concentrations could undoubtedly be achieved by varying the mass flow rates.

This result is significant since state-of-the-art processes for MIBK synthesis typically achieve less than 30 wt% MIBK in the product necessitating further refining.[23,24] Moreover, the downstream refining for these processes is problematic and expensive. Water for example is known to form azeotropic mixtures with MIBK.[1] In addition, the MIBK synthesis was carried out with great success at operating pressures much lower than state-of-the-art processes for MIBK.

The hydrogenation stage remains the controlling step in the overall MIBK synthesis via CD. The MIBK productivity and selectivity are strongly dependent on the hydrogen volumetric flow rate. Interestingly, the results show that the MO conversion is not only dependent on the hydrogen flow rate but also diminished with increasing reflux flow rate. This indicates that the liquid phase presents a barrier to hydrogen mass transfer. The MIBK selectivity is largely due to unreacted MO and is significantly improved by utilizing a multifunctional catalyst and from the enhancement of hydrogen mass transfer by maximizing the hydrogen flow rate and minimizing the reflux flow rate. At high MO conversions, the direct hydrogenation of acetone to produce IPA becomes significant since acetone and MO compete for the same active sites. In addition, consecutive reactions of MIBK to form MIBC and DIBK become apparent. These competing reactions, along with unreacted MO, constrained the MIBK selectivity to 90% for the condition of maximum MO conversion (97%).

In contrast to the first CD experiment using Amberlyst 15 to synthesize MO, the acid catalyzed reactions to produce MO are relatively insensitive to the reflux flow rate for the process conditions investigated utilizing the new CD

process. Although an external mass transfer effect is evident, the reaction appears to be approaching the regime of kinetic control. When operating with an overhead distillate stream, the average total productivity of all organic species over 8 steady state process conditions, ignoring an outlier with an unusually high productivity, was 0.41 [$g/h*g_{cat}$]. The maximum deviation from this average value was 13.8% .

The fact that MIBK and overall productivity is relatively insensitive to reflux flow rate is promising for CD technology. Operation at a lower reflux rate is more economical due to a reduction in energy consumption. In these experiments, the MIBK selectivity was maximized at a condition of minimal reflux flow rate and maximum hydrogen feed rate. For this condition 97% MO conversion was achieved and the MIBK selectivity in the reboiler product was 90% (neglecting acetone). The MIBK productivity for this condition was only 11% lower than the maximum MIBK productivity observed in the experiment when both the reflux flow rate and hydrogen flow rate were maximized.

Although water can be removed in the overhead distillate stream, the vast majority of organic species concentrate in the reboiler product. Only trace amounts of $C_9$ hydrocarbons are observed in the overhead distillate. IPA was only observed for the overhead distillate in one condition in one experiment. Samples obtained along the column major axis show that IPA becomes more concentrated towards the reboiler. Thus, the selectivity in the bottoms product is not significantly influenced by the *in situ* separation of organic species (other than acetone). However, the product distribution is strongly dependent on the reflux flow rate and hydrogen volumetric flow rate. The MIBK selectivity in the reboiler product ranged from 22.1 to 90.1% over the process conditions investigated.

# Chapter Nine

## Conclusions and Recommendations

### 9.1 Conclusions; Phase I – Elucidation of structure activity relationships

The effects of the most important catalyst parameters for dispersed niobia catalysts including the niobia loading, the calcination temperature, the nature of the oxide support and the support thermal pre-treatment temperature were investigated with the goal of elucidating the catalyst structure-activity relationships for MO synthesis. The catalyst activity, selectivity and stability for MO synthesis at 160°C were ascertained in a batch autoclave. The catalysts were characterized via EDXRF, XRD, $NH_3$/TPD, BET, Raman spectroscopy and *in situ* DRIFT spectroscopy of adsorbed pyridine probe molecules. The results demonstrate that each of the catalyst parameters had a significant effect on the catalyst properties and catalytic performance for MO synthesis.

Perhaps the most important of these catalyst parameters is the influence of the calcination temperature. Catalysts calcined at 500°C exhibited only Lewis acidity whereas catalysts calcined at 100°C exhibited very strong Bronsted acidity as well as Lewis acidity. The activity of silica catalysts for MO synthesis was found to be correlated to the strength of the acid sites. More importantly, catalysts exhibiting Bronsted acidity showed excellent stability for MO synthesis whereas those catalysts calcined at 500°C consistently deactivated and reached final acetone conversions dependent on the catalyst formulation. The effect of calcination at 500°C is irreversible. This implies that the annihilated Bronsted sites are not regenerated upon rehydration and that the resultant niobia structure is thermodynamically stable. It is postulated that in the hydrated state, there exists a boundary film several monolayers thick at the liquid-solid interface. It is proposed that the resultant catalyst stability associated with Bronsted acidity is due to a pseudo homogeneous reaction

occurring within the boundary film at the liquid solid interface as a consequence of the solvation of the niobium oxide phase and facilitated by facile proton exchange between the Bronsted sites and basic species in the liquid phase such as water or acetone which may be readily protonated. In contrast, the strong adsorption of water and other species on Lewis acid sites leads to catalyst deactivation.

The nature of the oxide support had a significant effect on the catalytic activity of the niobia catalysts. The most striking evidence of this is a comparison of the nature and strength of the acidity observed in niobia dispersed on fumed silica compared to niobia dispersed onto a Norpro SS 65137 silica catalyst carrier. On the catalyst carrier, the uptake of the niobia precursor was much less efficient. However, the niobium oxide phase on the catalyst carrier exhibited unique and very strong Bronsted acid sites not observed in the fumed silica catalyst or in other catalysts. *in situ* DRIFT spectra of adsorbed pyridine revealed that the Lewis acidity seen in the fumed silica catalysts was significantly diminished in the niobia dispersed onto the Norpro catalyst carrier. Evidently, the physico-chemical interaction between niobia and the catalyst carrier is distinct from its interaction with fumed silica. In the catalyst screening studies, the titania catalyst resulted in the highest activity per gram of niobia of the catalysts calcined at 500°C. It is interesting to note, that $TiO_2$ has a very low band gap compared to the other catalyst supports investigated, which may have lead to a strong metal-support interaction.

The thermal pre-treatment had a noticeable effect on the activity of catalysts for MO synthesis. Catalysts calcined at 500°C were more active for MO synthesis when the support was activated at elevated temperature (ca. 400°C) prior to reaction with niobium ethoxide precursor compared to those supports activated at 100°C. It is concluded that the increased surface coordinative unsaturation of the support oxide resulted in a stronger interaction with the surface oxide phase and consequently greater Lewis acidity. In the

case of silica catalysts, catalysts calcined at 500°C also showed greater initial activity when the support was activated at elevated temperature. However, for silica catalysts calcined at 100°C, the catalysts were more active when the support activation temperature was minimal but sufficient to remove physisorbed species (i.e. ca. 100°C). Since the thermal pre-treatment controls the surface hydroxyl concentration, the results suggest that the surface hydroxyl groups of the silica play a role in the generation of Bronsted acidity in the niobia overlayer.

In the case of $Nb_2O_5/\gamma\text{-}Al_2O_3$ catalysts, it is unclear if the niobium oxide phase acts as a catalyst or a promoter. The gamma alumina support had significant inherent Lewis acidity, exhibited significant activity for MO synthesis and should be considered as a co-catalyst. However the addition of a small amount of niobia less than 1/3 monolayer coverage to the gamma alumina resulted in a dramatic increase in the catalyst activity depending on the calcination temperature. Catalysts calcined at 500°C showed about double the initial activity for MO synthesis compared to the gamma alumina support while catalysts calcined at 100°C exhibited about three times the initial activity. Further addition of niobia beyond about 1/3 monolayer coverage resulted in a marked decrease in initial activity for MO synthesis for catalysts calcined at 100°C and a slight decrease with increasing niobia loading for catalysts calcined at 500°C.

The result for catalysts calcined at 500°C is consistent with the spectroscopic results of Datka et al.[91] who argued that after a critical optimum niobia loading, Lewis acid sites in the niobium oxide phase are created at the expense of relatively stronger Lewis acid sites on the alumina support. The catalysts calcined at 100°C exhibit Bronsted acidity, however Bronsted acidity was not observed in the alumina support. One would expect the activity to continue to increase with increasing niobia loading. Evidently, in the case of catalysts calcined at 100°C, highly dispersed niobia species are responsible for

the enhanced catalytic activity. A possible explanation is that the Bronsted sites of $Nb_2O_5/\gamma$-$Al_2O_3$ catalysts are associated with adlineation sites (Nb-OH-Al) located at the edges of the 2D niobia overlayer whose population diminish with increasing niobia loading beyond a critical niobia loading as the niobia overlayer is developed. In contrast, for silica catalysts the (Nb-OH-Nb) bridging hydroxyls in the niobia overlayer may be primarily responsible for catalytic activity. Thus the activity increases linearly with niobia content. Alternatively, the niobia may be highly dispersed on silica which prevents the complete development of a monolayer resulting in greater access to (Si-OH-Nb) bridging hydroxyls. The effect of the thermal pre-treatment temperature of the silica support indicates that the (Si-OH-Nb) bridging hydroxyls also contribute to the Bronsted acidity of the catalyst.

The initial activity of $Nb_2O_5/SiO_2$ catalysts calcined at 100°C for MO synthesis at 160°C were found to increase linearly with niobia loading up to half monolayer coverage. Catalysts calcined at 500°C also increased with niobia loading although the effect was less pronounced. The lack of an optimum niobia loading for $Nb_2O_5/SiO_2$ catalysts calcined at 100°C implies that the structure of the niobium oxide species responsible for catalytic activity in the silica catalysts is distinct from that in the alumina catalysts. Raman spectroscopic analysis of the $Nb_2O_5$/Norpro SS 65137 $SiO_2$ catalyst reveals Nb-OH-Nb bridging vibrations associated with the Bronsted acid sites and characteristic of a distorted octahedral structure. The Raman spectrum was unique in that the stretching vibration associated with the terminal Nb=O bond associated with Lewis acidity was not observed. Unfortunately, the Raman analysis of the fumed silica catalysts as well as the alumina catalysts was largely inconclusive due to excessive background fluorescence in these specimens.

## 9.2 Conclusions for Phase II - Kinetics and Catalyst Development

Silica and gamma alumina were identified as promising supports for catalysts for MO and MIBK syntheses. However, the gamma alumina support was eventually abandoned. Observations made during preliminary pilot scale CD experiments along with spectroscopic investigation of the adsorption properties of MIBK, acetone and other organic substrates on a $Pd/Al_2O_3$ catalyst showed that MIBK interacts very strongly with the Lewis acid sites of the alumina support. This was found to affect the retention time of products in the reactive section of the CD column. This property can adversely affect the product distribution and can potentially lead to coking. In addition, a $Nb_2O_5$/Norpro SA 6573 $\gamma$-$Al_2O_3$ raschig ring catalyst showed an exorbitantly low effectiveness factor (1.6%) for MO synthesis at 160°C in an autoclave reactor. In contrast, catalysts consisting of niobia dispersed onto silica raschig ring carriers showed very good activities for MO and MIBK syntheses, typically 0.9 to 1.3 [$g/hr*g_{cat}$] at 160°C in an FBR. The catalyst effectiveness factor was estimated to be 66% for MO synthesis at 160°C in an autoclave reactor. The disparity between the catalysts effectiveness factors of the silica and $\gamma$-$Al_2O_3$ raschig ring catalysts was attributed to the morphological characteristics of the carriers. The alumina carrier had a smaller mean pore diameter and a much higher surface area. The $Pd/Nb_2O_5/SiO_2$ raschig ring catalyst showed good stability in the pilot scale CD experiments, showing excellent activity even after 311 hours time on stream.

The macrokinetics of MO synthesis over a $Nb_2O_5$/Norpro SS 65137 silica raschig ring carrier catalyst was investigated in the liquid phase in an FBR for temperatures ranging from 140 to 180°C and weight hourly space velocities (WHSV) ranging from 3.9 to 28.5 $hr^{-1}$. The reaction rate was significantly inhibited at low space velocities but was found to become independent of flow rate at around 15 $hr^{-1}$ at 140°C and around 30 $hr^{-1}$ at 160°C. The results demonstrate that both MO selectivity and productivity can be maximized by minimizing the residence time in the reactor. A macrokinetic model was fit to

the experimental data via nonlinear regression analysis. The relatively high activation energy for MO synthesis suggests the inhibition of the reaction rate is a kinetic phenomenon rather than the result of external mass transfer effects.

A synergistic effect was observed when the one-step MIBK synthesis was carried out in a FBR using a multifunctional $Pd/Nb_2O_5$/Norpro SS 65137 silica raschig ring carrier catalyst. The catalyst activity for the collective production of all organic species was found to increase by 22% at 160°C and a WHSV of 8.6 $hr^{-1}$ when hydrogen was introduced into the system compared to operation in the absence of hydrogen. It is postulated that the rapid and irreversible hydrogenation of MO either shifts the equilibrium in favour of product formation and or increases the availability of acid sites for reaction by reducing the surface concentration of MO and its derivatives. Prolonged exposure of the catalyst to MO and its derivatives resulted in a marked loss of catalytic activity for MO hydrogenation. It is therefore recommended that the catalyst be protected by the presence of hydrogen during start up and regular operation.

The results of the autoclave experiments as well as the CD experiments confirm the claims of other authors, who suggest that a careful balance must be obtained between the sites responsible for aldol condensation, DAA dehydration and MO hydrogenation for a multifunctional catalyst. The results of the FBR experiments show that although the silica raschig ring catalyst showed excellent activity for MIBK synthesis, as high as 1.30 [$g/hr*g_{cat}$], the selectivity was constrained between 82 and 85 wt% due to the co-production of DIBK and IPA. In autoclave experiments, the rate of IPA production became comparable to the rate of MIBK production at a catalyst loading of around 1 wt% palladium. Since acetone and MO compete for the same active sites with MO being hydrogenated preferentially, IPA production can be mitigated by minimizing the palladium loading. The optimum palladium loading depends on the acidity of the niobium oxide phase and was estimated to be around 0.04 wt% Pd for the final catalyst formulation used in this work.

The intrinsic kinetics of the one step synthesis of MIBK from acetone were investigated over a $Pd/Nb_2O_5/SiO_2$ catalyst at 160°C and pressures ranging from 217 to 783 psia. Fumed silica was used as a support. The palladium loading was 0.047 wt% and the niobia loading was 15.2 wt%, which corresponds to ½ of a monolayer coverage. The catalyst exhibited excellent activity for MIBK synthesis at 160°C, as high as 6 times the benchmark activity of Amberlyst 15 for MO synthesis at its maximum operating temperature of 120°C. MIBK could be produced with essentially 100% selectivity up to acetone conversions around 20% for the conditions for which MO production was the controlling step. However, for conditions of high temperature and or low pressure, a significant amount of unreacted MO was present.

A kinetic model consisting of two rate expressions; one to account for MO synthesis and the other to account for MO hydrogenation was developed. The maximum likelihood estimates of the model parameters were ascertained using gProms advanced process modelling software. The model gave good prediction of water and acetone concentrations under all conditions. The model gave fair predictions of MIBK concentration for acetone conversions up to around 20% and above 500 psia but became unreliable at lower pressures. The absence of mass transfer effects was confirmed from calculation of the Mears and Weisz-Prater parameters as well as the low values of the Hatta number observed for the experiments. However, the results of the pilot plant CD experiments show that MIBK synthesis is controlled by the rate of external hydrogen mass transfer. Consequently a mass transport model for hydrogen is needed rather than a kinetic rate expression for hydrogenation, for CD process modelling of the one-step synthesis of MIBK.

### 9.3 Phase III – Pilot Scale CD Experiments

Moisture analysis of liquid samples obtained along the major axis of the CD column during MIBK production lead to the important observation that water

had accumulated in the top half of the reactor, with water concentrations in excess of 20 wt% observed in the rectification section and over 9 wt% in the reactive section. The accumulation of water in the reactive section inhibited the synthesis of MIBK due to the suppression of the DAA dehydration reaction. The accumulation of water in the top half of the CD column was an unexpected result, and is the opposite trend of what was expected based on experimental measurement and theoretical modelling of CD processes for MIBK synthesis and the aldol condensation of acetone disclosed in the literature at lower temperatures.[32,61,62,124] A process solution was developed whereby the water was rapidly separated *in situ* from the reaction zone via extraction in an overhead distillate stream with 83 to 97% reflux. This novel embodiment of the CD process involves two product streams and is distinct from the CD process design concepts for MIBK synthesis presented in the patent literature.[61,62]

MIBK synthesis utilizing two product streams resulted in a significant reduction in the water concentration in the reaction zone and directly resulted in an increase in the MIBK productivity by a factor of 21 compared to the initial benchmark where the process was operated at 100% reflux. In addition, the hydrogen utilization when operating with an overhead distillate stream was 10 to 19 times greater compared to when operating with 100% reflux. The hydrogenation selectivity improved from 81 (wt %) to values ranging from 93 to 100%. The *in situ* separation of water from the reaction zone highlights a unique and substantial advantage of CD technology over conventional fixed bed reactor technology used for MIBK synthesis. However, a comparison of the total organic productivity at 160°C observed in the CD experiments with water removal in the overhead distillate compared to the productivity observed in a fixed bed reactor with the catalyst fully wetted and in excess hydrogen at elevated pressure suggests an overall catalyst effectiveness factor of roughly 30%. Evidently, the catalyst was more effectively utilized in the fixed bed reactor. However, the low effectiveness factor may have been exacerbated by an initial catalyst deactivation during the CD experiments.

In the CD experiments utilizing an overhead distillate stream, MIBK was produced with over 50 wt% in the reboiler product and with as high as 90% selectivity (organic products neglecting acetone solvent). Perhaps more importantly, the reboiler product stream was essentially moisture free (ppm level). Water is known to form azeotropic mixtures with MIBK resulting in costly and difficult downstream separations. In addition, water is only slightly miscible with MIBK and can lead to phase splitting. Thus the *in situ* separation of water from the product stream is also a significant advantage of CD technology compared to conventional reactor technology.

The low operating pressure of the CD process appears to be another advantage over conventional reactor technology. One-step MIBK synthesis at 160°C via CD was carried out at system pressures around 1.3 to 1.4 MPa, when drawing an overhead distillate stream. It has been reported that state-of-the-art one-step processes are carried out in the liquid phase from 1 to 10 MPa in trickle bed reactors, which clearly places CD technology among the very low end of this scale.[23-25] The Veba-Chemie process for example, which perhaps represents the performance benchmark, is carried out at 135°C and 6 MPa, with an acetone conversion of 35% and 96% selectivity to MIBK.[1] The Deutsche Texaco process is similar but operates at 3 MPa pressure.[1] These so called "one-step" processes however, require several downstream distillation and phase splitting operations. Based on the results of the CD experiments of the present study, it may be concluded that the low operating pressure requirement of CD may be due to the enhanced hydrogen uptake efficiency, which is at least in part due to the *in situ* separation of water from the reactive section.

MIBK concentrations as high as 53 wt% were achieved in the reboiler product but could have easily been higher. In contrast, the MIBK concentration in the product streams of state-of-the-art reactors is typically less than 30 wt%, which necessitates further downstream refining. The separation of acetone from MIBK however, is relatively facile. The acetone conversion

was constrained for these CD experiments to less than 46% and was typically around 30 to 35% since the acetone feed rate was kept constant in the last three CD experiments. However, the first CD experiment demonstrated that MO could be produced with essentially 100% acetone conversion. It is reasonable to assume the same conversion could be achieved for MIBK synthesis via CD.

The results show that the CD process for one step MIBK synthesis is currently limited by hydrogen mass transfer. The MIBK productivity for the CD process was governed by the hydrogen feed rate. In addition, unreacted MO had the greatest adverse effect on the MIBK selectivity. The MO conversion is largely governed by the hydrogen flow rate. Moreover, the results also suggest that the presence of the liquid phase inhibits the transport of hydrogen to the active sites. At a constant hydrogen flow rate, the MO conversion was found to decrease with increasing reflux flow rate. This effect was more pronounced at lower hydrogen flow rates. However, the results show that the overall catalyst activity (all products) was relatively insensitive to the reflux flow rate. The MIBK selectivity (90%) and MO conversion (97%) were maximized due to improved hydrogen utilization when the reflux flow rate was minimized. This is promising for CD technology since the energy consumption of the process is greatly minimized from lower reboiler duty requirements at low reflux flow rate conditions. The reaction of MIBK on acid sites to produce DIBK and the direct hydrogenation of acetone to produce IPA were found to be significant competing reactions, even at palladium loading as low as 0.04 wt%. However, the high MIBK selectivity (90%) observed in the CD experiment was greater than that observed in the fixed bed flow reactor experiments for which the selectivity ranged from 82 to 85 wt% and was achieved at a much higher acetone conversion.

The results of this investigation suggest that currently the use of a multifunctional catalyst in a single reaction zone is preferred to the two-zone

approach. When utilizing two commercially available catalysts in two reaction zones, MO conversions from 4 to 15 wt% were observed. When a comparable amount of multifunctional catalyst was used in a single reaction zone at similar MIBK productivity a MO conversion of 86.6% was observed. The rapid hydrogenation of MO using a multifunctional catalyst not only enhances the MIBK selectivity but also results in a synergistic effect which enhances the overall catalytic activity as observed in the flow reactor experiments.

## 9.4 Recommendations

Future work should be directed towards enhancing hydrogen mass transfer. It is recommended that rather than using crushed catalyst contained within wire mesh bales, that the catalytic materials be dispersed onto catalyst carriers in the shape of distillation packings such as Raschig Rings or Berl Saddles. A kinetic enhancement for the hydrogenation step may be observed due to a reduction in the catalyst wetting efficiency with increasing characteristic dimension of the particle. An understanding of the relationships between catalyst particle size, shape and external surface area and the catalyst utilization is needed. Indeed the results of the CD experiments suggest an improved understanding of the interfacial phenomena which govern the catalytic processes, and their association with the reactor hydrodynamics is needed. It is recommended that the effects of the catalyst carrier hydrophobicity/hydrophillicity and morphological characteristics on the catalyst utilization be investigated. It is of particular interest to determine if the modification of surface tension and contact angles may lead to increased rates of hydrogen transport and kinetic enhancement from the reduction of both external and internal catalyst wetting. The silica carrier is recommended for future work since it showed excellent performance in FBR and CD reactor experiments. It is chemically inert and its surface hydrophobicity/hydrophillicity may be readily modified.

Since selectivity is largely a kinetic phenomenon, an improvement in MIBK selectivity will require optimization of the catalyst design. Future work should be directed towards the suppression of IPA production. The effects of the metal dispersion, reduction temperature, loading and morphological characteristics as well as its electronic properties on the MIBK yield should be investigated. Metals other than palladium should be considered such as nickel or copper. For example, the theory of Delbecq and Sautet [15] predicts that nickel would be more suitable than palladium for the selective hydrogenation of MO. An improved understanding of the relative adsorption strengths of the organic substrates on the hydrogenation catalyst and their association with the MIBK yield is needed.

The production of DIBK may be mitigated by optimizing the acid strength of the niobium oxide phase, achieving an improved balance between the hydrogenation and condensation functions. Alternatively, the MO hydrogenation may be conducted in a second reaction zone using the two-zone approach with the hydrogenation catalyst dispersed on an inert support. A two zone approach may be advantageous since depending on the catalyst and conditions, the synthesis of MO may be a liquid limited reaction, which would benefit from a reduction in catalyst size and increased catalyst wetting efficiency whereas MO hydrogenation is a gas limited reaction and may benefit from increased catalyst size and reduced catalyst wetting efficiency (i.e. competing design criteria). In addition, location of the hydrogenation zone at the bottom of the column where the MO is more concentrated may aid in the suppression of IPA production. Consequently, the optimization of two separate catalysts in two separate reaction zones may be beneficial. However, as mentioned in section 9.3, the results suggest a one-zone approach is currently preferred.

The effects of acetone feed rate and reflux ratio need to be further investigated for MIBK synthesis via CD. Preliminary results suggest a

significant enhancement in hydrogen uptake efficiency at very low reflux ratio (89%). At the end of this research project, plans for future work by the CD group for this project included investigation the effects of diluting the hydrogen feed stream with nitrogen on the process performance.

# References


1. Muthusamy, D. and Fisher, I., (2004), "Methyl Isobutyl Ketone", in The Kirk-Othmer Encyclopedia of Chemical Technology, 5th Edition, Vol.16, (Kroschwitz, J.I. Ed.) John Wiley and Sons, Inc., Hoboken, New Jersey, USA pp. 329-355.

2. Kirschner, M. (2004), "Methyl Isobutyl Ketone", *Chemical Market Reporter*, Feb 23, 2004; 265, 8, p. 27.

3. Moodley, N. (2007), "Sasol to Build New SA Chemicals Plant", in *Creamer Media's Engineering News*, published online 11 April, 2007, http://www.engineeringnews.co.za/article.php?a_id=107086.

4. Anonymous, (2005) *China Chemical Market Reporter*, (August 30, 2005) http://kaznak.web.infoseek.co.jp/china/china-5.htm

5. Zh, L. (2002), "Methyl Isobutyl Ketone Posts Insufficient Capacity", *China Chemical Week News*, http://www.sinocheminfo.com/topnews/w200201181007.htm

6. Anonymous, (2003) "Shell Invests $50 Million to Boost Solvents", *Chemical Market Reporter*, Jun 23, 2003; 263, 25, p. 3.

7. Landau, P. (1999), "Trend Towards Oxygenated Solvents Continue to Define Market", *Chemical Market Reporter*, Jun 7, 1999, 255, 23, p. 14.

8. Podrebarac, G.G., Ng, F.T.T. and Rempel, G.L., (1997) "A Kinetic Study of the Aldol Condensation of Acetone using an Anion Exchange Resin Catalyst", *Chem. Eng. Sci.*, **52(17)**, pp.2991-3002.

9. Craven, E.C. (1963), "The Alkaline Condensation of Acetone", *Journal of Applied Chemistry*, **13**, 71.

10. Klein, K.G. and Banchero, J.T., (1956), "Condensation of Acetone to Mesityl Oxide", *Industrial and Engineering Chemistry*., **48(8)**, pp. 1278-1286.

11. Kim, Y.K. and Hatfield, J.D. (1985), "Kinetics and Equilibrium Data of the Dehydration-Hydration Reaction between Diacetone Alcohol and Mesityl Oxide in Phosphoric Acid", *Journal of Chemical Engineering Data*, **30**, 149-153.

12. Canning, A.S., Gamman, J.J., Jackson, S.D., and Urquart, S, (2006) "Synthesis of Methyl Isobutyl Ketone over a Multifunctional Heterogeneous Catalyst: Effect of Metal and Base Components on Selectivity and Activity", in Chemical Industries, Catalysis of Organic Reactions, Vol. 115, (Schmidt., Ed.), CRC Press, Taylor and Francis, pp.67-75.

13. Canning, A.S., Jackson, S.D., McLeod, E. and Vass, E., (2005), "The Aldol Condensation of Acetone Over a $CsOH/SiO_2$ Solid Base Catalyst", in Chemical Industries, Catalysis of Organic Reactions, Vol. 104, (Sowa, J.R., Ed.), CRC Press, Taylor and Francis, pp.363-372.

14. Paulis, M., Martin, M., Soria, D.B., Diaz, A., Odriozola, J.A. and Montes, M., (1999), "Preparation and Characterization of Niobium Oxide for the Catalytic Aldol Condensation of Acetone", *Applied Catalysis A*, **180**, pp. 411-420.

15. Delbecq, F. and Sautet, P., (1995), "Competitive C=C and C=O Adsorption of α-β Unsaturated Aldehydes on Pt and Pd Surfaces in Relation with the Selelctivity of Hydrogenation Reactions: A Theoretical Approach", *Journal of Catalysis*, 152, pp.217-215.

16. Singh, U.K. and Vannice, M.A., (2001), "Kinetics of Liquid-Phase Hydrogenation Reactions Over Supported Metal Catalysts -a Review", *Applied Catalysis A*, **213**, pp.1-24.

17. Hegedus, L.S. (1999), Transition Metals in the Synthesis of Complex Organic Molecules, 2nd Ed., University Science Books, Sausalito, CA, USA, pp.1-34.

18. O'Keefe, W.K., Jiang, M., Ng, F.T.T. and Rempel, G.L., (2005), "Liquid Phase Kinetics for the Selective Hydrogenation of Mesityl Oxide to Methyl Isobutyl Ketone in Acetone over a $Pd/Al_2O_3$ Catalyst", *Chemical Engineering Science*, **60**, pp. 4131-4140.

19. Talwalkar, S. and Mahajani, S., (2006), "Synthesis of Methyl Isobutyl Ketone From Acetone over Metal-Doped Ion Exchange Resin", *Applied Catalysis A*, **302**, pp. 140-148.

20. Schmitt, K., Disteldorf, J., Schnurbusch, H. and Hilt, W. (1968), "Process for the Selective Hydrogenation of Unsaturated Ketones", U.S. Patent 3,361,822, Assigned to Schloven-Chemie Aktiengesellschaf, Gelsenkirchen-Buer, Germany.

21. Hwang, Y.L. and Bedard T.C., (2004), "Ketones", in The Kirk-Othmer Encyclopedia of Chemical Technology 5th Edition, Vol. 14, (Kroschwitz, J.I. Ed.) pp. 1-47.

22. Kocal, J.A. (2006), "Developing Sustainable Process Technology", in Chemical Industries, *Catalysis of Organic Reactions*, (Schmidt, S.R., Ed.), CRC Press, Taylor and Francis Group, New York, pp. 437-446.

23. Di Cosimo, J. I., Torres, G. and Apesteguia, C. R. (2002), "One-Step MIBK Synthesis: A New Process from 2-propanol", *Journal of Catalysis*, **208**, pp. 114-123.

24. Torres, G., Apesteguia, C.R. and Di Cosimo, J.I., (2007), "One-Step Methyl Isobutyl Ketone (MIBK) Synthesis from 2-Propanol: Catalyst and Reaction Conditions Optimization", *Applied Catalysis A*, **317**, pp. 161-170.

25. Lin, K.H and Ko, A.N., (1996), "Na Promotion of Pd/MgO Catalysts for Low-Pressure One-Step Synthesis of MIBK from Acetone and Hydrogen", *Applied Catalysis A.*, **147**, pp. 1259-1265.

26. Varga, M., Molnar, A., Mulas, G., Mohai, M., Bertoti, I. and Cocco, G., (2002), "Cu-MgO Samples Prepared by Mechanochemistry for Catalytic Application", *Journal of Catalysis*, **206**, pp. 71-81.

27. Das, N., Tichit, D., Durand, R., Graffin, P. and Coq, B., (2001) "Influence of the Metal Function in the 'one-pot' synthesis of 4-methyl-2-pentanone (methyl isobutyl ketone) from acetone over palladium supported on Mg(Al)O mixed oxides catalysts", *Catalysis Letters*, **71, No. 3-4,** pp. 181-185.

28. Molnar, A.; Varga, M.; Mulas, G.; Mohai, M.; Bertoti, I.; Lovas, A.; Cocco, G. (2001), "Cu-Mg powders and Ribbons Characterization and Catalytic Test Reactions." *Material Science and Engineering.* **A304-306**, pp. 1078-1082.

29. Chikan,V.; Molnar, A; Balazsik, K. (1999), "One-Step Synthesis of Methyl Isobutyl Ketone from Acetone and Hydrogen over Cu-on-MgO Catalysts." *Journal of Catalysis*, 184, pp. 134-143.

30. Mulas, G.; Deledda, S; Cocco, G. (1999). "The Mechanochemical Conversion of Acetone to Methyl Isobutyl Ketone over Cu-Mg based Substrates." *Material Science and Engineering*, **A267**, pp. 214-219.

31. Lemcoff, N. O; Cunningham, R. E. (1971), "Kinetics of Diacetone Alcohol Conversion to Mesityl Oxide Catalyzed by Ion Exchange Resin." *Journal of Catalysis*, **23**, pp. 81-92.

32. Lawson, K.H. and Nkosi, B. (1999), "Production of MIBK using Catalytic Distillation Technology", U.S. Patent 6,008,416, Assigned to Catalytic Distillation Technologies, (Pasadena, TX).

33. Nicol W. and Du Toit, E. (2004), "One-Step Methyl Isobutyl Ketone Synthesis from Acetone and Hydrogen using Amberlyst CH28." *Chemical Engineering and Processing*, **43**, pp. 1539-1545.

34. Chen,Y. Z., Hwang, C. M. and Liaw, C. W., (1998), "One-step Synthesis of Methyl Isobutyl Ketone from Acetone with Calcined Mg/Al Hydrotalcite Supported Palladium or Nickel Catalysts", *Applied Catalysis A*, **169**, pp. 207-214.

35. Martinez-Ortiz, M., Tichit, D., Gonzalez, P. and Coq, B., (2003), "The One-Pot Synthesis of 4-methyl-2-pentanone (Methyl Isobutyl Ketone) from Acetone over PdCu Catalysts Prepared from Layered Double Hydroxides", *Journal of Molecular Catalysis. A.*, **201**, pp. 199.

36. Unnikrishnan, R. and Narayanan, S. (1999), "Metal Containing Layered Double Hydroxides as Efficient Catalyst Precursors for the Selective Conversion of Acetone", *Journal of Molecular Catalysis A*, **144**, pp. 173-179.

37. Nikolopoulos, A.A., Jang, B.W.L. and Spivey, J.J., (2005), "Acetone Condensation and Selective Hydrogenation to MIBK on Pd and Pt Hydrotalcite-Derived Mg-Al Mixed Oxide Catalysts." *Applied Catalysis. A*, **296**, pp. 128-136.

38. Prinetto, P., Tichit, D, Tessier, R. and Coq, B., (2000), "Mg- and Ni- Containing Layered Double Hydroxides as Soda Substitutes in the Aldol Condensation of Acetone", *Catalysis Today*, **55**, pp. 103-116.

39. Winter, F., Van Dillen, A.J. and de Jong, K.P., (2004), "Single-Stage Liquid-Phase Synthesis of Methyl Isobutyl Ketone Under Mild Conditions", *Journal of Molecular Catalysis A*, 219, pp.273-281.

40. Winter, F., Koot, V., Van Dillen, A.J., Geus, J.W. and de Jong, K.P., (2005), "Hydrotalcites Supported on Carbon Nanofibres as Solid Base Catalysts for the Synthesis of MIBK", *Journal of Catalysis*, **236**, pp. 91-100.

41. Winter, F., Wolters, M., Van Dillen, A.J. and de Jong, K.P., (2006), "A Hydrotalcite-Based Catalyst System for the Single-Stage Liquid Phase Synthesis of MIBK", *Applied Catalysis A*, **307**, pp.231-238.

42. Chen, Y. Z. , Liaw, B. J., Tan, H.R. and Shen, K.L. (2001), "One-Step Synthesis of Methyl Isobutyl Ketone from Acetone and Hydrogen over Pd/($Nb_2O_5$/$SiO_2$) Catalysts", *Applied Catalysis A*, **205**, pp. 61-69.

43. Higashio, Y. and Nakayama, T., (1996), "One-Step Synthesis of Methyl Isobutyl Ketone Catalyzed by Palladium supported on Niobic Acid.", *Catalysis Today*, **28**, pp. 127-131.

44. Higashio, Y. and Nakayama, T. (1987), "Process for Production of Methyl Isobutyl Ketone", European Patent EP227868 (B1). [Also published as Japanese Patent JP610787745(A)], Assigned to Sumitomo Chemical Co., Japan.

45. Gandia, L. M. and Montes, M., (1994), "Effect of the Reduction Temperature on the Selectivity of the High Temperature Reaction of Acetone and Hydrogen over Alumina and Titania Supported Nickel and Cobalt Catalysts", *Journal of Molecular Catalysis*, **94**, pp. 347-367.

46. Narayanan, S. and Unnikrishnan, R. (1996), "Selective Hydrogenation of Acetone to Methyl Isobutyl Ketone (MIBK) over Co-Precipitated $Ni/Al_2O_3$ Catalysts. Appl. Catal. A. **145**, pp. 231-236.

47. Watanabe, Y. Matusumura, Y., Izumi, Y. and Mazutani, Y., (1974), "Synthesis of Methyl Isobutyl Ketone from Acetone and Hydrogen Catalyzed by Palladium Supported on Zirconium Phosphate", *Bulletin of the Chemical Society of Japan*, **47(12)**, pp. 2922-2925.

48. Mattos, L.V., Noronha, F.B. and Monterio, J.L.F., (2002), "Bifunctional Metal/Base Catalysts (Pt/X) for the Direct Synthesis of MIBK from Acetone", *Journal of Catalysis*, **209**, pp. 166-176.

49. Yang, S.M. and Wu, Y.M., (2000), "One-Step Synthesis of Methyl Isobutyl Ketone over Palladium Supported on ALPO4-11 and SAPO-11", *Applied Catlysis. A.*, **192**, pp. 211-220.

50. Melo, L., Magnoux, P., Giannetto, G., Alvarez, F. and Guisnet, M., (1997), "Transformation of Acetone over a 0.4 PtHMFI(60) Catalyst. Reaction Scheme.", *Journal of Molecular Catalysis. A.*, **124**, pp. 155-161.

51. Melo, L., Giannetto, G., Cardozo, L., Llanos, A., Garcia, L., Magnoux, P., Guisnet, M., and Alvarez, F., (1999), "Acetone transformation into Methyl Isobutyl Ketone over Pt/HFMI catalysts. IV. Effect of Density and Strength of Acid Sites", *Catalysis Letters*, **60**, pp. 217-222.

52. Melo, L., Llanos, A., Mediavilla, M. and Moronta, D., (2002), "Acetone Transformation over Pt/H[Al]ZSM5 and Pt/H[Ga]ZSM5 Catalysts. Evidences of a Pt-Ga Interaction", *Journal of Molecular Catalysis A*. **177**, pp. 281-287.

53. Melo, L., Velasquez, D., Llanos, A., Garcia, L., Giannetto, G., Guisnet, M., Magnoux, P. and Alvarez, F., (2002), "Acetone transformation over Pt/H[Al]ZSM5 catalysts. Effect of copper content", *Catalysis Letters*, **78**, pp. 57-63.

54. Chen, P.Y., Chu, S.J., Wu, K.C. and Lin, W.C., (1997), "Preparation of Methyl Isobutyl Ketone", U.S. Patent 5,684,207, Assigned to Industrial Technology Research Institute, (Hsinchu, TW).

55. Smith, L.A. and Adams, J.R., (1992), "Process for Conducting Heterogeneous Chemical Reactions", US Patent 5,118,872, Assigned to Chemical Research and Licensing, Co. (Houston, TX)

56. Podrebarac, G.G., (1996), "Development and Modeling of a New Catalytic Distillation Process", Ph.D. Thesis, The University of Waterloo. Waterloo, Ontario, Canada.

57. Taylor, R. and Krishna, R., (2000), "Modelling Reactive Distillation", *Chemical Engineering Science*, **55**, pp.5183-5229.

58. Ng, F.T.T. and Rempel, G.L., (2003), "Catalytic Distillation", in The Encyclopedia of Catalysis, Vol. 2, (Horvath, I.T., Ed.), Wiley-Interscience, Princeton, N.J., pp. 477-509.

59. Hiwale, R.S., Bhate, N.V., Mahajani, Y.S. and Mahajani, S.M., (2004), "Industrial Application of Reactive Distillation: Recent Trends", *International Journal of Chemical Reactor Engineering*, Vol. 2, Review R1, pp. 1-52.

60. Saayman, N., Grant, G.J. and Kindermans, S., (2003), "Process for the Production of MIBK using Catalytic Distillation Technology", U.S. Patent 6,518,462, Assigned to Catalytic Distillation Technologies (Pasadena, TX)

61. Saayman, N., Lund, G.J., and Kindermans, S., (2004), "Process for the Production of MIBK using Catalytic Distillation Technology", U.S. Patent, 6,762,328, Assigned to Catalytic Distillation Technologies (Pasadena, TX).

62. Shell Chemicals, (2005), "Methyl Isobutyl Ketone Data Sheet", Product code S1215 (North America), Issued April 7, 2005.

63. O'Keefe, W.K., Ng, F.T.T. and Rempel, G.L. (2007), "Experimental Studies on the Syntheses of Mesityl Oxide and Methyl Isobutyl Ketone via Catalytic Distillation", *Industrial and Engineering Chemistry Research*, **46(3)**, pp.716-725.

64. O'Keefe, W.K., M. Jiang, Ng, F.T.T. and Rempel, G.L., (2006), "The One Step Synthesis of MIBK via Catalytic Distillation: A Preliminary Pilot Scale Study", in Chemical Industries, *Catalysis of Organic Reactions*, **Vol. 115**, (Schmidt, S.R., Ed.), CRC Press, Taylor and Francis Group, (New York), pp. 365-374.

65. O'Keefe, W.K., Jiang, M., Ng, F.T.T. and Rempel, G.L., (2005), "A Catalytic Distillation Process for the One Step Synthesis of Methyl Isobutyl Ketone from Acetone: Liquid Phase Kinetics of the Hydrogenation of Mesityl Oxide". in Chemical Industries, *Catalysis of Organic Reactions*, **Vol. 104**, (Sowa, J.R., Ed.), CRC Press, Taylor and Francis Group, (New York), pp. 261-266.

66. Chakrabarti, A. and Sharma, M.M., (1993), "Cation Exchange Resins as Catalysts", *Reactive and Functional Polymers*, **20**, pp.1-45.

67. Tanabe, K., (2003), "Catalytic Application of Niobium Compounds", *Catalysis Today*, **78**, pp. 65-77.

68. Jehng, J. M. and Wachs, I. E. (1993), "Molecular Design of Supported Niobium Oxide Catalysts", *Catalysis Today*, **16**, pp. 417-426.

69. Ichikuni, N., Shirai, M. and Iwasawa, Y. (1996), "Surface Structures and Catalytic Properties of Supported Niobium Oxides", *Catalysis Today*, **28**, pp. 49-58.

70. Asakura, K. and Iwasawa, Y. (1991), "Synthesis, Characterization and Catalytic Properties of $SiO_2$-Attached One-Atomic-Layer Niobium Oxide Catalysts", *Journal of Physical Chemistry*, **95**, pp. 1711-1716.

71. Centi, G. and Perathoner, S. (2003), "Integrated Design for Solid Catalysts in Multiphase Reactions", Cattech,**7(3)**, pp.78-89.

72. Reed, T.B. (1971), "Free Energy of Formation of Binary Compounds. An Atlas of Charts for High Temperature Chemical Calculations", The MIT Press, Cambridge.

73. Nowak, I. and Ziolek, M. (1999), "Niobium Compounds: Preparation, Characterization and Application in Heterogeneous Catalysis", *Chemical Reviews*, **99**, pp. 3603-3624.

74. Ko, E.I. and Weissman, J.G. (1990) "Structures of Niobium Pentoxide and Their Implications on Chemical Behaviour", *Catalysis Today*, **8**, pp. 27-36.

75. Tanabe, K. (1987), "Niobic Acid as an Unusual Solid Material", *Materials Chemistry and Physics*, **17**, pp. 217-225.

76. Tanabe, K. and Okazaki, S. (1995), "Various Reactions Catalyzed by Niobium Compounds and Materials", *Applied Catalysis A*, **133**, pp. 191-218.

77. Tanabe, K. (1990), "Application of Niobium Oxides as Catalysts", *Catalysis Today*, **8**, pp.1-11.

78. Chen, Z., Iizuka, T. and Tanabe, K. (1984), "Niobic Acid as an Efficient Catalyst for the Vapour Phase Esterification of Ethyl Alcohol with Acetic Acid", *Chemistry Letters*, pp.1085-1088

79. Iizuka, T., Fujie, S, Ushikubo, T., Chen, Z. and Tanabe, T. (1986), "Esterification of Acrylic Acid with Methanol over a Niobic Acid Catalyst", *Applied Catalysis*, **28**, pp. 1-5.

80. Vedrine, J.C., Coudurier, G., Ouqour, A., Pries de Oliveira, P.G. and Volta, J.C. (1996), "Niobium Oxide Based Materials as Catalysts for Acidic and Partial Oxidation Reactions", *Catalysis Today*, **28**, pp. 3-15.

81. Soares, R.R., Frydman, A. and Schmal, M. (1993), "Effect of Preparation Method on a 5 wt% $Co/Nb_2O_5$ in Fischer Tropsch Synthesis (FTS)", *Catalysis Today*, **16**, pp. 361-370.

82. Carniti, P., Gervasini, A., Biella, S. and Auroux, A. (2006), "Niobic Acid and Niobium Phosphate as Highly Acidic Viable Catalysts in Aqueous Medium: Fructose Dehydration Reaction", Catalysis Today, 118, pp. 373-378.

83. Hanaoka, T., Takeuchi, K., Matsuzaki, T. and Sugi, Y. (1990), "Niobic Acid as a Solid Acid Catalyst for the Ring Opening Reactions of Phenyloxirane", *Catalysis Today*, **8**, pp.123-132.

84. Okazaki, S. and Wada, N. (1993), "Surface Properties and Catalytic Activities of Amorphous Niobium Phosphates and Comparison with those of $H_3PO_4$-treated Niobium Oxide", *Catalysis Today*, **16**, pp. 349-359.

85. Florentino, A., Cartraud P., Magnoux, P. and Guisnet, M. (1992), "Textural, Acidic and Catalytic Properties of Niobium Phosphate and of Niobium Oxide", *Applied Catalysis A*, **89**, pp. 143-153.

86. Okazaki, S., Kurimata, M., Iizuka, T. and Tanabe, K. (1987),"The Effect of Phosphoric Acid Treatment on the Catalytic Property of Niobic Acid", *Bulletin of the Chemical Society of Japan*, **60**, pp.37-41.

87. Jehng, J.M. and Wachs, I.E. (1990), "The Molecular Structures and Reactivity of Supported Niobium Oxide Catalysts", *Catalysis Today*, **8**, pp. 37-55.

88. Iizuka, T., Ogasawara, K. and Tanabe, K., (1983), "Acidic and Catalytic Properties of Niobium Pentaoxide", *Bulletin of the Chemical Society of Japan*, **56**, pp. 2927-2931.

89. Ko, E.I., Bafrali, R., Nuhfer, N.T. and Wagner, N.J., (1985), "The use of Niobia-Silica Surface-phase Oxide in Studying and Varying Metal Support Interactions in Supported Nickel Catalysts", *Journal of Catalysis*, **95**, pp. 260-270.

90. Burke, P.A. and Ko, E.I., (1991), "Acidic Properties of Oxides Containing Niobia on Silica and Niobia in Silica", *Journal of Catalysis*, **129**, pp.38-46.

91. Datka, J., Turek, A.M., Jehng, J.M. and Wachs, I.E. (1992), "Acidic Properties of Supported Niobium Oxide Catalysts: An Infrared Spectroscopy Investigation", *Journal of Catalysis*, **135**, pp.186-199.

92. da Silva, C.L.T., Camorim, V.L.L., Zotin, J.L., Pereira, M.L.R.D. and Faro, A.d.C. (2000), "Surface Acidic Properties of Alumina Supported Niobia Prepared by Chemical Vapour Deposition and Hydrolysis of Niobium Pentachloride", *Catalysis Today*, **57**, pp.209-217.

93. Shirai, M., Ichikuni, N., Asakura, K., and Iwasawa, Y. (1990), "Preparations and Catalytic Properties of Single, Pair and Monolayer Niobium Catalysts", *Catalysis Today*, **8**, pp.57-66.

94. Maki, T., Yokoyama, T. and Sumino, Y. (1988), "Production of Methyl Isobutyl Ketone", Japanese patent JP63068538, assigned to Mitsubishi Chemical Industries.

95. Maki, T., Yokoyama, T. and Sumino, Y. (1988), "Production of Methyl Isobutyl Ketone", Japanese patent JP63096146, assigned to Mitsubishi Chemical Industries.

96. Maki, T., Yokoyama, T. and Sumino, Y. (1988), "Production of Methyl Isobutyl Ketone", Japanese patent JP63068539, assigned to Mitsubishi Chemical Industries.

97. Jehng, J.M. and Wachs, I.E. (1991), "Structural Chemistry and Raman Spectra of Niobium Oxides", *Chemistry of Materials*, **3**, pp.100-107.

98. Wachs, I.E. (2005), "Recent Conceptual Advances in the Catalysis Science of Mixed Metal Oxide Materials", *Catalysis Today*, **100**, pp.79-94.

99. Turek, A.M., Wachs, I.E. and DeCanio, E., (1992), "Acidic Properties of Alumina Supported Metal Oxide Catalysts: An Infrared Spectroscopic Study", *Journal of Physical Chemistry*, **96**, pp. 5000-5007.

100. Jehng, J.M. and Wachs, I.E. (1991), "Molecular Structures of Supported Niobium Oxides under in situ Conditions", *Journal of Physical Chemistry*, **95**, pp. 7373-7379.

101. Ichikuni, N. and Iwasawa, Y. (1993), "Structures and Catalysis of New Nb Dimers on $SiO_2$", *Catalysis Today*, **16**, pp. 427-434.

102. Tanaka, T. Nojima, H., Yoshida, H., Nakagawa, H. Funabiki, T. and Yoshida, S. (1993), "Preparation of Highly Dispersed Niobium Oxide on Silica by Equilibrium Adsorption Method", *Catalysis Today*, **16**, pp. 297-307.

103. Burcham, L.J., Datka, J. and Wachs, I.E. (1999), "In Situ Vibrational Studies of Supported Niobium Oxide Catalysts", *Journal of Physical Chemistry B*, **103**, pp. 6015-6024

104. Banares, M.A. and Wachs, I.E. (2002), "Molecular Structures of Supported Metal Oxide Catalysts under Different Environments", *Journal of Raman Spectroscopy*, **33**, pp. 359-380.

105. Wachs, I.E. (1996), "Raman and IR studies of Surface of Metal Oxide Species on Oxide Supports: Supported Metal Oxide Catalysts", *Catalysis Today*, **27**, pp.437-455.

106. Ushikubo, T., Iizuka, T., Hattori, H. and Tanabe, K. (1993), "Preparation of Highly Acidic Hydrated Niobium Oxide", *Catalysis Today*, **16**, pp.291-295.

107. Ko, E.I. and Maurer, S.M. (1990), "Synthesis of Niobium Pentoxide Aerogels", *Journal of the Chemical Society Chemical Communications*, pp.1062-1063.

108. Uekawa, N., Kudo, T., Mori, F., Wu, Y.J. and Kakegawa, K., (2003), "Low Temperature Synthesis of Niobium Oxide Nanoparticles from Peroxo Niobic Acid Sol", *Journal of Colloid and Interface Science*, **264**, pp. 378-384.

109. Sokol'skii, D.V. (1958), "Mechanism of Catalytic Hydrogenation", *Trudy. Inst. Khim. Nauk., Akad. Nauk. Kazah. S.S.R.* **2**, pp. 3-52.

110. Sokol'skii, D.V. and Volkova, L.D., (1963), "Hydrogenation of Mesityl Oxide in Mixed Solvents", *Izv. Akad. Nauk. Kaz. S.S.R., Ser. Tekhn. i. Khim. Nauk.* **1**, pp. 3-7.

111. Dzhaparidze, G.L., Kenchadze, E., Gegenava, T.P., Nekrasov, N.V., Kostyukovskii, M.M. and Kiperman, S.L. (1985), Inst. Neorg. Khim. Elektrokhim, Tbilisi, USSR, Kinet. Katal., **26(3)**, pp. 673-679.

112. Macho, V. (1971), "Selective Hydrogenation of Mesityl Oxide to Methyl Isobutyl Ketone", *Vysk. Ustav. Petrochem., Novaky, Czech., Chem. Prum.* **21(1)**, pp. 9-11.

113. Hashimoto, K., Tsuto, K., Miyamoto, K., Hashimoto, N., Goto, N., Tada, T. and Nagata, S. (1969), "Kinetics of the Hydrogenation of Mesityl Oxide: Analysis of the Reaction Mechanism by Non-Linear Least Squares Method", Journal of Chemical Engineering of Japan, **2(2)**, pp. 158-163.

114. Kishida, S. and Teranishi, S., (1968), "A Kinetic Study of the Hydrogenation of Mesityl Oxide over Unpoisoned and Poisoned Raney Nickel Catalysts. Temperature Variation of the Reaction Order", Bulletin of the Chemical Society of Japan, 41(10), pp. 2528-2530.

115. Watanabe, Y., Okada, M., Izumi, Y. and Mizutani, Y., (1977), "Direct Synthesis of Methyl Isobutyl Ketone by Reductive Aldol Condensation: III Kinetics", Bulletin of the Chemical Society of Japan., 50(6), pp.1539-1544.

116. Lemcoff, N.O. and Cunningham, R.E., (1971), "Kinetics of DAA Conversion to Mesityl Oxide Catalyzed by Ion Exchange Resin", Journal of Catalysis, 23, pp. 81-92.

117. Kazanskaya, A.S., Ryabtseva, N.V., Panidl, I.S., Paushkin, Y.M., Sladkov, A.M. and Kudryavtsev, Y.P., (1971), *Dokl. Akad. Nauk. SSSR*, **198**, pp. 629-630.

118. Paushkin,Y.M, Panidi, I.S., Ryabtseva, N.V., Kazanskaya, A.S., Sladkov, A.M., Mescheryakov, S.V., Yatsko, O.I. and Lunin, A.F. (1970), *Kinet. Katal.*, **11**, pp. 1354-1356.

119. Traynelis, V.J., Hergenrother, W.L., Hanson, H.T. and Valicenti, J.A. (1964), "Dehydration of Alcohols, Diols and Related Compounds in Dimethyl Sulfoxide", *Journal of Organic Chemistry*, **29**, pp.123-129.

120. Scott, J.J. and Brower, K.R. (1967), "The Effect of Pressure on Rate and Equilibrium in Nucleophillic Addition to Mesityl Oxide", *Journal of the American Chemical Society*, **89**, pp. 2682-2685.

121. Jensen, J.L. and Carre, D.J. (1974), "Kinetics and Mechanisms of Reactions of 3-Butene-2-one and Related Compounds in Aqueous Perchloric Acid", *Journal of Organic Chemistry*, **39(14)**, pp. 2103-2107.

122. R.P. Bell, Preston, J. and Whitney, R.B. (1962), "Kinetics of the Hydration of Mesityl Oxide and Croton-aldehyde", *Journal of the Chemical Society*, pp.1166-1170.

123. Noyce, D.S. and Reed, W.L., (1958), "Carbonyl Reactions IV: Evidence for Alternate Mechanisms for the Dehydration of β-Hydroxy Ketones", *Journal of the American Chemical Society*, **80**, 5539-5542.

124. Thotla, S., Agarwal, V. and Mahajani, S.M. (2007), "Simultaneous production of Diacetone Alcohol and Mesityl Oxide from Acetone using Reactive Distillation", *Chemical Engineering Science*, **62,** pp. 5567-5574.

125. Davis, G.I. and Burrows, G.H., (1936), "Equilibrium Free Energy Relationships in the System Acetone-Diacetone Alcohol", *Journal of the American Chemical Society*, **58**, pp. 311-312.

126. Pressman, D., Brewer, L. and Lucas, H.J. (1942), "The Hydration of Unsaturated Compounds. The Role of Oxonium Complexes in the Hydration of Mesityl Oxide and the Dehydration of Diacetone Alcohol" *Journal of the American Chemical Society*, **64**, pp. 1122-1128.

127. du Toit, E., Schwarzer, R., and Nicol, W., (2004), "Acetone Condensation on a Cation Exchange Resin Catalyst: The Pseudo-Equilibrium Phenomenon", *Chemical Engineering Science*, **59**, pp. 5545-5550.

128. Pavnov, A.G. and Fripiat, J.J. (1998), "Acetone Condensation Reactions on Acid Catalysts", *Journal of Catalysis*, **178**, pp. 188-197.

129. Flego, C. and Perego, C. (2000), "Acetone Condensation as a Model Reaction for the Catalytic Behavior of Acidic Molecular Sieves: A UV- Vis Study", *Applied Catalysis A*, **192**, pp. 317-329.

130. Smith, E.F., (1950), "Process for Converting Lower Boiling Ketones to Higher Boiling Ketones", US Patent 2,499,172. Assigned to Commercial Solvents Co. Terre Haute, Industries, Maryland, USA.

131. L.V. Robbins and W.J. Porter, (1968), "Preparation of Higher Molecular Weight Ketones", US Patent 3,361,828. Assigned to Esso Research and Engineering Co., Delaware, USA.

132. Wollner, J., Kapellen, K.M. and Engelhardt, F., (1968), US Patent 3,405,178. Assigned to Rheinpreussen Aktiengeselschaft fur Bergbau und Chemie, Homberg, Germany.

133. Wollner, J., Moers, K.K. and Neier, W. (1971), "Production of Saturated Carbonyl Compounds", US Patent 3,574,763.

134. Schmitt, K., Disteldorf, J. and Flakus, W. (1976), "Process for Preparing Methyl Isobutyl Ketone and Catalyst", US Patent 3,953,517. Assigned to Veba-Chemie Aktiengesellschaft, Gelsenkirchen-Buer, Germany.

135. Tagaki, K, Murakami, M. and Iketani, K. (1972), "Method for Production of Methyl Isobutyl Ketone", US Patent 3,666,816. Assigned to Sumitomo Chemical Company Ltd., Osaka, Japan.

136. Porter, W.J. and Ellerbe, E.B. (1964), "Preparation of Ketones", US Patent 3,153,068. Assigned to Esso Research and Engineering Co., Delaware, USA.

137. Mertzweiller, J.K and Watts, R.N. (1967), "Synthesis of Higher Ketones", US Patent 3,316,303. Assigned to Esso Research and Engineering Co., Delaware, USA.

138. Hwang, Y.T. and Sandner, W.J. (1968), "Process for the Production of Higher Alkanones from Lower Alkanones", US Patent 3,379,766. Assigned to Union Oil Company of California, Los Angeles, CA, USA.

139. Nissen, A., Heilen, G., Sapper, E., Fliege, W and Wittwer, A. (1980), "Aldol Condensation and Hydrogenation Process Using a Catalyst of Nickel and Cobalt Together with Zinc Oxide and Another Metal of Groups VIII, IIB, IIIA, IVA and VA of the Periodic Table", US Patent 4,212,825. Assigned to BASF, Aktiengeselischaft, Germany.

140. Gefri, F.J., and Masilamani, D. (1987), "Process for the Production of Ketones and Carbinols", US Patent 4,704,480. Assigned to Allied Corporation, Morris Township, NJ, USA.

141. Huang, T.J. and Haag, O. (1982), "Conversion of Ketones Over Metal Containing Zeolites", US Patent 4,339,606, Assigned to Mobil Oil Co., New York, NY, USA.

142. Olson, K.D. (1987), "Process for the Condensation of Ketones", US Patent 4,704,478. Assigned to Union Carbide Co., Danburry, CT., USA

143. Isogai, N., Okawa, T. and Wakui, N., (1981), "Process for Producing Methylisobutylketone", US Patent, 4,289,911. Assigned to Mitsubishi, Gas Chemical Company.

144. Chen, P.Y., Chu, S.J., Chen, C.C., Chang, S.C., Lin, W.C. and Chuang, T.K. (1991), "Preparation of Methyl Isobutyl Ketone", US Patent 5,059,724.

145. Thornton, M. and Vandersall, J. (2005), "Metal Doped Sulfonated Ion Exchange Resin Catalysts", US Patent 6,977,314, Assigned to Rohm and Haas Company.

146. Brandes, G., Wollner, J., Neier, W. and Webers, W. (1981), "Method of Conducting Reactions in a Trickle-Type Reactor", US Patent 4,281,206. Assigned to Deutsche Texaco Aktiengesellschaft, Hamburg, Germany.

147. Kelly, G.J. (2004), "Aldol Condensation Reaction and Catalyst Therefor", US Patent 6,706,928, Assigned to Johnson Matthey PLC, London, GB.

148. Muthusamy, D., Wang, C.C., Swain, R.D. and Litzen, D.B. (1996), "Process of Making Ketones", US Patent 5,583,263. Assigned to Shell Oil Company, Houston, TX, USA.

149. Thotla, S., Argawal, V. and Mahajani, S.J., (2007), "Aldol Condensation of Acetone with Reactive Distillation using Water as a Selectivity Enhancer", *Industrial and Engineering Chemistry Research*, ASAP article in press.

150. O'Keefe, W.K., Ng, F.T.T. and Rempel, G.L. (2008), "Validation of a Gas Chromatography/Thermal Conductivity Detection Technique for the Determination of the Water Content of Oxygenated Solvents", *the Journal of Chromatography A*, **1182**, pp. 113-118.

151. Center for Drug Evaluation and Research (CDER),US Food and Drug Administration (FDA), (November 1994), "Reviewer Guidance: Validation of Chromatographic Methods", pp. 1-29. www.fda.gov/CDER

152. US Department of Health and Human Services, Food and Drug Administration Center for Veterinary Medicine (July 1999), "Guidance for Industry, Validation of Analytical Procedures: Methodology", pp. 1-13.

153. Center for Drug Evaluation and Research (CDER),US Food and Drug Administration (FDA), (November 1996), "Guidance for Industry, Q2B Validation of Analytical Methods Protocol: Methodology" pp. 1-13. http://www.fda.gov./CDER/guidance/index.htm

154. Brown, R., Caphart, M., Faustino, P., Frankewich, R., Gibbs, J., Leutzinger, E., Lunn, G., Ng, L., Rajagopalan, R., Chiu, Y. and Sheinin, E., (January 2001), "Analytical Procedures and Method Validation: Highlights of the FDA's Draft Guidance", *LCGC*, **19(1)**, pp. 74-79. www.chromatographyonline.com

155. Gambaro, V., Benvenuti, C., De Ferrari, L., Dell'Acqua, L. and Fare, F., (2003), "Validation of a GC/MS Method for the Determination of Tramadol in Human Plasma after Intravenous Bolus", *Il Farmaco*, **58**, pp. 947-950.

156. Agilent Technologies (2000), "Chapter One3, Evaluating System Suitability", in, Agilent Chemstation: Understanding your Chemstation, , pp.245-274.

157. Faro, A.C., Grange, P. and dos Santos, A.C.B. (2002), "Niobia Supported Nickel-Molybdenum Catalysts: Characterization of the Oxide Form", *Physical Chemistry Chemical Physics*, **4**, 3997-4007.

158. ASHE Analytics (2004), "Laboratory Analytical Procedure for X-Ray Fluorescence Analysis of Solid Media: 1. Laboratory-Grade Instrumentation Method", ASHE Analytics, PO Box 4172, Butte, MN, USA., pg.2

159. Wirtz, P., Wunder, F. and Warner, K.F. (1995), "Supported Catalyst, process for its preparation and its use for the preparation of vinyl acetate", U.S. Patent 5, 476, 963. Assigned to Hoechst, AG, Frankfurt, Germany.

160. Levin, I. and Brandon, D. (1998) "Metastable Alumina Polymorphs: Crystal Structures and Transitions Sequences", *Journal of the American Ceramic Society*, **81(8)**, pp. 1995-2012.

161. Smrcok, L., Langer, V. and Krestan, J. (2006), "$\gamma$-$Al_2O_3$: A Single-Crystal X-ray Diffraction Study", *Acta Crystallographica C, Crystal Structure Communications*, **62**, pp. i83-8-i84.

162. Soled, S. (1983), "$\gamma$-$Al_2O_3$ viewed as a Defect OxyHydroxide", Journal of Catalysis, 81, pp. 252-257.

163. Fang, C.M. and de Groot, R.A. (2007), "The Nature of Electron States in AlN and α-$Al_2O_3$" *Journal of Physics: Condensed Matter*, **19**, pp.1-6.

164. Dmitrieva, L.V., Vorotilova, L.S. and Razumeenko, M.V. (1997), "Measurement of the Chemical Shift and Quadrupole Coupling Tensor of $^{47}$Ti, $^{49}$Ti Nuclei in Anatase ($TiO_2$)" *Physics of the Solid State*, **39(7)**, pp.1057-1059.

165. James, M.A. and Hibma, T. (1999), "Thickness-Dependent Relaxation of NiO(001) Overlayers on MgO(001) studied by X-Ray Diffraction", *Surface Science*, **433-455**, pp. 718-722.

166. Menendez-Proupin, E. and Gutierrez, G. (2005), "Electronic Properties of Bulk γ-Al2O3", *Physical Review B*, **72**, pp. 035116-1 to 035116-9.

167. Chuah, G.K., Jaenicke, S. and Xu, T.H. (2000), "The Effect of Digestion on the Surface Area and Porosity of Alumina", *Microporous and Mesoporous Materials,* **37**, pp. 345-353.

168. Mullins, W.M. and Averbach, B.L. (1988), "Surface Properties of Silicon and Aluminum Oxide Powders", *Surface Science*, **206**, pp.41-51.

169. DiStefano, T.H. and Eastman, D.E. (1971), "The Band Edge of Amorphous $SiO_2$ by Photoinjection and Photoconductivity Measurements", *Solid State Communications*, **9**, pp. 2259-2261.

170. Karvinen, S., Hirva, P. and Pakkanen, T.A. (2003), "Ab initio Quantum Chemical Studies of Cluster Models for Doped Anatase and Rutile $TiO_2$", *Journal of Molecular Structure (Theochem)*, **626**, pp. 271-277.

171. Sempolinski, D.R., Kingery, W.D. and Tuller, H.L. (1980), "The Electronic Conductivity of Single Crystalline Magnesium Oxide", *Journal of the American Ceramic Society*, **63**, pp. 669-675.

172. Janner, A., Janssen, T. and de Wolff, P.M. (1983), "Wyckoff Positions used for the Classification of Bravais Classes of Modulated Cyrstals", *Acta Crystallographica*, **A39**, pp. 667-670.

173. Hall, S.R. (1981), "Space Group Notation with an Explicit Origin", *Acta Crystallographica*, **A37**, pp.517-525.

174. Sigma Aldrich, Product Information Sheet, Fumed Silica, Product Code 38,127-6. 06/03 (CKV)

175. Kung, H.H. (1989), "Transition Metal Oxides: Surface Chemistry and Catalysis", in Studies in Surface Science and Catalysis, Vol. 45, (Ed. Delmon, B. and Yates, J.T.), Elsevier Science, (New York). pp. 6-25.

176. Ruiz-Lopez, M.F. and Munoz-Paez, A. (1991), "A Theoretical Study of the XANES Spectra of Rutile and Anatase", *Journal of Physics: Condensed Matter*, **3**, pp. 8981-8990.

177. Fahmi, A., Mino, C., Silvi, B., and Causa, M. (1993), "Theoretical Analysis of the Structures of Titanium Dioxide Crystals", *Physical Review B*, **47(18)**, pp. 11717-11724.

178. Knozinger, H. and Ratnasamy, P. (1978), "Catalytic Aluminas: Surface Models and Characterization of Surface Sites", *Catalysis Reviews Science and Engineering*., **17**. pp.31.

179. Busca, G., Saussey, H., Saur, O., Lavalley, J.C. and Lorenzelli, V. (1985), "FT-IR Characterization of the Surface Acidity of Different Titanium Dioxide Anatase Preparations", *Applied Catalysis*, **14**, pp. 245-260.

180. Liu, Y., He, H., Xu, W. and Yu, Y. (2007), "Mechanism of Heterogeneous Reaction of Carbony Sulfide on Magnesium Oxide", *Journal of Physical Chemistry A*, **111**, pp.4333-4339.

181. Adachour, M., van Stee, L.L.P., Beens, J., Vreuls, R.J.J., Batenburg, M.A. and Brinkman, U.A.T. (2003), "Comprehensive Two-Dimensional Gas Chromatography with Time-of-flight Mass Spectrometric Detection for the Trace Analysis of Flavour Compounds in Food", *Journal of Chromatography A*., **1019**, pp. 157-172.

182. Cobb, G.W., (1998), Design and Analysis of Experiments, Springer, (New York), pg. 525.

183. Arena, F., Dario, R. and Parmaliana, A. (1998), "A Characterization Study of the Surface Acidity of Solid Catalysts by Temperature Programmed Methods", *Applied Catalysis A*, **170**, pp. 127-137.

184. Corma, A. (1995), "Inorganic Solid Acids and Their Use in Acid-Catalyzed Hydrocarbon Reactions", *Chemistry Reviews*, **95**, pp.559-614.

185. Ege, S. (1994), Organic Chemistry, 3rd Edition, D.C. Heath and Company, Toronto. "pKa Values"; Table of pKa values, inside front cover.

186. Baur, R., Taylor, R. and Krishna, R. (2001), "Influence of Column Hardware on the Performance of Reactive Distillation Columns", *Catalysis Today*, **66**, pp. 225-232.

187. Sundmacher, K. and Hoffman, U. (1994), "Multicomponent Mass and Energy Transport on Different Length Scales in a Packed Reactive Distillation Column for Heterogeneously Catalyzed Fuel Ether Production", *Chemical Engineering Science*, **49**, pp. 4443-4464.

188. Sundmacher, K. and Hoffman, U. (1996), "Development of a New Catalytic Distillation Process for Fuel Ethers via a Detailed Non-Equilibrium Model", *Chemical Engineering Science*, **51**, pp. 2359- 2368.

189. Huang, Chuncheng (1999), "Catalytic Distillation: Experimental Study and Theoretical Modelling", Ph. D. Thesis. The University of Waterloo; Waterloo, ON, Canada.

190. Autoclave Engineers, (August, 1996), "Autoclave Engineers Model BTRS-Jr/PC® Micro-Scale Bench-Top Reaction System: Installation, Operation and Maintenance Manual", Autoclave Engineers, 2930 West 22nd Street, Erie, PA, USA. Prepared for the University of Waterloo, S/N 96200924.

191. Duever, T.A. (2000), "Statistics in Engineering", Course notes for ChE 622, The University of Waterloo, Courseware Solutions, Waterloo, Ontario, Canada.

192. Brunner, E. (1985), "Solubility of Hydrogen in 10 Organic Solvents at 298.15, 323.15 and 373.15 K", *Journal of Chemical Engineering Data*, **30**, pp. 269-273.

193. Purwanto, Deshpande, R.M., Chaudhari, R.V. and Delmas, H. (1996), "Solubility of Hydrogen, Carbon Monoxide and 1-Octene in Various Solvents and Solvent Mixtures", *Journal of Chemical Engineering Data*, **41**, 1414-1417.

194. gPROMS Advanced User Guide, Process Systems Enterprise Ltd., pg. 46.

195. Fogler, H.S. (1992), Elements of Chemical Reaction Engineering 2nd Edition, Prentice Hall (Englewood Cliffs, New Jersey USA), pp. 625-628.

196. Geankoplis, C. (1993), Transport Processes and Unit Operations, Third Ed, Prentice Hall (Englewood Cliffs, New Jersey, USA), pp. 14-145, 450-453.

197. Sitaraman, R., Ibrahim, H. and Kuloor, R., (1963), *Journal of Chemical Engineering Data*., **8**, 198.

198. Guo, C.J. and De Kee, D. (1991), "Effect of Molecular Size and Free Volume on the Diffusion of Liquids", *Chemical Engineering Science*, **46**, pp. 2133-2141

199. Csiszar, P. "Postmixing Optimization and Solutions", www.postmixing.com

200. Radl, S., Koynov, A., Tryggvason, G. and Khinast, J.G. (2008), "DNS-Based Predictions of Selectivity of Fast Multiphase Reactions: Hydrogenation of Nitroarenes", *Chemical Engineering Science*, 63, pp. 3279-3291.

201. Perry, R.H and Green, D. (1984), Perry's Chemical Engineer's Handbook, 6th Ed., Mc Graw-Hill, Toronto, pg 14-22; Table 18-5, pg. 18-23; 3-280.

202. Hines, A.L. and Maddox, R.N. (1985), Mass Transfer Fundamentals and Applications, Prentice Hall, (Englewood Cliffs, New Jersey, USA), pp.19, 27-39.

203. Weisz, P.B. and Prater, C.D. (1954), *Advances in Catalysis*, **6**, 143.

204. Hudgins, R.R. (1968), "A General Criterion for the Absence of Diffusion Control in an Isothermal Catalyst Pellet", *Chemical Engineering Science*, **23,** pp. 93-94.

205. Mears, D.B. (1971) "Tests for Transport Limitations in Experimental Catalytic Reactors", *Industrial and Engineering Chemistry Process Design and Development*, **10,** pp. 541-547

206. Dooley, C., Fines, S., Trebacz, W. and Walker, R. (2005), "Improvements for a Catalytic Distillation Column Pilot Plant", Final Project Report for ChE 047, The University of Waterloo.

207. "Durlon Technical manual", (September 2005), Gasket Resources Incorporated, P.O. Box 565, Exton, PA, 19341-0565.

208. Ontario Regulation 213/07, The Ontario Fire code, section 4.3.12.10, *Fire Protection and Prevention Act*, (2007).

209. Industrial Accident Prevention Association, (July 2000), "Static Electricity: A Health and Safety Guideline for your Workplace", Toronto, Ontario. ISBN 1-55127-097-8.

210. Weast, R.C. and Astle, M.J. (1980), CRC Handbook of Chemistry and Physics, 60th Edition, CRC Press Inc. (Boca Raton, FL), pp. F-11, D-174; D-196, D-197

211. Felder, R.M. and Rousseau, R.W., (1986), Elementary Principles of Chemical Processes, 2nd Ed., John Wiley and Sons, (Toronto), pp. 366, 615.

212. Al-Dahhan, M.H., Larachi, F., Dudukovi, M.P. and Laurent, A. (1997), "High Pressure Trickle Bed Reactors: A Review", *Industrial and Engineering Chemistry Research*, **36**, pp. 3292-3314.

213. Wu, Y., Khadilkar, M.R. and Dudukovic, M.P. (1996), "Evaluation of Trickle Bed Reactor Models for a Liquid Limited Reaction", *Chemical Engineering Science*, **51**, pp. 2721-

214. Al-Dahhan, M.H. and Dudukovic, M.P. (1995), "Catalyst Wetting Efficiency in Trickle Bed Reactors at High Pressure", *Chemical Engineering Science*, **50**, pp. 2377-2389.

215. Lemcoff, N.O., Cukierman, A.L. and Martinez, O.M. (1988), "Effectiveness factor of partially wetted catalyst particles: Evaluation and application to the modeling of trickle bed reactors by a reaction method", *Catalysis Reviews – Science and Engineering*, **30(3)**, pp. 393-456.

216. Zhou, Z.M. Cheng, Z.M. Li, Z. and Yuan, W.K. (2004), "Determination of an Effectiveness Factor for a Partial Internal Wetting Catalyst from Adsorption Measurement", *Chemical Engineering Science*, **59**, pp. 4305-4311.

217. Jiang, M. and Ng, F.T.T. (2002), "Adsorption properties of a $Pd/Al_2O_3$ catalyst", unpublished internal communication

218. Howard, W.L. (2004), "Acetone", in The Kirk-Othmer Encyclopedia of Chemical Technology, 5th Edition, (Kroschwitz, J.I. Ed.) Vol.1, pp. 160-177.

# Appendix A

## Supplementary Data for Gas Chromatographic Methods

### A1 GC Parameters for GC/TCD and GC/FID Methods

**Table A1-1** GC Parameters for the GC/TCD method of Moisture Analysis

| | |
|---|---|
| Carrier Gas: | Helium |
| Carrier Flow Rate: | 20 mL/min |
| Inlet Temperature: | 250°C |
| Detector Temperature: | 250 °C |
| Reference flow: | 20 mL/min |
| Make-up flow: | 3 mL/min |
| Injection Volume: | 1 μL |
| **Oven Profile:** | |
| Initial Temperature: 140°C<br>Hold at initial temperature (140°C) for 2 minutes<br>Ramp to 220°C at 20°C/min | |

**Table A1-2** Parameter settings for the GC/FID method for the analysis of organic species

| | | |
|---|---|---|
| FID Detector | Temperature:<br>Makeup flow rate: | 300 °C<br>30 mL/min |
| Injector | Temperature:<br>Split Ratio:<br>Injection Volume: | 250 °C<br>100:1<br>1μL |
| Oven Thermal Profile | Initial temperature:<br>Isotherm:<br>Ramp:<br>Hold: | 40 °C<br>Hold at 40°C for 5 min<br>Ramp to 160°C at 10 °C/min<br>(at 160°C) for 2 min |
| Carrier Gas | Gas:<br>Mode:<br>Flow Rate: | Helium<br>Constant Flow Rate<br>35 cm/sec at 40°C<br>(i.e. 5.0 mL/min) |

## A2 Validation of the GC/TCD method of water analysis

**Table A2-1** Assessment of the background noise in the GC/TCD chromatograms of 5 calibration standards (21.09.2006)

| CALIBRATION STANDARD | BACKGROUND NOISE Over the interval from 0.7 to 1.1 min [x 25 μV] |
|---|---|
| 1 | 0.07439 |
| 2 | 0.07508 |
| 3 | 0.09334 |
| 4 | 0.09017 |
| 5 | 0.09204 |
| Average | 0.085004 |
| Standard Deviation | 0.0094449 |

**Table A2-2** y-intercepts obtained from 10 arbitrary GC/TCD calibration curves

| DATE | Y-INTERCEPT (WT%) |
|---|---|
| 10 September, 2006 | 0.056347 |
| 13 September, 2006 | 0.002601 |
| 19 September, 2006 | 0.003653 |
| 20 September, 2006 | 0.059043 |
| 21 September, 2006 | 0.004502 |
| 25 September, 2006 | 0.042766 |
| 26 September, 2006 | 0.017546 |
| 28 September, 2006 | 0.053174 |
| 3 October, 2006 | 0.060266 |
| 5 October, 2006 | 0.10928 |
| Standard Deviation (wt%) | 0.034152 |

## A3 Assays of Stock Solutions used to prepare GC/FID calibration standards

**Table A3-1** Stock solutions used to prepare calibration standards

| COMPONENT | Supplier | Product Number | Lot Number | Assay |
|---|---|---|---|---|
| DIPE | Aldrich | 398276 | 06034JO | 0.9988 |
| Acetone | Aldrich | 179124 | 01442JB | 0.9998 |
| 2- propanol (IPA) | Aldrich<br>Riedel de Haen | 320471<br>34965 | 01508PQ<br>530113 | 0.998<br>1.000 |
| MIBK | Aldrich | 293261 | 08461HC<br>15567TR | 0.9999<br>0.9981 |
| MO (MO) | Fluka<br>Aldrich | 63940<br>281832 | 432295<br>00706LL | 0.9150<br>0.9430 |
| MIBC | Aldrich | 109916 | 07825KI | 0.993 |
| DIBK | Aldrich | 273848 | 02813PI | 0.996 |
| Mesitylene (TMB) | Aldrich | M7200 | 00608TU | 0.990 |
| Diacetone Alcohol (DAA) | Aldrich | H41544 | 25603LB<br>16120PA | 0.999<br>0.988 |
| Phorone | Aldrich | 149233 | 09701BE | 0.999 |
| Isophorone | Fluka<br>Aldrich | 59190<br>I-1870-9 | 1168426<br>01702CU | 0.987<br>0.965 |
| Hexelene Glycol | Aldrich | 112100 | 06002DB | 0.999 |

## A4 Detailed Results of GC/FID Reliability and Reproducibility (R&R)

Calibration standards 1 and 7 were both analyzed 10 times each in succession in order to determine the repeatability (instrument precision) of the GC/FID technique.

Table A4-1: GC/FID Precision

**Calibration Std. 7**

| | | Area [pA*s] | | | | | | | | | |
|---|---|---|---|---|---|---|---|---|---|---|---|
| **Component** | **RetTime** | **1** | **2** | **3** | **4** | **5** | **6** | **7** | **8** | **9** | **10** |
| DIPE | 2.26 | 2154 | 2369 | 2396 | 2396 | 2421 | 2433 | 2495 | 2532 | 2435 | 2454 |
| Acetone | 3.55 | 38504 | 42573 | 43106 | 43226 | 43628 | 43915 | 45086 | 45796 | 44016 | 44466 |
| IPA | 6.17 | 1015 | 1121 | 1140 | 1147 | 1156 | 1163 | 1201 | 1218 | 1169 | 1185 |
| MIBK | 7.93 | 8396 | 8994 | 9289 | 9395 | 9449 | 9327 | 9621 | 9875 | 9515 | 9606 |
| IMO | 9.69 | 563 | 602 | 624 | 632 | 635 | 626 | 645 | 663 | 639 | 645 |
| MO | 10.60 | 7427 | 7877 | 8162 | 8277 | 8322 | 8166 | 8403 | 8667 | 8384 | 8442 |
| MIBC | 11.15 | 1558 | 1655 | 1714 | 1740 | 1750 | 1716 | 1767 | 1824 | 1766 | 1778 |
| DIBK | 11.28 | 2520 | 2619 | 2695 | 2732 | 2751 | 2685 | 2749 | 2841 | 2776 | 2779 |
| TMB | 12.53 | 2569 | 2686 | 2762 | 2799 | 2815 | 2755 | 2819 | 2913 | 2841 | 2848 |
| DAA | 14.34 | 1134 | 1206 | 1251 | 1274 | 1282 | 1248 | 1284 | 1337 | 1302 | 1300 |
| PHO | 16.12 | 1813 | 1860 | 1901 | 1930 | 1940 | 1895 | 1933 | 1990 | 1961 | 1954 |
| IPO | 17.55 | 2183 | 2231 | 2285 | 2319 | 2333 | 2277 | 2330 | 2389 | 2360 | 2351 |
| HG | 17.66 | 463 | 546 | 590 | 618 | 623 | 599 | 638 | 655 | 642 | 649 |

| | | | | 95% Confidence Interval | |
|---|---|---|---|---|---|
| **Component** | **Avg** | **stdev** | **RSD** | **+/- [pA*s]** | **+/- (%)** |
| DIPE | 2409 | 102 | 4.22 | 63 | 2.62 |
| Acetone | 43432 | 1977 | 4.55 | 1225 | 2.82 |
| IPA | 1151 | 56 | 4.86 | 35 | 3.01 |
| MIBK | 9347 | 407 | 4.36 | 253 | 2.70 |
| IMO | 627 | 28 | 4.41 | 17 | 2.73 |
| MO | 8213 | 346 | 4.21 | 214 | 2.61 |
| MIBC | 1727 | 75 | 4.32 | 46 | 2.68 |
| DIBK | 2715 | 91 | 3.36 | 57 | 2.08 |
| TMB | 2781 | 96 | 3.47 | 60 | 2.15 |
| DAA | 1262 | 57 | 4.53 | 35 | 2.81 |
| PHO | 1918 | 52 | 2.71 | 32 | 1.68 |
| IPO | 2306 | 63 | 2.72 | 39 | 1.68 |
| HG | 602 | 59 | 9.78 | 36 | 6.06 |

**Calibration Std. 1**

| | | Area [pA*s] | | | | | | | | | |
|---|---|---|---|---|---|---|---|---|---|---|---|
| **Species** | **RetTime** | **1** | **2** | **3** | **4** | **5** | **6** | **7** | **8** | **9** | **10** |
| DIPE | 2.26 | 170.2955 | 177.0414 | 178.2316 | 183.0322 | 186.8005 | 171.2105 | 178.171 | 192.3029 | 187.7883 | 183.7688 |
| Acetone | 3.54 | 65755.61 | 69273.13 | 69910.05 | 72095.44 | 73990.09 | 67115.24 | 70114.38 | 76918.46 | 74732.2 | 73378.84 |
| MIBK | 7.93 | 445.3198 | 460.0001 | 469.5972 | 470.0078 | 488.3635 | 458.9447 | 477.9686 | 504.342 | 484.6684 | 483.2624 |
| MO | 10.60 | 212.7771 | 218.2267 | 221.6226 | 220.4205 | 229.4572 | 216.2125 | 224.8548 | 236.6777 | 226.5673 | 226.6783 |
| DIBK | 11.29 | 137.9743 | 143.9586 | 145.9039 | 143.7178 | 147.284 | 142.233 | 146.6889 | 148.3872 | 143.881 | 144.1488 |
| TMB | 12.53 | 282.2475 | 292.4937 | 296.1881 | 293.6425 | 303.1412 | 289.0534 | 298.5901 | 307.7881 | 295.7501 | 295.7886 |
| PHO | 16.12 | 257.999 | 265.8101 | 267.3478 | 262.4207 | 268.713 | 261.2624 | 267.9382 | 271.5426 | 258.5373 | 260.0743 |

| | | | | 95% Confidence Interval | |
|---|---|---|---|---|---|
| **Component** | **Avg** | **stdev** | **RSD** | **+/- [pA*s]** | **+/- (%)** |
| DIPE | 181 | 7.16 | 3.96 | 4.44 | 2.45 |
| Acetone | 71328 | 3515 | 4.93 | 2179 | 3.05 |
| MIBK | 474 | 17.1 | 3.60 | 10.6 | 2.23 |
| MO | 223 | 6.99 | 3.13 | 4.33 | 1.94 |
| DIBK | 144 | 2.96 | 2.05 | 1.83 | 1.27 |
| TMB | 295 | 7.06 | 2.39 | 4.38 | 1.48 |
| PHO | 264 | 4.71 | 1.78 | 2.92 | 1.11 |

## A5 Validation of Liquid Sampling Technique by Direct Measurement of Effluent Composition via GC/FID

**Table A5-1** Raw data and experimental design for validation of liquid sampling technique by direct measurement of Effluent Concentration

| Retention Time [s] | Sample Order | GC Analysis Order | MO Peak Area [pA*s] |
|---|---|---|---|
| 0 | 14 | 1 | 544 |
| 5 | 1 | 12 | 565 |
| 10 | 7 | 14 | 567 |
| 30 | 4 | 8 | 601 |
| 60 | 11 | 7 | 602 |
| 0 | 12 | 3 | 565 |
| 5 | 10 | 6 | 598 |
| 10 | 2 | 15 | 580 |
| 30 | 13 | 1 | 576 |
| 60 | 8 | 4 | 571 |
| 0 | 6 | 5 | 578 |
| 5 | 9 | 10 | 540 |
| 10 | 3 | 2 | 591 |
| 30 | 15 | 13 | 570 |
| 60 | 5 | 9 | 561 |

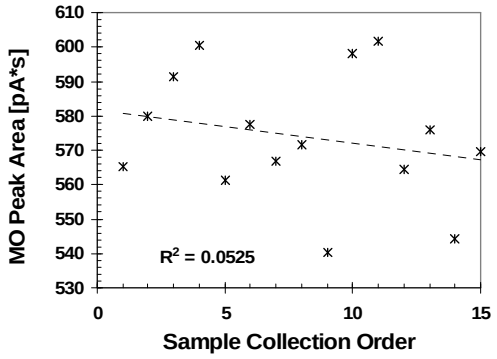


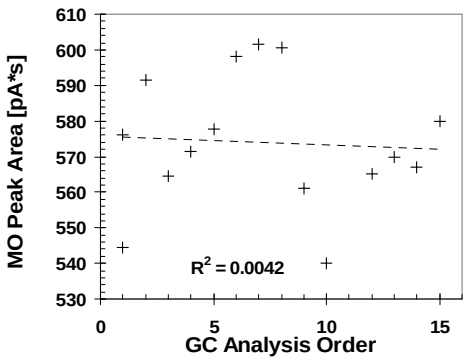


**Figure A5-1** (left) Effect of sample collection order on measured MO peak area

**Figure A5-2** (right) Effect of the GC analysis order on the measured MO peak area

# Appendix B
## Supplementary Data: Catalyst Preparation, UV-Vis Spectroscopy and EDXRF Analysis

### B1 EDXRF Method and Analysis

**Table B1-1** EDXRF method for the quantification of niobia loading (wt% $Nb_2O_5$) in supported or mixed metal oxide catalysts using a Lab-X 3000

| **EDXRF Method for the Quantification of Niobia Loading (wt% $Nb_2O_5$ ) on Transition Metal Oxide Supported Catalysts** | |
|---|---|
| Excitation Range | "Low" |
| Excitation Voltage | 10 kV |
| Beam Current | 90 μA |
| Helium purge | "on" |
| Filters | "W3" |
| Calibration Time | 200 seconds |
| Analysis Time | 200 seconds |
| Channels | 80 to 120 |

### B2. Catalyst Preparation Data

Reduction, thermal decomposition reaction and calcination were carried out in a calcinator (Figure 3-17)

The catalyst was dried in the calcinator with zero gas air flowing at 3.8 mL/min for 2 hours. Catalysts 35 to 41 were dried for 2 hours at 1.3 mL/min.

Thermal decomposition was carried out in flowing nitrogen ( 4.0 mL/min) for 2 hours

Calcination was carried out in flowing zero gas air (3.8 mL/min) for 2 hours

Treatment of the support with niobium ethoxide was carried out at room temperature in inert environment in a glove bag for 2 hours

After treatment with niobium ethoxide precursor, the catalyst was recovered by vacuum separation and dried in vacuo for 24 hours prior to calcination

The catalyst was not exposed to air at any time from drying until calcination was completed.

# Table B2-1 Niobia Catalyst Preparation Data

| Catalyst batch ID | Support | Pretreatment Temp (℃) | Support (g) | n-Hexane (mL) | Nb ethoxide (mL) | Thermal Decomp. (T) | Calcination Temp (T) | EDXRF wt% Nb2O5 |
|---|---|---|---|---|---|---|---|---|
| 001 | fumed silica | 200 | 2.824 | 30 | 1.0 | 400 | 500 | 23.8 |
| 002 | fumed silica | 400 | 2.516 | 30 | 0.9 | 400 | 500 | n/a |
| 003 | fumed silica | 400 | 2.088 | 22 | 0.8 | 400 | 500 | n/a |
| 004 | gamma alumina (acidic) | 400 | 4.539 | 20 | 4.0 | 400 | aborted | n/a |
| 005 | gamma alumina (acidic) | 400 | 4.255 | 40 | 5.5 | 400 | 500 | 41.33 |
| 006 | gamma alumina (acidic) | 250 | 1.906 | 3 | 1.0 | 400 | 500 | 15.52 |
| 007 | gamma alumina (basic) | 250 | 1.773 | 3 | 1.0 | 400 | 500 | 15.91 |
| 008 | gamma alumina (basic) | 250 | 1.768 | 3 | 1.0 | 400 | 500 | n/a |
| 009 | gamma alumina (basic) | 250 | 1.76 | 6 | 1.0 | 400 | 500 | 17.07 |
| 010 | alpha alumina | 450 | 1.99 | 6 | 1.0 | 400 | 500 | 4.21 |
| 011 | MgO | 400 | 1.701 | 6 | 1.0 | 400 | 500 | 6.21 |
| 012 | MgO | 400 | 1.85 | 6 | 1.0 | 400 | 500 | 12.88 |
| 013 | TiO2 | 400 | 1.984 | 6 | 1.0 | 400 | 500 | 11.84 |
| 014 | gamma alumina (acidic) | 400 | 2.03 | 6 | 1.0 | 400 | 500 | 16.98 |
| 015 | gamma alumina (basic) | 400 | 2.005 | 6 | 1.0 | 400 | 500 | 18.84 |
| 016 | gamma alumina (acidic) | 250 | 1.801 | 6 | 1.0 | 400 | 500 | 12.01 |
| 017 | alumina raschig ring | 250 | 2.022 | 8 | 1.0 | 400 | 500 | 22.33 |
| 018 | gamma alumina (acidic) | 250 | 2.881 | 9 | 1.5 | 400 | 500 | 17.09 |
| 019 | gamma alumina (acidic) | 250 | 2.848 | 6 | 0.3 | 400 | 500 | 6.7 |
| 020 | MS | 250 | 3.207 | 30 | 1.5 | 400 | 500 | n/a |
| 021 | fumed silica | 250 | 2.736 | 30 | 1.5 | 400 | 500 | 26.47 |
| 022 | MgO | 250 | 2.629 | 6 | 1.5 | 400 | 500 | 5.41 |
| 023 | TiO2 | 400 | 2.99 | 6 | 1.5 | 400 | 500 | 14.82 |
| 024 | alpha alumina | 250 | 2.77 | 6 | 1.5 | 400 | 500 | 4.38 |
| 025 | gamma alumina (acidic) | 250 | 2.788 | 6 | 0.3 | 400 | 500 | 7.05 |
| 026 | gamma alumina (acidic) | 250 | 2.815 | 6 | 0.1 | 400 | 500 | 2.65 |
| 027 | fumed silica | 250 | 2.585 | 30 | 0.3 | 400 | 500 | 12.47 |
| 028 | fumed silica | 250 | 2.685 | 30 | 0.1 | 400 | 500 | 5.82 |
| 029 | fumed silica | 250 | 2.488 | 30 | 0.3 | 200 | 100 | 16.65 |
| 030 | fumed silica | 250 | 2.739 | 30 | 0.1 | 200 | 100 | 12.3 |
| 031 | gamma alumina (acidic) | 250 | 2.742 | 6 | 0.3 | 200 | 100 | 6.29 |
| 032 | gamma alumina (acidic) | 250 | 1.66 | 6 | 0.1 | 200 | 100 | 3.79 |
| 033 | MS-3050 $SiO_2$ | 100 | 1.539 | 30 | 0.1 | 200 | 100 | 4.6 |
| 034 | MS-3050 $SiO_2$ | 250 | 1.891 | 30 | 0.2 | 200 | 300 | 12.47 |
| 035 | fumed silica | 250 | 2.39 | 30 | 0.2 | 200 | 300 | 7.68 |
| 036 | fumed silica | 100 | 1.973 | 30 | 0.1 | 200 | 100 | 4.52 |
| 037 | fumed silica | 250 | 2.047 | 30 | 0.2 | 200 | 300 | 6.82 |
| 038 | fumed silica | 100 | 2.12 | 30 | 0.2 | 200 | 100 | 9.06 |
| 039 | fumed silica | 100 | 1.952 | 30 | 0.1 | 200 | 100 | 5.11 |
| 040 | fumed silica | 250 | 4.661 | 60 | 0.5 | 200 | 100 | 10.17 |
| 041 | fumed silica | 250 | 2.914 | 45 | 0.3 | 400 | 500 | 8.98 |
| 044 | fumed silica | 400 | 1.998 | 30 | 0.2 | 200 | 100 | 7.63 |
| 045 | fumed silica | 250 | 1.966 | 30 | 0.2 | 200 | 300 | 5.55 |
| 047 | fumed silica | 400 | 2.11 | 30 | 0.1 | 200 | 100 | 3.93 |
| 048 | fumed silica | 400 | 2.06 | 30 | 0.1 | 400 | 500 | 3.4 |
| 049 | fumed silica | 100 | 1.89 | 30 | 0.2 | 400 | 500 | 7.96 |
| 050 | fumed silica | 100 | 1.97 | 30 | 0.1 | 400 | 500 | 2.8 |
| 052 | fumed silica | 250 | 4.98 | 75 | 0.8 | 200 | 100 | 13.96 |
| 054 | fumed silica | 250 | 14.86 | 225 | 2.2 | 200 | 100 | 15.21 |
| 055 | Norton SRK 13650 $SiO_2$ | 250 | 2.017 | 40 | 0.3 | 200 | 100 | 10.42 |
| 056 | Norton SRK 13650 $SiO_2$ | 250 | 1.98 | 40 | 0.3 | 200 | 100 | 4.12 |
| 057 | Norpro SS 65137 $SiO_2$ | 250 | 1.45 | 40 | 0.2 | 200 | 100 | 5.3 |
| 057-B | Norpro SS 65137 $SiO_2$ | 120 | 10 | 50 | 3.0 | 200 | 100 | n/a |
| 059 | fumed silica | 400 | 2.06 | 30 | 0.2 | 200 | 100 | 8.79 |
| 061 | Norpro SS 65137 $SiO_2$ | 120 | 9.92 | 50 | 3.0 | 200 | 100 | 5.97 |
| 063 | $TiO_2$ | 400 | 2.79 | 9 | 1.5 | 400 | 500 | 4.76 |

## Table B2-2. Multifunctional Catalyst Preparation Data

| Catalyst batch ID | Support | Pretreatment Temp (℃) | Support (g) | n-Hexane (mL) | Nb ethoxide (mL) | Thermal Decomp. (T) | Calcination Temp (T) | EDXRF wt% Nb2O5 |
|---|---|---|---|---|---|---|---|---|
| 042 | CAT 040 | 250 | 4.661 | 60 | 0.5 | 200 | 100 | 10.17 |
| 043 | CAT 032 | 250 | 1.660 | 6 | 0.1 | 200 | 100 | 3.79 |
| 046 | CAT 030 | 250 | 2.739 | 30 | 0.1 | 200 | 100 | 12.30 |
| 051 | fumed $SiO_2$ | 100 | 5.340 | 160 | 0.8 | 200 | 100 | 13.65 |
| 053 | CAT 052 | 250 | 4.980 | 75 | 0.8 | 200 | 100 | 13.96 |
| 054 | fumed SiO2 | 250 | 14.86 | 225 | 2.2 | 200 | 100 | 15.21 |
| 060 | Norpro SS 65137 $SiO_2$ | 120 | 10.00 | 50 | 3.0 | 200 | 100 | n/a |
| 062 | CAT 061 | 120 | 9.920 | 50 | 3.0 | 200 | 100 | 5.97 |
| 064 | Norpro SS 65137 $SiO_2$ | 120 | 9.940 | 50 | 3.0 | 200 | 100 | n/a |
| 065 | Norpro SS 65137 $SiO_2$ | 120 | 9.990 | 50 | 3.0 | 200 | 100 | 6.09 |
| 066-A | Norpro SS 65137 $SiO_2$ | 120 | 14.90 | 50 | 4.5 | 200 | 100 | |
| 066-B | Norpro SS 65137 $SiO_2$ | 120 | 14.92 | 50 | 4.5 | 200 | 100 | |
| 066-C | Norpro SS 65137 $SiO_2$ | 120 | 14.99 | 50 | 4.5 | 200 | 100 | |
| 066-D | Norpro SS 65137 $SiO_2$ | 120 | 15.01 | 50 | 4.5 | 200 | 100 | |
| 066_E | Norpro SS 65137 $SiO_2$ | 120 | 15.27 | 50 | 4.6 | 200 | 100 | |
| 066-F | Norpro SS 65137 $SiO_2$ | 120 | 14.96 | 50 | 4.5 | 200 | 100 | |
| 066-G | Norpro SS 65137 $SiO_2$ | 120 | 15.34 | 50 | 4.6 | 200 | 100 | |
| 067-A | Norpro SS 65137 $SiO_2$ | 120 | 14.87 | 50 | 4.5 | 200 | 100 | |
| 067-B | Norpro SS 65137 $SiO_2$ | 120 | 17.22 | 50 | 5.2 | 200 | 100 | |
| 067-C | Norpro SS 65137 $SiO_2$ | 120 | 17.98 | 50 | 5.4 | 200 | 100 | |
| 067-D | Norpro SS 65137 $SiO_2$ | 120 | 15.97 | 50 | 4.8 | 200 | 100 | |
| 067-E | Norpro SS 65137 $SiO_2$ | 120 | 15.14 | 50 | 4.5 | 200 | 100 | |
| 067-F | Norpro SS 65137 $SiO_2$ | 120 | 14.96 | 50 | 4.5 | 200 | 100 | |
| 067-G | Norpro SS 65137 $SiO_2$ | 120 | 16.34 | 50 | 4.9 | 200 | 100 | |
| 067-H | Norpro SS 65137 $SiO_2$ | 120 | 16.69 | 50 | 5.0 | 200 | 100 | |
| | | | | | | | CAT 066 | n/a |
| | | | | | | | CAT 067 | 5.75 |

**B3 Estimation of Palladium Loading via UV-Visible Spectroscopy (**Catalysts investigated in the Preliminary Experiments of Section 6.1.2)

The palladium loading of the catalysts used in the preliminary experiments described in sections 6.1.2 were estimated by UV-Vis Spectroscopy using a Hewlett Packard HP 8453 UV-Vis Spectrometer. The reader is strongly cautioned that this technique had not been validated and the accuracy and repeatability of the method is questionable. Consequently the results should be considered preliminary. However, the results provide insight and afford an explanation of the observations made in the preliminary autoclave experiments of Section 6.1.2. The palladium loading of catalysts used in critical kinetics experiments presented later in this chapter as well as the pilot scale catalytic distillation experiments presented in Chapter Eight were accurately measured via inductively coupled plasma (ICP) spectroscopy by an external laboratory (Galbraith Laboratories, Knoxville, TN).

The palladium loading of catalysts were inferred from the uptake of palladium (II) acetate during the impregnation procedure. The initial concentrations of palladium (II) acetate in the impregnation solutions were precisely known. The concentrations of palladium (II) acetate in the recovered supernatant liquid were determined by UV-Vis spectroscopy. The absorbance of light of wavelength 400 nm was correlated to the concentration of palladium (II) acetate in solution (Figure B3-1) in accordance with the Beer-Lambert Law. However, the specimen required dilution by a factor of 10 to carry out these measurements. The dilution with glacial acetic acid was done using volumetric pipettes and the amounts of specimen and acetic acid were determined by weighing the sealed vials with solution when empty, when specimen was added and when the additional solvent was added using a Sartorius balance (±0.00005 g). The dilution of the specimen introduced uncertainty in measurement and also necessitated a back calculation to determine the concentration of palladium (II) acetate in the undiluted specimen.

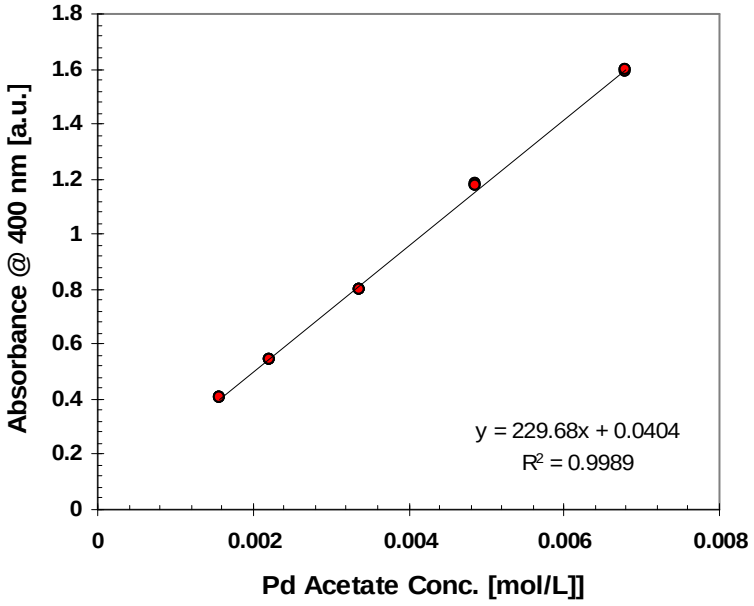


**Figure B3-1** Calibration curve for the determination of the concentration of Pd(II) acetate in glacial acetic acid solution via UV-Vis spectroscopy

The results of the UV-Vis measurements suggested that the palladium loading was only 0.15 wt% for catalyst 042 used in experiment 180 (Figure 6-2) for which the rate of IPA production was relatively low. In contrast, the palladium loading was 1.06 wt%, an order of magnitude higher, for catalyst 051 for which the IPA production rate was comparable to the MIBK production rate (Figure 6-4). A UV-Vis result for catalyst 046 used for experiment #185 (Figure 6-3) was inconclusive due to experimental error for which the back-calculation resulted in a dubious negative concentration. However, a comparison of Figures 6-3 to 6-4 suggests the results of catalyst 051 and 046 are similar. Therefore, catalyst 046 likely had a comparable loading to catalyst 051, around 1 wt% or probably slightly higher.

# Appendix C
## Supplementary Data: GC and GC/MS Data

### C1 Identification of Unknowns in Distillate Product (CD 005) via GC/MS

**Table C1-1 Results of GC/MS Analysis**

| 119D | one major peak | | |
|---|---|---|---|
| **Rank** | **Species** | **RSIM** | **Prob** |
| 1 | 2,4-dimethyl heptane | 867 | 47.66 |
| 2 | 3-ethyl hexane | 807 | 10.15 |
| 3 | 2,3,5-trimethyl hexane | 760 | 8.18 |
| 4 | 4,4-dimethyl heptane | 814 | 3.45 |
| 5 | 2,3-dimethyl heptane | 747 | 2.78 |

| 85D | peak (1/3) second largest peak, major peak | | |
|---|---|---|---|
| **Rank** | **Species** | **RSIM** | **Prob** |
| 1 | 2,4-dimethyl pentane | 868 | 22.29 |
| 2 | 3-ethyl-2,4-dimethyl pentane | 856 | 17.97 |
| 3 | 3-ethyl-hexane | 850 | 14.48 |

| 85D | peak (2/3) minor peak (smallest) | | |
|---|---|---|---|
| **Rank** | **Species** | **RSIM** | **Prob** |
| 1 | cyclohexane | 758 | 19.4 |
| 2 | dicyclopropyl carbinol | 738 | 15.36 |
| 3 | 2H,-pyran,2-(3-butynyloxy)tetrahydro | 739 | 12.6 |
| 4 | 2-cyclopropyl-pentane | | 10.15 |

| 85D | peak (3/3) major peak (largest) | | |
|---|---|---|---|
| **Rank** | **Species** | **RSIM** | **Prob** |
| 1 | 2,3,3-trimethyl hexane | 799 | 23.12 |
| 2 | 1,2,3,4,5-pentamethyl cyclopentane | 730 | 18.64 |
| 3 | 1,1'-bicyclopentyl-2-one | 709 | 12.78 |

| 47D | peak (1/3) minor peak | | |
|---|---|---|---|
| **Rank** | **Species** | **RSIM** | **Prob** |
| 1 | 1,2-dimethyl propyl-cyclopropane | 857 | 53.23 |
| 2 | *2-methyl-3-methylene-heptane* | 764 | 11.33 |
| 3 | dicyclopropyl carbinol | 753 | 6.87 |
| 4 | | | |
| 5 | 4,4,6-3-ethyl-4-methyl pentanol | 833 | |

| 47D | peak (2/3) minor peak | | |
|---|---|---|---|
| **Rank** | **Species** | **RSIM** | **Prob** |
| 1 | 2-cyclopropyl-pentane | 796 | 20.52 |
| 2 | cyclohexane | 764 | 16.54 |
| 3 | propyl-cyclopentane | 761 | 13.33 |

| 47D | peak (3/3) major peak | | |
|---|---|---|---|
| **Rank** | **Species** | **RSIM** | **Prob** |
| 1 | 2,3,3-trimethyl-1-hexene | 802 | 22.29 |
| 2 | 1,2,3,4,5-pentamethyl cyclopentane | 727 | 17.97 |
| 3 | 1,1'bicyclopentyl-2-one | 711 | 14.48 |
| 4 | 1,2-dimethyl propyl cyclopropane | 719 | 8.77 |

**Table C1-2 GC/MS Instrument Settings and Specifications**

Varian CP-3800 GC
Saturn 2000 MS
HP-5 column
flow: 1.5 mL/min
split ratio: 100:1
front injector: 200°C
Trap: 150°C
manifold: 100°C
transfer line: 170°C
Ionization Mode: Electron Impact (EI) auto
Oven Profile: isothermal 40°C; hold 20 min
cut out solvent peak from 1.38 to 1.43 min (3 sec)

## C2 GC Data from Autoclave Experiments

**Table C2-1 Results of GC analyses for autoclave experiments**

### Experiment #130

[T=160℃, W=2.1161 g CAT 005; 700 RPM, 400 psig N2, 78.1 g acetone charged]

**GC Results**

| Time | Mass Fractions (Wt%) | | | | | | |
|---|---|---|---|---|---|---|---|
| (min) | MO | IMO | DAA | MIBK | TMB | PHO | IPO |
| 80 | 6.07 | 0.66 | 0.35 | | | 0.34 | |
| 140 | 8.64 | 0.94 | 0.40 | | | 0.39 | |
| 200 | 9.58 | 1.04 | 0.40 | | | 0.41 | |
| 260 | 10.18 | 1.11 | 0.41 | | | 0.42 | |
| 320 | 10.64 | 1.16 | 0.40 | | | 0.43 | |
| 380 | 10.74 | 1.17 | 0.40 | | | 0.48 | |
| 440 | 10.90 | 1.19 | 0.41 | | | 0.48 | |

### Experiment #131

[T=160℃; W=1.0131 g CAT 006; 700 RPM, 400 psig N2, 100 mL acetone charged]

**GC Results**

| Time | Mass Fractions (Wt%) | | | | | | |
|---|---|---|---|---|---|---|---|
| (min) | MO | IMO | DAA | MIBK | TMB | PHO | IPO |
| 0 | | | | | | | |
| 31 | 0.5 | | | | | | |
| 60 | 5.02 | 0.6 | 0.32 | | | 0.31 | |
| 90 | 7.12 | 0.82 | 0.34 | | | 0.35 | |
| 124 | 8.05 | 0.93 | 0.34 | | | 0.37 | |
| 157 | 10.6 | 1.2 | 0.4 | | | 0.43 | |
| 216 | 11.9 | 1.34 | 0.4 | | | 0.48 | |
| 336 | 14.3 | 1.6 | 0.41 | | 0.23 | 0.54 | |
| 441 | problem with analysis | | | | | | |

## Experiment #134b

[T=160 C; W=.9585 g CAT 009; 400 psig N2; 700 RPM; 77.33 g acetone charged]

**GC Results**

| Time | Mass Fractions (Wt%) | | | | | | | | |
|---|---|---|---|---|---|---|---|---|---|
| (min) | MO | IMO | DAA | MIBK | TMB | PHO | IPO | H20 | Ac |
| 0 | 0.33 | | | | | | | 0.28 | 99.4 |
| 30 | 2.12 | 0.31 | 0.27 | | | | | 0.34 | 97 |
| 60 | 4.24 | 0.52 | 0.3 | | | | | 0.66 | 94.3 |
| 90 | 4.51 | 0.56 | 0.29 | | | | | 0.7 | 93.9 |
| 155 | 5.84 | 0.71 | 0.31 | | | 0.45 | | 0.83 | 91.9 |
| 214 | 6.36 | 0.78 | 0.29 | | | 0.46 | | 1 | 91.1 |
| 304 | 9.46 | 1.09 | 0.39 | | | 0.5 | | 1.3 | 87.3 |
| 480 | 9.46 | 1.1 | 0.35 | | | 0.5 | | 1.57 | 87 |

## Experiment #135

[T=160 C; W=1.0112 g CAT 010; 400 psig N2; 700 RPM; 77.09 g acetone charged]

**GC Results**

| Time | Mass Fractions (Wt%) | | | | | | | | |
|---|---|---|---|---|---|---|---|---|---|
| (min) | MO | IMO | DAA | MIBK | TMB | PHO | IPO | H20 | Ac |
| 0 | | | | | | | | 0.16 | 99.8 |
| 30 | 0.86 | | 0.91 | | | | | 0.21 | 98 |
| 60 | 0.83 | | 0.89 | | | | | 0.21 | 98.1 |
| 90 | 0.84 | | 0.89 | | | | | 0.21 | 98.1 |
| 120 | 0.82 | | 0.87 | | | | | 0.22 | 98.1 |
| 180 | 0.78 | | 0.86 | | | | | 0.22 | 98.1 |
| *300* | 0.93 | | 0.9 | | | | | 0.23 | 97.9 |
| *480* | 1.02 | | 0.88 | | | | | 0.25 | 97.9 |

## Experiment #136

[T=160 C; W=0.6563 g CAT 012; 400 psig N2; 700 RPM; 77.11 g acetone charged]

**GC Results**

| Time | Mass Fractions (Wt%) | | | | | | | | |
|---|---|---|---|---|---|---|---|---|---|
| (min) | MO | IMO | DAA | MIBK | TMB | PHO | IPO | H20 | Ac |
| 0 | 0.13 | | 0.19 | | | | | 0.18 | 99.5 |
| 30 | 0.13 | | 0.4 | | | | | 0.17 | 99.3 |
| 60 | 0.24 | | 0.39 | | | | | 0.17 | 99.2 |
| 90 | 0.29 | | 0.42 | | | | | 0.18 | 99.1 |
| 121 | 0.32 | | 0.41 | | | | | 0.18 | 99.1 |
| 181 | 0.37 | | 0.41 | | | | | 0.19 | 99 |
| 345 | 0.25 | | 0.28 | | | | | 0.21 | 99.3 |
| 468 | 0.13 | | 0.19 | | | | | 0.22 | 99.5 |

## Experiment #137

[T=160 C; W=0.8928 g, CAT 011; 400 psig N2; 700 RPM; 77.15 g acetone charged]
**GC Results:** No peaks reported; catalyst not active

## Experiment #138

[T=160 C; W=1.0250 g; CAT 013; 400 psig N2; 700 RPM; 78.28 g acetone charged]

**GC Results**

| Time | Mass Fractions (Wt%) | | | | | | | | |
|---|---|---|---|---|---|---|---|---|---|
| (min) | MO | IMO | DAA | MIBK | TMB | PHO | IPO | H20 | Ac |
| 0 | | | | | | | | 0.28 | 99.7 |
| 30 | | | | | | | | 0.34 | 99.7 |
| 60 | 2.23 | 0.31 | 0.42 | | | | | 0.66 | 96.4 |
| 91 | 2.75 | 0.35 | 0.44 | | | | | 0.7 | 95.8 |
| 121 | 3.11 | 0.39 | 0.43 | | | | | 0.83 | 95.2 |
| 180 | 4.11 | 0.5 | 0.44 | | | | | 1 | 93.9 |
| 300 | 4.92 | 0.6 | 0.44 | | | | | 1.3 | 92.7 |
| 481 | 6.6 | 0.79 | 0.46 | | | 0.43 | | 1.57 | 90.1 |

## Experiment #139

[T=160 C; W=1.0575 g; gamma alumina acidic support; 400 psig N2; 700 RPM; 77.55 g acetone charged]

**GC Results**

| Time | Mass Fractions (Wt%) | | | | | | | | |
|---|---|---|---|---|---|---|---|---|---|
| (min) | MO | IMO | DAA | MIBK | TMB | PHO | IPO | H20 | Ac |
| 0 | | | | | | | | 0.1 | 99.9 |
| 31 | 0.27 | | 0.19 | | | | | 0.16 | 99.4 |
| 60 | 1.92 | 0.23 | 0.41 | | | | | 0.51 | 96.9 |
| 92 | 2.49 | 0.29 | 0.44 | | | | | 0.63 | 96.2 |
| 123 | 2.79 | 0.33 | 0.43 | | | | | 0.69 | 95.8 |
| 180 | 3.27 | 0.38 | 0.42 | | | | | 0.77 | 95.2 |
| 241 | 4.32 | 0.49 | 0.46 | | | | | 0.95 | 93.8 |
| 480 | 4.8 | 0.54 | 0.45 | | | | | 1.15 | 93.1 |

## Experiment #140

[T=160 C; W=0.9978 g; CAT 014; P>400 psig N2; 700 RPM; 77.49 g acetone charged]

**GC Results**

| Time | Mass Fractions (Wt%) | | | | | | | |
|---|---|---|---|---|---|---|---|---|
| (min) | MO | IMO | DAA | MIBK | TMB | PHO | IPO | H20 |
| 0 | 0.35 | | | | | | | 0.16 |
| 30 | 3.9 | 0.32 | 0.27 | | | | | 1 |
| 61 | 5.14 | 0.46 | 0.26 | | | 0.26 | | 1.31 |
| 90 | 6.31 | 0.58 | 0.29 | | | 0.28 | | 1.49 |
| 120 | 7.31 | 0.69 | 0.31 | | | 0.31 | | 1.6 |
| 180 | 8.02 | 0.78 | 0.32 | | | 0.32 | | 1.9 |
| 327 | 7.98 | 0.8 | 0.27 | | | 0.31 | | 2.56 |
| 502 | 10.7 | 1.06 | 0.35 | | | 0.44 | | n/a |

## Experiment #141

[T=160 C; W=1.0084 g; CAT 015; P>400 psig N2; 700 RPM; 77.86 g acetone charged]

**GC Results**

| Time | Mass Fractions (Wt%) | | | | | | | |
|---|---|---|---|---|---|---|---|---|
| (min) | MO | IMO | DAA | MIBK | TMB | PHO | IPO | H20 |
| 0 | | | | | | | | 0.12 |
| 30 | 2.88 | 0.32 | 0.29 | | | | | 1.04 |
| 60 | 5.06 | 0.56 | 0.28 | | | 0.32 | | 1.54 |
| 90 | 6.54 | 0.71 | 0.32 | | | 0.34 | | 1.75 |
| 120 | 7.25 | 0.79 | 0.32 | | | 0.35 | | 1.9 |
| 182 | 8.35 | 0.91 | 0.34 | | | 0.38 | | 2.04 |
| 240 | 8.67 | 0.96 | 0.31 | | | 0.38 | | 2.56 |
| 480 | 10.6 | 1.15 | 0.38 | | | 0.48 | | 2.61 |

## Experiment #142

[T=160 C; W=0.9788 g; basic gamma alumina support; P>400 psig N2; 700 RPM; 76.98 g acetone charged]

**GC Results**

| Time | Mass Fractions (Wt%) | | | | | | | | |
|---|---|---|---|---|---|---|---|---|---|
| (min) | MO | IMO | DAA | MIBK | TMB | PHO | IPO | H20 | Ac |
| 1 | 1.59 | 0.23 | 0.35 | | | | | 0.12 | 97.7 |
| 20 | 4.09 | 0.49 | 0.48 | | | | | 1.04 | 93.9 |
| 70 | 5.99 | 0.7 | 0.42 | | | | | 1.54 | 91.3 |
| 90 | 6.35 | 0.73 | 0.47 | | | | | 1.75 | 90.7 |
| 120 | 6.83 | 0.78 | 0.47 | | | | | 1.9 | 90 |
| 180 | 7.46 | 0.85 | 0.48 | | | | | 2.04 | 89.2 |
| 300 | 8.15 | 0.91 | 0.49 | | | 0.33 | | 2.56 | 87.6 |
| 480 | 8.59 | 0.96 | 0.49 | | | 0.33 | | 2.61 | 87 |

## Experiment #143

[T=160 C; W=1.0048 g; CAT 016; P>400 psig N2; 700 RPM; 77.30 g acetone charged]

**GC Results**

| Time | Mass Fractions (Wt%) | | | | | | | |
|---|---|---|---|---|---|---|---|---|
| (min) | MO | IMO | DAA | MIBK | TMB | PHO | IPO | H20 |
| 1 | 0.71 | 0.13 | 0.28 | | | | | 0.68 |
| 33 | 2.93 | 0.39 | 0.31 | | | | | 1.01 |
| 60 | 4.31 | 0.53 | 0.31 | | | | | 1.34 |
| 90 | 4.48 | 0.55 | 0.28 | | | | | 1.39 |
| 120 | 5.35 | 0.64 | 0.3 | | | | | 1.45 |
| 180 | 5.04 | 0.62 | 0.27 | | | | | 0.13 |
| 302 | 5.27 | 0.64 | 0.27 | | | | | 3.33 |
| 480 | 6.05 | 0.73 | 0.28 | | | | | 2.24 |

## Experiment #149

[T=160 C; W=0.9672 g CAT 017; P>540 psig N2; 700 RPM; 77.19 g acetone charged]

**GC Results**

| Time | Mass Fractions (Wt%) | | | | | | | |
|---|---|---|---|---|---|---|---|---|
| (min) | MO | IMO | DAA | MIBK | TMB | PHO | IPO | H20 |
| 1 | 1.73 | 0.87 | 0.5 | | | 0.28 | | 0.49 |
| 1 | 1.71 | 0.87 | 0.49 | | | 0.28 | | 0.49 |
| 32 | 4.79 | 1.24 | 0.5 | | | 0.28 | | 1.26 |
| 32 | 4.88 | 1.25 | 0.5 | | | 0.28 | | 1.24 |

| | | | | | | | |
|---|---|---|---|---|---|---|---|
| 61 | 5.47 | 1.32 | 0.47 | | | 0.28 | 1.52 |
| 61 | 5.48 | 1.32 | 0.47 | | | 0.28 | 1.51 |
| 91 | 6.33 | 1.41 | 0.48 | | | 0.28 | 1.52 |
| 91 | 6.57 | 1.43 | 0.49 | | | 0.28 | 1.52 |
| 121 | 6.66 | 1.45 | 0.48 | | | 0.28 | 1.61 |
| 121 | 6.42 | 1.42 | 0.47 | | | 0.28 | 1.59 |
| 181 | 7.42 | 1.53 | 0.48 | | | 0.36 | 1.93 |
| 181 | 7.55 | 1.54 | 0.48 | | | 0.36 | 1.94 |
| 307 | 8.47 | 1.64 | 0.49 | | | 0.37 | 2.06 |
| 307 | 8.77 | 1.66 | 0.51 | | | 0.38 | 2.08 |
| 497 | 8.74 | 1.67 | 0.49 | | | 0.38 | 2.21 |
| 497 | 8.62 | 1.66 | 0.5 | | | 0.36 | 2.21 |

## Experiment #151

[T=160 C; W=1.0076 g CAT 018; P>400 psig N2; 700 RPM; 77.03 g acetone charged]

**GC Results**

| Time | Mass Fractions (Wt%) | | | | | | | |
|---|---|---|---|---|---|---|---|---|
| (min) | MO | IMO | DAA | MIBK | TMB | PHO | IPO | H20 |
| 0 | 0.96 | | 0.4 | | | | | 0.53 |
| 0 | 1 | | 0.41 | | | | | 0.53 |
| 31 | 3.11 | 0.63 | 0.37 | | | | | 1.08 |
| 31 | 3.33 | 0.65 | 0.39 | | | | | 1.08 |
| 60 | 4.22 | 0.75 | 0.37 | | | | | 1.27 |
| 60 | 4.31 | 0.76 | 0.37 | | | | | 1.26 |
| 90 | 4.52 | 0.79 | 0.35 | | | | | 1.38 |
| 90 | 5.04 | 0.84 | 0.39 | | | | | 1.35 |
| 121 | 4.9 | 0.83 | 0.35 | | | | | 1.55 |
| 121 | 4.99 | 0.84 | 0.35 | | | | | 1.55 |
| 180 | 5.54 | 0.91 | 0.34 | | | | | 1.7 |
| 180 | 5.83 | 0.93 | 0.37 | | | | | n/a |
| 300 | 6.16 | 0.97 | 0.37 | | | 0.44 | | 2.02 |
| 300 | 6.01 | 0.96 | 0.36 | | | 0.44 | | 2.01 |
| 480 | 5.69 | 0.94 | 0.3 | | | | | 2.15 |
| 480 | 5.85 | 0.95 | 0.32 | | | | | 2.1 |

## Experiment #152

[T=160 C; W=1.0007 g CAT 019; P>380 psig N2; 700 RPM; 77.63 g acetone charged]

**GC Results**

| Time | Mass Fractions (Wt%) | | | | | | | |
|---|---|---|---|---|---|---|---|---|
| (min) | MO | IMO | DAA | MIBK | TMB | PHO | IPO | H20 |
| 0 | 0.27 | | 0.19 | | | | | 0.42 |
| 0 | 0.29 | | 0.2 | | | | | 0.42 |
| 29 | 2.47 | 0.16 | 0.34 | | | | | 0.85 |
| 29 | 2.71 | 0.18 | 0.38 | | | | | 0.85 |
| 60 | 3.45 | 0.26 | 0.33 | | | | | 1 |
| 60 | 3.52 | 0.27 | 0.35 | | | | | 1 |
| 90 | 3.83 | 0.3 | 0.34 | | | | | 1.03 |
| 90 | 3.79 | 0.3 | 0.33 | | | | | 1.03 |
| 120 | 3.81 | 0.3 | 0.31 | | | | | 1.08 |

| | | | | | | | | |
|---|---|---|---|---|---|---|---|---|
| 120 | 3.89 | 0.31 | 0.32 | | | | 1.08 | |
| 180 | 4.53 | 0.38 | 0.31 | | | | 1.17 | |
| 180 | 4.38 | 0.36 | 0.32 | | | | 1.16 | |
| 300 | 5.79 | 0.51 | 0.34 | | | | 1.32 | |
| 300 | 5.26 | 0.45 | 0.3 | | | | 1.32 | |
| 480 | 6.15 | 0.55 | 0.34 | | | | 1.4 | |
| 480 | 6.1 | 0.54 | 0.34 | | | | 1.39 | |

## Experiment #153

[T=160 C; W=1.0157 g CAT 025; P~400 psig N2; 700 RPM; 77.95 g acetone charged]

**GC Results**

| Time | Mass Fractions (Wt%) | | | | | | | | |
|---|---|---|---|---|---|---|---|---|---|
| (min) | MO | IMO | DAA | MIBK | TMB | PHO | IPO | H20 | |
| 0 | 0.28 | | | | | | | *2.42* | *outlier, contamination?* |
| 0 | | | | | | | | *2.43* | |
| 30 | 1.71 | 0.3 | 0.33 | | | | | 1.01 | |
| 30 | 1.65 | 0.3 | 0.31 | | | | | 1.02 | |
| 60 | 3.12 | 0.46 | 0.29 | | | | | 1.07 | |
| 60 | 3.26 | 0.47 | 0.31 | | | | | 1.08 | |
| 90 | 3.51 | 0.5 | 0.29 | | | | | 1.14 | |
| 90 | 3.74 | 0.52 | 0.3 | | | | | 1.15 | |
| 120 | 4.17 | 0.56 | 0.31 | | | | | 1.15 | |
| 120 | 3.69 | 0.52 | 0.26 | | | | | 1.16 | |
| 185 | 4.52 | 0.6 | 0.28 | | | | | 1.35 | |
| 185 | 4.78 | 0.63 | 0.3 | | | | | 1.35 | |
| 300 | 4.89 | 0.64 | 0.29 | | | | | 1.78 | |
| 300 | 4.96 | 0.65 | 0.28 | | | | | 1.79 | |
| 485 | 5.93 | 0.75 | 0.3 | | | | | 1.63 | |
| 485 | 5.86 | 0.75 | 0.29 | | | | | 1.6 | |

## Experiment #154

[T=160 C; W=1.0104 g CAT 026; P>370 psig N2; 700 RPM; 77.37 g acetone charged]

**GC Results**

| Time | Mass Fractions (Wt%) | | | | | | | | |
|---|---|---|---|---|---|---|---|---|---|
| (min) | MO | IMO | DAA | MIBK | TMB | PHO | IPO | H20 | |
| 0 | 0.77 | | 0.26 | | | | | *4.53* | *outlier, contamination?* |
| 0 | 0.79 | | 0.28 | | | | | *4.65* | |
| 30 | 3.11 | 0.46 | 0.33 | | | | | 1.08 | |
| 30 | 3.42 | 0.49 | 0.38 | | | | | 1.09 | |
| 59 | 3.73 | 0.52 | 0.34 | | | | | 1.13 | |
| 59 | 3.75 | 0.52 | 0.34 | | | | | 1.14 | |
| 95 | 4.4 | 0.59 | 0.35 | | | | | 1.23 | |
| 95 | 4.51 | 0.61 | 0.36 | | | | | 1.25 | |
| 120 | 4.19 | 0.57 | 0.36 | | | | | 1.17 | |
| 120 | 4.37 | 0.59 | 0.38 | | | | | 1.18 | |
| 180 | 4.66 | 0.62 | 0.37 | | | | | 1.27 | |
| 180 | 4.78 | 0.63 | 0.37 | | | | | 1.24 | |
| 301 | 5.28 | 0.68 | 0.34 | | | | | 1.4 | |
| 301 | 5.14 | 0.67 | 0.32 | | | | | 1.38 | |
| 480 | 5.79 | 0.74 | 0.34 | | | | | 1.45 | |
| 480 | 6.03 | 0.76 | 0.36 | | | | | n/a | |

## Experiment #155

[T=160 C; W=0.9965 g CAT 021; P>370 psig N2; 700 RPM; 77.76 g acetone charged]

**GC Results**

| Time | Mass Fractions (Wt%) | | | | | | | | |
|---|---|---|---|---|---|---|---|---|---|
| (min) | MO | IMO | DAA | MIBK | TMB | PHO | IPO | H20 | |
| 0 | | | | | | | | *1.85* | *outlier, contamination?* |
| 0 | | | | | | | | *1.91* | |
| 35 | 2.41 | 0.16 | 0.23 | | | | | 0.98 | |
| 35 | 2.73 | 0.18 | 0.28 | | | | | 0.99 | |
| 60 | 3.18 | 0.18 | 0.2 | | | | | 0.93 | |
| 60 | 3.45 | 0.2 | 0.24 | | | | | 0.93 | |
| 90 | 4.41 | 0.3 | 0.25 | | | | | 1.11 | |
| 90 | 4.13 | 0.28 | 0.23 | | | | | 1.11 | |
| 120 | 4.4 | 0.31 | 0.18 | | | | | 1.24 | |
| 120 | 4.88 | 0.35 | 0.22 | | | | | 0.04 | |
| 180 | 5.98 | 0.49 | 0.21 | | | 0.45 | | 1.6 | |
| 180 | 6.68 | 0.55 | 0.26 | | | 0.46 | | 0.04 | |
| 306 | 7.17 | 0.61 | 0.21 | | | 0.48 | | 1.78 | |
| 306 | 7.2 | 0.61 | 0.21 | | | 0.48 | | 1.77 | |
| 490 | 9.34 | 0.89 | 0.23 | | 0.28 | 0.52 | | 2.39 | |
| 490 | 9.37 | 0.89 | 0.24 | | 0.28 | 0.52 | | n/a | |

## Experiment #156

[T=160 C; W=0.9967 g CAT 023; P>370 psig N2; 700 RPM; 77.70 g acetone charged]

**GC Results**

| Time | Mass Fractions (Wt%) | | | | | | | | |
|---|---|---|---|---|---|---|---|---|---|
| (min) | MO | IMO | DAA | MIBK | TMB | PHO | IPO | H20 | |
| 0 | | | | | | | | *7.75* | *outlier, contamination?* |
| 0 | | | | | | | | *7.82* | |
| 31 | 0.22 | | 0.17 | | | | | 2.67 | |
| 31 | 0.21 | | 0.15 | | | | | 2.68 | |
| 60 | 0.61 | | 0.23 | | | | | 1.19 | |
| 60 | 0.62 | | 0.23 | | | | | 1.18 | |
| 90 | 0.92 | | 0.24 | | | | | 0.68 | |
| 90 | 0.86 | | 0.23 | | | | | 0.68 | |
| 120 | 0.83 | | 0.2 | | | | | 0.55 | |
| 120 | 0.88 | | 0.22 | | | | | 0.56 | |
| 186 | 1.1 | | 0.21 | | | | | 0.59 | |
| 186 | 1.09 | | 0.21 | | | | | 0.58 | |
| 302 | 1.5 | | 0.23 | | | | | 0.76 | |
| 302 | 1.52 | | 0.23 | | | | | 0.76 | |
| 485 | 1.86 | 0.16 | 0.23 | | | | | 0.89 | |
| 485 | 1.76 | | 0.21 | | | | | n/a | |

## Experiment #157

[T=160 C; W=1.0009 g CAT 024; P>470 psig N2; 700 RPM; 77.35 g acetone charged]

**GC Results**

| Time | Mass Fractions (Wt%) | | | | | | | |
|---|---|---|---|---|---|---|---|---|
| (min) | MO | IMO | DAA | MIBK | TMB | PHO | IPO | H20 |
| 0 | | | 0.13 | | | | | 0.33 |
| 0 | | | 0.12 | | | | | 0.34 |
| 30 | 0.37 | | 0.25 | | | | | 0.36 |
| 30 | 0.41 | | 0.32 | | | | | 0.38 |
| 74 | 0.51 | | 0.24 | | | | | 0.37 |
| 74 | 0.5 | | 0.23 | | | | | 0.38 |
| 90 | 0.5 | | 0.22 | | | | | 0.37 |
| 90 | 0.54 | | 0.25 | | | | | 0.38 |
| 120 | 0.57 | | 0.21 | | | | | 0.38 |
| 120 | 0.58 | | 0.22 | | | | | 0.41 |
| 180 | 0.69 | | 0.2 | | | | | 0.42 |
| 180 | 0.68 | | 0.19 | | | | | 0.42 |
| 300 | | | | | | | | 0.45 |
| 300 | 0.88 | | 0.19 | | | | | 0.45 |
| 480 | 0.94 | | 0.18 | | | | | 0.45 |
| 480 | 0.96 | | 0.19 | | | | | 0.46 |

## Experiment #158

[T=160 C; W=0.9999 g CAT 022; P>470 psig N2; 700 RPM; 77.42 g acetone charged]

**GC Results**

| Time | Mass Fractions (Wt%) | | | | | | | |
|---|---|---|---|---|---|---|---|---|
| (min) | MO | IMO | DAA | MIBK | TMB | PHO | IPO | H20 |
| 1 | | | 0.27 | | | | | 0.28 |
| 1 | | | 0.27 | | | | | 0.29 |
| 37 | | | 0.36 | | | | | 0.29 |
| 37 | | | 0.39 | | | | | 0.29 |
| 60 | | | 0.38 | | | | | 0.29 |
| 60 | | | 0.4 | | | | | 0.3 |
| 90 | | | 0.4 | | | | | 0.29 |
| 90 | | | 0.4 | | | | | 0.31 |
| 120 | | | 0.4 | | | | | 0.29 |
| 120 | | | 0.4 | | | | | 0.3 |
| 180 | | | 0.39 | | | | | 0.3 |
| 180 | | | 0.4 | | | | | 0.3 |
| 300 | 0.12 | | 0.36 | | | | | 0.3 |
| 300 | 0.12 | | 0.37 | | | | | 0.31 |
| 480 | 0.14 | | 0.34 | | | | | 0.33 |
| 480 | 0.14 | | 0.31 | | | | | 0.32 |

* IPA contamination detected in this experiment (had used to clean autoclave)

## Experiment #159

[T=160 C; W=0.9997 g CAT 027; P~400 psig N2; 700 RPM; 77.36g acetone charged]

**GC Results**

| Time | Mass Fractions (Wt%) | | | | | | | |
|---|---|---|---|---|---|---|---|---|
| (min) | MO | IMO | DAA | MIBK | TMB | PHO | IPO | H20 |
| 1 | 0.15 | | 0.05 | | | | | 0.4 |
| 1 | 0.16 | | 0.06 | | | | | 0.43 |
| 26 | 1.07 | | 0.08 | | | | | 0.55 |
| 26 | 1.21 | | 0.12 | | | | | 0.57 |

| | | | | | |
|---|---|---|---|---|---|
| 61 | 1.95 | | 0.09 | | 0.72 |
| 61 | 2.01 | | 0.09 | | 0.74 |
| 98 | 2.49 | | 0.11 | | 0.79 |
| 98 | 2.46 | | 0.1 | | 0.81 |
| 122 | 2.87 | | 0.12 | | 0.84 |
| 122 | 2.67 | | 0.09 | | 0.85 |
| 181 | 3.22 | 0.17 | 0.1 | | 0.97 |
| 181 | | | | | 0.98 |
| 266 | 3.68 | 0.23 | 0.09 | | 1.05 |
| 266 | 3.89 | 0.24 | 0.12 | | n/a |
| 481 | 4.26 | 0.28 | 0.12 | | 1.1 |
| 481 | 4.06 | 0.27 | 0.1 | | 1.1 |

## Experiment #160

[T=160 C; W=1.0039 g CAT 028; P~400 psig N2; 700 RPM; 77.20g acetone charged]

**GC Results**

| Time | Mass Fractions (Wt%) | | | | | | | |
|---|---|---|---|---|---|---|---|---|
| (min) | MO | IMO | DAA | MIBK | TMB | PHO | IPO | H20 |
| 1 | | | | | | | | 0.38 |
| 1 | | | | | | | | 0.40 |
| 30 | 0.37 | | 0.12 | | | | | 0.36 |
| 30 | 0.40 | | 0.15 | | | | | 0.38 |
| 60 | 0.57 | | 0.14 | | | | | 0.39 |
| 60 | 0.60 | | 0.18 | | | | | 0.40 |
| 91 | 0.81 | | 0.18 | | | | | 0.42 |
| 91 | 0.79 | | 0.17 | | | | | 0.42 |
| 121 | 0.93 | | 0.20 | | | | | 0.44 |
| 121 | 0.81 | | 0.13 | | | | | 0.45 |
| 180 | 1.10 | | 0.17 | | | | | 0.48 |
| 180 | 1.13 | | 0.18 | | | | | 0.49 |
| 300 | 1.60 | | 0.17 | | | | | 0.59 |
| 300 | 1.62 | | 0.18 | | | | | 0.60 |
| 480 | 1.99 | | 0.19 | | | | | 0.65 |
| 480 | 1.83 | | 0.16 | | | | | 0.65 |

* IPA contamination detected in this experiment (had used to clean autoclave)

## Experiment #161

[T=160 C; W=0.9889 g CAT 029; P~400 psig N2; 700 RPM; 76.97g acetone charged]

**GC Results**

| Time | Mass Fractions (Wt%) | | | | | | | |
|---|---|---|---|---|---|---|---|---|
| (min) | MO | IMO | DAA | MIBK | TMB | PHO | IPO | H20 |
| 1 | 1.02 | 0.15 | 0.13 | | | | | 0.48 |
| 1 | 1.07 | 0.15 | 0.14 | | | | | 0.48 |
| 30 | 4.19 | 0.41 | 0.20 | | | 0.46 | | 1.14 |
| 30 | 4.35 | 0.42 | 0.23 | | | 0.47 | | 1.14 |
| 60 | 6.16 | 0.60 | 0.28 | | | 0.49 | | 1.50 |
| 60 | 6.01 | 0.59 | 0.29 | | | 0.50 | | 1.51 |
| 90 | 6.96 | 0.70 | 0.24 | | | 0.52 | | 1.65 |
| 90 | 6.64 | 0.68 | 0.20 | | | 0.51 | | 1.66 |
| 120 | 6.74 | 0.72 | 0.20 | | | 0.52 | | 1.83 |
| 120 | 7.07 | 0.75 | 0.21 | | | 0.52 | | 1.86 |

| | | | | | | | |
|---|---|---|---|---|---|---|---|
| 180 | 7.46 | 0.82 | 0.21 | | | 0.53 | 2.08 |
| 180 | 9.30 | 1.07 | 0.23 | | 0.24 | 0.57 | 2.09 |
| 276 | 8.53 | 0.96 | 0.24 | | | 0.55 | 2.35 |
| 276 | 8.80 | 0.98 | 0.26 | | | 0.56 | 2.35 |
| 480 | 9.46 | 1.08 | 0.23 | | 0.24 | 0.57 | 2.62 |
| 480 | 9.28 | 1.07 | 0.22 | | 0.23 | 0.56 | 2.62 |

## Experiment #162

[T=160 C; W=0.9979 g CAT 030; P>350 psig N2; 700 RPM; 78.38g acetone charged]

**GC Results**

| Time | Mass Fractions (Wt%) | | | | | | | |
|---|---|---|---|---|---|---|---|---|
| (min) | MO | IMO | DAA | MIBK | TMB | PHO | IPO | H20 |
| 1 | 0.93 | | 0.11 | | | | | 0.47 |
| 1 | 0.92 | | | | | | | 0.48 |
| 30 | 3.43 | 0.15 | 0.13 | | | | | 0.98 |
| 30 | 3.61 | 0.16 | 0.13 | | | | | 0.98 |
| 60 | 5.23 | 0.35 | 0.15 | | | 0.31 | | 1.40 |
| 60 | 5.12 | 0.34 | 0.15 | | | 0.32 | | 1.41 |
| 90 | 5.92 | 0.43 | 0.16 | | | 0.33 | | 1.57 |
| 90 | 6.19 | 0.45 | 0.17 | | | 0.34 | | 1.57 |
| 120 | 6.68 | 0.53 | 0.17 | | | 0.35 | | 1.73 |
| 120 | 6.69 | 0.53 | 0.17 | | | 0.36 | | 1.75 |
| 180 | 7.15 | 0.60 | 0.16 | | | 0.37 | | 1.84 |
| 180 | 7.38 | 0.62 | 0.18 | | | 0.38 | | 1.85 |
| 300 | 8.57 | 0.80 | 0.19 | | | 0.41 | | 2.29 |
| 300 | 8.29 | 0.77 | 0.18 | | | 0.41 | | 2.30 |
| 480 | 11.02 | 1.05 | 0.28 | | 0.16 | 0.48 | | 2.36 |
| 480 | 9.74 | 0.93 | 0.24 | | 0.15 | 0.43 | | 2.37 |

## Experiment #163

[T=160 C; W=1.0009 g CAT 031; P>400 psig N2; 700 RPM; 77.54g acetone charged]

**GC Results**

| Time | Mass Fractions (Wt%) | | | | | | | |
|---|---|---|---|---|---|---|---|---|
| (min) | MO | IMO | DAA | MIBK | TMB | PHO | IPO | H20 |
| 1 | 1.13 | | 0.23 | | | | | 0.38 |
| 1 | 1.12 | | 0.24 | | | | | 0.41 |
| 33 | 3.88 | 0.35 | 0.23 | | | | | 0.85 |
| 33 | 3.76 | 0.34 | 0.24 | | | | | 0.87 |
| 61 | 4.73 | 0.45 | 0.22 | | | | | 1.01 |
| 61 | 4.65 | 0.44 | 0.23 | | | | | 1.03 |
| 90 | 5.29 | 0.52 | 0.21 | | | | | 1.14 |
| 90 | 5.62 | 0.55 | 0.25 | | | | | 1.16 |
| 125 | 5.65 | 0.56 | 0.20 | | | | | 1.16 |
| 125 | 5.77 | 0.57 | 0.22 | | | | | 1.17 |
| 180 | 7.14 | 0.72 | 0.22 | | | | | 1.26 |
| 180 | 7.59 | 0.77 | 0.25 | | | 0.31 | | 1.26 |
| 269 | 8.72 | 0.90 | 0.23 | | | 0.34 | | 1.50 |
| 269 | 8.88 | 0.90 | 0.25 | | | 0.35 | | 1.51 |
| 480 | 11.14 | 1.18 | 0.23 | | | 0.39 | | 1.84 |
| 480 | 11.12 | 1.16 | 0.24 | | | 0.40 | | 1.82 |

## Experiment #164

[T=160 C; W=1.0031 g CAT 032; P>400 psig N2; 700 RPM; 77.50 g acetone charged]

**GC Results**

| Time | Mass Fractions (Wt%) | | | | | | | |
|---|---|---|---|---|---|---|---|---|
| (min) | MO | IMO | DAA | MIBK | TMB | PHO | IPO | H20 |
| 0 | | | 0.18 | | | | | 0.27 |
| 0 | | | 0.19 | | | | | 0.27 |
| 30 | 3.18 | 0.31 | 0.41 | | | | | 0.82 |
| 30 | 3.10 | 0.30 | 0.41 | | | | | 0.82 |
| 60 | 5.08 | 0.51 | 0.41 | | | | | 1.17 |
| 60 | 5.16 | 0.51 | 0.43 | | | | | 1.18 |
| 90 | 5.73 | 0.58 | 0.40 | | | | | 1.36 |
| 90 | 5.91 | 0.60 | 0.42 | | | | | 1.36 |
| 120 | 5.94 | 0.60 | 0.40 | | | | | 1.39 |
| 120 | 6.33 | 0.64 | 0.42 | | | | | 1.38 |
| 180 | 6.81 | 0.69 | 0.42 | | | 0.07 | | 1.46 |
| 180 | 7.11 | 0.72 | 0.43 | | | 0.07 | | 1.46 |
| 302 | 8.44 | 0.86 | 0.39 | | | 0.13 | | 1.92 |
| 302 | 8.43 | 0.86 | 0.39 | | | 0.13 | | 1.94 |
| 480 | 9.90 | 1.00 | 0.40 | | | 0.18 | | 2.07 |
| 480 | 10.05 | 1.02 | 0.41 | | | 0.18 | | 2.05 |

## Experiment #165

[T=160 C; W=1.0209 g, Nb (V) oxide uncalcined; P>400 psig N2; 700 RPM; 76.19 g acetone charged]

**GC Results**

| Time | Mass Fractions (Wt%) | | | | | | | |
|---|---|---|---|---|---|---|---|---|
| (min) | MO | IMO | DAA | MIBK | TMB | PHO | IPO | H20 |
| 1 | 1.96 | 1.96 | 1.22 | | | | | n/a |
| 1 | 1.96 | 1.96 | 1.22 | | | | | n/a |
| 30 | 2.39 | 1.96 | 1.46 | | | | | n/a |
| 30 | 2.37 | 1.96 | 1.46 | | | | | n/a |
| 61 | 1.96 | 1.96 | 1.22 | | | | | n/a |
| 61 | 1.96 | 1.96 | 1.22 | | | | | n/a |
| 90 | 2.92 | 1.96 | 1.44 | | | | | n/a |
| 90 | 2.96 | 1.96 | 1.44 | | | | | n/a |
| 120 | 2.87 | 1.96 | 1.42 | | | | | n/a |
| 120 | 2.75 | 1.96 | 1.39 | | | | | n/a |
| 180 | 2.26 | 1.96 | 1.46 | | | | | n/a |
| 180 | 2.28 | 1.96 | 1.47 | | | | | n/a |
| 308 | 2.29 | 1.96 | 1.50 | | | | | n/a |
| 308 | 2.38 | 1.96 | 1.59 | | | | | n/a |
| 480 | 2.70 | 1.96 | 1.22 | | | | | n/a |
| 480 | 2.73 | 1.96 | 1.22 | | | | | n/a |

## Experiment #166

Aborted experiment;  contamination in reactor.

## Experiment #167

[T=160 C; W=1.1920 g, fumed silica; P>400 psig N2; 700 RPM; 76.80 g acetone charged]

**GC Results**

| Time | Mass Fractions (Wt%) | | | | | | | |
|---|---|---|---|---|---|---|---|---|
| (min) | MO | IMO | DAA | MIBK | TMB | PHO | IPO | H20 |

| | | |
|---|---|---|
| 0 | | n/a |
| 0 | | n/a |
| 30 | | n/a |
| 30 | 0.07 | n/a |
| 62 | | n/a |
| 62 | | n/a |
| 92 | | n/a |
| 92 | | n/a |
| 120 | 0.07 | n/a |
| 120 | 0.08 | n/a |
| 190 | | n/a |
| 190 | 0.08 | n/a |
| 303 | 0.12 | n/a |
| 303 | 0.07 | n/a |
| 364 | 0.10 | n/a |
| 364 | 0.08 | n/a |

## Experiment #168

[T=160 C; W=2.6571 g; gamma alumina acidic support; P>400 psig N2; 700 RPM; 77.23 g acetone charged]

**GC Results**

Time Mass Fractions (Wt%)

| (min) | MO | IMO | DAA | MIBK | TMB | PHO | IPO | H20 |
|---|---|---|---|---|---|---|---|---|
| 0 | 2.83 | 0.25 | 0.29 | | | | | n/a |
| 0 | 2.59 | 0.23 | 0.25 | | | | | n/a |
| 30 | 6.51 | 0.64 | 0.35 | | | | | n/a |
| 30 | 5.71 | 0.56 | 0.29 | | | | | n/a |
| 60 | 8.76 | 0.87 | 0.32 | | | 0.07 | | n/a |
| 60 | 9.10 | 0.91 | 0.34 | | | 0.08 | | n/a |
| 97 | 10.07 | 1.00 | 0.31 | | | 0.12 | | n/a |
| 97 | 10.37 | 1.03 | 0.32 | | | 0.12 | | n/a |
| 128 | 10.83 | 1.09 | 0.30 | | | 0.15 | | n/a |
| 128 | 11.20 | 1.12 | 0.31 | | | 0.15 | | n/a |
| 186 | 9.45 | 0.94 | 0.24 | | | 0.13 | | n/a |
| 186 | 11.60 | 1.16 | 0.31 | | | 0.17 | | n/a |
| 300 | 12.97 | 1.30 | 0.31 | | | 0.23 | 0.15 | n/a |

## Experiment #169

[T=160 C; W=0.6804 g; CAT 033; P>400 psig N2; 700 RPM; 77.25 g acetone charged]

**GC Results**

| Time | Mass Fractions (Wt%) | | | | | | | |
|---|---|---|---|---|---|---|---|---|
| (min) | MO | IMO | DAA | MIBK | TMB | PHO | IPO | H20 |
| 1 | 0.38 | | 1.32 | | | | | 0.46 |
| 1 | 0.40 | | 1.36 | | | | | 0.45 |
| 31 | 1.44 | | 1.25 | | | | | 0.64 |
| 31 | 1.52 | | 1.28 | | | | | 0.65 |
| 60 | 1.77 | | 1.24 | | | | | 0.68 |
| 60 | 1.73 | | 1.24 | | | | | 0.68 |
| 90 | 1.75 | | 1.21 | | | | | 0.73 |
| 90 | 1.95 | | 1.23 | | | | | 0.74 |
| 120 | 2.31 | | 1.24 | | | | | 0.81 |
| 120 | 2.25 | | 1.24 | | | | | 0.90 |
| 180 | 3.03 | 0.40 | 1.27 | | | | | 0.90 |
| 180 | 3.09 | 0.40 | 1.27 | | | | | 1.08 |
| 301 | 3.78 | 0.49 | 1.27 | | | | | 1.09 |
| 301 | 3.29 | 0.45 | 1.23 | | | | | 1.11 |
| 480 | 4.11 | 0.52 | 1.26 | | | | | 1.09 |
| 480 | 4.52 | 0.55 | 1.29 | | | | | 1.10 |

## Experiment #170

[T=160 C; W=1.1166 g; Amberlyst 15; P>320 psig N2; 700 RPM; 77.44 g acetone charged]

**GC Results**

| Time | Mass Fractions (Wt%) | | | | | | | | |
|---|---|---|---|---|---|---|---|---|---|
| (min) | MO | IMO | DAA | MIBK | TMB | PHO | IPO | H20 | others |
| 1 | 0.72 | | 1.32 | | | | | 0.33 | |
| 1 | 0.78 | | 1.38 | | | | | 0.33 | |
| 31 | 2.11 | 0.61 | 1.36 | | | | | 0.75 | 0.24 |
| 31 | 2.12 | 0.61 | 1.35 | | | | | 0.74 | 0.25 |
| 61 | 4.52 | 0.77 | 1.35 | | | | | 1.45 | 0.33 |
| 61 | 4.95 | 0.81 | 1.38 | | | | | 1.43 | 0.34 |
| 90 | 7.16 | 0.94 | 1.44 | | | 0.27 | | 1.96 | 0.40 |
| 90 | 7.34 | 0.95 | 1.46 | | | 0.28 | | 1.94 | 0.39 |
| 120 | 6.73 | 0.90 | 1.41 | | | 0.27 | | 2.27 | 0.38 |
| 120 | 7.97 | 0.99 | 1.47 | | | 0.31 | | 2.55 | 0.40 |
| 180 | 8.93 | 1.05 | 1.53 | | | 0.35 | | 2.53 | 0.42 |
| 180 | 8.32 | 1.01 | 1.50 | | | 0.34 | | 2.89 | 0.40 |
| 305 | 8.24 | 1.00 | 1.51 | | | 0.36 | | 2.89 | 0.40 |
| 305 | 10.83 | 1.18 | 1.64 | | 0.14 | 0.44 | 0.20 | | 0.45 |
| 540 | 8.86 | 1.04 | 1.60 | | 0.22 | 0.42 | 0.24 | 3.64 | 0.39 |
| 540 | 11.37 | 1.21 | 1.75 | | 0.28 | 0.52 | 0.30 | 3.61 | 0.42 |

## Experiment #171

[T=160 C; W=0.9968 g; CAT 035; P>400 psig N2; 700 RPM; 76.19 g acetone charged]

**GC Results**

| Time | Mass Fractions (Wt%) | | | | | | | |
|---|---|---|---|---|---|---|---|---|
| (min) | MO | IMO | DAA | MIBK | TMB | PHO | IPO | H20 |
| 3 | 0.87 | | 0.19 | | | | | 0.44 |
| 3 | 0.87 | | | | | | | 0.15 |
| 29 | | | | | | | | 0.15 |
| 29 | 1.85 | | 0.18 | | | | | 0.65 |
| 60 | 3.03 | 0.63 | 0.21 | | | | | 1.00 |
| 60 | 2.97 | 0.62 | 0.19 | | | | | 1.00 |
| 90 | 2.86 | | 0.19 | | | | | 0.96 |
| 90 | 2.94 | | 0.19 | | | | | 0.96 |
| 120 | 5.04 | 0.78 | 0.27 | | | 0.21 | | 1.31 |
| 120 | 5.28 | 0.80 | 0.29 | | | 0.23 | | 1.45 |
| 180 | 6.07 | 0.87 | 0.27 | | | 0.27 | | 1.44 |
| 180 | 5.02 | 0.80 | 0.22 | | | 0.23 | | 0.15 |
| 300 | 7.06 | 1.04 | 0.26 | | | 0.35 | | 1.94 |
| 300 | 7.95 | 1.12 | 0.29 | | | 0.39 | | 0.15 |
| 480 | 6.28 | 1.02 | 0.20 | | 0.12 | 0.35 | | 2.28 |
| 480 | 6.75 | 1.06 | 0.21 | | 0.13 | 0.40 | | 2.35 |

## Experiment #172

[T=160 C; W=1.0729 g; Niobium (V) oxide, calcined; P>400 psig N2; 700 RPM; 77.52 g acetone charged]

**GC Results**

| Time | Mass Fractions (Wt%) | | | | | | | |
|---|---|---|---|---|---|---|---|---|
| (min) | MO | IMO | DAA | MIBK | TMB | PHO | IPO | H20 |
| 0 | | | | | | | | n/a |
| 0 | | | | | | | | n/a |

| | | | | | | | | |
|---|---|---|---|---|---|---|---|---|
| 30 | | | | | | | | n/a |
| 30 | | | | | | | | n/a |
| 60 | | | | | | | | n/a |
| 60 | | | | | | | | n/a |
| 91 | | | | | | | | n/a |
| 91 | | | | | | | | n/a |
| 121 | | | | | | | | n/a |
| 121 | | | | | | | | n/a |
| 180 | 0.57 | | | | | | | n/a |
| 180 | 0.58 | | | | | | | n/a |
| 301 | 0.60 | | 0.19 | | | | | n/a |
| 301 | 0.60 | | 0.18 | | | | | n/a |
| 480 | 0.71 | | 0.18 | | | | | n/a |
| 480 | 0.72 | | 0.18 | | | | | n/a |

## Experiment #173

[T=160 C; W=0.9886 g; CAT 036; P>400 psig N2; 700 RPM; 77.60 g acetone charged]

**GC Results**

| Time | Mass Fractions (Wt%) | | | | | | | |
|---|---|---|---|---|---|---|---|---|
| (min) | MO | IMO | DAA | MIBK | TMB | PHO | IPO | H20 |
| 1 | | | | | | | | 0.49 |
| 1 | | | | | | | | 0.50 |
| 31 | 1.68 | | 0.23 | | | | | 0.70 |
| 31 | 1.62 | | 0.21 | | | | | 0.70 |
| 60 | 2.53 | | 0.22 | | | | | 0.92 |
| 60 | 2.53 | | 0.21 | | | | | 0.89 |
| 90 | 3.26 | | 0.22 | | | | | 0.98 |
| 90 | 3.20 | | 0.22 | | | | | 0.98 |
| 124 | 3.81 | | 0.21 | | | | | 1.14 |
| 124 | 3.92 | 0.50 | 0.22 | | | | | 1.15 |
| 180 | 4.46 | 0.56 | 0.21 | | | | | 1.28 |
| 180 | 4.60 | 0.56 | 0.22 | | | | | 1.28 |
| 300 | 5.95 | 0.74 | 0.21 | | | 0.18 | | 1.67 |
| 300 | 5.64 | 0.71 | 0.21 | | | 0.18 | | |
| 517 | 7.02 | 0.84 | 0.23 | | | 0.25 | | 1.78 |
| 517 | 6.14 | 0.77 | 0.20 | | | 0.21 | | 1.77 |

## Experiment #174

[T=160 C; W=1.0086 g; CAT 037; P>400 psig N2; 700 RPM; 77.18 g acetone charged]

**GC Results**

| Time | Mass Fractions (Wt%) | | | | | | | |
|---|---|---|---|---|---|---|---|---|
| (min) | MO | IMO | DAA | MIBK | TMB | PHO | IPO | H20 |
| 0 | 1.03 | | | | | | | n/a |
| 0 | 1.05 | | | | | | | n/a |
| 31 | 2.50 | | | | | | | n/a |
| 31 | 2.51 | | | | | | | n/a |
| 60 | 3.55 | | | | | | | n/a |
| 60 | 3.84 | | 0.18 | | | | | n/a |
| 92 | 4.41 | 0.79 | | | | | | n/a |
| 92 | 4.30 | 0.79 | | | | | | n/a |
| 120 | 4.95 | 0.85 | 0.18 | | | | | n/a |

| | | | | | | | |
|---|---|---|---|---|---|---|---|
| 120 | 5.36 | 0.88 | 0.18 | | | | n/a |
| 180 | 5.89 | 0.96 | | | | 0.25 | n/a |
| 180 | 6.25 | 0.99 | 0.18 | | | 0.26 | n/a |
| 300 | 7.22 | 1.13 | | | | 0.32 | n/a |
| 300 | 6.74 | 1.10 | | | | 0.30 | n/a |
| 480 | 6.43 | 1.11 | | | | 0.31 | n/a |
| 480 | 6.49 | 1.12 | | | | 0.31 | n/a |

## Experiment #175

[T=160 C; W=1.0015 g; CAT 038; P>400 psig N2; 700 RPM; 77.47 g acetone charged]

**GC Results**

| Time | Mass Fractions (Wt%) | | | | | | | | |
|---|---|---|---|---|---|---|---|---|---|
| (min) | MO | IMO | DAA | MIBK | TMB | PHO | IPO | H20 | |
| *0* | 1.13 | | | | | | | 0.56 | |
| 0 | 1.36 | | | | | | | 0.58 | |
| 0 | 1.32 | | | | | | | - | |
| *34* | 3.83 | | | | | | | 1.17 | |
| 34 | 5.01 | | | | | | | 1.18 | |
| 34 | 4.50 | | | | | | | - | |
| *60* | 4.66 | 0.91 | | | | | | 1.41 | |
| 60 | 5.82 | 0.98 | | | | | | 1.42 | |
| 60 | 6.09 | 0.99 | | | | | | - | |
| *100* | 5.90 | 1.05 | | | | | | 1.73 | |
| 100 | 7.61 | 1.18 | | | | 0.15 | | 1.73 | |
| 100 | 7.78 | 1.19 | | | | 0.15 | | - | |
| *120* | 6.26 | 1.09 | | | | 0.11 | | 1.78 | |
| 120 | 7.74 | 1.20 | | | | 0.15 | | 1.80 | |
| 120 | 8.13 | 1.23 | | | | 0.17 | | - | |
| 180 | 10.23 | 1.47 | 0.41 | | | 0.28 | | 2.08 | |
| 180 | 9.26 | 1.40 | | | | 0.21 | | 2.08 | |
| 180 | 9.86 | 1.44 | | | | 0.28 | | - | |
| 302 | 11.69 | 1.68 | | | | 0.32 | | 2.35 | |
| 302 | 10.09 | 1.53 | | | | 0.28 | | 2.38 | |
| *302* | *57.30* | *5.74* | *0.99* | | *0.60* | *2.17* | | - | *obvious outlier* |
| *480* | 11.26 | 1.68 | 0.57 | | | | | 2.71 | |
| *480* | 5.60 | 1.14 | 0.44 | | | | | 2.75 | |
| *480* | 12.23 | 1.76 | 0.41 | | 0.15 | 0.42 | | - | |

## Experiment #176

[T=160 C; W=0.3574 g; CAT 040; P~400 psig N2; 700 RPM; 77.52 g acetone charged]

**GC Results**

| Time | Mass Fractions (Wt%) | | | | | | | |
|---|---|---|---|---|---|---|---|---|
| (min) | MO | IMO | DAA | MIBK | TMB | PHO | IPO | H20 |
| *1* | | | | | | | | 0.56 |
| 1 | | | | | | | | 0.58 |
| 23 | 1.16 | | 0.14 | | | | | 1.17 |
| *23* | 1.13 | | | | | | | 1.18 |
| 40 | 1.08 | | | | | | | 1.41 |
| 40 | 1.18 | | | | | | | 1.42 |
| *60* | 2.03 | | | | | | | 1.73 |
| 60 | 1.86 | | | | | | | 1.73 |

| | | | | |
|---|---|---|---|---|
| 80 | 2.50 | 0.14 | | 1.78 |
| *80* | 2.42 | | | 1.80 |
| 100 | 2.47 | | | 2.08 |
| 100 | 2.46 | 0.13 | | 2.08 |
| *120* | 2.90 | 0.13 | | 2.35 |
| 120 | 2.55 | | | 2.38 |

## Experiment #177

[T=160 C; W=0.3530 g; CAT 040-A; P>300 psig N2; 700 RPM; 77.87 g acetone charged]
CAT 040 treated with glacial acetic acid

**GC Results**

| Time | Mass Fractions (Wt%) | | | | | | |
|---|---|---|---|---|---|---|---|
| (min) | MO | IMO | DAA | MIBK | TMB | PHO | IPO |
| *0* | 0.48 | | | | | | |
| 0 | 0.48 | | | | | | |
| 20 | 1.04 | | | | | | |
| *20* | 1.07 | | | | | | |
| 40 | 1.74 | | 0.13 | | | | |
| 40 | 1.55 | | | | | | |
| *60* | 1.91 | | | | | | |
| 60 | 2.12 | | 0.16 | | | | |
| 80 | 2.70 | | 0.19 | | | | |
| *80* | 2.15 | | | | | | |
| 100 | 2.90 | | 0.18 | | | | |
| 100 | 2.54 | | 0.14 | | | | |
| *120* | 3.06 | | 0.17 | | | | |
| 120 | 3.07 | | 0.17 | | | | |

## Experiment #178

[T=160 C; W=0.3638 g, CAT 040-B; P>400 psig N2; 700 RPM; 77.34 g acetone charged]
CAT 040 treated with 1.0 M acetic acid

**GC Results**

| Time | Mass Fractions (Wt%) | | | | | | |
|---|---|---|---|---|---|---|---|
| (min) | MO | IMO | DAA | MIBK | TMB | PHO | IPO |
| 0 | | | | | | | |
| 0 | | | | | | | |
| 20 | 1.18 | | 0.16 | | | | |
| 20 | 1.12 | | 0.14 | | | | |
| 40 | 1.47 | | 0.16 | | | | |
| 40 | 1.48 | | 0.15 | | | | |
| 60 | 1.85 | | 0.15 | | | | |
| 60 | 1.80 | | 0.14 | | | | |
| 82 | 2.13 | | 0.15 | | | | |
| 82 | 2.14 | | 0.15 | | | | |
| 100 | 2.70 | | 0.18 | | | | |
| 100 | 2.49 | | 0.15 | | | | |
| 120 | 2.84 | | 0.16 | | | | |
| 120 | 2.80 | | 0.15 | | | | |

## Experiment #179

[T=160 C; W=0.3492 g, CAT 040; P>200 psig N2; 700 RPM; 77.29 g acetone charged]
CAT 040 control sample

**GC Results**

| Time | Mass Fractions (Wt%) | | | | | | |
|---|---|---|---|---|---|---|---|
| (min) | MO | IMO | DAA | MIBK | TMB | PHO | IPO |
| 0 | 0.50 | | | | | | |
| 0 | 0.50 | | | | | | |
| 20 | 1.39 | | 0.13 | | | | |
| 20 | 1.43 | | 0.14 | | | | |
| 40 | 2.30 | | 0.17 | | | | |
| 40 | 2.22 | | 0.16 | | | | |
| 60 | 2.39 | | 0.15 | | | | |
| 60 | 2.56 | | 0.17 | | | | |
| 80 | 3.01 | | 0.18 | | | | |
| 80 | 3.02 | | 0.17 | | | | |
| 100 | 3.52 | 0.51 | 0.19 | | | | |
| 100 | 3.31 | 0.49 | 0.17 | | | | |
| 120 | 3.40 | 0.51 | 0.16 | | | | |
| 120 | 4.07 | 0.54 | 0.20 | | | | |

## Experiment #180

[T=160 C; W=0.5974 g, CAT 042; P=600 psig H2; 700 RPM; 77.50 g acetone charged]

**GC Results**

| Time | Mass Fractions (Wt%) | | | | | | | | | | | |
|---|---|---|---|---|---|---|---|---|---|---|---|---|
| (min) | MO | IMO | DAA | MIBK | TMB | PHO | IPO | "others" | IPA | MIBC | DIBK | H2O |
| 0 | | | | | | | | | | | | 0.52 |
| 0 | | | | | | | | | | | | 0.52 |
| 30 | | | | 2.28 | | | | | | | | 0.88 |
| 30 | | | | 2.23 | | | | | | | | 0.88 |
| 60 | | | | 3.38 | | | | | | | | 1.09 |
| 60 | | | | 3.26 | | | | | | | | 1.08 |
| 90 | | | | 4.17 | | | | | | | | 1.28 |
| 90 | | | | 4.33 | | | | | | | | 1.28 |
| 120 | | | | 4.61 | | | | | | | | 1.31 |
| 120 | | | 0.21 | 5.17 | | | | | | | | 1.31 |
| 180 | | | 0.20 | 6.47 | | | | | 0.57 | | 0.19 | 1.64 |
| 180 | | | | 6.09 | | | | | 0.54 | | 0.18 | 1.64 |
| 300 | | | | 7.32 | | | | | 0.73 | | 0.21 | 1.79 |
| 300 | | | | 7.24 | | | | | 0.72 | | 0.21 | 1.79 |
| 584 | | | | 10.00 | 0.10 | | | | 1.25 | | 0.29 | 2.64 |
| 584 | | | | 9.77 | | | | | 1.22 | | 0.28 | 2.64 |

## Experiment #181

[T=160 C; W=0.7009 g, CAT 043; P=600 psig H2; 700 RPM; 77.23 g acetone charged]

**GC Results**

| Time | Mass Fractions (Wt%) | | | | | | | | | | | |
|---|---|---|---|---|---|---|---|---|---|---|---|---|
| (min) | MO | IMO | DAA | MIBK | TMB | PHO | IPO | "others" | IPA | MIBC | DIBK | H2O |
| 0 | | | | | | | | | | | | 0.51 |
| 0 | | | | | | | | | | | | 0.51 |
| 33 | | | | 1.32 | | | | | | | | 0.61 |
| 33 | | | 0.20 | 1.39 | | | | | | | | 0.6 |
| 61 | | | | 1.66 | | | | | | | | 0.66 |

| | | | | | | | | | | | |
|---|---|---|---|---|---|---|---|---|---|---|---|
| 61 | | | 0.20 | 1.70 | | | | | | | 0.66 |
| 90 | | | | 1.87 | | | | | | | 0.69 |
| 90 | | | | 1.86 | | | | | | | 0.7 |
| 120 | | | | 2.05 | | | | | | | 0.74 |
| 120 | | | | 1.98 | | | | | | | 0.74 |
| 180 | | | | 2.29 | | | | | | | 0.8 |
| 180 | | | | 2.31 | | | | | | | 0.8 |
| 300 | | | | 2.75 | | | | 0.50 | | | 0.91 |
| 300 | | | | 2.94 | | | | 0.52 | | | 0.9 |
| 480 | | | | 3.27 | | | | 0.72 | | | 1.02 |
| 480 | | | | 3.34 | | | | 0.76 | | | 1.01 |

## Experiment #182

[T=160 C; W=1.0080 g, CAT 039; P=600 psig H2; 700 RPM; 77.41 g acetone charged]

**GC Results**

| Time | Mass Fractions (Wt%) | | | | | | | | | | |
|---|---|---|---|---|---|---|---|---|---|---|---|
| (min) | MO | IMO | DAA | MIBK | TMB | PHO | IPO | "others" | IPA | MIBC | DIBK | H2O |
| 0 | | | | | | | | | | | | 0.41 |
| 0 | | | | | | | | | | | | 0.41 |
| 31 | 1.49 | | | | | | | | | | | 0.59 |
| 31 | 0.53 | | | | | | | | | | | 0.6 |
| 60 | 1.95 | | | 0.53 | | | | | | | | 0.79 |
| 60 | 1.82 | | | 0.49 | | | | | | | | 0.78 |
| 91 | 0.53 | | | -0.01 | | | | | | | | 0.99 |
| 91 | 0.53 | | | -0.01 | | | | | | | | 0.99 |
| 122 | 2.70 | | | 0.76 | | | | | | | | 1.05 |
| 122 | 2.91 | | | 0.84 | | | | | | | | 1.05 |
| 182 | 3.53 | 0.69 | | 1.36 | | | | | | | | 1.29 |
| 182 | 3.67 | 0.70 | | 1.38 | | | | | | | | 1.3 |
| 300 | | | | | | | | | | | | 1.53 |
| 300 | | | | | | | | | | | | 1.52 |
| 489 | 5.48 | 0.90 | | 2.26 | | 0.21 | | | | | | 1.92 |
| 489 | 5.30 | 0.89 | | 2.21 | | 0.20 | | | | | | 1.9 |

## Experiment #185

[T=160 C; W=0.6183 g, CAT 046; P=600 psig H2; 700 RPM; 77.46 g acetone charged]

**GC Results**

| Time | Mass Fractions (Wt%) | | | | | | | | | | |
|---|---|---|---|---|---|---|---|---|---|---|---|
| (min) | MO | IMO | DAA | MIBK | TMB | PHO | IPO | "others" | IPA | MIBC | DIBK | H2O |
| 1 | | | | | 0.02 | | | | | | | 0.46 |
| 1 | | | | | 0.02 | | | | | | | 0.46 |
| 31 | | | | 1.23 | 0.02 | | | | | | | 0.61 |
| 31 | | | | 1.24 | 0.02 | | | | | | | 0.61 |
| 61 | | | | 2.10 | 0.02 | | | | 0.65 | | | 0.77 |
| 61 | | | | 2.11 | 0.02 | | | | 0.65 | | | 0.77 |
| 91 | | | | 2.54 | 0.02 | | | | 0.85 | | | 0.85 |
| 91 | | | | 2.41 | 0.02 | | | | 0.82 | | | 0.86 |
| 121 | | | | 2.93 | 0.02 | | | | 1.12 | | | 0.9 |
| 121 | | | | 2.86 | 0.02 | | | | 1.07 | | | 0.94 |
| 181 | | | | 3.34 | 0.02 | | | | 1.74 | | | 0.99 |
| 181 | | | | 3.48 | 0.02 | | | | 1.81 | | | 1 |

| | | | | | | | | | | | |
|---|---|---|---|---|---|---|---|---|---|---|---|
| 301 | | | 3.95 | 0.02 | | | | 3.95 | | | 1.22 |
| 301 | | | 3.84 | 0.02 | | | | 3.83 | | | 1.22 |
| 600 | | | 4.31 | 0.02 | | | | 13.53 | | 0.30 | 1.25 |
| | | | | | | | | | | | 1.25 |

## Experiment #191

[T=160 C; W=0.5106 g, CAT 051; P=600 psig H2; 700 RPM; 75.89 g acetone charged]

**GC Results**

| Time | Mass Fractions (Wt%) | | | | | | | | | | |
|---|---|---|---|---|---|---|---|---|---|---|---|
| (min) | MO | IMO | DAA | MIBK | TMB | PHO | IPO | "others" | IPA | MIBC | DIBK | H2O |
| 0 | | | | 0.24 | | | | | 0.28 | | | 0.42 |
| 0 | | | | 0.24 | | | | | 0.28 | | | 0.4 |
| 40 | | | | 1.68 | | | | | 0.28 | | | 0.63 |
| 40 | | | | 1.71 | | | | | 0.65 | | | 0.63 |
| 65 | | | | 2.31 | | | | | 0.87 | | | 0.74 |
| 65 | | | | 2.38 | | | | | 0.90 | | | 0.73 |
| 90 | | | | 2.53 | | | | | 0.99 | | | 0.77 |
| 90 | | | | 0.24 | | | | | 0.28 | | | 0.77 |
| 120 | | | | 2.83 | | | | | 1.18 | | | 0.87 |
| 120 | | | | 2.91 | | | | | 1.19 | | | 0.87 |
| 180 | | | | 3.32 | | | | | 1.54 | | | 1.06 |
| 180 | | | | 3.38 | | | | | 1.55 | | | 1.04 |
| 300 | | | | 4.41 | | | | | 2.32 | | | 1.22 |
| 300 | | | | 4.61 | | | | | 2.49 | | | 1.22 |
| 482 | | | | 5.62 | | | | | 3.37 | | | 1.5 |
| 482 | | | | 5.26 | | | | | 3.78 | | | 1.48 |

## Experiment #192

[T=160 C; W=0.4383 g, CAT 051; P=600 psig H2; 700 RPM; 75.23 g acetone charged]

**GC Results**

| Time | Mass Fractions (Wt%) | | | | | | | | | | |
|---|---|---|---|---|---|---|---|---|---|---|---|
| (min) | MO | IMO | DAA | MIBK | TMB | PHO | IPO | "others" | IPA | MIBC | DIBK | H2O |
| 0 | | | | | | | | | | | | 0.14 |
| 0 | | | | | | | | | | | | 0.14 |
| 30 | | | | 2.07 | | | | | | | | 0.33 |
| 30 | | | | 2.09 | | | | | | | | 0.34 |
| 63 | | | | 2.53 | | | | | 0.86 | | | 0.54 |
| 63 | | | | 2.94 | | | | | 0.90 | | | 0.53 |
| 90 | | | | 0.67 | | | | | 0.28 | | | 0.63 |
| 90 | | | | 2.61 | | | | | 0.93 | | | 0.63 |
| 120 | | | | 3.68 | | | | | 1.39 | | | 0.64 |
| 120 | | | | 3.60 | | | | | 1.37 | | | 0.61 |
| 172 | | | | 3.80 | | | | | 1.64 | | | 0.65 |
| 172 | | | | 3.60 | | | | | 1.75 | | | 0.64 |
| 302 | | | | 4.73 | | | | | 2.83 | | | 0.77 |
| 302 | | | | 4.63 | | | | | 2.70 | | | 0.76 |
| 480 | | | | 3.85 | | | | | 3.87 | | | 0.89 |
| 480 | | | | 4.63 | | | | | 4.23 | | | 0.89 |

## Experiment #193

[T=160 C; W=1.00 g, CAT 051; P> 300 psig N2; 700 RPM; 75.8 g acetone charged]

**GC Results**

| Time | Mass Fractions (Wt%) | | | | | | | | | | |
|---|---|---|---|---|---|---|---|---|---|---|---|
| (min) | MO | IMO | DAA | MIBK | TMB | PHO | IPO | "others" | IPA | MIBC | DIBK | H2O |
| 0 | 0.09 | 0.09 | | | | | | | | | | 0.09 |
| 0 | 0.09 | 0.09 | | | | | | | | | | 0.08 |
| 32 | 3.31 | 0.27 | | | | | | | | | | 0.81 |
| 32 | 3.52 | 0.28 | | | | | | | | | | 0.81 |
| 60 | 5.27 | 0.45 | | | | | | | | | | 1.19 |
| 60 | 6.26 | 0.52 | | | | 0.26 | | | | | | 1.19 |
| 90 | 7.26 | 0.65 | | | | 0.30 | | | | | | 1.45 |
| 90 | 6.79 | 0.62 | | | | 0.28 | | | | | | 1.46 |
| 121 | 6.51 | 0.62 | | | | 0.29 | | | | | | 1.59 |
| 121 | 0.09 | 0.09 | | | | 0.02 | | | | | | 1.59 |
| 190 | 7.93 | 0.80 | | | | 0.36 | | | | | | 1.92 |
| 190 | 8.92 | 0.89 | | | | 0.37 | | | | | | 1.93 |
| 342 | 9.46 | 0.98 | | | | 0.44 | | | | | | n/a |
| 342 | 9.78 | 1.02 | | | | 0.43 | | | | | | n/a |
| 480 | 9.54 | 1.00 | | | 0.10 | 0.43 | | | | | | 2.43 |
| 480 | 10.55 | 1.10 | | | 0.11 | 0.50 | | | | | | 2.35 |

## Experiment #195

[T=160 C; W=0.6156 g, CAT 051; P= 600 psig H2; 700 RPM; 77.43 g acetone charged]

**GC Results**

| Time | Mass Fractions (Wt%) | | | | | | | | | | |
|---|---|---|---|---|---|---|---|---|---|---|---|
| (min) | MO | IMO | DAA | MIBK | TMB | PHO | IPO | "others" | IPA | MIBC | DIBK |
| 0 | 0.42 | | | 0.08 | | | | | | | |
| 0 | 0.40 | | | 0.08 | | | | | | | |
| 30 | 2.49 | 0.28 | | 1.99 | | | | | | | |
| 30 | 2.50 | 0.28 | | 1.99 | | | | | | | |
| 61 | 3.52 | 0.39 | | 3.09 | | | | | | | |
| 61 | 3.68 | 0.40 | | 3.21 | | | | | | | |
| 90 | 4.08 | 0.44 | | 4.62 | | | | | | | |
| 90 | 3.99 | 0.43 | | 4.52 | | | | | | | |
| 120 | 4.25 | 0.46 | | 5.93 | | | | | | | |
| 120 | 4.25 | 0.46 | | 5.93 | | | | | | | |
| 180 | 4.24 | 0.46 | | 8.13 | | | | | | | |
| 180 | 4.36 | 0.48 | | 8.39 | | | | | | | |
| 480 | 3.07 | 0.36 | | 13.58 | | | | | 0.68 | | 0.61 |
| 480 | 3.06 | 0.37 | | 13.53 | | | | | 0.67 | | 0.61 |
| 540 | 3.58 | 0.41 | | 14.91 | | | | | 0.50 | | 0.71 |

## Experiment #196

[T=135 C; W=0.4853 g, CAT 054; P= 388 psig H2; 700 RPM; 100 mL acetone charged]

**GC Results**

| Time | Mass Fractions (Wt%) | | | | | | | | | | | |
|---|---|---|---|---|---|---|---|---|---|---|---|---|
| (min) | MO | IMO | DAA | MIBK | TMB | PHO | IPO | "others" | IPA | MIBC | DIBK | H2O |
| 1 | | | | | | | | | | | | 0.11 |
| 1 | | | | | | | | | | | | 0.10 |
| 31 | | | | | | | | | | | | 0.11 |
| 31 | | | | | | | | | | | | 0.11 |
| 60 | | | | 1.24 | | | | | | | | 0.26 |

| | | | | | | | | | | | | |
|---|---|---|---|---|---|---|---|---|---|---|---|---|
| 60 | | | | 0.93 | | | | | | | | 0.26 |
| 90 | | | | 1.53 | | | | | | | | 0.33 |
| 90 | | | | 1.53 | | | | | | | | 0.33 |
| 120 | | | | 2.13 | | | | | | | | 0.43 |
| 120 | | | | 2.12 | | | | | | | | 0.43 |
| 180 | | | | 2.97 | | | | | | | | 0.58 |
| 180 | | | | 2.99 | | | | | | | | 0.57 |
| 300 | | | | 4.19 | | | | | | | | 0.82 |
| 300 | | | | 4.22 | | | | | | | | 0.83 |
| 480 | 0.56 | | | 5.67 | | | | | | | | 1.08 |
| 480 | 0.56 | | | 5.71 | | | | | | | | 1.08 |

## Experiment #197

[T=160 C; W=0.6327 g, CAT 054; P= 600 psig H2; 700 RPM; 76.15 acetone charged]

**GC Results**

| Time | Mass Fractions (Wt%) | | | | | | | "others" | | | | |
|---|---|---|---|---|---|---|---|---|---|---|---|---|
| (min) | MO | IMO | DAA | MIBK | TMB | PHO | IPO | 1.9 min | IPA | MIBC | DIBK | H2O |
| 0.5 | | | | 0.28 | | | | | | | | 0.28 |
| 0.5 | | | | 0.28 | | | | | | | | 0.27 |
| 32.5 | | | | 3.59 | | | | | | | | 0.65 |
| 32.5 | | | | 3.73 | | | | | | | | 0.66 |
| 60 | | | | 5.78 | | | | | | | | 0.99 |
| 60 | | | | 5.83 | | | | | | | | 0.99 |
| 90 | | | | 8.21 | | | | | | | | 1.33 |
| 90 | | | | 7.91 | | | | | | | | 1.35 |
| 120 | | | | 8.53 | | | | | | | | 1.54 |
| 120 | | | | 8.72 | | | | | | | | 1.54 |
| 180 | | | | 12.10 | | | | 0.23 | 0.60 | | | 2.03 |
| 180 | | | | 12.23 | | | | 0.23 | 0.60 | | | 2.02 |
| 335 | | | | 17.11 | | | | 0.28 | 0.94 | | 0.64 | 2.9 |
| 335 | | | | 16.67 | | | | 0.27 | 0.90 | | 0.63 | 2.88 |
| 480 | | | | 17.95 | | | | 0.2696 | 1.07 | | 0.68 | 3.27 |
| 480 | | | | 17.78 | | | | 0.26 | 1.05 | | 0.67 | 3.27 |

## Experiment #199

[T=155 C; W=0.4858 g, CAT 054; P= 500 psia H2; $P_{atm}$ = 102.7 kPa; 700 RPM; 76.31 acetone charged]

**GC Results**

| Time | Mass Fractions (Wt%) | | | | | | | "others" | | | | |
|---|---|---|---|---|---|---|---|---|---|---|---|---|
| (min) | MO | IMO | DAA | MIBK | TMB | PHO | IPO | 1.9 min | IPA | MIBC | DIBK | H2O |
| 0 | | | | | | | | | | | | 0.12 |
| 0 | | | | | | | | | | | | 0.11 |
| 33 | | | | 2.47 | | | | | | | | 0.45 |
| 33 | | | | 2.73 | | | | | | | | 0.45 |
| 60 | | | | 4.12 | | | | | | | | 0.74 |
| 60 | | | | 3.98 | | | | | | | | 0.73 |
| 90 | | | | 5.23 | | | | | | | | 0.93 |
| 90 | | | | 5.12 | | | | | | | | 0.94 |
| 120 | | | | 6.59 | | | | | | | | 1.16 |

| | | | | | | | | | | | | |
|---|---|---|---|---|---|---|---|---|---|---|---|---|
| 120 | | | | 6.27 | | | | | | | | 1.17 |
| 180 | | | | 9.31 | | | | | | | | 1.71 |
| 180 | | | | 9.08 | | | | | | | | 1.69 |
| 312 | | | | 11.84 | | | | | | | | 2.09 |
| 312 | | | | 11.27 | | | | | | | | 2.11 |
| 480 | 0.73 | | | 14.29 | | | | | | | 0.44 | 2.32 |
| 480 | 0.67 | | | 12.44 | | | | | | | | 2.29 |

## Experiment #200

[T=183 C; W=0.5050 g, CAT 054; P= 500 psia H2; $P_{atm}$ = 101.9 kPa; 700 RPM; 75.28 acetone charged]

**GC Results**

| Time | Mass Fractions (Wt%) | | | | | | | "others" | | | | |
|---|---|---|---|---|---|---|---|---|---|---|---|---|
| (min) | MO | IMO | DAA | MIBK | TMB | PHO | IPO | 1.9 min | IPA | MIBC | DIBK | H2O |
| 0 | | | | 0.33 | | | | | | | | 0.26 |
| 0 | | | | 0.33 | | | | | | | | 0.25 |
| 30 | 0.69 | | | 6.89 | | | | | | | | 1.42 |
| 30 | | | | 6.74 | | | | 0.19 | | | | |
| 61 | 0.66 | | | 10.48 | | | | 0.28 | | | | 2.18 |
| 61 | 0.74 | | | 12.02 | | | | 0.29 | | | | 2.18 |
| 90 | 0.69 | | | 14.42 | | | | 0.34 | | | 0.6 | 2.74 |
| 90 | 0.68 | | | 14.32 | | | | 0.35 | | | 0.6 | 2.78 |
| 120 | 0.63 | | | 15.56 | | | | 0.37 | | | 0.6 | 3.22 |
| 120 | 0.65 | | | 16.64 | | | | 0.39 | | | 0.7 | 3.22 |
| 180 | | | | 18.45 | | | | 0.41 | 0.58 | | 0.80 | 3.99 |
| 180 | | | | 17.27 | | | | 0.44 | 0.60 | | 0.69 | 3.97 |
| 301 | 0.75 | | | 20.60 | | | | 0.27 | 0.69 | | 0.90 | 4.32 |
| 301 | 0.68 | | | 17.83 | | | | 0.24 | 0.61 | | 0.78 | 4.35 |
| 480 | 1.58 | | | 22.61 | 0.35 | | | | 0.74 | | 0.98 | 4.19 |
| 480 | 1.57 | | | 22.45 | 0.35 | | | | 0.74 | | 0.98 | 4.03 |

## Experiment #201

[T=135 C; W=0.5050 g, CAT 054; P= 700 psia H2; $P_{atm}$ = 100.8 kPa; 700 RPM; 76.33 acetone charged]

**GC Results**

| Time | Mass Fractions (Wt%) | | | | | | | "others" | | | | |
|---|---|---|---|---|---|---|---|---|---|---|---|---|
| (min) | MO | IMO | DAA | MIBK | TMB | PHO | IPO | 1.9 min | IPA | MIBC | DIBK | H2O |
| 0 | | | | | | | | | | | | 0.1 |
| 0 | | | | | | | | | | | | 0.10 |
| 30 | 0.71 | | | 1.01 | | | | | | | | 0.25 |
| 30 | 0.76 | | | 1.08 | | | | | | | | 0.25 |
| 60 | 0.79 | | | 1.68 | | | | | | | | 0.39 |
| 60 | 0.81 | | | 1.73 | | | | | | | | 0.39 |
| 90 | 1.19 | | | 2.33 | | | | | | | | 0.52 |
| 90 | 1.08 | | | 2.15 | | | | | | | | 0.52 |
| 120 | 1.24 | | | 2.47 | | | | | | | | 1.02 |
| 120 | | | | 0.97 | | | | | | | | 1.02 |
| 180 | 2.05 | | | 4.10 | | | | | | | | 1.93 |
| 180 | | | | | | | | | | | | 1.94 |

Experiment terminated for maintenance; reactor leaking.

## Experiment #202

[T=183 C; W=0.4700 g, CAT 054; P= 500 psia H2; $P_{atm}$ = 102.1 kPa; 700 RPM; 77.11 acetone charged]

**GC Results**

| Time | Mass Fractions (Wt%) | | | | | | | "others" | | | | |
|---|---|---|---|---|---|---|---|---|---|---|---|---|
| (min) | MO | IMO | DAA | MIBK | TMB | PHO | IPO | 1.9 min | IPA | MIBC | DIBK | H2O |
| 0 | 0.75 | | | 0.70 | | | | | | | | 0.21 |
| 0 | 0.85 | | | 0.77 | | | | | | | | 0.22 |
| 30 | 1.68 | | | 2.50 | | | | | | | | 1.02 |
| 30 | 1.67 | | | 2.48 | | | | | | | | 1.01 |
| 61 | 2.69 | 0.42 | | 4.90 | | | | | | | | 1.39 |
| 61 | 2.66 | 0.42 | | 4.87 | | | | | | | | 1.39 |
| 90 | 2.91 | 0.46 | | 5.71 | | | | | | | | 1.72 |
| 90 | 3.08 | 0.48 | | 6.04 | | | | | | | | 1.73 |
| 120 | 2.79 | 0.47 | | 6.68 | | | | 0.20 | | | | 2.07 |
| 120 | 3.17 | 0.51 | | 7.42 | | | | 0.20 | | | | 2.07 |
| 180 | 2.88 | 0.48 | | 9.18 | | | | 0.24 | | | 0.32 | 2.56 |
| 180 | 2.87 | 0.47 | | 9.06 | | | | 0.23 | | | 0.32 | 2.58 |
| 300 | 1.03 | | | 8.23 | | | | 0.26 | | | | 4.79 |
| 300 | 1.06 | | | 8.60 | | | | 0.28 | | | | 4.82 |
| 480 | 0.73 | | | 25.39 | 0.39 | | | 0.1985 | 1.28 | | 1.24 | 5.88 |
| 480 | 0.72 | | | 24.75 | 0.38 | | | 0.20 | 1.25 | | 1.21 | 5.83 |

## Experiment #203

[T=135 C; W=0.4692 g, CAT 054; P= 700 psia H2; $P_{atm}$ = 100.7 kPa; 700 RPM; 75.45 acetone charged]

**GC Results**

| Time | Mass Fractions (Wt%) | | | | | | | "others" | | | | |
|---|---|---|---|---|---|---|---|---|---|---|---|---|
| (min) | MO | IMO | DAA | MIBK | TMB | PHO | IPO | 1.9 min | IPA | MIBC | DIBK | H2O |
| 1 | | | | | | | | | | | | 0.18 |
| 1 | | | | | | | | | | | | 0.18 |
| 31 | | | | 0.72 | | | | | | | | 0.24 |
| 31 | | | | 0.72 | | | | | | | | 0.24 |
| 60 | | | | 1.54 | | | | | | | | 0.35 |
| 60 | | | | 1.47 | | | | | | | | 0.35 |
| 90 | | | | 2.05 | | | | | | | | 0.45 |
| 90 | | | | 2.01 | | | | | | | | 0.45 |
| 120 | | | | 2.58 | | | | | | | | 0.53 |
| 120 | | | | 2.57 | | | | | | | | 0.54 |
| 172 | | | | 3.57 | | | | | | | | 0.72 |
| 172 | | | | 3.68 | | | | | | | | 0.74 |
| 310 | | | | 5.66 | | | | | | | | 1.14 |
| 310 | | | | 5.64 | | | | | | | | 1.17 |
| 480 | 0.88 | | | 7.15 | | | | | | | | 1.34 |
| 480 | problem with organic analysis 8b (480 min repeated) | | | | | | | | | | | 1.35 |

## Experiment #204

[T=135 C; W=0.4842 g, CAT 054; P= 300 psia H2; $P_{atm}$ = 101.0 kPa; 700 RPM; 76.32 acetone charged]

**GC Results**

| Time | Mass Fractions (Wt%) | | | | | | | "others" | | | | |
|---|---|---|---|---|---|---|---|---|---|---|---|---|
| (min) | MO | IMO | DAA | MIBK | TMB | PHO | IPO | 1.9 min | IPA | MIBC | DIBK | H2O |
| 1 | | | | | | | | | | | | 0.15 |
| 1 | | | | | | | | | | | | 0.16 |
| 31 | | | | 0.92 | | | | | | | | 0.24 |
| 31 | | | | 0.91 | | | | | | | | 0.24 |

| | | | | | | | | | | | | |
|---|---|---|---|---|---|---|---|---|---|---|---|---|
| 60 | 0.63 | | | 2.49 | | | | | | | | n/a |
| 60 | 0.63 | | | 2.46 | | | | | | | | 0.51 |
| 90 | | | | 2.26 | | | | | | | | 0.46 |
| 90 | | | | 2.18 | | | | | | | | 0.46 |
| 120 | | | | 3.01 | | | | | | | | 0.62 |
| 120 | 0.58 | | | 3.02 | | | | | | | | 0.62 |
| 192 | 0.62 | | | 5.65 | | | | | | | | 1.11 |
| 192 | 0.62 | | | 5.79 | | | | | | | | n/a |
| 380 | 0.58 | | | 9.39 | | | | | | | | 1.78 |
| 380 | 0.58 | | | 9.18 | | | | | | | | 1.78 |
| 480 | 0.63 | | | 8.99 | | | | | | | | 1.84 |
| 480 | 0.66 | | | 9.78 | | | | | | | 0.42 | 1.85 |

## Experiment #205

[T=175 C; W=0.4688 g, CAT 054; P= 700 psia H2; $P_{atm}$ = 101.9 kPa; 700 RPM; 75.69 acetone charged]

**GC Results**

| Time | Mass Fractions (Wt%) | | | | | | | "others" | | | | |
|---|---|---|---|---|---|---|---|---|---|---|---|---|
| (min) | MO | IMO | DAA | MIBK | TMB | PHO | IPO | 1.9 min | IPA | MIBC | DIBK | H2O |
| 1 | 0.78 | | | 0.91 | | | | | | | | 0.44 |
| 1 | 0.76 | | | 0.91 | | | | | | | | 0.43 |
| 30 | 0.82 | | | 4.01 | | | | | | | | 0.9 |
| 30 | 0.84 | | | 4.12 | | | | | | | | 0.9 |
| 60 | 1.02 | | | 8.03 | | | | | | | | 1.59 |
| 60 | 1.03 | | | 8.14 | | | | | | | | 1.57 |
| 90 | 0.95 | | | 9.97 | | | | | | | | 1.99 |
| 90 | 0.94 | | | 9.70 | | | | | | | | 2 |
| 120 | 0.94 | | | 11.25 | | | | 0.19 | | | 0.4 | 2.36 |
| 120 | 0.95 | | | 11.27 | | | | | | | 0.4 | 2.35 |
| 180 | 0.86 | | | 13.75 | | | | 0.23 | 0.55 | | 0.46 | 2.85 |
| 180 | 0.85 | | | 13.83 | | | | 0.23 | 0.56 | | 0.46 | 2.82 |
| 300 | 0.85 | | | 16.99 | | | | 0.21 | 0.85 | | 0.60 | 3.7 |
| 300 | 0.85 | | | 17.02 | | | | 0.22 | 0.85 | | 0.60 | 3.7 |
| 480 | 1.92 | 0.43 | | 20.33 | | | | | 1.24 | | 0.70 | 6.14 |
| 480 | 1.91 | 0.43 | | 20.19 | | | | | 1.23 | | 0.70 | 6.05 |

## Experiment #206

[T=155 C; W=0.4642 g, CAT 054; P= 500 psia H2; $P_{atm}$ = 101.1 kPa; 700 RPM; 76.09 acetone charged]

**GC Results**

| Time | Mass Fractions (Wt%) | | | | | | | "others" | | | | |
|---|---|---|---|---|---|---|---|---|---|---|---|---|
| (min) | MO | IMO | DAA | MIBK | TMB | PHO | IPO | 1.9 min | IPA | MIBC | DIBK | H2O |
| 1 | | | | | | | | | | | | 0.15 |
| 1 | | | | | | | | | | | | 0.14 |
| 30 | 0.64 | | | 1.46 | | | | | | | | 0.4 |
| 30 | 0.63 | | | 1.44 | | | | | | | | 0.4 |
| 60 | 1.05 | | | 2.86 | | | | | | | | 0.72 |
| 60 | 1.03 | | | 2.81 | | | | | | | | 0.71 |
| 91 | 1.48 | | | 4.21 | | | | | | | | 1.01 |
| 91 | 0.24 | | | | | | | | | | | 1.02 |
| 120 | 1.53 | | | 4.92 | | | | | | | | 1.19 |
| 120 | 1.50 | | | 4.80 | | | | | | | | 1.19 |
| 180 | 1.67 | | | 6.83 | | | | | | | | 1.63 |

| | | | | | | | | | | | | |
|---|---|---|---|---|---|---|---|---|---|---|---|---|
| 180 | 1.71 | | | 7.04 | | | | | | | | 1.65 |
| 300 | 1.97 | | | 9.71 | | | | | | | 0.35 | 2.26 |
| 300 | 1.96 | | | 9.66 | | | | | | | 0.35 | 2.28 |
| 480 | 2.20 | 0.42 | | 10.51 | | | | | | | 0.36 | 4.35 |
| 480 | n/a | n/a | n/a | n/a | n/a | n/a | n/a | n/a | n/a | n/a | n/a | 4.33 |

## Experiment #207

[T=127 C; W=0.4848 g, CAT 054; P= 500 psia H2; $P_{atm}$ = 101.7 kPa; 700 RPM; 75.68 acetone charged]

**GC Results**

| Time | Mass Fractions (Wt%) | | | | | | | "others" | | | | |
|---|---|---|---|---|---|---|---|---|---|---|---|---|
| (min) | MO | IMO | DAA | MIBK | TMB | PHO | IPO | 1.9 min | IPA | MIBC | DIBK | H2O |
| 1 | | | | | | | | | | | | 0.08 |
| 1 | | | | | | | | | | | | 0.07 |
| 30 | | | | | | | | | | | | 0.1 |
| 30 | | | | | | | | | | | | 0.1 |
| 60 | | | | 0.92 | | | | | | | | 0.15 |
| 60 | | | | 0.89 | | | | | | | | 0.15 |
| 90 | | | | 1.31 | | | | | | | | 0.24 |
| 90 | | | | 1.36 | | | | | | | | 0.23 |
| 120 | | | | 1.53 | | | | | | | | 0.29 |
| 120 | | | | 1.58 | | | | | | | | 0.29 |
| 180 | | | | 2.46 | | | | | | | | 0.48 |
| 180 | 0.47 | | | 2.73 | | | | | | | | 0.47 |
| 383 | 0.73 | | | 4.97 | | | | | | | | 0.94 |
| 383 | 0.73 | | | 4.99 | | | | | | | | 0.94 |
| 480 | 1.05 | | | 5.74 | | | | | | | | 1.44 |
| 480 | 1.04 | | | 5.65 | | | | | | | | 1.44 |

## Experiment #208

[T=155 C; W=0.4927 g, CAT 054; P= 217 psia H2; $P_{atm}$ = 100.8 kPa; 700 RPM; 75.21 acetone charged]
* used recycled catalyst “R208”

**GC Results**

| Time | Mass Fractions (Wt%) | | | | | | | "others" | | | | |
|---|---|---|---|---|---|---|---|---|---|---|---|---|
| (min) | MO | IMO | DAA | MIBK | TMB | PHO | IPO | 1.9 min | IPA | MIBC | DIBK | H2O |
| 1 | | | | | | | | | | | | 0.16 |
| 1 | | | | | | | | | | | | 0.16 |
| 34 | 0.76 | | | | | | | | | | | 0.27 |
| 34 | 0.78 | | | | | | | | | | | 0.27 |
| 60 | 2.12 | | | 1.39 | | | | | | | | 0.59 |
| 60 | 2.00 | | | 1.32 | | | | | | | | 0.59 |
| 90 | 2.26 | | | 1.71 | | | | | | | | 0.85 |
| 90 | 2.26 | | | 1.70 | | | | | | | | 0.84 |
| 120 | 3.00 | 0.40 | | 2.51 | | | | | | | | 1.1 |
| 120 | 2.87 | 0.39 | | 2.42 | | | | | | | | 1.09 |
| 180 | 3.50 | 0.45 | | 3.33 | | | | | | | | 1.39 |
| 180 | 3.49 | 0.45 | | 3.33 | | | | | | | | 1.39 |
| 301 | 3.94 | 0.50 | | 4.53 | | | | | | | | 1.95 |
| 301 | 3.99 | 0.50 | | 4.54 | | | | | | | | 1.98 |
| 480 | 4.40 | 0.55 | | 5.53 | | | | | | | | 2.38 |
| 480 | 4.39 | 0.55 | | 5.51 | | | | | | | | 2.35 |

## Experiment #209

[T=155 C; W=0.4862 g, CAT 054; P= 783 psia H2; $P_{atm}$ = 101.8 kPa; 700 RPM; 75.48 acetone charged]
* used recycled catalyst “R208”

**GC Results**

| Time | Mass Fractions (Wt%) | | | | | | | "others" | | | | |
|---|---|---|---|---|---|---|---|---|---|---|---|---|
| (min) | MO | IMO | DAA | MIBK | TMB | PHO | IPO | 1.9 min | IPA | MIBC | DIBK | H2O |
| 1 | | | | | | | | | | | | 0.16 |
| 1 | | | | | | | | | | | | 0.15 |
| 33 | 0.79 | | | 1.47 | | | | | | | | 0.43 |
| 33 | 0.82 | | | 1.51 | | | | | | | | 0.43 |
| 60 | 0.78 | | | 2.31 | | | | | | | | 0.62 |
| 60 | 0.78 | | | 2.31 | | | | | | | | 0.61 |
| 94 | 0.92 | | | 3.92 | | | | | | | | 0.93 |
| 94 | 0.94 | | | 4.01 | | | | | | | | 0.93 |
| 120 | 0.93 | | | 4.44 | | | | | | | | 0.97 |
| 120 | 0.92 | | | 4.41 | | | | | | | | 0.97 |
| 180 | 1.08 | | | 6.65 | | | | | | | | 1.48 |
| 180 | 0.96 | | | 5.96 | | | | | | | | 1.48 |
| 330 | 1.51 | | | 9.14 | | | | | 0.67 | | | 6.65 |
| 330 | 0.73 | | | 3.63 | | | | | | | | 6.67 |

## Experiment #210

[T=175 C; W=0.4723 g, CAT 054; P= 300 psia H2; $P_{atm}$ = 101.2 kPa; 700 RPM; 75.75 acetone charged]

**GC Results**

| Time | Mass Fractions (Wt%) | | | | | | | "others" | | | | |
|---|---|---|---|---|---|---|---|---|---|---|---|---|
| (min) | MO | IMO | DAA | MIBK | TMB | PHO | IPO | 1.9 min | IPA | MIBC | DIBK | H2O |
| 1 | 0.59 | | | | | | | | | | | 0.24 |
| 1 | 0.58 | | | | | | | | | | | 0.24 |
| 31 | 1.93 | | | 2.07 | | | | | | | | 0.78 |
| 31 | 2.04 | | | 2.19 | | | | | | | | 0.78 |
| 61 | 2.22 | 0.46 | | 3.09 | | | | | | | | 1.18 |
| 61 | 2.21 | 0.46 | | 3.06 | | | | | | | | 1.16 |
| 90 | 2.84 | 0.51 | | 5.60 | | | | | | | | 1.68 |
| 90 | 2.88 | 0.52 | | 5.72 | | | | | | | | 1.68 |
| 120 | 3.35 | 0.57 | | 6.57 | | | | | | | | 1.99 |
| 120 | 3.28 | 0.56 | | 6.38 | | | | | | | | 1.98 |
| 180 | 4.41 | 0.68 | | 7.51 | | | | 0.34 | | | 0.31 | 2.24 |
| 180 | 4.56 | 0.70 | | 7.77 | | | | 0.35 | | | 0.32 | 2.26 |
| 300 | 5.89 | 0.85 | | 8.41 | | | | 0.42 | | | 0.35 | 2.73 |
| 300 | 5.94 | 0.86 | | 8.54 | | | | 0.42 | | | 0.35 | 2.71 |
| 480 | 7.46 | 1.05 | | 8.91 | | 0.31 | | 0.4905 | | | 0.37 | 2.99 |
| 480 | 7.69 | 1.07 | | 9.19 | | 0.31 | | 0.50 | | | 0.38 | 2.95 |

## Experiment #211

[T=183 C; W=0.4865 g, CAT 054; P= 500 psia H2; $P_{atm}$ = 102.6 kPa; 700 RPM; 68.29 acetone charged]

**GC Results**

| Time | Mass Fractions (Wt%) | | | | | | | "others" | | | | |
|---|---|---|---|---|---|---|---|---|---|---|---|---|
| (min) | MO | IMO | DAA | MIBK | TMB | PHO | IPO | 1.9 min | IPA | MIBC | DIBK | H2O |
| 1 | 0.72 | | | 1.39 | | | | | | | | 0.47 |
| 1 | 0.75 | | | 1.46 | | | | | | | | 0.47 |
| 30 | 0.74 | | | 6.93 | | | | | | | | 1.51 |

| | | | | | | | | | | | | |
|---|---|---|---|---|---|---|---|---|---|---|---|---|
| 30 | 0.74 | | | 6.99 | | | | | | | | 1.52 |
| 60 | 0.75 | | | 10.30 | | | | 0.24 | | | 0.3 | 2.13 |
| 60 | 0.75 | | | 10.34 | | | | 0.23 | | | 0.3 | 2.14 |
| 90 | 0.72 | | | 12.08 | | | | 0.29 | | | 0.4 | 2.82 |
| 90 | 0.70 | | | 11.70 | | | | 0.29 | | | 0.4 | 2.77 |
| 120 | 0.78 | | | 14.00 | | | | 0.31 | | | 0.5 | 3.13 |
| 120 | 0.77 | | | 13.82 | | | | 0.30 | | | 0.4 | 3.14 |
| 180 | 0.76 | | | 16.02 | | | | 0.36 | 0.52 | | 0.54 | 3.82 |
| 180 | 0.74 | | | 15.42 | | | | 0.34 | 0.49 | | 0.53 | 3.79 |
| 300 | 1.03 | | | 17.19 | | | | 0.34 | 0.67 | | 0.58 | 4.78 |
| 300 | 1.04 | | | 17.21 | | | | 0.32 | 0.65 | | 0.60 | 4.84 |
| 480 | 1.52 | 0.33 | | 18.71 | | | | 0.2301 | 1.02 | | 0.62 | 6.96 |
| 480 | 1.50 | 0.32 | | 18.35 | | | | 0.23 | 1.06 | | 0.61 | 7.01 |

## Experiment #212

[T=160 C; W=0.9942 g, CAT 055; P= 600 psig N2; 700 RPM; 75.5 acetone charged]

**GC Results**

| Time | Mass Fractions (Wt%) | | | | | | | "others" | | | | |
|---|---|---|---|---|---|---|---|---|---|---|---|---|
| (min) | MO | IMO | DAA | MIBK | TMB | PHO | IPO | 1.9 min | IPA | MIBC | DIBK | H2O |
| 1 | 0.17 | | | | | | | | | | | 0.4 |
| 1 | 0.17 | | | | | | | | | | | 0.38 |
| 30 | 3.38 | 0.37 | | | | | | | | | | 0.59 |
| 30 | 3.29 | 0.37 | | | | | | | | | | 0.6 |
| 60 | 4.30 | 0.47 | | | | 0.21 | | | | | | 0.78 |
| 60 | 4.38 | 0.47 | | | | 0.21 | | | | | | 0.78 |
| 91 | 5.15 | 0.56 | | | | 0.24 | | | | | | 0.91 |
| 91 | 5.12 | 0.56 | | | | 0.24 | | | | | | 0.92 |
| 120 | 5.49 | 0.60 | | | | 0.25 | | | | | | 0.97 |
| 120 | 5.30 | 0.58 | | | | 0.24 | | | | | | 0.98 |
| 180 | 6.11 | 0.68 | | | | 0.25 | | | | | | 1.13 |
| 180 | 5.89 | 0.66 | | | | 0.26 | | | | | | 1.14 |
| 300 | 6.64 | 0.76 | | | | 0.28 | | | | | | 1.32 |
| 300 | 6.66 | 0.76 | | | | 0.28 | | | | | | 1.34 |
| 480 | 7.15 | 0.82 | | | | 0.31 | | | | | | 1.51 |
| 480 | 7.01 | 0.81 | | | | 0.30 | | | | | | 1.52 |

## Experiment #213

[T=160 C; W=0.8208 g, CAT 055; P= 600 psig N2; 700 RPM; 75.05 acetone charged]
CAT 055 Rings ground to powder to determine effectiveness factor

**GC Results**

| Time | Mass Fractions (Wt%) | | | | | | | "others" | | | | |
|---|---|---|---|---|---|---|---|---|---|---|---|---|
| (min) | MO | IMO | DAA | MIBK | TMB | PHO | IPO | 1.9 min | IPA | MIBC | DIBK | H2O |
| 1 | 0.69 | | | | | | | | | | | 0.28 |
| 1 | 0.75 | | | | | | | | | | | 0.27 |
| 30 | 2.71 | 0.13 | | | | | | | | | | 0.59 |
| 30 | 2.56 | 0.13 | | | | | | | | | | 0.59 |
| 60 | 3.46 | 0.13 | | | | | | | | | | 0.73 |
| 60 | 3.33 | 0.13 | | | | | | | | | | 0.72 |
| 90 | 4.14 | 0.36 | | | | | | | | | | 0.8 |
| 90 | 3.70 | 0.34 | | | | | | | | | | 0.8 |
| 120 | 3.99 | 0.38 | | | | | | | | | | 0.85 |
| 120 | 3.94 | 0.37 | | | | | | | | | | 0.86 |

| | | | | | | | | | | | | |
|---|---|---|---|---|---|---|---|---|---|---|---|---|
| 180 | 4.47 | 0.42 | | | | | | | | | | 0.9 |
| 180 | 4.37 | 0.42 | | | | | | | | | | 0.89 |
| 300 | 4.66 | 0.46 | | | | | | | | | | 0.95 |
| 300 | 4.68 | 0.47 | | | | | | | | | | 0.95 |
| 483 | 4.80 | 0.50 | | | | | | | | | | 1.04 |
| 483 | 0.13 | 0.13 | | | | | | | | | | 1.02 |

## Experiment #215

[T=160 C; W=1.0704 g, CAT 055; P= 600 psig N2; 100 RPM; 75.07acetone charged]

**GC Results**

| Time | Mass Fractions (Wt%) | | | | | | | "others" | | | | |
|---|---|---|---|---|---|---|---|---|---|---|---|---|
| (min) | MO | IMO | DAA | MIBK | TMB | PHO | IPO | 1.9 min | IPA | MIBC | DIBK | H2O |
| 1 | 0.40 | | | | | | | | | | | 0.21 |
| 1 | 0.39 | | | | | | | | | | | 0.20 |
| 30 | 0.77 | 0.10 | | | | | | | | | | 0.27 |
| 30 | 0.77 | 0.10 | | | | | | | | | | 0.28 |
| 64 | 1.90 | 0.10 | | | | | | | | | | 0.49 |
| 64 | 1.98 | 0.10 | | | | | | | | | | 0.49 |
| 90 | 2.78 | 0.10 | | | | | | | | | | 0.62 |
| 90 | 2.61 | 0.10 | | | | | | | | | | 0.61 |
| 120 | 2.90 | 0.28 | | | | | | | | | | 0.66 |
| 120 | 3.11 | 0.30 | | | | | | | | | | 0.66 |
| 248 | 3.73 | 0.37 | | | | | | | | | | 0.8 |
| 248 | 3.77 | 0.37 | | | | | | | | | | 0.81 |
| 301 | 3.50 | 0.36 | | | | | | | | | | 0.84 |
| 301 | 3.88 | 0.39 | | | | | | | | | | 0.84 |
| 482 | 4.31 | 0.44 | | | | | | | | | | 0.94 |
| 482 | 4.24 | 0.44 | | | | | | | | | | 0.96 |

## Experiment #216

[T=160 C; W=0.5845 g, CAT 056; P= 600 psig N2; 100 RPM; 74.57 acetone charged]

**GC Results**

| Time | Mass Fractions (Wt%) | | | | | | | "others" | | | | |
|---|---|---|---|---|---|---|---|---|---|---|---|---|
| (min) | MO | IMO | DAA | MIBK | TMB | PHO | IPO | 1.9 min | IPA | MIBC | DIBK | H2O |
| 1 | 0.18 | | | | | | | | | | | 0.19 |
| 1 | 0.18 | | | | | | | | | | | 0.18 |
| 37 | 0.71 | | | | | | | | | | | 0.26 |
| 37 | 0.72 | | | | | | | | | | | 0.26 |
| 60 | 1.06 | | | | | | | | | | | 0.32 |
| 60 | 1.09 | | | | | | | | | | | 0.32 |
| 92 | 1.18 | | | | | | | | | | | 0.35 |
| 92 | 0.65 | | | | | | | | | | | 0.34 |
| 120 | 1.37 | | | | | | | | | | | 0.4 |
| 120 | 1.40 | | | | | | | | | | | 0.4 |
| 180 | 1.43 | | | | | | | | | | | 0.4 |
| 180 | 1.43 | | | | | | | | | | | 0.4 |
| 300 | 1.59 | | | | | | | | | | | 0.43 |
| 300 | 1.56 | | | | | | | | | | | 0.43 |
| 480 | 1.78 | | | | | | | | | | | 0.47 |
| 480 | 1.82 | | | | | | | | | | | 0.48 |

## Experiment #217

[T=160 C; W=1.0149 g, CAT 057; P= 600 psig N2; 100 RPM; 75.51 acetone charged]

**GC Results**

| Time | Mass Fractions (Wt%) | | | | | | | "others" | | | | |
|---|---|---|---|---|---|---|---|---|---|---|---|---|
| (min) | MO | IMO | DAA | MIBK | TMB | PHO | IPO | 1.9 min | IPA | MIBC | DIBK | H2O |
| 1 | 0.17 | | | | | | | | | | | 0.15 |
| 1 | 0.18 | | | | | | | | | | | 0.15 |
| 30 | 0.80 | | | | | | | | | | | 0.35 |
| 30 | | | | | | | | | | | | 0.37 |
| 61 | 3.29 | 0.12 | | | | 0.31 | | | | | | 0.86 |
| 61 | 3.27 | 0.12 | | | | 0.31 | | | | | | 0.87 |
| 90 | 4.48 | 0.23 | | | | 0.35 | | | | | | 1.15 |
| 90 | 4.37 | 0.22 | | | | 0.34 | | | | | | 1.14 |
| 120 | 6.06 | 0.38 | | | | 0.40 | | | | | | 1.38 |
| 120 | 5.58 | 0.34 | | | | 0.39 | | | | | | 1.38 |
| 180 | 6.49 | 0.43 | | | | 0.42 | | | | | | 1.58 |
| 180 | 6.53 | 0.43 | | | | 0.42 | | | | | | 1.58 |
| 250 | 7.40 | 0.54 | | | | 0.45 | | | | | | 1.83 |
| 250 | 7.31 | 0.53 | | | | 0.44 | | | | | | 1.86 |
| 480 | 10.10 | 0.83 | | | 0.14 | 0.53 | | | | | | 2.38 |
| 480 | 10.06 | 0.83 | | | 0.14 | 0.53 | | | | | | 2.38 |

## Experiment #219

[T=160 C; W=0.3758 g, CAT 060; P= 600 psig H2; 100 RPM; 68.14 acetone charged]

**GC Results**

| Time | Mass Fractions (Wt%) | | | | | | | "others" | | | | |
|---|---|---|---|---|---|---|---|---|---|---|---|---|
| (min) | MO | IMO | DAA | MIBK | TMB | PHO | IPO | 1.9 min | IPA | MIBC | DIBK | H2O |
| 1 | | | | | | | | | | | | 0.25 |
| 1 | | | | | | | | | | | | 0.26 |
| 30 | | | | 0.48 | | | | | | | | 0.23 |
| 30 | | | | 0.52 | | | | | | | | 0.23 |
| 60 | | | | 1.78 | | | | | | | | 0.44 |
| 60 | | | | 1.74 | | | | | | | | 0.44 |
| 92 | | | | 2.43 | | | | | | | | 0.57 |
| 92 | | | | 2.57 | | | | | | | | 0.57 |
| 120 | | | | 3.42 | | | | | | | | 0.72 |
| 120 | | | | 3.50 | | | | | | | | 0.73 |
| 180 | | | | 4.69 | | | | | 0.46 | | | 0.95 |
| 180 | | | | 4.60 | | | | | 0.45 | | | 0.94 |
| 300 | | | | 7.22 | | | | | 0.80 | | 0.27 | 1.39 |
| 300 | | | | 7.98 | | | | | 0.88 | | 0.29 | 1.38 |
| 480 | | | | 9.56 | | | | | 1.12 | | 0.35 | 1.86 |
| 480 | n/a | n/a | n/a | n/a | n/a | n/a | n/a | n/a | n/a | n/a | n/a | 1.83 |

## Experiment #221

[T=160 C; W=0.7040 g, CAT 067; P= 600 psig; 614.7 psia; H2; 100 RPM; 74.98 acetone charged]

**GC Results**

| Time | Mass Fractions (Wt%) | | | | | | | "others" | | | | |
|---|---|---|---|---|---|---|---|---|---|---|---|---|
| (min) | MO | IMO | DAA | MIBK | TMB | PHO | IPO | 1.9 min | IPA | MIBC | DIBK | H2O |
| 1 | | | | | | | | | | | | n/a |
| 1 | | | | | | | | | | | | n/a |

| | | | |
|---|---|---|---|
| 30 | | | n/a |
| 30 | 1.11 | | n/a |
| 60 | 2.23 | | n/a |
| 60 | 2.30 | | n/a |
| 96 | 3.42 | 0.55 | n/a |
| 96 | 3.02 | 0.46 | n/a |
| 120 | 4.34 | 0.72 | n/a |
| 120 | 4.36 | 0.72 | n/a |

did not do GC/TCD analysis

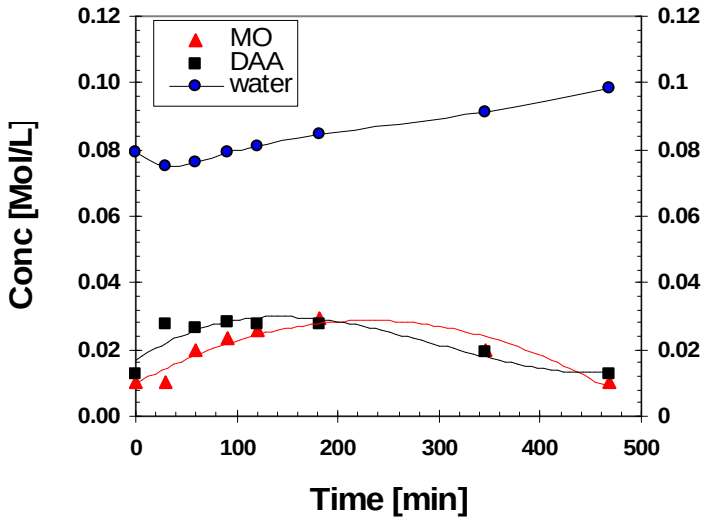


**Figure C2-1** Concentration versus time profile for Experiment #136 using a 12.9 wt% $Nb_2O_5$/MgO catalyst *The magnesia catalyst rapidly deactivated. The reverse aldol condensation reaction appears to occur after a relatively low acetone conversion. In experiment 137, no product was detected after 8 hours of operation using a 6.2 wt%* $Nb_2O_5$*/MgO catalyst. Evidently, the strongly basic support is not suitable for this application.*

# Appendix D
## Supplementary Data: TPD & DRIFT Spectroscopy Data

### D1. TPD Calibration

The calibration procedure consisted of 10 consecutive injections of 524.0 μL pulses of anhydrous ammonia through the analytical vent of the TPD instrument. The number of moles (n) of ammonia was calculated from the ideal gas law at the temperature in the sample loop measured by the instrument and assuming 1 atm pressure as advised by Altamira instruments. The pressure in the sample loop is not measured by the instrument. The measurement of the average area showed good repeatability with the 95% confidence bounds expressed as a percentage being ± 2.79%.

The ratio of the average area divided by the number of moles injected represents a GC/TCD response factor for ammonia which can be used to convert the deconvoluted peak area to the number of moles of ammonia desorbed. Assuming each mole of desorbed ammonia corresponds to one mole of acid sites, then the number of acid sites can be calculated.

The calibration used below was the only calibration used. However, the deconvolution of the TPD peaks introduces greater uncertainty to the measurement of acidity than does the GC detector drift. The calibration was carried out at a gain of 1 whereas the analysis of niobia samples was carried out at a gain of 20. Consequently the peak areas were divided by a factor of 20 before calculating the acidity.

**Table D1-1** TPD Instrument Calibration Data (09.12.2006)

| **INTEGRATION RESULTS (Automatic)** | | | | | | | |
|---|---|---|---|---|---|---|---|
| | Gain = 1 | | | **n** | | | |
| **PULSE** | **Area** | R2 | | μmol | Area/n | | |
| 1 | 537.3 | 0.970 | | 21.26 | 25.27 | | |
| 2 | 517.7 | 0.988 | | 21.24 | 24.38 | | |
| 3 | 480.0 | 0.981 | | 21.22 | 22.62 | | |
| 4 | 498.3 | 0.964 | | 21.20 | 23.51 | | |
| 5 | 498.0 | 0.988 | | 21.18 | 23.51 | | |
| 6 | 479.2 | 0.982 | | 21.16 | 22.64 | | |
| 7 | 529.7 | 0.965 | | 21.15 | 25.05 | | |
| 8 | 500.1 | 0.989 | | 21.13 | 23.67 | | |
| 9 | 485.2 | 0.979 | | 21.12 | 22.98 | | |
| 10 | 538.5 | 0.976 | | 21.10 | 25.52 | | |
| average | 506.401 | 0.978 | | avg | **23.91** | A/ μmol | 95% CI 0.668 |
| st dev | 22.89014 | | | stdev | 1.08 | | error % 2.79 |
| RSD | 4.52 | | | RSD | 4.51 | | |

### D2 Supplementary Data: TPD Results

**Table D2-1** Summary of TPD Results

| Specimen | Catalyst [g] | PEAKS Tm [℃] | | | | | PEAK AREAS (Gain = 20) | | | | Acidity [mmol/g] | | | | Total [µmol/g] |
|---|---|---|---|---|---|---|---|---|---|---|---|---|---|---|---|
| | | Peak 1 | Peak 2 | Peak 3 | Peak 4 | Artifact | Peak 1 | Peak 2 | Peak 3 | Peak 4 | Peak 1 | Peak 2 | Peak 3 | Peak 4 | |
| Alumina (acidic) | 0.1261 | | 234 | 326 | | 664 | | 3672 | 6201 | | 0.000 | 0.061 | 0.103 | 0.000 | 163.71 |
| CAT 059 | 0.0692 | | 246 | 325 | | 484 | | 323 | 850 | | 0.000 | 0.010 | 0.026 | 0.000 | 35.45 |
| CAT 057 | 0.1258 | | 274 | 396 | 461 | *510* | | 1254 | 1104 | 119 | 0.000 | 0.021 | 0.018 | 0.002 | 41.15 |
| CAT 050 | 0.1033 | 147 | 234 | 310 | | 497 | 58 | 283 | 735 | | 0.001 | 0.006 | 0.015 | 0.000 | 21.78 |
| CAT 049 | 0.1034 | | 243 | 338 | | 522 | | 1077 | 2761 | | 0.000 | 0.022 | 0.056 | 0.000 | 77.60 |
| CAT 048 | 0.0999 | 146 | 229 | 303 | | 490 | 64 | 255 | 994 | | 0.001 | 0.005 | 0.021 | 0.000 | 27.50 |
| CAT 047 | 0.1064 | 134 | 240 | 335 | | 484 | 115 | 675 | 679 | | 0.002 | 0.013 | 0.013 | 0.000 | 28.87 |
| CAT 047 (rpt) | 0.0658 | 136 | 258 | 362 | | 521 | 97 | 510 | 556 | | 0.003 | 0.016 | 0.018 | 0.000 | 36.97 |
| CAT 045 | 0.0899 | 151 | 254 | 352 | | 516 | 187 | 866 | 1938 | | 0.004 | 0.020 | 0.045 | 0.000 | 69.56 |
| CAT 044 | 0.0816 | 161 | 283 | 377 | | 507 | 179 | 2208 | 923 | | 0.005 | 0.057 | 0.024 | 0.000 | 84.81 |
| CAT 040 | 0.0710 | 154 | 270 | 375 | | 482 | 90 | 1368 | 472 | | 0.003 | 0.040 | 0.014 | 0.000 | 56.84 |
| CAT 040 (rpt) | 0.0741 | 138 | 262 | 369 | | 490 | 71 | 1439 | 559 | | 0.002 | 0.041 | 0.016 | 0.000 | 58.38 |
| CAT 038 | 0.0687 | | 242 | 360 | | 521 | | 874 | 2194 | | 0.000 | 0.027 | 0.067 | 0.000 | 93.37 |
| CAT 037 | 0.0631 | | 234 | 324 | | 500 | | 428 | 1114 | | 0.000 | 0.014 | 0.037 | 0.000 | 51.09 |
| CAT 036 | 0.0401 | | 249 | 378 | | 527 | | 324 | 1102 | | 0.000 | 0.017 | 0.057 | 0.000 | 74.35 |
| CAT 034 | 0.0720 | | 249 | 345 | | 543 | | 1207 | 3826 | | 0.000 | 0.035 | 0.111 | 0.000 | 146.14 |
| CAT 029 | 0.0331 | | 278 | 389 | | 507 | | 1606 | 756 | | 0.000 | 0.101 | 0.048 | 0.000 | 149.23 |
| CAT 022 | 0.0762 | | 250 | 349 | | | | 143 | 183 | | 0.000 | 0.004 | 0.005 | 0.000 | 8.92 |
| CAT 001 | 0.1071 | | 230 | 328 | | 536 | | 453 | 2922 | | 0.000 | 0.009 | 0.057 | 0.000 | 65.89 |
| CAT 026 | 0.1216 | | 253 | 296 | 368 | 502 | | 969 | 1838 | 2576 | 0.0000 | 0.0167 | 0.0316 | 0.0443 | 92.56 |
| CAT 005 | 0.0906 | | 275 | 353 | | | | 1627 | 2731 | | 0.0000 | 0.0375 | 0.0630 | 0.0000 | 100.57 |
| CAT 032 | 0.0682 | | 262 | 308 | 397 | 551 | | 984 | 2096 | 3246 | 0.0000 | 0.0302 | 0.0643 | 0.0995 | 193.94 |
| Alumina (wk Acidic) | 0.1261 | | 234 | 326 | | 664 | | 3672 | 6201 | | 0.000 | 0.061 | 0.103 | 0.000 | 163.71 |
| | | | | | | | | | | | | | | | |
| ***Rachig Rings*** | | | | | | | | | | | | | | | |
| CAT 057 | 0.1258 | | 274 | 396 | 460 | *510* | | 1254 | 1104 | 119 | 0.000 | 0.021 | 0.018 | 0.002 | 41.15 |
| CAT 066 | 0.0585 | 309 | 362 | 485 | 626 | 776 | 543 | 246 | 1821 | 616 | 0.019 | 0.009 | 0.065 | 0.022 | 115.29 |
| Norpro SS 65137 | 0.0529 | | | | | 514 | | | | 402 | 0.000 | 0.000 | 0.000 | 0.016 | 0 |
| Spent CAT 066 | 0.0754 | *283* | *376* | *497* | | *763* | 543 | 246 | 1821 | 616 | 0.015 | 0.007 | 0.051 | 0.017 | 89.45 |

**Figure D2-1** $NH_3$/TPD profile of Norpro SS 65137 Silica catalyst carrier support illustrating negligible acidity (W=0.0529 g)

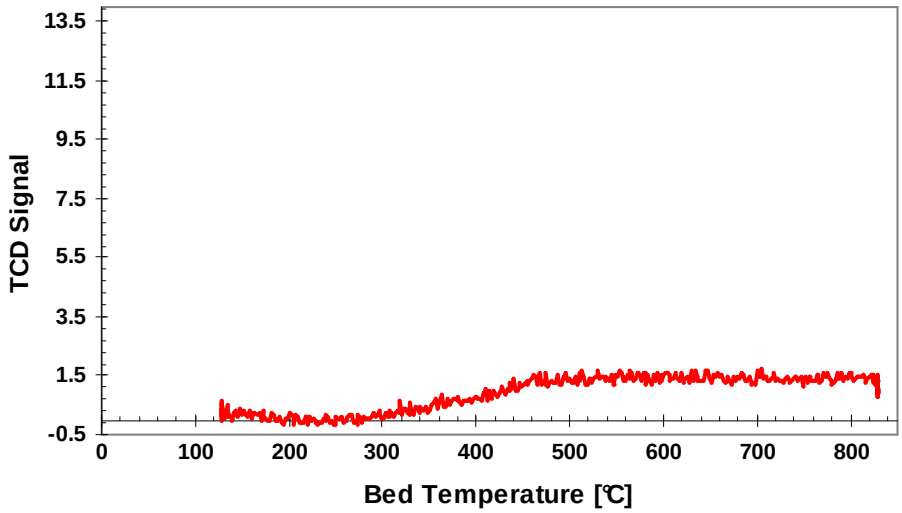


**Figure D2-2** $NH_3$/TPD profile of CAT 059 (W=0.0692 g)

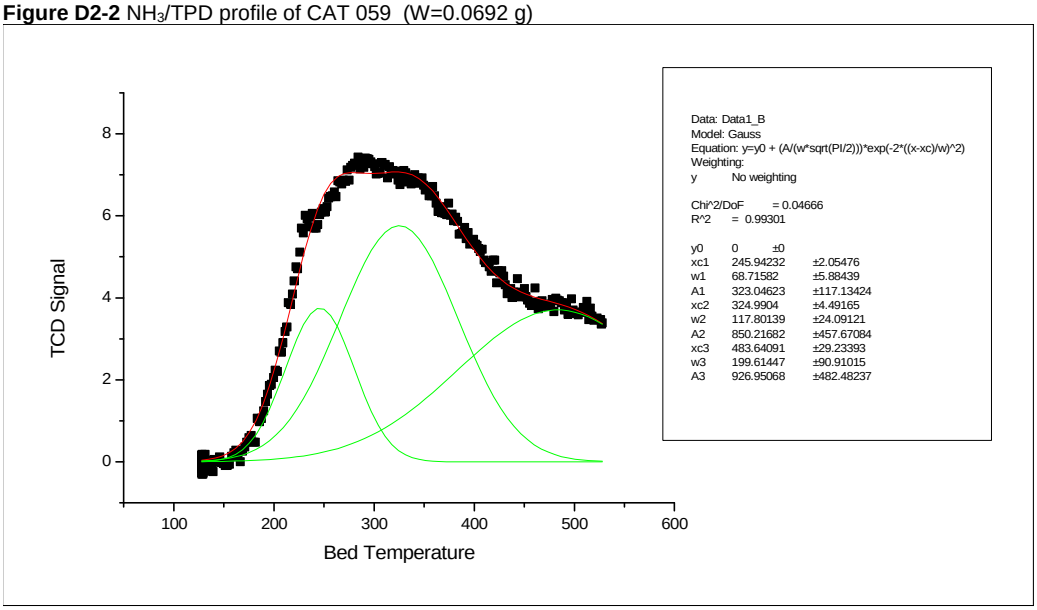

**Figure D2-3** $NH_3$/TPD profile of CAT 050 (W= 0.1033 g)

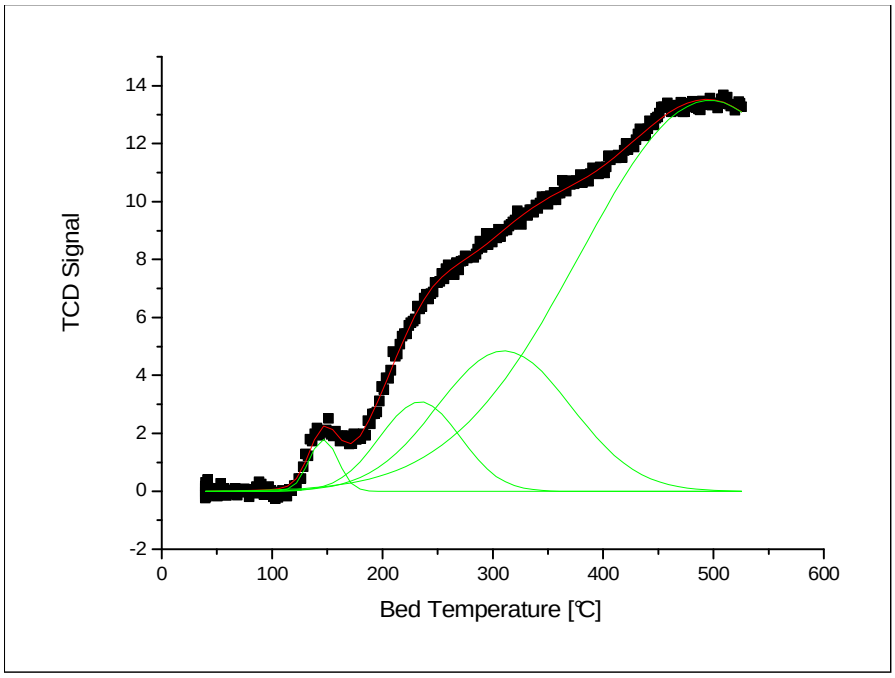


**Figure D2-4** $NH_3$/TPD profile of CAT 049 W=.1034 g

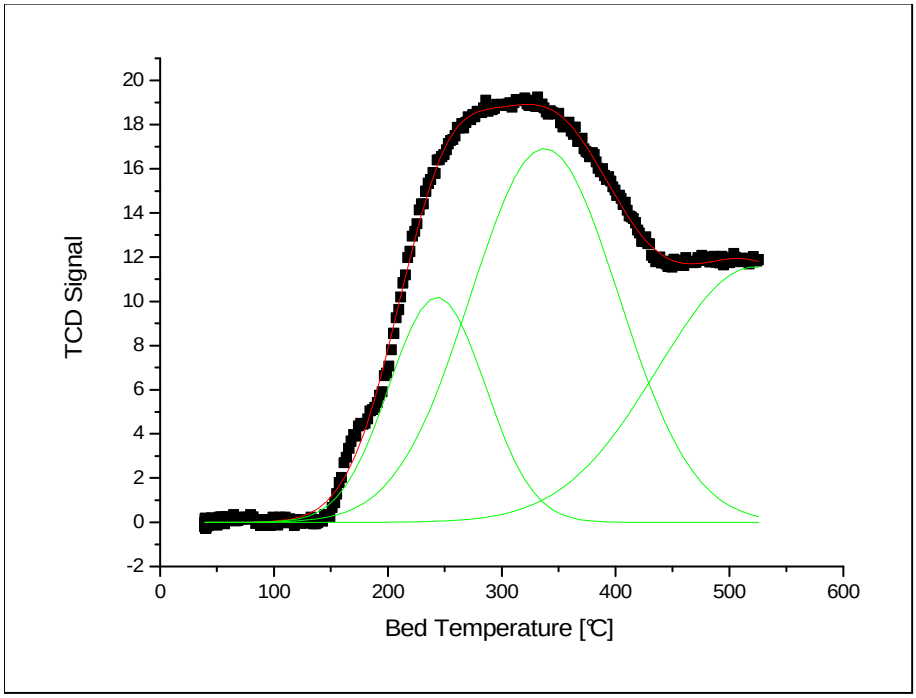

**Figure D2-5** $NH_3$/TPD profile of CAT 047 W=0.1064 g

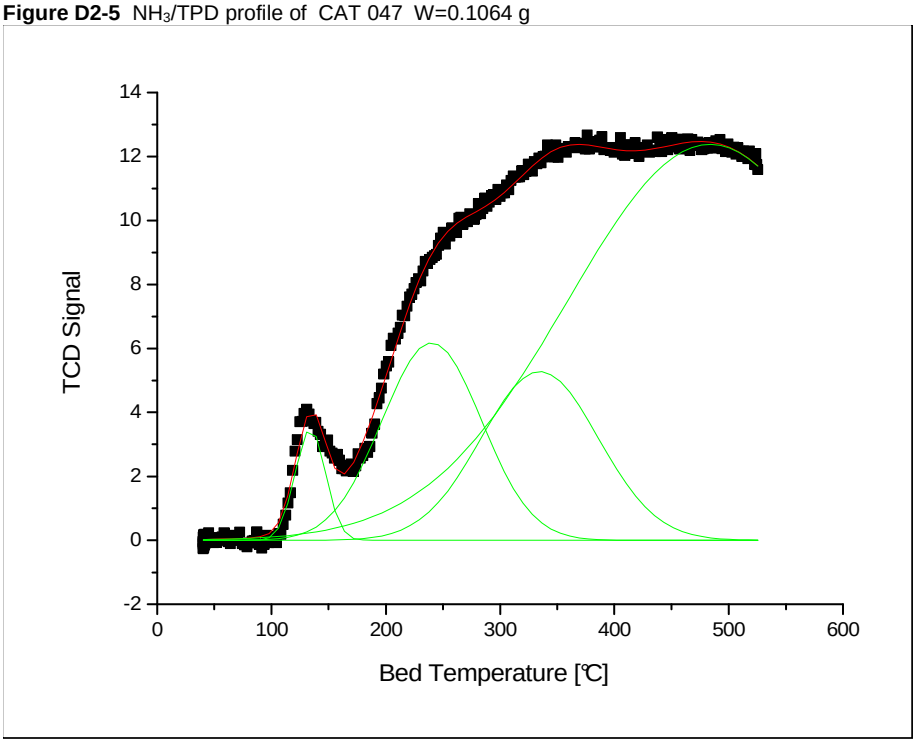


**Figure D2-6** $NH_3$/TPD profile of CAT 047 (repeated) W=0.0658 g

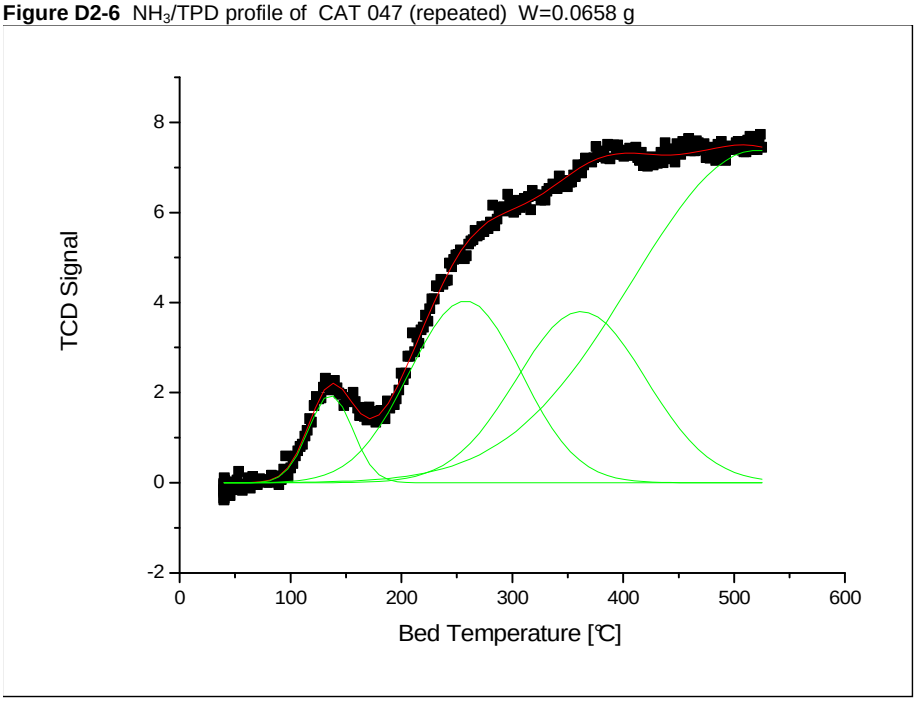

**Figure D2-7** $NH_3$/TPD profile of CAT 040 W=0.0741

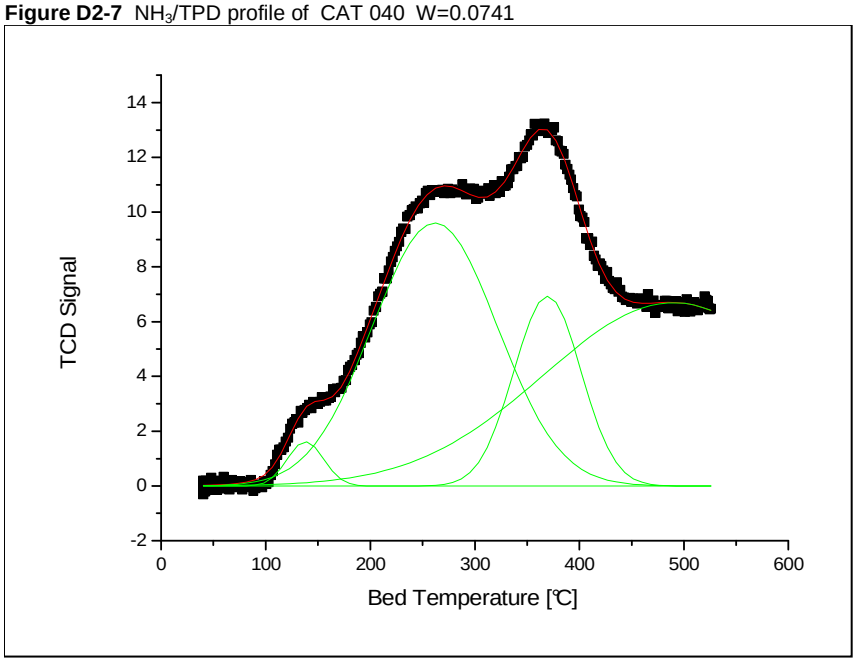


**Figure D2-8** $NH_3$/TPD profile of CAT 040 (repeated) W=0.0710

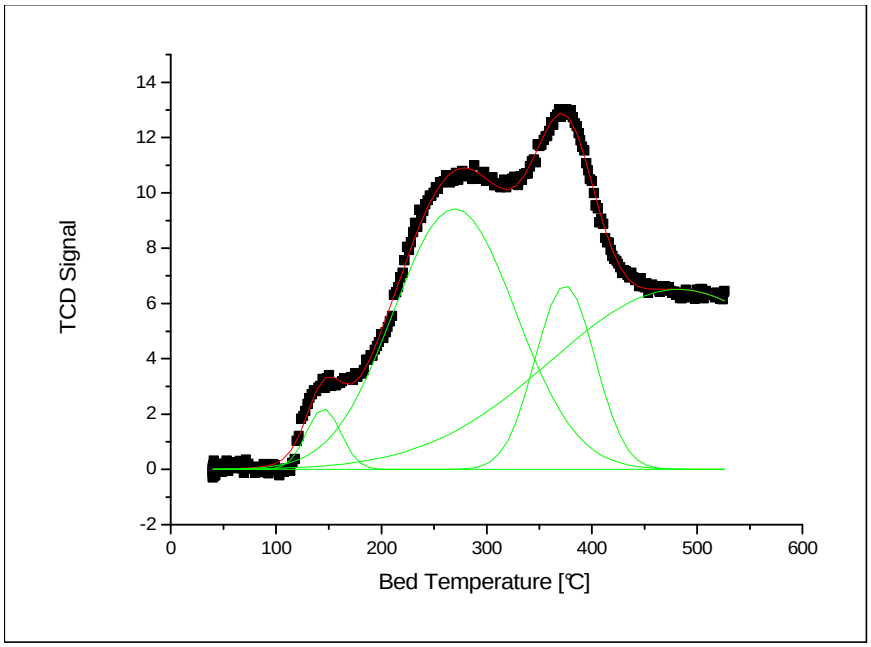

**Figure D2-9** $NH_3$/TPD profile of CAT 038 W =0.0687

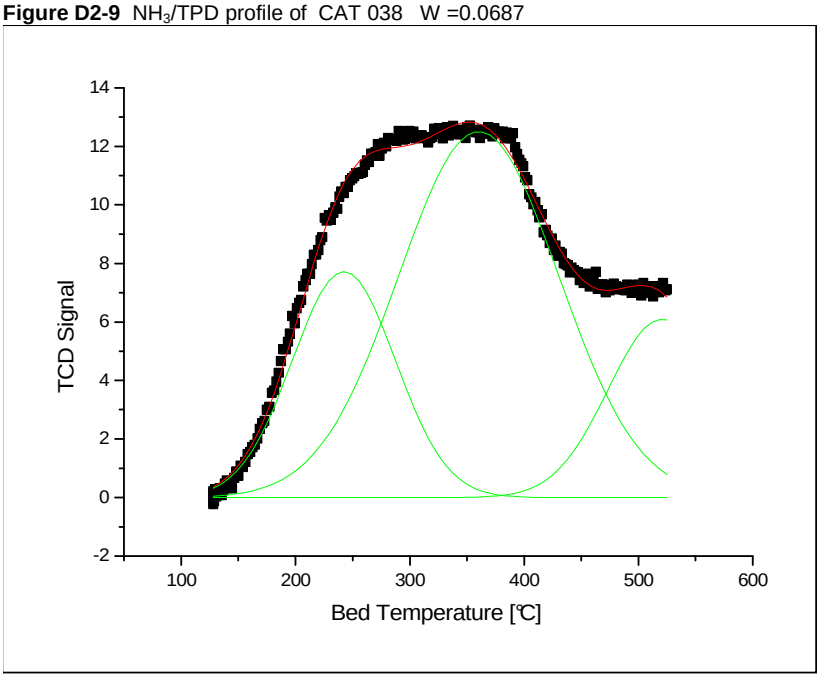


**Figure D2-10** $NH_3$/TPD profile of CAT 037 (W=0.0631 g)

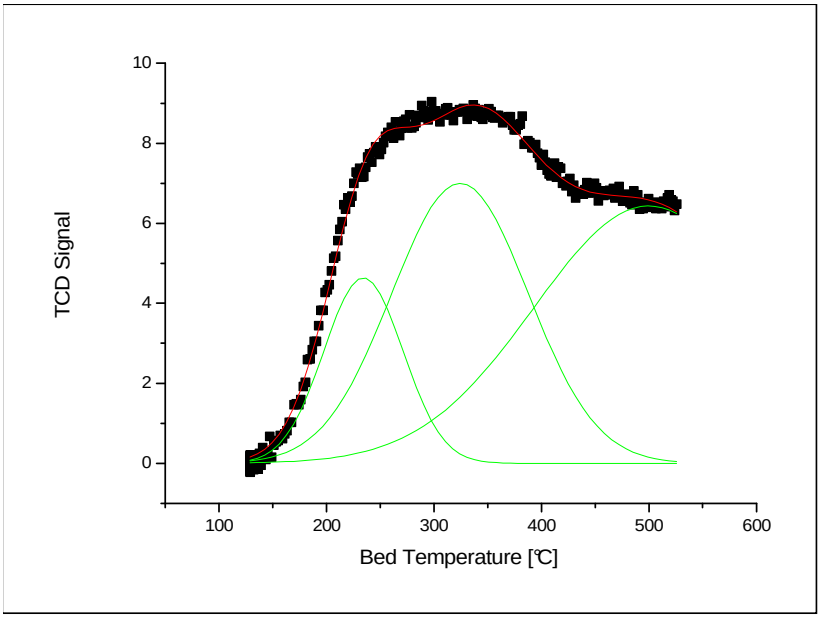

**Figure D2-11** $NH_3$/TPD profile of CAT 036 W=0.0401

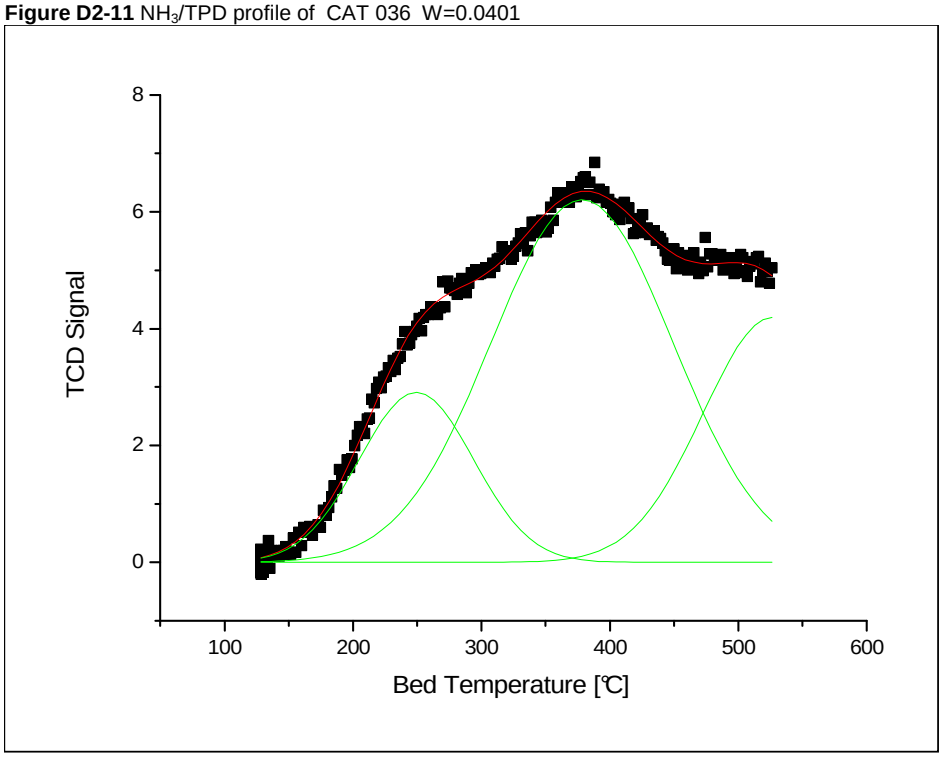


**Figure D2-12** $NH_3$/TPD profile of CAT 034 (W=0.0720 g)

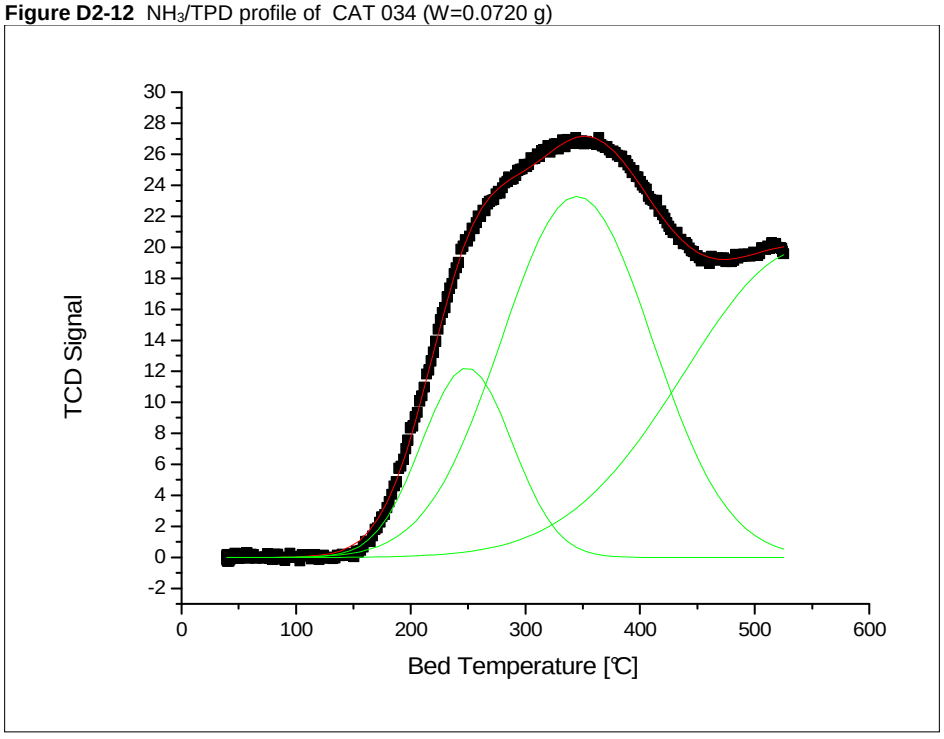

**Figure D2-13** $NH_3$/TPD profile of CAT 022 (W=0.0762 g)

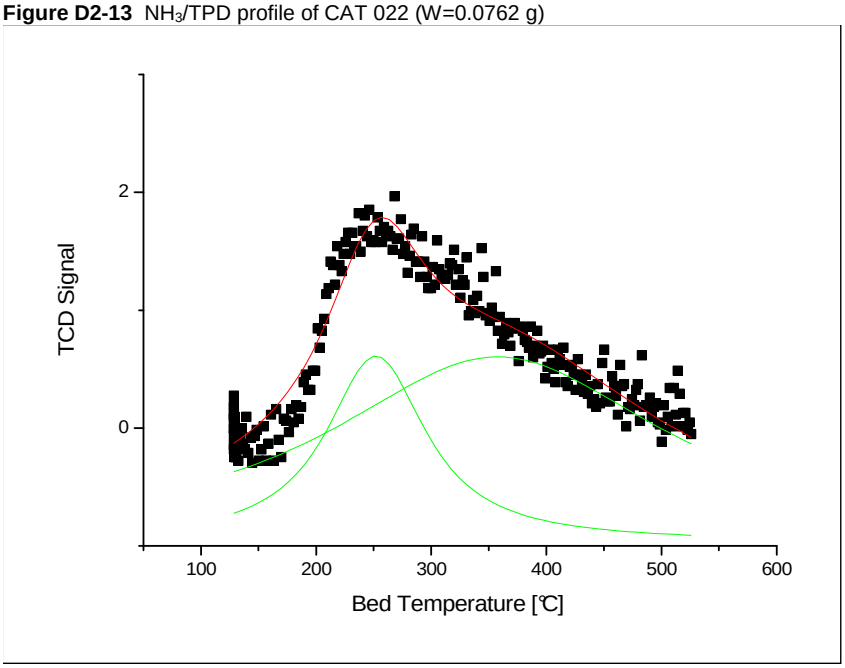


**Figure D2-14** $NH_3$/TPD profile of CAT 001 (W=0.1071 g)

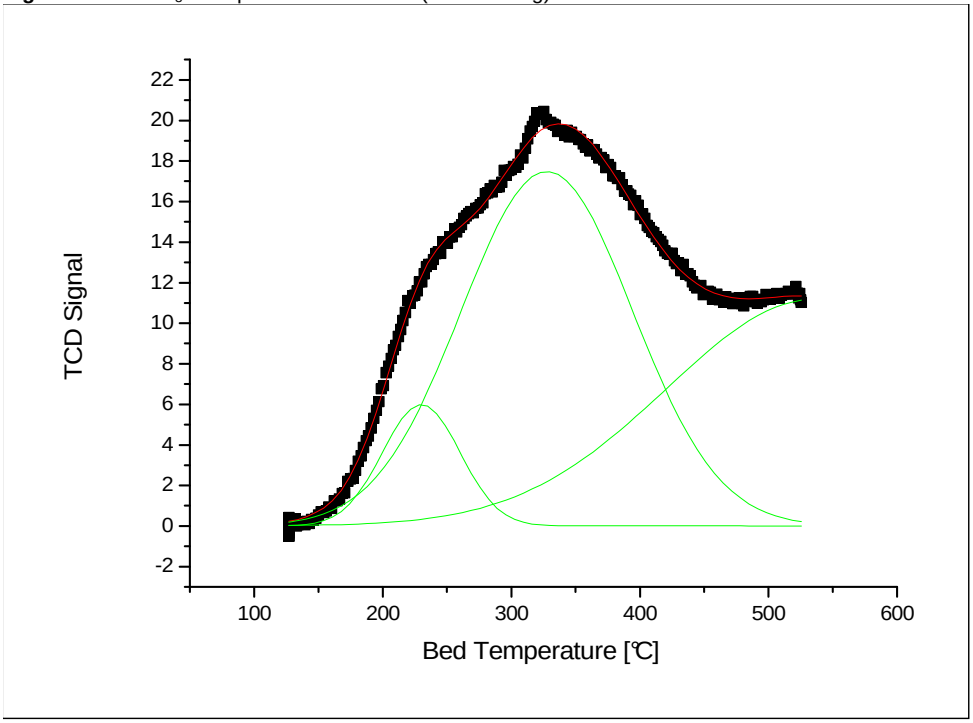

**Figure D2-15** $NH_3$/TPD profile of CAT 005 (W=0.0906 g)

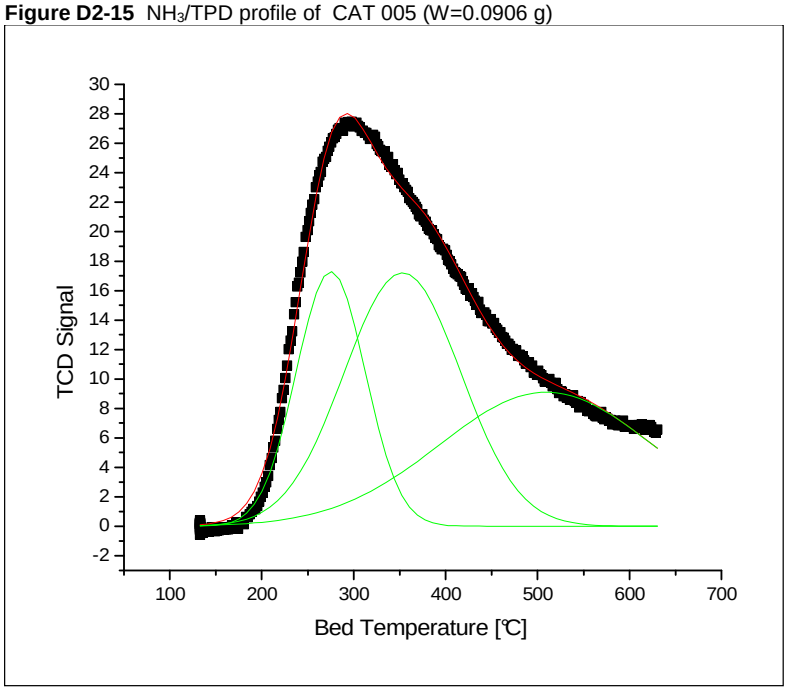


**Figure D2-16** $NH_3$/TPD profile of CAT 066 Spent (W=0.0754 g)

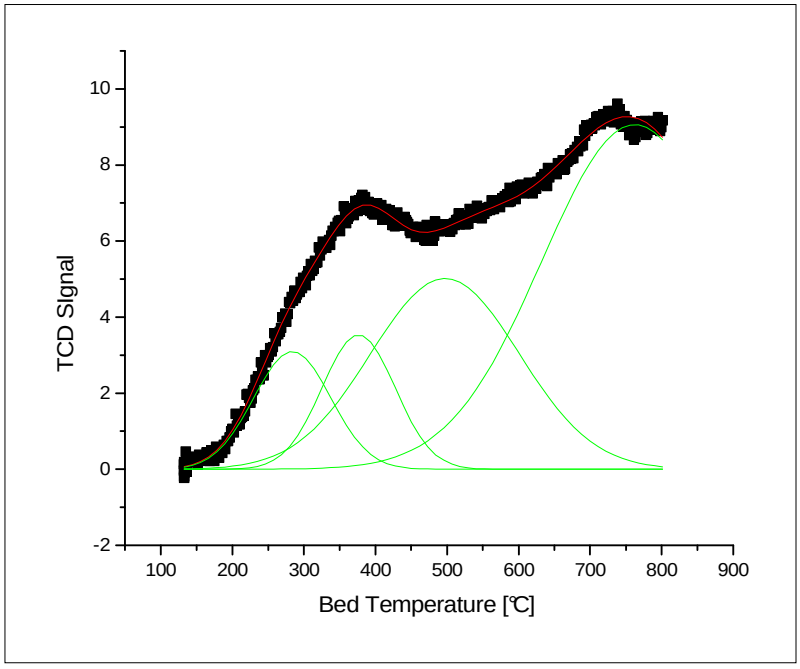

## D3 Supplementary Data: DRIFT Spectroscopy

**Figure D3-1** *in situ* drift spectrum of pyridine adsorbed on Aldrich weakly acidic gamma alumina support.

Specimen activated at 425°C for 2 hours at P ~ $10^{-3}$ Torr. Spectrum obtained after 15 minutes in vacuum after pulse adsorption at 200°.

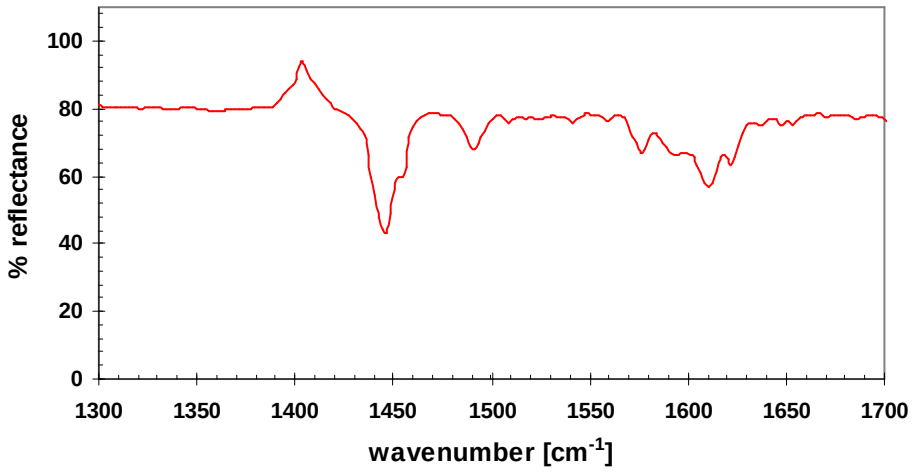


**Figure D3-2** *in situ* drift spectrum of pyridine adsorption on CAT 025

Specimen activated at 425°C for 2 hours at P ~ $10^{-3}$ Torr. Spectrum obtained after 15 minutes in vacuum after pulse adsorption at 200°.

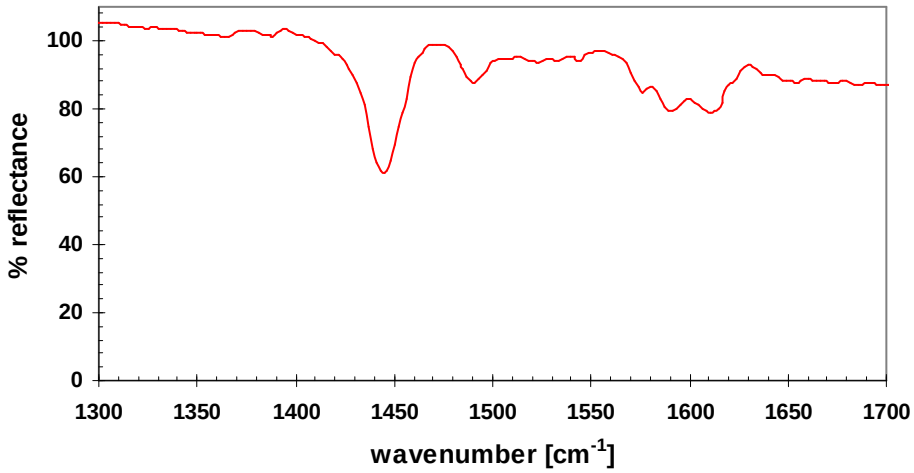

**Figure D3-3** in situ drift spectrum of pyridine adsorption on CAT 032

Specimen activated at 200°C for 2 hours at P ~ $10^{-4}$ Torr. Spectrum obtained after 15 minutes in vacuum after pulse adsorption at 200°.

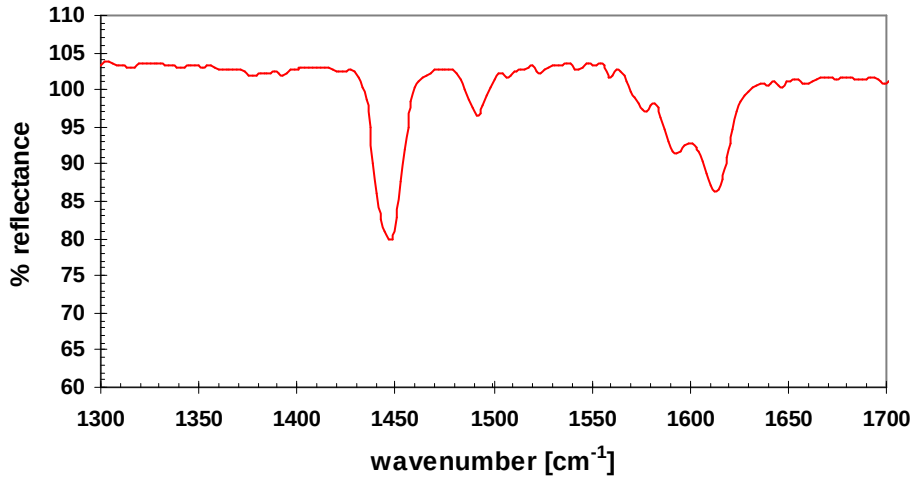


**Figure D3-4** in situ drift spectrum of pyridine adsorption on CAT 029

Specimen activated at 200°C for 2 hours at P ~ $10^{-4}$ Torr. Spectrum obtained after 15 minutes in vacuum after pulse adsorption at 200°.

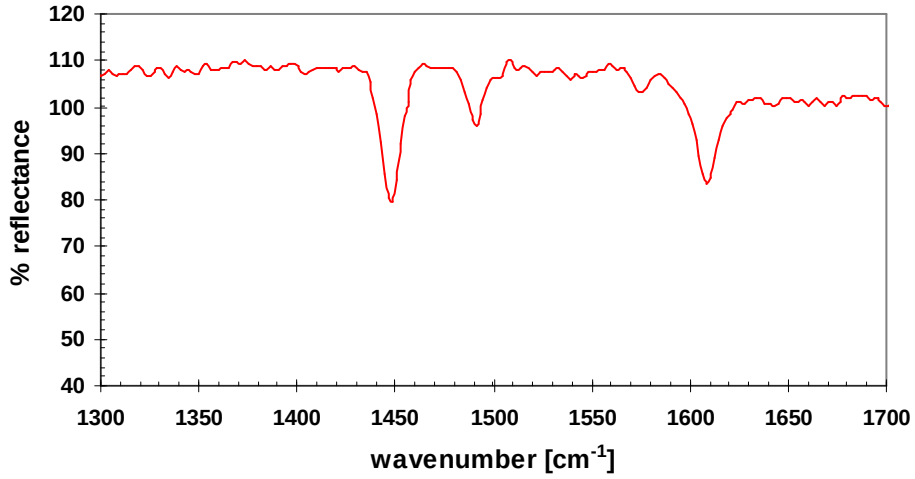

# Appendix E

## Supplementary Data: Chapter Six Kinetics and Catalyst Development

### E1. gProms code for kinetic modelling of batch autoclave

**PROCESS MODEL**

```
PARAMETER
    # Component densities
    Density            AS ARRAY(4) OF REAL

    # Reaction data
    # ArrheniusConstant  AS REAL
    # ActivationEnergy   AS REAL

    # Component stoichiometric coefficients
    Nu                 AS ARRAY(4,2) OF INTEGER

    # Ideal gas constant
    R                  AS REAL

  VARIABLE
    HoldUp             AS ARRAY(4) OF Moles
    C                  AS ARRAY(4) OF MolarConcentration
    TotalVolume        AS Volume
    ReactionRate       AS ARRAY(2) OF NoType
    ReactionConstant   AS ARRAY(2) OF NoType
#   ChemEquilConstant  AS NoType
    T                  AS Temperature
    Wcat               AS NoType
    CH2                AS NoType

    # Reaction data
    # ... variables for parameter estimation purposes
    ArrheniusConstant  AS ARRAY(2) OF NoType
    ActivationEnergy   AS ARRAY(2) OF NoType
#    EquilActivityEnergy  AS NoType
    Kw  AS NoType
    KM  AS NoType
    KI  AS NoType


  EQUATION
    # Mass balance
    FOR i := 1 TO 4 DO
      $HoldUp(i) =
(Nu(i,1)*ReactionRate(1)+Nu(i,2)*ReactionRate(2))*TotalVolume*Wcat ;
    END # For

    # Reaction rate
    ReactionRate(1) = ReactionConstant(1)*C(1)*C(1)/(1.0+Kw*C(3))^2;
    ReactionRate(2) = ReactionConstant(2)*C(2)*CH2/((1+(KM*C(2)))^4);

    # Reaction constant
    ReactionConstant(1) = ArrheniusConstant(1) * EXP(-
ActivationEnergy(1)/(R*T));
    ReactionConstant(2) = ArrheniusConstant(2) * EXP(-
ActivationEnergy(2)/(R*T));


    # Concentrations
    Holdup = C * TotalVolume ;
```

```
    TotalVolume = SIGMA(Holdup/Density) ;


UNIT # Equipment items
    R101 AS BatchReactor

  SET # Parameter values

    WITHIN R101 DO

      Density := [13.5985, 9.2135, 55.3710, 7.9872] ; #[kmol/m3]

      Nu := [ -2,  0,
              +1, -1,
              +1,  0,
               0, +1 ] ;

      R := 8.314 ;

    END # Within

  ASSIGN # Degrees of freedom - these may be overriden by gEST
    WITHIN R101 DO

      ArrheniusConstant(1) := 6.5E8 ;
      ArrheniusConstant(2) := 6.5E5 ;
      ActivationEnergy(1)  := 105262.0 ;
      ActivationEnergy(2)  := 75262.0 ;
      Kw := 2.0;
      KM := 0.47;
      KI := 0.1;

#     EquilActivityEnergy  := 20000.0 ;
      T := 456.0 ;
      Wcat :=0.51;
      CH2 := 0.3;
    END # Within

  INITIAL # Initial conditions - these may be overriden by experimental runs

    WITHIN R101 DO
      Holdup(1) = 1.352e-3;
      Holdup(2) = 0.0;
      Holdup(3) = 11.28e-5;
      Holdup(4) = 0.0;
    END # Within

  SOLUTIONPARAMETERS
#    INTEGRATOR := "SRADAU";
    ReportingInterval := 20;

  SCHEDULE # Operating procedure - this is ignored by gEST

    SEQUENCE
      CONTINUE FOR 500
      STOP
    END # Sequence
```

## E2 Supplementary Data for Flow Reactor Experiments

**Figure E2-1** Catalyst 061 activity vs Time on Stream for flow reactor experiment "BTRS-4" including repeated conditions 180℃ indica ting catalyst deactivation

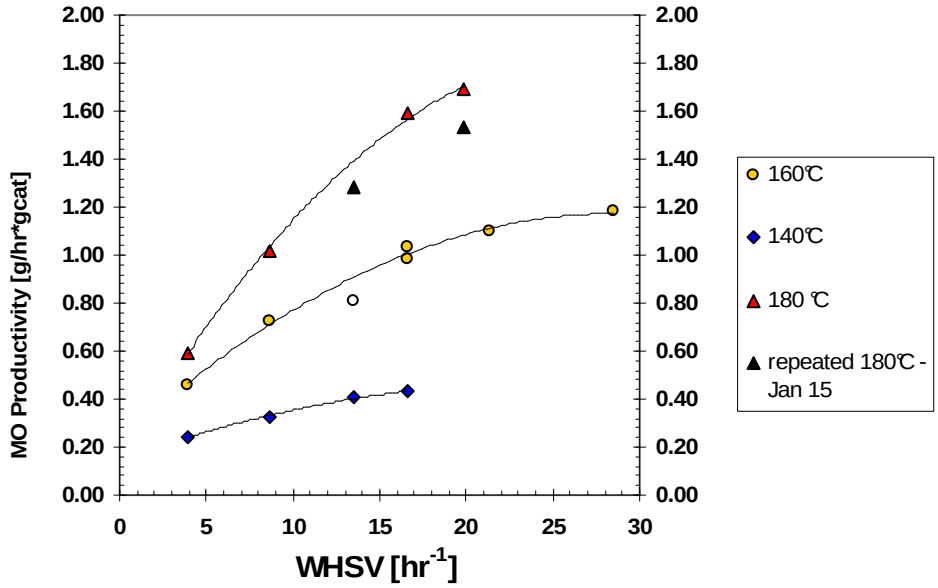


**Table E2-1** Supplementary process data for FBR experiment "BTRS-4"

Italics denote either GC analysis outlier or unsteady state data or anomaly not used in calculations of activity and selectivity. Time on stream does not include transient start up and shut down.

CAT 061 (W=3.006 g) 128 mm glass beads above catalyst bed; 86 mm below catalyst bed; 123 mm catalyst bed

| | TOS | Mass Fraction (wt%) | | | | selectivity | Acetone | Activity |
|---|---|---|---|---|---|---|---|---|
| ID | (hr) | IMO | MO | TMB | PHO | (wt %) | [mL/min] | [g/hr*gcat] |
| Condition 1 | [160℃,1.0 mL/min] | | | | | | | |
| 1 | 0.0 | 0.67 | 5.39 | | 0.28 | 95.6 | 1.05 | 1.01 |
| 1 | 0.0 | 0.69 | 5.57 | | 0.28 | 95.7 | 1.05 | 1.04 |
| 2 | 1.0 | 0.71 | 5.83 | | 0.28 | 95.9 | 1.05 | 1.08 |
| 2 | 1.0 | 0.71 | 5.88 | | 0.28 | 95.9 | 1.05 | 1.09 |
| 3 | 2.0 | 0.55 | 5.40 | | 0.23 | 96.3 | 1.05 | 0.99 |
| 3 | 2.0 | 0.54 | 5.23 | | 0.22 | 96.3 | 1.05 | 0.96 |
| 3 | 2.0 | 0.53 | 5.10 | | 0.22 | 96.3 | 1.05 | 0.93 |
| 4 | 3.0 | 0.54 | 5.32 | | 0.23 | 96.3 | 1.05 | 0.97 |
| 4 | 3.0 | 0.56 | 5.49 | | 0.22 | 96.4 | 1.05 | 1.00 |
| 5 | 4.0 | 0.53 | 5.16 | | 0.22 | 96.3 | 1.05 | 0.94 |
| 5 | 4.0 | 0.52 | 5.12 | | 0.22 | 96.3 | 1.05 | 0.94 |
| 6 | 6.8 | 0.50 | 4.80 | | | 100.0 | 1.05 | 0.88 |
| 6 | 6.8 | 0.51 | 5.01 | | 0.21 | 96.3 | 1.05 | 0.92 |

| | | | | | | | |
|---|---|---|---|---|---|---|---|
| Condition 2 [160℃, 0.8 mL/min] | | | | | | 0.00 | |
| 7 | 7.5 | 0.54 | 5.26 | 0.22 | 96.3 | 0.86 | 0.78 |
| 7 | 7.5 | 0.56 | 5.49 | 0.23 | 96.3 | 0.86 | 0.82 |
| 8 | 8.5 | 0.58 | 5.65 | 0.24 | 96.3 | 0.86 | 0.84 |
| 8 | 8.5 | 0.57 | 5.61 | 0.23 | 96.4 | 0.86 | 0.83 |
| 9 | 9.5 | 0.59 | 5.79 | 0.23 | 96.5 | 0.86 | 0.86 |
| 9 | 9.5 | 0.56 | 5.46 | 0.22 | 96.4 | 0.86 | 0.81 |
| 10 | 10.5 | 0.53 | 5.17 | 0.21 | 96.4 | 0.86 | 0.77 |
| 10 | 10.5 | 0.52 | 5.05 | 0.21 | 96.3 | 0.86 | 0.75 |
| 11 | 11.5 | 0.54 | 5.23 | 0.22 | 96.4 | 0.86 | 0.78 |
| 11 | 11.5 | 0.56 | 5.52 | 0.22 | 96.5 | 0.86 | 0.82 |
| | | | | | | | |
| Day 2: Condition 3, repeat initial condition [160°C, 1 mL/min] | | | | | | | |
| *12* | *14.5* | *0.46* | *4.45* | | *100.0* | *1.05* | *0.81* *GC outlier* |
| 12 | 14.5 | 0.52 | 5.24 | | 100.0 | 1.05 | 0.96 |
| 13 | 15.5 | 0.57 | 5.71 | 0.23 | 96.4 | 1.05 | 1.04 |
| 13 | 15.5 | 0.57 | 5.64 | 0.23 | 96.4 | 1.05 | 1.03 |
| 14 | 16.5 | 0.58 | 5.80 | 0.23 | 96.5 | 1.05 | 1.06 |
| 14 | 16.5 | 0.59 | 5.84 | 0.23 | 96.5 | 1.05 | 1.07 |
| | | | | | | | |
| Day 2: Condition 4, [160°, F=1.30 mL/min] | | | | | | | |
| 15 | 17.5 | 0.49 | 4.80 | | 100.0 | 1.36 | 1.13 |
| 15 | 17.5 | 0.47 | 4.68 | | 100.0 | 1.36 | 1.10 |
| 16 | 18.5 | 0.48 | 4.81 | | 100.0 | 1.36 | 1.13 |
| 16 | 18.5 | 0.48 | 4.69 | | 100.0 | 1.36 | 1.11 |
| 17 | 19.5 | 0.46 | 4.48 | | 100.0 | 1.36 | 1.06 |
| 17 | 19.5 | 0.46 | 4.53 | | 100.0 | 1.36 | 1.07 |
| | | | | | | | |
| Day 2: Condition 5, [160°, F=1.75 mL/min] | | | | | | | |
| 18 | 20.5 | 0.38 | 3.63 | | 100.0 | 1.81 | 1.14 |
| 18 | 20.5 | 0.40 | 3.89 | | 100.0 | 1.81 | 1.22 |
| 19 | 21.5 | 0.38 | 3.63 | | 100.0 | 1.81 | 1.14 |
| 19 | 21.5 | 0.38 | 3.62 | | 100.0 | 1.81 | 1.14 |
| 20 | 22.5 | 0.39 | 3.81 | | 100.0 | 1.81 | 1.20 |
| 20 | 22.5 | 0.40 | 3.92 | | 100.0 | 1.81 | 1.23 |
| | | | | | | | |
| Day 3: Condition 6, [160°, F=0.50 mL/min] | | | | | | | |
| 21 | 24.5 | 0.75 | 7.34 | 0.32 | 96.2 | 0.55 | 0.70 |
| 21 | 24.5 | 0.80 | 7.93 | 0.34 | 96.3 | 0.55 | 0.76 |
| 22 | 25.5 | 0.78 | 7.78 | 0.31 | 96.5 | 0.55 | 0.74 |
| 22 | 25.5 | 0.79 | 7.90 | 0.31 | 96.5 | 0.55 | 0.75 |
| 23 | 26.5 | 0.73 | 7.36 | 0.30 | 96.4 | 0.55 | 0.70 |
| 23 | 26.5 | 0.73 | 7.31 | 0.30 | 96.5 | 0.55 | 0.70 |
| | | | | | | | |
| Day 3: Condition 7, [160°, F=0.20 mL/min] | | | | | | | |
| 24 | 30.0 | 1.05 | 10.62 | 0.41 | 96.6 | 0.25 | 0.45 |
| 24 | 30.0 | 1.06 | 10.70 | 0.42 | 96.5 | 0.25 | 0.46 |
| 25 | 31.0 | 1.05 | 10.58 | 0.41 | 96.6 | 0.25 | 0.45 |
| 25 | 31.0 | 1.06 | 10.74 | 0.42 | 96.6 | 0.25 | 0.46 |
| 26 | 32.0 | 1.06 | 10.76 | 0.42 | 96.6 | 0.25 | 0.46 |

Day 4: Condition 8, [140 ℃, 1.0 ml/min ]

| | | | | | | | |
|---|---|---|---|---|---|---|---|
| 27 | 35.0 | | 2.22 | | 100.0 | 1.05 | 0.37 | |
| 27 | 35.0 | | 2.51 | | 100.0 | 1.05 | 0.42 | |
| 28 | 36.0 | | 2.46 | | 100.0 | 1.05 | 0.41 | |
| 28 | 36.0 | | 2.51 | | 100.0 | 1.05 | 0.42 | |
| 29 | 37.0 | | 2.33 | | 100.0 | 1.05 | 0.39 | |
| 29 | 37.0 | | 2.49 | | 100.0 | 1.05 | 0.41 | |

Day 4: Condition 9, [140 ℃, 0.8 ml/min ]

| | | | | | | | |
|---|---|---|---|---|---|---|---|
| 30 | 43.0 | | 2.89 | | 100.0 | 0.86 | 0.39 | |
| 30 | 43.0 | | 2.87 | | 100.0 | 0.86 | 0.39 | |
| 31 | 44.0 | | 2.97 | | 100.0 | 0.86 | 0.40 | |
| 31 | 44.0 | | 2.85 | | 100.0 | 0.86 | 0.38 | |
| 32 | 45.0 | | 2.80 | | 100.0 | 0.86 | 0.38 | |
| *32* | *45.0* | | *2.73* | | *100.0* | *0.86* | *0.37* | *GC outlier* |

Day 5: Condition 10, [140 ℃, 0.2 ml/min ]

| | | | | | | | | |
|---|---|---|---|---|---|---|---|---|
| *33* | *47.5* | | *3.91* | | *100.0* | *0.25* | *0.15* | Not steady |
| *33* | *47.5* | | *3.94* | | *100.0* | *0.25* | *0.16* | state |
| 34 | 48.5 | 0.45 | 5.30 | | 100.0 | 0.25 | 0.23 | |
| 34 | 48.5 | 0.46 | 5.63 | | 100.0 | 0.25 | 0.24 | |
| 35 | 49.5 | 0.47 | 5.57 | | 100.0 | 0.25 | 0.24 | |
| 35 | 49.5 | 0.48 | 5.64 | | 100.0 | 0.25 | 0.24 | |
| 36 | 50.5 | 0.49 | 5.77 | | 100.0 | 0.25 | 0.25 | |
| 36 | 50.5 | 0.51 | 6.13 | 0.23 | 96.7 | 0.25 | 0.26 | |

Day 5: Condition 11, [140 ℃, 0.5 ml/min ]

| | | | | | | | |
|---|---|---|---|---|---|---|---|
| 37 | 51.5 | | 3.73 | | 100.0 | 0.55 | 0.32 | |
| 37 | 51.5 | | 3.61 | | 100.0 | 0.55 | 0.31 | |
| 38 | 52.5 | | 3.45 | | 100.0 | 0.55 | 0.30 | |
| 38 | 52.5 | | 3.44 | | 100.0 | 0.55 | 0.30 | |
| 39 | 53.5 | | 3.61 | | 100.0 | 0.55 | 0.31 | |

Day 6: Condition 12, [160 ℃, 1.0 ml/min ] repea t initial condition

| | | | | | | | | |
|---|---|---|---|---|---|---|---|---|
| *40* | *55.5* | *0.47* | *4.59* | | *100.0* | *1.05* | *0.84* | not steady |
| *40* | *55.5* | *0.47* | *4.60* | | *100.0* | *1.05* | *0.84* | state |
| 41 | 56.5 | 0.48 | 4.74 | | 100.0 | 1.05 | 0.86 | |
| 41 | 56.5 | 0.51 | 5.16 | | 100.0 | 1.05 | 0.94 | |
| 42 | 58.0 | 0.49 | 4.83 | | 100.0 | 1.05 | 0.88 | |
| 42 | 58.0 | 0.51 | 5.11 | | 100.0 | 1.05 | 0.93 | |
| 43 | 58.5 | 0.51 | 5.07 | | 100.0 | 1.05 | 0.93 | |
| 43 | 58.5 | 0.51 | 5.20 | | 100.0 | 1.05 | 0.95 | |

Day 6: Condition 13, [180 ℃, 1.0 ml/min ]

| | | | | | | | |
|---|---|---|---|---|---|---|---|
| 44 | 59.5 | 0.98 | 8.42 | 0.33 | 96.6 | 1.05 | 1.56 |
| 44 | 59.5 | 1.02 | 8.77 | 0.34 | 96.6 | 1.05 | 1.62 |

Day 7: Condition 14, [160 ℃, 1.0 ml/min ] repea t initial condition

| | | | | | | | |
|---|---|---|---|---|---|---|---|
| 45 | 60.5 | 0.44 | 4.30 | 0.03 | 99.3 | 1.05 | 0.79 |

| | | | | | | | | | |
|---|---|---|---|---|---|---|---|---|---|
| 45 | 60.5 | 0.46 | 4.54 | | | 100.0 | 1.05 | 0.83 | |
| 46 | 61.5 | 0.49 | 4.79 | | | 100.0 | 1.05 | 0.88 | |
| 46 | 61.5 | 0.50 | 4.96 | | | 100.0 | 1.05 | 0.91 | |
| 47 | 62.5 | 0.46 | 4.57 | | | 100.0 | 1.05 | 0.83 | |
| 47 | 62.5 | 0.45 | 4.43 | | | 100.0 | 1.05 | 0.81 | |
| 48 | 63.5 | 0.48 | 4.70 | | | 100.0 | 1.05 | 0.86 | |
| 48 | 63.5 | 0.53 | 5.33 | | | 100.0 | 1.05 | 0.97 | |

Day 7: Condition 15, [180 ℃, 1.2 ml/min ]

| | | | | | | | | | |
|---|---|---|---|---|---|---|---|---|---|
| *49* | *65.5* | *0.84* | *7.18* | | *0.29* | *96.5* | *1.26* | *1.59* | *not steady* |
| *49* | *65.5* | *0.84* | *7.21* | | *0.29* | *96.6* | *1.26* | *1.60* | *state yet* |
| 50 | 66.5 | 0.89 | 7.62 | | 0.30 | 96.6 | 1.26 | 1.69 | |
| 50 | 66.5 | 0.91 | 7.82 | | 0.31 | 96.6 | 1.26 | 1.73 | |
| *51* | *67.5* | *0.83* | *5.54* | | *0.33* | *95.0* | *1.26* | *1.26* | *unsteady* |
| *51* | *67.5* | *0.86* | *5.78* | | *0.35* | *95.0* | *1.26* | *1.32* | sample clear |
| 52 | 68.5 | 0.90 | 7.77 | | 0.31 | 96.6 | 1.26 | 1.72 | |
| 52 | 68.5 | 0.90 | 7.74 | | 0.31 | 96.5 | 1.26 | 1.71 | |
| 53 | 69.0 | 0.86 | 7.33 | | 0.30 | 96.5 | 1.26 | 1.62 | |
| 53 | 69.0 | 0.87 | 7.44 | | 0.30 | 96.5 | 1.26 | 1.65 | |

Day 8: Condition 16, [180 ℃, 0.2 ml/min ]

| | | | | | | | | | |
|---|---|---|---|---|---|---|---|---|---|
| *55* | *73.0* | *1.50* | *12.59* | *0.39* | *0.49* | *94.1* | *0.25* | *0.55* | *not steady* |
| *55* | *73.0* | *1.56* | *13.16* | *0.40* | *0.49* | *94.3* | *0.25* | *0.57* | *state yet* |
| 56 | 74.0 | 1.57 | 13.31 | 0.43 | 0.69 | 93.0 | 0.25 | 0.58 | |
| 56 | 74.0 | 1.68 | 14.20 | 0.44 | 0.71 | 93.2 | 0.25 | 0.62 | |
| 57 | 75.0 | 1.68 | 14.29 | 0.45 | 0.74 | 93.1 | 0.25 | 0.62 | |
| 57 | 75.0 | 1.62 | 13.70 | 0.43 | 0.69 | 93.2 | 0.25 | 0.59 | |
| 58 | 76.0 | 1.61 | 13.62 | 0.42 | 0.50 | 94.3 | 0.25 | 0.59 | |
| 58 | 76.0 | 1.62 | 13.66 | 0.43 | 0.70 | 93.1 | 0.25 | 0.59 | |
| 59 | 77.0 | 1.57 | 13.23 | 0.41 | 0.48 | 94.3 | 0.25 | 0.57 | |
| 59 | 77.0 | 1.61 | 13.57 | 0.42 | 0.68 | 93.3 | 0.25 | 0.59 | |

Day 8: Condition 17, [180 ℃, 0.5 ml/min ]

| | | | | | | | | |
|---|---|---|---|---|---|---|---|---|
| 60 | 79.0 | 1.23 | 10.52 | 0.17 | 0.38 | 95.5 | 0.55 | 1.02 |
| 60 | 79.0 | 1.22 | 10.48 | 0.17 | 0.39 | 95.4 | 0.55 | 1.02 |
| 61 | 80.0 | 1.27 | 10.84 | 0.17 | 0.42 | 95.3 | 0.55 | 1.05 |
| 61 | 80.0 | 1.26 | 10.79 | 0.17 | 0.41 | 95.4 | 0.55 | 1.05 |
| 62 | 81.0 | 1.18 | 9.93 | 0.16 | 0.38 | 95.4 | 0.55 | 0.96 |
| 62 | 81.0 | 1.24 | 10.60 | 0.17 | 0.41 | 95.3 | 0.55 | 1.03 |
| 63 | 82.0 | 1.23 | 10.41 | 0.17 | 0.40 | 95.3 | 0.55 | 1.01 |
| 63 | 82.0 | 1.26 | 10.60 | 0.17 | 0.39 | 95.5 | 0.55 | 1.03 |

Day 9: Condition 18, [180 ℃, 0.8 ml/min ]

| | | | | | | | | | |
|---|---|---|---|---|---|---|---|---|---|
| *64* | *83.5* | *0.93* | *7.97* | | *0.31* | *96.6* | *0.86* | *1.20* | *GC outlier* |
| *64* | *83.5* | *0.95* | *8.18* | | *0.33* | *96.5* | *0.86* | *1.23* | *wait to* |
| *65* | *84.5* | *0.95* | *8.21* | | *0.32* | *96.7* | *0.86* | *1.24* | *ensure* |
| *65* | *84.5* | *0.95* | *8.11* | | *0.30* | *96.8* | *0.86* | *1.22* | *steady state* |
| 66 | 85.5 | 0.96 | 8.25 | | 0.32 | 96.7 | 0.86 | 1.24 | |
| 66 | 85.5 | 1.01 | 8.71 | | 0.33 | 96.7 | 0.86 | 1.31 | |

| | | | | | | | |
|---|---|---|---|---|---|---|---|
| 67 | 86.5 | 0.96 | 8.30 | 0.32 | 96.7 | 0.86 | 1.25 |
| 67 | 86.5 | 1.01 | 8.77 | 0.33 | 96.7 | 0.86 | 1.32 |

Day 9: Condition 19, [180 ℃, 1.2 ml/min ] (repe at condition 15)

| | | | | | | | |
|---|---|---|---|---|---|---|---|
| 68 | 88.0 | 0.78 | 6.82 | 0.26 | 96.7 | 1.26 | 1.51 |
| 68 | 88.0 | 0.80 | 6.92 | 0.27 | 96.7 | 1.26 | 1.53 |
| 69 | 89.0 | 0.84 | 7.25 | 0.27 | 96.7 | 1.26 | 1.60 |
| 69 | 89.0 | 0.82 | 7.04 | 0.26 | 96.7 | 1.26 | 1.56 |
| 70 | 90.0 | 0.73 | 6.17 | 0.24 | 96.6 | 1.26 | 1.37 |
| 70 | 90.0 | 0.78 | 6.75 | 0.26 | 96.7 | 1.26 | 1.49 |
| 71 | 91.0 | 0.83 | 7.18 | 0.28 | 96.7 | 1.26 | 1.59 |
| 71 | 91.0 | 0.84 | 7.24 | 0.27 | 96.8 | 1.26 | 1.60 |

Table E2-2 Process data for FBR experiment “BTRS-5”

Italics denote either GC analysis outlier or unsteady state data or anomaly not used in calculations of activity and selectivity. Hydrogen flow meter calibrated for methane. To convert set-point or measured value to actual hydrogen flow rate, multiply by 1.4027.

Catalyst 062 (W=2.582 g)

| | TOS | C9 | Mass Fraction (wt%) | | | | | | Sel | Ac | H2 | MO/MIBK | Total | |
|---|---|---|---|---|---|---|---|---|---|---|---|---|---|---|
| ID | (hr) | 1.8 min | IMO | MO | TMB | PHO | MIBK | DIBK | (wt %) | [mL/min] | (sccm) | | | |
| **Day 1; Condition #1 [T=160℃, VH=100 sccm; VA=1 mL/ min; P=555 psig]** | | | | | | | | | | | | | | |
| *1* | *1* | *0.15* | | | | | *5.11* | *0.82* | *84.0* | *1.05* | *147* | *0.99* | *1.17* | unsteady |
| *1* | *1.0* | *0.15* | | | | | *6.14* | *0.90* | *85.4* | *1.05* | *147* | *1.19* | *1.39* | |
| 2 | 2.0 | 0.16 | | | 0.23 | | 6.43 | 0.94 | 83.0 | 1.05 | 147 | 1.24 | 1.50 | |
| 2 | 2.0 | 0.16 | | | 0.23 | | 6.55 | 0.93 | 83.3 | 1.05 | 147 | 1.26 | 1.52 | |
| 3 | 3.0 | | | | 0.22 | | 6.54 | 0.92 | 85.2 | 1.05 | 147 | 1.26 | 1.48 | |
| 3 | 3.0 | | | | 0.22 | | 6.62 | 0.92 | 85.3 | 1.05 | 147 | 1.28 | 1.50 | |
| 4 | 4.0 | 0.15 | | | 0.24 | | 7.18 | 0.98 | 84.0 | 1.05 | 147 | 1.39 | 1.65 | |
| 4 | 4.0 | | | | 0.23 | | 6.81 | 0.95 | 85.2 | 1.05 | 147 | 1.32 | 1.54 | |
| 5 | 5.0 | 0.16 | | | 0.23 | | 7.05 | 0.96 | 83.9 | 1.05 | 147 | 1.36 | 1.62 | |
| 5 | 5.0 | 0.15 | | | 0.23 | | 6.92 | 0.95 | 83.8 | 1.05 | 147 | 1.34 | 1.60 | |
| 6 | 6.0 | | | | 0.22 | | 6.48 | 0.90 | 85.3 | 1.05 | 147 | 1.25 | 1.47 | |
| 6 | 6.0 | | | | 0.23 | | 6.97 | 0.95 | 85.5 | 1.05 | 147 | 1.35 | 1.57 | |
| 7 | 7.0 | | | | | | 6.48 | 0.87 | 88.1 | 1.05 | 147 | 1.25 | 1.42 | |
| 7 | 7.0 | | | | | | 6.57 | 0.88 | 88.2 | 1.05 | 147 | 1.27 | 1.44 | |

**Day 2 Shut down 1 hour after start-up due to PLC problem**

**Day 3; Condition #2 [T=160℃, VH=0 sccm; VA=1 mL/m in; P=555 psig]**

| | | | | | | | | | |
|---|---|---|---|---|---|---|---|---|---|
| 9 | 9.0 | 0.49 | 4.35 | 0.20 | 1.04 | 0.00 | 0.926 | 0.964 | |
| 9 | 9.0 | 0.49 | 4.31 | 0.20 | 1.04 | 0.00 | 0.934 | 0.957 | |
| 10 | 10.0 | 0.47 | 4.08 | 0.20 | 1.04 | 0.00 | 0.885 | 0.908 | |
| 10 | 10.0 | 0.49 | 4.30 | 0.20 | 1.04 | 0.00 | 0.933 | 0.956 | |
| 11 | 11.0 | 0.47 | 4.08 | 0.20 | 1.04 | 0.00 | 0.885 | 0.908 | |
| 11 | 11.0 | 0.49 | 4.26 | 0.19 | 1.04 | 0.00 | 0.925 | 0.945 | |
| 12 | 12.0 | 0.47 | 4.06 | 0.18 | 1.04 | 0.00 | 0.881 | 0.901 | |
| 12 | 12.0 | 0.46 | 3.98 | 0.18 | 1.04 | 0.00 | 0.864 | 0.884 | |

(cont'd)

| | | | | | | | | | | |
|---|---|---|---|---|---|---|---|---|---|---|
| **Day 3; Condition #3 [T=160℃, VH=100 sccm; VA=1 mL /min; P=555 psig]** | | | | | | | | | | |
| 13 | 14.5 | 0.50 | 4.96 | 0.59 | 82.0 | 1.05 | 147 | 0.958 | 1.17 | |
| 13 | 14.5 | 0.51 | 5.03 | 0.64 | 81.5 | 1.05 | 147 | 0.972 | 1.19 | |
| 14 | *15.5* | *0.44* | *4.41* | *0.54* | *81.8* | *1.05* | *147* | *0.851* | *1.04* | |
| 14 | *15.5* | 0.44 | 4.51 | 0.54 | 82.1 | 1.05 | 147 | 0.871 | 1.06 | |
| 15 | 16.5 | 0.50 | 5.15 | 0.65 | 81.7 | 1.05 | 147 | 0.994 | 1.22 | |
| 15 | 16.5 | 0.50 | 5.22 | 0.62 | 82.3 | 1.05 | 147 | 1.008 | 1.22 | |
| 16 | 17.5 | 0.45 | 4.74 | 0.57 | 82.2 | 1.05 | 147 | 0.916 | 1.11 | |
| 16 | 17.5 | 0.47 | 4.92 | 0.61 | 82.0 | 1.05 | 147 | 0.951 | 1.16 | |
| 17 | 10.5 | 0.48 | 5.07 | 0.60 | 82.4 | 1.05 | 147 | 0.979 | 1.19 | |

**Table E2-3** Process Data for FBR experiment "BTRS-6"

Catalyst 065, (W=2.988 g); 147 mm glass beads above catalyst bed; 58 mm of glass beads below catalyst bed; catalyst bed 154 mm

| | | | | | | | | | | | | | activity [g/hr*gcat] | |
|---|---|---|---|---|---|---|---|---|---|---|---|---|---|---|
| | **TOS** | **C9** | **Mass Fraction (wt%)** | | | | | | | **Select** | **Ac** | **H2** | MO/MIBK | Total |
| **ID** | **(hr)** | **1.8 min** | **IMO** | **MO** | **TMB** | **PHO** | **IPA** | **MIBK** | **DIBK** | **(wt %)** | **[mL/min]** | **(sccm)** | | |
| **Day 1; Condition #1 [T=160℃, VH=100 sccm; VA=1 mL/ min; P=555 psig]** | | | | | | | | | | | | | | |
| 1 | 1.0 | | | | | | 1.3 | 4.51 | 0.34 | 73.3 | 1.04 | 147 | 0.746 | 1.02 |
| 1 | 1.0 | | | | | | 1.29 | 4.53 | 0.34 | 73.5 | 1.04 | 147 | 0.749 | 1.02 |
| 2 | 2.0 | | | | | | 1.67 | 4.03 | 0.26 | 67.7 | 1.04 | 147 | 0.666 | 0.984 |
| 2 | 2.0 | | | | | | 1.62 | 3.96 | 0.25 | 67.8 | 1.04 | 147 | 0.654 | 0.965 |
| 3 | 3.0 | | | | | | 1.71 | 4.04 | 0.25 | 67.4 | 1.04 | 147 | 0.669 | 0.993 |
| 3 | 3.0 | | | | | | 1.71 | 4.20 | 0.26 | 68.1 | 1.04 | 147 | 0.695 | 1.02 |
| 4 | 4.0 | | | | | | 1.69 | 4.02 | 0.26 | 67.3 | 1.04 | 147 | 0.664 | 0.987 |
| 4 | 4.0 | | | | | | 1.71 | 4.04 | 0.26 | 67.2 | 1.04 | 147 | 0.668 | 0.994 |
| 5 | 5.0 | | | | | | 1.61 | 4.00 | 0.26 | 68.2 | 1.04 | 147 | 0.662 | 0.971 |
| 5 | 5.0 | | | | | | 1.75 | 4.39 | 0.29 | 68.3 | 1.04 | 147 | 0.727 | 1.06 |
| **Day 2; Condition #2 [T=160℃, VH=0 sccm; VA=1 mL/m in; P=555 psig]** | | | | | | | | | | | | | | |
| 6 | 7.0 | | 0.64 | 5.06 | | 0.26 | | | | 95.7 | 1.03 | 0 | 0.950 | 0.976 |
| 6 | 7.0 | | 0.65 | 5.15 | | 0.26 | | | | 95.8 | 1.03 | 0 | 0.966 | 0.992 |
| 7 | 8.0 | | 0.64 | 5.00 | | 0.23 | | | | 96.0 | 1.04 | 0 | 0.948 | 0.971 |
| **7** | 8.0 | | 0.64 | 5.01 | | 0.23 | | | | 96.1 | 1.04 | 0 | 0.949 | 0.970 |
| 8 | 9.0 | | 0.61 | 4.83 | | 0.23 | | | | 96.0 | 1.04 | 0 | 0.915 | 0.938 |
| 8 | 9.0 | | **0.63** | **5.07** | | **0.24** | | | | 96.0 | 1.04 | 0 | 0.958 | 0.981 |
| 9 | 10.0 | | 0.62 | 5.05 | | 0.23 | | | | 96.1 | 1.04 | 0 | 0.938 | 0.976 |
| 9 | 10.0 | | 0.62 | 5.03 | | 0.23 | | | | 96.1 | 1.04 | 0 | 0.951 | 0.973 |
| **Day 2; Condition #3 [T=160℃, VH=100 sccm; VA=1 mL /min; P=555 psig]** | | | | | | | | | | | | | | |
| 10 | 11.0 | | | | | | 0.79 | 5.65 | 0.41 | 82.4 | 1.04 | 147 | 0.935 | 1.134 |
| 10 | 11.0 | | | | | | 0.79 | 5.63 | 0.41 | 82.4 | 1.04 | 147 | 0.931 | 1.130 |
| 11 | 12.0 | | | | | | 0.69 | 5.44 | 0.41 | 83.2 | 1.04 | 147 | 0.899 | 1.081 |
| 11 | 12.0 | | | | | | 0.65 | 5.15 | 0.39 | 83.1 | 1.04 | 147 | 0.852 | 1.025 |
| 12 | 13.0 | | | | | | 0.62 | 5.34 | 0.40 | 83.9 | 1.04 | 147 | 0.88 | 1.05 |
| 12 | 13.0 | | | | | | 0.62 | 5.41 | 0.41 | 84.0 | 1.04 | 147 | 0.89 | 1.06 |
| 13 | 14.0 | | | | | | 0.56 | 5.39 | 0.42 | 84.7 | 1.04 | 147 | 0.892 | 1.05 |
| 13 | 14.0 | | | | | | 0.55 | 5.28 | 0.41 | 84.7 | 1.03 | 147 | 0.865 | 1.02 |

**Day 3; Condition #4 [T=160℃, VH=0 sccm; VA=0.5 mL /min; P=555 psig]**

| | | | | | | | | | | | |
|---|---|---|---|---|---|---|---|---|---|---|---|
| *14* | *16.0* | *0.70* | *5.70* | *0.26* | | *96.0* | *0.54* | 0 | *0.558* | *0.57* | *unsteady* |
| *14* | *16.0* | *0.70* | *5.68* | *0.27* | | *95.9* | *0.54* | 0 | *0.557* | *0.57* | |
| 15 | 17.0 | 0.78 | 6.55 | 0.29 | | 96.2 | 0.54 | 0 | 0.640 | 0.65 | |
| 15 | 17.0 | 0.75 | 6.19 | 0.28 | | 96.1 | 0.54 | 0 | 0.605 | 0.62 | |
| 16 | 18.0 | 0.74 | 6.12 | 0.27 | | 96.2 | 0.54 | 0 | 0.599 | 0.61 | |
| 16 | 18.0 | 0.75 | 6.21 | 0.28 | | 96.2 | 0.54 | 0 | 0.61 | 0.62 | |
| 17 | 19.0 | 0.77 | 6.44 | 0.28 | | 96.2 | 0.54 | 0 | 0.63 | 0.64 | |
| 17 | 19.0 | 0.76 | 6.22 | 0.28 | | 96.1 | 0.54 | 0 | 0.61 | 0.62 | |
| 18 | 20.0 | 0.78 | 6.58 | 0.29 | | 96.2 | 0.54 | 0 | 0.64 | 0.66 | |
| 18 | 20.0 | 0.74 | 6.04 | 0.27 | | 96.2 | 0.54 | 0 | 0.59 | 0.60 | |

**Day 3; Condition #5 [T=160℃, VH=100 sccm; VA=0.5 mL/min; P=555 psig]**

| | | | | | | | | | | | | |
|---|---|---|---|---|---|---|---|---|---|---|---|---|
| 19 | 21.0 | 0.2 | | 0.2 | 0.38 | 7.92 | 0.86 | 83.1 | 0.54 | 74 | 0.68 | 0.82 | |
| 19 | 21.0 | 0.2 | | | 0.39 | 8.02 | 0.87 | 85.0 | 0.54 | 74 | 0.69 | 0.81 | wait |
| 20 | 22.0 | 0.2 | | 0.3 | 0.39 | 8.81 | 1.02 | 82.7 | 0.54 | 74 | 0.76 | 0.91 | for steady |
| 20 | 22.0 | 0.2 | | 0.2 | 0.39 | 8.61 | 0.98 | 82.8 | 0.54 | 74 | 0.74 | 0.89 | state |
| 21 | 23.0 | 0.2 | | 0.3 | 0.36 | 8.93 | 1.08 | 82.3 | 0.54 | 74 | 0.77 | 0.93 | |
| 21 | 23.0 | 0.2 | | 0.3 | 0.37 | 8.98 | 1.09 | 82.4 | 0.54 | 74 | 0.77 | 0.94 | |
| 22 | 24.0 | 0.2 | | 0.3 | | 8.35 | 1.03 | 85.0 | 0.54 | 74 | 0.72 | 0.84 | |
| 23 | 25.0 | 0.2 | | 0.3 | | 9.39 | 1.19 | 84.8 | 0.54 | 74 | 0.81 | 0.95 | |

**Table E2-4** Process data for FBR experiment "BTRS-10"

The first condition in the data set below was a preliminary experiment "BTRS-9". Conditions 2-5 constitute "BTRS-10". Catalyst reduced in situ for 2 hrs at 100℃ before conditions #1,2 and 4.

Catalyst 066; (W=2.517 g)

| | | | | | | | | | | | | activity [g/hr*gcat] | |
|---|---|---|---|---|---|---|---|---|---|---|---|---|---|
| | TOS | C9 | Mass Fraction (wt%) | | | | | | | Select | Ac | H2 | MO/MIBK | Total |
| ID | (hr) | 1.9 min | IMO | MO | TMB | PHO | IPA | MIBK | DIBK | (wt %) | [mL/min] | (sccm) | | |
| **Day 1; Condition #1 [T=160℃, VH=120 sccm; VA=1.2 m L/min; P=555 psig]** | | | | | | | | | | | | | | |
| 1 | 8.0 | 0.19 | | | | | 0.61 | 5.91 | 0.59 | 81.0 | 1.24 | 177 | 1.379 | 1.70 |
| 1 | 8.0 | 0.07 | | | | | 0.76 | 6.96 | 0.62 | 82.8 | 1.24 | 177 | 1.623 | 1.96 |
| 2 | 9.0 | 0.07 | | | | | | 4.74 | 0.38 | 91.4 | 1.24 | 177 | 1.106 | 1.210 |
| 2 | 9.0 | 0.07 | | | | | | 4.80 | 0.39 | 91.2 | 1.24 | 177 | 1.120 | 1.228 |
| 3 | 10.0 | 0.19 | | | | | | 6.70 | 0.56 | 89.9 | 1.24 | 177 | 1.563 | 1.738 |
| 3 | 10.0 | 0.18 | | | | | | 6.43 | 0.55 | 89.8 | 1.24 | 177 | 1.500 | 1.67 |
| 4 | 11.0 | 0.18 | | | | | | 5.25 | 0.47 | 89.0 | 1.24 | 177 | 1.226 | 1.377 |
| **Day 2; Condition #2 [T=160℃, VH=105 sccm; VA=1.05 mL/min; P=600 psig]** | | | | | | | | | | | | | | |
| 1 | 13.0 | | | | 0.19 | | | 5.88 | 0.64 | 87.6 | 1.04 | 147 | 1.15 | 1.32 |
| 1B | 13.0 | | | | 0.19 | | | 5.84 | 0.63 | 87.7 | 1.04 | 147 | 1.15 | 1.31 |
| 2 | 14.0 | | | | 0.18 | | | 6.43 | 0.61 | 89.0 | 1.04 | 147 | 1.26 | 1.42 |
| 2B | 14.0 | | | | 0.18 | | | 6.51 | 0.62 | 89.0 | 1.04 | 147 | 1.28 | 1.44 |
| 3 | 15.0 | | | | 0.22 | | | 6.54 | 0.73 | 87.4 | 1.04 | 147 | 1.28 | 1.47 |
| 3B | 15.0 | | | | 0.21 | | | **5.96** | 0.69 | 87.0 | 1.04 | 147 | 1.17 | 1.35 |
| 4 | 16.0 | | | | | | | 5.48 | 0.57 | 90.5 | 1.04 | 147 | 1.08 | 1.19 |
| 4B | 16.0 | | | | 0.18 | | | 5.96 | 0.60 | 88.4 | 1.04 | 147 | 1.17 | 1.32 |

(cont'd)

**Day 2; Condition #3 [T=160℃, VH=105 sccm; VA=1.05 mL/min; P=15 psig]**

| | | | | | | | | | | | |
|---|---|---|---|---|---|---|---|---|---|---|---|
| 5 | 17.0 | | 1.54 | 1.65 | 0.37 | 46.4 | 1.04 | 147 | 0.325 | 0.700 | |
| 5b | 17.0 | | 1.68 | 1.83 | 0.39 | 46.8 | 1.04 | 147 | 0.359 | 0.766 | |
| 6 | 18.0 | | 1.60 | 1.48 | 0.33 | 43.5 | 1.04 | 147 | 0.291 | 0.670 | |
| 6b | 18.0 | | 1.69 | 1.57 | 0.34 | 43.6 | 1.04 | 147 | 0.308 | 0.707 | |
| 7 | 19.0 | | 1.86 | 1.58 | 0.33 | 41.9 | 1.04 | 147 | 0.31 | 0.74 | |
| 7b | 19.0 | | 1.91 | 1.61 | 0.33 | 41.8 | 1.04 | 147 | 0.32 | 0.76 | |
| 8 | 20.0 | | 1.57 | 1.31 | 0.27 | 41.6 | 1.04 | 147 | 0.257 | 0.62 | |
| 8b | 20.0 | | 1.58 | 1.31 | 0.28 | 41.5 | 1.04 | 147 | 0.258 | 0.62 | |

**Day 3; Condition #4[T=160℃, VH=105 sccm; VA=1.05 mL/min; P=120 psig]**

| | | | | | | | | | | | |
|---|---|---|---|---|---|---|---|---|---|---|---|
| 9 | 23.0 | | 1.34 | 4.51 | 0.62 | 69.8 | 1.04 | 147 | 0.886 | 1.27 | |
| 9b | 23.0 | | 1.21 | *3.95* | *0.56* | 69.1 | 1.04 | 147 | 0.776 | *1.12* | |
| 10 | 24.0 | | 1.14 | 4.30 | 0.57 | 71.6 | 1.04 | 147 | 0.844 | 1.18 | |
| 10b | 24.0 | | 1.21 | 4.67 | 0.61 | 71.9 | 1.04 | 147 | 0.916 | 1.27 | |
| 11 | 25.0 | | 1.15 | 4.26 | 0.56 | 71.4 | 1.04 | 147 | 0.836 | 1.17 | |
| 11b | 25.0 | | 1.05 | 3.77 | 0.51 | 70.7 | 1.04 | 147 | 0.74 | 1.05 | |
| 12 | 26.0 | | 1.12 | 4.50 | 0.58 | 72.6 | 1.04 | 147 | 0.88 | 1.22 | |
| 12b | 26.0 | | 1.01 | 3.80 | 0.53 | 71.1 | 1.04 | 147 | 0.75 | 1.05 | |

**Day 3; Condition #5 [T=160℃, VH=100 sccm; VA=0.5 mL/min; P=600 psig]**

| | | | | | | | | | | | |
|---|---|---|---|---|---|---|---|---|---|---|---|
| 13 | 27.0 | 0.5 | 0.30 | 9.75 | 1.20 | 83.2 | 1.04 | 147 | 1.91 | 2.30 | Preliminary |
| 13b | 27.0 | 0.4 | 0.26 | 7.78 | 1.02 | 82.4 | 1.04 | 147 | 1.53 | 1.85 | |

Problem with MFC; shut down

## E3 Analysis of Mass Transfer Effects for Kinetic Study in Batch Autoclave

**Table E3-1** Calculation of Hatta Number and Mears Parameter

**Test for Hydrogen Mass Transfer Limitation**

| Experiment | Wcat | T | r mibk | CH | k | kL | **Hatta** | **MEARS** | Sc | D |
|---|---|---|---|---|---|---|---|---|---|---|
| | | (K) | (kmol/kgcat*s) | (mol/L) | (m3/kmol*s) | (m/s) | **Ha** | parameter | | ($m^2$/s) |
| 199 | 0.4858 | 428 | 1.01294E-05 | 0.341188 | 1.27E-03 | 4.45E-05 | **0.099** | **0.010** | 27 | 1.53E-08 |
| 200 | 0.505 | 456 | 3.01E-05 | 0.418506 | 3.21E-03 | 4.64E-05 | **0.170** | **0.022** | 25 | 1.62E-08 |
| 201 | 0.4954 | 408 | 4.73E-06 | 0.412817 | 5.56E-04 | 4.31E-05 | **0.066** | **0.004** | 28 | 1.45E-08 |
| 203 | 0.4692 | 408 | 3.40E-06 | 0.412817 | 5.27E-04 | 4.31E-05 | **0.064** | **0.003** | 28 | 1.45E-08 |
| 204 | 0.4842 | 408 | 4.34E-06 | 0.176922 | 5.44E-04 | 4.31E-05 | **0.065** | **0.008** | 28 | 1.45E-08 |
| 205 | 0.4688 | 448 | 1.90E-05 | 0.552694 | 2.66E-03 | 4.59E-05 | **0.142** | **0.011** | 25 | 1.60E-08 |
| 206 | 0.4642 | 428 | 7.18E-06 | 0.341188 | 1.22E-03 | 4.45E-05 | **0.097** | **0.007** | 27 | 1.53E-08 |
| 207 | 0.4848 | 400 | 1.98E-06 | 0.278153 | 3.79E-04 | 4.26E-05 | **0.055** | **0.002** | 28 | 1.43E-08 |
| 208 | 0.4927 | 428 | 2.74E-06 | 0.148075 | 1.29E-03 | 4.45E-05 | **0.100** | **0.006** | 27 | 1.53E-08 |
| 209 | 0.4862 | 428 | 5.37E-06 | 0.5343 | 1.27E-03 | 4.45E-05 | **0.099** | **0.003** | 27 | 1.53E-08 |
| 210 | 0.4723 | 448 | 9.26E-06 | 0.236869 | 2.68E-03 | 4.59E-05 | **0.142** | **0.012** | 25 | 1.60E-08 |
| 211 | 0.4865 | 456 | 2.43457E-05 | 0.418506 | 3.68E-03 | 4.64E-05 | **0.167** | **0.018** | 25 | 1.62E-08 |
| 196 | 0.4853 | 408 | 2.44268E-06 | 0.228819 | 5.45E-04 | 4.31E-05 | **0.065** | **0.004** | 28 | 1.45E-08 |
| 197 | 0.6327 | 433 | 1.27887E-05 | 0.424634 | 2.02E-03 | 4.49E-05 | **0.125** | **0.010** | 26 | 1.54E-08 |

# Appendix F
## Supplementary Data: Chapter Eight

### F1 Soxhlet Extraction: Root cause analysis CD 003

Catalyst 066 used in pilot plant experiment CD 003 showed very low catalyst activity 0.02 [g/hr*gcat] after initially achieving an activity an order of magnitude higher after 5 hours TOS. A soxhlet extraction was carried to identify the chemical species adsorbed on the catalyst in order to identify any potential catalyst poisons.

19.2 g of catalyst was loaded into a thimble vial and inserted into a soxhlet extraction apparatus. HPLC toluene was boiled up and refluxed over the catalyst for one hour. After one hour the product was observed to be a bright amber colour. A sample of the extract was analyzed via GC/FID. The results are illustrated in Figure F1-1 and contrasted to a blank analysis of HPLC grade toluene.

**Figure F1-1** GC/FID analysis of soxhlet extract (Spent Catalyst 066; CD 003)

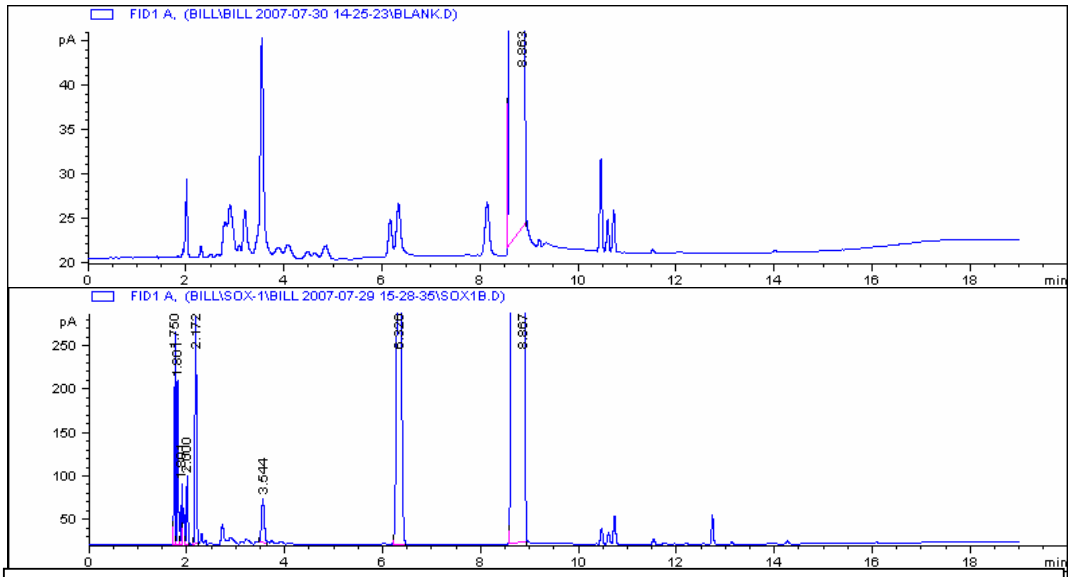


(top) GC/FID analysis of pure HPLC toluene used in soxhelete extraction

(bottom) GC/FID analysis of extract from soxhelete extra soxhlet

Unfortunately the ordinates are not scaled the soxhlet peak at 1.8 min (C9 hydrocarbon) and a peak around 12.7 min, possibly mesitylene, are observed in the soxhelete extract but not in the HPLC toluene blank. The peak at 2.1 min is much larger in the soxhelete extract compared to the HPLC toluene. However, there does not appear to be any conclusive indication of a catalyst poison in a significant concentration. The chromatogram beyond 15 minutes where phorones and other higher molecular mass species are usually observed is notably flat line for the GC/FID analysis of the soxhelete extract.

# Appendix G
## Permission to Re-print Copyrighted Material

### G1. Permission to reprint figures and data published previously in Chemical Industries *Catalysis of Organic Reactions* Volumes 104 and 115

Access Copyright have entered into agreement with the Copyright Clearance Center (CCC), a non-profit organization which manages the licensing and registration for the CRC Press publication "Catalysis of Organic Reactions", whereby Access Copyright act for CCC registered publishers in Canada. The legal department of Access Copyright has advised that since participation in the Theses Canada program is mandatory for Ph. D. and masters students at the University of Waterloo, then reproduction of the figures from these publications is covered by the University of Waterloo's comprehensive license and that no additional permission from the CRC Press, Taylor and Francis Group is required. The email correspondence with Access Copyright is attached below.

(continued next page)

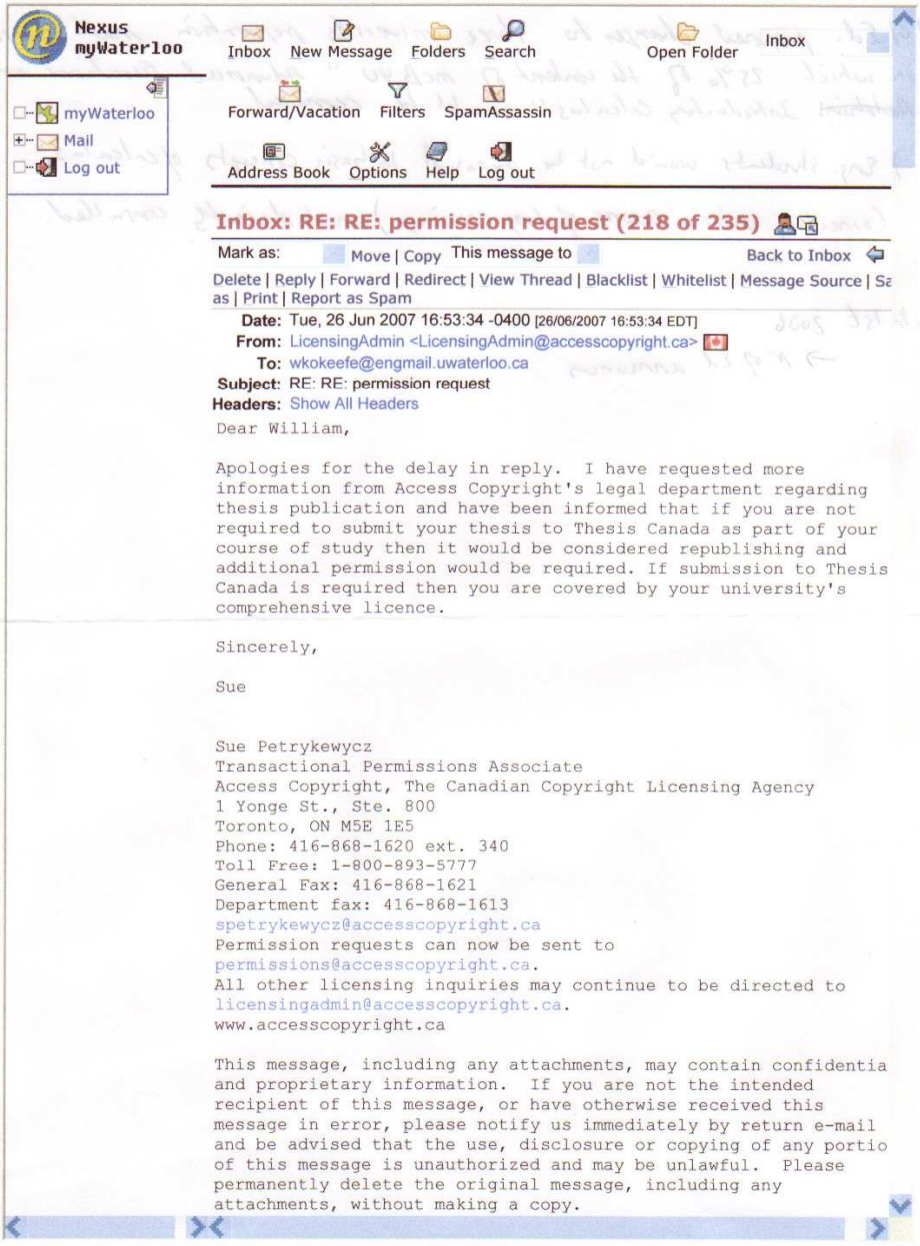

Nexus myWaterloo

Inbox | New Message | Folders | Search | Open Folder | Inbox

myWaterloo
Mail
Log out

Forward/Vacation | Filters | SpamAssassin

Address Book | Options | Help | Log out

**Inbox: RE: RE: permission request (218 of 235)**

Mark as: Move | Copy This message to Back to Inbox

Delete | Reply | Forward | Redirect | View Thread | Blacklist | Whitelist | Message Source | Sa as | Print | Report as Spam

**Date:** Tue, 26 Jun 2007 16:53:34 -0400 [26/06/2007 16:53:34 EDT]
**From:** LicensingAdmin <LicensingAdmin@accesscopyright.ca>
**To:** wkokeefe@engmail.uwaterloo.ca
**Subject:** RE: RE: permission request
**Headers:** Show All Headers

Dear William,

Apologies for the delay in reply. I have requested more information from Access Copyright's legal department regarding thesis publication and have been informed that if you are not required to submit your thesis to Thesis Canada as part of your course of study then it would be considered republishing and additional permission would be required. If submission to Thesis Canada is required then you are covered by your university's comprehensive licence.

Sincerely,

Sue

Sue Petrykewycz
Transactional Permissions Associate
Access Copyright, The Canadian Copyright Licensing Agency
1 Yonge St., Ste. 800
Toronto, ON M5E 1E5
Phone: 416-868-1620 ext. 340
Toll Free: 1-800-893-5777
General Fax: 416-868-1621
Department fax: 416-868-1613
spetrykewycz@accesscopyright.ca
Permission requests can now be sent to
permissions@accesscopyright.ca.
All other licensing inquiries may continue to be directed to
licensingadmin@accesscopyright.ca.
www.accesscopyright.ca

This message, including any attachments, may contain confidentia and proprietary information. If you are not the intended recipient of this message, or have otherwise received this message in error, please notify us immediately by return e-mail and be advised that the use, disclosure or copying of any portio of this message is unauthorized and may be unlawful. Please permanently delete the original message, including any attachments, without making a copy.

Dear William,

As dissertations and theses are considered to be unpublished works which students are required to complete for the purposes of their degree, this use is included under the incidental copying provisions of the comprehensive licence of your university. The work you would like to use is not on our excluded works list, and you wish to copy within the allowable limit (less than 10% of the entire original work).

The international copyright symbol ©, a credit to the author (including an identified artist or illustrator) and publisher must be included on all copies made under the licence, as well as the following notice "Copied under licence from Access Copyright. Further reproduction prohibited."

If however, you decide to publish the paper in a journal or in some other traditional way, then additional permission in the form of a transactional republication licence would be required.

Your school's comprehensive licence covers any unpublished use of your thesis. If you submit your completed thesis to Theses Canada, this is considered to be submission for publication as per the following from Theses Canada's website:

"The regulations for Legal Deposit do not require that theses be submitted to Library and Archives Canada since they are considered to be unpublished. Universities participating in the Theses Canada program voluntarily submit theses to LAC which then publishes the theses."

Your request would then be considered republishing and you would have to re-submit your republishing request to Access Copyright (using the attached form) and we would investigate the possibility of a transactional licence for you.

Yours sincerely,

Sue

Sue Petrykewycz
Transactional Permissions Associate
Access Copyright, The Canadian Copyright Licensing Agency
1 Yonge St., Ste. 800
Toronto, ON M5E 1E5
Phone: 416-868-1620 ext. 340
Toll Free: 1-800-893-5777
General Fax: 416-868-1621
Department fax: 416-868-1613
spetrykewycz@accesscopyright.ca
Permission requests can now be sent to
permissions@accesscopyright.ca.
All other licensing inquiries may continue to be directed to
licensingadmin@accesscopyright.ca.
www.accesscopyright.ca

-----Original Message-----
From: wkokeefe@engmail.uwaterloo.ca
[mailto:wkokeefe@engmail.uwaterloo.ca]
Sent: Monday, May 28, 2007 2:32 PM
To: LicensingAdmin
Subject: Fwd: RE: permission request

To whom it may concern,

I am a PhD student currently drafting my PhD dissertation and am writing to requrest permission in writing to use copyrighted material. Specifically, I would like to use figures published previously within two articles contained in separate volumes of "Cataylsis of Organic Reactions" (CRC Press,Taylor and
Francis) I am a co-author of both publications and intend to use these figures within my PhD thesis for academic credit. The specific figures and required information are outlined below.

Please be advised that the University of Waterloo receives a non-exclusive royalty free licence to: circulate the work as part of the University Library collection; make copies or representations of the work for academic purposes within the University; make copies of a thesis deposited in the University Library at the request of other universities or bona fide institutions; microfilm the work and submit the microfilm to the Library and Archives Canada; publish the abstract of any work which is a student thesis.

I would like to reproduce the following Figures from the following articles:
---
Publication: Catalysis of Organic Reactions, Chemical Industries,Vol. 115, pp.365-374.
Editor: Stephen R. Schmidt
Year: 2006
Publisher: CRC Press, Taylor and Francis Group
ISBN:10-0-8493-7557-6
Article: "The One-Step Synthesis of MIBK via Catalytic Distillation: A Prelimianry Pilot Scale Study"
Authors: W.K. O'Keefe, M. Jiang, F.T.T. Ng and G.L. Rempel
Request permission to reprint Figure 2 (page 367), Figures 4 and 5 (page 372) and Figure 6 (page 373)
---
Publication: Catalysis of Organic Reactions, in Chemical Industries,Vol. 104, pp. 261-266
Editor: John R. Sowa, Jr.
Year: 2005
Publisher: CRC Press, Taylor and Francis Group
ISBN:10-0-8493-7557-6
Article: "A Catalytic Distillation Process for the One-Step Synthesis of Methyl Isobutyl Ketone from Acetone:Liquid Phase Kinetics of the Selective Hydrogenation of MO"
Authors: W.K. O'Keefe, M. Jiang, F.T.T. Ng and G.L. Rempel
Request permission to reprint Figure 1 (page 263)

Best regards,
William K. O'Keefe, P.Eng.
PhD student

The University of Waterloo
Department of Chemical Engineering
519-888-4567 x.32879

----- Forwarded message from Brooke Whicher
<bwhicher@copyright.com> -----
    Date: Mon, 21 May 2007 15:43:19 -0400
    From: Brooke Whicher <bwhicher@copyright.com>
Reply-To: Brooke Whicher <bwhicher@copyright.com>
 Subject: RE: permission request
      To: wkokeefe@engmail.uwaterloo.ca

Dear William,

Copyright Clearance Center (CCC) has received your
correspondence requesting copyright permission.

I am pleased to inform you that CCC and the Canadian
Reproductive Rights Organizations, Access Copyright and
COPIBEC, have entered into reciprocal arrangements whereby
Access Copyright and COPIBEC act for CCC registered publishers
in Canada and, similarly, CCC acts for Canadian publishers
registered with them.  Access Copyright and COPIBEC have both
the relevant information about copyright compliance in Canada
and, the licensing systems available to simplify matters for
both rights owners and copyright users.

Inquiries from the province of Quebec should be directed to
COPIBEC, all others please contact Access Copyright:

Access Copyright,
The Canadian Copyright Licensing Agency
One Yonge Street, Suite 800
Toronto, Ontario M5E 1E5
Canada
Phone: 416-868-1620
or toll free 800-893-5777
Fax: 416-868-1621
Licensingadmin@accesscopyright.ca
www.accesscopyright.ca

COPIBEC
1290, Saint-Denis, 7th Floor
Montreal, Quebec H2X 3J7
Canada
Phone: 514-288-1644
or toll free 800-717-2022
Fax: 514-288-1699
www.copibec.qc.ca
Access Copyright or COPIBEC will provide a response to your
request for
copyright permission.

Sincerely,
Brooke Whicher
---
Copyright Clearance Center
www.copyright.com

-----Original Message-----
From: wkokeefe@engmail.uwaterloo.ca
[mailto:wkokeefe@engmail.uwaterloo.ca]
Sent: Saturday, May 19, 2007 12:07 AM
To: info@copyright.com

Delete | Reply | Reply to All | Forward | Redirect | Blacklist | Message Source | Save as | Print | Report as Spam

Back to INBOX

## G2. Permission to reprint figures previously published in Elsevier Science Journals

ELSEVIER

4 June 2007

Our ref: CT/SS/Jun 07/J001

William K. O'Keefe
155 Eramosa Rd
Guelph
Ontario
Canada, N1E 2M1

Dear Mr O'Keefe

***CATALYSIS TODAY, Vol 28, No 1-2, 1996, pp 49-58, Ichikuni et al, "Surface structures and…" Figure 1, schemes 1 & 2 only***
***CHEMICAL ENGINEERING SCIENCE, Vol 60, No 15, 2005, pp 4131-4140, O'Keefe et al, "Liquid phase kinetics…" Figures 4, 5 & 7 only***

As per your letter dated 10 May 2007, we hereby grant you permission to reprint the aforementioned material at no charge **in your thesis** subject to the following conditions:

1. If any part of the material to be used (for example, figures) has appeared in our publication with credit or acknowledgement to another source, permission must also be sought from that source. If such permission is not obtained then that material may not be included in your publication/copies.

2. Suitable acknowledgment to the source must be made, either as a footnote or in a reference list at the end of your publication, as follows:

   "This article was published in Publication title, Vol number, Author(s), Title of article, Page Nos, Copyright Elsevier (or appropriate Society name) (Year)."

3. Your thesis may be submitted to your institution in either print or electronic form.

4. Reproduction of this material is confined to the purpose for which permission is hereby given.

5. This permission is granted for non-exclusive world **English** rights only. For other languages please reapply separately for each one required. Permission excludes use in an electronic form other than submission. Should you have a specific electronic project in mind please reapply for permission.

6. This includes permission for the Library and Archives of Canada to supply single copies, on demand, of the complete thesis. Should your thesis be published commercially, please reapply for permission.

Yours sincerely

C. Truter

Clare Truter
Rights Manager, S&T

**Your future requests will be handled more quickly if you complete the online form at** www.elsevier.com/permissions

**Elsevier, Global Rights Department,** PO Box 800, Oxford OX5 1DX, UK
Tel +44 (0)1865 843830 | Fax +44 (0)1865 853333 | www.elsevier.com
vat no. 494 6272 12

## G3. Permission to reprint material previously published in ACS journals

**Arleen Courtney**


**From:** wkokeefe@engmail.uwaterloo.ca
**Sent:** Monday, June 04, 2007 12:50 PM
**To:** Copyright
**Subject:** permission to reprint figures

I am a PhD student currently preparing my PhD thesis for electronic submission (September 2007) for academic credit. I am writing to request permission in writing with authorizing signature to reprint copyrighted figures and data in Tables contained within an article from an ACS publication for which I am a co-author. The figures and data in Tables will be presented in the discussion of my thesis for academic credit.

I would like permission to reprint the following figures from W.K. O'Keefe, F.T.T. Ng and G.L. Rempel, "Experimental Studies on Syntheses of Mesityl Oxide and Methyl Isobutyl Ketone via Catalytic Distillation", Industrial and Engineering Chemistry Research, 46, (2007), pp.716-725.

Scheme 2
Figure 1
Figure 2
Figure 3
Figure 5
Figure 6
Figure 7
Figure 8

Data in Tables (in whole or in part)
Tables 1,2,3,4,5

Please be advised that I will be required to sign a Non-Exclusive License agreement that authorizes Library and Archives Canada to reproduce, communicate to the public on the Internet, loan, distribute or sell copies of my thesis, among other things."

Please send the written permission with authorizing signature to my home address below. Thank you for your assistance in this matter.

Best regards,
William K. O'Keefe
ACS member 2394938

155 Eramosa Rd
Guelph, Ontario, Canada, N1E 2M1

**PERMISSION TO REPRINT IS GRANTED BY THE AMERICAN CHEMICAL SOCIETY**

**ACS CREDIT LINE REQUIRED. Please follow this sample: Reprinted with permission from (reference citation). Copyright (year) American Chemical Society.**

"OR REPRINTED IN PART..."

**APPROVED BY:** *C. Arleen Courtney* 6/6/07
**ACS Copyright Office**

☐ **If box is checked, author permission is also required. See original article for address.**

1

## G4. Permission from MIT Press to reprint Figure from T.B. Reed (1971)

The MIT Press 55 Hayward Street Cambridge, Massachusetts 02142-1315

617 253 5646
617 258 6779 fax
http://mitpress.mit.edu

Massachusetts
Institute of
Technology

June 28, 2007

William O'Keefe
155 Eramosa Road
Guelph, Ontario
CANADA N1E 2M1

Dear William O'Keefe,

I am happy to grant you non-exclusive permission to reprint 1 figure from FREE ENERGY OF FORMATION OF BINARY COMPOUNDS, to appear in your thesis for The University of Waterloo. Please credit the reprinted figure to the author Thomas B. Reed, the book title, and The MIT Press. This permission allows the inclusion of your work in the Theses Canada library.

Please contact me if you have any questions.

Best regards,

Pamela Quick

Pamela Quick
MIT Press Permissions